nature

HANDOVER

New opportunities, new obligations

PHEROMONES AT FIFTY

On the track of human scent

HYBRID VIGOUR

Plants solve the day

THE STARS THAT WOULDN'T DIE

'Blue stragglers' explained

nature

www.nature.com/nature

Vol 457 | Issue no. 7227 | 15 January 2009

Science is not a spectator sport

As Barack Obama sets a fresh agenda for the US approach to climate change and energy, scientists must make sure that they do not merely watch from the sidelines.

For months now, US president-elect Barack Obama, his economic advisers and the incoming Congress have been in broad agreement. They believe that the worst recession in decades should be fought not just through short-term job creation, but by pouring hundreds of billions of dollars into long-term investments — including huge pushes in education, science and technology (see page 240).

That prospect has US scientists almost rubbing their hands in anticipation. But they would be wrong to view this simply as a chance to get more money. They will also need to help Obama clean up George W. Bush's legacy on science-related issues ranging from nuclear non-proliferation (see page 250) to endangered species (see page 252). And they must help him retool the scientific capabilities of agencies throughout the federal government. Some early road maps towards that goal can be found on page 258, where experts discuss issues from fixing the Food and Drug Administration to revitalizing the country's embryonic stem-cell research programme.

There is one area that definitely needs a well-organized and massive injection of funds: climate change. The United States now has an opportunity to wean itself off fossil fuels and move towards carbon-free sources of energy. But the government must commit itself to a rational, well-organized plan for doing so, and then sustain that plan into the future.

It is promising that Obama has already put an emphasis on energy efficiency. This is a priority of energy-secretary nominee Steven Chu (see page 241) and is the approach that offers by far the biggest energy saving per dollar invested. A less promising idea is the Advanced Research Projects Agency for Energy, or ARPA-E, which is meant to be modelled on the defence-research agency DARPA. Chu has supported this, congressional leaders are behind it, and on the surface it sounds like a good idea: putting bright minds in a single lean-and-mean agency to come up with radical energy innovations. But, as this journal has noted before, ARPA-E must be structured very carefully to escape gridlock from the competing industry interests that otherwise drag down federal efforts at energy reform (see *Nature* **438,** 129; 2005).

The biggest question, however, is how the United States will contain its greenhouse-gas emissions. A tax on carbon would be the most straightforward route, but is not politically feasible. Obama has advocated a cap-and-trade system for regulating emissions, a system that — at America's early insistence — has become the model of choice internationally. The United States must now learn the right lessons from the European emissions-trading system — don't give away allowances for free, for example, or sell them too cheaply — in order to institute its own system effectively.

"One area that definitely needs a well-organized and massive injection of funds is climate change."

Obama must also set up the infrastructure to support such a system and to drive a low-carbon economy. One top priority is expanding and improving the electricity grid to accommodate solar and wind energy. Another is a long-term adaptation strategy to help the nation's cities and states cope with the changing climate. But solving these and other such problems will require new policies and decades of reliable investment.

By putting these issues on the table before being sworn into office on 20 January, Obama has established climate as a major priority for his administration. Now he needs to follow through. Around Washington the talk is that climate is like health care in 1993, when incoming president Bill Clinton made it a signature issue and put his smartest people on it — only to watch it fail spectacularly. Scientists must help Obama ensure that climate action doesn't suffer the same fate. ■

The biggest threat?

The Obama administration must help prevent terrorists from building a nuclear device.

The US president should have someone reporting directly to him, who has no other mission other than "to wake up every morning thinking: 'What can I do today to keep nuclear weapons out of the hands of terrorists?'" That 2002 recommendation comes from a report co-authored by John Holdren, who is now scientific adviser to US president-elect Barack Obama. It is good news that Holdren understands the key nuclear non-proliferation issues, as bold US leadership is urgently needed to renew such efforts, especially given the damage done to these initiatives under the administration of George W. Bush (see page 250).

Holdren also understands that getting the international cooperation, and impetus, needed to revitalize non-proliferation will demand that the United States and other nuclear-weapons states make greater efforts to reduce their own arsenals and stockpiles. Obama could relay a strong message here by sending the Comprehensive Test Ban Treaty to the Senate for ratification.

Tangible steps could also be taken at once to substantially reduce the immediate threat of nuclear terrorism. What has been lacking is political will: a trade deal on bananas gets greater political priority than does non-proliferation. National and international measures to counter nuclear terrorism remain scandalously spartan and fragmented, and not remotely commensurate with the scale of the threat.

US support for all non-proliferation has been flat at between $1 billion and $1.5 billion annually over the past decade, or around 0.2% of

nature

www.nature.com/nature

Vol 457 | Issue no. 7227 | 15 January 2009

Science is not a spectator sport

As Barack Obama sets a fresh agenda for the US approach to climate change and energy, scientists must make sure that they do not merely watch from the sidelines.

For months now, US president-elect Barack Obama, his economic advisers and the incoming Congress have been in broad agreement. They believe that the worst recession in decades should be fought not just through short-term job creation, but by pouring hundreds of billions of dollars into long-term investments — including huge pushes in education, science and technology (see page 240).

That prospect has US scientists almost rubbing their hands in anticipation. But they would be wrong to view this simply as a chance to get more money. They will also need to help Obama clean up George W. Bush's legacy on science-related issues ranging from nuclear non-proliferation (see page 250) to endangered species (see page 252). And they must help him retool the scientific capabilities of agencies throughout the federal government. Some early road maps towards that goal can be found on page 258, where experts discuss issues from fixing the Food and Drug Administration to revitalizing the country's embryonic stem-cell research programme.

There is one area that definitely needs a well-organized and massive injection of funds: climate change. The United States now has an opportunity to wean itself off fossil fuels and move towards carbon-free sources of energy. But the government must commit itself to a rational, well-organized plan for doing so, and then sustain that plan into the future.

It is promising that Obama has already put an emphasis on energy efficiency. This is a priority of energy-secretary nominee Steven Chu (see page 241) and is the approach that offers by far the biggest energy saving per dollar invested. A less promising idea is the Advanced Research Projects Agency for Energy, or ARPA-E, which is meant to be modelled on the defence-research agency DARPA. Chu has supported this, congressional leaders are behind it, and on the surface it sounds like a good idea: putting bright minds in a single lean-and-mean agency to come up with radical energy innovations. But, as this journal has noted before, ARPA-E must be structured very carefully to escape gridlock from the competing industry interests that otherwise drag down federal efforts at energy reform (see *Nature* **438,** 129; 2005).

The biggest question, however, is how the United States will contain its greenhouse-gas emissions. A tax on carbon would be the most straightforward route, but is not politically feasible. Obama has advocated a cap-and-trade system for regulating emissions, a system that — at America's early insistence — has become the model of choice internationally. The United States must now learn the right lessons from the European emissions-trading system — don't give away allowances for free, for example, or sell them too cheaply — in order to institute its own system effectively.

"One area that definitely needs a well-organized and massive injection of funds is climate change."

Obama must also set up the infrastructure to support such a system and to drive a low-carbon economy. One top priority is expanding and improving the electricity grid to accommodate solar and wind energy. Another is a long-term adaptation strategy to help the nation's cities and states cope with the changing climate. But solving these and other such problems will require new policies and decades of reliable investment.

By putting these issues on the table before being sworn into office on 20 January, Obama has established climate as a major priority for his administration. Now he needs to follow through. Around Washington the talk is that climate is like health care in 1993, when incoming president Bill Clinton made it a signature issue and put his smartest people on it — only to watch it fail spectacularly. Scientists must help Obama ensure that climate action doesn't suffer the same fate. ■

The biggest threat?

The Obama administration must help prevent terrorists from building a nuclear device.

The US president should have someone reporting directly to him, who has no other mission other than "to wake up every morning thinking: 'What can I do today to keep nuclear weapons out of the hands of terrorists?'" That 2002 recommendation comes from a report co-authored by John Holdren, who is now scientific adviser to US president-elect Barack Obama. It is good news that Holdren understands the key nuclear non-proliferation issues, as bold US leadership is urgently needed to renew such efforts, especially given the damage done to these initiatives under the administration of George W. Bush (see page 250).

Holdren also understands that getting the international cooperation, and impetus, needed to revitalize non-proliferation will demand that the United States and other nuclear-weapons states make greater efforts to reduce their own arsenals and stockpiles. Obama could relay a strong message here by sending the Comprehensive Test Ban Treaty to the Senate for ratification.

Tangible steps could also be taken at once to substantially reduce the immediate threat of nuclear terrorism. What has been lacking is political will: a trade deal on bananas gets greater political priority than does non-proliferation. National and international measures to counter nuclear terrorism remain scandalously spartan and fragmented, and not remotely commensurate with the scale of the threat.

US support for all non-proliferation has been flat at between $1 billion and $1.5 billion annually over the past decade, or around 0.2% of

total US defence spending. Flat too has been support for the International Atomic Energy Agency — the watchdog responsible for ensuring that national civil nuclear efforts remain civil — which remains hamstrung by the lack of any official remit to tackle the newer threat of nuclear terrorism (see *Nature* **451,** 745; 2008).

The know-how to make a rudimentary nuclear weapon is already out there in the wild and cannot be recalled. But non-state players lack the means to produce the base fissile material needed: either highly enriched uranium (HEU) or plutonium. Blocking the theft or diversion of the vast stockpiles of these materials worldwide is therefore the most urgent issue for the international community.

HEU is the biggest worry. A plutonium device involves compressing a sphere of the metal with high explosives and would be a stretch for terrorists. An HEU device, by comparison, is child's play, demanding little more than a few dozen kilograms of the material and a simple mechanism to achieve a high-speed collision. Even a fizzle of an HEU device would take out most of Manhattan.

Incomprehensibly, there is no complete inventory of HEU stocks. But some 50 or so tonnes of it is thought to be stored in poorly secured civilian facilities worldwide, according to estimates by the Nuclear Threat Initiative in Washington DC. Most of that is used for research and medicine, for example in neutron sources and the production of medical isotopes. Low-enriched uranium (LEU) alternatives are available in almost all cases, but the extra costs involved, and the reactor redesign and extra research needed, have hampered efforts to switch over.

"Incomprehensibly, there is no complete inventory of stocks of highly enriched uranium."

That some 272 HEU reactors in 56 countries remain largely unsecured is simply unacceptable. All civilian HEU facilities must either promptly switch to LEU or be given military-level security.

Securing HEU is just one of many non-proliferation issues — from Iran and North Korea to reductions in arsenals and missile defence — that will be on Obama's plate. But the time is ripe for a renewed global non-proliferation effort to avoid the world having to ask the day after a nuclear terrorist attack: "How did we fail to see this coming; why didn't we do something about it before?" ■

A lifesaving arrangement

George Bush's AIDS programme needs leadership and support from the Obama administration.

The focus of president-elect Barack Obama's incoming administration is understandably green jobs and a stimulus package to revive the flagging economy. But officials should not neglect one of George W. Bush's few well-received initiatives: the President's Emergency Plan For AIDS Relief (PEPFAR).

Unveiled in 2003, PEPFAR is a massive international programme to help those infected with HIV. More than 2 million people have been treated under its auspices, and it is widely hailed for proving that lifesaving AIDS treatments can be administered anywhere in the world — even in very poor countries where health systems were thought to be inadequate for the task (see page 254). But the programme now faces a long list of challenges. The first is to rid itself of scientifically unsound restrictions that prevent it from meeting its full potential. Examples include rules, imposed to satisfy the US religious right, that committed part of its funds to education on sexual abstinence and that made it difficult for organizations receiving PEPFAR funds to work with people at high risk of contracting HIV, such as prostitutes. The abstinence provisions have now been softened, but many restrictions remain, such as ill-advised policies preventing PEPFAR funding recipients from integrating with family-planning groups.

Another challenge is to convince Congress to spend the $48 billion it authorized for the programme's continuation last summer — before the domestic and world economies imploded. Yet another is to expand PEPFAR to reach AIDS sufferers who still desperately need care.

Then there is the challenge of prevention, an area in which health officials acknowledge they have not made much headway, even as consensus grows that this is the key to stopping the epidemic. And perhaps most difficult of all is the challenge of sustaining PEPFAR in the future. AIDS cannot yet be cured, only held at bay. So PEPFAR must make a lifetime commitment to monitor the patients it is now serving, enrol them on antiretroviral treatment once they need it, and help them switch to new therapies as they develop drug resistance. This means that the programme will become much more expensive if it is to maintain its beneficial momentum.

For PEPFAR to navigate these challenges successfully, Obama will need to appoint a programme leader with scientific integrity and global stature. Meanwhile, PEPFAR's success abroad has led some to ask whether it is time for an equivalent programme within the United States, where public-health officials have stumbled badly in their efforts to fight the disease. Last year, the US Centers for Disease Control and Prevention in Atlanta, Georgia, revealed it had underestimated the number of new HIV infections by 40%. There are serious barriers to HIV testing, such as inadequate policies to ensure people get tested and pay for the tests, and hundreds of thousands of those infected with the virus don't know they have it. The death in December of Christine Maggiore, an HIV-positive Los Angeles woman who argued that HIV does not cause AIDS, highlighted the fact that the same stigma and denial driving the epidemic around the world can also be found in the United States.

"The same stigma and denial driving the AIDS epidemic around the world can also be found in the United States."

Doctors, activists and scientists have urged the United States to fill the vacant post of AIDS adviser at the White House to revitalize domestic efforts against the disease. They are also calling for a national AIDS policy to govern funding akin to PEPFAR's rules, under which aid recipients must explain how the funding fits their national goals to fight the epidemic. Obama should heed these calls, which would represent a significant step towards restoring the country's status as a leader in global health — both abroad and at home. ■

total US defence spending. Flat too has been support for the International Atomic Energy Agency — the watchdog responsible for ensuring that national civil nuclear efforts remain civil — which remains hamstrung by the lack of any official remit to tackle the newer threat of nuclear terrorism (see *Nature* **451,** 745; 2008).

The know-how to make a rudimentary nuclear weapon is already out there in the wild and cannot be recalled. But non-state players lack the means to produce the base fissile material needed: either highly enriched uranium (HEU) or plutonium. Blocking the theft or diversion of the vast stockpiles of these materials worldwide is therefore the most urgent issue for the international community.

HEU is the biggest worry. A plutonium device involves compressing a sphere of the metal with high explosives and would be a stretch for terrorists. An HEU device, by comparison, is child's play, demanding little more than a few dozen kilograms of the material and a simple mechanism to achieve a high-speed collision. Even a fizzle of an HEU device would take out most of Manhattan.

Incomprehensibly, there is no complete inventory of HEU stocks. But some 50 or so tonnes of it is thought to be stored in poorly secured civilian facilities worldwide, according to estimates by the Nuclear Threat Initiative in Washington DC. Most of that is used for research and medicine, for example in neutron sources and the production of medical isotopes. Low-enriched uranium (LEU) alternatives are available in almost all cases, but the extra costs involved, and the reactor redesign and extra research needed, have hampered efforts to switch over.

"Incomprehensibly, there is no complete inventory of stocks of highly enriched uranium."

That some 272 HEU reactors in 56 countries remain largely unsecured is simply unacceptable. All civilian HEU facilities must either promptly switch to LEU or be given military-level security.

Securing HEU is just one of many non-proliferation issues — from Iran and North Korea to reductions in arsenals and missile defence — that will be on Obama's plate. But the time is ripe for a renewed global non-proliferation effort to avoid the world having to ask the day after a nuclear terrorist attack: "How did we fail to see this coming; why didn't we do something about it before?" ■

A lifesaving arrangement

George Bush's AIDS programme needs leadership and support from the Obama administration.

The focus of president-elect Barack Obama's incoming administration is understandably green jobs and a stimulus package to revive the flagging economy. But officials should not neglect one of George W. Bush's few well-received initiatives: the President's Emergency Plan For AIDS Relief (PEPFAR).

Unveiled in 2003, PEPFAR is a massive international programme to help those infected with HIV. More than 2 million people have been treated under its auspices, and it is widely hailed for proving that lifesaving AIDS treatments can be administered anywhere in the world — even in very poor countries where health systems were thought to be inadequate for the task (see page 254). But the programme now faces a long list of challenges. The first is to rid itself of scientifically unsound restrictions that prevent it from meeting its full potential. Examples include rules, imposed to satisfy the US religious right, that committed part of its funds to education on sexual abstinence and that made it difficult for organizations receiving PEPFAR funds to work with people at high risk of contracting HIV, such as prostitutes. The abstinence provisions have now been softened, but many restrictions remain, such as ill-advised policies preventing PEPFAR funding recipients from integrating with family-planning groups.

Another challenge is to convince Congress to spend the $48 billion it authorized for the programme's continuation last summer — before the domestic and world economies imploded. Yet another is to expand PEPFAR to reach AIDS sufferers who still desperately need care.

Then there is the challenge of prevention, an area in which health officials acknowledge they have not made much headway, even as consensus grows that this is the key to stopping the epidemic. And perhaps most difficult of all is the challenge of sustaining PEPFAR in the future. AIDS cannot yet be cured, only held at bay. So PEPFAR must make a lifetime commitment to monitor the patients it is now serving, enrol them on antiretroviral treatment once they need it, and help them switch to new therapies as they develop drug resistance. This means that the programme will become much more expensive if it is to maintain its beneficial momentum.

For PEPFAR to navigate these challenges successfully, Obama will need to appoint a programme leader with scientific integrity and global stature. Meanwhile, PEPFAR's success abroad has led some to ask whether it is time for an equivalent programme within the United States, where public-health officials have stumbled badly in their efforts to fight the disease. Last year, the US Centers for Disease Control and Prevention in Atlanta, Georgia, revealed it had underestimated the number of new HIV infections by 40%. There are serious barriers to HIV testing, such as inadequate policies to ensure people get tested and pay for the tests, and hundreds of thousands of those infected with the virus don't know they have it. The death in December of Christine Maggiore, an HIV-positive Los Angeles woman who argued that HIV does not cause AIDS, highlighted the fact that the same stigma and denial driving the epidemic around the world can also be found in the United States.

"The same stigma and denial driving the AIDS epidemic around the world can also be found in the United States."

Doctors, activists and scientists have urged the United States to fill the vacant post of AIDS adviser at the White House to revitalize domestic efforts against the disease. They are also calling for a national AIDS policy to govern funding akin to PEPFAR's rules, under which aid recipients must explain how the funding fits their national goals to fight the epidemic. Obama should heed these calls, which would represent a significant step towards restoring the country's status as a leader in global health — both abroad and at home. ■

RESEARCH HIGHLIGHTS

Old Faithful Erebus

J. Volcanol. Geotherm. Res. **177,** 589–605 (2008)
Sited on the Terror rift of the Western Ross Sea, Antarctica, Mount Erebus is the continent's most active volcano and has a rare convecting magma lake at its summit. Peter Kelly of the New Mexico Institute of Mining and Technology in Socorro and his colleagues investigated the composition of this lake using lava bombs it spewed forth from 1972 to 2004.

Analysis of the glass and mineral composition of these bombs indicates that the temperature of the magma has been stable during this period, contradicting a previous suggestion of a cooling. Another analysis of 11 dated lava samples from the summit plateau ranging back to 17,000 years ago shows that the volcano has erupted lava with the same bulk composition for all this time.

G. STEINMETZ/CORBIS

CHEMICAL BIOLOGY

Fluorescent timers

Nature Chem. Biol. doi:10.1038/nchembio.138 (2009)
New fluorescent 'timers' that gradually change colour from blue to red could allow researchers to track the age and dynamic behaviour of proteins in living cells.

Previous work suggested that some red fluorescent proteins start out fluorescing blue, but then change to red as the protein is chemically modified over time. Vladislav Verkhusha and his colleagues at the Albert Einstein College of Medicine in New York mutated a red fluorescent protein called mCherry, then screened for mutants that had altered maturation rates from blue to red.

The researchers developed three fluorescent proteins, each with a specific maturation rate. The proteins were used to track newly synthesized proteins in mammalian cells grown in culture.

MICROSCOPY

Inside information

Phys. Rev. Lett. **102,** 018101 (2009)
Sliced chromosome is on the menu, thanks to a tour-de-force of X-ray microscopy. Yoshinori Nishino of the RIKEN SPring-8 Center in Hyogo, Japan, and his co-workers have recorded three-dimensional sectional images of a human chromosome (pictured right) using coherent X-ray diffraction microscopy.

Chromosomes are too dense for electron microscopes to see 'inside' them, and fluorescent light microscopy can reveal only selected features. By contrast, the X-ray diffraction method offers a full three-dimensional view of electron density in a single chromosome about 2 micrometres across, showing the internal structure with a resolution of about 120 nanometres.

AM. PHYS. SOC.

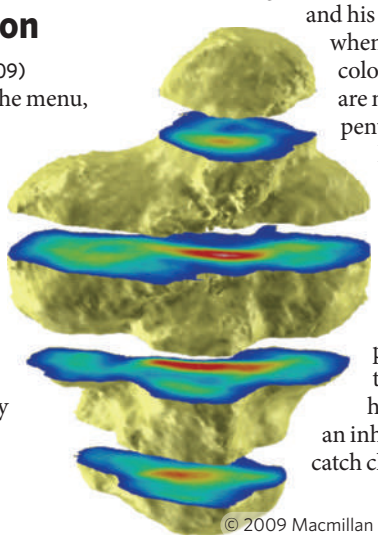

ANIMAL BEHAVIOUR

Caught red hydrocarboned

Curr. Biol. **19,** 78–81 (2009)
Ants, like other social creatures, strive to minimize antisocial behaviour by punishing cheaters. For example, fertile worker *Aphaenogaster cockerelli* ants that could undermine the unity of a colony with a single reproducing queen are attacked by nestmates. Although it has remained unclear how would-be cheats are identified, evidence suggested that variations in the hydrocarbons in ants' cuticles might be involved. Jürgen Liebig of Arizona State University in Tempe and his colleagues show that when *A. cockerelli* workers in colonies headed up by a queen are manually coated with pentacosane, a hydrocarbon linked with fertility, they are attacked by their nestmates.

Because ant eggs carry distinctive related hydrocarbons that prevent them from being identified and destroyed, cheaters probably cannot suppress their chemical profiles. Thus, hydrocarbons could provide an inherently reliable method to catch cheats.

MOLECULAR BIOLOGY

A bilingual genetic code

Science **323,** 259–261 (2009)
A ciliate called *Euplotes crassus* seems to have violated the rules of genetics.

Messenger RNA is used as a template to assemble proteins by means of three-letter sequences called codons. Each codon corresponds to either a single amino acid or a 'stop' signal. However, Vadim Gladyshev of the University of Nebraska in Lincoln and his colleagues found that in *E. crassus*, the codon UGA could encode two amino acids: cysteine or selenocysteine.

The codon could be read in both ways within the same gene, depending on its location within the mRNA strand and the presence and exposure of a specific sequence near the end of the mRNA molecule. The results suggest that the genetic code can be evolutionarily expanded.

ECOLOGICAL ACOUSTICS

Love buzz

Science doi:10.1126/science.1166541 (2009)
The buzz of flying female mosquitoes acts as a mating signal to attract males. When Ronald Hoy and his team at Cornell University in Ithaca, New York, listened closer, they found that when both sexes of *Aedes aegypti* get together, they change their buzz pitch to match, producing a courtship duet. But rather than duo at their usual wing beat frequencies — of around 400 hertz for females and 600 hertz in males — the mosquitoes take their acoustics up a notch to a shared harmonic frequency of 1,200 hertz.

Male mosquitoes were previously thought to be deaf to frequencies above 800 hertz.

RESEARCH HIGHLIGHTS

Old Faithful Erebus

J. Volcanol. Geotherm. Res. **177,** 589–605 (2008)
Sited on the Terror rift of the Western Ross Sea, Antarctica, Mount Erebus is the continent's most active volcano and has a rare convecting magma lake at its summit. Peter Kelly of the New Mexico Institute of Mining and Technology in Socorro and his colleagues investigated the composition of this lake using lava bombs it spewed forth from 1972 to 2004.

Analysis of the glass and mineral composition of these bombs indicates that the temperature of the magma has been stable during this period, contradicting a previous suggestion of a cooling. Another analysis of 11 dated lava samples from the summit plateau ranging back to 17,000 years ago shows that the volcano has erupted lava with the same bulk composition for all this time.

G. STEINMETZ/CORBIS

CHEMICAL BIOLOGY

Fluorescent timers

Nature Chem. Biol. doi:10.1038/nchembio.138 (2009)
New fluorescent 'timers' that gradually change colour from blue to red could allow researchers to track the age and dynamic behaviour of proteins in living cells.

Previous work suggested that some red fluorescent proteins start out fluorescing blue, but then change to red as the protein is chemically modified over time. Vladislav Verkhusha and his colleagues at the Albert Einstein College of Medicine in New York mutated a red fluorescent protein called mCherry, then screened for mutants that had altered maturation rates from blue to red.

The researchers developed three fluorescent proteins, each with a specific maturation rate. The proteins were used to track newly synthesized proteins in mammalian cells grown in culture.

MICROSCOPY

Inside information

Phys. Rev. Lett. **102,** 018101 (2009)
Sliced chromosome is on the menu, thanks to a tour-de-force of X-ray microscopy. Yoshinori Nishino of the RIKEN SPring-8 Center in Hyogo, Japan, and his co-workers have recorded three-dimensional sectional images of a human chromosome (pictured right) using coherent X-ray diffraction microscopy.

Chromosomes are too dense for electron microscopes to see 'inside' them, and fluorescent light microscopy can reveal only selected features. By contrast, the X-ray diffraction method offers a full three-dimensional view of electron density in a single chromosome about 2 micrometres across, showing the internal structure with a resolution of about 120 nanometres.

AM. PHYS. SOC.

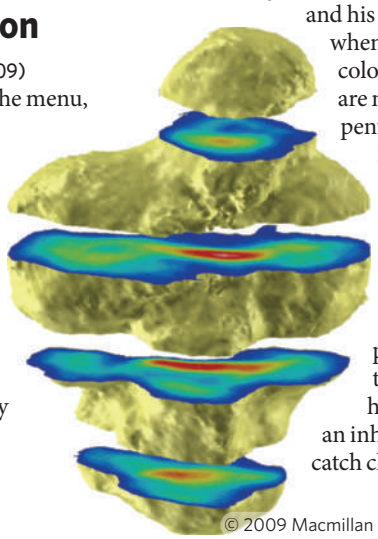

ANIMAL BEHAVIOUR

Caught red hydrocarboned

Curr. Biol. **19,** 78–81 (2009)
Ants, like other social creatures, strive to minimize antisocial behaviour by punishing cheaters. For example, fertile worker *Aphaenogaster cockerelli* ants that could undermine the unity of a colony with a single reproducing queen are attacked by nestmates. Although it has remained unclear how would-be cheats are identified, evidence suggested that variations in the hydrocarbons in ants' cuticles might be involved. Jürgen Liebig of Arizona State University in Tempe and his colleagues show that when *A. cockerelli* workers in colonies headed up by a queen are manually coated with pentacosane, a hydrocarbon linked with fertility, they are attacked by their nestmates.

Because ant eggs carry distinctive related hydrocarbons that prevent them from being identified and destroyed, cheaters probably cannot suppress their chemical profiles. Thus, hydrocarbons could provide an inherently reliable method to catch cheats.

MOLECULAR BIOLOGY

A bilingual genetic code

Science **323,** 259–261 (2009)
A ciliate called *Euplotes crassus* seems to have violated the rules of genetics.

Messenger RNA is used as a template to assemble proteins by means of three-letter sequences called codons. Each codon corresponds to either a single amino acid or a 'stop' signal. However, Vadim Gladyshev of the University of Nebraska in Lincoln and his colleagues found that in *E. crassus*, the codon UGA could encode two amino acids: cysteine or selenocysteine.

The codon could be read in both ways within the same gene, depending on its location within the mRNA strand and the presence and exposure of a specific sequence near the end of the mRNA molecule. The results suggest that the genetic code can be evolutionarily expanded.

ECOLOGICAL ACOUSTICS

Love buzz

Science doi:10.1126/science.1166541 (2009)
The buzz of flying female mosquitoes acts as a mating signal to attract males. When Ronald Hoy and his team at Cornell University in Ithaca, New York, listened closer, they found that when both sexes of *Aedes aegypti* get together, they change their buzz pitch to match, producing a courtship duet. But rather than duo at their usual wing beat frequencies — of around 400 hertz for females and 600 hertz in males — the mosquitoes take their acoustics up a notch to a shared harmonic frequency of 1,200 hertz.

Male mosquitoes were previously thought to be deaf to frequencies above 800 hertz.

RESEARCH HIGHLIGHTS

Old Faithful Erebus

J. Volcanol. Geotherm. Res. **177,** 589–605 (2008)
Sited on the Terror rift of the Western Ross Sea, Antarctica, Mount Erebus is the continent's most active volcano and has a rare convecting magma lake at its summit. Peter Kelly of the New Mexico Institute of Mining and Technology in Socorro and his colleagues investigated the composition of this lake using lava bombs it spewed forth from 1972 to 2004.

Analysis of the glass and mineral composition of these bombs indicates that the temperature of the magma has been stable during this period, contradicting a previous suggestion of a cooling. Another analysis of 11 dated lava samples from the summit plateau ranging back to 17,000 years ago shows that the volcano has erupted lava with the same bulk composition for all this time.

G. STEINMETZ/CORBIS

CHEMICAL BIOLOGY

Fluorescent timers

Nature Chem. Biol. doi:10.1038/nchembio.138 (2009)
New fluorescent 'timers' that gradually change colour from blue to red could allow researchers to track the age and dynamic behaviour of proteins in living cells.

Previous work suggested that some red fluorescent proteins start out fluorescing blue, but then change to red as the protein is chemically modified over time. Vladislav Verkhusha and his colleagues at the Albert Einstein College of Medicine in New York mutated a red fluorescent protein called mCherry, then screened for mutants that had altered maturation rates from blue to red.

The researchers developed three fluorescent proteins, each with a specific maturation rate. The proteins were used to track newly synthesized proteins in mammalian cells grown in culture.

MICROSCOPY

Inside information

Phys. Rev. Lett. **102,** 018101 (2009)
Sliced chromosome is on the menu, thanks to a tour-de-force of X-ray microscopy. Yoshinori Nishino of the RIKEN SPring-8 Center in Hyogo, Japan, and his co-workers have recorded three-dimensional sectional images of a human chromosome (pictured right) using coherent X-ray diffraction microscopy.

Chromosomes are too dense for electron microscopes to see 'inside' them, and fluorescent light microscopy can reveal only selected features. By contrast, the X-ray diffraction method offers a full three-dimensional view of electron density in a single chromosome about 2 micrometres across, showing the internal structure with a resolution of about 120 nanometres.

AM. PHYS. SOC.

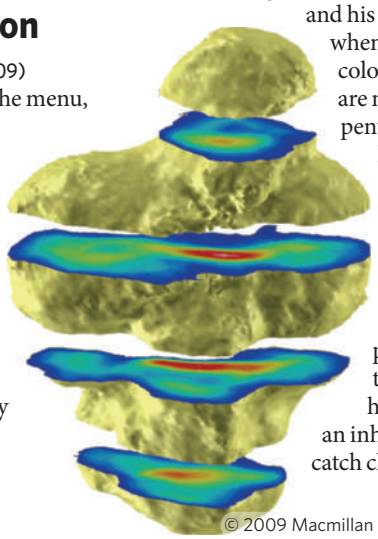

ANIMAL BEHAVIOUR

Caught red hydrocarboned

Curr. Biol. **19,** 78–81 (2009)
Ants, like other social creatures, strive to minimize antisocial behaviour by punishing cheaters. For example, fertile worker *Aphaenogaster cockerelli* ants that could undermine the unity of a colony with a single reproducing queen are attacked by nestmates. Although it has remained unclear how would-be cheats are identified, evidence suggested that variations in the hydrocarbons in ants' cuticles might be involved. Jürgen Liebig of Arizona State University in Tempe and his colleagues show that when *A. cockerelli* workers in colonies headed up by a queen are manually coated with pentacosane, a hydrocarbon linked with fertility, they are attacked by their nestmates.

Because ant eggs carry distinctive related hydrocarbons that prevent them from being identified and destroyed, cheaters probably cannot suppress their chemical profiles. Thus, hydrocarbons could provide an inherently reliable method to catch cheats.

MOLECULAR BIOLOGY

A bilingual genetic code

Science **323,** 259–261 (2009)
A ciliate called *Euplotes crassus* seems to have violated the rules of genetics.

Messenger RNA is used as a template to assemble proteins by means of three-letter sequences called codons. Each codon corresponds to either a single amino acid or a 'stop' signal. However, Vadim Gladyshev of the University of Nebraska in Lincoln and his colleagues found that in *E. crassus*, the codon UGA could encode two amino acids: cysteine or selenocysteine.

The codon could be read in both ways within the same gene, depending on its location within the mRNA strand and the presence and exposure of a specific sequence near the end of the mRNA molecule. The results suggest that the genetic code can be evolutionarily expanded.

ECOLOGICAL ACOUSTICS

Love buzz

Science doi:10.1126/science.1166541 (2009)
The buzz of flying female mosquitoes acts as a mating signal to attract males. When Ronald Hoy and his team at Cornell University in Ithaca, New York, listened closer, they found that when both sexes of *Aedes aegypti* get together, they change their buzz pitch to match, producing a courtship duet. But rather than duo at their usual wing beat frequencies — of around 400 hertz for females and 600 hertz in males — the mosquitoes take their acoustics up a notch to a shared harmonic frequency of 1,200 hertz.

Male mosquitoes were previously thought to be deaf to frequencies above 800 hertz.

RESEARCH HIGHLIGHTS

Old Faithful Erebus

J. Volcanol. Geotherm. Res. **177,** 589–605 (2008)
Sited on the Terror rift of the Western Ross Sea, Antarctica, Mount Erebus is the continent's most active volcano and has a rare convecting magma lake at its summit. Peter Kelly of the New Mexico Institute of Mining and Technology in Socorro and his colleagues investigated the composition of this lake using lava bombs it spewed forth from 1972 to 2004.

Analysis of the glass and mineral composition of these bombs indicates that the temperature of the magma has been stable during this period, contradicting a previous suggestion of a cooling. Another analysis of 11 dated lava samples from the summit plateau ranging back to 17,000 years ago shows that the volcano has erupted lava with the same bulk composition for all this time.

G. STEINMETZ/CORBIS

CHEMICAL BIOLOGY

Fluorescent timers

Nature Chem. Biol. doi:10.1038/nchembio.138 (2009)
New fluorescent 'timers' that gradually change colour from blue to red could allow researchers to track the age and dynamic behaviour of proteins in living cells.

Previous work suggested that some red fluorescent proteins start out fluorescing blue, but then change to red as the protein is chemically modified over time. Vladislav Verkhusha and his colleagues at the Albert Einstein College of Medicine in New York mutated a red fluorescent protein called mCherry, then screened for mutants that had altered maturation rates from blue to red.

The researchers developed three fluorescent proteins, each with a specific maturation rate. The proteins were used to track newly synthesized proteins in mammalian cells grown in culture.

MICROSCOPY

Inside information

Phys. Rev. Lett. **102,** 018101 (2009)
Sliced chromosome is on the menu, thanks to a tour-de-force of X-ray microscopy. Yoshinori Nishino of the RIKEN SPring-8 Center in Hyogo, Japan, and his co-workers have recorded three-dimensional sectional images of a human chromosome (pictured right) using coherent X-ray diffraction microscopy.

Chromosomes are too dense for electron microscopes to see 'inside' them, and fluorescent light microscopy can reveal only selected features. By contrast, the X-ray diffraction method offers a full three-dimensional view of electron density in a single chromosome about 2 micrometres across, showing the internal structure with a resolution of about 120 nanometres.

AM. PHYS. SOC.

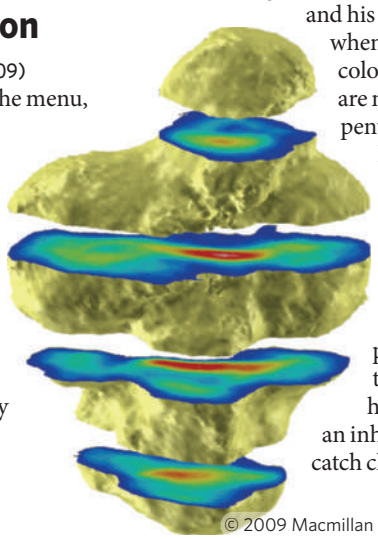

ANIMAL BEHAVIOUR

Caught red hydrocarboned

Curr. Biol. **19,** 78–81 (2009)
Ants, like other social creatures, strive to minimize antisocial behaviour by punishing cheaters. For example, fertile worker *Aphaenogaster cockerelli* ants that could undermine the unity of a colony with a single reproducing queen are attacked by nestmates. Although it has remained unclear how would-be cheats are identified, evidence suggested that variations in the hydrocarbons in ants' cuticles might be involved. Jürgen Liebig of Arizona State University in Tempe and his colleagues show that when *A. cockerelli* workers in colonies headed up by a queen are manually coated with pentacosane, a hydrocarbon linked with fertility, they are attacked by their nestmates.

Because ant eggs carry distinctive related hydrocarbons that prevent them from being identified and destroyed, cheaters probably cannot suppress their chemical profiles. Thus, hydrocarbons could provide an inherently reliable method to catch cheats.

MOLECULAR BIOLOGY

A bilingual genetic code

Science **323,** 259–261 (2009)
A ciliate called *Euplotes crassus* seems to have violated the rules of genetics.

Messenger RNA is used as a template to assemble proteins by means of three-letter sequences called codons. Each codon corresponds to either a single amino acid or a 'stop' signal. However, Vadim Gladyshev of the University of Nebraska in Lincoln and his colleagues found that in *E. crassus*, the codon UGA could encode two amino acids: cysteine or selenocysteine.

The codon could be read in both ways within the same gene, depending on its location within the mRNA strand and the presence and exposure of a specific sequence near the end of the mRNA molecule. The results suggest that the genetic code can be evolutionarily expanded.

ECOLOGICAL ACOUSTICS

Love buzz

Science doi:10.1126/science.1166541 (2009)
The buzz of flying female mosquitoes acts as a mating signal to attract males. When Ronald Hoy and his team at Cornell University in Ithaca, New York, listened closer, they found that when both sexes of *Aedes aegypti* get together, they change their buzz pitch to match, producing a courtship duet. But rather than duo at their usual wing beat frequencies — of around 400 hertz for females and 600 hertz in males — the mosquitoes take their acoustics up a notch to a shared harmonic frequency of 1,200 hertz.

Male mosquitoes were previously thought to be deaf to frequencies above 800 hertz.

RESEARCH HIGHLIGHTS

Old Faithful Erebus

J. Volcanol. Geotherm. Res. **177,** 589–605 (2008)
Sited on the Terror rift of the Western Ross Sea, Antarctica, Mount Erebus is the continent's most active volcano and has a rare convecting magma lake at its summit. Peter Kelly of the New Mexico Institute of Mining and Technology in Socorro and his colleagues investigated the composition of this lake using lava bombs it spewed forth from 1972 to 2004.

Analysis of the glass and mineral composition of these bombs indicates that the temperature of the magma has been stable during this period, contradicting a previous suggestion of a cooling. Another analysis of 11 dated lava samples from the summit plateau ranging back to 17,000 years ago shows that the volcano has erupted lava with the same bulk composition for all this time.

G. STEINMETZ/CORBIS

CHEMICAL BIOLOGY

Fluorescent timers

Nature Chem. Biol. doi:10.1038/nchembio.138 (2009)
New fluorescent 'timers' that gradually change colour from blue to red could allow researchers to track the age and dynamic behaviour of proteins in living cells.

Previous work suggested that some red fluorescent proteins start out fluorescing blue, but then change to red as the protein is chemically modified over time. Vladislav Verkhusha and his colleagues at the Albert Einstein College of Medicine in New York mutated a red fluorescent protein called mCherry, then screened for mutants that had altered maturation rates from blue to red.

The researchers developed three fluorescent proteins, each with a specific maturation rate. The proteins were used to track newly synthesized proteins in mammalian cells grown in culture.

MICROSCOPY

Inside information

Phys. Rev. Lett. **102,** 018101 (2009)
Sliced chromosome is on the menu, thanks to a tour-de-force of X-ray microscopy. Yoshinori Nishino of the RIKEN SPring-8 Center in Hyogo, Japan, and his co-workers have recorded three-dimensional sectional images of a human chromosome (pictured right) using coherent X-ray diffraction microscopy.

Chromosomes are too dense for electron microscopes to see 'inside' them, and fluorescent light microscopy can reveal only selected features. By contrast, the X-ray diffraction method offers a full three-dimensional view of electron density in a single chromosome about 2 micrometres across, showing the internal structure with a resolution of about 120 nanometres.

AM. PHYS. SOC.

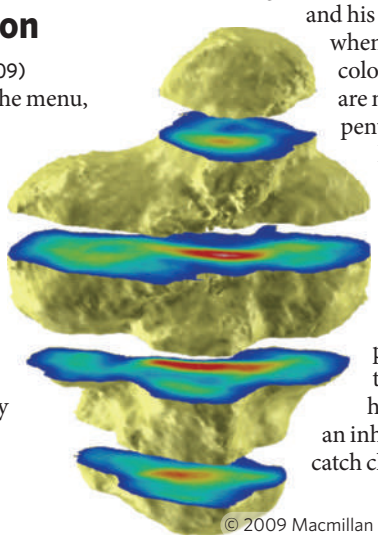

ANIMAL BEHAVIOUR

Caught red hydrocarboned

Curr. Biol. **19,** 78–81 (2009)
Ants, like other social creatures, strive to minimize antisocial behaviour by punishing cheaters. For example, fertile worker *Aphaenogaster cockerelli* ants that could undermine the unity of a colony with a single reproducing queen are attacked by nestmates. Although it has remained unclear how would-be cheats are identified, evidence suggested that variations in the hydrocarbons in ants' cuticles might be involved. Jürgen Liebig of Arizona State University in Tempe and his colleagues show that when *A. cockerelli* workers in colonies headed up by a queen are manually coated with pentacosane, a hydrocarbon linked with fertility, they are attacked by their nestmates.

Because ant eggs carry distinctive related hydrocarbons that prevent them from being identified and destroyed, cheaters probably cannot suppress their chemical profiles. Thus, hydrocarbons could provide an inherently reliable method to catch cheats.

MOLECULAR BIOLOGY

A bilingual genetic code

Science **323,** 259–261 (2009)
A ciliate called *Euplotes crassus* seems to have violated the rules of genetics.

Messenger RNA is used as a template to assemble proteins by means of three-letter sequences called codons. Each codon corresponds to either a single amino acid or a 'stop' signal. However, Vadim Gladyshev of the University of Nebraska in Lincoln and his colleagues found that in *E. crassus*, the codon UGA could encode two amino acids: cysteine or selenocysteine.

The codon could be read in both ways within the same gene, depending on its location within the mRNA strand and the presence and exposure of a specific sequence near the end of the mRNA molecule. The results suggest that the genetic code can be evolutionarily expanded.

ECOLOGICAL ACOUSTICS

Love buzz

Science doi:10.1126/science.1166541 (2009)
The buzz of flying female mosquitoes acts as a mating signal to attract males. When Ronald Hoy and his team at Cornell University in Ithaca, New York, listened closer, they found that when both sexes of *Aedes aegypti* get together, they change their buzz pitch to match, producing a courtship duet. But rather than duo at their usual wing beat frequencies — of around 400 hertz for females and 600 hertz in males — the mosquitoes take their acoustics up a notch to a shared harmonic frequency of 1,200 hertz.

Male mosquitoes were previously thought to be deaf to frequencies above 800 hertz.

RESEARCH HIGHLIGHTS

Old Faithful Erebus

J. Volcanol. Geotherm. Res. **177,** 589–605 (2008)
Sited on the Terror rift of the Western Ross Sea, Antarctica, Mount Erebus is the continent's most active volcano and has a rare convecting magma lake at its summit. Peter Kelly of the New Mexico Institute of Mining and Technology in Socorro and his colleagues investigated the composition of this lake using lava bombs it spewed forth from 1972 to 2004.

Analysis of the glass and mineral composition of these bombs indicates that the temperature of the magma has been stable during this period, contradicting a previous suggestion of a cooling. Another analysis of 11 dated lava samples from the summit plateau ranging back to 17,000 years ago shows that the volcano has erupted lava with the same bulk composition for all this time.

G. STEINMETZ/CORBIS

CHEMICAL BIOLOGY

Fluorescent timers

Nature Chem. Biol. doi:10.1038/nchembio.138 (2009)
New fluorescent 'timers' that gradually change colour from blue to red could allow researchers to track the age and dynamic behaviour of proteins in living cells.

Previous work suggested that some red fluorescent proteins start out fluorescing blue, but then change to red as the protein is chemically modified over time. Vladislav Verkhusha and his colleagues at the Albert Einstein College of Medicine in New York mutated a red fluorescent protein called mCherry, then screened for mutants that had altered maturation rates from blue to red.

The researchers developed three fluorescent proteins, each with a specific maturation rate. The proteins were used to track newly synthesized proteins in mammalian cells grown in culture.

MICROSCOPY

Inside information

Phys. Rev. Lett. **102,** 018101 (2009)
Sliced chromosome is on the menu, thanks to a tour-de-force of X-ray microscopy. Yoshinori Nishino of the RIKEN SPring-8 Center in Hyogo, Japan, and his co-workers have recorded three-dimensional sectional images of a human chromosome (pictured right) using coherent X-ray diffraction microscopy.

Chromosomes are too dense for electron microscopes to see 'inside' them, and fluorescent light microscopy can reveal only selected features. By contrast, the X-ray diffraction method offers a full three-dimensional view of electron density in a single chromosome about 2 micrometres across, showing the internal structure with a resolution of about 120 nanometres.

AM. PHYS. SOC.

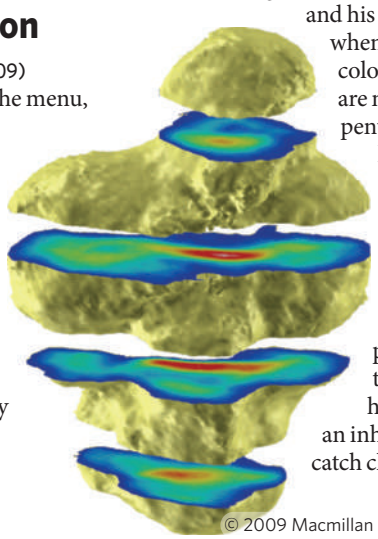

ANIMAL BEHAVIOUR

Caught red hydrocarboned

Curr. Biol. **19,** 78–81 (2009)
Ants, like other social creatures, strive to minimize antisocial behaviour by punishing cheaters. For example, fertile worker *Aphaenogaster cockerelli* ants that could undermine the unity of a colony with a single reproducing queen are attacked by nestmates. Although it has remained unclear how would-be cheats are identified, evidence suggested that variations in the hydrocarbons in ants' cuticles might be involved. Jürgen Liebig of Arizona State University in Tempe and his colleagues show that when *A. cockerelli* workers in colonies headed up by a queen are manually coated with pentacosane, a hydrocarbon linked with fertility, they are attacked by their nestmates.

Because ant eggs carry distinctive related hydrocarbons that prevent them from being identified and destroyed, cheaters probably cannot suppress their chemical profiles. Thus, hydrocarbons could provide an inherently reliable method to catch cheats.

MOLECULAR BIOLOGY

A bilingual genetic code

Science **323,** 259–261 (2009)
A ciliate called *Euplotes crassus* seems to have violated the rules of genetics.

Messenger RNA is used as a template to assemble proteins by means of three-letter sequences called codons. Each codon corresponds to either a single amino acid or a 'stop' signal. However, Vadim Gladyshev of the University of Nebraska in Lincoln and his colleagues found that in *E. crassus*, the codon UGA could encode two amino acids: cysteine or selenocysteine.

The codon could be read in both ways within the same gene, depending on its location within the mRNA strand and the presence and exposure of a specific sequence near the end of the mRNA molecule. The results suggest that the genetic code can be evolutionarily expanded.

ECOLOGICAL ACOUSTICS

Love buzz

Science doi:10.1126/science.1166541 (2009)
The buzz of flying female mosquitoes acts as a mating signal to attract males. When Ronald Hoy and his team at Cornell University in Ithaca, New York, listened closer, they found that when both sexes of *Aedes aegypti* get together, they change their buzz pitch to match, producing a courtship duet. But rather than duo at their usual wing beat frequencies — of around 400 hertz for females and 600 hertz in males — the mosquitoes take their acoustics up a notch to a shared harmonic frequency of 1,200 hertz.

Male mosquitoes were previously thought to be deaf to frequencies above 800 hertz.

The researchers then examined the 'ears' of *A. aegypti*, and confirmed that both sexes can hear up to 2,000 hertz. They call for more research on the mating behaviours of the mosquitoes, which carry yellow fever and dengue virus.

CHEMICAL SYNTHESIS

Take that, flu

Angew. Chem. Int. Edn doi:10.1002/anie.200804883 (2009)

With the constant threat of a flu pandemic, the quest for cheaper, more efficient routes by which to make the flu treatment Tamiflu is keeping chemists busy. Yujiro Hayashi and his team at the Tokyo University of Science report the highest-yielding route so far using inexpensive reagents and just nine reactions, all in three one-pot processes.

The first pot uses diphenylprolinol silyl ether, an organocatalyst — a class of catalysts that don't involve expensive and toxic metals. The organocatalyst helps the first two starting materials to react, and they go on to react with a third. The product goes into pot two to undergo a domino reaction — a cascade of reactions whereby each group of a molecule with many functional groups reacts in turn. In pot three, the final three reactions produce Tamiflu, or (–)-oseltamivir, in 57% yield.

The authors say that their scheme is ideal for large-scale production.

CELL BIOLOGY

Lost nuclei

J. Cell Biol. doi:10.1083/jcb.200811035 (2009)

Certain mutations in the gene *LMNA* cause a rare form of muscular dystrophy, possibly through improper positioning of cell nuclei. The disease, called autosomal dominant Emery-Dreifuss muscular dystrophy (AD-EDMD), and others like it are puzzling because the mutant proteins — in this case lamins A and C — are expressed throughout the body, not just in affected tissues.

Tom Misteli of the US National Cancer Institute in Bethesda, Maryland, and his colleagues looked at muscle fibres from mouse models of the disease and compared them with those of normal mice. Muscle fibres contain hundreds of nuclei, but a handful are recruited to the point where muscle and neuron meet, the neuromuscular junction. In the diseased mice, proteins found in muscle that mediate that recruitment don't associate properly with lamin A. The nuclei get misplaced, neuromuscular junctions become malformed and gene expression in the cells is disrupted.

EVOLUTIONARY BIOLOGY

Headstrong

PLoS ONE doi:10.1371/journal.pone.0003980 (2008)

Large body size confers obvious advantages in cricket fights, but Chinese gamblers have also looked to the head when placing their bets going back some eight centuries. New research bolsters the practice, providing the first evidence that males have developed larger heads — and mouth parts — as weaponry in aggressive turf battles.

Kevin Judge and Vanessa Bonanno at the University of Toronto Mississauga in Canada pitted fall field crickets (*Gryllus pennsylvanicus*) of similar body size against each other; those with bigger heads and mouth parts won 75% of battles that escalated to 'grappling'. The bigger the difference in head size, the more likely the head-strong cricket was to win.

But the team found no evidence of signalling that would influence disputes settled before grappling took place, suggesting that evolutionary selection takes place in the heat of the battle.

WANG YING/COLORCHINAPHOTO/NEWSCOM

CHEMISTRY

An aromatic hybrid

Angew. Chem. Int. Edn doi:10.1002/anie.200805554 (2008)

After years of trying, chemists have finally made a molecule somewhere between benzene (C_6H_6), and its inorganic boron/nitrogen equivalent borazine ($B_3N_3H_6$).

In the molecule, 1,2-dihydro-1,2-azaborine, one of benzene's carbon atoms is replaced with a nitrogen, and another with a boron atom. Scientists have been trying to make this compound since the 1960s, with no luck. David Dixon at the University of Alabama in Tuscaloosa, Lev Zakharov at the University of Oregon in Eugene and their colleagues have now succeeded. The compound, which they made by stabilizing the reactive intermediates with a chromium-based protecting unit, is stable, and like benzene is aromatic, although not as strongly.

JOURNAL CLUB

Jason W. Chin
MRC Laboratory of Molecular Biology, Cambridge, UK

A molecular biologist gets excited about making designer proteins in cells.

The genetic code describes the relationship between the heritable information in the genome and the amino acids that are strung together to make proteins. This code, like any that contains redundancy, is open to hacking, and I have long been fascinated by how the process of translation, by which cells string amino acids together, might be reprogrammed to make new polymers. Several labs have already manipulated cells to incorporate designer amino acids into their proteins.

But Peter Schultz and his colleagues at the Scripps Research Institute in La Jolla, California, have achieved something remarkable. Proteins are made from a set of 20 amino acids, each of which contains an amine and a carboxylic acid group flanking a central carbon atom. Schultz's team engineered a bacterial cell to work with amino-acid-like molecules called α-hydroxy acids that have an alcohol group where the amine would normally be. During translation, instead of forming an amide bond to link polymer subunits, this α-hydroxy acid forms an ester bond (J. Guo *et al. Angew. Chem.* **120,** 734–737; 2008).

Replacing a nitrogen and a hydrogen atom in a polymer chain with an oxygen atom might seem like a slight change, but it means that a protein can now be specifically cut at the ester bond in basic solution. Making esters from α-hydroxy acids may first have been achieved with ribosomes in a test tube in the 1970s, but turning the process into a heritable, genetic property is a major advance: it takes synthetic biologists closer to creating organisms with designer codes to make new polymers.

One day soon, the creativity and skill with which chemists can make molecules will be coupled to the selective power of organismal evolution. And we will watch new life forms boot up.

Discuss this paper at **http://blogs.nature.com/nature/journalclub**

The researchers then examined the 'ears' of *A. aegypti*, and confirmed that both sexes can hear up to 2,000 hertz. They call for more research on the mating behaviours of the mosquitoes, which carry yellow fever and dengue virus.

CHEMICAL SYNTHESIS

Take that, flu

Angew. Chem. Int. Edn doi:10.1002/anie.200804883 (2009)

With the constant threat of a flu pandemic, the quest for cheaper, more efficient routes by which to make the flu treatment Tamiflu is keeping chemists busy. Yujiro Hayashi and his team at the Tokyo University of Science report the highest-yielding route so far using inexpensive reagents and just nine reactions, all in three one-pot processes.

The first pot uses diphenylprolinol silyl ether, an organocatalyst — a class of catalysts that don't involve expensive and toxic metals. The organocatalyst helps the first two starting materials to react, and they go on to react with a third. The product goes into pot two to undergo a domino reaction — a cascade of reactions whereby each group of a molecule with many functional groups reacts in turn. In pot three, the final three reactions produce Tamiflu, or (–)-oseltamivir, in 57% yield.

The authors say that their scheme is ideal for large-scale production.

CELL BIOLOGY

Lost nuclei

J. Cell Biol. doi:10.1083/jcb.200811035 (2009)

Certain mutations in the gene *LMNA* cause a rare form of muscular dystrophy, possibly through improper positioning of cell nuclei. The disease, called autosomal dominant Emery-Dreifuss muscular dystrophy (AD-EDMD), and others like it are puzzling because the mutant proteins — in this case lamins A and C — are expressed throughout the body, not just in affected tissues.

Tom Misteli of the US National Cancer Institute in Bethesda, Maryland, and his colleagues looked at muscle fibres from mouse models of the disease and compared them with those of normal mice. Muscle fibres contain hundreds of nuclei, but a handful are recruited to the point where muscle and neuron meet, the neuromuscular junction. In the diseased mice, proteins found in muscle that mediate that recruitment don't associate properly with lamin A. The nuclei get misplaced, neuromuscular junctions become malformed and gene expression in the cells is disrupted.

EVOLUTIONARY BIOLOGY

Headstrong

PLoS ONE doi:10.1371/journal.pone.0003980 (2008)

Large body size confers obvious advantages in cricket fights, but Chinese gamblers have also looked to the head when placing their bets going back some eight centuries. New research bolsters the practice, providing the first evidence that males have developed larger heads — and mouth parts — as weaponry in aggressive turf battles.

Kevin Judge and Vanessa Bonanno at the University of Toronto Mississauga in Canada pitted fall field crickets (*Gryllus pennsylvanicus*) of similar body size against each other; those with bigger heads and mouth parts won 75% of battles that escalated to 'grappling'. The bigger the difference in head size, the more likely the head-strong cricket was to win.

But the team found no evidence of signalling that would influence disputes settled before grappling took place, suggesting that evolutionary selection takes place in the heat of the battle.

WANG YING/COLORCHINAPHOTO/NEWSCOM

CHEMISTRY

An aromatic hybrid

Angew. Chem. Int. Edn doi:10.1002/anie.200805554 (2008)

After years of trying, chemists have finally made a molecule somewhere between benzene (C_6H_6), and its inorganic boron/nitrogen equivalent borazine ($B_3N_3H_6$).

In the molecule, 1,2-dihydro-1,2-azaborine, one of benzene's carbon atoms is replaced with a nitrogen, and another with a boron atom. Scientists have been trying to make this compound since the 1960s, with no luck. David Dixon at the University of Alabama in Tuscaloosa, Lev Zakharov at the University of Oregon in Eugene and their colleagues have now succeeded. The compound, which they made by stabilizing the reactive intermediates with a chromium-based protecting unit, is stable, and like benzene is aromatic, although not as strongly.

JOURNAL CLUB

Jason W. Chin
MRC Laboratory of Molecular Biology, Cambridge, UK

A molecular biologist gets excited about making designer proteins in cells.

The genetic code describes the relationship between the heritable information in the genome and the amino acids that are strung together to make proteins. This code, like any that contains redundancy, is open to hacking, and I have long been fascinated by how the process of translation, by which cells string amino acids together, might be reprogrammed to make new polymers. Several labs have already manipulated cells to incorporate designer amino acids into their proteins.

But Peter Schultz and his colleagues at the Scripps Research Institute in La Jolla, California, have achieved something remarkable. Proteins are made from a set of 20 amino acids, each of which contains an amine and a carboxylic acid group flanking a central carbon atom. Schultz's team engineered a bacterial cell to work with amino-acid-like molecules called α-hydroxy acids that have an alcohol group where the amine would normally be. During translation, instead of forming an amide bond to link polymer subunits, this α-hydroxy acid forms an ester bond (J. Guo *et al. Angew. Chem.* **120,** 734–737; 2008).

Replacing a nitrogen and a hydrogen atom in a polymer chain with an oxygen atom might seem like a slight change, but it means that a protein can now be specifically cut at the ester bond in basic solution. Making esters from α-hydroxy acids may first have been achieved with ribosomes in a test tube in the 1970s, but turning the process into a heritable, genetic property is a major advance: it takes synthetic biologists closer to creating organisms with designer codes to make new polymers.

One day soon, the creativity and skill with which chemists can make molecules will be coupled to the selective power of organismal evolution. And we will watch new life forms boot up.

Discuss this paper at **http://blogs.nature.com/nature/journalclub**

The researchers then examined the 'ears' of *A. aegypti*, and confirmed that both sexes can hear up to 2,000 hertz. They call for more research on the mating behaviours of the mosquitoes, which carry yellow fever and dengue virus.

CHEMICAL SYNTHESIS

Take that, flu

Angew. Chem. Int. Edn doi:10.1002/anie.200804883 (2009)

With the constant threat of a flu pandemic, the quest for cheaper, more efficient routes by which to make the flu treatment Tamiflu is keeping chemists busy. Yujiro Hayashi and his team at the Tokyo University of Science report the highest-yielding route so far using inexpensive reagents and just nine reactions, all in three one-pot processes.

The first pot uses diphenylprolinol silyl ether, an organocatalyst — a class of catalysts that don't involve expensive and toxic metals. The organocatalyst helps the first two starting materials to react, and they go on to react with a third. The product goes into pot two to undergo a domino reaction — a cascade of reactions whereby each group of a molecule with many functional groups reacts in turn. In pot three, the final three reactions produce Tamiflu, or (–)-oseltamivir, in 57% yield.

The authors say that their scheme is ideal for large-scale production.

CELL BIOLOGY

Lost nuclei

J. Cell Biol. doi:10.1083/jcb.200811035 (2009)

Certain mutations in the gene *LMNA* cause a rare form of muscular dystrophy, possibly through improper positioning of cell nuclei. The disease, called autosomal dominant Emery-Dreifuss muscular dystrophy (AD-EDMD), and others like it are puzzling because the mutant proteins — in this case lamins A and C — are expressed throughout the body, not just in affected tissues.

Tom Misteli of the US National Cancer Institute in Bethesda, Maryland, and his colleagues looked at muscle fibres from mouse models of the disease and compared them with those of normal mice. Muscle fibres contain hundreds of nuclei, but a handful are recruited to the point where muscle and neuron meet, the neuromuscular junction. In the diseased mice, proteins found in muscle that mediate that recruitment don't associate properly with lamin A. The nuclei get misplaced, neuromuscular junctions become malformed and gene expression in the cells is disrupted.

EVOLUTIONARY BIOLOGY

Headstrong

PLoS ONE doi:10.1371/journal.pone.0003980 (2008)

Large body size confers obvious advantages in cricket fights, but Chinese gamblers have also looked to the head when placing their bets going back some eight centuries. New research bolsters the practice, providing the first evidence that males have developed larger heads — and mouth parts — as weaponry in aggressive turf battles.

Kevin Judge and Vanessa Bonanno at the University of Toronto Mississauga in Canada pitted fall field crickets (*Gryllus pennsylvanicus*) of similar body size against each other; those with bigger heads and mouth parts won 75% of battles that escalated to 'grappling'. The bigger the difference in head size, the more likely the head-strong cricket was to win.

But the team found no evidence of signalling that would influence disputes settled before grappling took place, suggesting that evolutionary selection takes place in the heat of the battle.

WANG YING/COLORCHINAPHOTO/NEWSCOM

CHEMISTRY

An aromatic hybrid

Angew. Chem. Int. Edn doi:10.1002/anie.200805554 (2008)

After years of trying, chemists have finally made a molecule somewhere between benzene (C_6H_6), and its inorganic boron/nitrogen equivalent borazine ($B_3N_3H_6$).

In the molecule, 1,2-dihydro-1,2-azaborine, one of benzene's carbon atoms is replaced with a nitrogen, and another with a boron atom. Scientists have been trying to make this compound since the 1960s, with no luck. David Dixon at the University of Alabama in Tuscaloosa, Lev Zakharov at the University of Oregon in Eugene and their colleagues have now succeeded. The compound, which they made by stabilizing the reactive intermediates with a chromium-based protecting unit, is stable, and like benzene is aromatic, although not as strongly.

JOURNAL CLUB

Jason W. Chin
MRC Laboratory of Molecular Biology, Cambridge, UK

A molecular biologist gets excited about making designer proteins in cells.

The genetic code describes the relationship between the heritable information in the genome and the amino acids that are strung together to make proteins. This code, like any that contains redundancy, is open to hacking, and I have long been fascinated by how the process of translation, by which cells string amino acids together, might be reprogrammed to make new polymers. Several labs have already manipulated cells to incorporate designer amino acids into their proteins.

But Peter Schultz and his colleagues at the Scripps Research Institute in La Jolla, California, have achieved something remarkable. Proteins are made from a set of 20 amino acids, each of which contains an amine and a carboxylic acid group flanking a central carbon atom. Schultz's team engineered a bacterial cell to work with amino-acid-like molecules called α-hydroxy acids that have an alcohol group where the amine would normally be. During translation, instead of forming an amide bond to link polymer subunits, this α-hydroxy acid forms an ester bond (J. Guo *et al. Angew. Chem.* **120,** 734–737; 2008).

Replacing a nitrogen and a hydrogen atom in a polymer chain with an oxygen atom might seem like a slight change, but it means that a protein can now be specifically cut at the ester bond in basic solution. Making esters from α-hydroxy acids may first have been achieved with ribosomes in a test tube in the 1970s, but turning the process into a heritable, genetic property is a major advance: it takes synthetic biologists closer to creating organisms with designer codes to make new polymers.

One day soon, the creativity and skill with which chemists can make molecules will be coupled to the selective power of organismal evolution. And we will watch new life forms boot up.

Discuss this paper at **http://blogs.nature.com/nature/journalclub**

The researchers then examined the 'ears' of *A. aegypti*, and confirmed that both sexes can hear up to 2,000 hertz. They call for more research on the mating behaviours of the mosquitoes, which carry yellow fever and dengue virus.

CHEMICAL SYNTHESIS

Take that, flu

Angew. Chem. Int. Edn doi:10.1002/anie.200804883 (2009)

With the constant threat of a flu pandemic, the quest for cheaper, more efficient routes by which to make the flu treatment Tamiflu is keeping chemists busy. Yujiro Hayashi and his team at the Tokyo University of Science report the highest-yielding route so far using inexpensive reagents and just nine reactions, all in three one-pot processes.

The first pot uses diphenylprolinol silyl ether, an organocatalyst — a class of catalysts that don't involve expensive and toxic metals. The organocatalyst helps the first two starting materials to react, and they go on to react with a third. The product goes into pot two to undergo a domino reaction — a cascade of reactions whereby each group of a molecule with many functional groups reacts in turn. In pot three, the final three reactions produce Tamiflu, or (–)-oseltamivir, in 57% yield.

The authors say that their scheme is ideal for large-scale production.

CELL BIOLOGY

Lost nuclei

J. Cell Biol. doi:10.1083/jcb.200811035 (2009)

Certain mutations in the gene *LMNA* cause a rare form of muscular dystrophy, possibly through improper positioning of cell nuclei. The disease, called autosomal dominant Emery-Dreifuss muscular dystrophy (AD-EDMD), and others like it are puzzling because the mutant proteins — in this case lamins A and C — are expressed throughout the body, not just in affected tissues.

Tom Misteli of the US National Cancer Institute in Bethesda, Maryland, and his colleagues looked at muscle fibres from mouse models of the disease and compared them with those of normal mice. Muscle fibres contain hundreds of nuclei, but a handful are recruited to the point where muscle and neuron meet, the neuromuscular junction. In the diseased mice, proteins found in muscle that mediate that recruitment don't associate properly with lamin A. The nuclei get misplaced, neuromuscular junctions become malformed and gene expression in the cells is disrupted.

EVOLUTIONARY BIOLOGY

Headstrong

PLoS ONE doi:10.1371/journal.pone.0003980 (2008)

Large body size confers obvious advantages in cricket fights, but Chinese gamblers have also looked to the head when placing their bets going back some eight centuries. New research bolsters the practice, providing the first evidence that males have developed larger heads — and mouth parts — as weaponry in aggressive turf battles.

Kevin Judge and Vanessa Bonanno at the University of Toronto Mississauga in Canada pitted fall field crickets (*Gryllus pennsylvanicus*) of similar body size against each other; those with bigger heads and mouth parts won 75% of battles that escalated to 'grappling'. The bigger the difference in head size, the more likely the head-strong cricket was to win.

But the team found no evidence of signalling that would influence disputes settled before grappling took place, suggesting that evolutionary selection takes place in the heat of the battle.

WANG YING/COLORCHINAPHOTO/NEWSCOM

CHEMISTRY

An aromatic hybrid

Angew. Chem. Int. Edn doi:10.1002/anie.200805554 (2008)

After years of trying, chemists have finally made a molecule somewhere between benzene (C_6H_6), and its inorganic boron/nitrogen equivalent borazine ($B_3N_3H_6$).

In the molecule, 1,2-dihydro-1,2-azaborine, one of benzene's carbon atoms is replaced with a nitrogen, and another with a boron atom. Scientists have been trying to make this compound since the 1960s, with no luck. David Dixon at the University of Alabama in Tuscaloosa, Lev Zakharov at the University of Oregon in Eugene and their colleagues have now succeeded. The compound, which they made by stabilizing the reactive intermediates with a chromium-based protecting unit, is stable, and like benzene is aromatic, although not as strongly.

JOURNAL CLUB

Jason W. Chin
MRC Laboratory of Molecular Biology, Cambridge, UK

A molecular biologist gets excited about making designer proteins in cells.

The genetic code describes the relationship between the heritable information in the genome and the amino acids that are strung together to make proteins. This code, like any that contains redundancy, is open to hacking, and I have long been fascinated by how the process of translation, by which cells string amino acids together, might be reprogrammed to make new polymers. Several labs have already manipulated cells to incorporate designer amino acids into their proteins.

But Peter Schultz and his colleagues at the Scripps Research Institute in La Jolla, California, have achieved something remarkable. Proteins are made from a set of 20 amino acids, each of which contains an amine and a carboxylic acid group flanking a central carbon atom. Schultz's team engineered a bacterial cell to work with amino-acid-like molecules called α-hydroxy acids that have an alcohol group where the amine would normally be. During translation, instead of forming an amide bond to link polymer subunits, this α-hydroxy acid forms an ester bond (J. Guo *et al. Angew. Chem.* **120,** 734–737; 2008).

Replacing a nitrogen and a hydrogen atom in a polymer chain with an oxygen atom might seem like a slight change, but it means that a protein can now be specifically cut at the ester bond in basic solution. Making esters from α-hydroxy acids may first have been achieved with ribosomes in a test tube in the 1970s, but turning the process into a heritable, genetic property is a major advance: it takes synthetic biologists closer to creating organisms with designer codes to make new polymers.

One day soon, the creativity and skill with which chemists can make molecules will be coupled to the selective power of organismal evolution. And we will watch new life forms boot up.

Discuss this paper at **http://blogs.nature.com/nature/journalclub**

The researchers then examined the 'ears' of *A. aegypti*, and confirmed that both sexes can hear up to 2,000 hertz. They call for more research on the mating behaviours of the mosquitoes, which carry yellow fever and dengue virus.

CHEMICAL SYNTHESIS

Take that, flu

Angew. Chem. Int. Edn doi:10.1002/anie.200804883 (2009)

With the constant threat of a flu pandemic, the quest for cheaper, more efficient routes by which to make the flu treatment Tamiflu is keeping chemists busy. Yujiro Hayashi and his team at the Tokyo University of Science report the highest-yielding route so far using inexpensive reagents and just nine reactions, all in three one-pot processes.

The first pot uses diphenylprolinol silyl ether, an organocatalyst — a class of catalysts that don't involve expensive and toxic metals. The organocatalyst helps the first two starting materials to react, and they go on to react with a third. The product goes into pot two to undergo a domino reaction — a cascade of reactions whereby each group of a molecule with many functional groups reacts in turn. In pot three, the final three reactions produce Tamiflu, or (–)-oseltamivir, in 57% yield.

The authors say that their scheme is ideal for large-scale production.

CELL BIOLOGY

Lost nuclei

J. Cell Biol. doi:10.1083/jcb.200811035 (2009)

Certain mutations in the gene *LMNA* cause a rare form of muscular dystrophy, possibly through improper positioning of cell nuclei. The disease, called autosomal dominant Emery-Dreifuss muscular dystrophy (AD-EDMD), and others like it are puzzling because the mutant proteins — in this case lamins A and C — are expressed throughout the body, not just in affected tissues.

Tom Misteli of the US National Cancer Institute in Bethesda, Maryland, and his colleagues looked at muscle fibres from mouse models of the disease and compared them with those of normal mice. Muscle fibres contain hundreds of nuclei, but a handful are recruited to the point where muscle and neuron meet, the neuromuscular junction. In the diseased mice, proteins found in muscle that mediate that recruitment don't associate properly with lamin A. The nuclei get misplaced, neuromuscular junctions become malformed and gene expression in the cells is disrupted.

EVOLUTIONARY BIOLOGY

Headstrong

PLoS ONE doi:10.1371/journal.pone.0003980 (2008)

Large body size confers obvious advantages in cricket fights, but Chinese gamblers have also looked to the head when placing their bets going back some eight centuries. New research bolsters the practice, providing the first evidence that males have developed larger heads — and mouth parts — as weaponry in aggressive turf battles.

Kevin Judge and Vanessa Bonanno at the University of Toronto Mississauga in Canada pitted fall field crickets (*Gryllus pennsylvanicus*) of similar body size against each other; those with bigger heads and mouth parts won 75% of battles that escalated to 'grappling'. The bigger the difference in head size, the more likely the head-strong cricket was to win.

But the team found no evidence of signalling that would influence disputes settled before grappling took place, suggesting that evolutionary selection takes place in the heat of the battle.

WANG YING/COLORCHINAPHOTO/NEWSCOM

CHEMISTRY

An aromatic hybrid

Angew. Chem. Int. Edn doi:10.1002/anie.200805554 (2008)

After years of trying, chemists have finally made a molecule somewhere between benzene (C_6H_6), and its inorganic boron/nitrogen equivalent borazine ($B_3N_3H_6$).

In the molecule, 1,2-dihydro-1,2-azaborine, one of benzene's carbon atoms is replaced with a nitrogen, and another with a boron atom. Scientists have been trying to make this compound since the 1960s, with no luck. David Dixon at the University of Alabama in Tuscaloosa, Lev Zakharov at the University of Oregon in Eugene and their colleagues have now succeeded. The compound, which they made by stabilizing the reactive intermediates with a chromium-based protecting unit, is stable, and like benzene is aromatic, although not as strongly.

JOURNAL CLUB

Jason W. Chin
MRC Laboratory of Molecular Biology, Cambridge, UK

A molecular biologist gets excited about making designer proteins in cells.

The genetic code describes the relationship between the heritable information in the genome and the amino acids that are strung together to make proteins. This code, like any that contains redundancy, is open to hacking, and I have long been fascinated by how the process of translation, by which cells string amino acids together, might be reprogrammed to make new polymers. Several labs have already manipulated cells to incorporate designer amino acids into their proteins.

But Peter Schultz and his colleagues at the Scripps Research Institute in La Jolla, California, have achieved something remarkable. Proteins are made from a set of 20 amino acids, each of which contains an amine and a carboxylic acid group flanking a central carbon atom. Schultz's team engineered a bacterial cell to work with amino-acid-like molecules called α-hydroxy acids that have an alcohol group where the amine would normally be. During translation, instead of forming an amide bond to link polymer subunits, this α-hydroxy acid forms an ester bond (J. Guo *et al. Angew. Chem.* **120,** 734–737; 2008).

Replacing a nitrogen and a hydrogen atom in a polymer chain with an oxygen atom might seem like a slight change, but it means that a protein can now be specifically cut at the ester bond in basic solution. Making esters from α-hydroxy acids may first have been achieved with ribosomes in a test tube in the 1970s, but turning the process into a heritable, genetic property is a major advance: it takes synthetic biologists closer to creating organisms with designer codes to make new polymers.

One day soon, the creativity and skill with which chemists can make molecules will be coupled to the selective power of organismal evolution. And we will watch new life forms boot up.

Discuss this paper at **http://blogs.nature.com/nature/journalclub**

The researchers then examined the 'ears' of *A. aegypti*, and confirmed that both sexes can hear up to 2,000 hertz. They call for more research on the mating behaviours of the mosquitoes, which carry yellow fever and dengue virus.

CHEMICAL SYNTHESIS

Take that, flu

Angew. Chem. Int. Edn doi:10.1002/anie.200804883 (2009)

With the constant threat of a flu pandemic, the quest for cheaper, more efficient routes by which to make the flu treatment Tamiflu is keeping chemists busy. Yujiro Hayashi and his team at the Tokyo University of Science report the highest-yielding route so far using inexpensive reagents and just nine reactions, all in three one-pot processes.

The first pot uses diphenylprolinol silyl ether, an organocatalyst — a class of catalysts that don't involve expensive and toxic metals. The organocatalyst helps the first two starting materials to react, and they go on to react with a third. The product goes into pot two to undergo a domino reaction — a cascade of reactions whereby each group of a molecule with many functional groups reacts in turn. In pot three, the final three reactions produce Tamiflu, or (–)-oseltamivir, in 57% yield.

The authors say that their scheme is ideal for large-scale production.

CELL BIOLOGY

Lost nuclei

J. Cell Biol. doi:10.1083/jcb.200811035 (2009)

Certain mutations in the gene *LMNA* cause a rare form of muscular dystrophy, possibly through improper positioning of cell nuclei. The disease, called autosomal dominant Emery-Dreifuss muscular dystrophy (AD-EDMD), and others like it are puzzling because the mutant proteins — in this case lamins A and C — are expressed throughout the body, not just in affected tissues.

Tom Misteli of the US National Cancer Institute in Bethesda, Maryland, and his colleagues looked at muscle fibres from mouse models of the disease and compared them with those of normal mice. Muscle fibres contain hundreds of nuclei, but a handful are recruited to the point where muscle and neuron meet, the neuromuscular junction. In the diseased mice, proteins found in muscle that mediate that recruitment don't associate properly with lamin A. The nuclei get misplaced, neuromuscular junctions become malformed and gene expression in the cells is disrupted.

EVOLUTIONARY BIOLOGY

Headstrong

PLoS ONE doi:10.1371/journal.pone.0003980 (2008)

Large body size confers obvious advantages in cricket fights, but Chinese gamblers have also looked to the head when placing their bets going back some eight centuries. New research bolsters the practice, providing the first evidence that males have developed larger heads — and mouth parts — as weaponry in aggressive turf battles.

Kevin Judge and Vanessa Bonanno at the University of Toronto Mississauga in Canada pitted fall field crickets (*Gryllus pennsylvanicus*) of similar body size against each other; those with bigger heads and mouth parts won 75% of battles that escalated to 'grappling'. The bigger the difference in head size, the more likely the head-strong cricket was to win.

But the team found no evidence of signalling that would influence disputes settled before grappling took place, suggesting that evolutionary selection takes place in the heat of the battle.

WANG YING/COLORCHINAPHOTO/NEWSCOM

CHEMISTRY

An aromatic hybrid

Angew. Chem. Int. Edn doi:10.1002/anie.200805554 (2008)

After years of trying, chemists have finally made a molecule somewhere between benzene (C_6H_6), and its inorganic boron/nitrogen equivalent borazine ($B_3N_3H_6$).

In the molecule, 1,2-dihydro-1,2-azaborine, one of benzene's carbon atoms is replaced with a nitrogen, and another with a boron atom. Scientists have been trying to make this compound since the 1960s, with no luck. David Dixon at the University of Alabama in Tuscaloosa, Lev Zakharov at the University of Oregon in Eugene and their colleagues have now succeeded. The compound, which they made by stabilizing the reactive intermediates with a chromium-based protecting unit, is stable, and like benzene is aromatic, although not as strongly.

JOURNAL CLUB

Jason W. Chin
MRC Laboratory of Molecular Biology, Cambridge, UK

A molecular biologist gets excited about making designer proteins in cells.

The genetic code describes the relationship between the heritable information in the genome and the amino acids that are strung together to make proteins. This code, like any that contains redundancy, is open to hacking, and I have long been fascinated by how the process of translation, by which cells string amino acids together, might be reprogrammed to make new polymers. Several labs have already manipulated cells to incorporate designer amino acids into their proteins.

But Peter Schultz and his colleagues at the Scripps Research Institute in La Jolla, California, have achieved something remarkable. Proteins are made from a set of 20 amino acids, each of which contains an amine and a carboxylic acid group flanking a central carbon atom. Schultz's team engineered a bacterial cell to work with amino-acid-like molecules called α-hydroxy acids that have an alcohol group where the amine would normally be. During translation, instead of forming an amide bond to link polymer subunits, this α-hydroxy acid forms an ester bond (J. Guo *et al. Angew. Chem.* **120,** 734–737; 2008).

Replacing a nitrogen and a hydrogen atom in a polymer chain with an oxygen atom might seem like a slight change, but it means that a protein can now be specifically cut at the ester bond in basic solution. Making esters from α-hydroxy acids may first have been achieved with ribosomes in a test tube in the 1970s, but turning the process into a heritable, genetic property is a major advance: it takes synthetic biologists closer to creating organisms with designer codes to make new polymers.

One day soon, the creativity and skill with which chemists can make molecules will be coupled to the selective power of organismal evolution. And we will watch new life forms boot up.

Discuss this paper at **http://blogs.nature.com/nature/journalclub**

NEWS

Science tipped to score in Obama cash stimulus

Researchers jockey for a piece of the US economic package.

The US research community stands to gain billions of dollars in funding, as Democratic leaders in Washington DC seek to lay the foundation for a greener, more competitive economy in a $750-billion stimulus package.

Scientific groups are actively pushing their argument that modernizing the nation's scientific infrastructure could help create the skilled workforce needed to address challenges such as global warming.

"It's amazing. The scientific community has a voice," says Maria Zuber, a geophysics professor at the Massachusetts Institute of Technology in Cambridge who testified before Nancy Pelosi, Speaker of the House of Representatives, and other Democratic leaders on 7 January. "The fact that we are invited to sit at the table with the economists when we are talking about the future of the US economy — it's like a new day."

Normally, the president proposes government spending levels in early February, and Congress adjusts and approves those over many months. The fiscal stimulus package introduced by Obama last week provides a shortcut.

The question is what kind of science and energy initiatives lawmakers will be willing to approve in a bill that is intended to provide a short-term jolt to the economy. Many Republicans are opposed to the scope of the package, and congressional Democrats have baulked at the notion of fast-tracking a bill sent down by the new administration. Pelosi said last week that she wants to see a bill by February, despite Obama's call to have it ready by his inauguration on 20 January.

Representatives from the American Physical Society began talking to Obama's transition team shortly after the November 2008 election, and have developed a short-list of desired projects at the Department of Energy, the National Science Foundation and the National Institute of Standards and Technology. The price tag stands at nearly $3.5 billion for dozens of projects, including renovations and upgrades at various Department of Energy labs and supercomputing work at the National Center for Atmospheric Research in Boulder, Colorado.

'Shovel-ready' projects such as these feature heavily in Obama's stimulus package, which would also include extensive tax cuts. "The only things that are in this list are approved projects" that have already gone through planning, says Michael Lubell, head of public affairs for the American Physical Society. He says the transition team warned against including anything that would constitute an ongoing funding commitment. "We are not talking about the long-term grant programmes or anything else," he says. "This is very, very short term, because those were the ground rules."

It is not clear whether calls for basic research funding, as opposed to infrastructure and technology, will make the cut. Several organizations, including the Association of American Medical Colleges and the Association of American Universities, last month asked Obama for $1.2 billion for some 3,200 grants at the National Institutes of Health, along with an additional $1.9-billion increase in the 2009 fiscal year.

G. HERBERT/AP

Bill Andresen, president of The Science Coalition, which represents 45 US universities, says that their goal is not a one-time boost but a rise for research funding that at least keeps up with inflation. "Whatever money is in the stimulus bill, we can spend quickly and create jobs immediately — while at the same time laying the groundwork for a more competitive economy," he says.

In their testimony last week, both Zuber and Norman Augustine, an aerospace engineer who chaired an influential National Academy of Sciences panel on US competitiveness, advocated boosting funding for the physical sciences. In 2007, Congress authorized a doubling of the physical-sciences budget under the American Competitiveness Initiative, which lawmakers have yet to fully fund. House Science Committee chairman Bart Gordon (Democrat, Tennessee) says he hopes Congress will include pieces of the initiative in the stimulus bill, although he doesn't specify which parts.

Lubell says that one area in which the incoming administration has shown a willingness for long-term projects is energy and climate, as have other countries (see 'Japan greens up'). Speaking last week at George Mason University in Fairfax, Virginia, Obama said his administration plans to double the production of renewable energy over the next three years while boosting energy efficiency in 2 million homes (1.6% of US housing) and in more than 75% of federal buildings.

Japan greens up

Last week, Japan's environment minister Tetsuo Saito hinted that green industrial development could play a major part in the ¥40-trillion (US$445 billion) stimulus package under discussion in parliament. He emphasized the importance of encouraging science and technology to enable Japan to recapture the world's top spot in photovoltaics and to promote wind energy, small hydroelectrics and next-generation cars.

As part of the stimulus, plans to expand the green industrial market from its current value of ¥70 trillion to ¥100 trillion, and to strengthen its workforce from 1.4 million to 2.2 million, might be brought forward from 2020 to 2015. The ministry is considering zero-interest loans for environmentally friendly companies and other measures to encourage green industry.

"Even in these harsh economic conditions, we cannot slow our efforts to deal with environmental problems," says Saito. "In fact, precisely because we have these conditions, we should make environmental protection the priming agent for explosive economic growth."

David Cyranoski

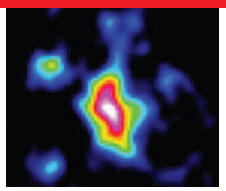

NRAO/AUI/NSF, SDSS

ASTRONOMY
Did black holes form before galaxies?
www.nature.com/news

Barack Obama and Congressional Democrats brought scientists and economists to the table.

Obama has also called for modernization of the electricity grid, an initiative that could cost upwards of $165 billion, according to the Electric Power Research Institute.

Democratic lawmakers are keen to include energy-efficiency initiatives, including weatherproofing assistance for homeowners, but questions remain about how to address renewable energy in the bill. Officials in the wind and solar energy industries say Obama's goal of doubling renewable-energy production was possible before the economic meltdown, but financing for new projects has since dried up, forcing some companies to lay off workers.

These industries are now pushing lawmakers to free up money by altering the structure of federal tax incentives that encourage the development of electricity from renewables — a move that could cost taxpayers an additional $1 billion over the next two years. Rhone Resch, who heads the Solar Energy Industries Association in Washington DC, says the industry is ready to go to work once it can get the financing. "The policies and the programmes that worked in the past economy will not work in today's dire economic environment," he says. ■

Jeff Tollefson

Steven Chu prepares for power

On 13 January, the US Senate Committee on Energy and Natural Resources was scheduled to hold a hearing on president-elect Barack Obama's nomination of Steven Chu for head of the Department of Energy (DoE). If confirmed as expected, Chu may well set sparks flying at the staid agency. Over the past four years, Chu has realigned the DoE's Lawrence Berkeley National Laboratory (LBNL) in California into a pioneer for alternative-energy research.

Using an ice-hockey analogy, Eddy Rubin, director both of the Joint Genome Institute in Walnut Creek, California, and of the genomics division at the LBNL, says: "You can't stay where the puck is — you have to skate where the puck is going to be. [Chu] had a compelling vision to put the lab where it needs to be."

Like many hockey greats, Chu isn't shy about asserting his position. "You say something stupid, he smacks you immediately," says one lab source who asked to remain anonymous. "I've seen him really embarrass people, to a fault."

Chu, 60, is not granting interviews until after his confirmation. But a week before Christmas, about 15 LBNL division heads and managers heard him explain how he visited Obama in Chicago around Thanksgiving, spending roughly 40 minutes alone with him. Obama was extremely knowledgeable about energy issues, Chu told the group, and their ideas for research on alternative sources were in sync.

LBNL

Steven Chu realigned the Lawrence Berkeley National Laboratory.

According to the division directors, Chu said he would take the job if he could select the approximately 15 political appointees who would direct key DoE components. In the early days of the Bush administration, vice-president Dick Cheney was behind most of those appointments. Instead, "Chu will get to select the smartest people he knows", says Rubin.

Chu is deeply interested in biology, having branched far beyond the laser-cooling work that won him his Nobel prize in 1997. And he is always delving into new fields, says geochemist Don DePaolo, a 20-year LBNL veteran appointed by Chu in 2007 to direct the Earth-sciences division. "In only four years at the LBNL, he learned so much about everything it is intimidating to talk to him," says DePaolo. "You can't tell him a story to patch over an issue; he zeroes in if it doesn't sound right."

But this focus has led to complaints of micromanagement. Colleagues say he "always has to be the smartest guy in the room", even privately voicing desires for a second Nobel in a biology-related field.

"He is an unabashed self-promoter," says Tad Patzek, a former researcher at the University of California, Berkeley, who clashed with Chu on bioenergy projects that Patzek considered to be 'nonsense' before moving last summer to the University of Texas at Austin. "But in fairness, he has been a very effective LBNL director, enlarging the scope of energy research."

Chu has mellowed in recent years, says Stephen Quake, a biophysicist at Stanford University in California, who studied under Chu. "Everything is about the science," Quake says. "I could go into his office and tell him why I thought something he requested wouldn't work; he listened."

Three years ago at the LBNL, Chu championed an initiative called Helios to develop new research frontiers in solar power. Its flagship facilities, to be built in partnership with the University of California, Berkeley, have been delayed by environmental lawsuits and community objections, but are now being re-reviewed.

In 2007, Chu was also instrumental in helping the university win US$500 million for bioenergy research from BP, one of the world's largest energy companies — a project that triggered controversy about the role of corporate financing in academic research (see *Nature* 445, 688–689; 2007). That research programme has begun on the Berkeley campus, but its building is delayed along with Helios. Last year, the LBNL did successfully open its $134-million Joint BioEnergy Institute in a gleaming facility at an industrial park in nearby Emeryville.

Chu's experience in setting up these initiatives may serve him well in Washington DC, which is full of people who think they are the smartest in the room. "He is going to take the DoE where it needs to go with new technologies," says Rubin. "He's a driver who doesn't take vacations." ■

Rex Dalton

For coverage of Steven Chu's confirmation hearing, see http://tinyurl.com/8dgwle.

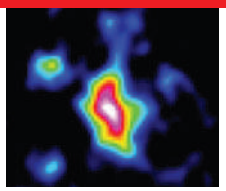

NRAO/AUI/NSF, SDSS

ASTRONOMY
Did black holes form before galaxies?
www.nature.com/news

Barack Obama and Congressional Democrats brought scientists and economists to the table.

Obama has also called for modernization of the electricity grid, an initiative that could cost upwards of $165 billion, according to the Electric Power Research Institute.

Democratic lawmakers are keen to include energy-efficiency initiatives, including weatherproofing assistance for homeowners, but questions remain about how to address renewable energy in the bill. Officials in the wind and solar energy industries say Obama's goal of doubling renewable-energy production was possible before the economic meltdown, but financing for new projects has since dried up, forcing some companies to lay off workers.

These industries are now pushing lawmakers to free up money by altering the structure of federal tax incentives that encourage the development of electricity from renewables — a move that could cost taxpayers an additional $1 billion over the next two years. Rhone Resch, who heads the Solar Energy Industries Association in Washington DC, says the industry is ready to go to work once it can get the financing. "The policies and the programmes that worked in the past economy will not work in today's dire economic environment," he says. ■

Jeff Tollefson

Steven Chu prepares for power

On 13 January, the US Senate Committee on Energy and Natural Resources was scheduled to hold a hearing on president-elect Barack Obama's nomination of Steven Chu for head of the Department of Energy (DoE). If confirmed as expected, Chu may well set sparks flying at the staid agency. Over the past four years, Chu has realigned the DoE's Lawrence Berkeley National Laboratory (LBNL) in California into a pioneer for alternative-energy research.

Using an ice-hockey analogy, Eddy Rubin, director both of the Joint Genome Institute in Walnut Creek, California, and of the genomics division at the LBNL, says: "You can't stay where the puck is — you have to skate where the puck is going to be. [Chu] had a compelling vision to put the lab where it needs to be."

Like many hockey greats, Chu isn't shy about asserting his position. "You say something stupid, he smacks you immediately," says one lab source who asked to remain anonymous. "I've seen him really embarrass people, to a fault."

Chu, 60, is not granting interviews until after his confirmation. But a week before Christmas, about 15 LBNL division heads and managers heard him explain how he visited Obama in Chicago around Thanksgiving, spending roughly 40 minutes alone with him. Obama was extremely knowledgeable about energy issues, Chu told the group, and their ideas for research on alternative sources were in sync.

LBNL

Steven Chu realigned the Lawrence Berkeley National Laboratory.

According to the division directors, Chu said he would take the job if he could select the approximately 15 political appointees who would direct key DoE components. In the early days of the Bush administration, vice-president Dick Cheney was behind most of those appointments. Instead, "Chu will get to select the smartest people he knows", says Rubin.

Chu is deeply interested in biology, having branched far beyond the laser-cooling work that won him his Nobel prize in 1997. And he is always delving into new fields, says geochemist Don DePaolo, a 20-year LBNL veteran appointed by Chu in 2007 to direct the Earth-sciences division. "In only four years at the LBNL, he learned so much about everything it is intimidating to talk to him," says DePaolo. "You can't tell him a story to patch over an issue; he zeroes in if it doesn't sound right."

But this focus has led to complaints of micromanagement. Colleagues say he "always has to be the smartest guy in the room", even privately voicing desires for a second Nobel in a biology-related field.

"He is an unabashed self-promoter," says Tad Patzek, a former researcher at the University of California, Berkeley, who clashed with Chu on bioenergy projects that Patzek considered to be 'nonsense' before moving last summer to the University of Texas at Austin. "But in fairness, he has been a very effective LBNL director, enlarging the scope of energy research."

Chu has mellowed in recent years, says Stephen Quake, a biophysicist at Stanford University in California, who studied under Chu. "Everything is about the science," Quake says. "I could go into his office and tell him why I thought something he requested wouldn't work; he listened."

Three years ago at the LBNL, Chu championed an initiative called Helios to develop new research frontiers in solar power. Its flagship facilities, to be built in partnership with the University of California, Berkeley, have been delayed by environmental lawsuits and community objections, but are now being re-reviewed.

In 2007, Chu was also instrumental in helping the university win US$500 million for bioenergy research from BP, one of the world's largest energy companies — a project that triggered controversy about the role of corporate financing in academic research (see *Nature* 445, 688–689; 2007). That research programme has begun on the Berkeley campus, but its building is delayed along with Helios. Last year, the LBNL did successfully open its $134-million Joint BioEnergy Institute in a gleaming facility at an industrial park in nearby Emeryville.

Chu's experience in setting up these initiatives may serve him well in Washington DC, which is full of people who think they are the smartest in the room. "He is going to take the DoE where it needs to go with new technologies," says Rubin. "He's a driver who doesn't take vacations." ■

Rex Dalton

For coverage of Steven Chu's confirmation hearing, see http://tinyurl.com/8dgwle.

On the record

Barack Obama's nominees for top federal positions are not speaking to the press until their appointments are confirmed, but they have spoken out before.

T. FITZSIMMONS

On the role of science:

John Holdren: "The toughest questions cannot be resolved by technical expertise, but the experts should clarify the options and the range of technical uncertainty as best they can."
In *Bulletin of the Atomic Scientists*, 1976

Steven Chu: "We seek solutions. We don't seek — dare I say this — just scientific papers any more."
In the *San Francisco Chronicle*, 2007

Jane Lubchenco: "Science alone does not hold the power to achieve the goal of greater sustainability, but scientific knowledge and wisdom are needed to help inform decisions that will enable society to move toward that end. A sustainable biosphere is one that is ecologically sound, economically feasible, and socially just."
In *Science*, 1998

Tom Daschle: "If history shows anything, it's that a bet against science is a bet you cannot win."
Lecture, 2004

On climate change:

Holdren: "The most dangerous and difficult of all environmental problems that have ever been created by human beings and probably ever will be created — full stop."
Lecture, 2007

Lawrence Summers: "My children are very alarmed about what's going to happen to Florida 60 years from now and they have great moral energy invested in 'the oceans are going to rise' and so forth. They are, except from what they hear from me, without concern and have not been led to be concerned about the fact that there are hundreds of thousands of girls like them who are becoming child prostitutes in the world every year, because of their poverty. This tremendous moral energy that is being inculcated in our youth is being channelled, almost exclusively in the United States to environmental questions. And I don't deny the force of environmental questions, but I think there are equally compelling and in some ways more immediate moral concerns that somehow don't get put on the same moral plane."
Panel debate, 2006

M. B. CENETA/AP

Lisa Jackson: "Perhaps the most crippling barrier we face is the false idea that we cannot reduce greenhouse gas emissions without hurting the economy. This has been a constant mantra of the current administration in Washington, but this is patently false."
Congressional testimony, 2007

Cass Sunstein: "The best way for the current generation to help posterity might be through reducing [carbon] emissions; but it might be through other methods, including approaches that make posterity richer and better able to adapt."
Working paper, 2008 (with David Weisbach)

Chu: "500 parts per million [atmospheric carbon dioxide] is very optimistic, and most of us don't think we will achieve this goal."
Lecture, 2008

On the environment and population:

J. LUBCHENCO

H. A. LINDQUIST/SIPA PRESS/NEWSCOM

Lubchenco: "We can no longer afford to have the environment be accorded marginal status on our agendas. The environment is not a marginal issue, it is the issue of the future, and the future is here now."
In *Science*, 1998

Holdren: "To ignore population today because the problem is a tough one is to commit ourselves to even gloomier prospects 20 years hence, when most of the 'easy' means to reduce per capita impact on the environment will have been exhausted."
In *Science*, 1971 (with Paul Ehrlich)

Chu: "The best birth control is economic prosperity ... rich people have fewer babies. We don't know why, but it cuts across every culture ... I personally think it has something to do with late-night TV."
Lecture, 2008

On investment:

Holdren: "We should be quadrupling to tentupling the amount of money we are putting in energy research and development on alternatives to provide the energy that people need to

Team Obama

John Holdren
Nominated for: assistant to the president for science and technology
Previously: professor, Harvard University

Steven Chu
Nominated for: secretary of energy Previously: director, Lawrence Berkeley National Laboratory

Carol Browner
Nominated for: assistant to the president for energy and climate change
Previously: director, Environmental Protection Agency

Tom Vilsack
Nominated for: secretary of agriculture
Previously: governor of Iowa

James Jones
Nominated for: National Security Advisor
Previously: four-star general

Lisa Jackson
Nominated for: head of the Environmental Protection Agency
Previously: head, New Jersey Department of Environmental Protection

Jane Lubchenco
Nominated for: administrator, National Oceanic and Atmospheric Administration
Previously: professor, Oregon State University

Tom Daschle
Nominated for: secretary, Health and Human Services
Previously: Senate majority leader

Lawrence Summers
Nominated for: head of the National Economic Council
Previously: president of Harvard University

Cass Sunstein
Nominated for: head of the Office of Information and Regulatory Affairs
Previously: professor, Harvard Law School

be prosperous without wrecking the climate."
The Late Show with David Letterman, 2008

Summers: "We need to identify those investments that stimulate demand in the short run and have a positive impact on productivity. These include renewable energy technologies and the infrastructure to support them, the broader application of biotechnologies and expanding broadband connectivity."
In his *Financial Times* column, 2008

On energy security:

James Jones: "Expanding domestic [oil] production will reduce our dependence on foreign oil and natural gas and significantly reduce the billions of dollars we send abroad each year."
Institute for 21st-Century Energy report, 2008

Tom Vilsack: "Iowa is one of the nation's leading producers of corn-based ethanol, and many people in my state have an economic stake in the expanded use of corn-based ethanol. But the reality is that corn-based ethanol will never be enough to reach our goals. Some have suggested that we import more sugar-based ethanol from Brazil and we should indeed consider all sources of available ethanol ... but if we are going to create energy security we can't simply replace one imported source of energy with another. That alone is not security ... the only way we can produce enough domestically is if we greatly improve the technology used to produce cellulosic ethanol."
Lecture, 2007

2008 OWEN SL/BLACK STAR/NEWSCOM

Chu: "We want to raise grasses; we do not want to use soybeans for diesel oil or corn for ethanol. That is not a good use of land."
Lecture, 2008

On regulation and markets:

Summers: "I tend to support a cap-and-trade system, and I think if we ever make progress against global warming — as I hope we will, as we need to — it will come through some kind of cap-and-trade system ... when I went to college or graduate school ... the assumption was, to address a problem like that you would use command and control regulation."
In *OnEarth* magazine, 2008

Carol Browner: "When the government steps up and it says that there is a requirement that you are going to have to take sulphur out of diesel fuel, you are going to have to get rid of CFCs (chlorofluorocarbons) by a certain date, what the government is doing is creating a market opportunity. And American innovation and American ingenuity have risen to that challenge inevitably more quickly and at less cost than was anticipated."
Lecture, 2008

AP

Chu: "[To reduce climate change] we really do need a combination of incentives to drive correct behaviour, but also fiscal policies and regulations and the most important is, of course, a price on carbon. Whether it is a tax or a cap and trade there has to be a price and ... there can't be any loopholes. And right now the industries who feel that their existence is threatened are working very hard to make sure there are safety valves and loopholes."
Lecture, 2008

Lubchenco: "I do believe that we can do a much better job of managing fisheries, and that in doing so, we can recover much of the bounty that has been lost."
In *The Oregonian*, 2007

Jones: "Our nation's demand for more and more energy compels us to move forward immediately on projects that will take years to finance and complete. Lengthy, excessive, and unnecessary regulatory delays and roadblocks during a project will only increase costs, which are ultimately passed on to consumers, and prolong the current imbalance of supply and demand, and imperil our economic progress."
Institute for 21st-Century Energy website

S. OLSON/GETTY IMAGES

On hope:

Browner: "I am a very optimistic person ... I think we'll ultimately get this right. I don't think we will be the first generation to lead to a world they cannot fix. But time is so of the essence. Scientists are telling us we do not have the luxury of time. We've wasted at least eight years. We've got to get going quickly."
Lecture, 2008

Holdren: "If I weren't optimistic, I would be out fishing today, Dave, and not talking to you."
The Late Show with David Letterman, 2008

Compiled by Emma Marris and Alexandra Witze.

See Editorial, page 235. References available online at: http://tinyurl.com/7gnvp2.

HAVE YOUR SAY
Comment on any of our news stories, online.
www.nature.com/news

Ocean study draws ire

A German research ship laden with 20 tonnes of iron sulphate has whipped up a storm of protest as it sails towards the Antarctic, where it intends to dump its cargo into the ocean late this week.

Scientists on the RV *Polarstern*, which set sail from Cape Town in South Africa on 7 January, plan an ocean-fertilization experiment that some argue will violate international agreements. But the scientists say that it will yield the very data necessary to assess the impact of the controversial geo-engineering technique, which aims to trap carbon dioxide from the atmosphere by encouraging the growth of algae.

The team, comprising about 50 scientists from Germany, India, Italy, Spain, Chile, France and Britain, is heading for a small patch of the Scotia Sea between Argentina and the Antarctic Peninsula. The eight-week experiment, called LOHAFEX, will be the sixth ocean-fertilization study conducted in the Southern Ocean since 1993.

In response to widespread environmental concerns, the 191 parties to the United Nations' Convention on Biological Diversity last year agreed to a moratorium on all ocean fertilization activities, with only small-scale scientific studies in coastal waters exempted.

Environmental campaigners say that LOHAFEX should not have received permission under these rules. "We're taken aback by this flagrant disregard of international law," says Mariam Mayet, director of the African Centre for Biosafety in Johannesburg.

But the Alfred Wegener Institute for Polar and Marine Research (AWI) in Bremerhaven, Germany, which operates the RV *Polarstern*, denies that the experiment falls under the UN moratorium.

The study will address, among other things, marine biology, the flow of carbonaceous particles, and biodiversity questions that have barely been analysed in previous experiments, says Karin Lochte, the director of the AWI. ■

Quirin Schiermeier

A longer version of this story appears at http://tinyurl.com/6upcrc.

be prosperous without wrecking the climate."
The Late Show with David Letterman, 2008

Summers: "We need to identify those investments that stimulate demand in the short run and have a positive impact on productivity. These include renewable energy technologies and the infrastructure to support them, the broader application of biotechnologies and expanding broadband connectivity."
In his *Financial Times* column, 2008

On energy security:

James Jones: "Expanding domestic [oil] production will reduce our dependence on foreign oil and natural gas and significantly reduce the billions of dollars we send abroad each year."
Institute for 21st-Century Energy report, 2008

Tom Vilsack: "Iowa is one of the nation's leading producers of corn-based ethanol, and many people in my state have an economic stake in the expanded use of corn-based ethanol. But the reality is that corn-based ethanol will never be enough to reach our goals. Some have suggested that we import more sugar-based ethanol from Brazil and we should indeed consider all sources of available ethanol ... but if we are going to create energy security we can't simply replace one imported source of energy with another. That alone is not security ... the only way we can produce enough domestically is if we greatly improve the technology used to produce cellulosic ethanol."
Lecture, 2007

2008 OWEN SL/BLACK STAR/NEWSCOM

Chu: "We want to raise grasses; we do not want to use soybeans for diesel oil or corn for ethanol. That is not a good use of land."
Lecture, 2008

On regulation and markets:

Summers: "I tend to support a cap-and-trade system, and I think if we ever make progress against global warming — as I hope we will, as we need to — it will come through some kind of cap-and-trade system ... when I went to college or graduate school ... the assumption was, to address a problem like that you would use command and control regulation."
In *OnEarth* magazine, 2008

Carol Browner: "When the government steps up and it says that there is a requirement that you are going to have to take sulphur out of diesel fuel, you are going to have to get rid of CFCs (chlorofluorocarbons) by a certain date, what the government is doing is creating a market opportunity. And American innovation and American ingenuity have risen to that challenge inevitably more quickly and at less cost than was anticipated."
Lecture, 2008

AP

Chu: "[To reduce climate change] we really do need a combination of incentives to drive correct behaviour, but also fiscal policies and regulations and the most important is, of course, a price on carbon. Whether it is a tax or a cap and trade there has to be a price and ... there can't be any loopholes. And right now the industries who feel that their existence is threatened are working very hard to make sure there are safety valves and loopholes."
Lecture, 2008

Lubchenco: "I do believe that we can do a much better job of managing fisheries, and that in doing so, we can recover much of the bounty that has been lost."
In *The Oregonian*, 2007

Jones: "Our nation's demand for more and more energy compels us to move forward immediately on projects that will take years to finance and complete. Lengthy, excessive, and unnecessary regulatory delays and roadblocks during a project will only increase costs, which are ultimately passed on to consumers, and prolong the current imbalance of supply and demand, and imperil our economic progress."
Institute for 21st-Century Energy website

S. OLSON/GETTY IMAGES

On hope:

Browner: "I am a very optimistic person ... I think we'll ultimately get this right. I don't think we will be the first generation to lead to a world they cannot fix. But time is so of the essence. Scientists are telling us we do not have the luxury of time. We've wasted at least eight years. We've got to get going quickly."
Lecture, 2008

Holdren: "If I weren't optimistic, I would be out fishing today, Dave, and not talking to you."
The Late Show with David Letterman, 2008

Compiled by Emma Marris and Alexandra Witze.

See Editorial, page 235. References available online at: http://tinyurl.com/7gnvp2.

HAVE YOUR SAY
Comment on any of our news stories, online.
www.nature.com/news

Ocean study draws ire

A German research ship laden with 20 tonnes of iron sulphate has whipped up a storm of protest as it sails towards the Antarctic, where it intends to dump its cargo into the ocean late this week.

Scientists on the RV *Polarstern*, which set sail from Cape Town in South Africa on 7 January, plan an ocean-fertilization experiment that some argue will violate international agreements. But the scientists say that it will yield the very data necessary to assess the impact of the controversial geo-engineering technique, which aims to trap carbon dioxide from the atmosphere by encouraging the growth of algae.

The team, comprising about 50 scientists from Germany, India, Italy, Spain, Chile, France and Britain, is heading for a small patch of the Scotia Sea between Argentina and the Antarctic Peninsula. The eight-week experiment, called LOHAFEX, will be the sixth ocean-fertilization study conducted in the Southern Ocean since 1993.

In response to widespread environmental concerns, the 191 parties to the United Nations' Convention on Biological Diversity last year agreed to a moratorium on all ocean fertilization activities, with only small-scale scientific studies in coastal waters exempted.

Environmental campaigners say that LOHAFEX should not have received permission under these rules. "We're taken aback by this flagrant disregard of international law," says Mariam Mayet, director of the African Centre for Biosafety in Johannesburg.

But the Alfred Wegener Institute for Polar and Marine Research (AWI) in Bremerhaven, Germany, which operates the RV *Polarstern*, denies that the experiment falls under the UN moratorium.

The study will address, among other things, marine biology, the flow of carbonaceous particles, and biodiversity questions that have barely been analysed in previous experiments, says Karin Lochte, the director of the AWI. ■

Quirin Schiermeier

A longer version of this story appears at http://tinyurl.com/6upcrc.

P. GARWOOD/WHO

DISEASE MODELLING
Fighting cholera by numbers.
www.nature.com/news

Brain imaging studies under fire

Social neuroscientists criticized for exaggerating links between brain activity and emotions.

A study attacking some of the most prominent research in the burgeoning field of social neuroscience is flawed and unfair, according to top scientists who have been accused of overselling their results.

Social neuroscience is the study of the neurobiological mechanisms underlying social behaviour. The field frequently uses functional magnetic resonance imaging (fMRI) to reveal which brain areas are activated while a subject is exposed to specific social interactions — for example, situations that may evoke jealousy or the perception of unfairness.

But a no-holds-barred paper[1], accepted for publication in *Perspectives on Psychological Science* and already circulating widely on the Internet, claims that many studies in the field are worthless because brain imaging data have been poorly analysed.

The paper was written by Edward Vul, a PhD student supervised by neuroscientist Nancy Kanwisher at the Massachusetts Institute of Technology in Cambridge, along with psychologists at the University of California, San Diego, including Harold Pashler.

The paper has touched a nerve: brain imaging studies were derided by some as "the new phrenology" when they became common 15 years ago, and interpretations of their highly complex data were denounced as naive. But those directly attacked say they are familiar with, and avoid, the pitfalls.

Vul and his co-authors say they wrote the paper because they were concerned by what they considered to be the "implausibly high correlations" reported between brain activation and particular forms of behaviour, and the lack of methodological details provided. So they selected 54 papers in social neuroscience and sent a brief questionnaire to the authors requesting details of their analyses.

They concluded that in a 'red list' of 31 cases — often in high-profile journals, including *Nature* and *Science* — the authors made fundamental errors in data handling and statistics.

They particularly criticize a 'non-independence error', in which bias is introduced by selecting data using a first statistical test and then applying a second non-independent statistical test to those data. This error, they say, arises from selecting small volumes of the brain, called voxels, on the basis of their high correlation with a psychological response, and then going on to report the magnitude of that correlation. "At present, all studies performed using these methods have large question marks over them," they write.

In a rebuttal[2], four authors of different red-list papers explain that there was no non-independence error because calculating the size of the correlation is not a statistical test.

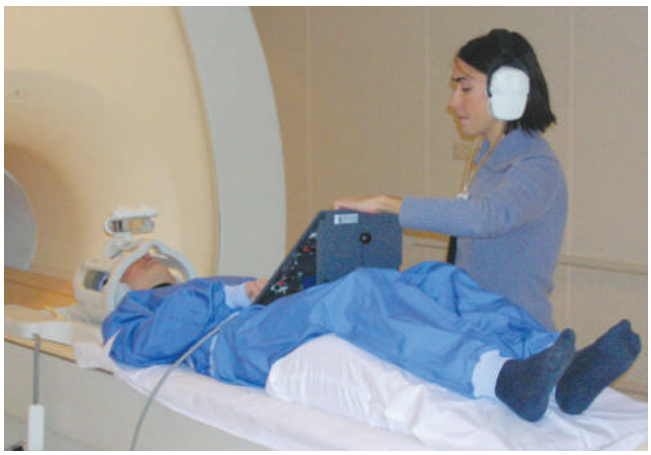

SOCIALBRAINLAB, UNIV. MED. CENTER GRONINGEN

Brain imaging is used to assess neural mechanisms in social behaviour.

Appropriate corrections ensure that the correlations between the selected voxels and psychological responses are likely to be real, and not noise, they add. And the strictness of the correction means that those correlations are necessarily less frequent and of higher magnitude — a situation far from implausible.

"This is not the way that scientific discourse should take place."

Vul and his colleagues also claim that the magnitude of correlation is limited by the average reliability of fMRI data generally. Not so, the accused respond: although the reliability of fMRI is very variable, the upper ceiling on data quality is extremely high.

The swift rebuttal was prompted by scientists' alarm at the speed with which the accusations have spread through the community. The provocative title — 'Voodoo correlations in social neuroscience' — and iconoclastic tone have attracted coverage on many blogs, including that of *Newsweek*. Those attacked say they have not had the chance to argue their case in the normal academic channels.

"I first heard about this when I got a call from a journalist," comments neuroscientist Tania Singer of the University of Zurich, Switzerland, whose papers on empathy are listed as examples of bad analytical practice. "I was shocked — this is not the way that scientific discourse should take place." Singer says she asked for a discussion with the authors when she received the questionnaire, to clarify the type of information needed, but got no reply.

"We didn't disclose all our potential criticisms before asking these people to tell us things that should have already been in their method sections," says an unrepentant Vul. "Would they have described their methods differently if we had?"

They would indeed, says biopsychologist Turhan Canli of Stony Brook University, New York, who has four papers on the red list. He argues that the questionnaire, which was billed as taking no more than a few minutes to complete, was not able to capture the rationale for using particular analyses.

The article is scheduled for publication in September, alongside one or more replies. But the accused scientists are concerned that the impression now being established through media reports will be hard to shake after the nine-month delay. "We are not worried about our close colleagues, who will understand the arguments. We are worried that the whole enterprise of social neuroscience falls into disrepute," says neuroscientist Chris Frith of University College London, whose *Nature* paper[3] on response to perceived fairness was called into question.

"On the other hand, we all agree that there is a kernel of truth in what Vul and his colleagues write about some of the literature being shaky," adds Christian Keysers of the University of Groningen in the Netherlands, whose 2007 paper in *NeuroImage* on empathy was highlighted[4]. "We can never be reminded often enough of the importance of good statistical practice." ■

Alison Abbott

1. Vul, E. *et al.* www.pashler.com/Articles/Vul_etal_2008inpress.pdf
2. Jabbi, M. *et al.* www.bcn-nic.nl/replyVul.pdf
3. Singer, T. *et al. Nature* **439,** 466–469 (2006).
4. Jabbi, M. *et al. NeuroImage* **34,** 1744–1753 (2007).

SPECIAL REPORT

Where the rubber meets the garden

China's leading conservation centre is facing down an onslaught of rubber plantations. **Jane Qiu** reports from Jinghong.

China's rainforests are being stripped to make way for rubber plantations.

ZI BO

With a combination of carefully groomed landscapes and the natural splendour of tropical rainforests, Xishuangbanna Tropical Botanical Garden (XTBG) in China's south-western Yunnan province is renowned for its exceptional beauty. The 900-hectare garden, which has a collection of 11,700 plant species, is the Chinese Academy of Sciences' flagship institute for conservation research. Around it, however, the forests have increasingly been being replaced by row upon row of rubber trees; from the air, they look like gigantic mazes hemming in the conservation centre.

The stark contrast between garden and rubber "is a painful reminder of the responsibility of botanical gardens in wider conservation efforts in the real world", says Joachim Gratzfeld, director of regional programmes at Botanic Gardens Conservation International in Richmond, UK. He was one of about 100 experts who gathered at the XTBG earlier this month to commemorate its fiftieth anniversary — and to discuss its future as rubber plantations proliferate.

Ironically, the garden owes its existence to rubber. During the 1950s, in a bid to produce its own rubber in the face of mounting international isolation, the Chinese government sent a team of botanists to Xishuangbanna — at the time a hinterland where diseases ran rampant — to test whether rubber trees could be grown at such high latitudes. The researchers discovered a tropical paradise and so set up the botanical garden as a research base.

But as rubber prices have tripled over the past decade, rubber plantations have boomed in Xishuangbanna. Now covering about 400,000 hectares, they occupy 20% of the prefecture's land. The economic gain from rubber is evident during a drive around Jinghong, the capital of Xishuangbanna 70 kilometres from the garden, with its luxury shops, roaming BMWs and Mercedes, and European-style villas in the suburbs. "The force of economic development is beyond our imagination," says Chen Jin, director of the XTBG. And as researchers push into other potential cash crops in the region — including jatropha and palm trees for biofuels — many worry that appropriate regulation and controls may come too late.

"Xishuangbanna will be pushed over the edge if no immediate action is taken to prevent further forest destruction," says Xu Jianchu, an ethnoecologist at the Kunming Institute of Botany and China's representative at the World Agroforestry Centre, an international think tank headquartered in Nairobi, Kenya.

Next month, the Xishuangbanna prefecture government will finish drafting a plan that would, if enacted, work to restore the region's ecosystems. But it is not clear whether environmental regulations will be enough to compete with the lucrative rubber crops. "We could make as many laws as we want," says Jiang Pusheng, the Communist party secretary of the prefecture. "But until we provide the farmers with appropriate compensation and alternative economic means, none of the laws can be effectively implemented."

To feed its booming automobile and tyre industry, China plans to increase its natural-rubber production by 30% from 2007 levels — to 780,000 tonnes per year by 2010 — and is investing aggressively in nearby countries such as Laos, Myanmar and Cambodia. To meet demand, scientists are looking into ways to breed and select rubber trees that can survive at higher elevations. They are also trying to raise output by making rubber trees mature faster than the current seven years.

The rainforest canopy in Xishuangbanna traps water vapour, helping plants to survive dry spells.

ZHU MIN

"The large-scale rubber cultivation has taken a heavy toll on the local environment," says Zhu Hua, an ecologist at the XTBG. Satellite studies show that between 1976 and 2003 forests were cleared at an average annual rate of almost 14,000 hectares, shrinking the total forest cover in Xishuangbanna to less than 50% and that of primary rainforests to 3.6% (refs 1, 2).

In Xishuangbanna, hydrological systems have been hardest hit. Average rainfall over the region is about 1,400 millimetres per year, and occurs mostly during the rainy season. In winter, a dense fog of water vapour trapped beneath the rainforest canopy keeps the myriad plant species alive.

Big drinkers

But the winter fog is becoming less pronounced as rubber trees take over the landscape, says Zhu. The non-native plants, known as 'water pumps' by the locals, suck up water and cause more surface runoff. As the soil water content is reduced, less evaporation takes place[3,4]. More water is also lost from the spaces between rubber trees, which grow farther apart than rainforest vegetation. As a result, streamflow has dropped and wells have dried up in many villages in Xishuangbanna.

Rainforest loss in Xishuangbanna also has implications for carbon dynamics and climate change in the region. Using a combination of remote sensing and forest inventory data, Ma Youxin, an ecologist at the XTBG, and his colleagues have calculated that 6 million tonnes of biomass carbon stock were lost in the prefecture between 1976 and 2003 (ref. 1). "This might be affecting the regional climate," he suggests.

Temperature and precipitation data from meteorological stations in Xishuangbanna

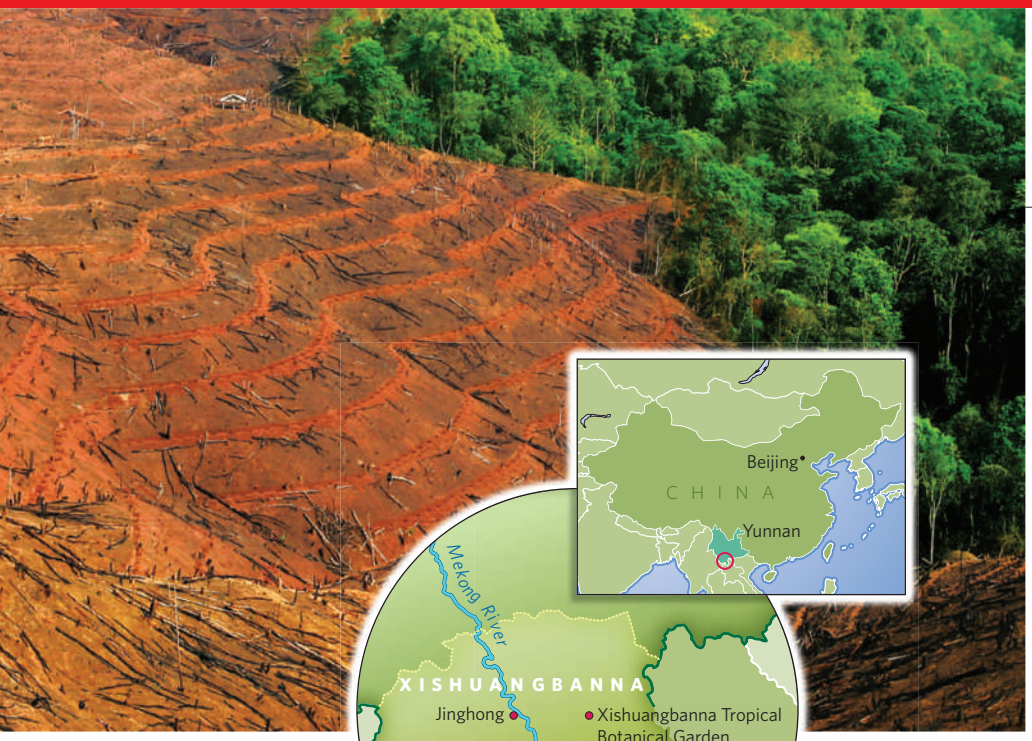

K. CAMPBELL/GETTY

GOT A NEWS TIP?
Send any article ideas for Nature's News section to **newstips@nature.com**

show that the region has been warming since the 1960s, with less rainfall and more severe droughts[5]. Ma notes that various factors may be contributing to those changes, but stresses that large-scale deforestation is likely to have a role.

"Destroying ecosystems will backfire and hit economic development in the long run," argues Cao Min, an ecologist at the XTBG. Hu Huabin, director of the garden's research-planning and foreign-affairs division, and his colleagues have calculated the changes in the value of ecosystem services — such as nutrient cycling, erosion control, climate regulation, water treatment and recreation — due to changes in land use in Menglun, a typical township of 33,500 hectares in Xishuangbanna. Between 1988 and 2006, rubber plantations increased from 12% of the total land cover to 46%, whereas forested areas dropped from 49% to 28% (ref. 6). As a result, the value of ecosystem services dropped by US$11.4 million. "We will soon hit the wall in an ecological credit crunch," says Cao. "This is hardly a viable investment."

But until recently, local officials were evaluated on just one criterion — gross domestic product — which largely determined the incentives and local policies they established. Although energy efficiency and the levels of industrial pollution discharges are now part of the assessment package, protection of natural resources remains optional. "This is a major problem," says Chen.

Jiang, the prefecture party secretary, is adamant that people in Xishuangbanna have the right to develop and lead a good life. He does, however, admit that the environmental problems caused by deforestation need to be tackled. "It's a tough call," he says.

Jiang is spearheading a regulatory plan due to be completed next month that would strengthen the control of forests in protected areas and restore some of those in the buffer zones of national nature reserves that have been converted to rubber plantations. It would also prevent the destruction of 'collective forests' — those that used to belong to villages but were, in a controversial move by the State Forestry Administration last year, allocated to individual farmers.

Still, rubber's sheer profitability means that any conservation efforts will be extremely challenging. Farmers in Xishuangbanna can earn a net income of 15,000 renminbi (US$2,200) per hectare for rubber a year, compared with 2,000–3,000 renminbi for rice or tea. Unless the market takes into account the value of ecosystem services lost owing to the cultivation of rubber and other crops, the conflict between development and conservation will never be reconciled, says Joachim Sauerborn, an agriculture researcher at the University of Hohenheim in Stuttgart, Germany.

"Destroying ecosystems will backfire and hit economic development in the long run." — Cao Min

Protection plan

"It is an uphill struggle — this is why conservation and poverty reduction go hand-in-hand," says Hasan Moinuddin of the Manila-based Asian Development Bank. Moinuddin, stationed in Bangkok, is the task leader of the bank's Biodiversity Conservation Corridors Initiative in the Greater Mekong Subregion. The scheme provides a revolving fund to villages that agree to establish new protection zones in their areas, to serve as crucial links between islands of existing nature reserves. A special village committee runs the fund, and farmers can borrow from it as microcredit. The initiative also tries to raise awareness of biodiversity among villagers and help them to plan and manage their land better.

"If villagers can get a few cows to care for, if they have clean water and their children can go to school, they are less likely to go around chopping down trees," says Hu, who runs the Xishuangbanna arm of the project.

Almost two years in, a pilot programme involving six villages in Xishuangbanna has shown some encouraging results. With a revolving fund of up to 50,000 renminbi each, the villages have agreed to protect and even restore the habitats of designated areas. Two new prefecture-level conservation corridors have also been approved by the Xishuangbanna government. The plan is to upscale the programme to another 40 villages, totalling 11,000 farmers and 8,000 hectares of forested areas, in the next five years. Other similar projects, such as the World Agroforestry Centre's Making Mekong Connected initiative, are exploring the potential of carbon trading and biodiversity offsets to help conserve the land and reduce poverty.

Meanwhile, Chen is looking to turn the XTBG into a Chinese version of the Panama-based Smithsonian Tropical Research Institute. This July, a brand new research centre is to open in Xishuangbanna at a cost of 90 million renminbi. It is to house 300 full-time researchers — twice the garden's current number — with greater capacity for visiting scholars, and cutting-edge facilities for conservation research.

The XTBG is also seeking a greater advocacy and policy role in biodiversity conservation in the region. Its system for evaluating its researchers, which is based solely on the number of publications in journals that use the Science Citation Index, will be reformed to encourage scientists to participate in regional development projects. "The future of the botanical garden is intimately linked to the future of the ecological environment of the region," says Chen. "The day when the forests are gone and rivers dried up would be the end of the XTBG." ■

1. Li, H., Ma, Y., Aide, T. M. & Liu, W. *Forest Ecol. Manag.* **255,** 16–24 (2008).
2. Li, H., Aide, T. M., Ma, Y., Liu, W. & Cao, M. *Biodivers. Conserv.* **16,** 1731–1745 (2007).
3. Liu. W., Meng, F.-R., Zhang, Y., Liu, Y. & Li, H. *J. Trop. Ecol.* **20,** 517–524 (2004).
4. Guardiola-Claramonte, M. *et al. Ecohydrology* **1,** 13–22 (2008).
5. He, Y. & Zhang, Y. *Mountain Res. Dev.* **25,** 341–348 (2005).
6. Hu, H., Liu, W. & Cao, M. *Environ. Monit. Assess.* **146,** 147–156 (2008).

Genome deal seeks to accelerate pore sequencing

Biotechnology company Illumina of San Diego, California, has bought exclusive rights to market, sell and distribute products based on the DNA sequencing technology of UK-based Oxford Nanopore Technologies (see *Nature* 456, 23–25; 2008).

Unlike conventional methods, the technique identifies sequences by passing DNA one base at a time through a tiny pore made from a protein. The process does not involve molecular tagging or intricate sample preparation, and the companies hope that it will ultimately allow them to sequence an entire human genome for less than US$1,000.

The deal includes an initial investment of $18 million from Illumina, followed by a second cash injection once Oxford Nanopore has demonstrated the commercial scope of the technique. Both firms will share profits from any sales.

Obama urged to make exports and visas a priority

The US National Research Council (NRC) has called on president-elect Barack Obama to overhaul the country's export-control system and to ease the visa process for foreign scientists.

In a report published on 8 January, the council warns that US security and economic growth are threatened by outdated export-control regulations, which restrict the flow of certain technologies and information to other countries. Rather than leaving items on the export-control list indefinitely, the NRC wants to see a 'sunset' rule imposed to reassess each item annually.

The report was co-chaired by former US national security adviser Brent Scowcroft and John Hennessy, president of Stanford University in California. It also suggests that Obama should speed up the processing of

Scheduling problems beset delayed Mars mission

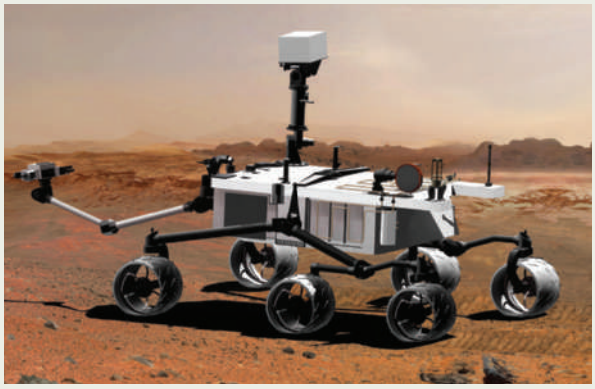

NASA/JPL-CALTECH

NASA's delayed Mars Science Laboratory mission (pictured) is experiencing further problems as it jostles for space in a crowded launch schedule.

The nuclear-powered rover, which will search for evidence of past life on Mars, is due to launch at the end of 2011, two years later than planned.

But the mission's first possible launch window, in October, would be tightly constrained by the August 2011 launch of Juno, a mission to study Jupiter's magnetic and gravitational fields. A second launch window is available in December, but that would favour landing sites in Mars's northern hemisphere, potentially reopening the debate over what part of the planet the rover should explore. Resolving the dilemma could add US$50 million to the already vastly over-budget mission, now expected to cost up to $2.3 billion over its lifetime.

For a longer version of this story, see http://tinyurl.com/9j3ptj.

Genome deal seeks to accelerate pore sequencing

Biotechnology company Illumina of San Diego, California, has bought exclusive rights to market, sell and distribute products based on the DNA sequencing technology of UK-based Oxford Nanopore Technologies (see *Nature* 456, 23–25; 2008).

Unlike conventional methods, the technique identifies sequences by passing DNA one base at a time through a tiny pore made from a protein. The process does not involve molecular tagging or intricate sample preparation, and the companies hope that it will ultimately allow them to sequence an entire human genome for less than US$1,000.

The deal includes an initial investment of $18 million from Illumina, followed by a second cash injection once Oxford Nanopore has demonstrated the commercial scope of the technique. Both firms will share profits from any sales.

Obama urged to make exports and visas a priority

The US National Research Council (NRC) has called on president-elect Barack Obama to overhaul the country's export-control system and to ease the visa process for foreign scientists.

In a report published on 8 January, the council warns that US security and economic growth are threatened by outdated export-control regulations, which restrict the flow of certain technologies and information to other countries. Rather than leaving items on the export-control list indefinitely, the NRC wants to see a 'sunset' rule imposed to reassess each item annually.

The report was co-chaired by former US national security adviser Brent Scowcroft and John Hennessy, president of Stanford University in California. It also suggests that Obama should speed up the processing of

Scheduling problems beset delayed Mars mission

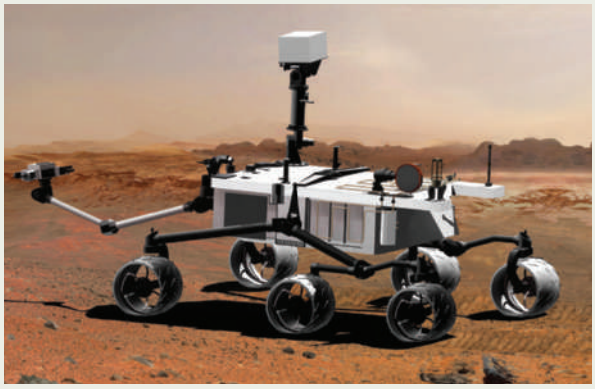

NASA/JPL-CALTECH

NASA's delayed Mars Science Laboratory mission (pictured) is experiencing further problems as it jostles for space in a crowded launch schedule.

The nuclear-powered rover, which will search for evidence of past life on Mars, is due to launch at the end of 2011, two years later than planned.

But the mission's first possible launch window, in October, would be tightly constrained by the August 2011 launch of Juno, a mission to study Jupiter's magnetic and gravitational fields. A second launch window is available in December, but that would favour landing sites in Mars's northern hemisphere, potentially reopening the debate over what part of the planet the rover should explore. Resolving the dilemma could add US$50 million to the already vastly over-budget mission, now expected to cost up to $2.3 billion over its lifetime.

For a longer version of this story, see http://tinyurl.com/9j3ptj.

visa applications for foreign researchers and give international science and engineering students an automatic one-year visa extension to seek work or advanced study.

Suspended urologist set to return to Austrian university

The urologist at the centre of Austria's biggest-ever research scandal can return to work at the Medical University of Innsbruck, a disciplinary committee has ruled.

Hannes Strasser was suspended from clinical, teaching and research duties in September 2008 following accusations of malpractice in a clinical trial using stem cells to treat urinary incontinence (see *Nature* 454, 922; 2008).

The national disciplinary committee responsible for university staff has now concluded that the suspension was not legally justified, as more than three years had passed since the alleged misdemeanour occurred.

Strasser, who is facing criminal charges relating to harming patients or putting them at risk of harm, is on paid leave until the end of January. He will not be allowed to treat patients until the criminal case is resolved — which is likely to take at least a year. An investigation by the Austrian National Academy of Sciences is also ongoing.

Coal conversion plant fires up in China

China's first coal-liquefaction plant is up and running. Located in Inner Mongolia, the facility is run by the state-owned Shenhua Group.

According to a statement issued by Shenhua last week, the plant has been turning coal into liquid fuel and chemical products since December. The technique, which is also widely used in South Africa, has been criticized for its high emissions of carbon dioxide.

Last year, the Chinese government issued a moratorium on new coal-liquefaction facilities, but allowed Shenhua to complete its Mongolia plant and continue work on a second. The company says it is developing ways to capture and store the CO_2 emitted during the process.

Italian universities lose freedom to appoint staff

Italian universities will have little say in choosing their own professors thanks to a law approved by parliament last week.

According to the new rules, a five-person selection committee will oversee each appointment. But a university recruiting a professor can appoint only one member to the board. The other four members will be picked at random from a list of twelve voted for by the relevant community of scientists across Italy.

The existing *concorsi* system is similar, but it allowed universities to have more control over selection — a privilege that was sometimes abused to make appointments based on local politics rather than on merit. Many academics had lobbied for a reform that would allow universities to make their own free choice, but lose funds if their chosen professors underperformed.

Corrections

The News round-up item 'Biodiversity gets catalogued online' (*Nature* **456,** 844–845; 2008) gave incorrect funding numbers for the Encyclopedia of Life. The total budget for the project's first five years is US$50 million; $2.5 million came from the Sloan Foundation and $10 million from the MacArthur Foundation in 2007.

The News story 'Good grades, but who gets the cash?' (*Nature* **457,** 13; 2009) incorrectly calculated the number of staff submitted by the University of Oxford who were rated world-leading and internationally excellent in the biological-sciences category of the 2008 Research Assessment Exercise. The correct number is 75, putting the university in second place behind the University of Cambridge.

Genome deal seeks to accelerate pore sequencing

Biotechnology company Illumina of San Diego, California, has bought exclusive rights to market, sell and distribute products based on the DNA sequencing technology of UK-based Oxford Nanopore Technologies (see *Nature* 456, 23–25; 2008).

Unlike conventional methods, the technique identifies sequences by passing DNA one base at a time through a tiny pore made from a protein. The process does not involve molecular tagging or intricate sample preparation, and the companies hope that it will ultimately allow them to sequence an entire human genome for less than US$1,000.

The deal includes an initial investment of $18 million from Illumina, followed by a second cash injection once Oxford Nanopore has demonstrated the commercial scope of the technique. Both firms will share profits from any sales.

Obama urged to make exports and visas a priority

The US National Research Council (NRC) has called on president-elect Barack Obama to overhaul the country's export-control system and to ease the visa process for foreign scientists.

In a report published on 8 January, the council warns that US security and economic growth are threatened by outdated export-control regulations, which restrict the flow of certain technologies and information to other countries. Rather than leaving items on the export-control list indefinitely, the NRC wants to see a 'sunset' rule imposed to reassess each item annually.

The report was co-chaired by former US national security adviser Brent Scowcroft and John Hennessy, president of Stanford University in California. It also suggests that Obama should speed up the processing of

Scheduling problems beset delayed Mars mission

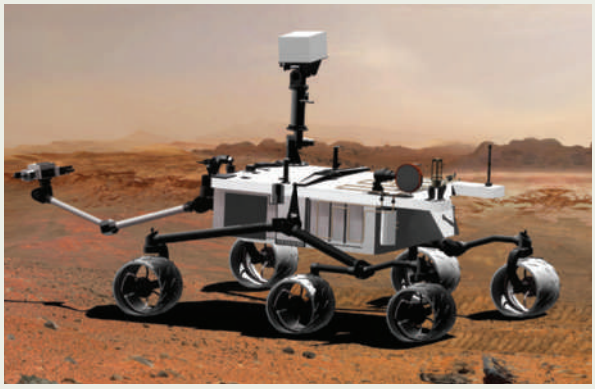

NASA/JPL-CALTECH

NASA's delayed Mars Science Laboratory mission (pictured) is experiencing further problems as it jostles for space in a crowded launch schedule.

The nuclear-powered rover, which will search for evidence of past life on Mars, is due to launch at the end of 2011, two years later than planned.

But the mission's first possible launch window, in October, would be tightly constrained by the August 2011 launch of Juno, a mission to study Jupiter's magnetic and gravitational fields. A second launch window is available in December, but that would favour landing sites in Mars's northern hemisphere, potentially reopening the debate over what part of the planet the rover should explore. Resolving the dilemma could add US$50 million to the already vastly over-budget mission, now expected to cost up to $2.3 billion over its lifetime.

For a longer version of this story, see http://tinyurl.com/9j3ptj.

visa applications for foreign researchers and give international science and engineering students an automatic one-year visa extension to seek work or advanced study.

Suspended urologist set to return to Austrian university

The urologist at the centre of Austria's biggest-ever research scandal can return to work at the Medical University of Innsbruck, a disciplinary committee has ruled.

Hannes Strasser was suspended from clinical, teaching and research duties in September 2008 following accusations of malpractice in a clinical trial using stem cells to treat urinary incontinence (see *Nature* 454, 922; 2008).

The national disciplinary committee responsible for university staff has now concluded that the suspension was not legally justified, as more than three years had passed since the alleged misdemeanour occurred.

Strasser, who is facing criminal charges relating to harming patients or putting them at risk of harm, is on paid leave until the end of January. He will not be allowed to treat patients until the criminal case is resolved — which is likely to take at least a year. An investigation by the Austrian National Academy of Sciences is also ongoing.

Coal conversion plant fires up in China

China's first coal-liquefaction plant is up and running. Located in Inner Mongolia, the facility is run by the state-owned Shenhua Group.

According to a statement issued by Shenhua last week, the plant has been turning coal into liquid fuel and chemical products since December. The technique, which is also widely used in South Africa, has been criticized for its high emissions of carbon dioxide.

Last year, the Chinese government issued a moratorium on new coal-liquefaction facilities, but allowed Shenhua to complete its Mongolia plant and continue work on a second. The company says it is developing ways to capture and store the CO_2 emitted during the process.

Italian universities lose freedom to appoint staff

Italian universities will have little say in choosing their own professors thanks to a law approved by parliament last week.

According to the new rules, a five-person selection committee will oversee each appointment. But a university recruiting a professor can appoint only one member to the board. The other four members will be picked at random from a list of twelve voted for by the relevant community of scientists across Italy.

The existing *concorsi* system is similar, but it allowed universities to have more control over selection — a privilege that was sometimes abused to make appointments based on local politics rather than on merit. Many academics had lobbied for a reform that would allow universities to make their own free choice, but lose funds if their chosen professors underperformed.

Corrections

The News round-up item 'Biodiversity gets catalogued online' (*Nature* **456,** 844–845; 2008) gave incorrect funding numbers for the Encyclopedia of Life. The total budget for the project's first five years is US$50 million; $2.5 million came from the Sloan Foundation and $10 million from the MacArthur Foundation in 2007.

The News story 'Good grades, but who gets the cash?' (*Nature* **457,** 13; 2009) incorrectly calculated the number of staff submitted by the University of Oxford who were rated world-leading and internationally excellent in the biological-sciences category of the 2008 Research Assessment Exercise. The correct number is 75, putting the university in second place behind the University of Cambridge.

visa applications for foreign researchers and give international science and engineering students an automatic one-year visa extension to seek work or advanced study.

Suspended urologist set to return to Austrian university

The urologist at the centre of Austria's biggest-ever research scandal can return to work at the Medical University of Innsbruck, a disciplinary committee has ruled.

Hannes Strasser was suspended from clinical, teaching and research duties in September 2008 following accusations of malpractice in a clinical trial using stem cells to treat urinary incontinence (see *Nature* 454, 922; 2008).

The national disciplinary committee responsible for university staff has now concluded that the suspension was not legally justified, as more than three years had passed since the alleged misdemeanour occurred.

Strasser, who is facing criminal charges relating to harming patients or putting them at risk of harm, is on paid leave until the end of January. He will not be allowed to treat patients until the criminal case is resolved — which is likely to take at least a year. An investigation by the Austrian National Academy of Sciences is also ongoing.

Coal conversion plant fires up in China

China's first coal-liquefaction plant is up and running. Located in Inner Mongolia, the facility is run by the state-owned Shenhua Group.

According to a statement issued by Shenhua last week, the plant has been turning coal into liquid fuel and chemical products since December. The technique, which is also widely used in South Africa, has been criticized for its high emissions of carbon dioxide.

Last year, the Chinese government issued a moratorium on new coal-liquefaction facilities, but allowed Shenhua to complete its Mongolia plant and continue work on a second. The company says it is developing ways to capture and store the CO_2 emitted during the process.

Italian universities lose freedom to appoint staff

Italian universities will have little say in choosing their own professors thanks to a law approved by parliament last week.

According to the new rules, a five-person selection committee will oversee each appointment. But a university recruiting a professor can appoint only one member to the board. The other four members will be picked at random from a list of twelve voted for by the relevant community of scientists across Italy.

The existing *concorsi* system is similar, but it allowed universities to have more control over selection — a privilege that was sometimes abused to make appointments based on local politics rather than on merit. Many academics had lobbied for a reform that would allow universities to make their own free choice, but lose funds if their chosen professors underperformed.

Corrections

The News round-up item 'Biodiversity gets catalogued online' (*Nature* **456,** 844–845; 2008) gave incorrect funding numbers for the Encyclopedia of Life. The total budget for the project's first five years is US$50 million; $2.5 million came from the Sloan Foundation and $10 million from the MacArthur Foundation in 2007.

The News story 'Good grades, but who gets the cash?' (*Nature* **457,** 13; 2009) incorrectly calculated the number of staff submitted by the University of Oxford who were rated world-leading and internationally excellent in the biological-sciences category of the 2008 Research Assessment Exercise. The correct number is 75, putting the university in second place behind the University of Cambridge.

visa applications for foreign researchers and give international science and engineering students an automatic one-year visa extension to seek work or advanced study.

Suspended urologist set to return to Austrian university

The urologist at the centre of Austria's biggest-ever research scandal can return to work at the Medical University of Innsbruck, a disciplinary committee has ruled.

Hannes Strasser was suspended from clinical, teaching and research duties in September 2008 following accusations of malpractice in a clinical trial using stem cells to treat urinary incontinence (see *Nature* 454, 922; 2008).

The national disciplinary committee responsible for university staff has now concluded that the suspension was not legally justified, as more than three years had passed since the alleged misdemeanour occurred.

Strasser, who is facing criminal charges relating to harming patients or putting them at risk of harm, is on paid leave until the end of January. He will not be allowed to treat patients until the criminal case is resolved — which is likely to take at least a year. An investigation by the Austrian National Academy of Sciences is also ongoing.

Coal conversion plant fires up in China

China's first coal-liquefaction plant is up and running. Located in Inner Mongolia, the facility is run by the state-owned Shenhua Group.

According to a statement issued by Shenhua last week, the plant has been turning coal into liquid fuel and chemical products since December. The technique, which is also widely used in South Africa, has been criticized for its high emissions of carbon dioxide.

Last year, the Chinese government issued a moratorium on new coal-liquefaction facilities, but allowed Shenhua to complete its Mongolia plant and continue work on a second. The company says it is developing ways to capture and store the CO_2 emitted during the process.

Italian universities lose freedom to appoint staff

Italian universities will have little say in choosing their own professors thanks to a law approved by parliament last week.

According to the new rules, a five-person selection committee will oversee each appointment. But a university recruiting a professor can appoint only one member to the board. The other four members will be picked at random from a list of twelve voted for by the relevant community of scientists across Italy.

The existing *concorsi* system is similar, but it allowed universities to have more control over selection — a privilege that was sometimes abused to make appointments based on local politics rather than on merit. Many academics had lobbied for a reform that would allow universities to make their own free choice, but lose funds if their chosen professors underperformed.

Corrections

The News round-up item 'Biodiversity gets catalogued online' (*Nature* **456,** 844–845; 2008) gave incorrect funding numbers for the Encyclopedia of Life. The total budget for the project's first five years is US$50 million; $2.5 million came from the Sloan Foundation and $10 million from the MacArthur Foundation in 2007.

The News story 'Good grades, but who gets the cash?' (*Nature* **457,** 13; 2009) incorrectly calculated the number of staff submitted by the University of Oxford who were rated world-leading and internationally excellent in the biological-sciences category of the 2008 Research Assessment Exercise. The correct number is 75, putting the university in second place behind the University of Cambridge.

visa applications for foreign researchers and give international science and engineering students an automatic one-year visa extension to seek work or advanced study.

Suspended urologist set to return to Austrian university

The urologist at the centre of Austria's biggest-ever research scandal can return to work at the Medical University of Innsbruck, a disciplinary committee has ruled.

Hannes Strasser was suspended from clinical, teaching and research duties in September 2008 following accusations of malpractice in a clinical trial using stem cells to treat urinary incontinence (see *Nature* 454, 922; 2008).

The national disciplinary committee responsible for university staff has now concluded that the suspension was not legally justified, as more than three years had passed since the alleged misdemeanour occurred.

Strasser, who is facing criminal charges relating to harming patients or putting them at risk of harm, is on paid leave until the end of January. He will not be allowed to treat patients until the criminal case is resolved — which is likely to take at least a year. An investigation by the Austrian National Academy of Sciences is also ongoing.

Coal conversion plant fires up in China

China's first coal-liquefaction plant is up and running. Located in Inner Mongolia, the facility is run by the state-owned Shenhua Group.

According to a statement issued by Shenhua last week, the plant has been turning coal into liquid fuel and chemical products since December. The technique, which is also widely used in South Africa, has been criticized for its high emissions of carbon dioxide.

Last year, the Chinese government issued a moratorium on new coal-liquefaction facilities, but allowed Shenhua to complete its Mongolia plant and continue work on a second. The company says it is developing ways to capture and store the CO_2 emitted during the process.

Italian universities lose freedom to appoint staff

Italian universities will have little say in choosing their own professors thanks to a law approved by parliament last week.

According to the new rules, a five-person selection committee will oversee each appointment. But a university recruiting a professor can appoint only one member to the board. The other four members will be picked at random from a list of twelve voted for by the relevant community of scientists across Italy.

The existing *concorsi* system is similar, but it allowed universities to have more control over selection — a privilege that was sometimes abused to make appointments based on local politics rather than on merit. Many academics had lobbied for a reform that would allow universities to make their own free choice, but lose funds if their chosen professors underperformed.

Corrections

The News round-up item 'Biodiversity gets catalogued online' (*Nature* **456,** 844–845; 2008) gave incorrect funding numbers for the Encyclopedia of Life. The total budget for the project's first five years is US$50 million; $2.5 million came from the Sloan Foundation and $10 million from the MacArthur Foundation in 2007.

The News story 'Good grades, but who gets the cash?' (*Nature* **457,** 13; 2009) incorrectly calculated the number of staff submitted by the University of Oxford who were rated world-leading and internationally excellent in the biological-sciences category of the 2008 Research Assessment Exercise. The correct number is 75, putting the university in second place behind the University of Cambridge.

THE WASTED YEARS

In the first of three features on the legacy of the Bush administration, **Declan Butler** looks at the United States' failure to deal with the risks of nuclear proliferation.

"Where do I start? One could write a book," sighs Frank von Hippel, a nuclear-weapons expert at Princeton University in New Jersey. He rattles off a litany of the ways in which he believes the administration of George W. Bush has harmed the cause of nuclear non-proliferation. The list includes the Iraq war, the administration's scuttling of the Nuclear Non-Proliferation Treaty (NPT), its opposition to the Comprehensive Test Ban Treaty, its pursuit of missile-defence schemes and a nuclear deal with India, and its foot-dragging on reductions in nuclear weapons. "The Bush administration did about as much damage to non-proliferation as one could imagine anybody doing," says von Hippel.

That gloomy assessment is largely shared by other experts. "For non-proliferation, the Bush administration has represented at best stagnation, and in many places retrogression," says Christopher Paine, a nuclear-weapons expert at the Natural Resources Defense Council in Washington DC. "All in all, not a good record." And for Daryl Kimball, executive director of the Washington-based Arms Control Association, the Bush administration has "left the world demonstrably less secure today than it was a decade ago with respect to nuclear-weapons-related threats".

The international nuclear non-proliferation regime depends on an interconnected, fragile system of trust, confidence, and diplomatic and regulatory checks and balances built up over decades around the NPT, Kimball explains. Although cheats of the NPT regime, such as North Korea, have rightly attracted prominent concern, eight years of less-conspicuous non-proliferation deregulation under Bush has undermined the regime itself, say experts.

"The Bush administration did about as much damage to non-proliferation as one could imagine anybody doing." — Frank von Hippel

Indeed, some find the situation depressingly similar to the recent carnage in the financial markets. One such example is Joseph Cirincione, president of the Ploughshares Fund, a grant-making facility in San Francisco, California, that supports projects to prevent the spread and use of nuclear weapons. Writing last November in *Arms Control Today*, Cirincione said that Bush non-proliferation officials are leaving "office like financiers fleeing busted Wall Street banks, with precious assets squandered on risky ventures, once-solid institutions crumbling, surpluses turned into gaping deficits, and a string of problems mismanaged into crises that threaten to bring down a decades-old global regime".

OFFICE OF THE PRESIDENCY OF IRAN/GETTY IMAGES

President Mahmoud Ahmadinejad of Iran (centre) has overseen an expansion of the country's uranium-enrichment facility.

"The Bush administration effectively walked away from proven arms-control and disarmament agreements," says Kimball — most obviously the NPT. Kimball and other arms-control experts are the first to admit that the NPT regime and its related legislation are far from perfect. But they argue that the treaty has succeeded in creating a diplomatic space and norms that have largely prevented the appearance of new nuclear-weapons states. Although India, Pakistan, Israel and North Korea have developed nuclear weapons since the treaty came into effect in 1970, these experts say, many more nations have renounced their programmes to develop nuclear weapons. Without this non-proliferation system, the world might contain 30–40 nuclear-weapons states, they say. And should the system founder, they add, many new nuclear-weapons states would probably emerge, and this in turn would increase the risk of terrorists getting their hands on a bomb.

Despite that risk, says Rebecca Johnson, founding director of the London-based Acronym Institute for Disarmament Diplomacy, the Bush White House viewed multilateral arms-control agreements as constraining US action yet offering the nation few benefits. So after the terrorist attacks of 11 September 2001, the administration effectively repudiated the 'grand bargain' that is the core of the NPT.

Give and take

That bargain calls for the United States, Russia, the United Kingdom, France and China — the five states that had developed nuclear weapons before the NPT came into effect — to work to eliminate their stocks. In addition, these states undertook, albeit unofficially, to use their weapons only as a last resort in the event of a nuclear attack. In return, other states agreed not to develop nuclear weapons, and were guaranteed an 'inalienable right' to use nuclear energy for peaceful purposes.

In 2002, however, reviews of US defence and nuclear policy enshrined a new 'Bush doctrine'. On the plus side, the doctrine formalized the post-cold-war reality: nuclear weapons were no longer central to foreign policy with Russia and China, who had ceased to be the nation's

mortal enemies. And it accurately reflected the new, twenty-first-century reality: the immediate threat was no longer full-scale nuclear war, but that terrorists might obtain and use a nuclear bomb. The problem was how the doctrine responded to this new reality. It has been a "disaster", says Paine. It has "completely backfired" in terms of non-proliferation.

For example, the doctrine authorized preemptive war against states considered to be developing weapons of mass destruction. It also left open for the first time the possibility of using nuclear weapons against states that did not have them, and blurred the historic red line between nuclear and conventional weapons by allowing tactical nuclear weapons to be used to attack enemy targets such as hardened bunkers. In doing so, the doctrine directly encouraged proliferation by countries in the US sights, says Bates Gill, director of the Stockholm International Peace Research Institute. He argues that it helped to convince countries such as Iran and North Korea that they needed to have nuclear weapons as deterrents to stave off potential US attacks. But if these two countries acquire nuclear arsenals it could trigger new nuclear-arms races in Asia and the Middle East, and perhaps beyond.

Bush initially refused to negotiate with either country, which "exacerbated" the problem, says Kimball. At least partly as a result of that missed opportunity, North Korea exploded a nuclear test device in 2006, and Iran now stands just months away from having enriched enough uranium for a bomb. Only recently has the United States started talks with North Korea, and it has now made tentative moves to negotiate with Iran.

On a broader level, say non-proliferation experts, the Bush doctrine's undermining of the NPT had a chilling effect on global non-proliferation efforts. It contributed directly to the collapse of the 2005 review conference of the NPT, in which member states failed to make any progress on a series of 13 measures that they had agreed to at the previous review conference five years earlier. These measures included the Comprehensive Nuclear-Test-Ban Treaty and a Fissile Material Cut-Off Treaty to outlaw the production of new weapons material.

Bush delivered another blow to the NPT when he signed a deal with India to force the lifting of an international ban on nuclear trade with the country, says Gill. The deal set a dangerous precedent by rewarding a country that has refused to sign the NPT and that has developed nuclear weapons, he adds. It also alienated countries that had abandoned their nuclear-weapons programmes to join the NPT. "In a word it has been negative," Gill says.

Dismantling the multilateral non-proliferation system further, in 2002, the United States withdrew from the Anti-Ballistic Missile Treaty negotiated with the Soviet Union in 1972, so that it could pursue its plans to build missile-defence shields against nuclear warheads. "This set a very dangerous precedent of a major country withdrawing from a major arms-control agreement," says Pavel Podvig, an expert on Russian nuclear affairs at the Center for International Security and Cooperation at Stanford University in California.

North Korea's 2006 nuclear test was a cause of celebration for the regime.

STR/AFP/GETTY IMAGES

The Bush administration has also "basically dropped the ball" on nuclear-arms reductions with Russia, says Podvig. Large reductions in arsenals were negotiated as part of the Strategic Arms Reduction Treaty initiated by Ronald Reagan in 1982. But the treaty expires at the end of this year, and no follow-up has been pursued. "The Bush administration consciously made the decision that it was not going to seek any new agreement," says Podvig. And the beneficial scientific and political dialogue that the agreements opened between the signatories has atrophied, he says.

> **"We have an opportunity to shift directions, and to repair our nuclear non-proliferation and disarmament strategies."**
> — Daryl Kimball

Positive progress

There are some bright spots in the Bush legacy. Behind-the-scenes US and British diplomacy helped to persuade Libya to give up its programme of weapons of mass destruction in 2003. That same year, the United States helped to dismantle the vast black-market network of uranium enrichment and nuclear-weapons technologies run by Abdul Qadeer Khan, former head of Pakistan's nuclear programme. And initiatives to secure stocks of nuclear-weapons material worldwide have also progressed somewhat, says von Hippel.

Another positive development — albeit one started during the previous administration of Bill Clinton — is the maturing of the stockpile stewardship programme launched in 1994 to maintain the US arsenal through simulation and physics rather than nuclear testing. The programme has defied sceptics, says von Hippel, and has been largely successful in demonstrating that existing US nuclear warheads are reliable enough not to need imminent replacement.

But perhaps the most significant development in non-proliferation has emerged in the United States not because of the Bush administration, but despite it. This is the bipartisan groundswell for a major new commitment to disarmament, says Johnson. Consensus is growing that nuclear weapons are more of a liability than an asset now that the major threat to the country is a terrorist nuclear attack. The continued existence of massive nuclear arsenals, and the huge and inadequately secured stockpiles of weapons-grade fissile material around the world make this threat even more severe.

The result is a movement to develop a comprehensive roadmap catalysed by Sam Nunn, former chairman of the Senate Committee on Armed Services and co-chair of the Nuclear Threat Initiative, a non-profit organization that aims to reduce the threat of nuclear and other weapons of mass destruction; George Schultz and Henry Kissinger, former secretaries of state; and William Perry, a former secretary of defence. The project aims to disarm the nuclear-weapons states, and in so doing gain multilateral support for a tougher international regime to counter nuclear terrorism and nuclear proliferation. Adding momentum, the Global Zero campaign put in place to back the plan was launched in Paris last month by prominent world figures, including former US president Jimmy Carter and other former heads of state.

The next NPT review conference, in 2010, will test whether such efforts are paying off. Experts have high expectations for the meeting, as US president-elect Barack Obama made the reinforcement of multilateral non-proliferation and disarmament efforts a central part of his election campaign (see page 235). "We have an opportunity here in the United States to shift directions, and to repair our nuclear non-proliferation and disarmament strategies," says Kimball. "You can never make up completely for lost time," says von Hippel, "but there certainly is a feeling that we now have to do the best we can to make up for the lost time of the Bush administration." ■

Declan Butler is a senior reporter at *Nature*, based in France.

See Editorial, page 235.

43 BY THE NUMBERS

A look at George W. Bush's legacy in science.

Although a president's influence extends only so far in determining the United States' research agenda, most if not all areas of science and environmental management feel some impact. In the eight years since he became the United States' 43rd president, George W. Bush has supported major increases in portions of the federal research budget, but he has also attracted serious criticism for some environmental policies and the degree to which policy decisions in his administration have been informed — or not — by the best available science. A full appreciation of his policies' impacts on a given field may take years. However, the raw data available now lend some insights as to what history is likely to judge as high and low points of the Bush administration's scientific legacy.

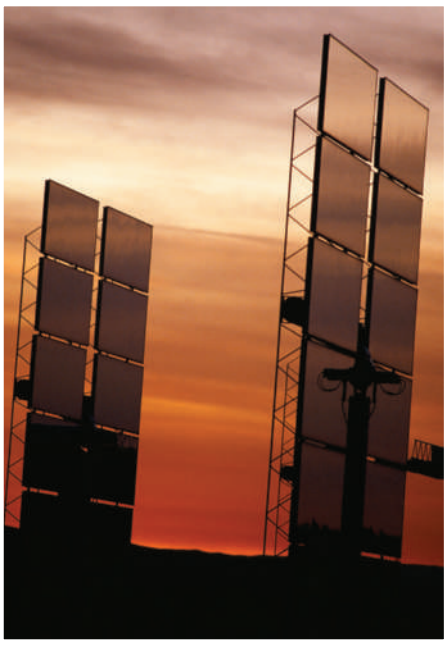

J. SOHM/VISIONSOFAMERICA/GETTY IMAGES

ALTERNATIVE ENERGY

The Bush years saw significant increases in energy production from such alternatives as wind, solar and biomass, driven in large part by skyrocketing oil and natural-gas prices. The Bush administration supported incentives to encourage continued expansion through tax credits and other approaches, but no provisions for permanent incentives were established. Total US renewable-energy production — which is dominated by hydropower and biomass — remains less than 7% of the country's overall energy consumption.

Increase in total installed capacity for wind, solar, geothermal, hydroelectric, wood and waste power generation during the administration of Bill Clinton (1993–2001): 3.07%

Increase during the current Bush administration, to 2007: 12.5%

MARINE RESERVES

In 2006 Bush declared the Northwest Hawaiian Islands as the Papahānaumokuākea Marine National Monument — the culmination of a long process that began well before he took office. On 6 January, the administration declared three additional, massive marine national monuments in remote areas of the Pacific that include coral reefs around several uninhabited islands and the Mariana Trench. No president has ever protected more ocean area, but the value of the protections will be largely determined by the extent to which the areas are ultimately managed and policed under future administrations.

Area of the Papahanaumokuakea Marine National Monument: 362,072 square kilometres

Area of the new Mariana Islands, Pacific Remote Islands, and Rose Atoll Marine National Monuments: 505,773 square kilometres

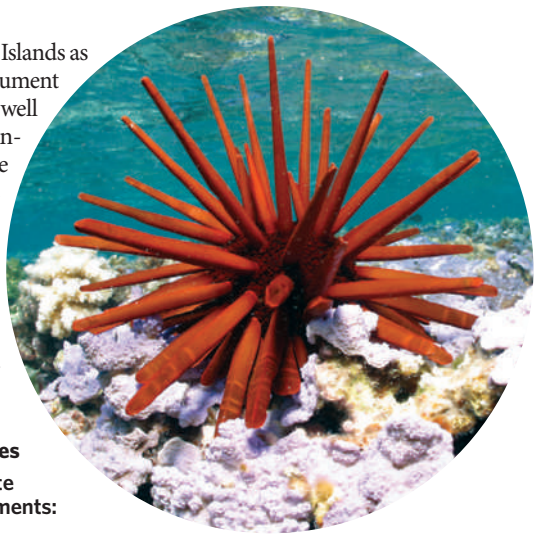

E. VUCCI/AP

J. D. WATT, TRUST

STEM CELLS

Academics have struggled to quantify the detrimental effects of Bush's decision in 2001 to restrict federal funding for research on human embryonic stem cells to those lines in existence at the time. Aaron Levine, a public-policy professor at the Georgia Institute of Technology in Atlanta, recently studied the stem-cell research contributions of various countries. His work suggests that, relative to other similar research areas such as RNA interference, the US contribution to the field is deficient. Perhaps not surprisingly, all five countries showing the highest performance rates in the field — Singapore, the United Kingdom, Israel, China and Australia — permit the creation of new embryonic stem-cell lines.

FALLING BEHIND

Percentage of publications with the corresponding author from a given country, as measured by citations of key initial biomedical papers (1998–2006).

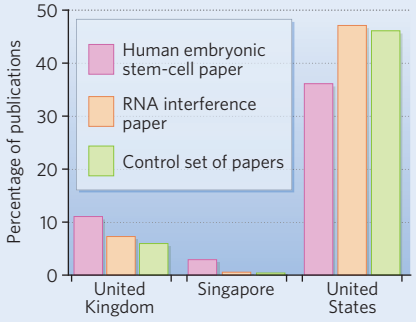

SOURCE: A. LEVINE

NASA

RESEARCH FUNDING

For the first few years of his administration, despite tight budgets and calls to expand into other research areas, Bush continued the substantial funding increases at the National Institutes of Health (NIH) that were begun under Clinton. By 2005, the NIH budget had levelled off, and the past few years have seen flat to negative funding once biomedical inflation is accounted for.

In 2006, Bush kicked off a focus on physical-sciences research by announcing the American Competitiveness Initiative. Among other goals, this aimed to double by 2016 the budgets for the National Science Foundation (NSF), the Department of Energy (DoE) Office of Science, and core funding for the National Institute of Standards and Technology. But whereas the president's proposed budgets each year were on track towards doubling, the budgets enacted by Congress have fallen well short of this mark for the NSF and the DoE.

The fate of all agency budgets will remain unclear until the new president makes his annual budget request in early February.

COMPETING PRIORITIES

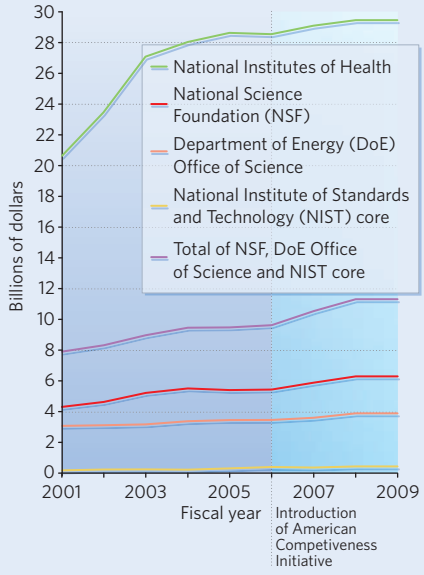

SPACE

As part of his new 'Vision for Space Exploration', Bush announced in 2004 that the United States would send humans back to the Moon by 2020. The resulting surge in US lunar interest and activities, combined with a cadre of Moon probes launched by other countries such as China, Japan and India, mean that the coming years will see a massive flood of Moon-related data to analyse.

The Lunar Reconnaissance Orbiter (LRO; above) and the Lunar Crater Observation and Sensing Satellite (LCROSS) are slated to launch together in late April. LRO will characterize the Moon's surface from orbit with an eye to finding safe landing and base sites for future astronauts; LCROSS will send two impactors plummeting to the surface to hunt for water ice in the shadowy craters near the lunar poles. Whether the larger vision of returning to the Moon is sustained depends on how Barack Obama crafts his space policy — an unknown at this time.

Number of US missions under development for lunar research, in 2001: 0

Number in 2008: 2

BIOSECURITY

One clear result of the 9/11 terrorist attacks was an increased focus on potential means of terrorism and a drastically heightened interest in research aimed at preventing and responding to attacks. From 2001 onwards there were huge increases in funding for civilian biodefence programmes (see chart below), although many of those also serve broader purposes in preparing for infectious-disease outbreaks or other disaster scenarios.

Even so, experts in the field say additional money is needed to address key needs such as development of medical countermeasures for attacks. A recent report on terrorism threats — *World at Risk*, put out by the bipartisan Commission on the Prevention of Weapons of Mass Destruction Proliferation and Terrorism — concluded that a biological attack is likely somewhere in the world in the next five years.

BE PREPARED

Funding for preparedness in civilian biodefence and pandemic influenza, from the Department of Health and Human Services.

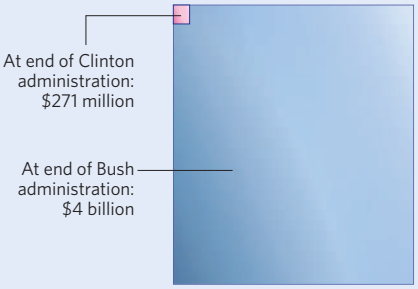

ENDANGERED SPECIES

Endangered-species listings slowed to a trickle during the Bush administration; critics have blamed an increase in bureaucratic hurdles and a failure at times to act according to scientists' recommendations. Officials say the decrease is due largely to litigation that forced the Fish and Wildlife Service to focus most available funding and energy on completing critical habitat designations — which did increase dramatically — for previously listed species. Having addressed much of this backlog, the agency says that more than 50 endangered-species listings are in the works for 2009.

Average number of endangered species listed per year:

Clinton administration: 65

Bush administration: 8

B. MOOSE PETERSON /ARDEA

The endangered Santa Catalina Island fox

Reported by Mark Schrope, a freelance writer in Florida.

See Editorial, page 235.

J. SCOTT APPLEWHITE/AP; B. STIRTON/GETTY IMAGES

An unlikely champion

Was setting up PEPFAR — a massive HIV treatment programme — the best thing that President Bush ever did? **Erika Check Hayden** investigates.

On 1 December 2008, a parade of luminaries appeared on screen in Washington DC to pay video tributes to President George W. Bush on World AIDS day. It was the twilight of his administration, and an obvious time for reflection. But for these people — including former US president Bill Clinton, United Nations secretary-general Ban Ki-moon, rock star Bono and US President-elect Barack Obama — this was not dutiful lip-service. They were heaping praise on Bush's signature programme to fight AIDS, and what many view as his most significant positive achievement of the past eight years.

By the next day though, the compliments had been eclipsed. The front pages of major newspapers were dominated by photos of Obama embracing Hillary Clinton, his pick for Secretary of State. None featured the accolades for Bush, or the new figures showing that his programme — the US President's Emergency Plan For AIDS Relief, or PEPFAR — had put more than two million HIV-positive people on antiretroviral treatments since Bush established it in 2003.

The episode underscores the complicated legacy that Bush has left with his HIV programme, variously praised, criticized and overshadowed. PEPFAR is credited with being the first and largest bilateral foreign-aid programme to try to treat chronic disease on a mass scale, with US$18.8 billion spent so far. But it has also been highly controversial because of stipulations on how its funds should be spent. And now, as Obama takes over and with PEPFAR's leadership likely to change, the programme faces a challenging future.

Unlike smallpox or polio, which were brought under control by vaccines that could be administered in a just a few doses, HIV drugs have to be delivered for life. "Once you start people on treatment, you can't stop — you have made a long-term commitment to supporting therapy for these people," says Chris Beyrer, director of the Johns Hopkins Center for Public Health and Human Rights in Baltimore, Maryland. Such therapy could get increasingly expensive as those already on treatment become resistant to their current medications and have to switch to pricey alternatives. And many hope that in addition to covering these drugs, the programme will expand to reach the millions who are still not receiving any treatment at all — a costly scale-up at just the time when the world's economy is in sharp decline and the United States is in a recession. How to sustain this scale-up, says Anthony Fauci, director of the US National Institute of Allergy and Infectious Diseases in Bethesda, Maryland, "is something that I dream about, think about, while I'm eating, sleeping — all the time". For Obama, then, PEPFAR could prove a complicated inheritance.

In 2003, only 400,000 people in poor countries had access to antiretroviral treatment, and the world was spending less than half of what was needed to reach their goals for combating AIDS by 2005, according to the Joint United Nations Programme on HIV/AIDS (UNAIDS). When Bush announced in his January 2003 State of the Union address his intention to create the $15-billion PEPFAR programme, he "completely changed the landscape", says Peter Piot, founder of UNAIDS. "The most powerful man in the world moved from the 'm' word to the 'b' word — from millions to billions. In that sense, PEPFAR not only brought money, but elevated AIDS issues to one of the big political themes of our time."

Stormy start

The programme was dogged by controversy from the outset. Bush became interested in putting together a large AIDS programme partly because the disease was becoming a big issue among Republican leaders and some of his conservative supporters. Yet some of those same supporters baulked at the prospect of supplying condoms, and with it the implicit endorsement of premarital sex. They found a compromise in a public-health approach called ABC — Abstinence, Be faithful, Correct and consistent condom use — that had been credited with helping to cut HIV prevalence in Uganda[1]. When lawmakers enacted the legislation that enabled PEPFAR, they dictated that

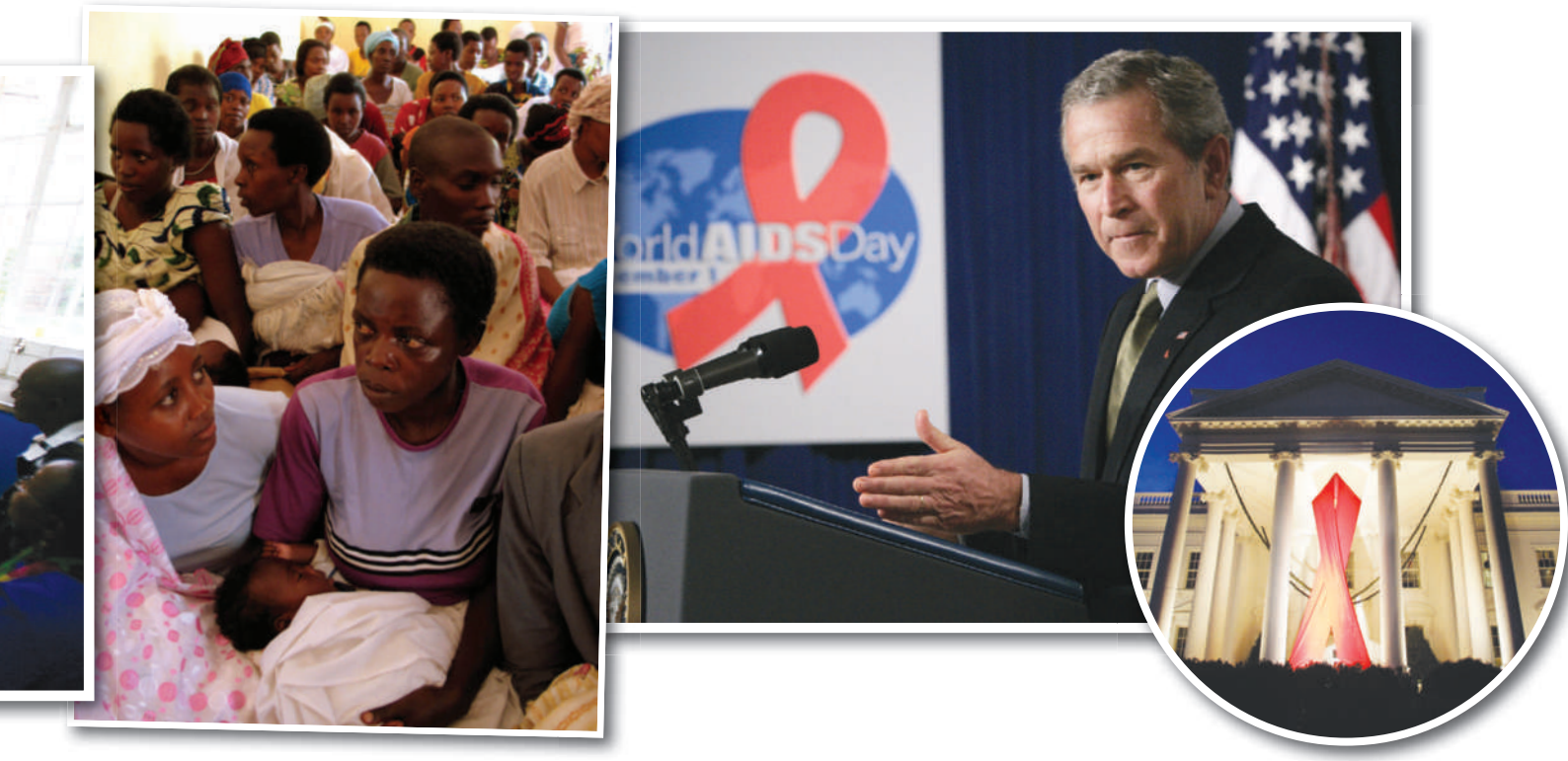

S. BENGALI/MCT/NEWSCOM; C. DHARAPAK/AP; R. EDMONDS/AP

one-third of the 20% spent on prevention must be used for abstinence education programmes. They also required organizations who would receive aid from PEPFAR to pledge their opposition to prostitution — ruling out support for any group trying to reach out to sex workers. And none of the money could go to groups that support abortion, under the 'gag' rule enacted by Bush on his first day in office.

"It's probably true that PEPFAR never would have gotten through Congress had it not been for these political compromises," says Lawrence Gostin, faculty director of the O'Neill Institute for National and Global Health Law at Georgetown University in Washington DC. But for many activists, these compromises confirmed their suspicions that PEPFAR was little more than a ploy to curry favour for the United States abroad after its internationally unpopular invasion of Iraq. If that was the intention, it backfired, says Thomas Coates, director of the Program in Global Health at the David Geffen School of Medicine at the University of California, Los Angeles. "The directives made the United States look ridiculous to the world," he says. "It was like, 'There they go again — being generous on the one hand and then earmarking these moral dictates on the other.'".

"Bush's directives made the United States look ridiculous to the world."
— Thomas Coates

The taint of moral hypocrisy deepened when Randall Tobias, the first head of PEPFAR, who left in 2006, resigned from government a year later after being linked to a prostitution ring. Tobias, a former chief executive of the pharmaceutical company Eli Lilly, had publicly questioned the effectiveness of condoms and the reliability of generic drugs. He was replaced at PEPFAR by Mark Dybul, an intense young doctor who specialized in infectious disease and who had helped to work out the nuts and bolts of the PEPFAR programme with Fauci. Dybul was seen as being more in touch with the reality of AIDS. "As a gay man who lived through the epidemic, he had a professional and personal connection to it in a way that Tobias didn't have," says long-time activist Gregg Gonsalves, now with the International Treatment & Preparedness Coalition in New Haven, Connecticut. "He helped to give [PEPFAR] a more clinical focus and strip it of some of its ideology."

By 2008, PEPFAR was estimated to have prevented infection in 240,000 babies born to HIV infected mothers and provided health care to 9.7 million people, on top of the two million receiving antiretroviral treatment. The programme targets 15 of the most stricken "focus countries" in Africa, Asia and the Caribbean. In addition to providing an overwhelming sum of money, PEPFAR also seems to have succeeded in setting and meeting targets from the outset, establishing a type of accountability that is often missing from aid efforts. "The PEPFAR strategy was to make sure that promises were kept, and that was new in international health," Gostin says.

Yet the controversy surrounding PEPFAR never let up. In 2006, a study[2] commissioned by the World Health Organization (WHO) found "little evidence of the effectiveness of abstinence-only programmes in developing countries". And in Uganda, critics say, restrictions on PEPFAR-funded organizations compelled the groups to place too much focus on abstinence and too little on condoms, helping to trigger a resurgence of the epidemic. PEPFAR officials counter that they always promoted the ABC strategy as a whole. "Our policy was never abstinence only," Dybul says, "anyone who read any of our documents could see that — we supplied more than 2 billion condoms."

Poaching partners

The abstinence provisions aren't the only source of contention. Some have alleged that PEPFAR is poaching scarce workers from countries' own health programmes. Others complain that by focusing resources on AIDS alone, the programme neglects other, equally vital aspects of the health system, such as childhood vaccinations or other infectious diseases. PEPFAR was also criticized for introducing its own process for approving generic drugs, meaning that drugs bought with PEPFAR money were mostly expensive brand-name ones. But some PEPFAR beneficiaries have said that such policies were possible to work around. Agnes Binagwaho, former head of Rwanda's AIDS-control commission, says that her country purchased cheap generic drugs with money from other donors, such as the Global Fund to Fight AIDS, Tuberculosis and Malaria and the World Bank. Rwanda used some of its $30 million from PEPFAR when it needed to purchase brand-name drugs to treat patients who had developed resistance to their original treatments. "There are so many needs, there is always something else the money can be used for," Binagwaho says.

The 'B' part of ABC — be faithful — has also received some credit. Interest in how to encourage people to change their sexual behaviour is growing throughout the world, led by public-health researchers such as Edward Green, director of the AIDS Prevention Research Project at the Harvard Center for Population

P.-A. PETTERSSON/GETTY IMAGES

US lawmakers dictated that one-third of HIV prevention funds be used to promote abstinence.

and Development Studies in Cambridge, Massachusetts. Green and others argue[3] that AIDS spreads more slowly in regions where people are encouraged to favour monogamous relationships — even if they are serial relationships — over multiple concurrent long-term sexual relationships. The theory is that the virus will spread more quickly between multiple partners in the acute infectious stage. And Green, who has been an adviser to PEPFAR, says that the organization has been in the vanguard here by advancing the idea that people need to change their behaviour in ways more radical than the wider use of condoms. "PEPFAR is the only major donor that has promoted this," he says.

Congressional credit

Three influential reports released since 2006 — two by the non-partisan US Government Accountability Office[4,5] and one by the US Institute of Medicine[6] — have praised the programme's results, but faulted its spending directives for lessening the initiative's potential impact. And in July 2008, Congress finally responded, stripping PEPFAR of the abstinence provision during the programme's required re-authorization.

The new law authorized $48 billion in new PEPFAR spending over the next five years — more than three times the original sum and a massive affirmation of the initiative's success. It still asks countries to explain themselves if they spend less than half of their prevention funds on abstinence and fidelity projects, but critics hope that this will not restrict distribution of the money. It also includes provisions that seem to counter other arguments against PEPFAR, setting targets to train 140,000 health workers, link AIDS and nutrition programmes and authorize $5 billion for malaria and $4 billion for tuberculosis.

The challenge now is to build on PEPFAR's success. Programme officials acknowledge that the people they have reached so far may be the 'low-hanging fruit' — those that can travel to clinics, for example. Many more live a long way from roads or services and will be difficult to reach. The WHO estimates that two-thirds of the nearly 10 million people who need treatment in developing countries still have no access to it. There is also a rising chorus of calls for PEPFAR to expand its remit beyond HIV and begin providing services such as maternal care, clean water, basic sanitation and food. Some even want it to be folded into a new US department of international development with a broader portfolio. "No matter what we do with PEPFAR, it will still ignore many of the fundamental things we need," says Gostin.

But such broad ambitions seem unlikely to be realized. Tight financial times leave no room for Obama to start bold new initiatives in global health, and some worry that Congress won't even appropriate the $48 billion authorized for PEPFAR. Who will lead the programme also remains uncertain. Observers say that Dybul's strong defence of the ABC initiative may have doomed his chances of staying on under Obama, and several people have been rumoured as potential replacements. Among the most prominent names is Jim Yong Kim, director of the François-Xavier Bagnoud Center for Health and Human Rights at Harvard School of Public Health in Boston, Massachusetts.

Whoever takes over, observers anticipate that the programme will improve under the Obama administration, and that many of the problematic aspects, such as the prostitution pledge and the anti-family planning bent, will be eliminated. "The good stuff will be salvaged, the bad stuff will be thrown out and PEPFAR will emerge a very different beast," predicts Stephen Lewis, co-director of the advocacy group AIDS-Free World, based in Boston.

Even as the beast it is, the PEPFAR legacy continues to win Bush a level of regard that was only rarely voiced during his administration. "I can't stand him," Gonsalves says, "but Bush has done something unprecedented." And for Fauci, the praise is most apparent in the places where HIV is hitting the hardest. "If you go to Africa," he says, "into villages where PEPFAR has had a major impact, people look at you and say, 'Thank you, and thank God for the United States of America.'". ■

T. SLOAN/AFP/GETTY IMAGES

As head of Bush's HIV programme, Mark Dybul (right) was credited with giving it a clinical focus.

Erika Check Hayden is a senior reporter for *Nature* based in San Francisco.

1. Stoneburner, R. L. & Low-Beer, D. *Science* **304,** 714–718 (2004).
2. O'Reilly, K., Medley, A., Dennison, J. & Sweat, M. Paper given at XVI International AIDS Conference 2006; abstract at http://www.aids2006.org/PAG/Abstracts.aspx?AID=17422.
3. Green, E. C., Halperin, D. T., Nantulya, V. & Hogle, J. A. *AIDS Behav.* **10,** 335–346 (2006).
4. United States Government Accountability Office *Global Health: Spending Requirement Presents Challenges for Allocating Prevention Funding under the President's Emergency Plan for AIDS Relief* (GAO, 2006).
5. United States Government Accountability Office *Global HIV/AIDS: A More Country-Based Approach Could Improve Allocation of PEPFAR Funding* (GAO, 2008).
6. Committee for the Evaluation of the President's Emergency Plan for AIDS Relief (PEPFAR) Implementation *PEPFAR Implementation: Progress and Promise* (National Academies Press, 2007).

See Editorial, page 236.

CORRESPONDENCE

Choosing between batteries or biomass to stay on the road

SIR — Nothing would please me more than to see batteries break out of their traditional markets and propel our cars, a goal described in your News Feature 'Charging up the future' (*Nature* **456,** 436–440; 2008). In my view, this will not happen, however, because of the weakness of electrochemical power storage. The best lithium-ion battery provides energy at the rate of 100 watt-hours per kilogram. For liquid fuels such as petrol and diesel the energy density is around 12,000 watt-hours per kilogram. Even after dividing the latter figure by four because of Carnot-cycle losses in the conventional car engine, you are still at least 30 times better off with petrol than with the best and most expensive battery.

Would people be willing to pay significantly more for cars that perform worse than current versions? How likely are they to charge their batteries with 'green' power, which costs up to 10 times more than conventional electricity? The truth is that electric cars may fill a niche market for idealistic commuters, but for longer trips they are out of the question.

Synthetic fuels made of non-edible biomass are the best way to free cars of carbon dioxide emissions with existing technologies. Although the enzymes needed for splitting cellulose into sugar (the source of ethanol) are still much too expensive, the Fischer–Tropsch technology for making synthetic fuels from waste wood, straw or grass has been around for 70 years. Controlled burning with the addition of water yields a mixture of carbon monoxide and hydrogen that can be catalytically converted into any desired liquid fuel suitable for conventional internal-combustion engines.

The infrastructure for distributing such fuels is already in place. And enough biomass grows each year to supply the world's entire car fleet.

Lucien F. Trueb In der Oberwis 9, 8123 Ebmatingen, Switzerland
e-mail: lucien.trueb@bluewin.ch

Genetic records threaten patients' privacy

SIR — The philosophical issues involved in privacy of genetic data are debated in your Editorial 'My genome. So what?' (*Nature* **456,** 1; 2008) and in Patrick Taylor's Commentary 'When consent gets in the way' (*Nature* **456,** 32–33; 2008). But practical concerns are an issue too.

Hospitals increasingly often have electronic databases accessible by all doctors and nurses on the staff and some administrators. Someone who had had an abortion, for example, could find this information available to thousands. Privacy is likewise denied to cancer patients who don't want their illness to be common knowledge.

Penalties for snooping are hard to enforce. Medical information sneaks out, particularly about celebrities: anyone in medicine can find out exactly what type of pancreatic tumour afflicted Steve Jobs of Apple, as well as the details of his operation.

The FBI is currently investigating a criminal network allegedly trying to extort money from patients who used a medical-benefits management company called Express Scripts; the company's computer records were, apparently, pilfered. People receiving medication for conditions such as herpesvirus were targeted.

Adding genetic information that can be interpreted in different ways will simply increase the exposure of patients to a system that is already faulty in practice.

Tom Goffman Cancer Intelligence and Research, 3830 Jefferson Boulevard, Virginia Beach, Virginia 23455, USA
e-mail: tetomtg@yahoo.com

Japan should intensify embryonic stem-cell investigations

SIR — Your News story 'Japan ramps up patent effort to keep iPS lead' (*Nature* **453,** 962–963; 2008) concerned research on human induced pluripotent stem (iPS) cells. For international research on these cells to progress, it is essential to have a thriving research programme on human embryonic stem (ES) cells.

However, the contribution to international research on ES cells between 1980 and 2006 by the United States and China was 20% and 20.8%, respectively, whereas Japan's was only 2.1% (see Japanese Ministry of Economy, Trade and Industry press release at http://tinyurl.com/6lphqw, in Japanese). If the Japanese government insists on having more restrictive regulations for human ES-cell research than other countries (see *Nature* **438,** 263; 2005), Japan is in danger of being overtaken in the field of human iPS-cell research.

Hisashi Moriguchi Laboratory for Systems Biology and Medicine, University of Tokyo, Japan, and Department of Analytical Health Science, Tokyo Medical and Dental University, Japan
e-mail: moriguchi@lsbm.org
Chifumi Sato Department of Analytical Health Science, Tokyo Medical and Dental University, Japan

Research on primate brains is scrutinized and must be justified

SIR — Ulrike Gross, in her Correspondence 'Public opinion and the ethics of primate brain research' (*Nature* **456,** 443; 2008), says that monkey brain research similar to that conducted by Andreas Kreiter has been 'prohibited' in Zurich. This is not the case.

As reported in your News story 'Swiss court bans work on macaque brains' (*Nature* **453,** 833; 2008), the Veterinary Office of the Canton of Zurich did grant licences for experiments involving macaques, but their decision was successfully challenged by some members of an advisory committee. These include the chair of the committee, Klaus Peter Rippe, who also chairs the Federal Ethics Committee on Non-Human Biotechnology that reported on the dignity of plants (*Nature* **453,** 824; 2008).

The same Zurich advisory committee did not object to the granting of licences to other Zurich groups that used similar methods to Kreiter's. There is therefore no objection in principle to experiments with monkeys in Zurich.

The issue at present centres on the balance of cost and benefit, particularly on whether fundamental research is less valuable than applied research even when the former has long-term potential for contributing to human health and welfare. The Zurich case is currently under consideration by the Swiss Federal Court.

Gross says that the monkeys in Zurich are suffering. They are not, as the protocols of unannounced inspection visits by members of the cantonal Veterinary Office advisory committee affirm.

She also says, "Even a prominent scientist such as Andreas Kreiter must justify his use of animals". In Europe there are many levels at which such justification is required: the research institutions, the funding organizations, the licensing authorities (where her interests are usually represented), and the journals where the research is peer reviewed. In our society, science is the activity that is probably subject to the widest scrutiny and review by both experts and laypeople alike.

Kevan A. C. Martin Institute of Neuroinformatics, UZH/ETH, Winterthurerstrasse 190, 8057 Zurich, Switzerland

Contributions may be submitted to correspondence@nature.com.

CORRESPONDENCE

Choosing between batteries or biomass to stay on the road

SIR — Nothing would please me more than to see batteries break out of their traditional markets and propel our cars, a goal described in your News Feature 'Charging up the future' (*Nature* **456,** 436–440; 2008). In my view, this will not happen, however, because of the weakness of electrochemical power storage. The best lithium-ion battery provides energy at the rate of 100 watt-hours per kilogram. For liquid fuels such as petrol and diesel the energy density is around 12,000 watt-hours per kilogram. Even after dividing the latter figure by four because of Carnot-cycle losses in the conventional car engine, you are still at least 30 times better off with petrol than with the best and most expensive battery.

Would people be willing to pay significantly more for cars that perform worse than current versions? How likely are they to charge their batteries with 'green' power, which costs up to 10 times more than conventional electricity? The truth is that electric cars may fill a niche market for idealistic commuters, but for longer trips they are out of the question.

Synthetic fuels made of non-edible biomass are the best way to free cars of carbon dioxide emissions with existing technologies. Although the enzymes needed for splitting cellulose into sugar (the source of ethanol) are still much too expensive, the Fischer–Tropsch technology for making synthetic fuels from waste wood, straw or grass has been around for 70 years. Controlled burning with the addition of water yields a mixture of carbon monoxide and hydrogen that can be catalytically converted into any desired liquid fuel suitable for conventional internal-combustion engines.

The infrastructure for distributing such fuels is already in place. And enough biomass grows each year to supply the world's entire car fleet.

Lucien F. Trueb In der Oberwis 9, 8123 Ebmatingen, Switzerland
e-mail: lucien.trueb@bluewin.ch

Genetic records threaten patients' privacy

SIR — The philosophical issues involved in privacy of genetic data are debated in your Editorial 'My genome. So what?' (*Nature* **456,** 1; 2008) and in Patrick Taylor's Commentary 'When consent gets in the way' (*Nature* **456,** 32–33; 2008). But practical concerns are an issue too.

Hospitals increasingly often have electronic databases accessible by all doctors and nurses on the staff and some administrators. Someone who had had an abortion, for example, could find this information available to thousands. Privacy is likewise denied to cancer patients who don't want their illness to be common knowledge.

Penalties for snooping are hard to enforce. Medical information sneaks out, particularly about celebrities: anyone in medicine can find out exactly what type of pancreatic tumour afflicted Steve Jobs of Apple, as well as the details of his operation.

The FBI is currently investigating a criminal network allegedly trying to extort money from patients who used a medical-benefits management company called Express Scripts; the company's computer records were, apparently, pilfered. People receiving medication for conditions such as herpesvirus were targeted.

Adding genetic information that can be interpreted in different ways will simply increase the exposure of patients to a system that is already faulty in practice.

Tom Goffman Cancer Intelligence and Research, 3830 Jefferson Boulevard, Virginia Beach, Virginia 23455, USA
e-mail: tetomtg@yahoo.com

Japan should intensify embryonic stem-cell investigations

SIR — Your News story 'Japan ramps up patent effort to keep iPS lead' (*Nature* **453,** 962–963; 2008) concerned research on human induced pluripotent stem (iPS) cells. For international research on these cells to progress, it is essential to have a thriving research programme on human embryonic stem (ES) cells.

However, the contribution to international research on ES cells between 1980 and 2006 by the United States and China was 20% and 20.8%, respectively, whereas Japan's was only 2.1% (see Japanese Ministry of Economy, Trade and Industry press release at http://tinyurl.com/6lphqw, in Japanese). If the Japanese government insists on having more restrictive regulations for human ES-cell research than other countries (see *Nature* **438,** 263; 2005), Japan is in danger of being overtaken in the field of human iPS-cell research.

Hisashi Moriguchi Laboratory for Systems Biology and Medicine, University of Tokyo, Japan, and Department of Analytical Health Science, Tokyo Medical and Dental University, Japan
e-mail: moriguchi@lsbm.org
Chifumi Sato Department of Analytical Health Science, Tokyo Medical and Dental University, Japan

Research on primate brains is scrutinized and must be justified

SIR — Ulrike Gross, in her Correspondence 'Public opinion and the ethics of primate brain research' (*Nature* **456,** 443; 2008), says that monkey brain research similar to that conducted by Andreas Kreiter has been 'prohibited' in Zurich. This is not the case.

As reported in your News story 'Swiss court bans work on macaque brains' (*Nature* **453,** 833; 2008), the Veterinary Office of the Canton of Zurich did grant licences for experiments involving macaques, but their decision was successfully challenged by some members of an advisory committee. These include the chair of the committee, Klaus Peter Rippe, who also chairs the Federal Ethics Committee on Non-Human Biotechnology that reported on the dignity of plants (*Nature* **453,** 824; 2008).

The same Zurich advisory committee did not object to the granting of licences to other Zurich groups that used similar methods to Kreiter's. There is therefore no objection in principle to experiments with monkeys in Zurich.

The issue at present centres on the balance of cost and benefit, particularly on whether fundamental research is less valuable than applied research even when the former has long-term potential for contributing to human health and welfare. The Zurich case is currently under consideration by the Swiss Federal Court.

Gross says that the monkeys in Zurich are suffering. They are not, as the protocols of unannounced inspection visits by members of the cantonal Veterinary Office advisory committee affirm.

She also says, "Even a prominent scientist such as Andreas Kreiter must justify his use of animals". In Europe there are many levels at which such justification is required: the research institutions, the funding organizations, the licensing authorities (where her interests are usually represented), and the journals where the research is peer reviewed. In our society, science is the activity that is probably subject to the widest scrutiny and review by both experts and laypeople alike.

Kevan A. C. Martin Institute of Neuroinformatics, UZH/ETH, Winterthurerstrasse 190, 8057 Zurich, Switzerland

Contributions may be submitted to correspondence@nature.com.

CORRESPONDENCE

Choosing between batteries or biomass to stay on the road

SIR — Nothing would please me more than to see batteries break out of their traditional markets and propel our cars, a goal described in your News Feature 'Charging up the future' (*Nature* **456,** 436–440; 2008). In my view, this will not happen, however, because of the weakness of electrochemical power storage. The best lithium-ion battery provides energy at the rate of 100 watt-hours per kilogram. For liquid fuels such as petrol and diesel the energy density is around 12,000 watt-hours per kilogram. Even after dividing the latter figure by four because of Carnot-cycle losses in the conventional car engine, you are still at least 30 times better off with petrol than with the best and most expensive battery.

Would people be willing to pay significantly more for cars that perform worse than current versions? How likely are they to charge their batteries with 'green' power, which costs up to 10 times more than conventional electricity? The truth is that electric cars may fill a niche market for idealistic commuters, but for longer trips they are out of the question.

Synthetic fuels made of non-edible biomass are the best way to free cars of carbon dioxide emissions with existing technologies. Although the enzymes needed for splitting cellulose into sugar (the source of ethanol) are still much too expensive, the Fischer–Tropsch technology for making synthetic fuels from waste wood, straw or grass has been around for 70 years. Controlled burning with the addition of water yields a mixture of carbon monoxide and hydrogen that can be catalytically converted into any desired liquid fuel suitable for conventional internal-combustion engines.

The infrastructure for distributing such fuels is already in place. And enough biomass grows each year to supply the world's entire car fleet.

Lucien F. Trueb In der Oberwis 9, 8123 Ebmatingen, Switzerland
e-mail: lucien.trueb@bluewin.ch

Genetic records threaten patients' privacy

SIR — The philosophical issues involved in privacy of genetic data are debated in your Editorial 'My genome. So what?' (*Nature* **456,** 1; 2008) and in Patrick Taylor's Commentary 'When consent gets in the way' (*Nature* **456,** 32–33; 2008). But practical concerns are an issue too.

Hospitals increasingly often have electronic databases accessible by all doctors and nurses on the staff and some administrators. Someone who had had an abortion, for example, could find this information available to thousands. Privacy is likewise denied to cancer patients who don't want their illness to be common knowledge.

Penalties for snooping are hard to enforce. Medical information sneaks out, particularly about celebrities: anyone in medicine can find out exactly what type of pancreatic tumour afflicted Steve Jobs of Apple, as well as the details of his operation.

The FBI is currently investigating a criminal network allegedly trying to extort money from patients who used a medical-benefits management company called Express Scripts; the company's computer records were, apparently, pilfered. People receiving medication for conditions such as herpesvirus were targeted.

Adding genetic information that can be interpreted in different ways will simply increase the exposure of patients to a system that is already faulty in practice.

Tom Goffman Cancer Intelligence and Research, 3830 Jefferson Boulevard, Virginia Beach, Virginia 23455, USA
e-mail: tetomtg@yahoo.com

Japan should intensify embryonic stem-cell investigations

SIR — Your News story 'Japan ramps up patent effort to keep iPS lead' (*Nature* **453,** 962–963; 2008) concerned research on human induced pluripotent stem (iPS) cells. For international research on these cells to progress, it is essential to have a thriving research programme on human embryonic stem (ES) cells.

However, the contribution to international research on ES cells between 1980 and 2006 by the United States and China was 20% and 20.8%, respectively, whereas Japan's was only 2.1% (see Japanese Ministry of Economy, Trade and Industry press release at http://tinyurl.com/6lphqw, in Japanese). If the Japanese government insists on having more restrictive regulations for human ES-cell research than other countries (see *Nature* **438,** 263; 2005), Japan is in danger of being overtaken in the field of human iPS-cell research.

Hisashi Moriguchi Laboratory for Systems Biology and Medicine, University of Tokyo, Japan, and Department of Analytical Health Science, Tokyo Medical and Dental University, Japan
e-mail: moriguchi@lsbm.org
Chifumi Sato Department of Analytical Health Science, Tokyo Medical and Dental University, Japan

Research on primate brains is scrutinized and must be justified

SIR — Ulrike Gross, in her Correspondence 'Public opinion and the ethics of primate brain research' (*Nature* **456,** 443; 2008), says that monkey brain research similar to that conducted by Andreas Kreiter has been 'prohibited' in Zurich. This is not the case.

As reported in your News story 'Swiss court bans work on macaque brains' (*Nature* **453,** 833; 2008), the Veterinary Office of the Canton of Zurich did grant licences for experiments involving macaques, but their decision was successfully challenged by some members of an advisory committee. These include the chair of the committee, Klaus Peter Rippe, who also chairs the Federal Ethics Committee on Non-Human Biotechnology that reported on the dignity of plants (*Nature* **453,** 824; 2008).

The same Zurich advisory committee did not object to the granting of licences to other Zurich groups that used similar methods to Kreiter's. There is therefore no objection in principle to experiments with monkeys in Zurich.

The issue at present centres on the balance of cost and benefit, particularly on whether fundamental research is less valuable than applied research even when the former has long-term potential for contributing to human health and welfare. The Zurich case is currently under consideration by the Swiss Federal Court.

Gross says that the monkeys in Zurich are suffering. They are not, as the protocols of unannounced inspection visits by members of the cantonal Veterinary Office advisory committee affirm.

She also says, "Even a prominent scientist such as Andreas Kreiter must justify his use of animals". In Europe there are many levels at which such justification is required: the research institutions, the funding organizations, the licensing authorities (where her interests are usually represented), and the journals where the research is peer reviewed. In our society, science is the activity that is probably subject to the widest scrutiny and review by both experts and laypeople alike.

Kevan A. C. Martin Institute of Neuroinformatics, UZH/ETH, Winterthurerstrasse 190, 8057 Zurich, Switzerland

Contributions may be submitted to correspondence@nature.com.

CORRESPONDENCE

Choosing between batteries or biomass to stay on the road

SIR — Nothing would please me more than to see batteries break out of their traditional markets and propel our cars, a goal described in your News Feature 'Charging up the future' (*Nature* **456,** 436–440; 2008). In my view, this will not happen, however, because of the weakness of electrochemical power storage. The best lithium-ion battery provides energy at the rate of 100 watt-hours per kilogram. For liquid fuels such as petrol and diesel the energy density is around 12,000 watt-hours per kilogram. Even after dividing the latter figure by four because of Carnot-cycle losses in the conventional car engine, you are still at least 30 times better off with petrol than with the best and most expensive battery.

Would people be willing to pay significantly more for cars that perform worse than current versions? How likely are they to charge their batteries with 'green' power, which costs up to 10 times more than conventional electricity? The truth is that electric cars may fill a niche market for idealistic commuters, but for longer trips they are out of the question.

Synthetic fuels made of non-edible biomass are the best way to free cars of carbon dioxide emissions with existing technologies. Although the enzymes needed for splitting cellulose into sugar (the source of ethanol) are still much too expensive, the Fischer–Tropsch technology for making synthetic fuels from waste wood, straw or grass has been around for 70 years. Controlled burning with the addition of water yields a mixture of carbon monoxide and hydrogen that can be catalytically converted into any desired liquid fuel suitable for conventional internal-combustion engines.

The infrastructure for distributing such fuels is already in place. And enough biomass grows each year to supply the world's entire car fleet.

Lucien F. Trueb In der Oberwis 9, 8123 Ebmatingen, Switzerland
e-mail: lucien.trueb@bluewin.ch

Genetic records threaten patients' privacy

SIR — The philosophical issues involved in privacy of genetic data are debated in your Editorial 'My genome. So what?' (*Nature* **456,** 1; 2008) and in Patrick Taylor's Commentary 'When consent gets in the way' (*Nature* **456,** 32–33; 2008). But practical concerns are an issue too.

Hospitals increasingly often have electronic databases accessible by all doctors and nurses on the staff and some administrators. Someone who had had an abortion, for example, could find this information available to thousands. Privacy is likewise denied to cancer patients who don't want their illness to be common knowledge.

Penalties for snooping are hard to enforce. Medical information sneaks out, particularly about celebrities: anyone in medicine can find out exactly what type of pancreatic tumour afflicted Steve Jobs of Apple, as well as the details of his operation.

The FBI is currently investigating a criminal network allegedly trying to extort money from patients who used a medical-benefits management company called Express Scripts; the company's computer records were, apparently, pilfered. People receiving medication for conditions such as herpesvirus were targeted.

Adding genetic information that can be interpreted in different ways will simply increase the exposure of patients to a system that is already faulty in practice.

Tom Goffman Cancer Intelligence and Research, 3830 Jefferson Boulevard, Virginia Beach, Virginia 23455, USA
e-mail: tetomtg@yahoo.com

Japan should intensify embryonic stem-cell investigations

SIR — Your News story 'Japan ramps up patent effort to keep iPS lead' (*Nature* **453,** 962–963; 2008) concerned research on human induced pluripotent stem (iPS) cells. For international research on these cells to progress, it is essential to have a thriving research programme on human embryonic stem (ES) cells.

However, the contribution to international research on ES cells between 1980 and 2006 by the United States and China was 20% and 20.8%, respectively, whereas Japan's was only 2.1% (see Japanese Ministry of Economy, Trade and Industry press release at http://tinyurl.com/6lphqw, in Japanese). If the Japanese government insists on having more restrictive regulations for human ES-cell research than other countries (see *Nature* **438,** 263; 2005), Japan is in danger of being overtaken in the field of human iPS-cell research.

Hisashi Moriguchi Laboratory for Systems Biology and Medicine, University of Tokyo, Japan, and Department of Analytical Health Science, Tokyo Medical and Dental University, Japan
e-mail: moriguchi@lsbm.org
Chifumi Sato Department of Analytical Health Science, Tokyo Medical and Dental University, Japan

Research on primate brains is scrutinized and must be justified

SIR — Ulrike Gross, in her Correspondence 'Public opinion and the ethics of primate brain research' (*Nature* **456,** 443; 2008), says that monkey brain research similar to that conducted by Andreas Kreiter has been 'prohibited' in Zurich. This is not the case.

As reported in your News story 'Swiss court bans work on macaque brains' (*Nature* **453,** 833; 2008), the Veterinary Office of the Canton of Zurich did grant licences for experiments involving macaques, but their decision was successfully challenged by some members of an advisory committee. These include the chair of the committee, Klaus Peter Rippe, who also chairs the Federal Ethics Committee on Non-Human Biotechnology that reported on the dignity of plants (*Nature* **453,** 824; 2008).

The same Zurich advisory committee did not object to the granting of licences to other Zurich groups that used similar methods to Kreiter's. There is therefore no objection in principle to experiments with monkeys in Zurich.

The issue at present centres on the balance of cost and benefit, particularly on whether fundamental research is less valuable than applied research even when the former has long-term potential for contributing to human health and welfare. The Zurich case is currently under consideration by the Swiss Federal Court.

Gross says that the monkeys in Zurich are suffering. They are not, as the protocols of unannounced inspection visits by members of the cantonal Veterinary Office advisory committee affirm.

She also says, "Even a prominent scientist such as Andreas Kreiter must justify his use of animals". In Europe there are many levels at which such justification is required: the research institutions, the funding organizations, the licensing authorities (where her interests are usually represented), and the journals where the research is peer reviewed. In our society, science is the activity that is probably subject to the widest scrutiny and review by both experts and laypeople alike.

Kevan A. C. Martin Institute of Neuroinformatics, UZH/ETH, Winterthurerstrasse 190, 8057 Zurich, Switzerland

Contributions may be submitted to correspondence@nature.com.

COMMENTARY

Your inbox, Mr President

Rejuvenate the Environmental Protection Agency. End the stem-cell ban. Re-engage with the UN on climate change. Six leading voices tell *Nature* what the new US president needs to do to move beyond the Bush legacy.

Christine Todd Whitman
Former administrator of the US Environmental Protection Agency.

Clarify who will speak for the President on environmental matters.

It is clear from everything he has said, that President-elect Barack Obama considers environment and energy issues to be at the top of his agenda. The importance of the commitments he has made cannot be understated and all of them have to be considered in light of the current economic crisis that we are facing.

In terms of key policy matters, the administration must decide how far the Environmental Protection Agency (EPA) should go on meeting the Supreme Court's decision that the EPA has the legal right to regulate carbon dioxide. Although congressional legislation setting a limit on carbon emissions and establishing a trading system or carbon tax would be the best way to move forward, that is unlikely given both the complexity of the issue and the other challenges facing the new Congress.

An early indication of how aggressively the administration will move forwards will be their decision on whether to allow the EPA to grant California a waiver so the state can enforce stricter vehicle-emission standards than those required by the federal government — the state's proposal is a 30% decrease in emissions by 2016. At least 16 other states are anxious to join California, citing the US Clean Air Act, although car-makers in Detroit have fought the regulation vigorously, and successfully, until now.

The Obama administration will also want to look at all the pending regulations moved out in the last few months of the Bush administration, such as those on New Source review — governing when power-plant facilities must install pollution-control technologies — and drilling in wilderness areas. In analyzing these regulations and ensuring both that the work that led to them was complete and that the regulations represent policy supported by the new administration, the incoming appointees would do well to listen carefully to career staff. Such staff are knowledgeable and, for the most part, interested more in a policy agenda than a political one.

Additionally, Obama needs to clarify who will be determining environmental policy — the EPA, the Council on Environmental Quality (CEQ) or the newly created energy tsar Carol Browner. Environment and energy are inextricably linked and, although there is always need for administration-wide coordination, it must be clearly delineated as to who speaks for the president on these issues. Too many voices create confusion and allow issues to fall between the cracks. Although President George W. Bush originally told me that the EPA would be the administration's representative on the environment, subsequent actions by the vice-president and the CEQ proved otherwise. In fact, towards the end of my tenure at the EPA I was told in no uncertain terms that when the CEQ spoke, it was speaking for the president even if on an issue that the EPA felt needed more work. Although I believe that the EPA administrator should be the voice of environmental policy, the president must ultimately decide — and that delineation should be clear and consistent throughout the administration's term.

Finally, the Obama administration needs to be clear on its directives and expectations for the EPA. Morale is low for a host of reasons, not the least of which is because environment was not a priority for the Bush administration. The mood will get worse if staff and appointees feel that they are not part of the crucial discussion and that all decisions are coming from the White House. Incoming administrator Lisa Jackson will find at the EPA many highly talented people whose skills, ideas and extensive institutional knowledge should be cultivated. There are some tremendous public servants there and their contributions should be welcomed and encouraged.

P. FOY/AP PHOTO

2009: the year of climate change?

Timothy E. Wirth
President of the United Nations Foundation, Washington DC, USA.

The United States must lead the way to a new climate deal at Copenhagen.

President-elect Obama has affirmed his intention to lead the United States back into the fight against climate change. His appointments in this area have been nothing short of brilliant, and just two weeks after the election, he told a California climate conference: "Delay is no longer an option. Denial is no longer an acceptable response. The stakes are too high. The consequences, too serious."

The downturn in the economy, far from being an insurmountable obstacle to definitive climate action, is setting the stage for previously unthinkable levels of capital investment that could put the United States on the road to a clean-energy economy, built on rapidly improving technologies and jobs that will remain at home.

Notwithstanding strong climate commitments by the European Union, the rest of the world has been adrift, waiting for the United States to wake from its eight-year sleep. This new American engagement must start with China. The world's two largest emitters have both the capacity and the need to take action, and finding ways to move forwards together would make a broader global agreement achievable.

Such collaboration may be difficult in areas where venture capital is driving innovation and intellectual property is the prize — novel solar technologies, for example. But where the scale of the challenge demands government engagement, such as with technologies for capturing carbon emissions from coal-fired power plants, the two countries could work closely together.

Internationally, some interim steps would be useful en route to a larger deal. Broad-based

commitments to energy efficiency and renewable-energy targets have been torpedoed by American objections in the past but would be constructive building blocks today. A new round of funding to help poorer countries adapt to climate change, delivered (not just pledged) by industrialized countries through the Global Environment Facility, would restore the trust that has been eroded by previously unmet promises. Creating a network of regional technology-innovation centres, as proposed by the United Kingdom's Carbon Trust, would reassure developing countries that they will have access to the technologies they need to respond to climate change.

American leadership on these confidence-building measures would improve the prospect of success in Copenhagen, where the United Nations climate talks resume in December 2009. UN secretary-general Ban Ki-moon has made this one of his highest priorities and has declared 2009 to be the "year of climate change".

The new US administration will have little time to prepare for Copenhagen, but agreement can be reached on the basic elements of a deal — commitments by industrialized countries to emissions targets, credit for avoided deforestation, financial support for adaptation and technology development, along with commensurate actions by rapidly developing countries. The finer details can be given the required attention in the following months, while still leaving enough time for ratification to avoid a post-2012 lapse when the existing commitments end under the Kyoto protocol.

Addressing climate change will require real political leadership domestically and in global negotiations. The commitment Obama has already made to action is remarkable and gives hope to a suffering planet.

Matthew Meselson
Co-director of the Harvard Sussex Program on chemical and biological weapons, Harvard University, USA.

Vast biosecurity expenditures require better oversight and monitoring.

It is seven years since envelopes containing anthrax spores were mailed to news media offices and to two US Senators, causing 11 cases of identified inhalation anthrax, five of which were fatal. In August 2008, the FBI announced that they had traced the source of the spores to the United States Army Medical Research Institute of Infectious Diseases at Fort Detrick in Maryland, one of the many US facilities conducting biodefence research. Although there has been no repetition of such attacks, the episode underscores the need for better oversight of biodefence activities and of the individuals conducting them.

Federal expenditure for civilian biodefence during 2001–08, conducted mainly by the departments of health and human services, homeland security, and defence is estimated at about US$50 billion, of which roughly one-third was for research[1]. Department of Defense (DoD) outlays for biodefence research, development and testing for strictly military objectives currently run at several hundred million dollars per year[2]. Relevant expenditures by the various intelligence agencies have not been made public.

Oversight of biodefence — to ensure that activities comply with existing laws and international agreements — varies from agency to agency, with perhaps the most advanced being that of the Department of Homeland Security (DHS). In addition to scientific peer-review to assess scientific merit, the DHS has a Compliance Review Group (CRG) that reviews all DHS-sponsored research for compliance with the 1972 Biological Weapons Convention and with US criminal law. It also applies the criteria of the National Science Advisory Board for Biosecurity in assessing proposed projects that have potential for hostile misuse. The CRG meets at least twice a year, and before each meeting there is a call for abstracts of proposed projects to be submitted by their respective principal investigators, who at the same time are reminded of their responsibility to ensure compliance with treaty commitments and applicable US law.

CRG members, therefore, are informed about all projects before they commence and the group continues to oversee them as they evolve. Projects deemed by CRG staff to pose risks of actual or perceived non-compliance, or which are likely to pose a dual-use potential for misapplication, are individually briefed to the group and, in some cases, the CRG members are required to acknowledge personal responsibility by signing their names to decisions regarding approval or denial of support for a project.

The compliance procedures in other departments are not as rigorous and there is no process to ensure consistency across government agencies. The DoD, for example, reviews biodefence projects at a broader 'programme' level rather then reviewing individual projects.

Oversight of biodefence activities is likely to come under examination by the new Congress, which could devise guidelines and procedures applicable throughout government. Topics to be considered should include the authority and composition of compliance review boards, criteria for approval of projects, harmonization of procedures, procedures for ensuring the reliability of personnel engaged in biodefence work, provision for site visits, a requirement for periodic reports, and the inclusion of State and Justice Department observers to promote both independence from parochial influences and familiarity with treaty commitments and applicable US law.

The resulting procedure could then serve as a model for consideration by the state parties of the Biological Weapons Convention at its seventh review conference in Geneva, Switzerland, in 2011. The aim would be to agree on a requirement for detailed periodic submissions from each nation describing the oversight procedures

K. LAMBERT/AP PHOTO

Federal expenditure for civilian biodefence during the Bush years totalled more than $50 billion.

it employs to ensure compliance with the convention. The objective would be to increase awareness of the need for improved oversight and to facilitate the development of international measures for enhanced exchange and transparency regarding implementation of the convention.

1. Franco, C. *Biosecur. Bioterror.* **6,** 131–146 (2008).
2. *Roles and Responsibilities Associated with the Chemical and Biological Defense (CBD) Program (CBDP)*, Department of Defense Directive 5160.05E (2008). Available at: www.dtic.mil/whs/directives/corres/pdf/516005p.pdf

Contaminated heparin led to many adverse events in 2008.

Steven E. Nissen
Chairman of the department of cardiovascular medicine, Cleveland Clinic, Ohio, USA.

An end to secrecy will revive the Food and Drug Administration.

After an unprecedented series of revelations about drug and device safety issues, many observers consider the Food and Drug Administration (FDA) a failed agency. The Obama administration has the opportunity to reinvigorate the FDA, but only through major restructuring and policy changes that are designed to protect the agency from undue influence, and to promote transparency.

The next FDA commissioner should serve a fixed six-year term to insulate the agency from political influence. Moreover, the system by which pharmaceutical companies fund a major portion of the FDA's budget through user fees requires re-evaluation.

Secrecy is antithetical to both science and good government, but much of what the FDA knows about drugs, it never publicly discloses. The agency must cease to regard clinical-trial data as proprietary and provide access to all available information on safety and efficacy. This policy should apply to information gathered during approval for drugs, and to post-approval surveillance. The agency needs better harmonization between its Office of Surveillance and Epidemiology, which monitors post-marketing safety, and its Office of New Drugs, which is responsible for post-marketing regulatory decisions.

The current voluntary mechanism for adverse-event reporting is relatively ineffective, because only 1%–10% of events are actually reported. Partnerships with large health-care providers, such as health maintenance organizations that supply care through hospitals, doctors and other providers, are needed to prospectively assess drug safety.

The approaches used to approve drugs need attention. Drug approvals are often based on placebo-controlled clinical trials. However, appropriate use of therapies requires understanding comparative effectiveness. The FDA has increasingly used 'non-inferiority' study designs to support efficacy. In these, a treatment is considered 'approvable' if it retains 50% or more of the effectiveness of a comparable product, which may represent too lenient a standard. The agency has also increasingly used 'surrogate endpoints' (biomarkers or laboratory measures) to support approvals without subsequently requiring more informative clinical-outcome studies.

For medical devices, the agency has authority to clear a product for market if it is deemed 'substantially equivalent' to devices already being sold. This rule has become the principal approach used to approve medical devices. However, even small changes to a device can affect safety, which has resulted in major safety recalls, such as for defective pacemaker leads.

Stronger enforcement capabilities are required throughout the agency. The Division of Drug Marketing, Advertising, and Communications needs the right to restrict direct-to-consumer advertising during the first two years a drug is marketed and to preview advertising to ensure it is not misleading. An FDA policy introduced in 2008 unwisely allows off-label promotion of drugs and devices through distribution of article reprints, an approach that may encourage unsafe use for unapproved indications and discourage appropriate clinical trials to establish new indications.

Currently, about 1,600 facilities in China manufacture drugs or components of drugs marketed in the United States. Recent high-profile cases — such as contaminated heparin — poignantly illustrate the risks inherent in globalization. The FDA must increase inspections and foreign governments must be held accountable for setting regulatory and safety standards for local manufacturing. All of these initiatives require more robust funding of the FDA, which currently has a budget of $2.3 billion with which the Agency must regulate $1 trillion worth of food, drugs, cosmetics and medical devices. The agency's budget is quarter that of the Centers for Disease Control and Prevention, which has a significantly more limited mission. Congress must re-evaluate priorities and recognize that ensuring the safety of food and drugs is a crucial national priority.

NEWSCOM

Calestous Juma
Director of the Science, Technology, and Globalization Project, Harvard Kennedy School, Cambridge, Massachusetts, USA.

A smart focus on infrastructure at home means more winners globally.

In the current economic climate, you might think that prospects for US science and technology cooperation with developing countries look grim. An immediate consequence of the recession is that there will be fewer consumers in richer countries for technology exports from the developing world. At the same time, an Obama administration, poised to make historic investments in US jobs and infrastructure, may decide that funding international scientific cooperation is less of a priority as it focuses on fixing problems at home.

Such a view, although understandable, couldn't be more wrong. Far from shutting out the rest of the world, we are about to witness perhaps the most audacious example of the collective insights from world science being applied to policy-making since the US administrations of the early 1960s. Moreover, large-scale investment in infrastructure projects such as transport systems and public housing in the United States is poised to benefit science — and infrastructure — in developing nations.

How? Part of the answer lies in President-elect Barack Obama's choice of science advisers. In choosing John Holdren from the Harvard Kennedy School, as well as the biologists Jane Lubchenco, Harold Varmus and Eric Lander, the president has chosen a quartet of advisers who will think globally and act both globally and locally — perhaps more so than any of their predecessors. The choices indicate that taking action to reduce the rate of biodiversity loss, to tackle climate change and to ensure that the poorest receive the best health care are regarded by the new administration as the right things to do. For each of these advisers and for their wider teams, the national interest and the international interest

will now overlap to a considerable degree.

Such overlapping priorities apply equally to another area of public policy that the Obama team will make their own. In the next few years, US industry and policy-makers will immerse themselves in a task that is usually associated with developing countries: nation-building. The predominant images in the United States for the next few years will be those of men and women in hard-hats upgrading roads, rail networks, schools, hospitals, postal systems, power plants and more.

Some regions of the United States have infrastructure challenges that are similar to those of developing countries. The lessons learned from these regions will offer additional opportunities for global learning. Development needs more than money, it needs skilled and experienced people. Right now, this is what so much international development lacks. Indeed, one reason why genetically modified crops have been slow to take off in Africa is because research and development in richer nations (especially in Europe) isn't happening. All in all, America is set to become a more credible international development partner in the eyes of many poorer countries.

International development for the United States will become an extension of local development — just as it is for China's current efforts in Africa, and just as it was during the birth of the Green Revolution in agriculture, when US scientists took a lead in developing technologies for high-yielding crop varieties and these invariably spread to help the rest of the world.

Domestic economic policy and the aspirations of developing countries will converge over the next few years. The Obama administration — and the many development cooperation institutions in the United States — cannot afford to miss out on this historic opportunity to do the right thing.

J. SCHYTTE/STILL PICTURES

Nation building could become an important US export.

George Daley
Associate Professor, Children's Hospital Boston, Massachusetts, USA.

Put the NIH in charge of stem-cell guidance and oversight.

The Obama administration has given every indication that it will swiftly eliminate restrictions on federal funding for research on human embryonic stem cells. This could potentially allow labs to study the nearly 1,000 cell lines that have been derived since August 2001, the arbitrary cut-off date chosen by president George W. Bush's administration. Newer cell lines have important properties that make them valuable for medical research. For example, lines generated from preimplantation genetic diagnosis can be used to model human diseases such as fragile X syndrome, neurofibromatosis and various forms of bone-marrow failure.

Still, significant challenges remain in harmonizing stem-cell research and reasserting the United States's role as a leading force in this field. Under the Bush policy, a number of US states have stepped in to fund embryonic stem-cell research — California, most prominently, but also states including New Jersey, New York, Wisconsin, Connecticut, Illinois, Maryland and, most recently, Massachusetts. That has created a Balkanized set of principles for regulation and protocol, and has obfuscated financial administration in laboratories that must keep these funding streams separate. Moreover, ethical guidelines for deriving and maintaining human stem-cell lines have taken a parochial turn, with subtle but sometimes meaningful discrepancies that could complicate future collaboration across state and international boundaries.

The situation reflects the fact that the National Institutes of Health (NIH) — which should have been the main arbiter in charge of oversight of stem-cell research in the United States — has largely been sidelined during some of the most dramatic and game-changing discoveries and debates of the past eight years.

The best policy outcome would be to return the NIH to its rightful role as arbiter of stem-cell research in the United States, making funding decisions based on scientific merit rather than ideology, and ensuring uniform standards of ethical oversight, most readily by endorsing the Guidelines from the National Academy of Science and the International Society for Stem Cell Research. Because so many countries look to the leadership of the NIH to set principles for how they operate within their own borders, this would have an enormous impact on policies worldwide.

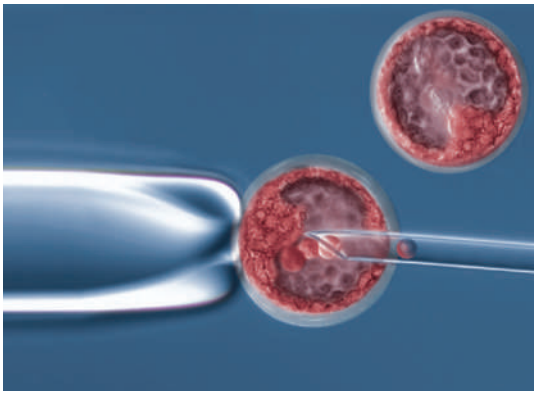

Work with human embryos will remain restricted.

ILLUSTRATION: FOTOFINDER/MEDICALPICTURE

A second issue looms on the horizon. The Dickey amendment, which has been a rider on the Department of Health and Human Services appropriations bill since 1995, precludes using federal money for the creation or destruction of human embryos for research purposes. So although hundreds of cell lines could be approved for federally funded research projects, subject to NIH approval, the amendment bars funding for research such as somatic cell nuclear transfer or work on embryos discarded from *in vitro* fertilization procedures to derive new cell lines.

In my opinion, this legislative barrier represents a blockade to essential forms of embryo research that could aid health care for birth defects, women's infertility and some cancers. The political reality may dictate that the few labs doing this (mine included) will have to continue to rely on state or private funding in the near term for this work. But the new Obama administration would be well advised to commission a comprehensive and thoughtful analysis of the scientific, medical and ethical issues pertinent to human-embryo research, and to act on the recommendations in the best interest of society as a whole.

Beyond the stem-cell issue, there is a pressing need for increased funding for all areas of biomedical research, given the inadequate NIH budgets of the past few years. It would be a Pyrrhic victory to win expanded federal funding of embryonic stem-cell research without seeing a greater overall investment in the NIH. Even in the current financial crisis, funding for biomedical research is a smart investment that is certain to yield handsome returns. ■

See Editorial, page 235, and visit http://tinyurl.com/7ct8h7 to respond to these Commentaries.

ESSAY

Fifty years of pheromones

Powerful chemical signals have been identified in moths, elephants and fish, recounts **Tristram D. Wyatt**. But, contrary to stories in the popular press, the race is still on to capture human scents.

Fifty years ago this month, Peter Karlson and Martin Lüscher proposed a new word for the chemicals used to communicate between individuals of the same species: pheromones[1]. Since then, pheromones have been found across the animal kingdom, sending messages between courting lobsters, alarmed aphids, suckling rabbit pups, mound-building termites and trail-following ants. They are also used by algae, yeast, ciliates and bacteria.

The new word met a pressing need. Karlson had discussed it with his colleague Adolf Butenandt, who was about to publish the first chemical identification of a pheromone — bombykol, the sex pheromone of the silk moth *Bombyx mori*. The bombykol paper showed the equivalent of Koch's postulates for establishing causal relationships for pheromones: isolation, identification, synthesis and bioassay confirmation of activity[2]. Butenandt's work established that chemical signals between animals exist and can be identified, marking the start of modern pheromone research. Popular speculation about human pheromones, still going strong today, began too.

The idea of chemical communication was not new in 1959. The ancient Greeks knew that the secretions of a female dog in heat attracted males. Charles Butler had warned in *The Feminine Monarchie* (1609) that if you are stung by one honeybee, "other Bees smelling the ranke favour of the poison cast out with the sting will come about you as thick as haile". In *The Descent of Man, and Selection in Relation to Sex* (1871), Charles Darwin included chemical signals alongside visual and auditory ones as outcomes of sexual selection, describing the success of the smelliest among breeding male crocodiles, ducks, goats and elephants. Jean-Henri Fabre, also in the 1870s, described how male emperor moths flocked around a female moth hidden behind wire-gauze, but ignored visible females sealed under glass. Surely her smell was the attraction.

In 1932, the physiologist Albrecht Bethe had proposed the broad term 'ectohormone' to cover many kinds of chemical interaction, including communication or attraction of an animal to a food smell. Karlson and Lüscher wanted a term that more narrowly covered communication between members of the same species, but more broadly allowed for those chemicals to be created by a variety of organs ('hormones' by definition come from the endocrine glands). Their new term, from the Greek *pherein* for 'to transfer', and *hormōn* 'to excite', at a stroke replaced ectohormone. 'Pheromone' was sonorous, and close enough to 'hormone' to imply some similarities along with the differences: like hormones, pheromones could be expected to be specific, and active in minute amounts. They defined pheromones as: "substances which are secreted to the outside by an individual and received by a second individual of the same species, in which they release a specific reaction, for example, a definite behaviour or a developmental process." The new word and definition stuck.

Feast for the senses

Karlson and Lüscher were far-sighted, noting that pheromones were likely to be used by a wide range of animals, including fish and underwater crustaceans as well as land mammals and insects. They predicted that most pheromones would act via the conventional senses of smell or taste, but that some might be ingested and act directly on the brain or other organs — as happens in termites, whose pheromones affecting caste development are passed round by mouth through the colony.

All these anticipations have been borne out, although Karlson and Lüscher might have been amazed at the range of molecules identified as pheromones since 1959, including everything from low-molecular-weight formic acid to polypeptides. We now know that many pheromones (including the sex pheromones of most moths) are not single compounds, but rather a species-specific combination of molecules in a precise ratio.

> "Controversy over mammalian pheromones has been almost as heated as the 'stink wars' between opposing troops of ring-tailed lemurs."

The ubiquity and variety of pheromones can be explained by natural selection. The evolutionary development of sex pheromones in a fish, for example, might have started with male fish detecting sex hormones leaking from a female about to spawn. The most sensitive males would get there first. Over generations, there would be selection for increased sensitivity of the receiver and increased production of the signal by the sender.

Chemical communication can also be exploited by other species. For example, some orchids, which benefit from attracting pollinators, produce a mixture of compounds that mimics female-wasp pheromones. The mimicry is so good that duped males will ejaculate on the flowers.

Karlson also catalysed a completely new field of study in biology, by asking a young biologist neighbour, Dietrich Schneider, if he could invent an electrophysiological way to assess Butenandt's silk-moth extracts for activity. Schneider's solution was the electroantennogram, still used today: wires inserted into both ends of a moth antenna are used to measure electrical signals as different extracts are presented. Recordings of activity in single antennal sensory cells followed in later years, as moths and their pheromones became a key model system in neurobiology.

The pursuit of pheromone science has not been entirely sweet and easy. The concept has faced key periods of controversy over mammalian pheromones, in battles almost as heated as the 'stink wars' between opposing troops of ring-tailed lemurs, which wave their pheromone-coated tails to assert their dominance.

In the 1970s, a group of researchers studying mammals argued that the term 'pheromones' should not be used for mammalian chemical signals, citing in particular the complex, highly variable odours that mammals use to distinguish littermate from stranger, for example for altruism or mate choice. These individual odours, including some related to the immune system, need to be learnt for recognition, and did not seem to fit Karlson and Lüscher's definition. Some researchers even doubted that complex mammals, including humans, could have their behaviour altered by something as simple as an instinctive reaction to a smell.

Debate continues among those in the field. I now agree that these variable odours are not pheromones, and instead are better termed 'signature odours' (the same holds for complex variable odours in social insects such as ants and bees, which also have to be learnt and are used for colony recognition). But species-specific small molecules that do fit the classic pheromone definition have now been identified for mammals. Most spectacular was the 1996 discovery that the female Asian elephant's sex pheromone is a small molecule — (*Z*)-7-dodecen-1-yl acetate — also used by some

K. CHEUNG

140 species of moth as a component of their female sex pheromones. Signature odours and pheromones can be mixed. Some mammals, including elephants and mice, present their small-molecule pheromones in the cleft of highly variable urinary (or other lipocalin) proteins. As well as overlaying the anonymous pheromone signals with individual signature odours, the proteins release the small molecules slowly, making them last longer.

Person-to-person

A second group of researchers — mainly molecular biologists — accepted the idea that mammals have pheromones, but proposed that these are exclusively detected by a specialized sensory system, the vomeronasal organ (VNO), rather than the main olfactory epithelium in the nose. This view perhaps arose because some pheromones in mice do act via the VNO, and the mouse is a widely used model. As humans do not have a VNO, this theory would exclude them from sensing and responding to pheromone signals.

This argument persisted despite extensive evidence from behavioural studies and neurobiologists that information from the VNO and the main olfactory system was integrated in the rodent brain, and that some mammal pheromones, such as the rabbit mammary pheromone, acted via the nose. Finally, in 2005, a series of molecular studies in mice, using combinations of genetic markers and knockouts, confirmed that pheromones can stimulate both systems, which are integrated in the brain. So humans wouldn't need a VNO to receive pheromone signals after all.

The identification and synthesis of pheromones have been put to good use, giving the greenest way to control pests ranging from moths in cotton fields to lampreys in the Great Lakes of North America. Pheromones can be used to lure pests into a death trap or confuse males so that they never find a female; pheromones' high specificity and low toxicity leave ecosystems intact.

> **"A compound in women's armpit extract could potentially open the door to sniffable contraceptives."**

Advances in analytical techniques have enabled progress. Butenandt's team needed 500,000 female silk moths to produce 12 milligrams of material for the first pheromone identification. Today, one moth might do. New tools will power new discoveries. For example, we can now follow the chemical signals emitted by fighting wasps, in real time. Microarray genomics shows genes switching on and off in the honeybee brain in response to pheromones. But challenges remain. Correct synthesis of pheromone molecules is harder than their identification. We can record and play back the audible calls of an animal easily enough, but we don't have a video or MP3 equivalent for recreating chemical signals.

What about humans? As we're mammals, we are likely to use pheromones. Our armpits are prime candidates as sources, as their smells develop along with other changes at puberty. However, both human behaviour and our chemical emissions are so complex that the research is challenging: so far, no pheromones have been conclusively identified, despite stories in the popular press. A strong contender for the first real human pheromone is some compound in women's armpit extract that apparently causes menstrual synchrony in females living in close quarters. Its identification is keenly awaited, not least as it could potentially open the door to sniffable contraceptives. There may never be a magic potion to make us irresistible, but I'm sure human pheromones will surprise us yet. ■

Tristram D. Wyatt is in the Department of Zoology of the University of Oxford, UK, and is the author of *Pheromones and Animal Behaviour*.
e-mail: tristram.wyatt@zoo.ox.ac.uk

1. Karlson, P. & Lüscher, M. *Nature* **183,** 55–56 (1959).
2. Butenandt, A., Beckmann, R., Stamm, D. & Hecker, E. *Z. Naturforsch. B* **14,** 283–284 (1959).

See http://tinyurl.com/9bll5d for further reading.

BOOKS & ARTS

How to end the copyright wars

A high-profile copyright activist is fighting for traditional publishers to stop criminalizing their own readers, explains **Jonathan Zittrain**.

Remix: Making Art and Commerce Thrive in the Hybrid Economy
by Lawrence Lessig
Penguin: 2008. 352 pp. £25.95

LIBRARY OF CONGRESS; P. M. MONSIVAIS/AP PHOTO

Media moguls such as Mitch Bainwol, Jack Valenti and LL Cool J (left to right) fight today's copying culture — seen as flattery in maestro John P. Sousa's time (inset).

By its own account, the Recording Industry Association of America (RIAA) has threatened thousands of people — many of them teenagers — with lawsuits for sharing copies of copyrighted music without permission. Most individuals pay several thousand dollars to settle out of court. In the only such case to go to trial in the United States, the jury awarded the RIAA $222,000 in a verdict against a woman from Duluth, Minnesota, who shared 24 songs that had a retail value of $23.76. Massachusetts youth Joel Tenenbaum has also refused to settle, and his trial will soon begin — more than $1 million is at stake for allegations that he shared seven songs.

In *Remix*, Lawrence Lessig says 'enough' to this situation, arguing for a hybrid approach that differentiates private and commercial use. His book is an important and urgent work of radical moderation. It seeks to get both sides to stand down and respect one another, using arguments couched in terms of each party's values. Lessig wants to persuade traditional publishers — the purveyors of 'read-only' culture — that they should not fear their own fans. Publishers stand to make more money by embracing those who make new works from old standards than they do by criminalizing them. More subtly, Lessig argues that a strict divide between the world of sharing and the world of commerce is counterproductive. He wants to refocus attention away from the stalemated copyright wars and towards a more vibrant 'read–write culture' that remixes rather than replaces what came before. The future lies with hybrid enterprises that wisely blend the mercenary 'me' and the charitable 'thee'.

Lessig points out that the act of writing is near-universal. We teach our children how to write at an early age, and the tools to do so have long been accessible. With so much writing going on, there is bound to be appropriation of others' work, but its universal character has meant that no one minds, as long as it is attributed. The accessibility of new tools of digital literacy — and with them the ability to remix audiovisual works — is a much more recent phenomenon. Here, Lessig says, our instincts are too often wrongly grounded in the elaborate rules of copyright and licensing practices that date from an era when only big publishers could effectively edit such works. Lessig claims that the new is actually the old: before the rise of mass media, people naturally reworked audiovisual works as they sang the songs or performed the plays of the day. Even the most orthodox copyright proponents did not object. Some, such as composer John P. Sousa, thought this remixing crucial, lest the new "infernal machines" of mass media led to a world only of "the mechanical device and the professional executants". The loss of amateur 'yeoman creators', says Lessig, cheapens and flattens our culture, and worse, alienates us from our kids.

Lessig's ingenious framing makes the late-twentieth-century dominance of read-only culture the outlier, a rut caused by historical accident. It was a particular combination of technological development and some unintended language — the word 'copies' — by the drafters of the US Copyright Act of 1909 that vastly expanded the scope of regulation. Free markets and democracy are the respective private- and public-sector innovations that ensure the past does not unduly dominate the future. Lessig fears that if read–write culture is marginalized by the law, this will detrimentally reinforce the status quo; the tenet of 'what is now, ought to be' is one of Lessig's main enemies, as in nearly all of his works. He is desperate for us to reflect on what counts as normal, and what counts as depraved, in a zone too often defined and dominated by soulless lawyers.

The sharing economy that has thrived alongside the Internet greatly intrigues Lessig. Although he concedes that no one has yet fully understood its magic, he is concerned that too much purism can kill it. Here, one can find a quiet remonstrance that content and code are different creatures, and thus some of the types of licence that sharing-oriented people might choose for free software might not be suited to content that is shared. Lessig is the founder of Creative Commons, a non-profit organization that provides creators with flexible copyright licences. In *Remix*, he outlines the case for licences that make one's work free for non-commercial use but reserve any right

to commercial exploitation to the author — something that is traditionally anathema to the free-software movement.

Lessig approves of sharing activities that fall beneath a corporate umbrella, as long as they are in touch with their volunteer communities, and he sketches what can make them work. In one quietly controversial paragraph, he advocates that the current allocation of copyright infringement liability in these situations should be reversed. For example, YouTube ought to answer more for the copyright infringement of its users because it profits from such transgressions, whereas the infringing users should be protected because their activities amount to non-commercial sharing.

Successful hybrid enterprises abound. Yahoo! Answers is a web-based service to which people post questions and others answer them for payment in the form of non-monetary points. Interestingly, the similar service Google Answers sought to pay contributors outright, and it folded. One wonders what would have happened in the late 1990s if Microsoft's Encarta encyclopaedia had started paying for corrections and improvements from the world at large — would users of the nascent Wikipedia have felt they were doing for free what otherwise ought to be charged? Other hybrid phenomena — such as the classified-advertising network Craigslist, wiki-hosting service Wikia and even Google itself — will soon find themselves competing not only with pure community enterprises such as Wikipedia, but also with a new set of mercenary but distributed services. These include InnoCentive, which awards bounties to those who can solve particular problems, usually in exchange for transferring all rights to the solutions to those paying for them; Amazon's Mechanical Turk, a marketplace for people to do mind-numbing work that still only a human can do; and LiveOps, a 'virtual call centre' that creates communities of independent contractors, each in their own homes, who might take pizza orders one moment and staff a hotline for hurricane survivors the next.

Ultimately, Lessig seeks to shed his copyright-fighter's reputation, acquired in part through his challenge — for which I was a co-counsel — to the Sonny Bono Copyright Term Extension Act in the United States. The case was lost in 2003 at the US Supreme Court by a majority of 7–2. Lessig's goal is not to overthrow the current system so much as to temper its shortsighted excesses and to give a little something to everyone. *Remix* is dedicated both to L. Ray Patterson, a copyright historian who would no doubt have agreed with Lessig's prescriptions for copyright reform, and to Jack Valenti, the late president of the Motion Picture Association of America. Lessig and Valenti debated several times, and agreed on nothing except the observation that our children's values are out of touch with read-only culture and the law that tilts so far in its favour. Lessig hopes to appeal to the Sousa within Valenti's successor and partners, yet as the founder of modern cyberlaw, he has a more ambitious agenda: dealing with what he sees as a more general corruption of the democratic political system originally intended to save us from our economic, legal and cultural ruts. Perhaps Lessig's smaller battle is being won: in late December it was reported that the RIAA was abandoning new lawsuits against individual file sharers. But Joel Tenenbaum's trial continues. ■

Jonathan Zittrain is professor of law at Harvard Law School, Cambridge, Massachusetts 02138, USA. He is a founder of Harvard's Berkman Center for Internet and Society and author of *The Future of the Internet — And How to Stop It.*
e-mail: zittrain@law.harvard.edu

Fusion history beyond the fiascos

Sun in a Bottle: The Strange History of Fusion and the Science of Wishful Thinking
by Charles Seife
Viking: 2008. 304 pp. $25.95

It is 50 years since the first international symposium on fusion energy research took place in Geneva, Switzerland, as part of the second United Nations 'Atoms for Peace' conference. There, the United Kingdom, the Soviet Union and the United States announced the declassification of controlled fusion research, raising the hope of clean and limitless energy for mankind.

In his new history of fusion research, journalist Charles Seife argues that such grand hopes push researchers to make unjustified claims of major advances. But in pursuing the controversies generated by a few isolated individuals, *Sun in a Bottle* neglects the more important story of the wider fusion community.

At the first Atoms for Peace conference in 1955, its chairman Homi Bhabha said: "I venture to predict that a method will be found for liberating fusion energy in a controlled manner within the next two decades." But the proceedings of the second conference in 1958 remind us that the scientific leaders of the main delegations were much less optimistic. Edward Teller from the United States said that the state of controlled fusion was "similar to the stage at which flying was about 100 years ago", and that the technical difficulties of fusion "are likely to make the released energy so costly that an economic exploitation of controlled thermonuclear reactions may not turn out to be possible before the end of the twentieth century". Similarly, reviewing work in the Soviet Union, Lev Artsimovich stressed that "worldwide collaboration is needed for progress".

"Fusion scientists have not lived quiet lives."

Soon after, a network of collaborations under the auspices of the International Atomic Energy Agency, the International Energy Agency and Euratom (the European atomic-energy community) was established in the domain of magnetic fusion. Results were openly shared and, two decades later, a major European facility, the Joint European Torus (JET), was constructed at Culham, UK. Scientific progress since then has been impressive — the foundations of a new 'plasma science' have been established. We now have a fundamental understanding of the complex collective processes prevailing in the hot, electrically charged gases known as plasmas, and have made significant technological advances in magnets, materials and high-power electrical systems. Consequently, fusion machines have improved greatly in their performance, both in fusion power and plasma duration. The US Tokamak Fusion Test Reactor (TFTR) and its European competitor JET, both of which use deuterium and tritium fuels, demonstrated power exceeding 10 megawatts, but only for short periods set by the limits of the auxiliary systems, notably the magnets. Other, smaller tokamaks and stellarator devices use superconducting magnets to confine the plasma and can be operated stably for much longer periods — 5 hours in the case of the Japanese tokamak TRIAM 1-M. Plasma science also provides industrial spin-offs. Plasmas are now common in low-consumption light bulbs, television screens and, through plasma processing, in nearly all electronic equipment.

Although JET and the TFTR have produced large amounts of power, these were less than the power consumed to heat the plasmas initially. A larger experiment, ITER — meaning 'the way' in Latin — was therefore designed with the aim of having a fusion power output that is ten times greater than the input power. ITER was originally designed by scientists

to commercial exploitation to the author — something that is traditionally anathema to the free-software movement.

Lessig approves of sharing activities that fall beneath a corporate umbrella, as long as they are in touch with their volunteer communities, and he sketches what can make them work. In one quietly controversial paragraph, he advocates that the current allocation of copyright infringement liability in these situations should be reversed. For example, YouTube ought to answer more for the copyright infringement of its users because it profits from such transgressions, whereas the infringing users should be protected because their activities amount to non-commercial sharing.

Successful hybrid enterprises abound. Yahoo! Answers is a web-based service to which people post questions and others answer them for payment in the form of non-monetary points. Interestingly, the similar service Google Answers sought to pay contributors outright, and it folded. One wonders what would have happened in the late 1990s if Microsoft's Encarta encyclopaedia had started paying for corrections and improvements from the world at large — would users of the nascent Wikipedia have felt they were doing for free what otherwise ought to be charged? Other hybrid phenomena — such as the classified-advertising network Craigslist, wiki-hosting service Wikia and even Google itself — will soon find themselves competing not only with pure community enterprises such as Wikipedia, but also with a new set of mercenary but distributed services. These include InnoCentive, which awards bounties to those who can solve particular problems, usually in exchange for transferring all rights to the solutions to those paying for them; Amazon's Mechanical Turk, a marketplace for people to do mind-numbing work that still only a human can do; and LiveOps, a 'virtual call centre' that creates communities of independent contractors, each in their own homes, who might take pizza orders one moment and staff a hotline for hurricane survivors the next.

Ultimately, Lessig seeks to shed his copyright-fighter's reputation, acquired in part through his challenge — for which I was a co-counsel — to the Sonny Bono Copyright Term Extension Act in the United States. The case was lost in 2003 at the US Supreme Court by a majority of 7–2. Lessig's goal is not to overthrow the current system so much as to temper its shortsighted excesses and to give a little something to everyone. *Remix* is dedicated both to L. Ray Patterson, a copyright historian who would no doubt have agreed with Lessig's prescriptions for copyright reform, and to Jack Valenti, the late president of the Motion Picture Association of America. Lessig and Valenti debated several times, and agreed on nothing except the observation that our children's values are out of touch with read-only culture and the law that tilts so far in its favour. Lessig hopes to appeal to the Sousa within Valenti's successor and partners, yet as the founder of modern cyberlaw, he has a more ambitious agenda: dealing with what he sees as a more general corruption of the democratic political system originally intended to save us from our economic, legal and cultural ruts. Perhaps Lessig's smaller battle is being won: in late December it was reported that the RIAA was abandoning new lawsuits against individual file sharers. But Joel Tenenbaum's trial continues. ■

Jonathan Zittrain is professor of law at Harvard Law School, Cambridge, Massachusetts 02138, USA. He is a founder of Harvard's Berkman Center for Internet and Society and author of *The Future of the Internet — And How to Stop It.*
e-mail: zittrain@law.harvard.edu

Fusion history beyond the fiascos

Sun in a Bottle: The Strange History of Fusion and the Science of Wishful Thinking
by Charles Seife
Viking: 2008. 304 pp. $25.95

It is 50 years since the first international symposium on fusion energy research took place in Geneva, Switzerland, as part of the second United Nations 'Atoms for Peace' conference. There, the United Kingdom, the Soviet Union and the United States announced the declassification of controlled fusion research, raising the hope of clean and limitless energy for mankind.

In his new history of fusion research, journalist Charles Seife argues that such grand hopes push researchers to make unjustified claims of major advances. But in pursuing the controversies generated by a few isolated individuals, *Sun in a Bottle* neglects the more important story of the wider fusion community.

At the first Atoms for Peace conference in 1955, its chairman Homi Bhabha said: "I venture to predict that a method will be found for liberating fusion energy in a controlled manner within the next two decades." But the proceedings of the second conference in 1958 remind us that the scientific leaders of the main delegations were much less optimistic. Edward Teller from the United States said that the state of controlled fusion was "similar to the stage at which flying was about 100 years ago", and that the technical difficulties of fusion "are likely to make the released energy so costly that an economic exploitation of controlled thermonuclear reactions may not turn out to be possible before the end of the twentieth century". Similarly, reviewing work in the Soviet Union, Lev Artsimovich stressed that "worldwide collaboration is needed for progress".

"Fusion scientists have not lived quiet lives."

Soon after, a network of collaborations under the auspices of the International Atomic Energy Agency, the International Energy Agency and Euratom (the European atomic-energy community) was established in the domain of magnetic fusion. Results were openly shared and, two decades later, a major European facility, the Joint European Torus (JET), was constructed at Culham, UK. Scientific progress since then has been impressive — the foundations of a new 'plasma science' have been established. We now have a fundamental understanding of the complex collective processes prevailing in the hot, electrically charged gases known as plasmas, and have made significant technological advances in magnets, materials and high-power electrical systems. Consequently, fusion machines have improved greatly in their performance, both in fusion power and plasma duration. The US Tokamak Fusion Test Reactor (TFTR) and its European competitor JET, both of which use deuterium and tritium fuels, demonstrated power exceeding 10 megawatts, but only for short periods set by the limits of the auxiliary systems, notably the magnets. Other, smaller tokamaks and stellarator devices use superconducting magnets to confine the plasma and can be operated stably for much longer periods — 5 hours in the case of the Japanese tokamak TRIAM 1-M. Plasma science also provides industrial spin-offs. Plasmas are now common in low-consumption light bulbs, television screens and, through plasma processing, in nearly all electronic equipment.

Although JET and the TFTR have produced large amounts of power, these were less than the power consumed to heat the plasmas initially. A larger experiment, ITER — meaning 'the way' in Latin — was therefore designed with the aim of having a fusion power output that is ten times greater than the input power. ITER was originally designed by scientists

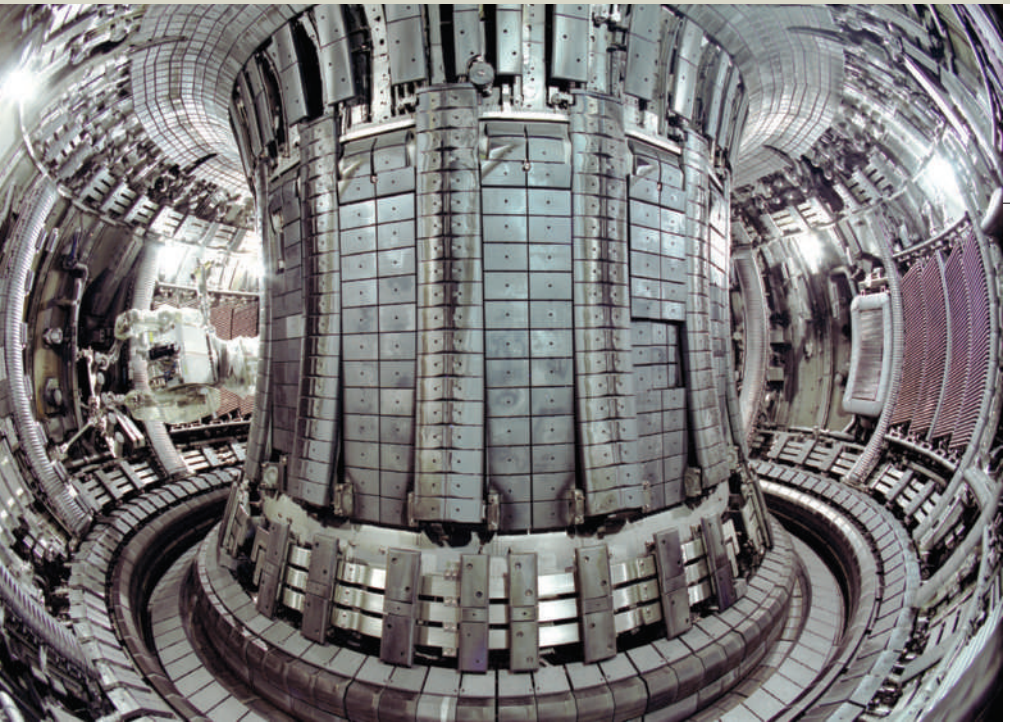

Fusion force: inside the tokamak used to confine plasma at the Joint European Torus, Culham, UK.

EFDA JET

from Europe, Japan, Russia and the United States. Its dimensions were defined by scaling laws derived from data collected worldwide. In 2004 and 2005, these four partners were joined by China, South Korea and India. Soon after, the seven partners agreed to construct ITER at Cadarache in the south of France. The ITER international organization, which was established by treaty in 2006, is a collaboration of unprecedented scale. Its seven partners represent more than half of the world's population. The annual budget for ITER construction is about €0.5 billion (US$0.7 billion). This may seem high, but it is a tiny investment compared with the annual worldwide cost of electricity, which stands at around €2 trillion based on the average cost per kilowatt hour in 2007 in the European Union.

The fiftieth anniversary of international fusion research was marked in October 2008 with many lectures on the history of fusion (see http://fire.pppl.gov), which showed that fusion scientists have not lived quiet lives during this time. Teller and Artsimovich were right — the physics and technology of fusion are challenging, but the fusion community can be proud of its progress.

Yet this community will not recognize its own history in Seife's book. As admitted in the title, it is a rather strange history. After relating at length the early years of fusion research, it concentrates disproportionately on two table-top fusion fiascos — cold fusion and bubble fusion — generated by isolated individuals.

The book leads without proof to the dubious conclusion that "Over and over again, desperate scientists have deceived themselves and their peers — and cheated — in hopes to keep their fusion quest alive". Yet it focuses on outsiders to the field, who thought they had made a major discovery and who, after having been proven wrong when their results could not be repeated by others, did not have the courage to admit their errors. Thankfully, the book does not identify any scandal within magnetic fusion research, the main line for fusion energy. But as a result, it pays too little attention to this large international community. Whereas the dream of limitless energy may afflict isolated scientists, it is certainly not applicable to all fusion researchers as the author suggests.

The book identifies correctly that peer review is a necessary prerequisite for preventing fiascos. Scientists who call on journalists to make announcements without having had the traditional discussions with colleagues followed by publication in a peer-reviewed journal are in danger of damaging their reputation. Yet peer review may not always be sufficient. In addition to internal reviewing, in the late 1980s JET set up an internal database on which its experimental data were made available. Researchers within the organization can easily cross-check a scientific claim made by their colleagues. An open, international, multidevice database followed in the early 1990s, which has proven to be a sound basis for progress in fusion research. Such a system protects scientists from the insidious distortion of reality that can be provoked when they remain too isolated. Maybe Seife himself is a victim of 'wishful thinking' and should have sought peer review before publishing such a strange thesis. ■

Jean Jacquinot is scientific adviser to the French High Commissioner for Atomic Energy at the Commissariat a l'Energie Atomique (CEA), 91191 Gif-sur-Yvette, France, and the former director of both JET and the CEA magnetic fusion research group.
e-mail: jean.jacquinot@cea.fr

Our culture of obsession

Obsession: A History
by Lennard J. Davis
University of Chicago Press: 2008. 296 pp. $27.50, £16

A battle for the public good has been waged for centuries between qualified doctors of medicine with formal training and their 'quack' counterparts. As scientific analysis has come to be accepted, we have demanded more evidence from our physicians. Despite a lingering love-affair with alternative medicines such as homeopathy, patient-consumers today expect more than snake oil and bedside charm. Into this market lands Lennard Davis's latest book, *Obsession*.

The stereotypical view of a scientist, which rings true of many, is of an obsessive individual working long hours, worrying about minutiae and trying to replicate experiments against an approaching deadline. Davis looks at this form of obsession and others. He discusses the mania of novel writing in the nineteenth century, when prolific authors such as Émile Zola would write for days and nights at a time. The obsessive Zola became a subject of obsessive study by his contemporaries, and Davis guides us through the sociocultural evolution of the disease now known as obsessive–compulsive disorder. There are fascinating examples throughout the book, not least in his discussion of obsessive love and sex.

Davis tries to untangle the central question of what constitutes obsession. If I check my car doors are locked a couple of times before I leave it parked each morning, am I being obsessive? What about washing my hands repeatedly? Where is the line between obsession as a harmless fact of life, and when it becomes a mental illness? It is far from normal to wash one's hands so often one develops skin diseases, or to be unable to leave the house because of fears one has left the doors unlocked.

Obsession provides an insightful and nuanced review of the history of this tragic illness by exposing obsessive behaviour and contrasting it with the common, mildly obsessive behaviours we all engage in. The question of difference, and thus definition, is a recurring

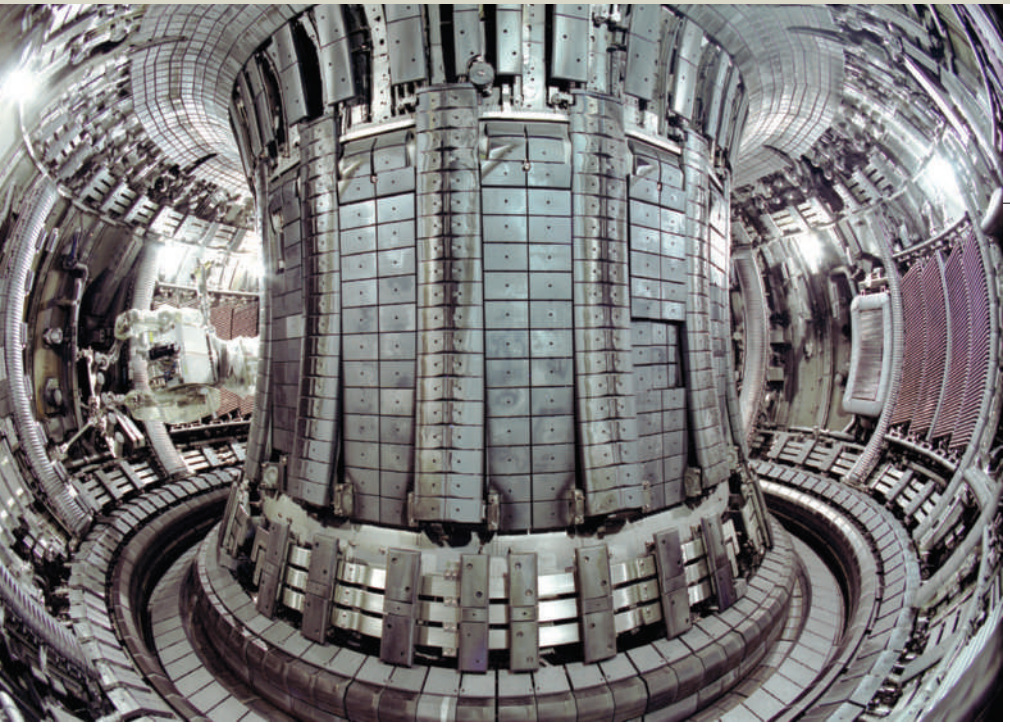

Fusion force: inside the tokamak used to confine plasma at the Joint European Torus, Culham, UK.

EFDA JET

from Europe, Japan, Russia and the United States. Its dimensions were defined by scaling laws derived from data collected worldwide. In 2004 and 2005, these four partners were joined by China, South Korea and India. Soon after, the seven partners agreed to construct ITER at Cadarache in the south of France. The ITER international organization, which was established by treaty in 2006, is a collaboration of unprecedented scale. Its seven partners represent more than half of the world's population. The annual budget for ITER construction is about €0.5 billion (US$0.7 billion). This may seem high, but it is a tiny investment compared with the annual worldwide cost of electricity, which stands at around €2 trillion based on the average cost per kilowatt hour in 2007 in the European Union.

The fiftieth anniversary of international fusion research was marked in October 2008 with many lectures on the history of fusion (see http://fire.pppl.gov), which showed that fusion scientists have not lived quiet lives during this time. Teller and Artsimovich were right — the physics and technology of fusion are challenging, but the fusion community can be proud of its progress.

Yet this community will not recognize its own history in Seife's book. As admitted in the title, it is a rather strange history. After relating at length the early years of fusion research, it concentrates disproportionately on two table-top fusion fiascos — cold fusion and bubble fusion — generated by isolated individuals.

The book leads without proof to the dubious conclusion that "Over and over again, desperate scientists have deceived themselves and their peers — and cheated — in hopes to keep their fusion quest alive". Yet it focuses on outsiders to the field, who thought they had made a major discovery and who, after having been proven wrong when their results could not be repeated by others, did not have the courage to admit their errors. Thankfully, the book does not identify any scandal within magnetic fusion research, the main line for fusion energy. But as a result, it pays too little attention to this large international community. Whereas the dream of limitless energy may afflict isolated scientists, it is certainly not applicable to all fusion researchers as the author suggests.

The book identifies correctly that peer review is a necessary prerequisite for preventing fiascos. Scientists who call on journalists to make announcements without having had the traditional discussions with colleagues followed by publication in a peer-reviewed journal are in danger of damaging their reputation. Yet peer review may not always be sufficient. In addition to internal reviewing, in the late 1980s JET set up an internal database on which its experimental data were made available. Researchers within the organization can easily cross-check a scientific claim made by their colleagues. An open, international, multidevice database followed in the early 1990s, which has proven to be a sound basis for progress in fusion research. Such a system protects scientists from the insidious distortion of reality that can be provoked when they remain too isolated. Maybe Seife himself is a victim of 'wishful thinking' and should have sought peer review before publishing such a strange thesis. ■

Jean Jacquinot is scientific adviser to the French High Commissioner for Atomic Energy at the Commissariat a l'Energie Atomique (CEA), 91191 Gif-sur-Yvette, France, and the former director of both JET and the CEA magnetic fusion research group.
e-mail: jean.jacquinot@cea.fr

Our culture of obsession

Obsession: A History
by Lennard J. Davis
University of Chicago Press: 2008. 296 pp. $27.50, £16

A battle for the public good has been waged for centuries between qualified doctors of medicine with formal training and their 'quack' counterparts. As scientific analysis has come to be accepted, we have demanded more evidence from our physicians. Despite a lingering love-affair with alternative medicines such as homeopathy, patient-consumers today expect more than snake oil and bedside charm. Into this market lands Lennard Davis's latest book, *Obsession*.

The stereotypical view of a scientist, which rings true of many, is of an obsessive individual working long hours, worrying about minutiae and trying to replicate experiments against an approaching deadline. Davis looks at this form of obsession and others. He discusses the mania of novel writing in the nineteenth century, when prolific authors such as Émile Zola would write for days and nights at a time. The obsessive Zola became a subject of obsessive study by his contemporaries, and Davis guides us through the sociocultural evolution of the disease now known as obsessive–compulsive disorder. There are fascinating examples throughout the book, not least in his discussion of obsessive love and sex.

Davis tries to untangle the central question of what constitutes obsession. If I check my car doors are locked a couple of times before I leave it parked each morning, am I being obsessive? What about washing my hands repeatedly? Where is the line between obsession as a harmless fact of life, and when it becomes a mental illness? It is far from normal to wash one's hands so often one develops skin diseases, or to be unable to leave the house because of fears one has left the doors unlocked.

Obsession provides an insightful and nuanced review of the history of this tragic illness by exposing obsessive behaviour and contrasting it with the common, mildly obsessive behaviours we all engage in. The question of difference, and thus definition, is a recurring

motif. Davis is a professor at the University of Illinois in the departments of English, Medical Education, and Disability and Human Development, and has an interesting broad perspective. He insists that to treat an illness effectively, we must understand its history and evolution in a cultural context. Obsession has evolved from being subjacent to demonic possession into something to be almost proud of, to want even. Obsession is the hallmark of genius, of industry and perhaps of modern life, such as our need to regularly check e-mail.

Davis argues for the provision of a narrative framework to medicine, to understand both the disease entity itself and the illness that results from it. This raises the interesting question of whether we need a new type of clinician to help a patient understand their disease through such a narrative.

Davis also asks us to agree with a reclassification of obsession and thereby most, if not all, mental illness. But it is not clear into what. He asks us to assume that science and medical knowledge are responsible for the creation of obsessive culture because of their reductionist approach that observes too strictly the one gene, one disease schema. By this logic, it follows that scientists and physicians are themselves obsessive and unable to render any judgement. He addresses them in his introduction: "some clinicians and researchers who have miraculously persisted in reading my introduction up to this point will all the while have been shaking their heads at the ignorant insouciance of my project." Unfortunately, he is right. His elegant approach to reclassifying obsession, and by extension obsessive–compulsive disorders, is clouded by a post-modernist demonization of science.

Many facts and statements in the book are misleading. For example, "We are in the very early days of understanding the neurochemical and electrical activity of the brain," says Davis. But our current understanding of human physiology and disease follows centuries of study and analysis. The diagnoses we render now are based on an infinitely larger body of knowledge than those of our forebears who prescribed a good bleeding when one was feeling melancholic; hardly early days.

Davis gives us a witty and interesting historical tour of a fascinating subject. However, by presenting science as excessively reductionist and as responsible for the mis- or over-diagnosis of obsession, his arguments for reclassifying the disease remain incomplete and lack scientific rigour. ■

Ian Brooks is a neuroscientist at the Clinical and Translational Science Institute, University of Tennessee Health Science Center, Memphis, Tennessee 38163, USA.
e-mail: ibrooks1@utmem.edu

Q&A: Chemistry in the kitchen

Voted the world's best restaurant, Spain's elBulli near Barcelona offers an unusual culinary experience, from hot velvet-crab aspic with mini-corncob couscous to ice-cold liquorice nitro-dragon dessert. Innovative head chef **Ferran Adrià** explains how science and haute cuisine can work together.


ELBULLI

What will a guest find at elBulli?
It's not just about the food, it's an experience in itself. Cooking is a language. I'm expressing myself and everyone perceives it in a different way, like a piece of theatre. Each person takes away something new. In most human activities it would be normal to find humour, irony and deception. The one place this isn't expected is in the kitchen.

What are you doing now?
At the moment my team and I are working with a very strange ingredient, veal cartilage. We're also designing a new version of the Chinese 'thousand-year-old egg' [traditionally an egg preserved in clay, salt, ash, tea and lime]. I spend half the year composing at my workshop in Barcelona, and the other half interpreting in the kitchen at elBulli.

How hard is it to develop new dishes?
Last year we ran 4,000 tests and only about 300 of them panned out. Everyone learns from their mistakes — it's a necessary consequence of being creative. The important thing is to have lots of ideas simmering. Some of these ideas will work, and from these we build our new dishes.

Do you ever seek advice?
As with any other art, when my creative team needs something specific we go to an expert such as a scientist or historian. But when it comes to everyday ingredients, we don't usually consult researchers. Our work is systematic: you have to be very organized to achieve a sense of anarchism. It's not possible to grasp our work without seeing it for yourself — it would be like trying to describe eating an Amazonian fruit you've never tried.

Where do you find new ingredients?
I recently went to the Amazon, which has incredible fruits, some of them unknown to science. Under jungle conditions, many fruits ferment naturally. I also studied them in museums, in markets and with biologists.

Has your work raised any scientific questions?
It is having an influence in the world of science. I visited the physics department at Harvard University last month to talk about this. The dialogue between science and cooking is not new. Bread making has been considered a chemical process for hundreds of years, and the food industry has relied on chemists for almost a century. But only recently has there been a dialogue between science and haute cuisine. ■

Interview by **Jascha Hoffman**, a writer based in New York.

A Day At elBulli
by Ferran Adrià, Albert Adrià and Juli Soler
Phaidon Press: 2008. 600 pp. £29.95, €45


F. GUILLAMET

Ferran Adrià's 'Folie' salad combines tuna-oil foam, air-bag dough and yoghurt nodules.

motif. Davis is a professor at the University of Illinois in the departments of English, Medical Education, and Disability and Human Development, and has an interesting broad perspective. He insists that to treat an illness effectively, we must understand its history and evolution in a cultural context. Obsession has evolved from being subjacent to demonic possession into something to be almost proud of, to want even. Obsession is the hallmark of genius, of industry and perhaps of modern life, such as our need to regularly check e-mail.

Davis argues for the provision of a narrative framework to medicine, to understand both the disease entity itself and the illness that results from it. This raises the interesting question of whether we need a new type of clinician to help a patient understand their disease through such a narrative.

Davis also asks us to agree with a reclassification of obsession and thereby most, if not all, mental illness. But it is not clear into what. He asks us to assume that science and medical knowledge are responsible for the creation of obsessive culture because of their reductionist approach that observes too strictly the one gene, one disease schema. By this logic, it follows that scientists and physicians are themselves obsessive and unable to render any judgement. He addresses them in his introduction: "some clinicians and researchers who have miraculously persisted in reading my introduction up to this point will all the while have been shaking their heads at the ignorant insouciance of my project." Unfortunately, he is right. His elegant approach to reclassifying obsession, and by extension obsessive–compulsive disorders, is clouded by a post-modernist demonization of science.

Many facts and statements in the book are misleading. For example, "We are in the very early days of understanding the neurochemical and electrical activity of the brain," says Davis. But our current understanding of human physiology and disease follows centuries of study and analysis. The diagnoses we render now are based on an infinitely larger body of knowledge than those of our forebears who prescribed a good bleeding when one was feeling melancholic; hardly early days.

Davis gives us a witty and interesting historical tour of a fascinating subject. However, by presenting science as excessively reductionist and as responsible for the mis- or over-diagnosis of obsession, his arguments for reclassifying the disease remain incomplete and lack scientific rigour. ■

Ian Brooks is a neuroscientist at the Clinical and Translational Science Institute, University of Tennessee Health Science Center, Memphis, Tennessee 38163, USA.
e-mail: ibrooks1@utmem.edu

Q&A: Chemistry in the kitchen

Voted the world's best restaurant, Spain's elBulli near Barcelona offers an unusual culinary experience, from hot velvet-crab aspic with mini-corncob couscous to ice-cold liquorice nitro-dragon dessert. Innovative head chef **Ferran Adrià** explains how science and haute cuisine can work together.


ELBULLI

What will a guest find at elBulli?
It's not just about the food, it's an experience in itself. Cooking is a language. I'm expressing myself and everyone perceives it in a different way, like a piece of theatre. Each person takes away something new. In most human activities it would be normal to find humour, irony and deception. The one place this isn't expected is in the kitchen.

What are you doing now?
At the moment my team and I are working with a very strange ingredient, veal cartilage. We're also designing a new version of the Chinese 'thousand-year-old egg' [traditionally an egg preserved in clay, salt, ash, tea and lime]. I spend half the year composing at my workshop in Barcelona, and the other half interpreting in the kitchen at elBulli.

How hard is it to develop new dishes?
Last year we ran 4,000 tests and only about 300 of them panned out. Everyone learns from their mistakes — it's a necessary consequence of being creative. The important thing is to have lots of ideas simmering. Some of these ideas will work, and from these we build our new dishes.

Do you ever seek advice?
As with any other art, when my creative team needs something specific we go to an expert such as a scientist or historian. But when it comes to everyday ingredients, we don't usually consult researchers. Our work is systematic: you have to be very organized to achieve a sense of anarchism. It's not possible to grasp our work without seeing it for yourself — it would be like trying to describe eating an Amazonian fruit you've never tried.

Where do you find new ingredients?
I recently went to the Amazon, which has incredible fruits, some of them unknown to science. Under jungle conditions, many fruits ferment naturally. I also studied them in museums, in markets and with biologists.

Has your work raised any scientific questions?
It is having an influence in the world of science. I visited the physics department at Harvard University last month to talk about this. The dialogue between science and cooking is not new. Bread making has been considered a chemical process for hundreds of years, and the food industry has relied on chemists for almost a century. But only recently has there been a dialogue between science and haute cuisine. ■

Interview by **Jascha Hoffman**, a writer based in New York.

A Day At elBulli
by Ferran Adrià, Albert Adrià and Juli Soler
Phaidon Press: 2008. 600 pp. £29.95, €45


F. GUILLAMET

Ferran Adrià's 'Folie' salad combines tuna-oil foam, air-bag dough and yoghurt nodules.

NEWS & VIEWS

STEM CELLS

Tailor-made diseased neurons

Michael Sendtner

How can we investigate a disease affecting neurons, which cannot be isolated from patients for analysis? As the study of one neurological disorder shows, a first step might be to make patient-specific neurons.

Spinal muscular atrophy (SMA) is among the most common inherited neurological disorders that can cause death in childhood. Although the most severe form of the condition is known to be due to mutations in both copies of the *SMN1* gene, an understanding of how SMA develops has been slow. On page 277 of this issue, Ebert *et al.*[1] describe an elegant method in which skin cells taken from a patient with SMA were used to generate neurons of the same genetic make-up and characteristic features as the neurons affected in this disorder. The approach will not only lead to a better understanding of SMA, but should also aid the testing and development of drugs for its treatment.

For genetic reasons, SMA is unique to humans. Whereas rodents, flies and worms have only one version of the gene that is mutated in SMA, the human genome has two — *SMN1* and *SMN2*. These two genes differ in three nucleotides, one of which affects the genes' expression. Consequently, whereas *SMN1* expression predominantly produces the full-length SMN protein, *SMN2* expression results in only 10% occurring as full-length protein, with the rest being a truncated, non-functional protein. The severity of SMA in humans varies according to the number of copies of *SMN2* the patient carries — the more copies of *SMN2* there are, the better the patient can cope with the SMA-associated *SMN1* mutation. As mice carry only one copy of the *Smn* gene, its deletion results in early embryonic death[2]. Furthermore, if SMN expression is reduced in cells not normally affected by the disease, the cells die[3]. Therefore, a mouse model of SMA can be produced only by artificially introducing the human *SMN2* gene, or mutant or truncated versions of the human *SMN1* gene, into mice lacking the *Smn* gene.

Another problem in elucidating the mechanism underlying SMA stems from the fact that, although the SMN protein is ubiquitously expressed and is essential for the assembly of the machinery for processing messenger RNA, its absence in SMA predominantly affects spinal motor neurons. And clearly, unlike blood cells or skin fibroblast cells, for example, human neurons cannot simply be isolated for analysis.

A breakthrough came in 2006, when it was found that, by introducing four specific gene transcription factors, mouse fibroblasts could be reprogrammed to become induced pluripotent stem (iPS) cells, which have the ability to differentiate into any cell type[4]. Progress in stem-cell research has since been impressive, allowing previously unresolved problems in biomedicine to be addressed. For example, a mutation in the gene for haemoglobin was corrected in reprogrammed fibroblasts to treat sickle-cell anaemia in a mouse model[5]. Moreover, patient-specific iPS cells have been generated from the cells of patients with other disorders, including amyotrophic lateral sclerosis[6], a neurodegenerative disease that also affects motor neurons.

Ebert *et al.*[1] isolated fibroblasts from a child with SMA and from the child's healthy mother, and reprogrammed each set of cells to become iPS cells. From the iPS cells, they then derived motor neurons of the same genetic make-up as that of each donor. The authors found that, compared with the motor-neuron-like cells derived from the mother, those of the child showed the abnormalities typical of SMA motor neurons — a finding that makes the iPS cell line an invaluable tool for studying this disease.

"This observation is indeed exciting, as it suggests that the same approach could be used to test the efficacy of drug candidates before their use in patients."

Can this approach[1] be used to develop therapies? To investigate this possibility, the authors treated their iPS-cell-derived motor neurons with valproic acid or tobramycin, two drugs that increase the expression of both full-length and truncated versions of the SMN protein. In the cells derived from the patient with SMA, they observed increased production of full-length SMN and alterations in SMN-containing nuclear structures. By contrast, the equivalent cells from the mother did not show the same increase. This observation is indeed exciting, as it suggests that the same approach could be used to test the efficacy of drug candidates before their use in patients. As is often the case, however, the situation is not so simple.

Ebert and colleagues' motor-neuron-like cells indeed express markers of bona fide developing spinal motor neurons, such as the transcription factors OLIG2, ISLET1, HB9 and HOXB4, as well as the SMI-32 protein and the enzyme choline acetyltransferase. But what remains unclear is whether, *in vivo*, the cells surrounding the motor neurons and making contact with them — including other neurons, skeletal-muscle cells and support cells called glia — signal to the motor neurons to mediate their differentiation and the development of disease-specific features.

Take amyotrophic lateral sclerosis, for example. Experience with a mouse model of this disease, in which expression of a mutant form of the enzyme SOD-1 is increased, has shown[7] that the disease process is not limited to intrinsic defects in neurons, and that other cell types — in particular glial cells called astrocytes — also contribute. The same phenomenon was observed *in vitro* in motor neurons generated from iPS cell lines from patients with amyotrophic lateral sclerosis[8]. These motor neurons are sensitive to the toxic effects of astrocytes and other glial cells that carry a mutation in the SOD-1 gene[8].

Determining the contribution of cells other than motor neurons to the development of SMA is therefore important, not least because, even in the most severe form of the disorder, symptoms do not usually appear until a few weeks after birth — long after these neurons have begun to express their specific markers, developed axonal processes and made contact with skeletal-muscle cells. The availability of iPS cell lines should allow researchers to elucidate the contribution of other cells to motor-neuron differentiation as the neurons become affected in SMA, and to identify signals that act later in the development of embryonic motor neurons in the spinal cord.

The availability of protocols for inducing iPS cells to differentiate into motor neurons — using factors such as retinoic acid, the sonic hedgehog protein, GDNF and BDNF — is a first step towards resolving these issues. Moreover, additional strategies for tracking the

differentiation of other subcellular structures[9,10] in iPS-cell-derived motor neurons should help to determine why the disease is specific to motor neurons, with other types of neurons being unaffected. ■

Michael Sendtner is at the Institute of Clinical Neurobiology, University of Würzburg, Zinklesweg 10, 97078 Würzburg, Germany.
e-mail: sendtner_m@klinik.uni-wuerzburg.de

1. Ebert, A. D. *et al. Nature* **457,** 277–280 (2009).
2. Schrank, B. *et al. Proc. Natl Acad. Sci. USA* **94,** 9920–9925 (1997).
3. Wang, J. & Dreyfuss, G. *J. Biol. Chem.* **276,** 9599–9605 (2001).
4. Takahashi, K. & Yamanaka, S. *Cell* **126,** 663–676 (2006).
5. Hanna, J. *et al. Science* **318,** 1920–1923 (2007).
6. Dimos, J. T. *et al. Science* **321,** 1218–1221 (2008).
7. Lobsiger, C. S. & Cleveland, D. W. *Nature Neurosci.* **10,** 1355–1360 (2007).
8. Di Giorgio, F. P., Boulting, G. L., Bobrowicz, S. & Eggan, K. C. *Cell Stem Cell* **3,** 637–648 (2008).
9. Nishimune, H., Sanes, J. R. & Carlson, S. S. *Nature* **432,** 580–587 (2004).
10. Jablonka, S., Beck, M., Lechner, B. D., Mayer, C. & Sendtner, M. *J. Cell Biol.* **179,** 139–149 (2007).

FLUID DYNAMICS

Rotating convection on the edge

Peter L. Read

Turbulent convection in a rotating body is a common but poorly understood phenomenon in astrophysical and geophysical settings. Consideration of boundary effects offers a fresh angle on this thorny problem.

Heat energy is transported by three basic processes: conduction, radiation and convection. But which of them is likely to dominate in any given circumstance? In particular, how can we quantify the relative efficiency of each process, not least of convection, which is inherently nonlinear and turbulent? This problem is especially challenging for understanding the evolution and interior structure of stars and planets — a task that is further complicated by the fact that most stars and planets are rotating, which may modify the style of convection and influence its efficiency.

In a study that combines laboratory measurements and numerical simulations over an unusually wide range of parameters, King and colleagues (page 301 of this issue)[1] have systematically investigated the behaviour of convective heat transport in a rotating fluid. They focus on exploring the hypothesis that the type of convection that occurs is primarily governed by the ratio of the characteristic thicknesses of the principal (rotationally controlled) boundary layers (Fig. 1).

It is traditional in fluid mechanics to characterize quantities in terms of dimensionless ratios. So the total heat flux carried by a fluid can be quantified by comparing it with that obtained by conduction alone in a solid with the same thermal properties. The resulting ratio is known as the Nusselt number, Nu. This is convenient because, for many problems, the conductive heat flux is relatively easy to calculate from basic geometrical and physical properties of the fluid. Nu = 1 then corresponds to a thermal efficiency that is no better than conduction alone, whereas for convection on domestic or industrial scales, Nu takes typical values from about 10 up to several thousand.

But how should we extrapolate estimates of this convective efficiency to systems on the scale of planets or stars? From nearly 100 years of measurements and theory, several semi-empirical scaling laws have emerged that relate Nu to another dimensionless parameter, the Rayleigh number, Ra, which effectively measures the ratio of buoyancy to viscous forces in a fluid and is proportional to the imposed temperature contrast. In a non-rotating fluid, Nu has been measured[2,3] to vary as $\sim \mathrm{Ra}^{\alpha}$, where α can take a range of values ($2/7 \le \alpha \le 0.31$). The measurements cover an enormous range, including the extreme so-called 'hard' turbulence regime at values of $\mathrm{Ra} > 10^8$. This might seem to provide a good indication of how to extrapolate estimates of Nu to values of $\mathrm{Ra} \sim 10^{25}$–10^{30}, typical of planets and stars.

However, if convection takes place in a rapidly rotating fluid, things are much more complicated. This is because rapid rotation imparts an extra 'rigidity' to a fluid, but only in a direction parallel to the axis of rotation (Fig. 1). This directional rigidity changes the turbulent motions in ways that are still poorly understood, but that may profoundly influence the efficiency of convective heat transport, suggesting a scaling law closer to $\sim \mathrm{Ra}^{6/5}$ under some conditions. Such a difference in scaling exponent can change the extrapolated Nusselt number by orders of magnitude, rendering estimates of planetary or stellar heat flow extremely uncertain.

According to conventional wisdom, the force balance between buoyancy effects in the interior of the convecting region and Coriolis forces (which, for example, cause the air flow around low-pressure centres in Earth's atmosphere to circulate in the same sense as Earth's rotation) is the main factor governing the influence of rotation on the convection — notably, its efficiency as measured by Nu. King *et al.*[1] have examined whether this interior force balance provides a quantitative criterion for determining whether Nu scales either in the non-rotating limit as $\sim \mathrm{Ra}^{2/7}$ or in the rotating limit as $\sim \mathrm{Ra}^{6/5}$, but find that it doesn't predict the observed changeover between regimes.

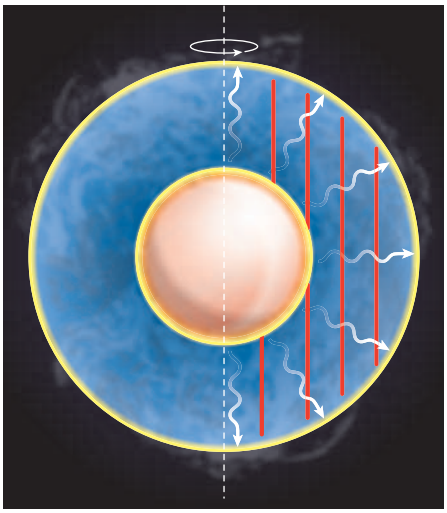

Figure 1 | Thermal convection in a spherical shell of fluid, rotating about a vertical axis. This is a situation such as might occur inside a gas-giant planet, or a stellar convection zone, and might for instance influence the planet's or star's magnetic field and other phenomena. Turbulent convective heat transfer (white arrows) is directed radially outwards, and loses heat to space. But rotation imparts a 'rigidity' parallel to the rotation axis (red bars), which may profoundly affect heat transfer. Boundary layers are shown as thick yellow lines at the inner and outer edges of the spherical shell, within which heat is added or removed and flow has to adjust to the mechanical conditions. King *et al.*[1] propose that it is the fluid dynamics at these boundary layers that constitutes the primary control on convection.

In contrast, they concentrate on the role of the boundary layers in the problem. Typical convective flows are not generally compatible with the mechanical and thermal boundary conditions imposed at the edges of the convective region. The fluid generally gets around this by creating thin regions of adjustment, known as boundary layers, in which diffusive effects (viscous or thermal) become large enough to allow the interior flow to match the imposed boundary conditions. Two types of boundary layer seem to be of most significance: first, a thermal boundary layer, dominated by thermal conduction, whose thickness $\delta_T \approx D/\mathrm{Nu}$, where D is a typical dimension of the convecting system, independent of rotation; and, second, the Ekman layer, within which viscous forces are comparable in size to Coriolis forces and whose thickness scales as $\delta_E \sim (\nu/\Omega)^{1/2}$, where Ω is the rotation rate and ν the kinematic viscosity.

King *et al.* have accumulated impressive evidence from their laboratory and numerical modelling experiments to show that the scaling dependence of Nu on Ra depends on whether $\delta_E > \delta_T$, or vice versa. This relationship seems to apply over a wide range of conditions, and even seems to work for systems bounded by stress-free boundaries, representing an idealization of

differentiation of other subcellular structures[9,10] in iPS-cell-derived motor neurons should help to determine why the disease is specific to motor neurons, with other types of neurons being unaffected. ■

Michael Sendtner is at the Institute of Clinical Neurobiology, University of Würzburg, Zinklesweg 10, 97078 Würzburg, Germany.
e-mail: sendtner_m@klinik.uni-wuerzburg.de

1. Ebert, A. D. *et al. Nature* **457,** 277–280 (2009).
2. Schrank, B. *et al. Proc. Natl Acad. Sci. USA* **94,** 9920–9925 (1997).
3. Wang, J. & Dreyfuss, G. *J. Biol. Chem.* **276,** 9599–9605 (2001).
4. Takahashi, K. & Yamanaka, S. *Cell* **126,** 663–676 (2006).
5. Hanna, J. *et al. Science* **318,** 1920–1923 (2007).
6. Dimos, J. T. *et al. Science* **321,** 1218–1221 (2008).
7. Lobsiger, C. S. & Cleveland, D. W. *Nature Neurosci.* **10,** 1355–1360 (2007).
8. Di Giorgio, F. P., Boulting, G. L., Bobrowicz, S. & Eggan, K. C. *Cell Stem Cell* **3,** 637–648 (2008).
9. Nishimune, H., Sanes, J. R. & Carlson, S. S. *Nature* **432,** 580–587 (2004).
10. Jablonka, S., Beck, M., Lechner, B. D., Mayer, C. & Sendtner, M. *J. Cell Biol.* **179,** 139–149 (2007).

FLUID DYNAMICS

Rotating convection on the edge

Peter L. Read

Turbulent convection in a rotating body is a common but poorly understood phenomenon in astrophysical and geophysical settings. Consideration of boundary effects offers a fresh angle on this thorny problem.

Heat energy is transported by three basic processes: conduction, radiation and convection. But which of them is likely to dominate in any given circumstance? In particular, how can we quantify the relative efficiency of each process, not least of convection, which is inherently nonlinear and turbulent? This problem is especially challenging for understanding the evolution and interior structure of stars and planets — a task that is further complicated by the fact that most stars and planets are rotating, which may modify the style of convection and influence its efficiency.

In a study that combines laboratory measurements and numerical simulations over an unusually wide range of parameters, King and colleagues (page 301 of this issue)[1] have systematically investigated the behaviour of convective heat transport in a rotating fluid. They focus on exploring the hypothesis that the type of convection that occurs is primarily governed by the ratio of the characteristic thicknesses of the principal (rotationally controlled) boundary layers (Fig. 1).

It is traditional in fluid mechanics to characterize quantities in terms of dimensionless ratios. So the total heat flux carried by a fluid can be quantified by comparing it with that obtained by conduction alone in a solid with the same thermal properties. The resulting ratio is known as the Nusselt number, Nu. This is convenient because, for many problems, the conductive heat flux is relatively easy to calculate from basic geometrical and physical properties of the fluid. Nu = 1 then corresponds to a thermal efficiency that is no better than conduction alone, whereas for convection on domestic or industrial scales, Nu takes typical values from about 10 up to several thousand.

But how should we extrapolate estimates of this convective efficiency to systems on the scale of planets or stars? From nearly 100 years of measurements and theory, several semi-empirical scaling laws have emerged that relate Nu to another dimensionless parameter, the Rayleigh number, Ra, which effectively measures the ratio of buoyancy to viscous forces in a fluid and is proportional to the imposed temperature contrast. In a non-rotating fluid, Nu has been measured[2,3] to vary as $\sim \mathrm{Ra}^{\alpha}$, where α can take a range of values ($2/7 \le \alpha \le 0.31$). The measurements cover an enormous range, including the extreme so-called 'hard' turbulence regime at values of $\mathrm{Ra} > 10^8$. This might seem to provide a good indication of how to extrapolate estimates of Nu to values of $\mathrm{Ra} \sim 10^{25}$–10^{30}, typical of planets and stars.

However, if convection takes place in a rapidly rotating fluid, things are much more complicated. This is because rapid rotation imparts an extra 'rigidity' to a fluid, but only in a direction parallel to the axis of rotation (Fig. 1). This directional rigidity changes the turbulent motions in ways that are still poorly understood, but that may profoundly influence the efficiency of convective heat transport, suggesting a scaling law closer to $\sim \mathrm{Ra}^{6/5}$ under some conditions. Such a difference in scaling exponent can change the extrapolated Nusselt number by orders of magnitude, rendering estimates of planetary or stellar heat flow extremely uncertain.

According to conventional wisdom, the force balance between buoyancy effects in the interior of the convecting region and Coriolis forces (which, for example, cause the air flow around low-pressure centres in Earth's atmosphere to circulate in the same sense as Earth's rotation) is the main factor governing the influence of rotation on the convection — notably, its efficiency as measured by Nu. King *et al.*[1] have examined whether this interior force balance provides a quantitative criterion for determining whether Nu scales either in the non-rotating limit as $\sim \mathrm{Ra}^{2/7}$ or in the rotating limit as $\sim \mathrm{Ra}^{6/5}$, but find that it doesn't predict the observed changeover between regimes.

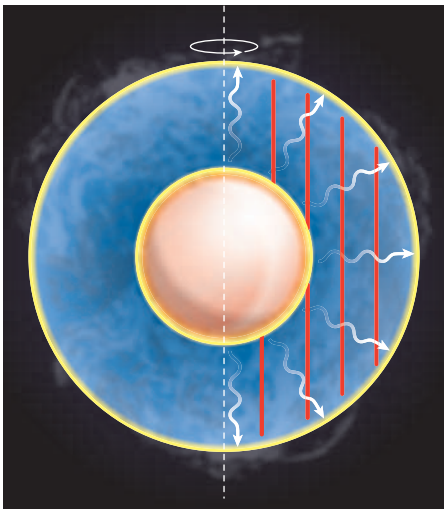

Figure 1 | Thermal convection in a spherical shell of fluid, rotating about a vertical axis. This is a situation such as might occur inside a gas-giant planet, or a stellar convection zone, and might for instance influence the planet's or star's magnetic field and other phenomena. Turbulent convective heat transfer (white arrows) is directed radially outwards, and loses heat to space. But rotation imparts a 'rigidity' parallel to the rotation axis (red bars), which may profoundly affect heat transfer. Boundary layers are shown as thick yellow lines at the inner and outer edges of the spherical shell, within which heat is added or removed and flow has to adjust to the mechanical conditions. King *et al.*[1] propose that it is the fluid dynamics at these boundary layers that constitutes the primary control on convection.

In contrast, they concentrate on the role of the boundary layers in the problem. Typical convective flows are not generally compatible with the mechanical and thermal boundary conditions imposed at the edges of the convective region. The fluid generally gets around this by creating thin regions of adjustment, known as boundary layers, in which diffusive effects (viscous or thermal) become large enough to allow the interior flow to match the imposed boundary conditions. Two types of boundary layer seem to be of most significance: first, a thermal boundary layer, dominated by thermal conduction, whose thickness $\delta_T \approx D/\mathrm{Nu}$, where D is a typical dimension of the convecting system, independent of rotation; and, second, the Ekman layer, within which viscous forces are comparable in size to Coriolis forces and whose thickness scales as $\delta_E \sim (\nu/\Omega)^{1/2}$, where Ω is the rotation rate and ν the kinematic viscosity.

King *et al.* have accumulated impressive evidence from their laboratory and numerical modelling experiments to show that the scaling dependence of Nu on Ra depends on whether $\delta_E > \delta_T$, or vice versa. This relationship seems to apply over a wide range of conditions, and even seems to work for systems bounded by stress-free boundaries, representing an idealization of

the top of the atmosphere of a planet or star.

The notion that the ratio δ_E/δ_T might determine the character and properties of rotating, stratified flows is not especially new. It was applied[4] in the 1980s to such problems as models of the circulation in the ocean thermocline, which is currently the subject of a controversy concerning Sandström's theorem on the nature and energetics of the thermohaline ocean circulation[5,6]. In that problem, the (highly turbulent) Ekman and thermal boundary layers play a clear role in the oceanic meridional circulation, so their importance in governing convective heat flow is not surprising.

In the convective problem considered by King *et al.*, however, it is less clear precisely what role the Ekman boundary layers play in the detailed transport of mass and heat. So the authors' results are all the more surprising and impressive. In the problems they have considered, however, heat enters or leaves the convecting region strictly by thermal conduction through the bounding walls, which is not exactly how heat is introduced or extracted in real planets or stars. So it remains to be seen to what extent their results can be applied to more general mechanisms for driving convection. ■

Peter L. Read is in the Subdepartment of Atmospheric, Oceanic and Planetary Physics, University of Oxford, Clarendon Laboratory, Parks Road, Oxford OX1 3PU, UK.
e-mail: p.read1@physics.ox.ac.uk

1. King, E. M., Stellmach, S., Noir, J., Hansen, U. & Aurnou, J. M. *Nature* **457,** 301–304 (2009).
2. Tilgner, A., Belmonte, A. & Libchaber, A. *Phys. Rev. E* **47,** 2253–2256 (1993).
3. Niemela, J. J., Skrbek, L., Sreenivasan, K. R. & Donnelly, R. J. *Nature* **404,** 837–840 (2000).
4. Hignett, P., Ibbetson, A. & Killworth, P. D. *J. Fluid Mech.* **109,** 161–187 (1981).
5. Wunsch, C. & Ferrari, R. *Annu. Rev. Fluid Mech.* **36,** 281–314 (2004).
6. Coman, M. A., Griffiths, R. W. & Hughes, G. O. *J. Mar. Res.* **64,** 783–796 (2006).

SYNTHETIC BIOLOGY

The yin and yang of nature

Jeff Gore and Alexander van Oudenaarden

Oscillations in gene expression regulate various cellular processes and so must be robust and tunable. Interactions between both negative and positive feedback loops seem to ensure these features.

Periodic oscillations are the basis of timekeeping. For many millennia, the main timekeeper was the water clock, in which time is recorded by the regular dripping of water into or out of a basin. In the seventeenth century, the water clock was replaced by the pendulum clock, following Galileo's famous discovery that the period of a pendulum's swing is independent of the size of the swing. This clock offered a substantial improvement because pendulum oscillations are robust and the period can be altered by changing the length of the pendulum arm. As three papers[1–3] now indicate, similar improvements are occurring in our ability to generate increasingly robust and tunable oscillations in biological systems. On page 309 of this issue, Tigges *et al.*[1] demonstrate this feat in mammalian cells, and not long ago Stricker *et al.*[2] reported it in bacteria. These two advances are nicely complemented by Tsai and colleagues' recent detailed theoretical study[3], which elucidates the essential 'design principles' underlying oscillatory networks in nature.

The simplest way to generate oscillations is by negative feedback with a delay. We are probably all familiar with this phenomenon from our attempts to maintain the proper water temperature in the shower. Because of the delay inherent in the system, we often overshoot, leading to a sometimes comical oscillation between scalding and freezing temperatures. An early example of a synthetic biological oscillator was a network called the repressilator[4], in which three genes sequentially repressed one another. The three repressive interactions led to net negative feedback, with a delay due to the multiple biochemical processes involved in gene expression. The repressilator did indeed oscillate, but the oscillations were not robust. Only half of the cells had observable oscillations, and those oscillations that did occur were variable. Moreover, the repressilator is not tunable; changing the rate constants of the various reactions generally abolishes the oscillation rather than changing its frequency[3].

Nonetheless, both robustness and tunability are important features of an oscillatory system, whether it be a gene circuit or a clock. For example, despite slight variations in the individual components of a clock, the oscillation period must remain a precise number of seconds. Similarly, if the physical environment changes, it may be necessary to retune the system to compensate: moving a pendulum clock from the ground floor to the top floor of a tall building requires retuning the clock, to correct for the small change in the acceleration due to gravity.

In the recent set of papers[1–3], a common theme is that supplementing the core negative feedback circuit with a positive feedback loop can make the oscillations both robust and tunable. Stricker *et al.*[2] demonstrated this experimentally by implementing a simple transcriptional circuit in the bacterium *Escherichia coli*. Their oscillator was composed of two genes driven by the same hybrid promoter sequence: the gene encoding the LacI protein generated the core negative feedback loop to suppress transcription, whereas that encoding the AraC protein generated the positive feedback loop. The resulting oscillation period could be tuned between 13 and 100 minutes depending on the concentration of the molecules used to induce transcription and on the temperature of the system. This oscillator design was based on a previously published theoretical study[5], although the authors[2] found it necessary to explicitly model intermediate steps such as multimerization, translation and protein folding.

Tigges *et al.*[1] construct a tunable oscillator in mammalian cells — using sense/antisense logic — by supplementing a central time-delayed negative feedback loop with a positive feedback loop. Here, negative feedback was provided by post-transcriptional repression of the gene encoding tTA by antisense RNA, whereas positive feedback was present because tTA enhanced its own transcription. The authors could tune the oscillation period by varying the number of copies of the genes encoding components of the oscillator. Whether varying the concentration of transcription inducers, while keeping the copy number of genes constant, would allow tuning of the oscillation period remains an intriguing question.

In their theoretical study, Tsai *et al.*[3] computationally analysed many different network topologies that might lead to oscillations, and also concluded that a positive feedback loop is likely to be necessary for tunable oscillations. The authors pointed out that bioengineers are simply learning tricks discovered by evolution long ago. Many biological networks that drive oscillations of variable period (such as the cell cycle) have a positive feedback loop, in addition to the central negative feedback loop that is mainly responsible for generating the oscillation. Indeed, Tsai and colleagues found that such a positive feedback loop is present in many oscillatory networks that do not require tunability (such as the circadian rhythm that tracks the day–night cycle). A possible function of the extra feedback loop in these networks of fixed frequency could be to make the oscillations robust — that is, more resistant to changes in kinetic parameters — thus perhaps increasing the 'evolvability' of the oscillation.

Advances in generating biological oscillations are similar to those made in the seventeenth century that led to our widespread adoption of the pendulum clock. What advances lie in store for our ability to construct synthetic biological oscillations? In the latest experiments[1–3], the phase of the oscillations was partly passed on to daughter cells, although individual cells gradually lost their synchronization. For any coordinated action, it is desirable for the population to oscillate in phase, thus requiring some

the top of the atmosphere of a planet or star.

The notion that the ratio δ_E/δ_T might determine the character and properties of rotating, stratified flows is not especially new. It was applied[4] in the 1980s to such problems as models of the circulation in the ocean thermocline, which is currently the subject of a controversy concerning Sandström's theorem on the nature and energetics of the thermohaline ocean circulation[5,6]. In that problem, the (highly turbulent) Ekman and thermal boundary layers play a clear role in the oceanic meridional circulation, so their importance in governing convective heat flow is not surprising.

In the convective problem considered by King *et al.*, however, it is less clear precisely what role the Ekman boundary layers play in the detailed transport of mass and heat. So the authors' results are all the more surprising and impressive. In the problems they have considered, however, heat enters or leaves the convecting region strictly by thermal conduction through the bounding walls, which is not exactly how heat is introduced or extracted in real planets or stars. So it remains to be seen to what extent their results can be applied to more general mechanisms for driving convection. ■

Peter L. Read is in the Subdepartment of Atmospheric, Oceanic and Planetary Physics, University of Oxford, Clarendon Laboratory, Parks Road, Oxford OX1 3PU, UK.
e-mail: p.read1@physics.ox.ac.uk

1. King, E. M., Stellmach, S., Noir, J., Hansen, U. & Aurnou, J. M. *Nature* **457,** 301–304 (2009).
2. Tilgner, A., Belmonte, A. & Libchaber, A. *Phys. Rev. E* **47,** 2253–2256 (1993).
3. Niemela, J. J., Skrbek, L., Sreenivasan, K. R. & Donnelly, R. J. *Nature* **404,** 837–840 (2000).
4. Hignett, P., Ibbetson, A. & Killworth, P. D. *J. Fluid Mech.* **109,** 161–187 (1981).
5. Wunsch, C. & Ferrari, R. *Annu. Rev. Fluid Mech.* **36,** 281–314 (2004).
6. Coman, M. A., Griffiths, R. W. & Hughes, G. O. *J. Mar. Res.* **64,** 783–796 (2006).

SYNTHETIC BIOLOGY

The yin and yang of nature

Jeff Gore and Alexander van Oudenaarden

Oscillations in gene expression regulate various cellular processes and so must be robust and tunable. Interactions between both negative and positive feedback loops seem to ensure these features.

Periodic oscillations are the basis of timekeeping. For many millennia, the main timekeeper was the water clock, in which time is recorded by the regular dripping of water into or out of a basin. In the seventeenth century, the water clock was replaced by the pendulum clock, following Galileo's famous discovery that the period of a pendulum's swing is independent of the size of the swing. This clock offered a substantial improvement because pendulum oscillations are robust and the period can be altered by changing the length of the pendulum arm. As three papers[1–3] now indicate, similar improvements are occurring in our ability to generate increasingly robust and tunable oscillations in biological systems. On page 309 of this issue, Tigges *et al.*[1] demonstrate this feat in mammalian cells, and not long ago Stricker *et al.*[2] reported it in bacteria. These two advances are nicely complemented by Tsai and colleagues' recent detailed theoretical study[3], which elucidates the essential 'design principles' underlying oscillatory networks in nature.

The simplest way to generate oscillations is by negative feedback with a delay. We are probably all familiar with this phenomenon from our attempts to maintain the proper water temperature in the shower. Because of the delay inherent in the system, we often overshoot, leading to a sometimes comical oscillation between scalding and freezing temperatures. An early example of a synthetic biological oscillator was a network called the repressilator[4], in which three genes sequentially repressed one another. The three repressive interactions led to net negative feedback, with a delay due to the multiple biochemical processes involved in gene expression. The repressilator did indeed oscillate, but the oscillations were not robust. Only half of the cells had observable oscillations, and those oscillations that did occur were variable. Moreover, the repressilator is not tunable; changing the rate constants of the various reactions generally abolishes the oscillation rather than changing its frequency[3].

Nonetheless, both robustness and tunability are important features of an oscillatory system, whether it be a gene circuit or a clock. For example, despite slight variations in the individual components of a clock, the oscillation period must remain a precise number of seconds. Similarly, if the physical environment changes, it may be necessary to retune the system to compensate: moving a pendulum clock from the ground floor to the top floor of a tall building requires retuning the clock, to correct for the small change in the acceleration due to gravity.

In the recent set of papers[1–3], a common theme is that supplementing the core negative feedback circuit with a positive feedback loop can make the oscillations both robust and tunable. Stricker *et al.*[2] demonstrated this experimentally by implementing a simple transcriptional circuit in the bacterium *Escherichia coli*. Their oscillator was composed of two genes driven by the same hybrid promoter sequence: the gene encoding the LacI protein generated the core negative feedback loop to suppress transcription, whereas that encoding the AraC protein generated the positive feedback loop. The resulting oscillation period could be tuned between 13 and 100 minutes depending on the concentration of the molecules used to induce transcription and on the temperature of the system. This oscillator design was based on a previously published theoretical study[5], although the authors[2] found it necessary to explicitly model intermediate steps such as multimerization, translation and protein folding.

Tigges *et al.*[1] construct a tunable oscillator in mammalian cells — using sense/antisense logic — by supplementing a central time-delayed negative feedback loop with a positive feedback loop. Here, negative feedback was provided by post-transcriptional repression of the gene encoding tTA by antisense RNA, whereas positive feedback was present because tTA enhanced its own transcription. The authors could tune the oscillation period by varying the number of copies of the genes encoding components of the oscillator. Whether varying the concentration of transcription inducers, while keeping the copy number of genes constant, would allow tuning of the oscillation period remains an intriguing question.

In their theoretical study, Tsai *et al.*[3] computationally analysed many different network topologies that might lead to oscillations, and also concluded that a positive feedback loop is likely to be necessary for tunable oscillations. The authors pointed out that bioengineers are simply learning tricks discovered by evolution long ago. Many biological networks that drive oscillations of variable period (such as the cell cycle) have a positive feedback loop, in addition to the central negative feedback loop that is mainly responsible for generating the oscillation. Indeed, Tsai and colleagues found that such a positive feedback loop is present in many oscillatory networks that do not require tunability (such as the circadian rhythm that tracks the day–night cycle). A possible function of the extra feedback loop in these networks of fixed frequency could be to make the oscillations robust — that is, more resistant to changes in kinetic parameters — thus perhaps increasing the 'evolvability' of the oscillation.

Advances in generating biological oscillations are similar to those made in the seventeenth century that led to our widespread adoption of the pendulum clock. What advances lie in store for our ability to construct synthetic biological oscillations? In the latest experiments[1–3], the phase of the oscillations was partly passed on to daughter cells, although individual cells gradually lost their synchronization. For any coordinated action, it is desirable for the population to oscillate in phase, thus requiring some

mode of cell-to-cell communication to synchronize oscillations. More generally, a way to entrain or pause the oscillations is often necessary. For example, circadian oscillations must be entrained by daylight, and the cell-cycle oscillation must be paused under low-nutrient conditions. Further advances combining theoretical modelling with experimental synthetic biology will both increase our understanding of natural networks and allow us to use the cell as a platform for future developments in biological engineering. ■

Jeff Gore and Alexander van Oudenaarden are in the Department of Physics, Massachusetts Institute of Technology, Cambridge, Massachusetts 02139, USA.
e-mail: avano@mit.edu

1. Tigges, M., Marquez-Lago, T. T., Stelling, J. & Fussenegger, M. *Nature* **457,** 309–312 (2009).
2. Stricker, J. *et al. Nature* **456,** 516–519 (2008).
3. Tsai, T. Y.-C. *et al. Science* **321,** 126–129 (2008).
4. Elowitz, M. B. & Leibler, S. *Nature* **403,** 335–338 (2000).
5. Hasty, J., Dolnik, M., Rottschäfer, V. & Collins, J. J. *Phys. Rev. Lett.* **88,** 148101 (2002).

CONDENSED-MATTER PHYSICS

Going with the flow

Jonathan Keeling and Natalia G. Berloff

Observations of superfluid behaviour — flow without friction — of unusual character in a condensed-matter system pave the way to investigations of superfluidity in systems that are out of thermal equilibrium.

When in 1937 liquid helium was first observed to flow with negligible viscosity through a narrow gap, it was clear that, at low temperatures, helium was different from ordinary fluids. This prompted Pyotr Kapitza to name the phenomenon superfluidity[1] by analogy with superconductivity. Since then, experiments on liquid helium and cold atoms have revealed other aspects of superfluidity (Table 1), including quantized vortices, undisturbed flow past an obstacle (for example, a structural defect), and (metastable) persistent flow in a doughnut-shaped geometry.

Experiments by Amo *et al.*[2], reported on page 291 of this issue, reveal a new variety of dissipationless flow in semiconductor microcavity polaritons — entities comprising both matter and light. The properties of the polariton fluid demonstrated by Amo *et al.* have their origin in the way polariton–polariton interactions modify the propagation of these quasiparticles, preventing scattering from structural defects in the microcavity. The question of how the finite lifetime of polaritons distinguishes these systems from previous examples of superfluidity provokes questions about the relationships between different aspects of superfluidity[3].

The system studied by Amo *et al.* is a semiconductor microcavity, consisting of a pair of mirrors (built from layers of semiconductors with alternating refractive indices) and a semiconductor quantum well, placed between these mirrors. The quantum well confines excitons (electronic excitations in the semiconductor) and the mirrors confine light. Because excitons can recombine and emit light, and light can create new excitons, repeated interconversion leads to new quasiparticles: microcavity polaritons[4,5]. These quasiparticles inherit properties from both of their constituents: from light comes their very small effective mass (about 0.0001 that of the electron); from the exciton come the polariton–polariton interactions.

Polaritons also have properties that neither of their constituents has alone. Crucially for

Table 1 | Superfluidity checklist

	Quantized vortices	Landau critical velocity	Metastable persistent flow	Two-fluid hydrodynamics	Local thermal equilibrium	Solitary waves
Superfluid ^{4}He/cold atom Bose–Einstein condensate	✓	✓	✓	✓	✓	✓
Non-interacting Bose–Einstein condensate	✓	✗	✗	✗	✓	✗
Classical irrotational fluid	✗	✓	✗	✓	✓	✓
Incoherently pumped polariton condensates	✓	✗	?	?	✗	?
Parametrically pumped polariton condensates	?	✓	?	?	✗	✓

Aspects of superfluid-like behaviour that have been demonstrated (ticks), shown not to exist (crosses), or remain to be verified (question marks) in different condensed-matter systems. Amo *et al.*[2] add a new system (red) to the table.

50 YEARS AGO

In 1949 it was found that water applied to the tongue of the frog elicited an electrical response from the glossopharyngeal nerve. This response was produced by specific fibres. It was first thought that these 'water' fibres might serve a particular purpose in water regulation in amphibians living in fresh water. These findings also revived the old problem of whether warm-blooded animals and man possess similar specific taste fibres mediating what we might call a water taste. The late Prof. David Katz of Stockholm, who believed this to be the case, often asked in his examinations: What is the taste of water? The correct answer was 'wet' ... It seems to us most likely that water does not elicit any positive taste sensation. The action must be of negative character in that water abolishes or decreases the resting activity of taste fibres ... The specific effect of water on taste in man can thus be looked upon as being of the same nature as that of blackness upon vision.

ALSO:

The world low air temperature record of −102.1 °F at the South Pole ... was exceeded in the polar night of 1958 at the Russian International Geophysical Year Antarctic stations Sovetskaya and Vostok. The Sovetskaya station recorded −86.7 °C (−124.1 °F) between 1900 and 2000 L.M.T. on August 9.
From *Nature* 17 January 1959.

100 YEARS AGO

At the recent conference on the conservation of resources which met at the White House at the invitation of the President of the United States, notes of warning were sounded concerning the coming exhaustion of coal, wood, ores, and soils. Whether or not we accept as exact the estimates furnished by experts on that impressive occasion, there is no doubt that we are approaching the end of our available resources, and that the near future will have momentous problems to face.
From *Nature* 14 January 1909.

50 & 100 YEARS AGO

mode of cell-to-cell communication to synchronize oscillations. More generally, a way to entrain or pause the oscillations is often necessary. For example, circadian oscillations must be entrained by daylight, and the cell-cycle oscillation must be paused under low-nutrient conditions. Further advances combining theoretical modelling with experimental synthetic biology will both increase our understanding of natural networks and allow us to use the cell as a platform for future developments in biological engineering. ■

Jeff Gore and Alexander van Oudenaarden are in the Department of Physics, Massachusetts Institute of Technology, Cambridge, Massachusetts 02139, USA.
e-mail: avano@mit.edu

1. Tigges, M., Marquez-Lago, T. T., Stelling, J. & Fussenegger, M. *Nature* **457,** 309–312 (2009).
2. Stricker, J. *et al. Nature* **456,** 516–519 (2008).
3. Tsai, T. Y.-C. *et al. Science* **321,** 126–129 (2008).
4. Elowitz, M. B. & Leibler, S. *Nature* **403,** 335–338 (2000).
5. Hasty, J., Dolnik, M., Rottschäfer, V. & Collins, J. J. *Phys. Rev. Lett.* **88,** 148101 (2002).

CONDENSED-MATTER PHYSICS

Going with the flow

Jonathan Keeling and Natalia G. Berloff

Observations of superfluid behaviour — flow without friction — of unusual character in a condensed-matter system pave the way to investigations of superfluidity in systems that are out of thermal equilibrium.

When in 1937 liquid helium was first observed to flow with negligible viscosity through a narrow gap, it was clear that, at low temperatures, helium was different from ordinary fluids. This prompted Pyotr Kapitza to name the phenomenon superfluidity[1] by analogy with superconductivity. Since then, experiments on liquid helium and cold atoms have revealed other aspects of superfluidity (Table 1), including quantized vortices, undisturbed flow past an obstacle (for example, a structural defect), and (metastable) persistent flow in a doughnut-shaped geometry.

Experiments by Amo *et al.*[2], reported on page 291 of this issue, reveal a new variety of dissipationless flow in semiconductor microcavity polaritons — entities comprising both matter and light. The properties of the polariton fluid demonstrated by Amo *et al.* have their origin in the way polariton–polariton interactions modify the propagation of these quasiparticles, preventing scattering from structural defects in the microcavity. The question of how the finite lifetime of polaritons distinguishes these systems from previous examples of superfluidity provokes questions about the relationships between different aspects of superfluidity[3].

The system studied by Amo *et al.* is a semiconductor microcavity, consisting of a pair of mirrors (built from layers of semiconductors with alternating refractive indices) and a semiconductor quantum well, placed between these mirrors. The quantum well confines excitons (electronic excitations in the semiconductor) and the mirrors confine light. Because excitons can recombine and emit light, and light can create new excitons, repeated interconversion leads to new quasiparticles: microcavity polaritons[4,5]. These quasiparticles inherit properties from both of their constituents: from light comes their very small effective mass (about 0.0001 that of the electron); from the exciton come the polariton–polariton interactions.

Polaritons also have properties that neither of their constituents has alone. Crucially for

Table 1 | Superfluidity checklist

	Quantized vortices	Landau critical velocity	Metastable persistent flow	Two-fluid hydrodynamics	Local thermal equilibrium	Solitary waves
Superfluid ^{4}He/cold atom Bose–Einstein condensate	✓	✓	✓	✓	✓	✓
Non-interacting Bose–Einstein condensate	✓	✗	✗	✗	✓	✗
Classical irrotational fluid	✗	✓	✗	✓	✓	✓
Incoherently pumped polariton condensates	✓	✗	?	?	✗	?
Parametrically pumped polariton condensates	?	✓	?	?	✗	✓

Aspects of superfluid-like behaviour that have been demonstrated (ticks), shown not to exist (crosses), or remain to be verified (question marks) in different condensed-matter systems. Amo *et al.*[2] add a new system (red) to the table.

50 YEARS AGO

In 1949 it was found that water applied to the tongue of the frog elicited an electrical response from the glossopharyngeal nerve. This response was produced by specific fibres. It was first thought that these 'water' fibres might serve a particular purpose in water regulation in amphibians living in fresh water. These findings also revived the old problem of whether warm-blooded animals and man possess similar specific taste fibres mediating what we might call a water taste. The late Prof. David Katz of Stockholm, who believed this to be the case, often asked in his examinations: What is the taste of water? The correct answer was 'wet' ... It seems to us most likely that water does not elicit any positive taste sensation. The action must be of negative character in that water abolishes or decreases the resting activity of taste fibres ... The specific effect of water on taste in man can thus be looked upon as being of the same nature as that of blackness upon vision.

ALSO:

The world low air temperature record of −102.1 °F at the South Pole ... was exceeded in the polar night of 1958 at the Russian International Geophysical Year Antarctic stations Sovetskaya and Vostok. The Sovetskaya station recorded −86.7 °C (−124.1 °F) between 1900 and 2000 L.M.T. on August 9.
From *Nature* 17 January 1959.

100 YEARS AGO

At the recent conference on the conservation of resources which met at the White House at the invitation of the President of the United States, notes of warning were sounded concerning the coming exhaustion of coal, wood, ores, and soils. Whether or not we accept as exact the estimates furnished by experts on that impressive occasion, there is no doubt that we are approaching the end of our available resources, and that the near future will have momentous problems to face.
From *Nature* 14 January 1909.

50 & 100 YEARS AGO

MATERIALS SCIENCE

Bend, fold and stretch

It is tempting to view graphene as the material of choice for the next generation of electronic devices. The fact that it forms strong, bendable sheets — made from carbon atoms arranged in a honeycomb lattice — together with its remarkable electronic properties makes it a promising starting point for flexible electronic applications.

However, the high-performance electronic graphene devices reported so far are made from tiny, micrometre-sized pieces of graphene, obtained using a rather cumbersome method that involves peeling off layers from a larger graphite substrate. In a paper published online in *Nature*, Byung Lee Hong and his colleagues now describe an alternative and more versatile method to produce graphene films with excellent electronic properties and with large, centimetre-scale areas (K. S. Kim *et al. Nature* doi:10.1038/nature07719; 2009).

Although chemical-processing techniques already exist for producing large-area graphene material, the electronic properties of such materials have been disappointing. But Hong *et al.* have perfected an approach known as chemical-vapour deposition. In this technique, a gaseous mixture of hydrocarbons flows over heated nickel foils and breaks down into atomic carbon, which in turn rearranges into graphene. Rapid cooling of the substrate then ensures that films just a few layers thick are formed. These ultrathin films are optically transparent and have high electrical conductivity, similar to that of mechanically cleaved graphene.

The main promise of Hong and colleagues' method lies in large-area applications, notably transparent, flexible electrodes such as that pictured. Hong *et al.* show that the graphene films can be radically bent and stretched without affecting their optical and electronic properties. And crucially, with this fabrication method the graphene can be easily transferred to other materials, because the underlying nickel can simply be etched away and the graphene film picked up and placed elsewhere. In addition, nanoscale patterns can be made in the graphene films by pre-patterning the nickel substrate with standard lithography techniques.

This combination of straightforward processing techniques and desirable properties increases the prospects of inexpensive, flexible and reliable electronic devices. Future applications, such as in photovoltaics, or as sensors and displays that are wearable or foldable, suddenly don't seem to require such a stretch of the imagination.

Liesbeth Venema

JI HYE HONG

Amo and colleagues' experiment, the polariton dispersion relation (the dependence of energy on momentum) does not take the simple quadratic form that a free particle takes. This means that a pair of polaritons injected at one energy is able to scatter to one high-energy polariton state and one low-energy state, in a process known as parametric scattering[6]. The rate of scattering depends on the type of quantum statistics particles obey. Because polaritons behave as bosons and thus obey Bose–Einstein statistics, the rate of scattering goes up as the populations of the final states increase. Amo *et al.* used this property to create a small seed population in the high-energy state. This, in turn, triggered parametric scattering of polaritons from the injected energy (pump state) to a lower-energy and a higher-energy state, producing a pulse of low-energy polaritons that travelled through the microcavity, continually fed by the parametric scattering.

Previous experiments on microcavity polaritons, in which polaritons were injected (incoherently) in a range of high-energy states instead of by parametric scattering, showed that they can form a Bose–Einstein condensate[7] (BEC): a form of matter that emerges when particles obeying Bose–Einstein statistics are cooled to very low temperatures and collapse into the same lowest-energy state, behaving as a single, coherent whole. Recently, quantized vortices have also been seen[8] in these systems, a feature associated with superfluidity.

The phenomenon of superfluidity is closely related, but not equivalent, to Bose–Einstein condensation[3]. In an interacting BEC, the occupation of a single quantum state by a large fraction of bosons means that the system is described by a single quantum wavefunction that satisfies a nonlinear equation for classical waves. Ubiquitous in nonlinear physics, this equation is known as the nonlinear Schrödinger equation[9]. This equation, written in terms of the density and velocity of the condensate, has a form almost equivalent to the usual Euler equation for the dynamics of a non-viscous fluid. Thus, one has the ingredients necessary to produce many of the aspects of superfluidity, such as frictionless flow below the Landau critical velocity (Table 1).

Frictionless flow has been observed in liquid helium using moving ions as probes[10], and in BECs of dilute atoms using laser beams[11]. At subcritical velocities, the superfluid flow around such an obstacle is symmetrical fore and aft of the direction of motion, so there is no drag. This absence of drag on moving objects is known as d'Alembert's paradox. In a classical fluid, drag does arise, because viscosity breaks the fore–aft symmetry. In their experiments, Amo and co-workers observed that a cloud of polaritons passed an obstacle — a structural defect in the microcavity — without any detectable drag, realizing d'Alembert's paradox in a condensate out of thermal equilibrium. In superfluid helium and atomic BECs, the drag above the critical velocity has been attributed to the shedding of vortices around the obstacle[10]. Although no such vortices have been directly observed in the polariton experiments of Amo *et al.*, it remains plausible that drag at speeds between the critical and sound velocities could arise from vortex formation in polariton fluids.

Amo and colleagues' experiments differ from previous investigations of superfluids in several ways. Most obviously, the polaritons have a finite lifetime. But this alone need not preclude many of the regular signatures of superfluidity. Perhaps most remarkably, the linearization of the relevant part of the polariton's dispersion relation, and thus the quasiparticle's immunity to scattering from structural microcavity defects, results from the nonlinear interactions of the low-energy polaritons with the pump polaritons as well as interactions among the low-energy polaritons. By contrast, for liquid helium or cold atoms, such linearization arises entirely as a result of interactions between the low-energy particles. The question of whether such polariton fluids can be called superfluid is, to us, less interesting than investigating the properties that these out-of-thermal-equilibrium polariton fluids possess. While experiments continue apace to explore these properties, it seems better to go with the flow. ■

Jonathan Keeling is in the Department of Physics, University of Cambridge, Cambridgeshire CB3 0HE, UK. Natalia G. Berloff is in the Department of Applied Mathematics and Theoretical Physics, University of Cambridge, Cambridgeshire CB3 0WA, UK.
e-mails: jmjk2@cam.ac.uk; n.g.berloff@damtp.cam.ac.uk

1. Kapitza, P. *Nature* **141,** 74 (1938).
2. Amo, A. *et al. Nature* **457,** 291–295 (2009).
3. Leggett, A. J. *Rev. Mod. Phys.* **71,** S318–S323 (1999).
4. Björk, G., Machida, S., Yamamoto, Y. & Igeta, K. *Phys. Rev. A* **44,** 669–681 (1991).
5. Weisbuch, C., Nishioka, M., Ishikawa, A. & Arakawa, Y. *Phys. Rev. Lett.* **69,** 3314–3317 (1992).
6. Savvidis, P. G. *et al. Phys. Rev. Lett.* **84,** 1547–1550 (2000).
7. Kasprzak, J. *et al. Nature* **443,** 409–414 (2006).
8. Lagoudakis, K. G. *et al. Nature Phys.* **4,** 706–710 (2008).
9. Pitaevskii, L. P. & Stringari, S. *Bose–Einstein Condensation* (Clarendon, 2003).
10. Rayfield, G. W. & Reif, F. *Phys. Rev.* **136,** A1194–A1208 (1964).
11. Raman, C. *et al. Phys. Rev. Lett.* **83,** 2502–2505 (1999).

mode of cell-to-cell communication to synchronize oscillations. More generally, a way to entrain or pause the oscillations is often necessary. For example, circadian oscillations must be entrained by daylight, and the cell-cycle oscillation must be paused under low-nutrient conditions. Further advances combining theoretical modelling with experimental synthetic biology will both increase our understanding of natural networks and allow us to use the cell as a platform for future developments in biological engineering. ■

Jeff Gore and Alexander van Oudenaarden are in the Department of Physics, Massachusetts Institute of Technology, Cambridge, Massachusetts 02139, USA.
e-mail: avano@mit.edu

1. Tigges, M., Marquez-Lago, T. T., Stelling, J. & Fussenegger, M. *Nature* **457,** 309–312 (2009).
2. Stricker, J. *et al. Nature* **456,** 516–519 (2008).
3. Tsai, T. Y.-C. *et al. Science* **321,** 126–129 (2008).
4. Elowitz, M. B. & Leibler, S. *Nature* **403,** 335–338 (2000).
5. Hasty, J., Dolnik, M., Rottschäfer, V. & Collins, J. J. *Phys. Rev. Lett.* **88,** 148101 (2002).

CONDENSED-MATTER PHYSICS

Going with the flow

Jonathan Keeling and Natalia G. Berloff

Observations of superfluid behaviour — flow without friction — of unusual character in a condensed-matter system pave the way to investigations of superfluidity in systems that are out of thermal equilibrium.

When in 1937 liquid helium was first observed to flow with negligible viscosity through a narrow gap, it was clear that, at low temperatures, helium was different from ordinary fluids. This prompted Pyotr Kapitza to name the phenomenon superfluidity[1] by analogy with superconductivity. Since then, experiments on liquid helium and cold atoms have revealed other aspects of superfluidity (Table 1), including quantized vortices, undisturbed flow past an obstacle (for example, a structural defect), and (metastable) persistent flow in a doughnut-shaped geometry.

Experiments by Amo *et al.*[2], reported on page 291 of this issue, reveal a new variety of dissipationless flow in semiconductor microcavity polaritons — entities comprising both matter and light. The properties of the polariton fluid demonstrated by Amo *et al.* have their origin in the way polariton–polariton interactions modify the propagation of these quasiparticles, preventing scattering from structural defects in the microcavity. The question of how the finite lifetime of polaritons distinguishes these systems from previous examples of superfluidity provokes questions about the relationships between different aspects of superfluidity[3].

The system studied by Amo *et al.* is a semiconductor microcavity, consisting of a pair of mirrors (built from layers of semiconductors with alternating refractive indices) and a semiconductor quantum well, placed between these mirrors. The quantum well confines excitons (electronic excitations in the semiconductor) and the mirrors confine light. Because excitons can recombine and emit light, and light can create new excitons, repeated interconversion leads to new quasiparticles: microcavity polaritons[4,5]. These quasiparticles inherit properties from both of their constituents: from light comes their very small effective mass (about 0.0001 that of the electron); from the exciton come the polariton–polariton interactions.

Polaritons also have properties that neither of their constituents has alone. Crucially for

Table 1 | Superfluidity checklist

	Quantized vortices	Landau critical velocity	Metastable persistent flow	Two-fluid hydrodynamics	Local thermal equilibrium	Solitary waves
Superfluid ^{4}He/cold atom Bose–Einstein condensate	✓	✓	✓	✓	✓	✓
Non-interacting Bose–Einstein condensate	✓	✗	✗	✗	✓	✗
Classical irrotational fluid	✗	✓	✗	✓	✓	✓
Incoherently pumped polariton condensates	✓	✗	?	?	✗	?
Parametrically pumped polariton condensates	?	✓	?	?	✗	✓

Aspects of superfluid-like behaviour that have been demonstrated (ticks), shown not to exist (crosses), or remain to be verified (question marks) in different condensed-matter systems. Amo *et al.*[2] add a new system (red) to the table.

50 YEARS AGO

In 1949 it was found that water applied to the tongue of the frog elicited an electrical response from the glossopharyngeal nerve. This response was produced by specific fibres. It was first thought that these 'water' fibres might serve a particular purpose in water regulation in amphibians living in fresh water. These findings also revived the old problem of whether warm-blooded animals and man possess similar specific taste fibres mediating what we might call a water taste. The late Prof. David Katz of Stockholm, who believed this to be the case, often asked in his examinations: What is the taste of water? The correct answer was 'wet' ... It seems to us most likely that water does not elicit any positive taste sensation. The action must be of negative character in that water abolishes or decreases the resting activity of taste fibres ... The specific effect of water on taste in man can thus be looked upon as being of the same nature as that of blackness upon vision.

ALSO:

The world low air temperature record of −102.1 °F at the South Pole ... was exceeded in the polar night of 1958 at the Russian International Geophysical Year Antarctic stations Sovetskaya and Vostok. The Sovetskaya station recorded −86.7 °C (−124.1 °F) between 1900 and 2000 L.M.T. on August 9.
From *Nature* 17 January 1959.

100 YEARS AGO

At the recent conference on the conservation of resources which met at the White House at the invitation of the President of the United States, notes of warning were sounded concerning the coming exhaustion of coal, wood, ores, and soils. Whether or not we accept as exact the estimates furnished by experts on that impressive occasion, there is no doubt that we are approaching the end of our available resources, and that the near future will have momentous problems to face.
From *Nature* 14 January 1909.

50 & 100 YEARS AGO

MATERIALS SCIENCE

Bend, fold and stretch

It is tempting to view graphene as the material of choice for the next generation of electronic devices. The fact that it forms strong, bendable sheets — made from carbon atoms arranged in a honeycomb lattice — together with its remarkable electronic properties makes it a promising starting point for flexible electronic applications.

However, the high-performance electronic graphene devices reported so far are made from tiny, micrometre-sized pieces of graphene, obtained using a rather cumbersome method that involves peeling off layers from a larger graphite substrate. In a paper published online in *Nature*, Byung Lee Hong and his colleagues now describe an alternative and more versatile method to produce graphene films with excellent electronic properties and with large, centimetre-scale areas (K. S. Kim *et al. Nature* doi:10.1038/nature07719; 2009).

Although chemical-processing techniques already exist for producing large-area graphene material, the electronic properties of such materials have been disappointing. But Hong *et al.* have perfected an approach known as chemical-vapour deposition. In this technique, a gaseous mixture of hydrocarbons flows over heated nickel foils and breaks down into atomic carbon, which in turn rearranges into graphene. Rapid cooling of the substrate then ensures that films just a few layers thick are formed. These ultrathin films are optically transparent and have high electrical conductivity, similar to that of mechanically cleaved graphene.

The main promise of Hong and colleagues' method lies in large-area applications, notably transparent, flexible electrodes such as that pictured. Hong *et al.* show that the graphene films can be radically bent and stretched without affecting their optical and electronic properties. And crucially, with this fabrication method the graphene can be easily transferred to other materials, because the underlying nickel can simply be etched away and the graphene film picked up and placed elsewhere. In addition, nanoscale patterns can be made in the graphene films by pre-patterning the nickel substrate with standard lithography techniques.

This combination of straightforward processing techniques and desirable properties increases the prospects of inexpensive, flexible and reliable electronic devices. Future applications, such as in photovoltaics, or as sensors and displays that are wearable or foldable, suddenly don't seem to require such a stretch of the imagination.

Liesbeth Venema

JI HYE HONG

Amo and colleagues' experiment, the polariton dispersion relation (the dependence of energy on momentum) does not take the simple quadratic form that a free particle takes. This means that a pair of polaritons injected at one energy is able to scatter to one high-energy polariton state and one low-energy state, in a process known as parametric scattering[6]. The rate of scattering depends on the type of quantum statistics particles obey. Because polaritons behave as bosons and thus obey Bose–Einstein statistics, the rate of scattering goes up as the populations of the final states increase. Amo *et al.* used this property to create a small seed population in the high-energy state. This, in turn, triggered parametric scattering of polaritons from the injected energy (pump state) to a lower-energy and a higher-energy state, producing a pulse of low-energy polaritons that travelled through the microcavity, continually fed by the parametric scattering.

Previous experiments on microcavity polaritons, in which polaritons were injected (incoherently) in a range of high-energy states instead of by parametric scattering, showed that they can form a Bose–Einstein condensate[7] (BEC): a form of matter that emerges when particles obeying Bose–Einstein statistics are cooled to very low temperatures and collapse into the same lowest-energy state, behaving as a single, coherent whole. Recently, quantized vortices have also been seen[8] in these systems, a feature associated with superfluidity.

The phenomenon of superfluidity is closely related, but not equivalent, to Bose–Einstein condensation[3]. In an interacting BEC, the occupation of a single quantum state by a large fraction of bosons means that the system is described by a single quantum wavefunction that satisfies a nonlinear equation for classical waves. Ubiquitous in nonlinear physics, this equation is known as the nonlinear Schrödinger equation[9]. This equation, written in terms of the density and velocity of the condensate, has a form almost equivalent to the usual Euler equation for the dynamics of a non-viscous fluid. Thus, one has the ingredients necessary to produce many of the aspects of superfluidity, such as frictionless flow below the Landau critical velocity (Table 1).

Frictionless flow has been observed in liquid helium using moving ions as probes[10], and in BECs of dilute atoms using laser beams[11]. At subcritical velocities, the superfluid flow around such an obstacle is symmetrical fore and aft of the direction of motion, so there is no drag. This absence of drag on moving objects is known as d'Alembert's paradox. In a classical fluid, drag does arise, because viscosity breaks the fore–aft symmetry. In their experiments, Amo and co-workers observed that a cloud of polaritons passed an obstacle — a structural defect in the microcavity — without any detectable drag, realizing d'Alembert's paradox in a condensate out of thermal equilibrium. In superfluid helium and atomic BECs, the drag above the critical velocity has been attributed to the shedding of vortices around the obstacle[10]. Although no such vortices have been directly observed in the polariton experiments of Amo *et al.*, it remains plausible that drag at speeds between the critical and sound velocities could arise from vortex formation in polariton fluids.

Amo and colleagues' experiments differ from previous investigations of superfluids in several ways. Most obviously, the polaritons have a finite lifetime. But this alone need not preclude many of the regular signatures of superfluidity. Perhaps most remarkably, the linearization of the relevant part of the polariton's dispersion relation, and thus the quasiparticle's immunity to scattering from structural microcavity defects, results from the nonlinear interactions of the low-energy polaritons with the pump polaritons as well as interactions among the low-energy polaritons. By contrast, for liquid helium or cold atoms, such linearization arises entirely as a result of interactions between the low-energy particles. The question of whether such polariton fluids can be called superfluid is, to us, less interesting than investigating the properties that these out-of-thermal-equilibrium polariton fluids possess. While experiments continue apace to explore these properties, it seems better to go with the flow. ■

Jonathan Keeling is in the Department of Physics, University of Cambridge, Cambridgeshire CB3 0HE, UK. Natalia G. Berloff is in the Department of Applied Mathematics and Theoretical Physics, University of Cambridge, Cambridgeshire CB3 0WA, UK.
e-mails: jmjk2@cam.ac.uk; n.g.berloff@damtp.cam.ac.uk

1. Kapitza, P. *Nature* **141,** 74 (1938).
2. Amo, A. *et al. Nature* **457,** 291–295 (2009).
3. Leggett, A. J. *Rev. Mod. Phys.* **71,** S318–S323 (1999).
4. Björk, G., Machida, S., Yamamoto, Y. & Igeta, K. *Phys. Rev. A* **44,** 669–681 (1991).
5. Weisbuch, C., Nishioka, M., Ishikawa, A. & Arakawa, Y. *Phys. Rev. Lett.* **69,** 3314–3317 (1992).
6. Savvidis, P. G. *et al. Phys. Rev. Lett.* **84,** 1547–1550 (2000).
7. Kasprzak, J. *et al. Nature* **443,** 409–414 (2006).
8. Lagoudakis, K. G. *et al. Nature Phys.* **4,** 706–710 (2008).
9. Pitaevskii, L. P. & Stringari, S. *Bose–Einstein Condensation* (Clarendon, 2003).
10. Rayfield, G. W. & Reif, F. *Phys. Rev.* **136,** A1194–A1208 (1964).
11. Raman, C. *et al. Phys. Rev. Lett.* **83,** 2502–2505 (1999).

OBITUARY

Edwin Salpeter (1924–2008)

Multi-talented astrophysicist and public servant.

Edwin Ernest Salpeter, who perhaps more than anyone put the physics into astrophysics, died on 26 November 2008 at the age of 83. Among his many accomplishments was figuring out how giant stars burn helium to form carbon in the 'triple-alpha process' (named after the three helium nuclei — alpha particles — that fuse together in the process). Before this discovery, the origin of the elements beyond helium in the periodic table was a mystery.

Salpeter was born on 3 December 1924 in Vienna. In 1939 his family fled to Australia after the Nazi takeover of Austria the previous year. He earned bachelor's and master's degrees at the University of Sydney, and then went to the University of Birmingham, UK, where he earned his doctorate in theoretical physics under the supervision of Rudolf Peierls in 1948. On Peierls' advice, he went to Cornell University in New York to work with fellow theoretical physicist Hans Bethe. He stayed at Cornell for nearly 60 years, and for most of this time occupied the same office assigned to him on his arrival.

Salpeter's most important work from his early years at Cornell led to the Bethe–Salpeter equation, which describes bound states of particles in quantum field theory. But despite his success in theoretical particle physics, Salpeter felt that he did not have the right talents or temperament for the subject. He started to look for a field that, in his own words, "was more controversial, more open-ended and new, where quick was useful and sloppy did not matter too much because it would all change soon anyway". He found it in astrophysics.

In 1939, Bethe published his Nobel-prizewinning work showing how the conversion of hydrogen to helium powers main-sequence stars such as the Sun. He subsequently received much correspondence on the subject. When Salpeter became the most junior of Bethe's postdocs, he was often delegated to respond to this correspondence, sparking his interest in nuclear astrophysics. Beginning in 1951, Salpeter started spending summers at the Kellogg Radiation Laboratory of the California Institute of Technology in Pasadena, working with Bethe's friend, the nuclear experimentalist Willy Fowler.

One of the key problems at the time was working out how elements heavier than helium (^{4}He) are generated in giant stars that have finished fusing hydrogen (^{1}H) to form helium. It was already known that there were no stable nuclei of atomic mass 5 or 8, and so there was no way that nuclei could form through the fusion of ^{1}H and ^{4}He, or through

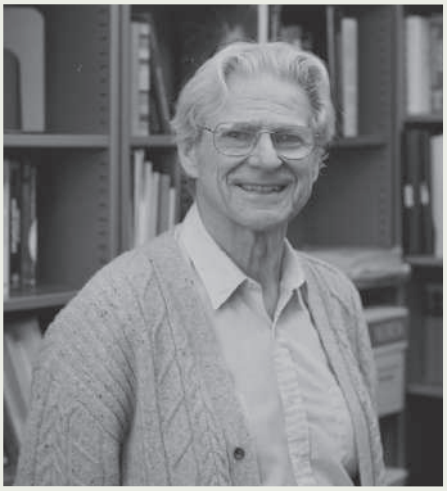

CORNELL UNIV.

the fusion of two ^{4}He nuclei. Furthermore, the probability of three helium nuclei coming together directly to produce ^{12}C was much too low to be feasible.

While studying Fowler's experimental data, Salpeter realized that the beryllium nucleus ^{8}Be — the fusion product of two helium nuclei — is actually metastable, and would exist in low concentrations inside red-giant stars. The ^{8}Be nucleus could therefore capture another helium nucleus to make ^{12}C. In 1997, Salpeter won the Royal Swedish Academy of Sciences' Crafoord prize for his discovery of this triple-alpha process. He shared the award with the astronomer Fred Hoyle, who predicted that ^{12}C must have a specific energy-level structure for the rate of the process to correspond to the known temperature of giant stars.

As the new field of nuclear astrophysics burgeoned, a vital question was how much heavy-element enrichment of the interstellar gas occurs when massive stars die. The answer hinges on how many stars of a given mass have been born — the 'initial mass function'. In 1955, Salpeter provided an answer to this crucial question as a simple power-law distribution. This "sloppy" treatment has turned out to be remarkably good, and is still widely used today. Salpeter also showed how electron screening affects both thermonuclear reaction rates in stars and the equation describing the state of dense matter, such as in white dwarfs and planetary interiors.

Whereas Salpeter's early research in astrophysics focused on questions related to stars, in the 1960s he began to study larger-scale problems in astronomy. Some of his most important work concerned the physical chemistry of interstellar gases, especially the condensation of the gases into dust grains, and the pivotal role of these grains as sites of chemical reactions. In the 1970s and 1980s, Salpeter turned towards still-larger scales of galaxies and the Universe, writing crucial papers on dark matter, on the rotational velocities of galaxies, and on the development of galaxy clusters and superclusters.

Salpeter's work in astrophysics was characterized by a combination of 'broad-brush' semi-quantitative estimates, theoretical rigour and, always, attention to unexplained observations — some of which he, his students and his collaborators made themselves. But he often predicted new and unexpected phenomena while thinking about what might become observable. Perhaps his most famous prediction (also made independently by Yakov Zel'dovich in the Soviet Union) was made in 1964, when he predicted that black holes could be detected indirectly by the radiation emitted by gas accreting onto them. This has become a standard method for detecting black holes.

Among his numerous contributions to public service, Salpeter's most important role was in the rigorous technical studies of anti-ballistic missile defence systems, starting in the 1960s. This impressed on him the limitations of such systems, and in the 1980s he participated in an influential study by the American Physical Society that debunked the feasibility of the 'Star Wars' Strategic Defense Initiative. Salpeter sparked some controversy by referring to the "dishonesty without outright lies" that pervaded the anti-ballistic missile defence community, then and now.

Late in his career, Salpeter became increasingly interested in neurobiology, collaborating with his wife, Miriam (Mika, then professor of neurobiology and behaviour at Cornell University), on research into the interactions between nerves and muscle fibres. He also worked on epidemiology and the statistical analysis of clinical trials, both in collaboration with his daughter Shelley Salpeter, a physician, and recently with his grandson, Nicholas Buckley. Of this work, Salpeter said, "My switch to epidemiology was not as radical a change as you might think. Humans coughing tuberculosis mycobacteria into the air at different ages required similar mathematical treatment to stars of different lifetimes disbursing heavy elements into the interstellar medium."

Salpeter trained many students during his magnificent career, including numerous faculty members at leading universities worldwide. And yet, no matter how eminent he became, Salpeter retained his modesty and sense of fun.

Saul A. Teukolsky and Ira Wasserman
Saul A. Teukolsky and Ira Wasserman are in the Departments of Physics and Astronomy, Space Sciences Building, Cornell University, Ithaca, New York 14853, USA.
e-mails: saul@astro.cornell.edu; ira@astro.cornell.edu

ARTICLES

Induced pluripotent stem cells from a spinal muscular atrophy patient

Allison D. Ebert[1,2], Junying Yu[3], Ferrill F. Rose Jr[4], Virginia B. Mattis[4], Christian L. Lorson[4], James A. Thomson[2,3,5] & Clive N. Svendsen[1,2,5,6]

Spinal muscular atrophy is one of the most common inherited forms of neurological disease leading to infant mortality. Patients have selective loss of lower motor neurons resulting in muscle weakness, paralysis and often death. Although patient fibroblasts have been used extensively to study spinal muscular atrophy, motor neurons have a unique anatomy and physiology which may underlie their vulnerability to the disease process. Here we report the generation of induced pluripotent stem cells from skin fibroblast samples taken from a child with spinal muscular atrophy. These cells expanded robustly in culture, maintained the disease genotype and generated motor neurons that showed selective deficits compared to those derived from the child's unaffected mother. This is the first study to show that human induced pluripotent stem cells can be used to model the specific pathology seen in a genetically inherited disease. As such, it represents a promising resource to study disease mechanisms, screen new drug compounds and develop new therapies.

Spinal muscular atrophy (SMA) is an autosomal recessive genetic disorder caused by mutations in the survival motor neuron 1 gene (*SMN1*) significantly reducing SMN protein expression[1,2] and resulting in the selective degeneration of lower α-motor neurons[3]. Clinically, patients with SMA 1 typically show symptoms at 6 months of age and die by age 2 (ref. 4). The *SMN2* gene is almost identical to *SMN1* except that *SMN2* has a single nucleotide difference that results in only 10% of the full-length protein being produced and high levels of a truncated, unstable protein lacking exon 7 (SMNΔ7)[5]. However, patients with several copies of SMN2 produce more full-length protein and have a less severe phenotype[6]. Although current model systems using worms, flies or mice have provided invaluable data concerning the genetic cause of SMA, the mechanisms of motor neuron death and potential drug therapies[7], they have important limitations. For example, mice, flies and worms lack the *SMN2* gene and thus animal models require complicated knockout and over-expression strategies[8–12]. As some therapies aim to target activation of endogenous *SMN2* as a potential disease modifier, a human cell-based assay system would be very beneficial. Although SMA patient fibroblasts are available for study, fibroblasts do not show the same vulnerability as motor neurons, and the processing and functioning of the SMN protein probably has unique features in a neural context that is highly relevant for understanding disease mechanisms.

Induced pluripotent stem (iPS) cells, which show marked similarities to embryonic stem cells, can now be derived from human adult somatic tissues[13–17], and recent studies have been successful in generating patient-specific iPS cells from a variety of diseases including amyotrophic lateral sclerosis, muscular dystrophy and Huntington's disease[18,19]. None of these reports, however, has shown any disease-specific changes in cell survival or function. In the current study we successfully established iPS cells from a type 1 SMA patient and his unaffected mother, and showed that these cells retained the capacity to generate differentiated neural tissue and motor neurons while maintaining a lack of SMN1 expression and the disease phenotype of selective motor neuron death. These cells also responded to compounds known to increase SMN protein. Together, these results will allow disease modelling and drug screening for SMA in a far more relevant system[20].

Characterization of iPS cells

We generated iPS cells from primary fibroblasts from a type 1 SMA patient and his unaffected mother after infection with lentiviral constructs encoding *OCT4* (also known as *POU5F1*), *SOX2*, *NANOG* and *LIN28* (ref. 16) (Supplementary Fig. 1). Two SMA clones (3.5 and 3.6) and one wild-type clone (4.2) propagated robustly when maintained on mouse embryonic fibroblasts. Quantitative PCR with reverse transcription (qRT–PCR), teratoma formation, DNA fingerprinting and microarray analysis all indicated that reprogramming of wild-type and SMA fibroblasts to a pluripotent state occurred, along with repression of the exogenously introduced genes (Fig. 1f–j, Supplementary Tables 1–3 and Supplementary Figs 2–4). Only the 3.6 clone (iPS-SMA) and the 4.2 clone (iPS-WT; Fig. 1a–c) were used for further evaluation in this study. Both the iPS-SMA and iPS-WT cells grew at similar rates and maintained a normal karyotype for at least 12 weeks (Fig. 1d, e).

Cells from SMA patients have significantly reduced levels of SMN transcripts that contain all 9 exons (full-length transcripts) due to loss of the *SMN1* gene[1,2]. To test whether the derivation of iPS cells affected SMN production, iPS and fibroblast SMN RNA was analysed. RT–PCR analysis showed that iPS-WT had comparable SMN levels to the wild-type fibroblasts (Fib-WT), whereas iPS-SMA had lower levels that were similar to the Fib-SMA cells (Fig. 2a). As expected owing to the maintenance of *SMN2* function in this disorder[1,2], transcripts for some full-length SMN and the alternatively spliced product lacking exon 7 (Δ7) were identified in all samples (Fig. 2a). Furthermore, specific digestion of full-length bands produced the expected *SMN2* cleavage products in all samples, confirming that *SMN2* produces full-length SMN in both the wild-type and SMA cells (Fig. 2b). Intact *SMN1* was detected only in the wild-type cells, thus verifying the absence of *SMN1* in SMA cells and recapitulating SMA and carrier

[1]The Waisman Center, and [2]The Stem Cell and Regenerative Medicine Center, University of Wisconsin-Madison, 1500 Highland Avenue, Madison, Wisconsin 53705, USA. [3]The Genome Center and Wisconsin National Primate Research Center, University of Wisconsin-Madison, 425 Henry Mall, Madison, Wisconsin 53706, USA. [4]Department of Veterinary Pathobiology, Bond Life Sciences Center, University of Missouri, 1201 Rollins Road, Columbia, Missouri 65211, USA. [5]Department of Anatomy, University of Wisconsin-Madison, 1300 University Avenue Madison, Wisconsin 53706, USA. [6]Department of Neurology, University of Wisconsin-Madison, 600 North Highland Avenue, Madison, Wisconsin 53792, USA.

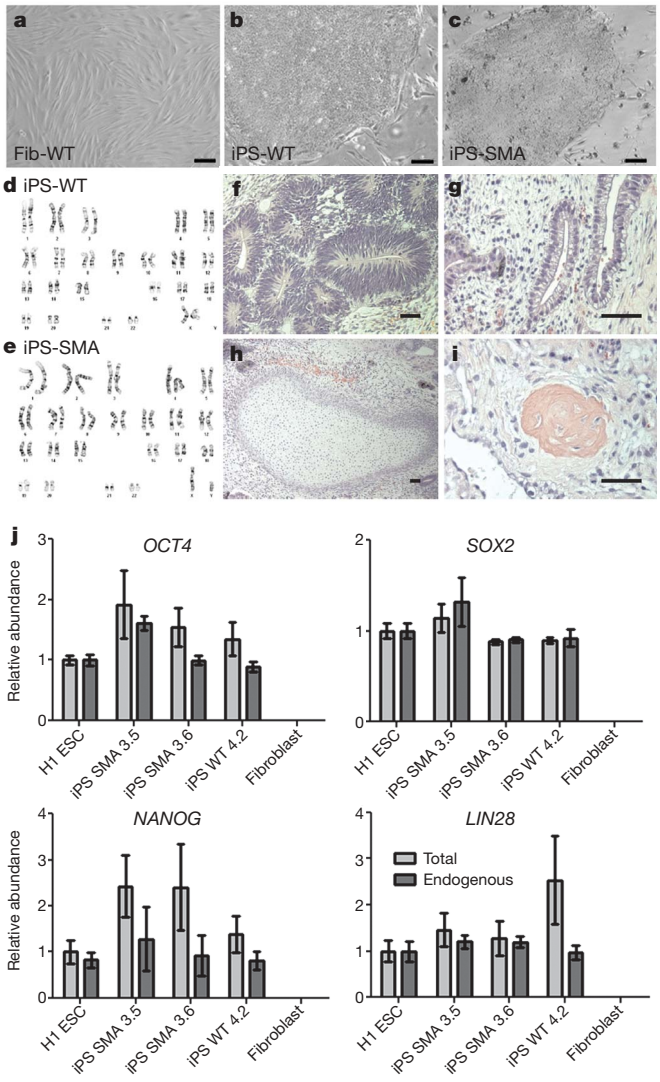

Figure 1 | Newly generated iPS cells were fully reprogrammed. **a**–**c**, iPS-WT and iPS-SMA cells formed tightly packed colonies in contrast to the spindle morphology of fibroblasts. **d**, **e**, No karyotypic abnormalities were observed. **f**–**i**, After transplantation, all iPS cells generated teratomas showing (**f**) neural tissue (ectoderm), (**g**) primitive gut (endoderm), (**h**) cartilage (mesoderm), and (**i**) bone (mesoderm). **j**, qRT–PCR showed induction of endogenous transcripts of *OCT4*, *SOX2*, *NANOG* and *LIN28*. 'Endogenous' refers to primers recognizing the 3′ untranslated region, whereas 'total' identifies both the endogenous and exogenously expressed transgene. ESC, embryonic stem cells. Data are expressed as mean ± s.e.m. Scale bars, 50 μm.

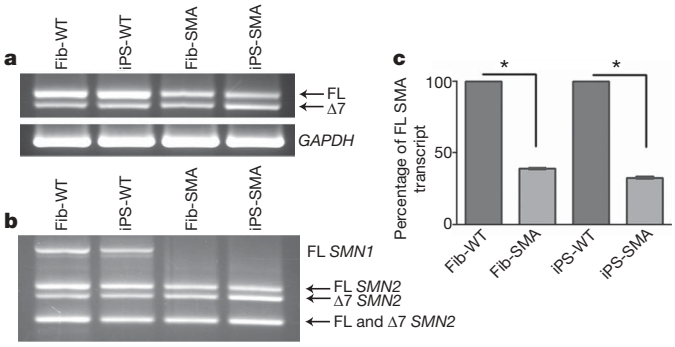

Figure 2 | iPS-SMA cells show decreased SMN transcripts. **a**, iPS-WT and iPS-SMA cells had levels of full-length (FL) and truncated, exon 7 deleted (Δ7) *SMN* transcripts similar to their respective fibroblast lines (Fib-WT and Fib-SMA, respectively). **b**, Additionally, both Fib-SMA and iPS-SMA cells showed a specific lack of *SMN1*, although *SMN2* full-length and Δ7 transcripts were still present in all samples. **c**, qRT–PCR showed reduced full-length SMN transcript in both fibroblasts (61.1% ± 0.6 reduced) and iPS cells (67.4% ± 0.8 reduced) when compared to wild-type cultures (*$P < 0.001$, Student's *t*-test). Data are presented as mean ± s.e.m.

transcript patterns[21] (Fig. 2b). qRT–PCR further confirmed the significantly reduced level of full-length *SMN* transcript in SMA cells (32–39% reduced compared to wild-type, Fig. 2c). These data are consistent with full-length *SMN* mRNA levels observed in SMA peripheral blood mononuclear cells[22]. Taken together, these data demonstrate that the generation of iPS cells does not alter the critical gene expression profiles or alternative splicing events of *SMN1* and *SMN2* in unaffected or disease-specific contexts.

Neuronal differentiation of iPS cells

To establish whether the lack of SMN1 may affect neuronal differentiation or survival in this new model, we next generated neurons and astrocytes from both iPS-SMA and iPS-WT cells (Supplementary Fig. 1). Traditional embryoid body formation was found to be very inefficient for neural differentiation from iPS cultures and so an alternate protocol was developed. The iPS cultures were first removed from their feeder layers and grown as floating iPS spheres in a defined media for a minimum of 2 weeks. These could be continually passaged using a chopping method that avoids losing cell–cell contact known to be important for maintaining both neural and embryonic stem cell proliferation[23,24]. These cultures were then dissociated and plated onto laminin-coated coverslips. The iPS-SMA and iPS-WT spheres generated nestin-positive cells indicative of a neural stem cell phenotype[25] (Fig. 3a, b). On further differentiation, Tuj1-positive neurons and GFAP-positive astrocytes were also found (Fig. 3c, d). The iPS spheres were simple to expand, remarkably stable over time and maintained the ability to produce neural progeny for more than 20 passages.

As SMA adversely affects motor neurons, we next addressed whether the iPS cells could be lineage-restricted towards a motor neuron fate (Supplementary Fig. 1). Basing our differentiation model on a previously published report using human embryonic stem cells[26], iPS spheres were grown in a neural induction medium containing retinoic acid for 1 week, followed by a further week of retinoic acid and sonic hedgehog (SHH). Spheres were then seeded onto laminin-coated coverslips for another 2–6 weeks (totalling 4–8 weeks of differentiation), and grown in the presence of retinoic acid, SHH, cyclic AMP, ascorbic acid, glial cell line-derived neurotrophic factor and brain-derived neurotrophic factor. One week after plating, long fine processes resembling neuronal axons were observed and neural-like cells were seen migrating out from the sphere. Both iPS-SMA and iPS-WT spheres generated cells that expressed the motor neuron transcription factors HOXB4, OLIG2, ISLET1 (also known as ISL1) and HB9 (refs 27, 28) during the differentiation process (Fig. 3e, f and Supplementary Fig. 5). The presumptive motor neurons were then immunostained with SMI-32 and choline acetyltransferase (ChAT), which are established markers for mature motor neurons[29]. Both SMI-32 and ChAT staining identified positive neurons in all cultures after 4 weeks of differentiation (Fig. 3e–h). At this point there was no significant difference between the iPS-SMA and iPS-WT cultures in the number of motor neurons (12.6% ± 2.2 and 9.5% ± 2.4, respectively) or their size (641.0 μm^2 ± 81.3 and 669.8 μm^2 ± 59.1, respectively, Fig. 3k, l) suggesting that iPS-SMA cells are capable of generating motor neurons, which is similar to the human condition and mouse models in which functional motor neurons are generated at early developmental times[30].

To develop the system further, we cultured the cells for another 2 weeks and again analysed motor neuron number and size. Notably, at this time the iPS-SMA cultures had significantly fewer motor neurons (4.3% ± 2.0) with a reduced size (383.1 μm^2 ± 38.6) compared to the iPS-WT cultures (24.2% ± 4.0, 654.8 μm^2 ± 32.6, Fig. 3k, l). However, there was no difference in the number of total Tuj1-positive neurons in either iPS-WT or iPS-SMA cells at 6 weeks of differentiation (15.78% ± 2.9 and 15.55% ± 2.8, respectively), suggesting that there is a specific effect of the SMA phenotype on

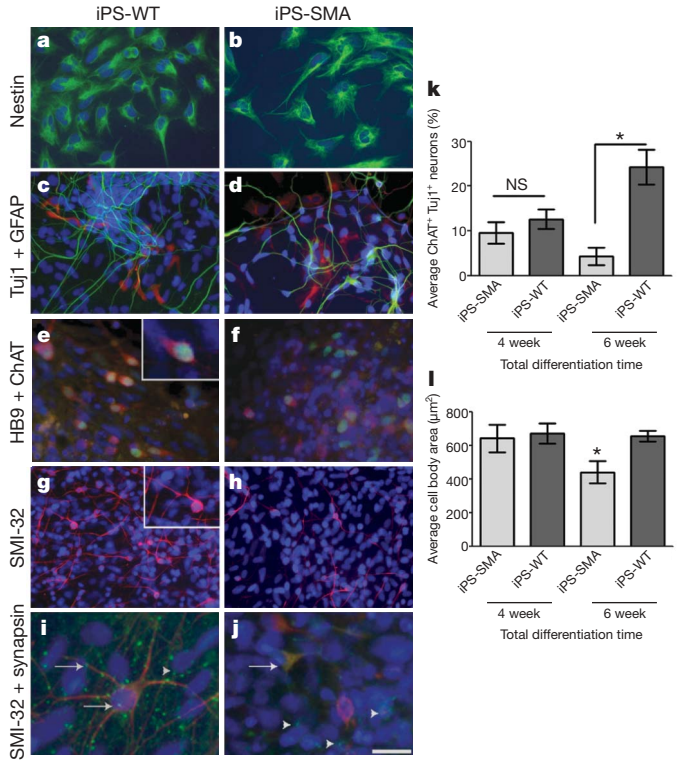

Figure 3 | iPS-WT and iPS-SMA cells can generate cells in the neural lineage. **a**, **b**, iPS-WT and iPS-SMA cells generated nestin-positive neural progenitor cells (green). **c**, **d**, Tuj1-positive neurons (green) and GFAP-positive astrocytes (red) are shown. **e**–**h**, At 4–6 weeks of differentiation, HB9 (green) and ChAT (red) double-positive motor neurons (**e**, **f**), and SMI-32-positive (red) motor neurons (**g**, **h**) are shown, with magnified images shown in insets **e**, **g**. **i**, At 8 weeks, punctate synapsin (green) staining on SMI-32-positive motor neurons (red) was identified on iPS-WT cells (arrows). **j**, However, only diffuse synapsin (green) staining was observed on SMI-32-positive motor neurons (red) in iPS-SMA cells (arrows). Arrowheads in **i** and **j** denote punctate synapsin staining on SMI-32-negative cells. Nuclei are labelled with Hoechst nuclear dye (blue). **k**, **l**, iPS-SMA-derived motor neurons are significantly reduced in number and size at 6 weeks compared to iPS-WT cells ($n = 3$, $^*P < 0.05$, analysis of variance (ANOVA)). All data are presented as mean ± s.e.m. Scale bar, 50 μm (**a**–**h**) and 25 μm (**i**, **j**).

motor neurons. Taken together, these data show that iPS-SMA cells can produce similar numbers of neurons and motor neurons initially, but that the disease phenotype selectively hinders motor neuron production and/or increases motor neuron degeneration at later time points. Although synapses were not observed after 6 weeks of differentiation, by 8 weeks synapses were identified by punctate synapsin staining on iPS-WT SMI-32-positive motor neurons and non-motor neurons (Fig. 3i and Supplementary Fig. 6), suggesting that pre-synaptic maturation of the neurons was occurring in this system. Notably, synapsin staining remained diffuse on the iPS-SMA SMI-32-positive motor neurons (Fig. 3j), although some punctate synapsin staining was observed on SMI-32 negative cells (Fig. 3j), again suggesting a specific motor neuron deficit in the SMA cultures.

Drug induced increase of SMN protein

Finally, we assessed whether SMN-inducing compounds could increase SMN levels in the iPS-SMA cellular context because this would be an important proof-of-principle for the further development of drug screens. SMN protein is found in both the cytoplasm and nuclear aggregate structures called gems, and the number of gems present is inversely correlated to disease severity[2]. We therefore assessed nuclear gem localization in iPS-SMA- and iPS-WT-derived neurons and astrocytes in the presence or absence of 1 mM valproic acid or 320 μM tobramycin: two compounds shown to increase SMN protein levels[31–33]. Using an antibody against SMN, untreated Fib-WT and iPS-WT cells showed an abundance of nuclear gems that characterize the normal distribution of this protein (Fig. 4a, c). Both untreated Fib-SMA and iPS-SMA cells showed the expected lack of nuclear gems (Fig. 4b, d) providing further support for reliable disease modelling using iPS-SMA cells. After 2 days of drug treatment, there was no significant increase in gem localization in treated (Fig. 4e, g, i) compared to untreated (Fig. 4c, i) iPS-WT cells. However, valproic acid and tobramycin significantly increased the number of gems in treated compared to untreated iPS-SMA cells (Fig. 4d, f, h, i). We further verified this increase by examining SMN protein by western blot analysis. Two days after drug treatment, total SMN protein was far higher in iPS-WT cells than in iPS-SMA cells (Fig. 4j, k), owing to the lack of SMN1 expression in the latter (Fig. 2b). iPS-SMA cells treated with either valproic acid or tobramycin showed a significant 2- or 3-fold increase, respectively, in SMN protein levels compared to untreated iPS-SMA cells (Fig. 4j, k). We are at present assessing gem formation in differentiating motor neurons and have shown that they can indeed be detected (Supplementary Fig. 7). Together these data suggest that iPS-SMA cells respond to drug treatment in a similar fashion to Fib-SMA cells and could be useful for new drug screening specifically on motor neurons in future studies.

Discussion

Previous efforts to understand the mechanisms of SMA in human tissues have relied on fibroblasts from patients or immortalized non-motor neuron cell lines. However, one of the most fascinating aspects of the disease is that a ubiquitous loss of SMN protein from all cells in the body results in the specific degeneration of motor neurons. SMN has been shown to form complexes involved in the production of small nuclear RNA proteins that make up the splicesosome[34–36]. More recently, SMN has also been shown to traffic to neuronal processes of motor neurons and may have other important roles in motor axons yet to be fully determined[37,38]. Using human motor neurons carrying

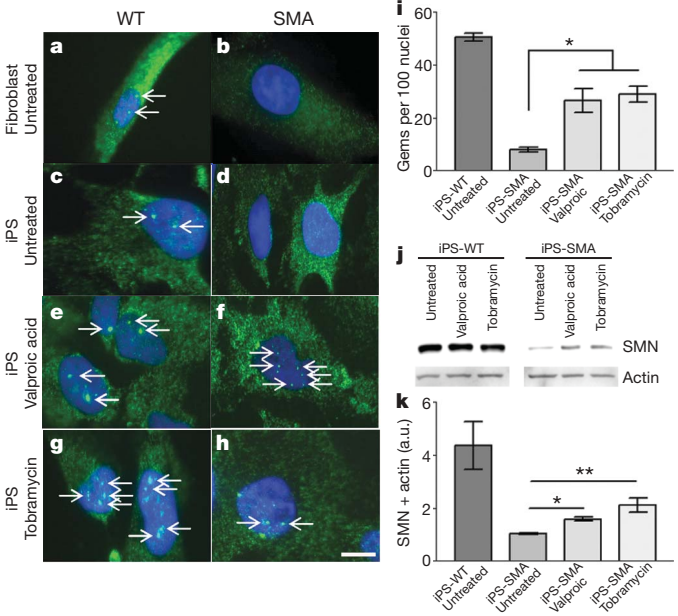

Figure 4 | iPS-WT and iPS-SMA cells increase SMN protein in response to drug treatment. **a**–**d**, Untreated Fib-WT and iPS-WT cells show nuclear gem localization (**a**, **c**; gems indicated by arrows), whereas untreated Fib-SMA and iPS-SMA lack nuclear gems (**b**, **d**). **e**–**i**, After valproic acid (**e**, **f**) or tobramycin (**g**, **h**) treatment, iPS-SMA cells show a significant increase in the number of gems ($P < 0.05$, ANOVA, **i**). **j**, **k**, Western blot analysis showed a significant 2–3-fold increase in SMN protein in valproic acid or tobramycin treated iPS-SMA cells compared to untreated iPS-SMA cells ($n = 3$, $^*P < 0.05$, $^{**}P < 0.01$, ANOVA). a.u., arbitrary units. Data are presented as mean ± s.e.m. Scale bar, 50 μm.

the SMA phenotype generated from a virtually limitless source of iPS cells described here should help to clarify further this new role for SMN in disease initiation and progression.

This is, to our knowledge, the first report to observe disease-specific effects on human motor neuron survival and drug induced increases in protective proteins, thus validating that the iPS model can recapitulate at least some aspects of this genetically inherited disorder. Although the motor neurons generated in the current study show appropriate morphology, specific markers and synapsin staining, experiments are at present underway to more fully assess their function including electrophysiology and co-cultures with muscle fibres. More clones from this and other patient sources also need to be studied. These are important next steps to ensure that the reprogramming has not subtly affected the ability of the motor neurons to function normally. However, this new model should provide a unique platform for studies aimed at both understanding SMA disease mechanisms that lead to motor neuron dysfunction and death, and the potential discovery of new compounds to treat this devastating disorder. It also points to a future in which iPS technology could be used to better understand and develop treatments for several other genetically inherited diseases.

METHODS SUMMARY

Detailed methods are included in the Methods section. SMA and wild-type fibroblast cell lines were from Coriell Institute for Medical Research. Lentiviral infection of the fibroblasts and iPS cell culture was performed as described previously[16]. PCR was performed according to standard procedures using primers specific for *OCT4*, *SOX2*, *NANOG*, *LIN28*, *HOXB4*, *SMN* and *GAPDH* as published previously[16,22] and shown in the Supplementary Information. Gene expression profiling, DNA fingerprinting and microarray analysis were performed following standard protocols. Neural induction was modified from previously published methods[26], and immunological analyses were performed using standard protocols for nestin (Chemicon, 1:10,000), Tuj1 (Sigma, 1:5,000), GFAP (Dako, 1:1,000), OLIG2 (Santa Cruz, 1:1,000), HB9 (Hybrodoma bank, 1:100), ISLET1 (Hybrodoma bank, 1:100), ChAT (Chemicon, 1:250), SMI-32 (Covance, 1:500), SMN (4B7 (ref. 33), 1:10), and synapsin (Calbiochem, 1:250). Neuron counts and measurements were analysed using Metamorph software, and statistical calculations were performed using Prizm software.

Full Methods and any associated references are available in the online version of the paper at www.nature.com/nature.

Received 17 September; accepted 1 December 2008.
Published online 21 December 2008.

1. Lefebvre, S. *et al.* Identification and characterization of a spinal muscular atrophy-determining gene. *Cell* **80,** 155–165 (1995).
2. Coovert, D. D. *et al.* The survival motor neuron protein in spinal muscular atrophy. *Hum. Mol. Genet.* **6,** 1205–1214 (1997).
3. Crawford, T. O. & Pardo, C. A. The neurobiology of childhood spinal muscular atrophy. *Neurobiol. Dis.* **3,** 97–110 (1996).
4. Munsat, T. L. & Davies, K. E. International SMA consortium meeting. (26–28 June 1992, Bonn, Germany). *Neuromuscul. Disord.* **2,** 423–428 (1992).
5. Lorson, C. L., Hahnen, E., Androphy, E. J. & Wirth, B. A single nucleotide in the SMN gene regulates splicing and is responsible for spinal muscular atrophy. *Proc. Natl Acad. Sci. USA* **96,** 6307–6311 (1999).
6. Lefebvre, S. *et al.* Correlation between severity and SMN protein level in spinal muscular atrophy. *Nature Genet.* **16,** 265–269 (1997).
7. Schmid, A. & DiDonato, C. J. Animal models of spinal muscular atrophy. *J. Child Neurol.* **22,** 1004–1012 (2007).
8. Schrank, B. *et al.* Inactivation of the survival motor neuron gene, a candidate gene for human spinal muscular atrophy, leads to massive cell death in early mouse embryos. *Proc. Natl Acad. Sci. USA* **94,** 9920–9925 (1997).
9. DiDonato, C. J. *et al.* Cloning, characterization, and copy number of the murine survival motor neuron gene: homolog of the spinal muscular atrophy-determining gene. *Genome Res.* **7,** 339–352 (1997).
10. Hsieh-Li, H. M. *et al.* A mouse model for spinal muscular atrophy. *Nature Genet.* **24,** 66–70 (2000).
11. Monani, U. R. *et al.* The human centromeric survival motor neuron gene (*SMN2*) rescues embryonic lethality in $Smn^{-/-}$ mice and results in a mouse with spinal muscular atrophy. *Hum. Mol. Genet.* **9,** 333–339 (2000).
12. Le, T. T. *et al.* SMNΔ7, the major product of the centromeric survival motor neuron (*SMN2*) gene, extends survival in mice with spinal muscular atrophy and associates with full-length SMN. *Hum. Mol. Genet.* **14,** 845–857 (2005).
13. Park, I. H. *et al.* Reprogramming of human somatic cells to pluripotency with defined factors. *Nature* **451,** 141–146 (2008).
14. Jaenisch, R. & Young, R. Stem cells, the molecular circuitry of pluripotency and nuclear reprogramming. *Cell* **132,** 567–582 (2008).
15. Takahashi, K. *et al.* Induction of pluripotent stem cells from adult human fibroblasts by defined factors. *Cell* **131,** 861–872 (2007).
16. Yu, J. *et al.* Induced pluripotent stem cell lines derived from human somatic cells. *Science* **318,** 1917–1920 (2007).
17. Lowry, W. E. *et al.* Generation of human induced pluripotent stem cells from dermal fibroblasts. *Proc. Natl Acad. Sci. USA* **105,** 2883–2888 (2008).
18. Dimos, J. T. *et al.* Induced pluripotent stem cells generated from patients with ALS can be differentiated into motor neurons. *Science* **321,** 1218–1221 (2008).
19. Park, I. H. *et al.* Disease-specific induced pluripotent stem cells. *Cell* **134,** 877–886 (2008).
20. Jakel, R. J., Schneider, B. L. & Svendsen, C. N. Using human neural stem cells to model neurological disease. *Nature Rev. Genet.* **5,** 136–144 (2004).
21. Gavrilov, D. K., Shi, X. Y., Das, K., Gilliam, T. C. & Wang, C. H. Differential SMN2 expression associated with SMA severity. *Nature Genet.* **20,** 230–231 (1998).
22. Sumner, C. J. *et al.* SMN mRNA and protein levels in peripheral blood: biomarkers for SMA clinical trials. *Neurology* **66,** 1067–1073 (2006).
23. Fox, V. *et al.* Cell-cell signaling through NOTCH regulates human embryonic stem cell proliferation. *Stem Cells* **26,** 715–723 (2008).
24. Svendsen, C. N. *et al.* A new method for the rapid and long term growth of human neural precursor cells. *J. Neurosci. Methods* **85,** 141–152 (1998).
25. Lendahl, U., Zimmerman, L. B. & McKay, R. D. G. Cns stem-cells express a new class of intermediate filament protein. *Cell* **60,** 585–595 (1990).
26. Li, X. J. *et al.* Specification of motoneurons from human embryonic stem cells. *Nature Biotechnol.* **23,** 215–221 (2005).
27. Jessell, T. M. Neuronal specification in the spinal cord: Inductive signals and transcriptional codes. *Nature Rev. Genet.* **1,** 20–29 (2000).
28. Wichterle, H., Lieberam, I., Porter, J. A. & Jessell, T. M. Directed differentiation of embryonic stem cells into motor neurons. *Cell* **110,** 385–397 (2002).
29. Carriedo, S. G., Yin, H. Z. & Weiss, J. H. Motor neurons are selectively vulnerable to AMPA/kainate receptor-mediated injury *in vitro*. *J. Neurosci.* **16,** 4069–4079 (1996).
30. Monani, U. R. Spinal muscular atrophy: a deficiency in a ubiquitous protein; a motor neuron-specific disease. *Neuron* **48,** 885–896 (2005).
31. Brichta, L. *et al.* Valproic acid increases the SMN2 protein level: a well-known drug as a potential therapy for spinal muscular atrophy. *Hum. Mol. Genet.* **12,** 2481–2489 (2003).
32. Sumner, C. J. *et al.* Valproic acid increases SMN levels in spinal muscular atrophy patient cells. *Ann. Neurol.* **54,** 647–654 (2003).
33. Wolstencroft, E. C., Mattis, V., Bajer, A. A., Young, P. J. & Lorson, C. L. A non-sequence-specific requirement for SMN protein activity: the role of aminoglycosides in inducing elevated SMN protein levels. *Hum. Mol. Genet.* **14,** 1199–1210 (2005).
34. Pellizzoni, L., Yong, J. & Dreyfuss, G. Essential role for the SMN complex in the specificity of snRNP assembly. *Science* **298,** 1775–1779 (2002).
35. Fischer, U., Liu, Q. & Dreyfuss, G. The SMN–SIP1 complex has an essential role in spliceosomal snRNP biogenesis. *Cell* **90,** 1023–1029 (1997).
36. Liu, Q., Fischer, U., Wang, F. & Dreyfuss, G. The spinal muscular atrophy disease gene product, SMN, and its associated protein SIP1 are in a complex with spliceosomal snRNP proteins. *Cell* **90,** 1013–1021 (1997).
37. Carrel, T. L. *et al.* Survival motor neuron function in motor axons is independent of functions required for small nuclear ribonucleoprotein biogenesis. *J. Neurosci.* **26,** 11014–11022 (2006).
38. Zhang, H. *et al.* Multiprotein complexes of the survival of motor neuron protein SMN with gemins traffic to neuronal processes and growth cones of motor neurons. *J. Neurosci.* **26,** 8622–8632 (2006).

Supplementary Information is linked to the online version of the paper at www.nature.com/nature. A summary figure is also included.

Acknowledgements We thank J. Meyer for helpful discussions and B. Shelley, B. Heins and E. McMillan for technical assistance. We also thank WiCell Research Institute for karyotype analysis, Cell Line Genetics for DNA fingerprinting, R. Stewart, S. Tian and V. Ruotti at the Morgridge Institute for Research for microarray analysis, and Promega Corp. for qRT–PCR analysis (all at Madison, Wisconsin). The MNR2/HB9 (81.5C10) and the ISLET1 (40.2D6) monoclonal antibodies (both developed by T. Jessell) were obtained from the Developmental Studies Hybridoma Bank. Funding support was provided by the Amyotrophic Lateral Sclerosis Association (to C.N.S.), the National Institutes of Neurological Disorders and Stroke (P01NS057778 to C.N.S. and R01NS41584 to C.L.L.), National Institutes of Child Health and Human Development (R01HD054413 to C.L.L.), and National Institutes of General Medical Sciences (T32GM008396 for F.F.R.).

Author Contributions A.D.E. participated in all aspects and prepared the manuscript; J.Y. generated and aided in the characterization of iPS-SMA and iPS-WT clones; F.F.R., V.B.M. and C.L.L. performed SMN analysis and manuscript preparation; J.A.T. participated in the generation of the iPS clones; C.N.S. conceived the project and participated in planning, data analysis and manuscript preparation.

Author Information Microarray data have been deposited in GEO under accession number GSE13828. Reprints and permissions information is available at www.nature.com/reprints. Correspondence and requests for materials should be addressed to A.D.E. (ebert@waisman.wisc.edu) or C.N.S. (cnsvendsen@wisc.edu).

METHODS

iPS cell culture and lentiviral infection. iPS cells were maintained on irradiated mouse embryonic fibroblasts as previously described[16]. Fibroblast cells (GM03813 and GM03814, Coriell Inst.) were cultured in Minimum Essential Medium (Eagle) (Invitrogen) supplemented with 10% heat-inactivated fetal bovine serum (HyClone Laboratories). Lentiviral transduction of fibroblast cells was performed as previously described[16].

Neural differentiation. iPS spheres were generated by lifting intact iPS colonies from the feeder layers after collagenase treatment (1 mg ml^{-1}, Gibco) and placing them directly into a human neural progenitor growth medium (Stemline, Sigma) supplemented with 2% B27 (Gibco), 100 ng ml^{-1} basic fibroblast growth factor (bFGF, Chemicon), 100 ng ml^{-1} epidermal growth factor (EGF, Chemicon), and 5 μg ml^{-1} heparin (Sigma) in polyhema-coated flasks to prevent attachment and were passaged weekly using a chopping technique[24]. To induce neuron and astrocyte differentiation, spheres were dissociated with accutase (Chemicon) and plated onto poly-ornithine/laminin (Sigma)-coated coverslips in Stemline/2% B27 without bFGF, EGF and heparin for 1 week. To induce motor neuron differentiation, spheres were placed in neural induction medium (1:1 DMEM/F12 and 1% N2 supplement (Gibco)) in the presence of retinoic acid (0.1 μM) for 1 week followed by the addition of sonic hedgehog (SHH, 100 ng ml^{-1}, R&D) for another week. Spheres were then plated onto poly-ornithine/laminin-coated coverslips in retinoic acid and SHH medium supplemented with cAMP (1 μM), ascorbic acid (200 ng ml^{-1}), brain-derived neurotrophic factor and glial cell line-derived neurotrophic factor (both 10 ng ml^{-1}, PeproTech Inc.) for a further 2–6 weeks.

RNA isolation and PCR analysis. Total RNA was isolated using the RNeasy Mini Kit (Qiagen) with on-column DNase I digestion or Tri reagent (Sigma). Complementary DNA was generated from 1–4 μg total RNA using SuperScript III (Invitrogen). RT–PCR and/or qRT–PCR were performed using specific primer sequences (Supplementary Table 3). Full-length and Δ7 *SMN* products were gel purified and digested with Dde1 specifically cleaving *SMN2*, giving expected band sizes of 713 nucleotides (undigested full-length), 436 and 277 nucleotides (*SMN2* full-length), and 382 and 277 nucleotides (*SMN2* Δ7).

Karyotyping and DNA fingerprinting. Standard G-banding chromosome analysis was performed in the Cytogenetics Lab at WiCell Research Institute. To confirm the fibroblast origins of the iPS-SMA and iPS-WT cells, short tandem repeat (STR) analysis was performed by Cell Line Genetics.

Teratoma formation. Two 10-cm dishes of iPS-WT clone 4.2, iPS-SMA clone 3.5, and clone 3.6 (~50% confluent) grown on irradiated mouse embryonic fibroblasts were injected into the hind limb muscle of two mice. All iPS clones gave rise to teratomas. Control mice injected with $\sim 8.5 \times 10^6$ Fib-WT and 11×10^6 Fib-SMA failed to form teratomas. Haematoxylin and eosin staining of teratoma sections was performed after 7–10 weeks.

Microarray analysis. Human genome U133 Plus 2.0 GeneChip arrays carrying 54,675 probe sets (Affymetrix) were used for microarray hybridizations to examine the global gene expression. Approximately 3 μg of RNA from each sample was labelled using the MessageAmp Biotin II-Enhanced IVT kit (Ambion) following manufacturer's instructions. All arrays were hybridized at 45 °C for 16 h and scanned using an AFX GC3000 G7 scanner.

The gene expression raw data were extracted using the AFX Expression Console software. Quality control was done on the basis of Affymetrix quality control metrics. The qualified data sets were then analysed in the R statistical environment, freely available under the GNU General Public Licence (http://www.r-project.org) using bioconductor libraries (http://www.bioconductor.org). All chips were normalized by the quantile method[39] and background corrected using robust multi-array analysis (RMA)[40] followed by summarization using median polish[40] to get the probe set level measurement. A total of 54,675 probe sets was collapsed to 51,337 transcripts by taking the average log intensity values for probe sets representing common accession numbers. Hierarchical cluster analyses were carried out with 1-PCC (Pearson correlation coefficient) as the distance measurement. The maximum distance between cluster members was used as the basis to merge lower-level clusters (complete linkage) into higher-level clusters. Multiscale bootstrap resampling (10,000 bootstraps) was applied to the hierarchical clustering, *P* values of hypotheses were calculated, and bootstrap probabilities were determined for each cluster[41].

HeatMap generation and data visualization. For each gene, the average expression level was calculated across five normal human embryonic stem cell lines and the two SMA or wild-type fibroblast cell lines. The fold changes were calculated for all the genes in the SMA and wild-type fibroblast cell lines over the corresponding average in human embryonic stem cells. The top 25 genes most specifically expressed in SMA and wild-type fibroblasts and 30 genes that are known to be enriched in human embryonic stem cells were selected for the HeatMap generation. The log intensities of these 55 genes were standardized so that their expression values across all samples have mean 0 and standard deviation 1. The standardized values were reordered and displayed in a heat map, with the spectrum ranging from green (low level) to red (high level).

Immunocytochemistry. Cells were fixed in 4% paraformaldehyde or 1:1 acetone/methanol for 20 min at room temperature and rinsed with PBS. Nonspecific labelling was blocked and the cells were permeabilized with 5% normal goat serum and/or 5% normal donkey serum containing 0.2% Triton X-100 in PBS for 30 min at room temperature. Cells were rinsed with PBS and then incubated with primary antibodies for 1 h at room temperature or overnight at 4 °C. Cells were then labelled with the appropriate fluorescently tagged secondary antibodies. Hoechst nuclear dye was used to label nuclei. Gems were counted in 100 nuclei, and positively stained neurons were counted and measured on five areas on each of three coverslips using Metamorph software. All data were analysed using Prizm statistical software.

Protein isolation and western blot analysis. Cells were isolated, suspended in 1% Triton X-100 lysis buffer supplemented with 1% protease inhibitor cocktail (Sigma), triturated and centrifuged at 16,060*g* for 10 min at 4 °C. Ten to twenty micrograms of protein was separated on 12% SDS-polyacrylamide gel, transferred to a nitrocellulose membrane and probed with a primary antibody against SMN (mouse monoclonal), followed by a horseradish-peroxidase-conjugated secondary antibody (Promega), and then visualized using ECL chemiluminescence (Amersham). As a control, the membrane was stripped and re-probed for β-actin. For semiquantitative analysis, SMN signal intensity was analysed and corrected with respect to β-actin.

39. Bolstad, B. M., Irizarry, R. A., Astrand, M. & Speed, T. P. A comparison of normalization methods for high density oligonucleotide array data based on variance and bias. *Bioinformatics* **19**, 185–193 (2003).
40. Irizarry, R. A. *et al.* Exploration, normalization, and summaries of high density oligonucleotide array probe level data. *Biostatistics* **4**, 249–264 (2003).
41. Suzuki, R. & Shimodaira, H. Pvclust: an R package for assessing the uncertainty in hierarchical clustering. *Bioinformatics* **22**, 1540–1542 (2006).

ARTICLES

Photon capture and signalling by melanopsin retinal ganglion cells

Michael Tri H. Do[1,3], Shin H. Kang[1], Tian Xue[1,3], Haining Zhong[1]†, Hsi-Wen Liao[1]†, Dwight E. Bergles[1] & King-Wai Yau[1,2,3]

A subset of retinal ganglion cells has recently been discovered to be intrinsically photosensitive, with melanopsin as the pigment. These cells project primarily to brain centres for non-image-forming visual functions such as the pupillary light reflex and circadian photoentrainment. How well they signal intrinsic light absorption to drive behaviour remains unclear. Here we report fundamental parameters governing their intrinsic light responses and associated spike generation. The membrane density of melanopsin is 10^4-fold lower than that of rod and cone pigments, resulting in a very low photon catch and a phototransducing role only in relatively bright light. Nonetheless, each captured photon elicits a large and extraordinarily prolonged response, with a unique shape among known photoreceptors. Notably, like rods, these cells are capable of signalling single-photon absorption. A flash causing a few hundred isomerized melanopsin molecules in a retina is sufficient for reaching threshold for the pupillary light reflex.

In mammals, non-image-forming vision operates alongside conventional image-forming vision and drives processes such as the pupillary light reflex and circadian photoentrainment[1]. It is mediated largely by the intrinsically photosensitive retinal ganglion cells (ipRGCs)[2–5], which transmit signals from rods and cones but also are photoreceptors themselves—indeed, the only other known photoreceptors in mammals besides rods and cones[6]. IpRGCs express the pigment melanopsin[3,7–13] and depolarize to light[2], opposite to rods and cones but similar to most invertebrate photoreceptors. They are also less photosensitive than rods and cones[14,15]. Much fundamental information remains outstanding for these unique cells. First, their melanopsin content, which determines photon catch and therefore sensitivity, is unknown. The pigment content is difficult to measure biochemically or spectroscopically[16] because ipRGCs are sparse (~700 per mouse retina[3]), but it can be evaluated electrophysiologically if the response to a single absorbed photon is measurable. Second, the properties of this 'single-photon response' are unknown. This unitary response is the building block of all light responses, with its amplitude reflecting the signal amplification and its kinetics the phototransduction time course. Defining the single-photon-response kinetics is particularly important given the supposed bistability of melanopsin[9,11,12,17–19], whereby photon absorption by active melanopsin can revert it to the inactive state. Bistability can therefore terminate the photoresponse prematurely if two photons in the same stimulus are absorbed sequentially by the same melanopsin molecule. This complication is avoided for single-photon responses, thus revealing the full forward-phototransduction kinetics. Finally, the efficiency of signalling intrinsic light absorption by the ipRGCs is unknown. Unlike rods and cones, ipRGCs signal via spikes, so spike threshold can potentially limit sensitivity. We address all of these questions in this study.

Flash sensitivity of ipRGCs

To identify the sparse ipRGCs, we generated bacterial artificial chromosome (BAC)-transgenic mice[20] expressing the fluorescent protein tdTomato[21] (λ_{max} of 554 nm, far from 480 nm for melanopsin[2,10,22,23]), under the control of the melanopsin promoter (Supplementary Information S1 and Supplementary Fig. 1). The labelling was specific, and ipRGC properties seemed unaffected by tdTomato expression (Fig. 1; see also Supplementary Information S1). We used perforated-patch recording, which avoided washout of the photoresponse observed in whole-cell recording[2,24,25] (Supplementary Information S1), to make voltage-clamp measurements of current from *in situ* ipRGCs in flat-mount retinae (with synaptic blockers to eliminate rod and cone signals) or from dissociated cells.

A brief flash (one in which intensity and duration are interchangeable without affecting the response[26–28]) of increasing intensity elicited a transient inward current of progressively larger amplitude and shorter time-to-peak, the latter indicating light adaptation[27,29] (Fig. 2a, top panel; *in situ* cell, diffuse light covering the entire dendritic field). As with rods and cones, the Michaelis equation fit the peak intensity–response relationship[22,27] (open circles in Fig. 2a, bottom panel) but has no simple mechanistic interpretation because the time-to-peak changes with flash intensity[27,30]. The 'instantaneous' intensity–response relationship measured at a fixed time in the response rising phase[26,30] followed roughly a saturating exponential function (filled triangles in Fig. 2a, bottom panel), similar to rods[30]. One interpretation, albeit not unique, is that an active melanopsin molecule activates a spatially restricted domain within which transduction essentially saturates[30]. In any case, the intensity–response relationship had a linear foot, that is, the dim-flash responses had an invariant waveform and summed arithmetically (Fig. 2b; verified in 51 *in situ* and 13 dissociated cells), suggesting that the underlying single-photon response might be deducible from fluctuation analysis (see below).

The diffuse 480-nm flash intensity ($I_{1/2}$) that half-saturated the photoresponse was similar for *in situ* cells ($2.9 \pm 1.4 \times 10^7$ photons μm^{-2}, mean ± s.d., 3 cells) and dissociated cells (comprising mainly soma, $4.4 \pm 1.9 \times 10^7$ photons μm^{-2}, 6 cells) (Fig. 2c), suggesting comparable sensitivities of soma and dendrites, and no ill effect of the

[1]Solomon H. Snyder Department of Neuroscience, [2]Department of Ophthalmology, and [3]Center for Sensory Biology, The Johns Hopkins University School of Medicine, Baltimore, Maryland 21205, USA. †Present addresses: Janelia Farm Research Campus, HHMI, Ashburn, Virginia 20147, USA (H.Z.); Department of Neurobiology, Children's Hospital Boston, Harvard Medical School, Boston, Massachusetts 02115, USA (H.-W.L.).

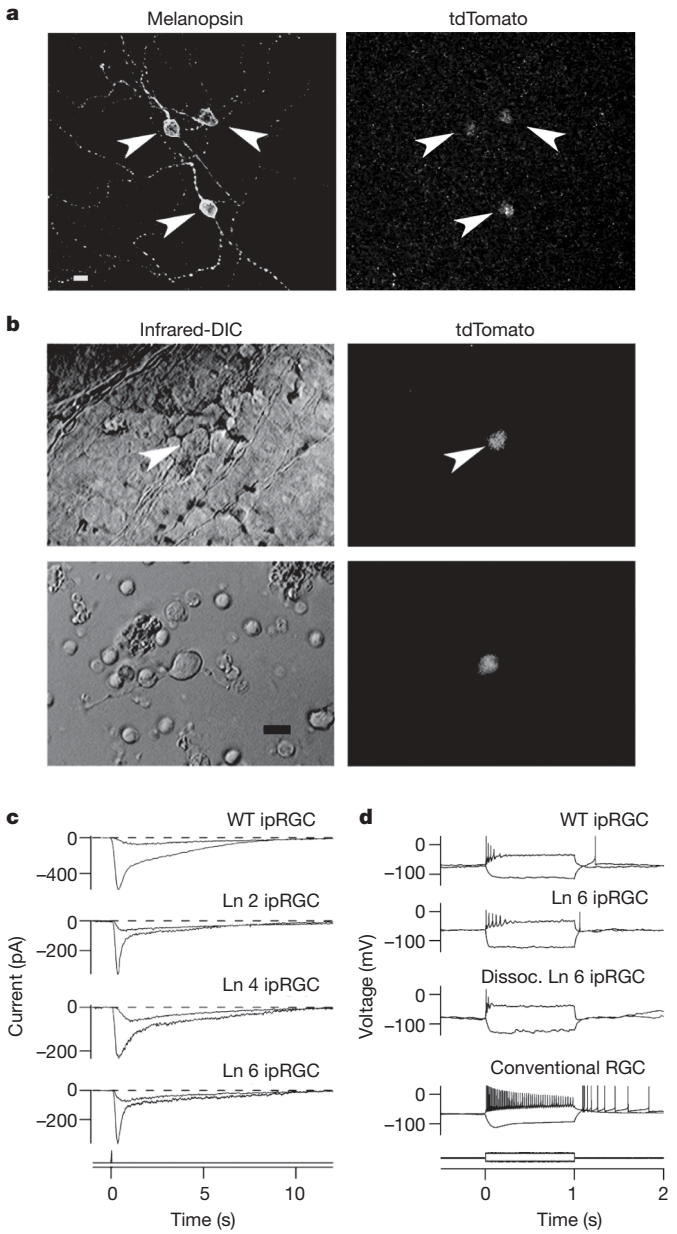

Figure 1 | IpRGCs of melanopsin–tdTomato transgenic mice. **a**, Stacked confocal view of ipRGCs (transgenic line 6 (Ln 6); Supplementary Information S1) in flat-mount transgenic retina, showing melanopsin immunoreactivity and tdTomato fluorescence. **b**, Top panels: live *in situ* (line 6) tdTomato cell in flat-mount retina (inner limiting membrane overlying cell removed); bottom panels: live, dissociated tdTomato cell. Infrared-DIC (left) and tdTomato fluorescence (right) are shown. Scale bars: 10 μm. **c**, Whole-cell or perforated-patch recordings of intrinsic photoresponses to dim and bright flashes (at time 0) from *in situ* wild-type (WT) ipRGCs (retrograde-labelled from the suprachiasmatic nucleus) and tdTomato ipRGCs of three transgenic lines (lines 2, 4 and 6). 50-ms flash; −80 mV holding voltage. **d**, Responses to current injection recorded from retrograde-labelled wild-type ipRGC, *in situ* and dissociated tdTomato ipRGCs (line 6), and conventional RGC retrograde-labelled from optic chiasm. Current monitor is shown below. Steady injected current gave ~−70 mV resting voltage and stimulus currents were adjusted to give similar membrane polarization for all cells. Temperature, 23 °C. Synaptic blockers were present for *in situ* cells.

dissociation procedure. The variation in $I_{1/2}$ values could reflect subpopulations of ipRGCs with different sensitivities[23,31] (we targeted small cells, with brighter tdTomato fluorescence). These $I_{1/2}$ values are ~10^6 times that of mouse rods[32] and ~10^4 times that of mouse cones[33].

Single-photon response

To determine if the low sensitivity of ipRGCs came from a low amplification in phototransduction, we estimated the single-photon response by fluctuation analysis[34]. We illuminated an ipRGC with repeated, identical flashes in the linear range (Fig. 3a; dissociated cell, diffuse light; complete response trials in Supplementary Fig. 2) and computed the response ensemble mean, $m(t)$, and variance, $\sigma^2(t)$ (Fig. 3b, middle and top panels). The time courses of $m^2(t)$ and $\sigma^2(t)$ were similar (Fig. 3b, bottom panel), not inconsistent with trial-to-trial fluctuations arising predominantly from stochastic variations in the number of absorbed photons, with each photon giving a stereotypical unitary response. Recording stability (Fig. 3c, top panel) allowed the fluctuations to be quantified, with the σ^2/m ratio at response peak giving a unitary amplitude of 0.4 pA. As expected, the measured amplitude histogram broadly fit the Poisson distribution predicted from this σ^2/m value (Fig. 3c, bottom panel) (Methods). From four dissociated cells with diffuse light, σ^2/m was 0.3 ± 0.1 pA (mean ± s.d.). *In situ* cells stimulated with a 40- or 100-μm light spot centred on the soma gave a similar σ^2/m of 0.4 ± 0.3 pA (10 cells), as did dendritic stimulation with a 40-μm spot centred at 100 μm from the soma ($\sigma^2/m = 0.3 \pm 0.2$ pA, 4 cells) (Fig. 3d). 620- or 420-nm light produced the same σ^2/m as well (Fig. 3d). Some dispersion in the σ^2/m value was probably due to the limited number of trials achievable. As expected, σ^2/m was independent of m within the linear range (Fig. 3e, 5 cells).

To support the above analysis, we tried to observe the single-photon response directly by using a flash so dim that most trials elicited no response or just one unit. We experimented at 35 °C, which made the dim-flash responses faster and larger by ~3-fold (see below and Fig. 4b), although stable recordings were rare. The light response showed all-or-none behaviour, with a high probability of failure (black traces in Fig. 3f; *in situ* ipRGC, local 40-μm spot on soma; only partial series shown, see Supplementary Fig. 3 for complete trials). In Fig. 3f, the unitary amplitude from σ^2/m was 2.3 pA. The grey traces give the expected unitary-response profile (see legend). Comparing this profile to each response yielded the apparent failures (indicated by an asterisk) and uncertain failures (absent in trials shown; see Supplementary Information S1 for detections based on the criteria of current, charge and a least-squares fit). Some responses matched the profile well, indicating that they were singletons. The mean number of unitary responses per flash (that is, the mean 'quantal content' of the response), ζ, was given by $m^2/\sigma^2 = 0.31$. From the Poisson distribution (Methods), the predicted probability of failure, P_0, was $P_0 = e^{-\zeta} = 0.74$, similar to the observed P_0 (0.74 in Fig. 3f with apparent failures counted, and 0.85 if uncertain failures are also included). This agreement supported the identification of the unitary response. The non-zero peak in the amplitude histograms (Fig. 3g) also roughly matched the σ^2/m value. Two other experiments are shown in Supplementary Fig. 4. Altogether, seven *in situ* cells at 35 °C gave similar results: the predicted/observed P_0 ratio being 0.96 ± 0.17 with apparent failures counted, and 0.79 ± 0.11 with uncertain failures also included, suggesting accurate detection of the unitary response. The unitary response was 0.7–2.5 pA (mean ± s.d. = 1.6 ± 0.8 pA) from σ^2/m and 0.6–2.8 pA (1.5 ± 0.8 pA) from identified singletons. These values approximated the 1.0–1.3 pA from correcting the mean unitary response (0.3–0.4 pA, see earlier) at room temperature (23 °C) to 35 °C by multiplying by 3 (see below and Fig. 4b), supporting the overall quantal analysis. On the basis of the current–voltage relationship for the light response[24], a unitary amplitude of ~1.5 pA should decrease by at most ~30% (to ~1 pA) on correcting from our holding voltage of −80 mV to the physiological membrane potential (presumably as high as −30 mV, because the ipRGCs showed basal firing; see Supplementary Information S7).

A single-photon response of ~1.0 pA (35 °C) is larger than that of mouse rods[35] and ~100 times that of ground-squirrel cones[36]. For dissociated cells (consisting largely of soma), the saturated response to bright flashes was 80 ± 70 pA (6 cells) at 23 °C. A unitary response of 0.3–0.4 pA at 23 °C is thus ~1% of maximum. With a surface area of

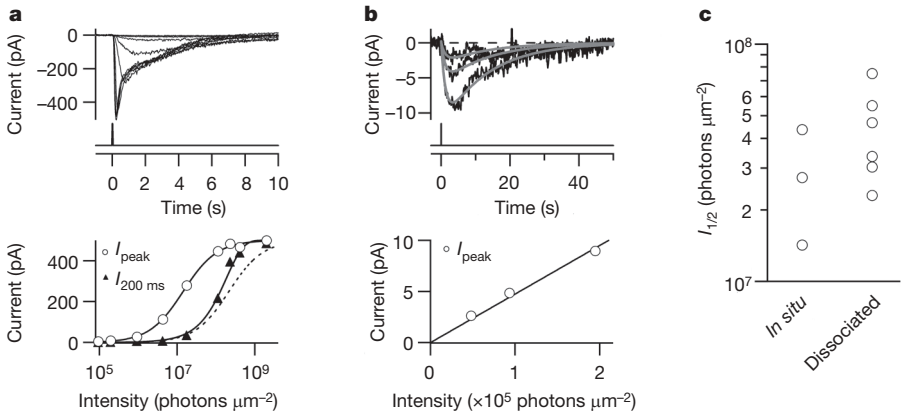

Figure 2 | Intensity–response relationships of ipRGCs. **a**, Top: responses of an *in situ* tdTomato-labelled cell to diffuse 50-ms flashes at different intensities. Light monitor is shown below. Flashes were at 480 nm except for the brightest three flashes, which were white but converted to equivalent 480-nm light (Methods). Bottom: intensity–response relationships plotted from the top panel. Open circles, peak response–intensity relationship fit with Michaelis equation, $R = R_{max}I/(I + I_{1/2})$, with $R_{max} = 500$ pA and $I_{1/2} = 1.8 \times 10^7$ photons μm^{-2}. Filled triangles, instantaneous intensity–response relationship at 200 ms from flash onset, fit with a saturating exponential function, $1-e^{-I/I_0}$, with $I_0 = 2.1 \times 10^8$ photons μm^{-2}. The dashed curve is a Michaelis fit aligned for comparison with saturating exponential fit. **b**, Top: three smallest (dim-flash) responses from **a**, elicited by successive approximate doublings of flash intensity, on expanded ordinate and longer time base. Fits are $A(e^{-t/1.3} - e^{-t/12.9})$ with A = −12.2, −5.9 and −3.0 pA, respectively (see Fig. 4a), according to the relative flash intensities. Bottom: peak intensity–response relationship from the top panel, fit with a straight line through the origin to indicate linearity. **c**, Collected $I_{1/2}$. For *in situ* cells, $I_{1/2}$ was measured as in **a**. For dissociated cells, $I_{1/2}$ was calculated from dim and saturated responses based on the Michaelis equation. All diffuse illumination; perforated-patch recording. Holding voltage, −80 mV; temperature, 23 °C. Synaptic blockers were present for *in situ* cells.

520 ± 80 μm^2 for three dissociated cells (from capacitance measurements), and assuming homogeneity, the transduction domain for one photon therefore would span ~5 μm^2 or more on the somatic surface. The saturated response of *in situ* cells to diffuse light was 490 ± 110 pA (3 cells, 23 °C), or ~10 times that of dissociated cells and matching the ratio between total and somatic surface areas of rodent ipRGCs (Supplementary Information S6). Thus, phototransduction seems uniform over the entire cell surface.

Kinetics of single-photon response

The single-photon response of ipRGCs was very slow, especially in the decline phase. The response waveform followed the convolution of two single-exponential decays (Fig. 4a, top panel; time constants of 1.0 s and 14.1 s, 23 °C), simpler than four stages for the rod response[34] or five stages for the cone response[36]; the quantum bumps of invertebrate photoreceptors are likewise more complex[37,38] (Supplementary Information S8). This kinetics was quite stereotyped (Fig. 4a, bottom panel, 20 cells, with average time constants of 1.5 s (±1.0 s) and 17.3 s (±6.8 s), *in situ* or dissociated, 23 °C). Two time constants does not necessarily mean that phototransduction in ipRGCs has only two steps, but rather that there are two particularly slow steps, the nature of which are unknown. When acutely warmed from 23 °C to 35 °C, the dim-flash response increased in size by 3.2 ± 1.0 times and in speed by ~3 times (Fig. 4b; time constants of 0.4 ± 0.2 s and 6.6 ± 4.4 s at 35 °C, 5 cells). The response integration time (t_i), a measure of its effective duration and given by $\int f(t)dt/f_p$, where $f(t)$ is the waveform and f_p is its transient peak amplitude[39], was 21.7 ± 6.7 s (20 cells) at 23 °C and 7.6 ± 3.5 s (5 cells) at 35 °C. The t_i at 35 °C was 20 times that of mouse rods[32] and >100 times that of rodent cones[33,36].

For a dim flash eliciting few unitary responses, the probability of two photons hitting the same melanopsin molecule is extremely small (Supplementary Information S5), so the kinetics of the dim-flash response (and the single-photon response) should only reflect forward phototransduction. This property explains the spectral univariance of the dim-flash response amplitude (see earlier) and kinetics (Fig. 4c), as in rods[34]. The response kinetics was similar for dissociated cells and *in situ* cells stimulated at the dendrites, suggesting little distortion of these small and slow currents by cell geometry and space-clamp issues (Supplementary Information S1).

Melanopsin density

To estimate membrane pigment density, we asked how many incident photons (I_ϕ) were required for a unitary response. From the 11 *in situ* cells giving σ^2/m estimates with a 40-μm spot (23 °C or 35 °C), $I_\phi = 1.2 \times 10^4$–2.7×10^6 (mean ± s.d. $= 3.7 \pm 7.8 \times 10^5$) photons μm^{-2} (480 nm). Some I_ϕ value spread might be due to the 40-μm spot (smallest possible aperture) stimulating the variable proximal dendrites (Supplementary Information S6). From six dissociated cells with diffuse light (23 °C), $I_\phi = 1.2$–5.6×10^5 ($3.4 \pm 1.5 \times 10^5$) photons μm^{-2}. Thus, *in situ* and dissociated cells both gave $I_\phi \approx 4 \times 10^5$ photons μm^{-2} for the soma. The pigment density, ρ_m, can be calculated from $r^2 I_\phi \rho_m \times 3 \times 10^{-8} = 1$, or $\rho_m = 10^8/(3r^2 I_\phi)$, where r is somatic radius (Methods). Adopting $r \approx 5$ μm, we obtained $\rho_m \approx 3$ μm^{-2}, best viewed as an order-of-magnitude estimate (Methods and Supplementary Information S2 and S3). This value is 10^4-fold lower than the pigment density in rods and cones (~25,000 μm^{-2}; ref. 40). The melanopsin density on dendrites should be similar (Methods), suggested also by the comparable melanopsin immunostainings on soma and dendrites[3,8,41].

High-efficiency signalling to the brain

To examine the efficiency of signalling by ipRGCs, we recorded spikes from *in situ* cells in the flat-mount retina (with synaptic blockers present; see earlier) using loose-patch recording for minimal perturbation (Methods; 35 °C). IpRGCs spiked spontaneously in darkness (2.3 ± 2.0 Hz, range 0.2–9.5 Hz, 19 cells; Supplementary Information S7). In Fig. 5, a flash (40-μm spot centred on soma) transiently increased spike rate at intensities of 1.9×10^4 photons μm^{-2} (480 nm) and higher. From three cells, the threshold was $1.9 \pm 3.0 \times 10^5$ photons μm^{-2}, producing a transient peak firing rate of 7.7 ± 1.2 Hz. Remarkably, this threshold intensity approximates the $\sim 4 \times 10^5$ photons μm^{-2} required for triggering a single-photon response (previous section), suggesting that ipRGCs can signal single-photon absorption to the brain.

From ipRGC signalling to behaviour

We compared the intrinsic sensitivity of a single ipRGC to the behavioural threshold for the melanopsin system, using the pupillary light reflex as a model[14,15,42].

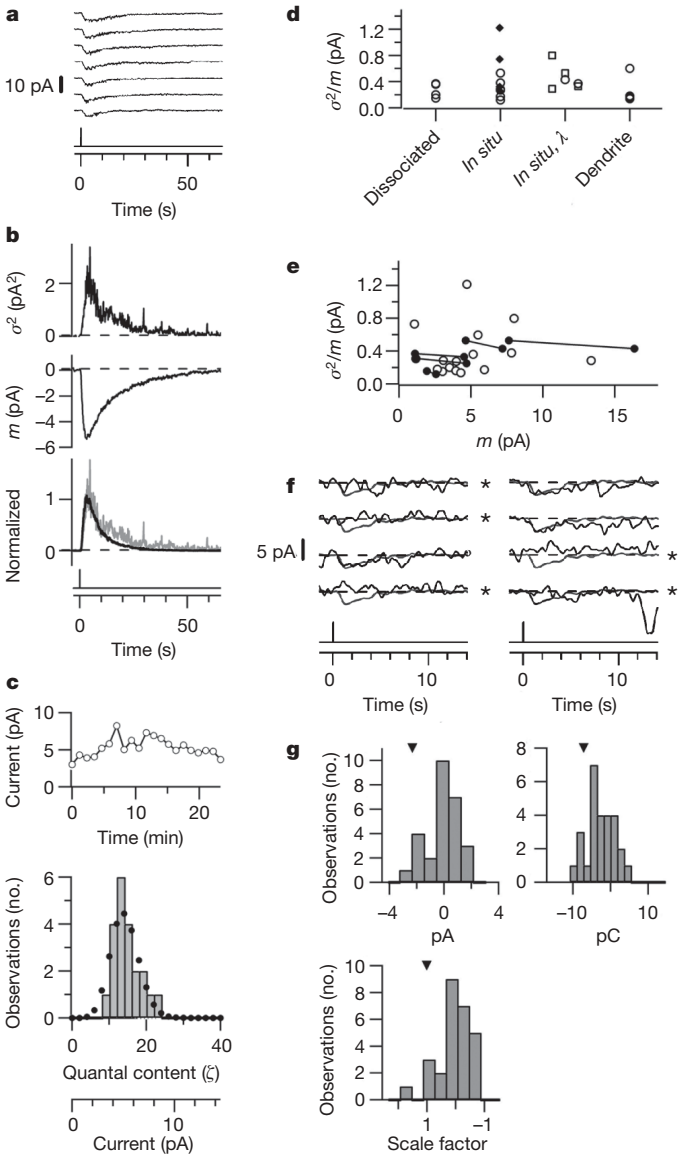

Figure 3 | Single-photon response of ipRGCs. **a**–**e**, Fluctuation analysis of dissociated ipRGC at 23 °C; **f**, **g**, Directly resolved single-photon response from *in situ* ipRGC at 35 °C. **a**, Partial series of responses to identical dim flashes (full series in Supplementary Fig. 2). 50-ms, 480-nm diffuse flash delivering 6.2×10^6 photons μm^{-2}. **b**, Top and middle: response ensemble variance, $\sigma^2(t)$, and mean, $m(t)$. Bottom, overlaid and scaled $\sigma^2(t)$ and $m^2(t)$ showing similar waveforms. **c**, Top: response amplitudes over time to indicate stationarity. Bottom: amplitude histogram (bars). The dotted profile is the Poisson distribution from $\zeta = m^2/\sigma^2 = 13.5$ (see Methods). **d**, Collected σ^2/m values. 'Dissociated', diffuse light; '*In situ*', 40-μm spot (filled diamonds) and 100-μm spot (open circles); '*In situ*, λ', 100-μm spot at 620 nm (left, open squares) or 620 nm/420 nm compared for a given cell (paired square/circle on middle and right); *in situ* 'Dendrite', 40-μm spot at 100 μm from soma. **e**, σ^2/m values from **d** plotted against m. Same-cell measurements are connected by lines. **f**, Partial series of responses of an *in situ* ipRGC to identical flashes (full series in Supplementary Fig. 3), mostly too dim to elicit a response. Temperature, 35 °C. 8.2×10^5 photons μm^{-2} at 480 nm, 40-μm spot. The single-photon response from σ^2/m was 2.3 pA. The grey trace superimposed on each trial (black trace) is the mean response to a dim flash fourfold brighter (for better resolution) and scaled to 2.3 pA, thus representing the expected profile of the unitary response. Apparent failures marked by an asterisk were judged according to three detection algorithms (Supplementary Information S1). **g**, Histograms from complete trial series based on the algorithms over a ~2-s window capturing the peak of the expected unitary–response profile. Arrowheads indicate the respective parameters of expected unitary profile.

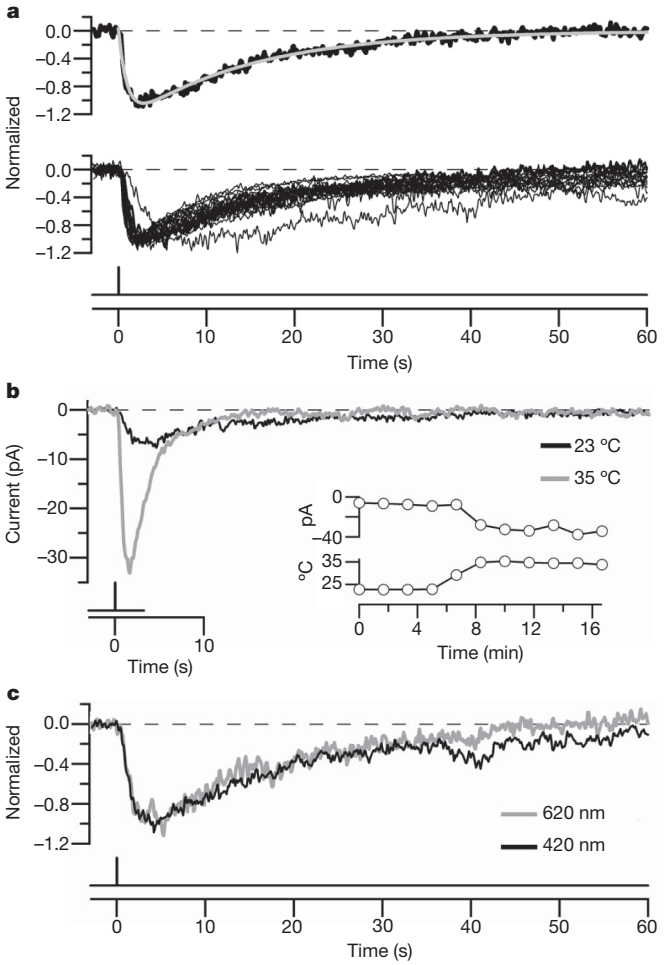

Figure 4 | Kinetics of dim-flash response. **a**, Top: dim-flash response at 23 °C fit with the convolution of two single-exponentials, $A(e^{-t/\tau_1} - e^{-t/\tau_2})$, with $A = -1.4$, $\tau_1 = 1.0$ s and $\tau_2 = 14.2$ s. Bottom: normalized and superposed dim-flash responses at 23 °C from 20 *in situ* or dissociated ipRGCs used in σ^2/m measurements (and with $m \geq 2$ pA for better signal resolution). Dissociated cells, diffuse illumination; i*n situ* cells, 40- or 100-μm spot centred on soma, or 40-μm spot on dendrites. The reason for the unusually slow kinetics of one cell is unknown. **b**, Dim-flash responses of an *in situ* ipRGC at 23 °C and 35 °C. Inset: time course of the same experiment showing peak photocurrent above and temperature below. Diffuse illumination. **c**, Normalized dim-flash responses of an *in situ* ipRGC stimulated with interleaved 420 nm and 620 nm light. 100-μm spot; 200-ms flash.

We first noted that, with diffuse light, the flash intensity for triggering a single-photon response in an *in situ* ipRGC should be ~10-fold lower than with somatic stimulation alone, the ratio between *in situ* cell area to somatic area being ~10 (Supplementary Information S6). Sensitivity also increases 3.5-fold after chromophore application (Supplementary Information S2 and Supplementary Fig. 5). Thus, for diffuse light under full dark adaptation, the flash intensity for a single-photon response (hence signalling to the brain) is $\sim 4 \times 10^5 / 35 = 11{,}000$ photons μm^{-2}. With a continuous step of light (not shown), the corresponding threshold intensity was, after correction, $1{,}510 \pm 1{,}490$ photons $\mu m^{-2} s^{-1}$ (4 cells), consistent with the 1,375 photons $\mu m^{-2} s^{-1}$ from dividing the above flash threshold of 11,000 photons μm^{-2} by the 8-s integration time. Both values are similar to the ~1,000 photons $\mu m^{-2} s^{-1}$ measured with multielectrode-array recording from dark-adapted *rd/rd* mouse retina[23] (with all rods and most cones degenerated), which used diffuse light and did not require fluorescence for ipRGC identification.

For the consensual pupillary light reflex (Methods and Fig. 6a), we used a *Gnat1*$^{-/-}$ *cl* mouse[43], with non-transducing rods and diphtheria-toxin-ablated cones (a more thorough cone removal than the *rd/rd* line)

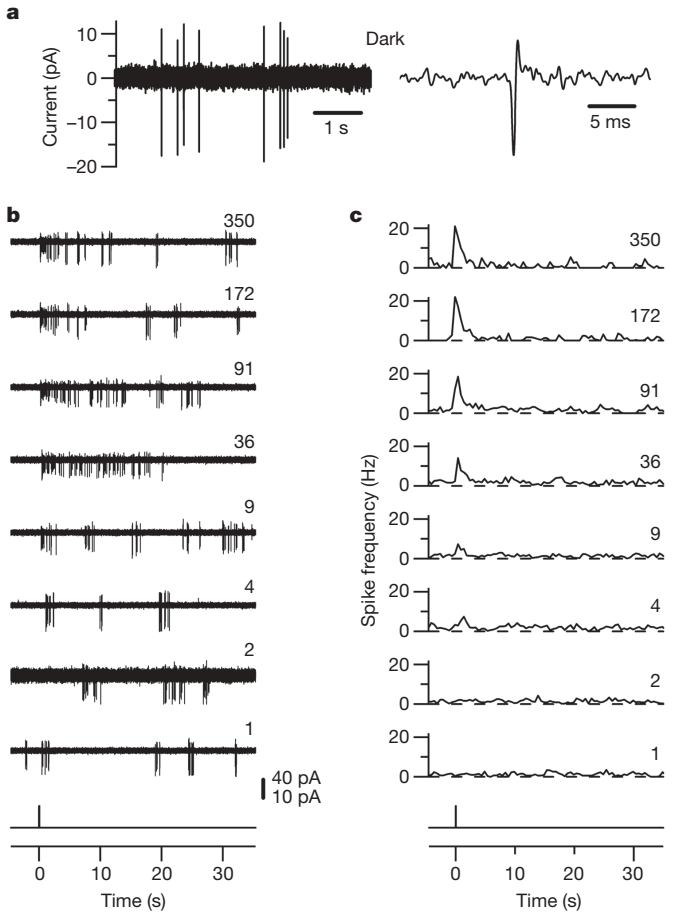

Figure 5 | Flash threshold for modulation of ipRGC spike frequency. Loose-patch recordings from an *in situ* ipRGC at 35 °C. **a**, Left: spontaneous firing in darkness. Right: a single spike from the left panel on an expanded abscissa. **b**, Effect of different-intensity flashes (50 ms, 480 nm, 40-μm diameter spot centred on soma). Flash monitor is shown at the bottom. Relative flash intensity is indicated on the right of each trace. 40-pA scale bar for all traces except relative intensity '2', where it is 10 pA owing to a transient decrease in contact resistance with the cell. **c**, Peri-stimulus time histograms for flash intensities in **b**. 4–15 trials averaged, 500-ms bins. Threshold modulation of spike frequency occurs at the relative flash intensity '4', or 1.9×10^4 photons μm^{-2}.

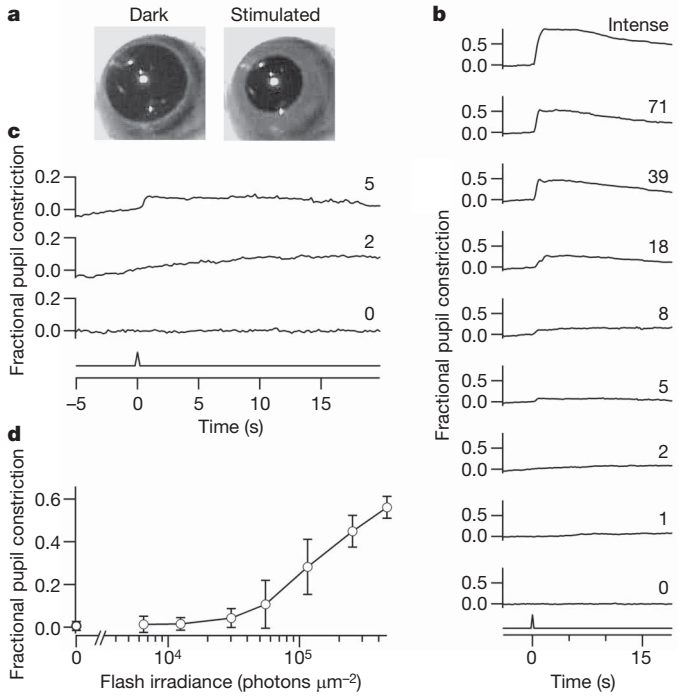

Figure 6 | Flash threshold for ipRGC-driven consensual pupillary light reflex. Unanaesthetized *Gnat1*$^{-/-}$*cl* mice. **a**, Infrared image of pupil before and after an intermediate-intensity flash. **b**, Pupil reflex at the relative flash intensities indicated (50 ms; 480 nm except for 'intense', which was white). Ordinate: maximum pupillary constriction within 2 s after flash, averaged over 800 ms. Traces are averages from six mice. Fractional pupil constriction: '0' refers to mean dark pupil area (3.7 mm^2) during 1 s preceding flash; '1' refers to mean minimal pupil area (0.5 mm^2) elicited with a step of white light. **c**, Reflex measurements on expanded axes for three selected traces in **b**: no flash ('0'), just below reflex threshold ('2'), and at reflex threshold ('5'), with the last corresponding to a corneal flash irradiance of 30,200 photons μm^{-2}. **d**, Fractional constriction plotted against corneal flash irradiance. Error bars are s.d.

to isolate the melanopsin signal. To correlate strictly with single-cell recordings, we stimulated the dark-adapted eye also with 50-ms flashes (Fig. 6b). Pupil constriction was first detectable (~4% of maximal constriction) at a corneal Ganzfeld flash irradiance (480 nm) of 3×10^4 photons μm^{-2} (6 mice averaged). Dividing this threshold irradiance by the integration time (8 s) of the dim-flash response gives a predicted corneal steady irradiance of ~3,750 photons $\mu m^{-2}\,s^{-1}$ at reflex threshold, comparable to previous measurements on an analogous mouse line (*rd/rd cl*; ref. 14).

The corneal flash irradiance of 3×10^4 photons μm^{-2} corresponds to a diffuse intraocular flash intensity of 7,200 photons μm^{-2} (Supplementary Information S1). Because 11,000 photons μm^{-2} were required for a single-photon response (see earlier), the mean number of single-photon responses per ipRGC at reflex threshold was 7,200/11,000 ~ 0.7. With ~700 ipRGCs per retina[3], this threshold corresponds to ~500 single-photon responses over all ipRGCs (or lower: see Supplementary Information S2). With both eyes stimulated, it would be ~250 per eye because the pupillary light reflex is bilaterally driven[44]. How many ipRGCs are activated at this reflex threshold? From the Poisson distribution, the probability of one or more single-photon responses in any ipRGC is $1 - P_0 = 1 - e^{-0.7} = 0.5$, or ~350 cells. Depending on how ipRGC signals are processed at the olivary pretectal nucleus[3] and beyond, a few intense-firing ipRGCs may be equally effective.

Conclusions

This work provides a quantitative foundation for understanding ipRGCs, including basic parameters governing their absolute sensitivity. Their single-photon response is even larger than that of rods. The extremely slow response kinetics provides long temporal integration and suits non-image-forming visual functions, where high temporal resolution is non-critical or even undesirable. The density of melanopsin seems to be exceedingly low, with just several molecules per square micrometre of surface membrane. Compounded by the lack of pigment-containing intracellular membrane stacks[41], the photon-capture probability of ipRGCs is more than 10^6-fold lower than that of rods and cones per unit area of retinal illumination. In principle, the melanopsin density could increase by orders of magnitude without degrading the image on the underlying rods and cones. However, ipRGCs may not need high intrinsic sensitivity. First, rod and cone pathways do drive these cells synaptically at low light levels[22,41,45,46]. Second, at least the pupillary light reflex is specifically designed for higher light levels. Even with circadian photoentrainment, it is not obvious that high photosensitivity is an advantage.

Remarkably, a single absorbed photon is sufficient for the spike-generating ipRGC to signal to the brain—as efficient as rods, which signal in analogue fashion. The ipRGC achieves this feat by operating near spike threshold in darkness, firing spontaneously at a low rate, such that the small depolarization (~1 mV) caused by one photon can increase the spike rate by several-fold. The slow decay of the response also prolongs this effect. Some dissociated ipRGCs fired

spontaneously, suggesting that this is an intrinsic property, perhaps expressly for high-efficiency signalling. From the Poisson distribution, the signalling efficiency of ipRGCs at low light intensities is exceedingly sensitive to the threshold number of absorbed photons required for spike modulation. Even a small elevation of this threshold would decrease light signalling efficiency by orders of magnitude (Supplementary Information S9).

As an exemplary non-image-forming visual function at the system level, the pupillary light reflex first appeared with several hundred photoisomerized melanopsin molecules over the entire retina, corresponding to about the same number of activated ipRGCs. This threshold number of active ipRGCs is considerably higher than the several rods, and therefore ganglion cells, active at the psychophysical threshold of light detection by a dark-adapted human subject[47]. However, with respect to the pupil reflex, the number of rods and ganglion cells active at threshold in the wild-type mouse is probably very much higher as well (Supplementary Information S10). In other words, the number of required driver cells is task-specific.

METHODS SUMMARY

To label ipRGCs, a linearized mouse BAC[20] containing *tdTomato* was injected into B6SJL embryos, with transgenics backcrossed to C57BL/6J. Melanopsin immunostaining[3] confirmed specific expression. For recordings, mice (~P20–90) were dark-adapted overnight, anaesthetized, enucleated and killed. The retina was flat-mounted or dissociated (Supplementary Information S1). Aerated, heated bicarbonate-buffered Ames' solution, containing synaptic blockers for flat-mount experiments, ran at ~5 ml min^{-1} through a 1-ml chamber. IpRGCs were visualized with seconds of fluorescence followed by infrared differential interference contrast (DIC) (Supplementary Information S1). Patch-clamp recordings used a KCl-based pipette solution (pH 7.2; see Methods) supplemented with (in mM): 2 glutathione, 4 MgATP, and 0.3 Tris-GTP for whole-cell recordings or, alternatively, 125–250 μM amphotericin B for perforated-patch recording. For loose-patch recordings, the pipette contained HEPES-buffered Ames' solution. Pipettes were parafilm-wrapped, and an Axopatch 200B in voltage-clamp or fast-current-clamp was used (Supplementary Information S1). Recording stability was checked periodically with a test flash, and series resistance monitored. V_{hold} was −80 mV, initially for improving signal resolution, although the photocurrent current–voltage relationship was later shown to be rather shallow between −90 mV and −30 mV (ref. 24). Liquid-junction potential was corrected. Photocurrent was low-pass filtered at 2 Hz (dim flashes) or 10 Hz (bright flashes) and membrane voltage at 10 kHz. Loose-patch recording bandwidth was 10 Hz–1 kHz, sometimes with a notch filter. Sampling exceeded the Nyquist minimum. Flashes (10-nm bandwidth or occasionally white) were diffuse (730-μm diameter spot) or local (40- or 100-μm diameter), temporally spaced for full recovery between flashes (30–120 s). White flashes, for response saturation, were converted to equivalent 480-nm flashes by response matching (Supplementary Information S1). Consensual pupillary light reflex measurements followed previous work[14], with one eye of the unanaesthetized mouse videoed under infrared and the other stimulated by Ganzfeld light (Supplementary Information S1). Data are mean ± s.d.

Full Methods and any associated references are available in the online version of the paper at www.nature.com/nature.

Received 4 September; accepted 8 December 2008.
Published online 31 December 2008.

1. Hankins, M. W., Peirson, S. N. & Foster, R. G. Melanopsin: an exciting photopigment. *Trends Neurosci.* **31,** 27–36 (2008).
2. Berson, D. M., Dunn, F. A. & Takao, M. Phototransduction by retinal ganglion cells that set the circadian clock. *Science* **295,** 1070–1073 (2002).
3. Hattar, S., Liao, H. W., Takao, M., Berson, D. M. & Yau, K. W. Melanopsin-containing retinal ganglion cells: architecture, projections, and intrinsic photosensitivity. *Science* **295,** 1065–1070 (2002).
4. Guler, A. D. *et al.* Melanopsin cells are the principal conduits for rod–cone input to non-image-forming vision. *Nature* **453,** 102–105 (2008).
5. Hatori, M. *et al.* Inducible ablation of melanopsin-expressing retinal ganglion cells reveals their central role in non-image forming visual responses. *PLoS ONE* **3,** e2451 (2008).
6. Hattar, S. *et al.* Melanopsin and rod-cone photoreceptive systems account for all major accessory visual functions in mice. *Nature* **424,** 76–81 (2003).
7. Provencio, I., Jiang, G., De Grip, W. J., Hayes, W. P. & Rollag, M. D. Melanopsin: An opsin in melanophores, brain, and eye. *Proc. Natl Acad. Sci. USA* **95,** 340–345 (1998).
8. Provencio, I., Rollag, M. D. & Castrucci, A. M. Photoreceptive net in the mammalian retina. This mesh of cells may explain how some blind mice can still tell day from night. *Nature* **415,** 493 (2002).
9. Melyan, Z., Tarttelin, E. E., Bellingham, J., Lucas, R. J. & Hankins, M. W. Addition of human melanopsin renders mammalian cells photoresponsive. *Nature* **433,** 741–745 (2005).
10. Qiu, X. *et al.* Induction of photosensitivity by heterologous expression of melanopsin. *Nature* **433,** 745–749 (2005).
11. Panda, S. *et al.* Illumination of the melanopsin signaling pathway. *Science* **307,** 600–604 (2005).
12. Fu, Y. *et al.* Intrinsically photosensitive retinal ganglion cells detect light with a vitamin A-based photopigment, melanopsin. *Proc. Natl Acad. Sci. USA* **102,** 10339–10344 (2005).
13. Gooley, J. J., Lu, J., Chou, T. C., Scammell, T. E. & Saper, C. B. Melanopsin in cells of origin of the retinohypothalamic tract. *Nature Neurosci.* **4,** 1165 (2001).
14. Lucas, R. J. *et al.* Diminished pupillary light reflex at high irradiances in melanopsin-knockout mice. *Science* **299,** 245–247 (2003).
15. Panda, S. *et al.* Melanopsin is required for non-image-forming photic responses in blind mice. *Science* **301,** 525–527 (2003).
16. Walker, M. T., Brown, R. L., Cronin, T. W. & Robinson, P. R. Photochemistry of retinal chromophore in mouse melanopsin. *Proc. Natl Acad. Sci. USA* **105,** 8861–8865 (2008).
17. Qiu, X. & Berson, D. M. Melanopsin bistability in ganglion cell photoreceptors. *Invest. Ophthalmol. Vis. Sci.* **48,** E-Abstract 612 (2007).
18. Koyanagi, M., Kubokawa, K., Tsukamoto, H., Shichida, Y. & Terakita, A. Cephalochordate melanopsin: evolutionary linkage between invertebrate visual cells and vertebrate photosensitive retinal ganglion cells. *Curr. Biol.* **15,** 1065–1069 (2005).
19. Mure, L. S., Rieux, C., Hattar, S. & Cooper, H. M. Melanopsin-dependent nonvisual responses: evidence for photopigment bistability *in vivo*. *J. Biol. Rhythms* **22,** 411–424 (2007).
20. Yang, X. W., Model, P. & Heintz, N. Homologous recombination based modification in *Escherichia coli* and germline transmission in transgenic mice of a bacterial artificial chromosome. *Nature Biotechnol.* **15,** 859–865 (1997).
21. Shaner, N. C. *et al.* Improved monomeric red, orange and yellow fluorescent proteins derived from *Discosoma* sp. red fluorescent protein. *Nature Biotechnol.* **22,** 1567–1572 (2004).
22. Dacey, D. M. *et al.* Melanopsin-expressing ganglion cells in primate retina signal colour and irradiance and project to the LGN. *Nature* **433,** 749–754 (2005).
23. Tu, D. C. *et al.* Physiologic diversity and development of intrinsically photosensitive retinal ganglion cells. *Neuron* **48,** 987–999 (2005).
24. Warren, E. J., Allen, C. N., Brown, R. L. & Robinson, D. W. Intrinsic light responses of retinal ganglion cells projecting to the circadian system. *Eur. J. Neurosci.* **17,** 1727–1735 (2003).
25. Schmidt, T. M., Taniguchi, K. & Kofuji, P. Intrinsic and extrinsic light responses in melanopsin-expressing ganglion cells during mouse development. *J. Neurophysiol.* **100,** 371–384 (2008).
26. Baylor, D. A., Hodgkin, A. L. & Lamb, T. D. The electrical response of turtle cones to flashes and steps of light. *J. Physiol.* **242,** 685–727 (1974).
27. Baylor, D. A., Lamb, T. D. & Yau, K. W. The membrane current of single rod outer segments. *J. Physiol.* **288,** 589–611 (1979).
28. Luo, D.-G., Kefalov, V. & Yau, K.-W. in *The Senses: A Comprehensive Reference* (ed. Basbaum, A. I.) (Elsevier/Academic Press, 2008).
29. Wong, K. Y., Dunn, F. A. & Berson, D. M. Photoreceptor adaptation in intrinsically photosensitive retinal ganglion cells. *Neuron* **48,** 1001–1010 (2005).
30. Lamb, T. D., McNaughton, P. A. & Yau, K. W. Spatial spread of activation and background desensitization in toad rod outer segments. *J. Physiol.* **319,** 463–496 (1981).
31. Wong, K. Y., Ecker, J. L., Dumitrescu, O. N., Berson, D. M. & Hattar, S. Multiple morphological types of melanopsin ganglion cells with distinct light responses and axonal targets. *Invest. Ophthalmol. Vis. Sci.* 49, E-Abstract 1518 (2008).
32. Raport, C. J. *et al.* Downregulation of cGMP phosphodiesterase induced by expression of GTPase-deficient cone transducin in mouse rod photoreceptors. *Invest. Ophthalmol. Vis. Sci.* **35,** 2932–2947 (1994).
33. Nikonov, S. S., Kholodenko, R., Lem, J. & Pugh, E. N. Jr. Physiological features of the S- and M-cone photoreceptors of wild-type mice from single-cell recordings. *J. Gen. Physiol.* **127,** 359–374 (2006).
34. Baylor, D. A., Lamb, T. D. & Yau, K. W. Responses of retinal rods to single photons. *J. Physiol.* **288,** 613–634 (1979).
35. Chen, C. K. *et al.* Abnormal photoresponses and light-induced apoptosis in rods lacking rhodopsin kinase. *Proc. Natl Acad. Sci. USA* **96,** 3718–3722 (1999).
36. Kraft, T. W. Photocurrents of cone photoreceptors of the golden-mantled ground squirrel. *J. Physiol. (Lond.)* **404,** 199–213 (1988).
37. Hardie, R. C. & Postma, M. in *The Senses: A Comprehensive Reference* (ed. Basbaum, A. I.) (Elsevier Science/Academic Press, 2008).
38. Dorlochter, M. & Stieve, H. The Limulus ventral photoreceptor: light response and the role of calcium in a classic preparation. *Prog. Neurobiol.* **53,** 451–515 (1997).
39. Baylor, D. A. & Hodgkin, A. L. Detection and resolution of visual stimuli by turtle photoreceptors. *J. Physiol.* **234,** 163–198 (1973).
40. Liebman, P. A., Parker, K. R. & Dratz, E. A. The molecular mechanism of visual excitation and its relation to the structure and composition of the rod outer segment. *Annu. Rev. Physiol.* **49,** 765–791 (1987).
41. Belenky, M. A., Smeraski, C. A., Provencio, I., Sollars, P. J. & Pickard, G. E. Melanopsin retinal ganglion cells receive bipolar and amacrine cell synapses. *J. Comp. Neurol.* **460,** 380–393 (2003).

42. Lucas, R. J., Douglas, R. H. & Foster, R. G. Characterization of an ocular photopigment capable of driving pupillary constriction in mice. *Nature Neurosci.* **4,** 621–626 (2001).
43. Cahill, H. & Nathans, J. The optokinetic reflex as a tool for quantitative analyses of nervous system function in mice: application to genetic and drug-induced variation. *PLoS ONE* **3,** e2055 (2008).
44. Grozdanic, S. *et al.* Characterization of the pupil light reflex, electroretinogram and tonometric parameters in healthy mouse eyes. *Curr. Eye Res.* **26,** 371–378 (2003).
45. Wong, K. Y., Dunn, F. A., Graham, D. M. & Berson, D. M. Synaptic influences on rat ganglion-cell photoreceptors. *J. Physiol.* **582,** 279–296 (2007).
46. Perez-Leon, J. A., Warren, E. J., Allen, C. N., Robinson, D. W. & Lane Brown, R. Synaptic inputs to retinal ganglion cells that set the circadian clock. *Eur. J. Neurosci.* **24,** 1117–1123 (2006).
47. Hecht, S., Shlaer, S. & Pirenne, M. H. Energy, quanta, and vision. *J. Gen. Physiol.* **25,** 819–840 (1942).

Supplementary Information is linked to the online version of the paper at www.nature.com/nature.

Acknowledgements Supported by an NRSA fellowship and a VNTP Training Grant to M.T.H.D., and NIH grants to K.-W.Y. and D.E.B. We thank Y. Koutalos, V. Bhandawat, D.-G. Luo, V. Kefalov, D. Liu, G. Maimon and C.-Y. Su for discussions, and Y. Wang, J. Hsieh and N. Nishiyama for technical assistance. We also thank J. Nathans and R. Reeves for suggestions on transgenic lines, J. Nathans and H. Cahill for the *Gnat1*$^{-/-}$ *cl* mouse line, and T. Shelley for machining. We dedicate this work to the Champalimaud Foundation, Portugal.

Author Contributions M.T.H.D. and K.-W.Y. designed the experiments and wrote the paper. All experiments were performed by M.T.H.D., except for pupil measurements, which were done by T.X. and M.T.H.D. The melanopsin-tdTomato BAC-transgenic mouse was generated by S.H.K. in the laboratory of D.E.B. Important early observations of the intensity–response relationship and kinetics were made by H.Z. using animals retrograde-labelled by H.-W.L.

Author Information Reprints and permissions information is available at www.nature.com/reprints. Correspondence and requests for materials should be addressed to M.T.H.D. (mdo@jhmi.edu) or K.-W.Y. (kwyau@mail.jhmi.edu).

METHODS

Solutions. For whole-cell and perforated-patch recordings, the unsupplemented pipette solution was (in mM): 110 KCl, 13 NaCl, 2 $MgCl_2$, 1 $CaCl_2$, 10 EGTA, 10 HEPES, pH 7.2 with KOH. For loose-patch recordings, it was an 'ionic Ames' containing (in mM): 140 NaCl, 3.1 KCl, 0.5 KH_2PO_4, 1.5 $CaCl_2$, 1.2 $MgSO_4$, 6 glucose, 10 HEPES, pH 7.4 with NaOH. Fast synaptic transmission was blocked by adding to the bath 50 μM D,L-APV, 20 μM CNQX, 100 μM hexamethonium bromide, 100 μM picrotoxin, and often 1 μM strychnine. 3 mM kynurenate sometimes replaced the first three. On rare occasions, some synaptic transmission persisted in this cocktail (evidenced by a short-latency, transient light response preceding the intrinsic light response), and was abolished by adding 100 μM D,L-AP4.

Fluctuation/quantal analyses. These were as described for retinal rods[34]. At 23 °C, the single-photon response was not individually resolvable, but estimated from the ensemble variance-to-mean ratio, σ^2/m, at the peak of the mean response, $m(t)$, to dim flashes. The quantal content of $m(t)$, ζ, is given by $\zeta = m/(\sigma^2/m) = m^2/\sigma^2$. The predicted Poisson distribution for comparison with the amplitude histogram was calculated from $P_n = \zeta^n e^{-\zeta}/n!$, where $n = 0, 1, 2$, etc., and P_n is the probability of n unitary responses in any trial. NP_n was then plotted against $n(\sigma^2/m)$, where N is the total number of stimulus trials. At 35 °C, the single-photon response was just resolvable, as were the failures, so σ^2/m could be directly compared to the singletons. The method to identify the singletons is described in Supplementary Information S1.

Melanopsin-density calculations. Melanopsin is supposed to be situated only on the plasma membrane[41]. The Beer–Lambert Law states that $OD = \log_{10}(I_i/I_t) = \varepsilon CL$, where OD is optical density, I_i and I_t are incident and transmitted intensities, ε is the molar extinction coefficient, C is molar concentration, and L is path length[48]. For dilute pigment, this equation approximates to $I_a/I_i = 2.3\varepsilon CL$, where I_a is the absorbed intensity. Suppose R is the total number of pigment molecules in a planar membrane of volume V (litres), then $C = R/(6 \times 10^{23} \times V)$ mol litre^{-1}. L (μm) is given by $(V \times 10^{15})/A$, where A is membrane surface area (μm^2). Thus, for incident light normal to the planar membrane, $I_a/I_i = 3.83 \times 10^{-9} \times \varepsilon \times \rho_m$, where $\rho_m = R/A$ is the pigment density on membrane. Taking into account the quantum efficiency of isomerization, Q_{isom}, and assuming that every isomerized pigment molecule triggers an electrical response (as in rods, cones and invertebrate photoreceptors; see Supplementary Information S3), the number of single-photon responses triggered by I_i is given by $3.83 \times 10^{-9} \times \varepsilon \times \rho_m \times Q_{isom} \times I_i A$.

For rhodopsin (randomly oriented) in solution, $\varepsilon \approx 42{,}000$ M^{-1} cm^{-1} for photons at λ_{max} (ref. 49). For a planar membrane, the chromophore (11-*cis*-retinal) of all pigment molecules is oriented roughly parallel to the membrane surface, so that for unpolarized light at normal incidence, the probability of absorption is 50% higher than in solution[50], giving an ε of ~63,000 M^{-1} cm^{-1}, or 6.3 mol^{-1} litre^{-1} μm^{-1} at λ_{max}. This parameter is unlikely to be very different between rhodopsin and melanopsin at their respective λ_{max} values (Supplementary Information S3), because it depends mostly on the chromophore, and melanopsin uses also 11-*cis*-retinal[16]. For the same reason, Q_{isom} should be similar between rhodopsin (0.67; see ref. 50) and melanopsin, and, indeed, across a wide variety of pigments (Supplementary Information S3). To apply the calculations to ipRGCs, we need to consider two more factors. First, for a spherical membrane (as of a cell soma), the average probability of absorption for roughly collimated light is lower by a factor of 2 compared with planar membrane (Supplementary Information S4). Second, there was a 3.5-fold increase in ipRGC sensitivity with 9-*cis*-retinal incubation, suggesting that some pigment was without chromophore, or bleached, at the beginning of recording (although the true correction factor may be less than 3.5; see Supplementary Information S2). Substituting all of the above parameters into the final expression in the previous paragraph, and with $A = 4\pi r^2$, where r (in μm) is the somatic radius, we arrive at the number of single-photon responses produced by a flash of intensity I_i (photons μm^{-2}) at λ_{max} (480 nm) on the ipRGC soma as being $3.83 \times 10^{-9} \times 6.3 \times \rho_m \times 0.67 \times I_i \times 4\pi r^2 = 3 \times 10^{-8} \times r^2 I_i \rho_m$. From the measured I_i for triggering one single-photon response (I_ϕ, see main text), ρ_m can be evaluated. If not every isomerized melanopsin molecule triggers an electrical response, the estimated melanopsin density should scale up proportionally. We consider the above calculations as an order-of-magnitude estimate.

The melanopsin density on the dendrites is unlikely to be very different from that on the soma, as can be seen from the following. The Michaelis equation (the exact relation is non-critical, as long as linearity holds at low flash intensities) describing the intensity–response relationship is:

$$R = R_{max} I/(I + I_{1/2})$$

where R_{max} is the saturated response. For small I, this becomes $R = R_{max}(I/I_{1/2})$. Suppose, for local illumination on soma, $R_{\phi,s}$ is the single-photon-response amplitude elicited by $I_{\phi,s}$ photons μm^{-2} on soma, and $I_{1/2,s}$ and $R_{max,s}$ are the half-saturating flash intensity and the saturated response on the soma, respectively; likewise, suppose $R_{\phi,d}$, $I_{\phi,d}$, $I_{1/2,d}$ and $R_{max,d}$ have the same meanings for dendritic illumination. Thus,

$$R_{\phi,s} = R_{max,s}(I_{\phi,s}/I_{1/2,s})$$

$$\text{and } R_{\phi,d} = R_{max,d}(I_{\phi,d}/I_{1/2,d})$$

Combining these two equations—and because we found (see main text) $R_{\phi,s} \approx R_{\phi,d}$, $I_{1/2,s} \approx I_{1/2,d}$ and $R_{max,s}/R_{max,d} \approx A_s/A_d$, where A_s and A_d are the somatic and dendritic light-collecting areas—we have

$$I_{\phi,s} A_s \approx I_{\phi,d} A_d$$

Thus, roughly the same overall number of photons is required for producing the single-photon response on the somatic surface as on the dendrites. The parsimonious interpretation is a similar melanopsin density in both locations.

48. Lisman, J. E. & Bering, H. Electrophysiological measurement of the number of rhodopsin molecules in single Limulus photoreceptors. *J. Gen. Physiol.* 70, 621–633 (1977).
49. Harosi, F. I. Absorption spectra and linear dichroism of some amphibian photoreceptors. *J. Gen. Physiol.* 66, 357–382 (1975).
50. Dartnall, H. J. A. in *Photochemistry of Vision* (ed. Dartnall, H. J. A.) 122–145 (Springer, 1972).

LETTERS

A binary origin for 'blue stragglers' in globular clusters

Christian Knigge[1], Nathan Leigh[2] & Alison Sills[2]

Blue stragglers in globular clusters are abnormally massive stars that should have evolved off the stellar main sequence long ago. There are two known processes that can create these objects: direct stellar collisions[1] and binary evolution[2]. However, the relative importance of these processes has remained unclear. In particular, the total number of blue stragglers found in a given cluster does not seem to correlate with the predicted collision rate[3,4], providing indirect support for the binary-evolution model. Yet the radial distributions of blue stragglers in many clusters are bimodal, with a dominant central peak[5–7]: this has been interpreted as an indication that collisions do dominate blue straggler production, at least in the high-density cluster cores[7,8]. Here we report that there is a clear, but sublinear, correlation between the number of blue stragglers found in a cluster core and the total stellar mass contained within it. From this we conclude that most blue stragglers, even those found in cluster cores, come from binary systems. The parent binaries, however, may themselves have been affected by dynamical encounters. This may be the key to reconciling all of the seemingly conflicting results found to date.

In both models of blue straggler formation, the numbers and properties of the resultant blue stragglers can shed light on the dynamical histories of their host clusters. The conclusions drawn from the observed blue straggler populations depend on which formation mechanism is dominant. Unfortunately, even though a number of potential formation tracers have been proposed, a simple observational distinction between collisional and binary blue stragglers has yet to be found[9–14]. In general, it is impossible to tell whether an individual blue straggler was formed by means of a stellar collision or a binary merger.

However, it should be possible to determine the dominant formation channel statistically, by studying the relationship between the size of a blue straggler population and the properties of its host cluster. Here, we focus on blue stragglers found in the cores of clusters, where collisions should be most frequent. If most blue stragglers are formed as a result of single–single stellar collisions, their number in a particular cluster core should be approximately $N_{\rm BS,coll} \approx \tau_{\rm BS}/\tau_{\rm coll}$, where $\tau_{\rm BS}$ is the typical blue straggler lifetime and $\tau_{\rm coll}$ is the timescale on which single–single collisions occur in the core. Conversely, if most core blue stragglers are the progeny of binary stars, their number may be expected to scale simply as $N_{\rm BS,bin} \propto f_{\rm bin} M_{\rm core}$, where $f_{\rm bin}$ is the binary fraction in the core and $M_{\rm core}$ is the total stellar mass contained in the core. These predictions are applicable to the simplest versions of the competing models, but note that more complex, intermediate channels could also contribute (for example blue stragglers produced as a result of dynamical encounters involving binary stars). We will return to this subtlety below.

To test these simple predictions, we used our existing database of core blue straggler counts[4], which are derived from a large set of colour–magnitude diagrams based on images from NASA's Hubble Space Telescope[15]. Figure 1 confirms that there is no global correlation between the observed core blue straggler numbers and those

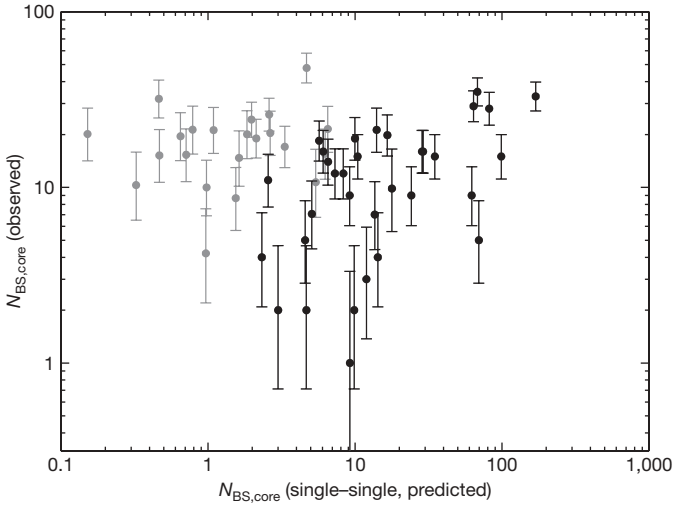

Figure 1 | The observed number of core blue stragglers versus the number expected from single–single collisions. Black points correspond to high-density clusters ($\rho_0 > 10^4 M_\odot\ {\rm pc}^{-3}$), grey points to low-density clusters ($\rho_0 < 10^4 M_\odot\ {\rm pc}^{-3}$). The error bars shown are approximate 68% Poisson confidence intervals[22]. There is no correlation between observed and predicted numbers across the full sample (Spearman's rank test yields $\rho_{\rm S} = -0.03$, $P = 0.6$, $N = 56$). For the subset of dense clusters, a correlation does exist ($\rho_{\rm S} = 0.52$, $P = 8 \times 10^{-4}$, $N = 34$). In calculating the predicted numbers, we took the timescale between collisions to be[23]

$$\tau_{\rm coll} = 1.1 \times 10^{10} \left(\frac{r_{\rm c}}{1\ {\rm pc}}\right)^{-3} \left(\frac{n_0}{10^3\ {\rm pc}^{-3}}\right)^{-2} \left(\frac{\sigma_0}{5\ {\rm km\ s}^{-1}}\right) \left(\frac{M_*}{M_\odot}\right)^{-1} \left(\frac{R_*}{R_\odot}\right)^{-1} {\rm yr}$$

Here $r_{\rm c}$ is the core radius, n_0 is the central number density in stars per cubic parsec, σ_0 is the central velocity dispersion, M_* is the average stellar mass (taken to be $0.5M_\odot$) and R_* is the average stellar radius (taken to be $0.5R_\odot$; $R_\odot$, solar radius). Core radii and central luminosity densities were taken from the McMaster Globular Cluster Catalogue[24]. Core number densities were estimated by adopting a fixed mass-to-light ratio of two[25]. Central velocity dispersions were taken primarily from the compilation of ref. 26, but supplemented with data from ref. 27. The typical blue straggler lifetime in a cluster was taken to be 1.5 Gyr (refs 28, 29). Note that for high-concentration clusters, the observational definition of the core radius can be somewhat arbitrary. However, this should not have a significant impact on our analysis, as long as the associated central densities and velocity dispersions remain reasonable averages over the relevant regions.

[1]University of Southampton, School of Physics and Astronomy, Southampton SO17 1BJ, UK. [2]McMaster University, Department of Physics and Astronomy, 1280 Main Street West, Hamilton, Ontario L8S 4M1, Canada.

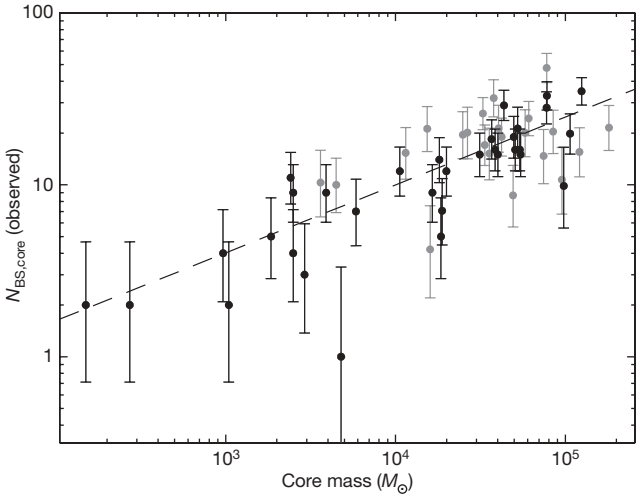

Figure 2 | The observed number of core blue stragglers versus the estimated core mass. Black points correspond to high-density clusters ($\rho_0 > 10^4 M_\odot\,\mathrm{pc}^{-3}$), grey points to low-density clusters ($\rho_0 < 10^4 M_\odot\,\mathrm{pc}^{-3}$). The error bars shown are approximate 68% Poisson confidence intervals[22]. Blue straggler numbers and core masses are strongly correlated ($\rho_S = 0.71$, $P = 4 \times 10^{-10}$, $N = 56$), as is expected if blue stragglers are descended from binary systems. The correlation with core mass also holds for the subset of dense clusters ($\rho_S = 0.84$, $P = 3 \times 10^{-10}$, $N = 34$), and in both cases is stronger than that with collision rate. The dashed line is a power-law fit to the full set of clusters, obtained by a method appropriate for this type of data set[30]. The best-fit power law is $N_{BS} \propto M_{core}^{0.38 \pm 0.04}$.

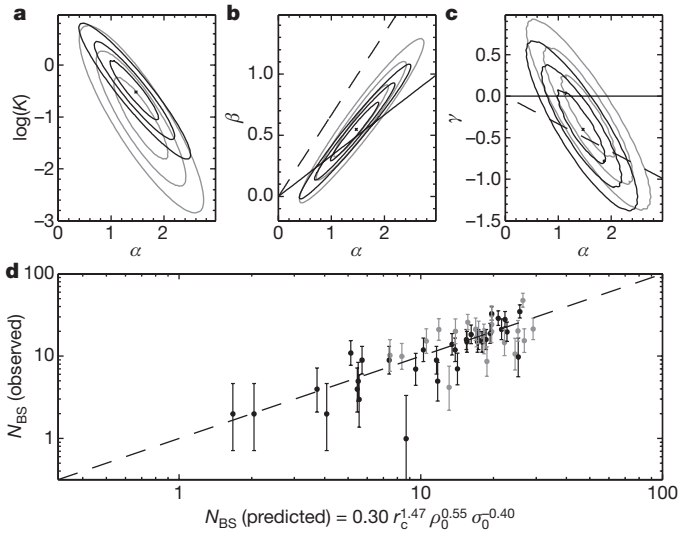

Figure 3 | Results of fitting the generalized model $N_{BS} \propto K r_c^{\alpha} \rho_0^{\beta} \sigma_0^{\gamma}$ to the observed blue straggler number. **a**, **b**, **c**, Projections of the four-dimensional parameter space. The contours in each panel represent 1 s.d., 2 s.d. and 3 s.d. joint confidence intervals for the two parameters being considered. Black contours correspond to the full cluster sample, grey contours to the dense cluster sample ($\rho_0 > 10^4 M_\odot\,\mathrm{pc}^{-3}$). The straight lines in **b** and **c** show the parameter relationships expected for a power-law dependence on collision rate (dashed lines) and core mass (solid lines). The best-fit power-law indices are $\alpha = 1.47 \pm 0.29$, $\beta = 0.55 \pm 0.15$ and $\gamma = -0.40 \pm 0.27$. **d**, Observed blue straggler number versus the best-fit model prediction for the full sample. Black points correspond to high-density clusters ($\rho_0 > 10^4 M_\odot\,\mathrm{pc}^{-3}$), grey points to low-density clusters ($\rho_0 < 10^4 M_\odot\,\mathrm{pc}^{-3}$). The error bars shown are approximate 68% Poisson confidence intervals[22]. The dashed line marks the identity relation, that is, N_{BS} (observed) = N_{BS} (predicted). We also carried out a separate fit to the subset of dense clusters ($\rho_0 > 10^4 M_\odot\,\mathrm{pc}^{-3}$). This yielded $\alpha = 1.59 \pm 0.33$, $\beta = 0.63 \pm 0.19$ and $\gamma = -0.28 \pm 0.31$, consistent with the values obtained for the complete cluster sample. Note that, even within this subset, there is no evidence for a dependence of blue straggler numbers on σ_0.

predicted by the collision model[3,4]. In particular, the predicted numbers are very different for high- and low-density clusters, in contradiction to the observations. Figure 2 shows that, by contrast, the observed numbers do correlate strongly with the cluster core masses, as is expected if most blue stragglers are the progeny of binary stars. A power-law fit suggests that $N_{BS} \propto M_{core}^{0.38 \pm 0.04}$.

When consideration is restricted to dense cores ($\rho_0 > 10^4 M_\odot\,\mathrm{pc}^{-3}$; $M_\odot$, solar mass), the collisional predictions are, in fact, significantly correlated with observed blue straggler numbers (see the black points in Fig. 1). However, even for these dense cores, the correlation with core mass remains stronger (Fig. 2). Thus, not only is core mass the only successful global predictor for core blue straggler number, it also remains a better predictor than collision rate even for dense clusters.

One way to distinguish even more clearly between collisional and binary models is to isolate the key cluster parameters that drive the observed correlations and quantify their respective impacts on the observed sizes of the core blue straggler populations. For example, even though collision rate and core mass are correlated parameters, only collision rate depends fundamentally on a cluster's central velocity dispersion. We therefore carried out a direct fit to the observed core blue straggler numbers, using the generalized model $N_{BS} = K r_c^{\alpha} \rho_0^{\beta} \sigma_0^{\gamma}$, where K, α, β and γ are all treated as free parameters. For purely collisional blue straggler formation, we expect that $\alpha \approx 3$, $\beta \approx 2$ and $\gamma \approx -1$, whereas pure binary formation implies that $\alpha \approx 3$, $\beta \approx 1$ and $\gamma \approx 0$. These relationships rely on the binary fraction being uniform across clusters; we will return to this assumption below. Allowing for a more general power-law dependence on collision rate or core mass, we predict that $\alpha \approx 1.5\beta \approx -3\gamma$ for collisional blue straggler formation and that $\alpha \approx 3\beta$ with $\gamma \approx 0$ for binary blue straggler formation.

Figure 3 shows the results of this fit. The best-fit power-law indices are $\alpha = 1.47 \pm 0.29$, $\beta = 0.55 \pm 0.15$ and $\gamma = -0.40 \pm 0.27$. These coefficients are consistent with a power-law dependence on M_{core} but not with one on collision rate. (Note that because r_c, ρ_0 and σ_0 are correlated parameters, α, β and γ are also correlated.) There is no evidence for a significant dependence of blue straggler number on velocity dispersion. A fit to only the dense clusters yielded results consistent with the values obtained for the complete cluster sample.

We find that blue straggler number depends strongly on core mass, but not on collision rate. We argue that this is strong evidence for a binary, as opposed to a collision, origin for blue stragglers in globular clusters. We note that the core-mass dependence can be approximated as $N_{BS} \propto M_{core}^{\delta}$ with $\delta \approx 0.4$–0.5. The sublinear dependence of blue straggler number on core mass is interesting. For ordinary populations of single stars, a roughly linear dependence would be expected, and we have verified that this is the case for the red giant and horizontal branch populations in our cluster sample. In the context of the binary model of blue straggler formation, the simplest way to account for this sublinearity is to posit that core binary fractions decrease with increasing core mass, that is, $f_{bin} \propto M_{core}^{-\varepsilon}$ with $\varepsilon \approx 0.5$–0.6.

This is a testable prediction. There have been two recent efforts to estimate core binary fractions in a consistent way from homogeneous, deep Hubble Space Telescope Advanced Camera for Surveys observations of globular clusters[16,17]. One of these[16] is restricted to a set of 13 low-density clusters (sample one). The other[17] is still preliminary, but is based on a larger set of 35 clusters that span a wider range in density and other dynamical parameters (sample two). Promisingly, from our perspective, a correlation between blue straggler frequency and core binary fraction has already been reported for sample one[18], and an anticorrelation between core binary fraction and total cluster mass has been reported for sample two[17]. Because sample one spans only a narrow dynamic range and the binary fractions reported for sample two are available only in graphical form, we could make only a preliminary attempt to infer the dependence of f_{bin} on M_{core} from these samples. Nevertheless, our power law estimate is $f_{bin} \propto M_{core}^{-0.35}$ for both samples, which is close to the predicted

relation, albeit with considerable scatter. Thus, the number of blue stragglers found in the cores of globular clusters scales roughly as $N_{BS} \propto f_{bin} M_{core}$, just as would be expected if most core blue stragglers were descended from binary systems.

There are several ways to build on the analysis presented above. First, binary–single and binary–binary interactions may actually produce more blue stragglers in clusters than single–single collisions, because the interaction cross-sections are larger. The expected numbers of binary–single and binary–binary collisions scale like the number of single–single collisions times f_{bin} and, respectively, f_{bin}^2. A better determination of the dependence of binary fractions on cluster parameters is clearly warranted to test these predictions fully. However, on the basis of the preliminary analysis of the observed binary fractions described above, it currently seems unlikely that binary–single and binary–binary interaction numbers can produce the observed scaling of blue straggler numbers with cluster parameters.

Second, the effects of mass segregation have been ignored in our analytical predictions. Massive stars at any particular location in a cluster will sink to the core on roughly the local relaxation time. Thus, some of the blue stragglers found today in cluster cores may actually have been formed outside the core[7,8,19]. Moreover, clusters evolve, so the present-day cluster parameters may not always be close approximations to what should ideally be suitably weighted averages over the blue straggler lifetime. As a first test of this, we have split our cluster sample into objects with half-mass relaxation times less than and, respectively, greater than the blue straggler lifetime. If mass segregation were responsible for masking an underlying trend with collision rate, we might expect the clusters with long relaxation timescales to reveal this trend, and those with short relaxation timescales to exhibit enhanced blue straggler numbers (at a given collision rate). We find no evidence for either of these effects. It is also worth noting that our result for core blue stragglers is actually consistent with the behaviour of the total (core plus peripheral) blue straggler populations, which also seem to show a sublinear correlation with total cluster mass[19].

Our results do not imply that dynamical interactions are unimportant in blue straggler formation. The properties of the core binary populations from which blue stragglers are probably descended may themselves be strongly affected by dynamical encounters. There is a wide spectrum of possible paths within the family of binary channels. Whereas some 'binary blue stragglers' may be the direct descendants of primordial binaries that evolved essentially in isolation, others may exist only as a result of multiple strong interactions and exchanges[20,21].We are not the first to point out this subtlety (though it has sometimes been obscured by the terminology used). For example, the collisional blue straggler population invoked in the model of refs 7, 8 could be produced through encounters involving binaries, and the primordial binary channel described in ref. 19 explicitly allows for dynamical interactions. Our results do, however, argue against the simple scaling of blue straggler numbers with any collision rate. Clearly, a key challenge for future work will be to determine whether dynamically active binaries can produce blue straggler numbers consistent with the trends found here.

Received 3 June; accepted 6 November 2008.

1. Hills, J. G. & Day, C. A. Stellar collisions in globular clusters. *Astrophys. Lett.* **17,** 87–93 (1976).
2. McCrea, W. H. Extended main-sequence of some stellar clusters. *Mon. Not. R. Astron. Soc.* **128,** 147–155 (1964).
3. Piotto, G. *et al.* Relative frequencies of blue stragglers in galactic globular clusters: Constraints for the formation mechanisms. *Astrophys. J.* **604,** L109–L112 (2004).
4. Leigh, N., Sills, A. & Knigge, C. Where the blue stragglers roam: Searching for a link between formation and environment. *Astrophys. J.* 661, 210–221 (2007); erratum **678,** 564–566 (2008).
5. Ferraro, F. R. *et al.* Blue stragglers in the Galactic globular clusters M3: Evidence for two populations. *Astron. J.* **106,** 2324–2334 (1993).
6. Ferraro, F. R. *et al.* Discovery of another peculiar radial distribution of blue stragglers in globular clusters: The case of 47 Tucanae. *Astrophys. J.* **603,** 127–134 (2004).
7. Mapelli, M. *et al.* The radial distribution of blue straggler stars and the nature of their progenitors. *Mon. Not. R. Astron. Soc.* **373,** 361–368 (2006).
8. Mapelli, M. *et al.* The contribution of primordial binaries to the blue straggler population in 47 Tucanae. *Astrophys. J.* **605,** L29–L32 (2004).
9. Benz, W. & Hills, J. G. Three-dimensional hydrodynamical simulations of stellar collisions. I - Equal-mass main-sequence stars. *Astrophys. J.* **323,** 614–628 (1987).
10. Leonard, P. J. T. & Livio, M. The rotational rates of blue stragglers produced by physical stellar collisions. *Astrophys. J.* **447,** L121–L123 (1995).
11. Sills, A. P., Bailyn, C. D. & Demarque, P. Are blue stragglers mixed during collisions? *Astrophys. J.* **455,** L163–L165 (1995).
12. Sandquist, E. L., Bolte, M. & Hernquist, L. Composition mixing during blue straggler formation and evolution. *Astrophys. J.* **477,** 335–345 (1997).
13. Sills, A. & Bailyn, C. D. The distribution of collisionally induced blue stragglers in the color-magnitude diagram. *Astrophys. J.* **513,** 428–441 (1999).
14. Ferraro, F. R. *et al.* Discovery of carbon/oxygen-depleted blue straggler stars in 47 Tucanae: The chemical signature of a mass transfer formation process. *Astrophys. J.* **647,** L53–L56 (2006).
15. Piotto, G. *et al.* HST color-magnitude diagrams of 74 galactic globular clusters in the HST F439W and F555W bands. *Astron. Astrophys.* **391,** 945–965 (2002).
16. Sollima, A., Beccari, G., Ferraro, F. R., Fusi Pecci, F. & Sarajedini, A. The fraction of binary systems in the core of 13 low-density Galactic globular clusters. *Mon. Not. R. Astron. Soc.* **380,** 781–791 (2007).
17. Milone, A. P., Piotto, G., Bedin, L. R. & Sarajedini, A. in *XXI Century Challenges for Stellar Evolution* (eds Cassisi, S & Salaris, M.) 623–627 (Società Astronomica Italiana, 2008).
18. Sollima, A., Lanzoni, B., Beccari, G., Ferraro, F. R. & Fusi Pecci, F. The correlation between blue straggler and binary fractions in the core of Galactic globular clusters. *Astron. Astrophys.* **481,** 701–704 (2008).
19. Davies, M. B., Piotto, G. & de Angeli, F. Blue straggler production in globular clusters. *Mon. Not. R. Astron. Soc.* **349,** 129–134 (2004).
20. Knigge, C. *et al.* A blue straggler binary with three progenitors in the core of a globular cluster? *Astrophys. J.* **641,** 281–287 (2006).
21. Knigge, C. *et al.* Stellar exotica in 47 Tucanae. *Astrophys. J.* **683,** 1006–1030 (2008).
22. Gehrels, N. Confidence limits for small numbers of events in astrophysical data. *Astrophys. J.* **303,** 336–346 (1986).
23. Leonard, P. J. T. Stellar collisions in globular clusters and the blue straggler problem. *Astron. J.* **98,** 217–226 (1989).
24. Harris, W. E. A catalog of parameters for globular clusters in the Milky Way. *Astron. J.* **112,** 1487–1488 (1996).
25. McLaughlin, D. E. & van der Marel, R. P. Resolved massive star clusters in the Milky Way and its satellites: Brightness profiles and a catalog of fundamental parameters. *Astrophys. J. Suppl. Ser.* **161,** 304–360 (2005).
26. Pryor, C. & Meylan, G. in *Structure and Dynamics of Globular Clusters* (eds Djorgovski, S. G. & Meylan, G.) 357–371 (Astronomical Society of the Pacific, 1993).
27. Webbink, R. F. in *Dynamics of Star Clusters* (eds Goodman, J. & Hut, P.) 541–577 (Reidel, 1985).
28. Sills, A. *et al.* Evolution of stellar collision products in globular clusters. I. Head-on collisions. *Astrophys. J.* **487,** 290–303 (1997).
29. Sills, A., Faber, J. A., Lombardi, J. C. Jr, Rasio, F. A. & Warren, A. R. Evolution of stellar collision products in globular clusters. II. Off-axis collisions. *Astrophys. J.* **548,** 323–334 (2001).
30. Verbunt, F. W. M. Observational evidence for origin of stellar exotica in globular clusters. *Highlights Astron.* **14,** 440–441 (2007).

Acknowledgements Research support for C.K. was provided by the UK Science and Technology Facilities Council. A.S. and N.L. are supported by the Natural Sciences and Engineering Research Council of Canada. C.K. would like to thank T. Maccarone for discussions.

Author Information Reprints and permissions information is available at www.nature.com/reprints. Correspondence and requests for materials should be addressed to C.K. (christian@astro.soton.ac.uk).

LETTERS

Collective fluid dynamics of a polariton condensate in a semiconductor microcavity

A. Amo[1], D. Sanvitto[1], F. P. Laussy[2], D. Ballarini[1], E. del Valle[2], M. D. Martin[1], A. Lemaître[3], J. Bloch[3], D. N. Krizhanovskii[4], M. S. Skolnick[4], C. Tejedor[2] & L. Viña[1]

Semiconductor microcavities offer unique systems in which to investigate the physics of weakly interacting bosons. Their elementary excitations, polaritons—mixtures of excitons and photons—can accumulate in macroscopically degenerate states to form various types of condensate in a wide range of experimental configurations, under either incoherent[1,2] or coherent[3,4] excitation. Condensates of polaritons have been put forward as candidates for superfluidity[5,6], and the formation of vortices[7] as well as elementary excitations with linear dispersion[8] are actively sought as evidence to support this. Here, using a coherent excitation triggered by a short optical pulse, we have created and set in motion a macroscopically degenerate state of polaritons that can be made to collide with a variety of defects present in the microcavity. Our experiments show striking manifestations of a coherent light–matter packet, travelling at high speed (of the order of one per cent of the speed of light) and displaying collective dynamics consistent with superfluidity, although one of a highly unusual character as it involves an out-of-equilibrium dissipative system. Our main results are the observation of a linear polariton dispersion accompanied by diffusionless motion; flow without resistance when crossing an obstacle; suppression of Rayleigh scattering; and splitting into two fluids when the size of the obstacle is comparable to the size of the wave packet. This work opens the way to the investigation of new phenomenology of out-of-equilibrium condensates.

Below a critical temperature, bosons of a sufficiently high number density undergo Bose–Einstein condensation (BEC). Under this condition, the particles collapse into a macroscopic condensate with a common phase, showing collective quantum behaviour like superfluidity, quantised vortices, interference, and so on. Until recently, BEC was only observed in dilute atomic gases at microkelvin temperatures. Following the recent observations of non-equilibrium BEC in semiconductor microcavities at temperatures of $\sim$10 K, using momentum-[1] and real-space[2] trapping, the goal is now to observe new quantum phenomena associated with condensates of polaritons. For the same reasons that these particles benefit from having features especially favourable for condensation, such as very high critical temperatures, it is expected that their superfluid properties would similarly be manifest with altogether different magnitudes, such as very high critical velocities. Because in their Bose-condensed phase they have shown many deviations from the cold-atom systems, it is a priori not clear to what extent their properties would coincide with or depart from those observed in atoms, among which quantized vortices[9], frictionless motion[10], linear dispersion of the elementary excitations[11] or, more recently, Čerenkov emission of a condensate flowing at supersonic velocities[12] are the clearest signatures of quantum fluid propagation.

Microcavity polaritons are two-dimensional bosons, of mixed electronic and photonic nature, formed by the strong coupling of excitons—confined in semiconductor quantum wells—with photons trapped in a micrometre-scale resonant cavity[13]. Owing to their photon fractions, polaritons can easily be excited by an external laser source and detected by light emission. However, unlike photons, they experience strong interparticle interactions, owing to their partially electronic fractions. The deep polariton dispersion causes the effective masses of these particles to be 10^4–10^5 times smaller than the free electron mass, resulting in a very low density of states. This allows for a high state occupancy even at relatively low excitation intensities. However, polaritons can exist for only a few picoseconds in the cavity before decaying into photons and thermal equilibrium is therefore never achieved. In this respect, a macroscopically degenerate state of polaritons departs strongly from an atomic Bose-condensed phase, especially in our experiment, where the condensate is formed from a coherent excitation. The experimental observations of spectral and momentum narrowing, spatial coherence and long-range order—which have been used as evidence for polariton BEC—have also been seen in a pure photonic laser[14]. The recent observation of long-range spatial coherence[15], vortices[7] and the loss of coherence with increasing density in the condensed phase[16,17] are in accordance with macroscopic phenomena observed in interacting, coherent bosons. However, a study of the fluid dynamics of coherent states of this kind is still missing.

In this work, using a combination of temporally and spatially resolved spectroscopic techniques in a GaAs microcavity[18], we are able to probe directly the dynamics of the motion of a condensed droplet of polaritons by tracking its space-time evolution. We report a shape-preserving, non-diffusive propagation of matter, dressed by the light field, moving at a speed of the order of $10^6\,\mathrm{m\,s^{-1}}$. Collisions with obstacles of different sizes provide further insights into the dynamics of this system: the collective behaviour shown here is expected from a condensate of polaritons, as suggested by our theoretical analysis in terms of a nonlinear Schrödinger equation. Our findings are a class of new phenomena that, like some previously observed[7,8], are consistent with superfluidity and nonlinear optical effects[19]. However, our work, which probes the dynamics of a condensate, adds insight into the extent to which the polariton condensate exhibits superfluid-like properties.

Our experiments are based on the continuous replenishment of a polariton fluid, at energy E_S and momentum $\hbar\mathbf{k}_S$, from a higher-lying state, at E_P and $\hbar\mathbf{k}_P$, driven coherently by a continuous-wave laser and set in motion by a short trigger pulse (2 ps) at the idler state, E_I and $\hbar\mathbf{k}_I$, in a configuration of a triggered optical parametric oscillator (TOPO; see Fig. 1 and Supplementary Information)[20]. This experimental arrangement allows the study of the propagation of the signal

[1]Departamento Física de Materiales, [2]Departamento Física Teórica de la Materia Condensada, Universidad Autonóma de Madrid, 28049 Madrid, Spain. [3]LPN/CNRS, Route de Nozay, 91460 Marcoussis, France. [4]Department of Physics & Astronomy, University of Sheffield, Sheffield S3 7RH, UK.

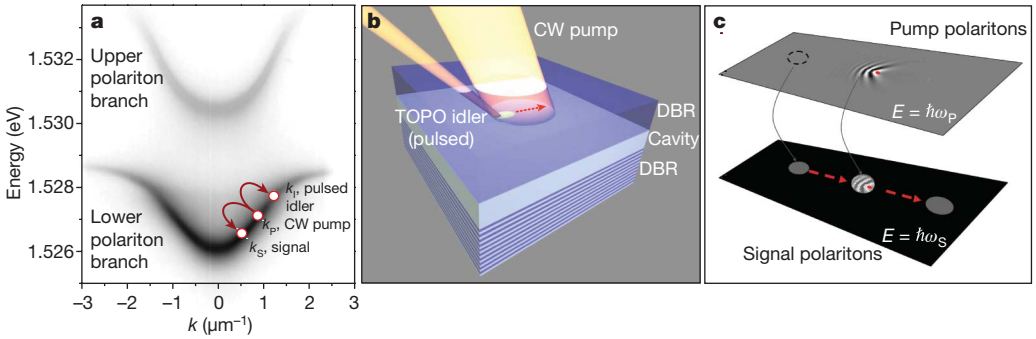

Figure 1 | Experimental configuration of the TOPO. a, Experimental microcavity dispersion of the two polariton branches, showing the condition of excitation of the continuous pump and the formation of a polariton state at the continuous-wave (CW) pump energy, which feeds the signal polaritons at a lower energy, fulfilling the conditions $2k_P = k_S + k_I$ and $2E_P = E_S + E_I$. This process is initialised by a pulse at the idler state. **b**, Diagram of the experimental set-up. The two laser beams are shown impinging on the sample surface at an arbitrary direction (x) in the plane of the cavity (x, y). The polaritons are created in the cavity region (light green circle), which is surrounded by two highly reflective distributed Bragg reflectors (DBRs). **c**, Sketch of the motion of two fluids, pump polaritons (upper) and signal polaritons (lower), against a defect depicted by the red point. Although the two fluids are spatially in the same plane, they are shown separately in the figure to emphasize their energy difference. The movement of the signal polariton fluid, at $E_S = \hbar\omega_S$, is represented by the circle moving from left to right on the black plane. The continuous feeding from the pump polaritons at $E_P = \hbar\omega_P$, shown in the grey plane, makes it possible to detect this motion. $\hbar$, Planck's constant (h) divided by 2π.

polaritons, which can have any, specifically selected, in-plane momentum $\hbar\mathbf{k}$ given by the phase matching conditions shown in the caption of Fig. 1. Owing to the polariton light emission, we are able to probe continuously and in real time features such as the motion of the droplet and its dispersion.

The experimental dispersions of the light emitted by the polaritons in different regimes are depicted in Fig. 2a. The false-colour graph in the upper panel shows the emission of the polariton fluid generated by the TOPO, after the trigger pulse has disappeared; in the lower panel this is compared with the standard parabolic dispersion of the photoluminescence obtained under non-resonant, low-power excitation. The most striking feature, under TOPO conditions, is the clear linearization of the dispersion around the signal state. This dispersion arises from the nonlinear response as a manifestation of dominant interactions that strongly dress the states, and resembles the Bogoliubov dispersion for elementary excitations of a superfluid. In the latter case, linearization leads to suppression of weak scattering and therefore to motion without dissipation. In our case, the dispersion reflects the dynamics of the whole system, rather than that of its excitations only. Figure 2a also shows that, for the TOPO, polaritons are blueshifted ($\Delta E = 0.6$ meV at $k \equiv |\mathbf{k}| = 0$), owing to polariton–polariton interactions, and that the intensity peaks strongly at $k_S = 0.6\,\mu\text{m}^{-1}$, which is determined by the phase-matching conditions ($2k_P = k_S + k_I$).

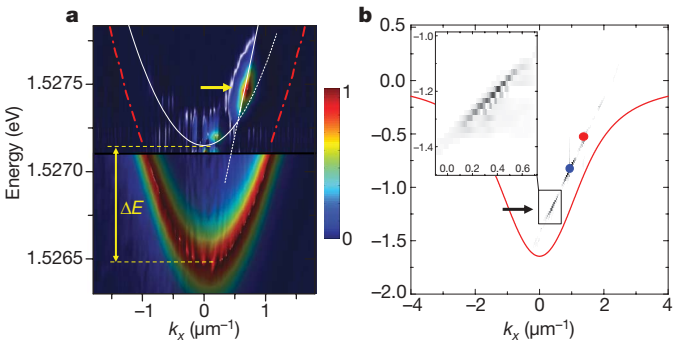

Figure 2 | Experimental and theoretical dispersions. a, Upper panel: false-colour plot of the polariton dispersion under TOPO conditions, showing intensity of emitted light (arbitrary units); lower panel: dispersion obtained under non-resonant, low-power excitation, for which polaritons are not in a condensed state. It is important to notice that the dispersion in which the signal polaritons are moving (bright spot denoted by the arrow in the upper panel) is different from the bare dispersion and shows a linear dependence on k_x. The energy blueshift, $\Delta E = 0.6$ meV, is due to polariton–polariton interactions. **b**, Computer simulation of $|\psi(k_x, E)|^2$ showing the linearization of the signal polariton dispersion due to stimulated scattering processes occurring between a CW pump (blue circle) and a probe (red circle) after the pulse has disappeared. The vertical axis shows the bare exciton energy. An expanded plot of the region around the signal is depicted in the inset. The red line describes the bare dispersion relation of polaritons.

Our system involves macroscopically degenerate states of bosons coupled through exciton–exciton interactions. It can therefore be described theoretically using a nonlinear Schrödinger equation for the polariton wavefunction, $\psi(x, t)$, in the presence of a continuous pump, F_P, and a pulse, F_I, that are incident on the microcavity with respective momenta $\hbar\mathbf{k}_P$ and $\hbar\mathbf{k}_I$, have frequencies ω_P and ω_I, and are localized in Gaussian spots located at x_P and x_I, with spatial extensions σ_P and σ_I. The pulse hits the microcavity at time t_I with a Gaussian profile of root-mean-square duration σ_t. The Schrödinger equation is thus

$$i\hbar\frac{\partial\psi(x,t)}{\partial t} = \left(D - i\hbar\frac{\gamma}{2} + V|\psi(x,t)|^2\right)\psi(x,t) + F_P e^{-(x-x_P)^2/2\sigma_P^2} e^{i(k_P x - \omega_P t)} + F_I e^{-(x-x_I)^2/2\sigma_I^2} e^{-(t-t_I)^2/2\sigma_t^2} e^{i(k_I x - \omega_I t)} \quad (1)$$

where the operator D is the free-propagation energy of the particles; in our case, it provides the dispersion relation specific to polariton branches. The lower branch gives rise to the OPO ($F_I = 0$) or TOPO ($F_I \neq 0$) physics of phase-matched scattering. The two last terms are responsible for maintaining the system out of equilibrium against the decay rate γ. The inclusion of these terms is a crucial difference between our case and the usual case of atomic condensates. Figure 2b shows the calculated dispersion in TOPO conditions, which reproduces both the linearization induced by the interactions and a strong signal-idler emission that proves the triggering of OPO scattering.

In Fig. 3, real-space images of the signal polaritons are shown along with their counterparts in momentum space. The images show that the polariton droplet undergoes unperturbed motion without diffusion in either the x or the y direction, proving that the dispersion around the signal state has lost its locally parabolic character. At the same time, the packet also conserves a well-defined momentum during the propagation time (Fig 3b). This confirms that the polariton signal has a linearized dispersion, as predicted theoretically and observed experimentally (see Fig. 2). By contrast, at low pump powers (without linearization of the dispersion), we observe the very fast appearance of the Rayleigh scattering circle in reciprocal space[6] and the absence of collective motion in real space (Supplementary

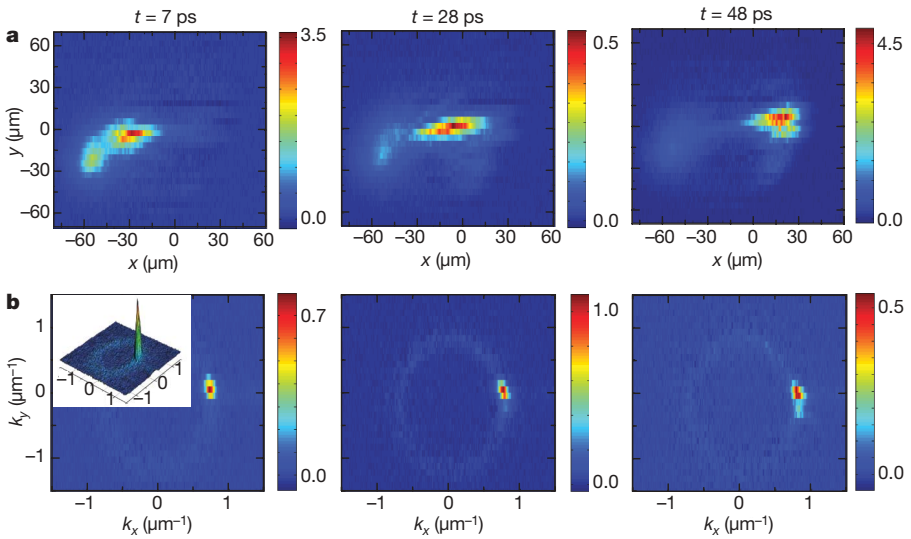

Figure 3 | Free movement of a polariton droplet. a, Spectrally selected observation at the TOPO signal energy of a coherent polariton gas moving at group velocity $v_g = 1.2 \times 10^6\,m\,s^{-1}$ from left to right without being perturbed. Colour scale is as in Fig. 2. The images, recorded under similar conditions to those of Fig. 2, are real-space shots taken at different times (shown) after the pulse arrival ($t = 0$). The total polariton density (pump, signal and idler) is estimated to be of the order of $10^2\,\mu m^{-2}$. **b**, Same conditions as in **a** but in momentum space. The inset displays a three-dimensional view which shows the narrow k distribution. Supplementary Videos 3 and 4 show the free polariton motion.

Videos 1, 2). This observation demonstrates the suppression of scattering as we cross the threshold into the coherent regime.

This propagation is reproduced by our numerical simulation, as seen in Fig. 4a, where a snapshot of the signal is shown at regular intervals of times. To observe the motion of the signal, we take advantage of its separation in energy from both the idler and the pump by filtering the emission in a window of energy, as done in the experiments. Clear propagation within the excitation spot is sustained from the time the pulse triggers the OPO (~2 ps), until the time the signal reaches the edge of the excitation spot. It has a constant speed of $(0.95 \pm 0.1) \times 10^6\,m\,s^{-1}$, in agreement with that obtained experimentally ($(1.2 \pm 0.3) \times 10^6\,m\,s^{-1}$). In Fig. 4b, the spread of the polariton wave packet is plotted as a function of time both from the experimental data and according to calculations based on a parabolic or linear dispersion. The calculation shows that, without the linearization due to interactions, the wave packet would expand more than twice as much during the same time of flight. Moreover, the agreement with the experiments using equation (1) implies that polariton interactions are responsible for the linearization of the signal state.

The excitations of the polariton fluids created with a TOPO can be studied by observing their collisions with structural defects, which are naturally present in the sample. Figure 5a shows images obtained in the near field of a polariton fluid colliding with a defect occurring in the middle of its trajectory. In the course of its propagation, the signal shows unambiguous signs of passing through a defect. However, it clearly maintains its cohesion in this process. This is most strikingly observed in momentum space (Fig. 5b), where the signal is left completely unaltered until the very end of the trajectory, when the single-state occupancy starts spreading as the signal dies by moving off the edge of the pump laser region.

We note that the images reflect the addition of two different contributions: that of the pump polaritons (extended in an area of $\sim 8 \times 10^3\,\mu m^2$) and that of the signal polaritons themselves, which, being constantly fed by the pump, reflect its density fluctuations. Figure 1c illustrates how these two contributions are detected at the signal polariton energy. The fringes observed around the defect appear as a result of the local change in density of the pump polaritons, which is reflected in the spatial structure of the signal.

The pump polaritons are injected in a coherent state, at high energy, density and momenta and with a group velocity greater than the speed of sound, $v_s = 3 \times 10^6\,m\,s^{-1}$ (estimated from the blueshift

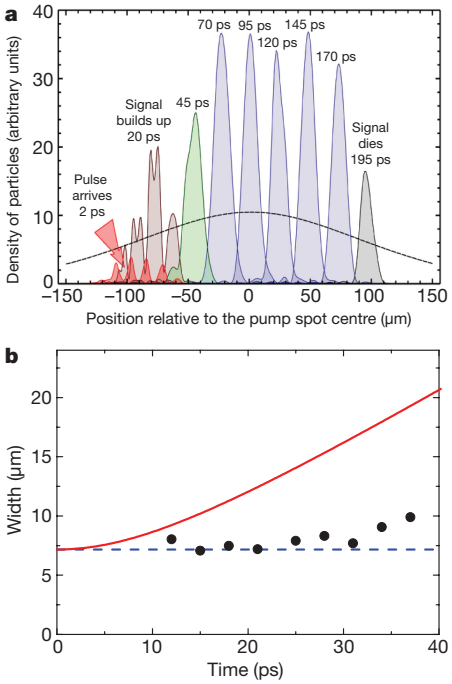

Figure 4 | Simulation of the travelling signal polariton state within the pump spot. a, Computer simulation showing the spatial extent of the pump polaritons (black dashed line) and the evolution of the signal wave packet. The signal is created (red) after a pulse has excited the microcavity at $k_I = 2k_P - k_S$, builds up (orange) and develops into a well-defined Gaussian-like wave packet (green) that subsequently travels over hundreds of micrometres (blue) while inside the pump polariton area. The wave packet dies as it reaches the edge of the pump spot (grey). The animation of the simulated polariton dynamics in real and momentum space can be seen in the Supplementary Video 5. **b**, The measured width (black points) of the coherent polariton droplet as it flows unperturbed, plotted as a function of time. The blue dashed line shows the evolution expected for a fluid with a linear dispersion. The red solid line depicts the size of a polariton wave packet as obtained from the Schrödinger equation with a quadratic dispersion (diffusive regime).

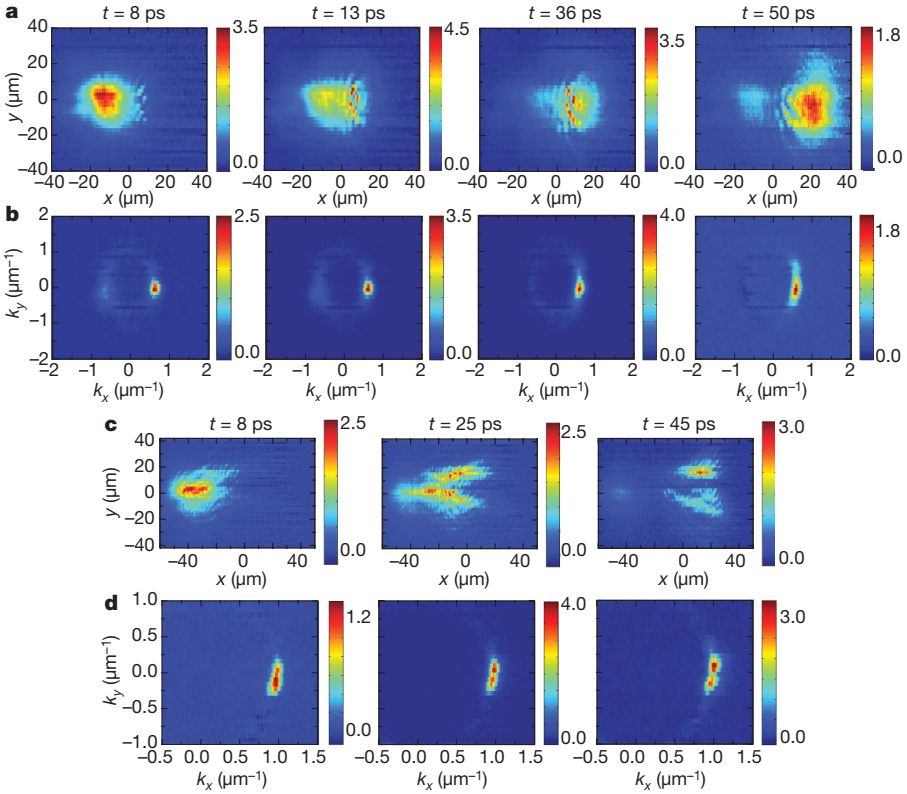

Figure 5 | Images of a polariton droplet colliding against native defects. **a**, **b**, A small structural defect in the sample is encountered in the trajectory of the polariton condensate moving at a velocity of 0.9×10^6 m s^{-1}. Colour scale is as in Fig. 2. The position of the obstacle is revealed, in real space (**a**), by Čerenkov waves caused by the pump polaritons, which are travelling at a supersonic speed. However, the signal polaritons pass through the defect in a superfluid fashion without changing direction or scattering against the obstacle (clearer evidence of this phenomenon can be observed in Supplementary Video 6). This fact is confirmed by the images taken at the same times in momentum space (**b**). It is clear that the momentum vector does not change significantly when the condensate crosses the obstacle (Supplementary Video 7). **c**, **d**, The polariton fluid encounters a defect of a size comparable to its own: the condensed state fully experiences the defect potential, which strongly perturbs the trajectory in real space (**c**) showing the appearance of two independent polariton states with different momentum vectors (**d**); see also Supplementary Videos 8 and 9.

of the polariton dispersion), giving rise, in the presence of a defect, to characteristic quantum interferences resembling Čerenkov waves, which are observed through the emission of the signal polaritons. Similar shock waves have been reported recently for an atomic BEC flowing against a potential barrier at Mach numbers greater than one[12]. It is important to note that the visibility of these waves does not imply that the signal polaritons are also in the 'Čerenkov regime'. By contrast, for the signal polaritons (which are at lower energy and momentum), the group velocity (0.9×10^6 m s^{-1}) is less than v_s, and the signal polariton droplet can thus be expected to behave as a superfluid: excitations in the droplet are inhibited while it passes through the obstacle.

In Fig. 5c, d, a more striking collision is observed: one in which the size of the defect is comparable to that of the polariton packet. The finite-size travelling polariton fluid scatters coherently and elastically on the potential and is split in two after the collision. We note that the process is dissipationless. A normal polariton fluid[21,22] would diffuse both in real and reciprocal space in this configuration. Our macroscopically degenerate droplet, the dispersion of which has been linearized, instead follows coherent and diffusionless trajectories, as borne out by our experiments and clearly shown in the real-space images of Fig. 5c, albeit with two new momenta (see Fig. 5d). The linear dispersion is the key element of this coherent propagation, as any scattered particle from the wave packet remains in phase with the others and at the same group velocity, precluding diffusion both in real and in reciprocal space. We again note that this concerns the wave packet itself, not only its excitations, as is the case in the Landau picture of helium superfluidity. The system exhibits the dynamics of a condensate, but many new features arise from the specific properties of polaritons. Until now, theoretical analysis of the scattering has only been made in the perturbative regime[6,23], with regard to the elementary excitations of the polariton condensate.

Our findings call for further work, both experimental and theoretical, to reveal other properties of this unusual state of matter: a coherent, macroscopically occupied Bose fluid propagating at ultrahigh speed. We have demonstrated that semiconductor microcavities are ideal candidates to study exotic bosonic phenomena. Although the physics associated with condensed phases of polaritons presents both fundamental and subtle deviations from the atomic case, these may prove to be assets in their future study. For instance, in a dissipative system, particle number conservation is lifted and a well-defined phase can be externally imprinted onto polaritons, allowing the investigation of symmetry-breaking mechanisms.

METHODS SUMMARY

Time- and space-resolved emission is obtained at 5 K under simultaneous continuous-wave and pulsed laser excitation. The polariton fluid, at energy E_S and momentum k_S, is continuously replenished from a higher-lying state, at E_P and k_P, by the continuous-wave laser and set in motion by a short trigger pulse (2 ps) at the idler state, E_I and k_I, in a configuration of a TOPO (Fig. 1). Typically, the pump injects a coherent polariton state into the lower polariton branch at an angle of 10° relative to the normal to the cavity plane; the pulse arrives at time $t = 0$ in resonance with the branch at 16°, triggering the OPO and generating a polariton signal with a finite momentum at 4°. Images of the near and far fields of a GaAs-based microcavity are projected on to the entrance slit of a 0.5-m imaging spectrometer attached to a streak camera, thus allowing for simultaneous collection of two-dimensional, time-resolved images at a given energy. To avoid problems caused by detection at the pulsed laser energy, which would bleach the streak camera, the pulsed laser is made resonant with the idler rather than with

the signal state of the triggered OPO. Furthermore, to retain only the light emission from the TOPO signal, the OPO-only emission coming from the pump field, contributing at $k = 0$, is subtracted from all the images.

To solve the nonlinear Schrödinger equation, equation (1) is integrated numerically, first in the absence of the pulse ($F_I = 0$), until a steady state is reached for $|\psi(x, t)|^2$. We obtain the energy/momentum-density plot of the system by Fourier-transforming $\psi(x, t)$. At a given time, t_I, we release a Gaussian pulse ($F_I \neq 0$) that triggers OPO processes. We track the new evolution of $\psi(x, t)$ until the steady state is restored, and Fourier-transform again during this time. In order to compare with the experiment, we subtract the two dispersions.

Full Methods and any associated references are available in the online version of the paper at www.nature.com/nature.

Received 26 August; accepted 13 November 2008.

1. Kasprzak, J. *et al.* Bose–Einstein condensation of exciton polaritons. *Nature* **443,** 409–414 (2006).
2. Balili, R., Hartwell, V., Snoke, D., Pfeiffer, L. & West, K. Bose-Einstein condensation of microcavity polaritons in a trap. *Science* **316,** 1007–1010 (2007).
3. Stevenson, R. M. *et al.* Continuous wave observation of massive polariton redistribution by stimulated scattering in semiconductor microcavities. *Phys. Rev. Lett.* **85,** 3680–3683 (2000).
4. Saba, M. *et al.* High-temperature ultrafast polariton parametric amplification in semiconductor microcavities. *Nature* **414,** 731–735 (2001).
5. Kavokin, A., Malpuech, G. & Laussy, F. P. Polariton laser and polariton superfluidity in microcavities. *Phys. Lett. A* **306,** 187–199 (2003).
6. Carusotto, I. & Ciuti, C. Probing microcavity polariton superfluidity through resonant Rayleigh scattering. *Phys. Rev. Lett.* **93,** 166401 (2004).
7. Lagoudakis, K. G. *et al.* Quantised vortices in an exciton–polariton fluid. *Nature Phys.* **4,** 706–710 (2008).
8. Utsunomiya, S. *et al.* Observation of Bogoliubov excitations in exciton-polariton condensates. *Nature Phys.* **4,** 700–705 (2008).
9. Abo-Shaeer, J. R., Raman, C., Vogels, J. M. & Ketterle, W. Observation of vortex lattices in Bose-Einstein condensates. *Science* **292,** 476–479 (2001).
10. Onofrio, R. *et al.* Observation of superfluid flow in a Bose-Einstein condensed gas. *Phys. Rev. Lett.* **85,** 2228–2231 (2000).
11. Steinhauer, J., Ozeri, R., Katz, N. & Davidson, N. Excitation spectrum of a Bose-Einstein condensate. *Phys. Rev. Lett.* **88,** 120407 (2002).
12. Carusotto, I., Hu, S. X., Collins, L. A. & Smerzi, A. Bogoliubov-Cerenkov radiation in a Bose-Einstein condensate flowing against an obstacle. *Phys. Rev. Lett.* **97,** 260403 (2006).
13. Weisbuch, C., Nishioka, M., Ishikawa, A. & Arakawa, Y. Observation of the coupled exciton-photon mode splitting in a semiconductor quantum microcavity. *Phys. Rev. Lett.* **69,** 3314–3317 (1992).
14. Bajoni, D., Senellart, P., Lemaître, A. & Bloch, J. Photon lasing in GaAs microcavity: Similarities with a polariton condensate. *Phys. Rev. B* **76,** 201305(R) (2007).
15. Lai, C. W. *et al.* Coherent zero-state and π-state in an exciton–polariton condensate array. *Nature* **450,** 529–532 (2007).
16. Krizhanovskii, D. N. *et al.* Dominant effect of polariton-polariton interactions on the coherence of the microcavity optical parametric oscillator. *Phys. Rev. Lett.* **97,** 097402 (2006).
17. Porras, D. & Tejedor, C. Linewidth of a polariton laser: Theoretical analysis of self-interaction effects. *Phys. Rev. B* **67,** 161310 (2003).
18. Perrin, M., Senellart, P., Lemaître, A. & Bloch, J. Polariton relaxation in semiconductor microcavities: Efficiency of electron-polariton scattering. *Phys. Rev. B* **72,** 075340 (2005).
19. Bolda, E. L., Chiao, R. Y. & Zurek, H. Dissipative optical flow in a nonlinear Fabry-Pérot cavity. *Phys. Rev. Lett.* **86,** 416–419 (2001).
20. Ballarini, D. *et al.* Observation of long-lived polariton states in semiconductor microcavities across the parametric threshold. Preprint at ⟨http://arxiv.org/abs/arXiv:0807.3224⟩ (2008).
21. Freixanet, T., Sermage, B., Tiberj, A. & Planel, R. In-plane propagation of excitonic cavity polaritons. *Phys. Rev. B* **61,** 7233–7236 (2000).
22. Langbein, W. *et al.* Polarization beats in ballistic propagation of exciton-polaritons in microcavities. *Phys. Rev. B* **75,** 075323 (2007).
23. Szymanska, M. H., Keeling, J. & Littlewood, P. B. Nonequilibrium quantum condensation in an incoherently pumped dissipative system. *Phys. Rev. Lett.* **96,** 230602 (2006).

Supplementary Information is linked to the online version of the paper at www.nature.com/nature.

Acknowledgements We thank I. Carusotto, M. Wouters and N. Berloff for discussions and D. Steel for a critical reading of the manuscript. This work was partially supported by the Spanish Ministerio de Educación y Ciencia (MEC) (MAT2005-01388, NAN2004-09109-C04-04 & QOIT-CSD2006-00019), the Comunidad Autónoma de Madrid (S-0505/ESP-0200) and the IMDEA-Nanociencia. D.B. and E.d.V. acknowledge a scholarship (Formacion de Profesorado Universitario) of the Spanish MEC. D.S. and M.D.M. thank the Ramón y Cajal Programme.

Author Information Reprints and permissions information is available at www.nature.com/reprints. Correspondence and requests for materials should be addressed to D.S. (daniele.sanvitto@uam.es).

METHODS

Sample. The studied microcavity is composed of an AlAs $\lambda/2$ cavity with top and bottom Bragg mirrors of 15 and, respectively, 25 $Al_{0.1}Ga_{0.9}As$/AlAs pairs, grown on a GaAs substrate. A 20-nm-thick GaAs quantum well is embedded at the antinode position of the cavity mode. When the sample is kept at a temperature of 10 K, the heavy-hole excitons of the quantum well are strongly coupled with the cavity mode, with a Rabi splitting of 4.4 meV. The wedge-shaped cavity allows for fine-tuning of the resonance between the quantum well exciton and the cavity mode by changing the position of the excitation spot on the sample.

Experiments. To make polaritons flow, we have to address three important issues: the very short polariton dwell time in the cavity ($<$2–5 ps), which hinders detection of their dynamics; creation of polaritons in a state with a well-defined momentum; and spatial inhomogeneities produced by sample strain and/or defects. The signal polaritons, fed by the pump in resonance with the lower polariton branch, last for more than 10^{-9} s after the trigger pulse of 2 ps, thus allowing for the detection of the polariton flow dynamics. This approach addresses the first issue listed above: although the lifetime of a single particle of the polariton droplet remains short (a few picoseconds), the packet itself lasts hundreds of picoseconds. To reduce the effect of spatial inhomogeneities, which are present in all semiconductor microcavities[24,25], we keep the pump power at an intensity high enough that most of the potential fluctuations are smoothed out[26]. Scattering centres are nevertheless still present with an approximate density of $10^{-2}\,\mu m^{-2}$, but, as shown in the main text, they can help to reveal the peculiar quantum nature of the polariton fluid.

TOPO. A TOPO is an optical parametric amplifier (for an experimental description of a polariton OPA obtained under CW conditions, see ref. 27) in which the continuous-wave seed provided by an external probe at the idler state is substituted by a short pulse (2 ps), which simply initializes the system, inducing a population at the signal state. After the pulse has disappeared, the signal state is left macroscopically occupied, and the final-state stimulation of the pump polaritons to the signal polaritons carries on for hundreds of picoseconds even if the pulse is no longer present (see Supplementary Fig. 1). Our experimental TOPO configuration differs from the conventional realization of atomic Bose–Einstein condensates and superfluids formed spontaneously in thermal equilibrium without the action of any external driving field. In our case, owing to the lossy character of polaritons, an external coherent source must drive the system. Furthermore, the fluid has a finite spatial extension and propagates as a whole; hence, we are investigating the explicit kinematics of a droplet of BEC, rather than the indirect propagation of a defect inside an infinite-size system.

The propagation of a signal whose shape remains unaltered over great distances is suggestive of a soliton surfing on the steady-state OPO; this picture correctly includes the notion of a non-perturbative excitation (triggered by the pulse). However, elements that are crucial for the stability of a soliton, such as attractive rather than repulsive interactions or the dependence on the dimensionality of the system or on the particle densities, are not present in our case, and a plethora of different shapes, widths and heights of the wave packets can also be sustained on the same dispersion. Therefore, interactions serve the main purpose of replenishing the signal rather than holding it together, and the soliton description is thus not adequate. Instead, this system provides a coherent and macroscopic population of bosons isolated in energy on a linear dispersion. Both ingredients are essential in accounting for the experimental findings.

24. Gurioli, M. *et al.* Weak localization of light in a disordered microcavity. *Phys. Rev. Lett.* **94,** 183901 (2005).
25. Sanvitto, D. *et al.* Spatial structure and stability of the macroscopically occupied polariton state in the microcavity optical parametric oscillator. *Phys. Rev. B* **73,** 241308(R) (2006).
26. Malpuech, G., Solnyshkov, D. D., Ouerdane, H., Glazov, M. M. & Shelykh, I. Bose glass and superfluid phase of cavity polaritons. *Phys. Rev. Lett.* **98,** 206402 (2007).
27. Sanvitto, D., Whittaker, D. M., Skolnick, M. S. & Roberts, J. S. Continuous wave pump-probe experiment on a planar microcavity. *Phys. Stat. Sol. (a)* **202,** 353–356 (2005).

Vol 457|15 January 2009|doi:10.1038/nature07644

LETTERS

Competition between the pseudogap and superconductivity in the high-T_c copper oxides

Takeshi Kondo[1], Rustem Khasanov[2], Tsunehiro Takeuchi[3,4], Jörg Schmalian[1] & Adam Kaminski[1]

In a classical Bardeen–Cooper–Schrieffer superconductor, pairing and coherence of electrons are established simultaneously below the critical transition temperature (T_c), giving rise to a gap in the electronic energy spectrum. In the high-T_c copper oxide superconductors, however, a pseudogap[1–8] extends above T_c. The relationship between the pseudogap and superconductivity is one of the central issues in this field[9–17]. Spectral gaps arising from pairing precursors are qualitatively similar to those caused by competing electronic states, rendering a standard approach to their analysis inconclusive[10–16]. The issue can be settled, however, by studying the correlation between the weights associated with the pseudogap and superconductivity spectral features. Here we report a study of two spectral weights using angle-resolved photoemission spectroscopy. The weight of the superconducting coherent peak increases away from the node following the trend of the superconducting gap, but starts to decrease in the antinodal region. This striking non-monotonicity reveals the presence of a competing state. We demonstrate a direct correlation, for different values of momenta and doping, between the loss in the low-energy spectral weight arising from the opening of the pseudogap and a decrease in the spectral weight associated with superconductivity. We therefore conclude that the pseudogap competes with the superconductivity by depleting the spectral weight available for pairing.

The traditional approach of using spectral features measured by angle-resolved photoemission spectroscopy (ARPES) to determine whether or not the pseudogap consists of a state of preformed pairs has failed to yield conclusive results[10–13,15,16] because the spectral gaps due to, for example, states with charge or spin order can have spectral features qualitatively similar to those characterizing a paired state: back-bending of the dispersion[15] and a symmetric gap[16]. For example, gaps at points on the Fermi surface connected by a density-wave ordering vector are particle–hole symmetric, just as in the case of a pairing gap[16]. The distinguishing factors are subtle, quantitative details such as the precise location of the gap minimum and the degree of symmetry of the spectral function about the chemical potential (μ). Because pairing always leads to a particle–hole-symmetric gap at all points on the Fermi surface[15], the asymmetry of the pseudogap away from the antinodes reported in ref. 16 seems to contradict the data in ref. 15 and a pairing origin of the pseudogap in that region of momentum space.

Although the presence of a Bardeen–Cooper–Schrieffer-like superconducting gap that closes at T_c was unambiguously demonstrated in the nodal regions[11,12], the question about the relationship between the pseudogap and superconductivity was left unanswered owing to the very limited data available in the antinodal region. Similarly, the muon spin relaxation results[14] suggested that the temperature dependence of the superfluid density in optimally doped $(Bi,Pb)_2(Sr,La)_2CuO_{6+\delta}$ (Bi2201) is inconsistent with a fully gapped Fermi surface, but did not show what caused this behaviour, and no connection to the pseudogap was established because muon spin relaxation is a momentum-integrated technique.

Superconductivity in the copper oxides manifests itself in the appearance of a narrow peak in the ARPES spectra[18,19], whereas the pseudogap depletes the low-energy spectral weight below the pseudogap energy[2–4,12]. In Fig. 1 we examine the temperature dependence of the spectral line shape in overdoped Bi2201 ($T_c = 29$ K). Above the pseudogap temperature ($T^* \approx 110$ K), the symmetrized EDCs[4] show a peak centred at μ, consistent with the metallic state of the sample. On cooling below T^*, the low-energy spectral weight for the energies in the range from -20 to 20 meV decreases, leading to a characteristic dip that signifies the opening of an energy gap, as shown in Fig. 1d. As the temperature is decreased below T_c, a small but very sharp peak with a width of $\sim$10 meV appears at an energy of -15 meV (Fig. 1e). The intensity of this peak increases as temperature decreases. This peak appears below T_c and no significant changes in the spectral line shape are observed in this energy range above T_c, as in Bi2212 (ref. 18).

Whereas ARPES measures the single-particle spectral function, it is experimentally well established that the temperature dependence of the weight of the coherent peak is related to that of the superfluid density, a two-particle response function that reflects the robustness of superconductivity[20,21]. Additional evidence supporting this is provided in Fig. 2i, where we compare the doping dependence of the weight of the coherent peak integrated over the Fermi surface with the superfluid density measured in Bi2201 using muon spin relaxation[14,22].

To conduct a quantitative analysis of the spectral weight, we subtract from each EDC in Fig. 1d and Fig. 1e an EDC obtained at T^* (110 K) and one obtained slightly above T_c (41 K), respectively. The results are shown in Fig. 1f, g. From this data, we can extract the respective fractions of the spectral weight lost because of the opening of the pseudogap (W_{PG}) and the coherent spectral weight (W_{CP}). These are plotted in Fig. 1h, i, with the associated areas defined in the insets. We use this method to examine the momentum dependence of both quantities by plotting in Fig. 2a, c, e the symmetrized EDCs below and above T_c (at 11 K and 40 K), measured around the Fermi surface for slightly overdoped (OD29K), optimally doped (OP35K) and underdoped (UD23K) Bi2201, which have respective T_cs of 29 K, 35 K and 23 K. The evolution of the coherent peak around the Fermi surface (Fig. 2g) can be visualized by plotting the difference between the EDCs below and above T_c, as shown in Fig. 2b, d, f. The weight of the coherent peak has a very unexpected momentum dependence, which varies significantly with doping. In the overdoped sample (Fig. 2b), the weight of the coherent peak increases away from the node (top curve) and saturates near the antinode (bottom curve). By contrast, in the optimally and underdoped samples (Fig. 2d, f, respectively) W_{CP} is highly non-monotonic. It initially increases away

[1]Ames Laboratory and Department of Physics and Astronomy, Iowa State University, Ames, Iowa 50011, USA. [2]Laboratory for Muon Spin Spectroscopy, Paul Scherrer Institute, CH-5232 Villigen PSI, Switzerland. [3]Department of Crystalline Materials Science, [4]EcoTopia Science Institute, Nagoya University, Nagoya 464-8603, Japan.

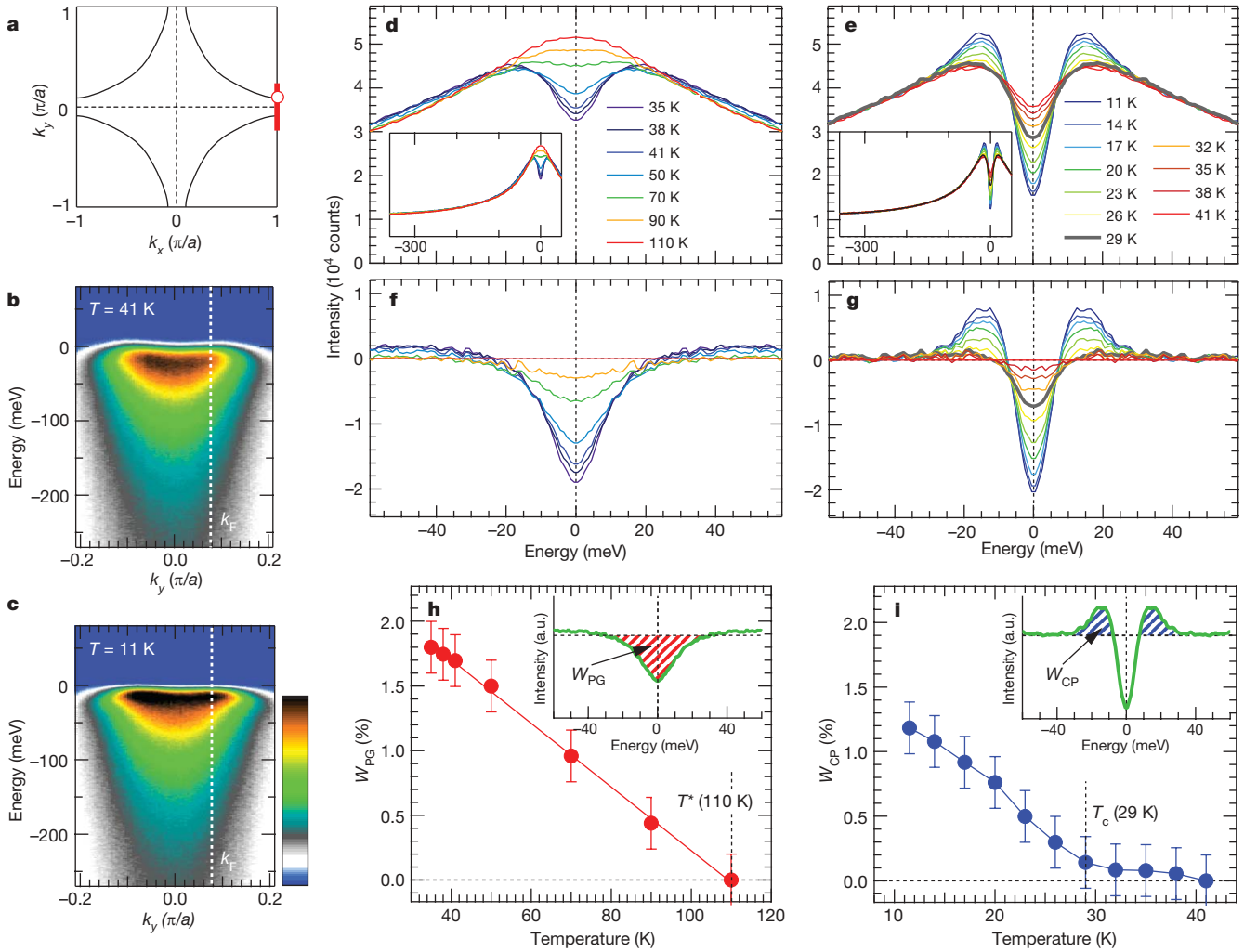

Figure 1 | Temperature dependence of the spectral weight in the superconducting and pseudogap states of overdoped Bi2201 ($T_c = 29$ K). Details of the symmetrization and normalization procedures are provided in Supplementary Information. Location of the Fermi momentum (k_F) for all our data was determined using the peak position of the momentum dispersion curves. The x and y axes lie along the Cu–O bond directions; a, lattice parameter. **a**, Schematic diagram of the Brillouin zone. The red line indicates the cut along which the data in **b** and **c** was acquired. The open circle indicates the antinodal point where the data in **d** and **e** was acquired. k_x and k_y, components of momentum. **b**, **c**, ARPES intensity plots (colour bar shows intensity, increasing from bottom to top), along the cut indicated in **a**, above (**b**) and below (**c**) T_c. The presence of the coherent peak in the superconducting state is evident as a sharp line of strong intensity at −15 meV. **d**, Temperature dependence of the symmetrized energy dispersion curves (EDCs) at antinodal k_F in the pseudogap state. A single peak at the chemical potential is present at 110 K, which corresponds to T^*. **e**, Temperature dependence of the symmetrized EDCs at the antinodal k_F in the superconducting state and slightly above T_c. Note that the coherent peak appears only below T_c and that spectra in this energy range are essentially independent of temperature above T_c. Insets in **d** and **e** show the same data over a wide energy range. **f**, Difference spectra obtained by subtracting the EDC at $T^* = 110$ K from the curves in **d**. **g**, Difference spectra obtained by subtracting the EDC at 41 K from the curves in **e**. **h**, **i**, Temperature dependences of the low-energy spectral weight lost in the pseudogap state (W_{PG}, **h**) and the weight of the coherent peak (W_{CP}, **i**), as fractions of the total area of the symmetrized EDCs in the range −0.3 eV to 0.3 eV (Supplementary Information). We note that W_{PG} is a linear function of temperature below T^*, whereas W_{CP} is zero above T_c and increases with decreasing temperature only below T_c. We note that, by itself, the difference in temperature dependence between W_{PG} and W_{CP} does not provide information about the relationship between the pseudogap and superconductivity. Error bars reflect the maximum uncertainty due to normalization. a.u., arbitrary units.

from the node, just as in the overdoped case, but then is abruptly suppressed in the antinodal region.

This is quite striking, as in all our samples the magnitude of the spectral gap (the overall gap obtained from the peak position) is monotonic (Fig. 3a–c); the weight of the coherent peak might therefore be expected to remain constant or to increase monotonically around the Fermi surface with the largest value at the antinode for all dopings.

We quantify these results by plotting W_{CP} for the three samples as a function of Fermi angle, ϕ, in Fig. 2h. We note that the coherent peak is present at the antinode in optimally and overdoped Bi2201 samples, consistent with previous results[19]. Our measurements reveal that suppression of the coherent peak near the antinode ($\phi = 0$) occurs even in the overdoped samples and becomes stronger with underdoping. This remarkable non-monotonicity and suppression of the weight of the coherent peak is our most significant experimental observation. Because the size of the d-wave superconducting gap is a monotonic function of momentum between the node and antinode, the momentum dependence of the weight of the coherent peak can only be explained by the presence of a state that competes with superconductivity in those regions near the antinode.

We now identify this state. In Fig. 3 a–c, we plot the momentum dependence of the spectral gap below and above T_c. The spectral gap has two components[12]: a d-wave superconducting gap and a pseudogap. In optimally and underdoped samples, the pseudogap dominates the spectra in the antinodal regions[12]. In Fig. 3 d–f, we plot W_{PG} as extracted from the data in Fig. 2a, c, e (see Fig. 1h inset) and compare its momentum dependence with that of W_{CP} for the three dopings. W_{PG} is zero near the node for all three dopings because the

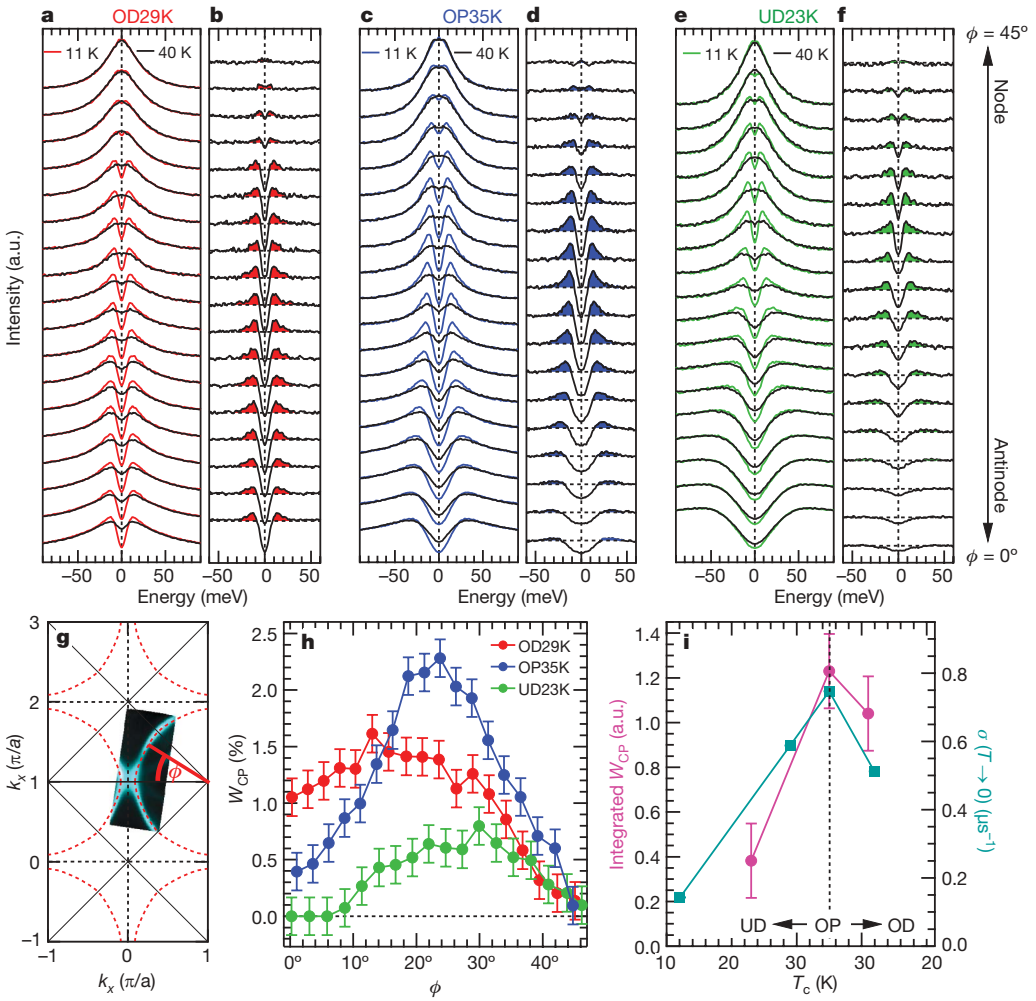

Figure 2 | Momentum dependence of the coherent spectral weight in overdoped, optimally doped and underdoped Bi2201 samples. **a**, Symmetrized EDCs below and above T_c for the overdoped sample ($T_c = 29$ K). **b**, Difference between the curves in **a** (intensity at 11 K minus intensity at 40 K). The area of coherent spectral weight is marked in red. **c**, Symmetrized EDCs below and above T_c for the optimally doped sample ($T_c = 35$ K). **d**, Difference between the curves in panel **c** (as in **b**) The area of coherent spectral weight is marked in blue. **e**, Symmetrized EDCs below and above T_c for the underdoped sample ($T_c = 23$ K). **f**, Difference between the curves in panel **e** (as in **b**). The area of coherent spectral weight is marked in green. The shaded regions **b**, **d** and **e** indicate the areas of the coherent spectral weight (see Fig. 1i inset). **g**, Fermi surface map for the OD29K sample, and definition of the Fermi surface angle, ϕ. This plot represents the ARPES intensity integrated between $\mu - 10$ meV and $\mu + 10$ meV and measured at $T = 40$ K. The bright areas correspond to higher photoelectron intensities and mark the location of the Fermi surface. **h**, Momentum dependence of the weight of the coherent peak (extracted from data in **b**, **d** and **f** between the antinode and node for the three dopings). **i**, Comparison of the weight of the coherent peak from **h** integrated over the Fermi surface (pink) and superfluid density (proportional to muon spin relaxation rate, σ (T → 0); turquoise) measured on similar Bi2201 samples using muon spin relaxation (data from refs 14, 22). UD, underdoped; OP, optimally doped; OD, overdoped. Error bars reflect the maximum uncertainty due to normalization.

superconducting gap closes at T_c, creating a Fermi arc. W_{PG} increases towards the antinode and reaches a maximum there. This behaviour contrasts with that of W_{CP}. In fact, consistently for all dopings, the onset of the suppression of W_{CP} coincides with the increase of the weight lost to the pseudogap. To examine the relationship between the two quantities in more detail, we plot W_{CP} versus W_{PG} (Fig. 3g). Surprisingly, we find an almost perfect linear anticorrelation between the two quantities in all three samples. A similar anticorrelation can be also demonstrated as a function of doping. In Fig. 3h, we plot the ratio of the coherent spectral weight to the total change in the spectral weight ($W_{CP} + W_{PG}$). Here the angle ϕ, where the pseudogap suppresses the coherent component, decreases, as both the pseudogap and T^* become larger; this is clear evidence that the pseudogap competes with superconductivity for the low-energy spectral weight, causing a shrinkage of the coherent part of the Fermi surface as carrier concentration decreases. This explains the unusual temperature dependence of the superfluid density reported in recent muon spin relaxation measurements[14] on the same samples, as well as the suppression of the coherent peak at the antinode in Bi2212 (ref. 10).

In Fig. 4, we sketch the anticorrelation between the pseudogap and the coherent peak in momentum space. An obvious reason for the superconductivity and pseudogap state to compete is that they are due to different microscopic interactions. However, another explanation is possible. The same microscopic interaction that provides the pairing mechanism may also lead to a competing state in which the coherent quasiparticle weight and superconductivity are suppressed. A classical analogue is that, although the electron–phonon coupling gives rise to conventional superconductivity, if it increases it leads to the formation of polaronic states or charge-density order that competes with the superconductivity. We note that pseudogap formation owing to preformed Cooper pairs[1,15,16,23] is clearly inconsistent with our results. In that case, a spectrum with a pseudogap above T_c should transform into that of a fully coherent superconductor below T_c, in contradiction to our findings. Similarly, in the resonating-valence-bond picture[8], at least in its most elementary version, the superconducting coherency should be positively correlated with the pseudogap behaviour. Instead, our data demonstrate that the pseudogap is due to the formation of a competing state such

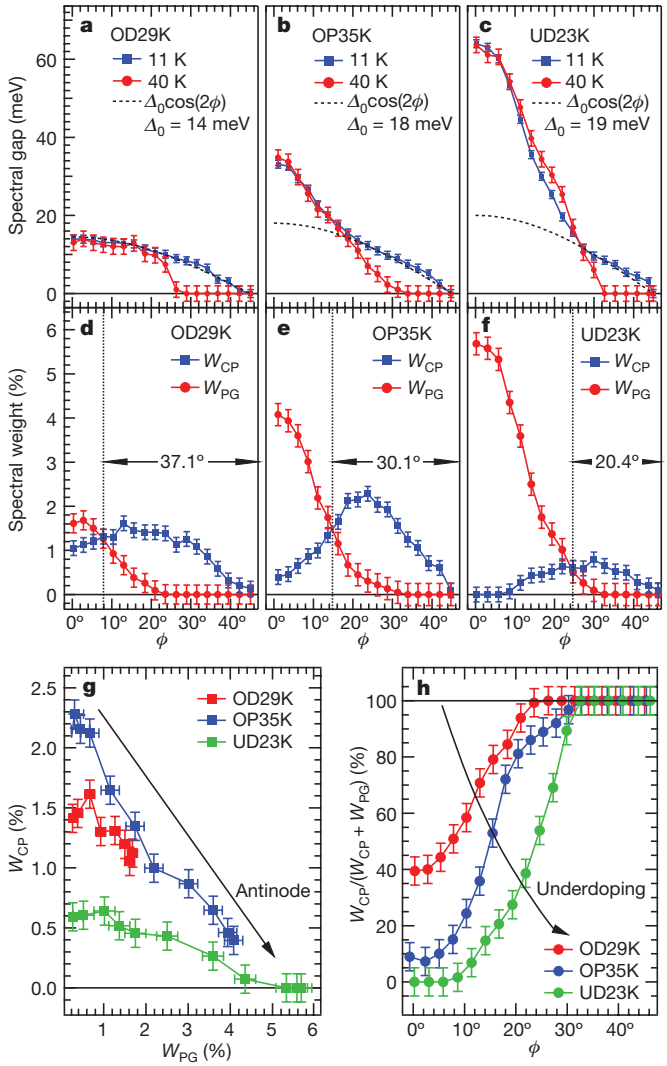

Figure 3 | Momentum dependence of the magnitudes of spectral gap and the coherent and pseudogap spectral weights in overdoped, optimally doped and underdoped Bi2201 samples. **a**–**c**, Momentum dependence of the spectral gap below and above T_c in samples OD29K (**a**), OP35K (**b**) and UD23K (**c**). Dotted lines represent a $\cos(2\phi)$ fit to data in the nodal region. Error bars in **a**–**c** are estimated at ± 1 meV in the superconducting state and ± 2 meV in the pseudogap state, and account for the uncertainty in the fitting procedure. **d**–**f**, Spectral weight lost to the pseudogap (red) and the coherent spectral weight (blue) plotted as a function of the Fermi surface angle, ϕ, and expressed as a percentage of the total spectral weight integrated between $\mu - 300$ meV and $\mu + 300$ meV for the overdoped ($T_c = 29$ K, **d**), optimally doped ($T_c = 35$ K, **e**) and underdoped ($T_c = 23$ K, **f**) samples. Low-energy spectral weight loss in the pseudogap state was obtained by subtracting spectra measured above T^* from those obtained at 40 K and then integrating over an energy range where the difference was negative (see Fig. 1h inset). For the OD29K, OP35K and UD23K samples, the values of T^* were respectively 110 K, 130 K and 240 K (see Supplementary Fig. 1). The arrows indicate the ϕ range of the coherent Fermi surface (that is, where the weight of the coherent peak dominates over the pseudogap weight). We note that this range shrinks with underdoping. **g**, Plot of W_{CP} versus W_{PG}, demonstrating the anticorrelation between the two quantities. The data points correspond to the range of Fermi angles, where weight lost to the pseudogap is finite: $\phi < 15^\circ$ for OD29K, $\phi < 25^\circ$ for OP35K, $\phi < 30^\circ$ for UD23K. **h**, Ratio of W_{CP} to the total change in the spectral weight ($W_{CP} + W_{PG}$) for the three doping levels. Error bars in **d**–**h** reflect the maximum uncertainty due to normalization.

as a density-wave state[24–29] or an ordered dimer state[30]. It is because of this competition that some parts of the Fermi surface do not develop superconducting coherence, which leads to the unusual superconducting response of the underdoped copper oxides[14,22].

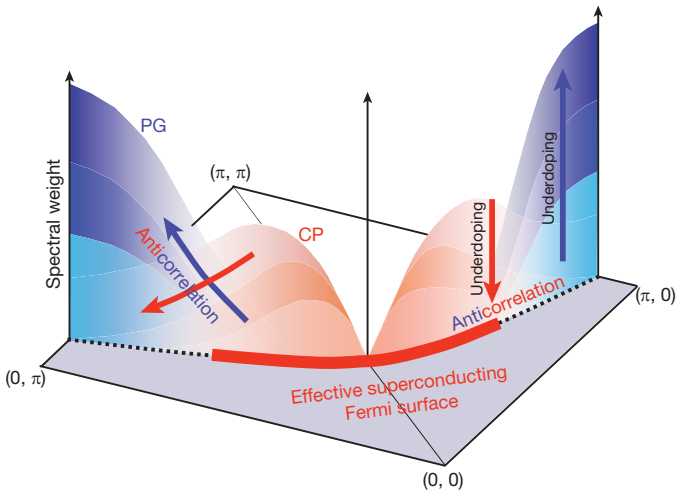

Figure 4 | The momentum and doping evolution of the coherent and pseudogap spectral weights and the effective region of the superconducting quasiparticles. The arrows mark the anticorrelation between pseudogap and high temperature superconductivity in momentum space (k_x, k_y) and with varying doping level. PG, pseudogap; CP, coherent peak.

Received 12 August; accepted 10 November 2008.

1. Emery, V. J. & Kivelson, S. A. Importance of phase fluctuations in superconductors with small superfluid density. *Nature* **374**, 434–437 (1995).
2. Ding, H. *et al.* Spectroscopic evidence for a pseudogap in the normal state of underdoped high-T_c superconductors. *Nature* **382**, 51–54 (1996).
3. Loeser, A. G. *et al.* Excitation gap in the normal state of underdoped $Bi_2Sr_2CaCu_2O_{8+x}$. *Science* **273**, 325–329 (1996).
4. Norman, M. R. *et al.* Destruction of the Fermi surface in underdoped high-T_c superconductors. *Nature* **392**, 157–160 (1998).
5. Timusk, T. & Statt, B. The pseudogap in high-temperature superconductors: an experimental survey. *Rep. Prog. Phys.* **62**, 61–122 (1999).
6. Damascelli, A., Hussain, Z. & Shen, Z.-X. Angle-resolved photoemission studies of the cuprate superconductors. *Rev. Mod. Phys.* **75**, 473–541 (2003).
7. Campuzano, J. C., Norman, M. R. & Randeria, M. in *The Physics of Superconductors* Vol. II (eds Bennemann, K. H. & Ketterson, J. B.) 167–273 (Springer, 2004).
8. Anderson, P. W. *et al.* The physics behind high-temperature superconducting cuprates: The "plain vanilla" version of RVB. *J. Phys. Condens. Matter* **16**, R755–R769 (2004).
9. Le Tacon, M. *et al.* Two energy scales and two distinct quasiparticle dynamics in the superconducting state of underdoped cuprates. *Nature Phys.* **2**, 537–543 (2006).
10. Tanaka, K. *et al.* Distinct Fermi-momentum-dependent energy gaps in deeply underdoped Bi2212. *Science* **314**, 1910–1913 (2006).
11. Lee, W. S. *et al.* Abrupt onset of a second energy gap at the superconducting transition of underdoped Bi2212. *Nature* **450**, 81–84 (2007).
12. Kondo, T., Takeuchi, T., Kaminski, A., Tsuda, S. & Shin, S. Evidence for two energy scales in the superconducting state of optimally doped $(Bi,Pb)_2(Sr,La)_2CuO_{6+x}$. *Phys. Rev. Lett.* **98**, 267004 (2007).
13. Boyer, M. C. *et al.* Imaging the two gaps of the high-temperature superconductor $Bi_2Sr_2CuO_{6+x}$. *Nature Phys.* **3**, 802–806 (2007).
14. Khasanov, R. *et al.* Evidence for competition between the superconducting and the pseudogap state in $(BiPb)_2(SrLa)_2CuO_{6+\delta}$ from muon-spin rotation experiments. *Phys. Rev. Lett.* **101**, 227002 (2008).
15. Kanigel, A. *et al.* Evidence for pairing above T_c from the dispersion in the pseudogap phase of cuprates. *Phys. Rev. Lett.* **101**, 137002 (2008).
16. Johnson, P. D. *et al.* Emergence of preformed Cooper pairs from the doped Mott insulating state in $Bi_2Sr_2CaCu_2O_{8+\delta}$. *Nature* **456**, 77–80 (2008).
17. Norman, M. R., Pines, D. & Kallin, C. The pseudogap: friend or foe of high T_c? *Adv. Phys.* **54**, 715–733 (2005).
18. Loeser, A. G. *et al.* Temperature and doping dependence of the Bi-Sr-Ca-Cu-O electronic structure and fluctuation effects. *Phys. Rev. B* **56**, 14185–14189 (1997).
19. Wei, J. *et al.* Superconducting coherence peak in the electronic excitations of a single layer cuprate superconductor $Bi_2Sr_{1.6}La_{0.4}CuO_{6+\delta}$. *Phys. Rev. Lett.* **101**, 097005 (2008).
20. Feng, D. L. *et al.* Signature of superfluid density in the single-particle excitation spectrum of $Bi_2Sr_2CaCu_2O_{8+x}$. *Science* **289**, 277–281 (2000).
21. Ding, H. *et al.* Coherent quasiparticle weight and its connection to high-T_c superconductivity from angle-resolved photoemission. *Phys. Rev. Lett.* **87**, 227001 (2001).
22. Russo, P. L. *et al.* Muon spin relaxation study of superconducting $Bi2Sr_{2-x}La_xCuO_{6+x}$. *Phys. Rev. B* **75**, 054511 (2007).
23. Shi, M. *et al.* The coherent d-wave superconducting gap in underdoped $La_{2-x}Sr_xCuO_4$ as studied by angle-resolved photoemission. *Phys. Rev. Lett.* **101**, 047002 (2008).

24. Varma, C. M. Non-Fermi-liquid states and pairing instability of a general model of copper oxide metals. *Phys. Rev. B* **55,** 14554–14580 (1997).
25. Schmalian, J., Pines, D. & Stojkovic, B. Weak pseudogap behavior in the underdoped cuprate superconductors. *Phys. Rev. Lett.* **80,** 3839–3842 (1998).
26. Emery, V. J., Kivelson, S. A. & Tranquada, J. M. Stripe phases in high-temperature superconductors. *Proc. Natl Acad. Sci. USA* **96,** 8814–8817 (1999).
27. Chakravarty, S., Laughlin, R. B., Morr, D. K. & Nayak, C. Hidden order in the cuprates. *Phys. Rev. B* **63,** 094503 (2001).
28. Hanaguri, T. *et al.* A 'checkerboard' electronic crystal state in lightly hole-doped $Ca_{2-x}Na_xCuO_2Cl_2$. *Nature* **430,** 1001–1005 (2004).
29. Wise, W. D. *et al.* Charge-density-wave origin of cuprate checkerboard visualized by scanning tunnelling microscopy. *Nature Phys.* **4,** 696–699 (2008).
30. Balents, L., Bartosch, L., Burkov, A., Sachdev, S. & Sengupta, K. Putting competing orders in their place near the Mott transition. II. The doped quantum dimer model. *Phys. Rev. B* **71,** 144509 (2005).

Supplementary Information is linked to the online version of the paper at www.nature.com/nature.

Acknowledgements We thank A. J. Millis, C. Varma and H. M. Fretwell for discussions. This work was supported by Basic Energy Sciences, US Department of Energy. The Ames Laboratory is operated for the US Department of Energy, Basic Energy Sciences, by Iowa State University under contract no. DE-AC02-07CH11358.

Author Contributions T.K., R.K. and A.K. designed the experiment. T.K. and T.T. grew the high-quality single crystals. T.K. acquired the experimental data and T.K. and A.K. performed the data analysis. T.K., A.K. and J.S. wrote the manuscript. All authors discussed the results and commented on the manuscript.

Author Information Reprints and permissions information is available at www.nature.com/reprints. Correspondence and requests for materials should be addressed to A.K. (kaminski@ameslab.gov) or T.K. (kondo@ameslab.gov).

LETTERS

Boundary layer control of rotating convection systems

Eric M. King[1], Stephan Stellmach[2]†, Jerome Noir[1], Ulrich Hansen[2] & Jonathan M. Aurnou[1]

Turbulent rotating convection controls many observed features of stars and planets, such as magnetic fields, atmospheric jets and emitted heat flux patterns[1–6]. It has long been argued that the influence of rotation on turbulent convection dynamics is governed by the ratio of the relevant global-scale forces: the Coriolis force and the buoyancy force[7–12]. Here, however, we present results from laboratory and numerical experiments which exhibit transitions between rotationally dominated and non-rotating behaviour that are not determined by this global force balance. Instead, the transition is controlled by the relative thicknesses of the thermal (non-rotating) and Ekman (rotating) boundary layers. We formulate a predictive description of the transition between the two regimes on the basis of the competition between these two boundary layers. This transition scaling theory unifies the disparate results of an extensive array of previous experiments[8–15], and is broadly applicable to natural convection systems.

Rapidly rotating convection is typically organized by the Coriolis force into tall, thin, coherent convection columns that are aligned with the rotation axis (Fig. 1a). This organizing effect is thought, for example, to be responsible for the strength and structure of magnetic fields generated by convection in planetary interiors[16]. As thermal forcing is increased, the relative influence of rotation weakens, and three-dimensional, turbulent convection can occur (Fig. 1b). It is commonly assumed that rotational effects will dominate convection dynamics when the ratio of the global buoyancy force to the Coriolis forces is less than unity[7–12]. Here we argue, by means of a coupled set of laboratory and numerical experiments, that the boundary layer dynamics, not the global force balance, control the style of convection.

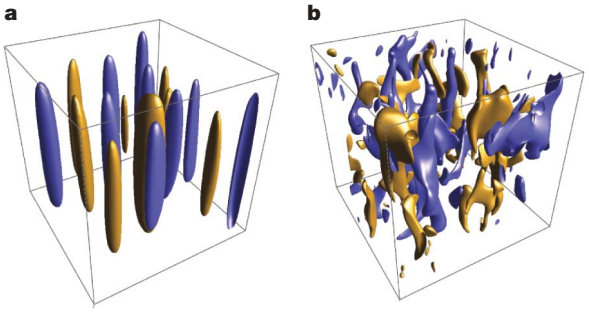

Figure 1 | Iso-surfaces of vertical velocity, from numerical experiments. **a**, $E = 10^{-4}$, $\mathrm{Ra} = 5 \times 10^6$, $\mathrm{Pr} = 7$. Here we see large-scale, coherent, axially aligned velocity structures typical of rotationally dominated convection. $\mathrm{Ro_c} = 0.08$, $\mathrm{Ra/Ra_t} = 0.36$. **b**, $E = 10^{-4}$, $\mathrm{Ra} = 2.1 \times 10^8$, $\mathrm{Pr} = 7$. Here we see predominantly three-dimensional convective structures typical of non-rotating convection, despite a ratio of global buoyancy to Coriolis force of $\mathrm{Ro_c} = 0.5$. However, the boundary-layer-transition hypothesis predicts this breakdown of rotational control, as $\mathrm{Ra/Ra_t} = 14$.

Many previous studies of heat transfer exist for rotating convection systems[8–10,12–15]. However, no unified description of rotating convective heat transfer exists. Often, such studies seek scaling laws for heat transfer efficiency as a function of thermal driving, $\mathrm{Nu} \propto \mathrm{Ra}^{\alpha}$. The Nusselt number, Nu, characterizes the efficiency of convective heat transfer, and is given by the ratio of the total heat transfer to the conductive heat transfer. Thus, $\mathrm{Nu} = 1$ for purely conductive heat transfer, and higher values of Nu correspond to more efficient convective heat transfer. The strength of buoyancy forcing is characterized by the ratio of buoyancy to diffusion, quantified by the Rayleigh number, Ra. In thermal convection, $\mathrm{Ra} = \alpha_T g \Delta T D^3/\nu\kappa$, where α_T is the fluid's thermal expansion coefficient, g is the acceleration due to gravity, ΔT is the temperature drop across the fluid layer, D is the length scale of the system, ν is the fluid's viscous diffusivity and κ is the fluid's thermal diffusivity. Many non-rotating convection studies yield a scaling exponent of $\alpha \approx 2/7$ (refs 10, 17, 18). Some rotating convection studies still find the $\alpha \approx 2/7$ scaling[8–10], whereas comparable studies have found a markedly different, $\alpha \approx 6/5$, scaling[12–14]. Extrapolating these two empirical scaling laws to astrophysical or geophysical parameters yields predictions that disagree by many orders of magnitude.

In this Letter, we show that this apparent discrepancy can be explained in terms of boundary layer dynamics. A convecting fluid volume consists of two distinct dynamical regions: the interior (or bulk) fluid, and the boundary layers[1,19]. Typically, most of the convecting volume is contained in the bulk, and the boundary layers are thin regions where the interior fluid meets the bounding surfaces and diffusion is important. In turbulent, non-rotating convection, diffusive effects are negligible in the bulk of the fluid. Ideally, strongly turbulent motions result in a well-mixed, isothermal interior, corresponding to an effective thermal short cut across the fluid layer[1]. The only remaining limitation to heat transfer, then, is in the quasi-static thermal boundary layers. In this system, it can be shown that $\mathrm{Nu} \propto D/\delta_\kappa$, where δ_κ is the thermal boundary layer thickness[1], such that the thermal boundary layer becomes thinner as the vigour of convection is increased (see Supplementary Information, section 2). In rotating fluid dynamics, the strength of rotation is characterized by the ratio of the viscous force to the Coriolis force, namely the Ekman number, $E = \nu/2\Omega D^2$, where Ω is the angular rate of rotation. In rapidly rotating systems, the important boundary layer is the Ekman layer, which promotes communication between the rotating container and the bulk fluid, permitting an interior flow that is controlled by rotation[9,19]. The Ekman boundary layer has thickness $\delta_E \propto E^{1/2}D$, such that the Ekman layer becomes thinner as the system's rotation rate increases.

Following refs 20–22, we hypothesize that the effects of rotation dominate convection dynamics when the Ekman layer is thinner than the thermal boundary layer, that is, when $\delta_E < \delta_\kappa$. By contrast, when

[1]Department of Earth and Space Sciences, University of California, Los Angeles, California 90095-1567, USA. [2]Institut für Geophysik, WWU Münster, AG Geodynamik Corrensstrasse 24, Münster 48149, Germany. †Present address: Department of Applied Mathematics and Statistics, and Institute of Geophysics and Planetary Physics, University of California, Santa Cruz, California 95064, USA.

the thermal boundary layer is thinner than the Ekman layer, $\delta_\kappa < \delta_E$, the uppermost part of the Ekman layer is mixed with the bulk. This mixing truncates the influence of the Ekman layer, and therefore rotation, on the interior fluid dynamics[20,22]. The transition between rotationally controlled and non-rotating convection dynamics therefore occurs when $\delta_\kappa \approx \delta_E$. We solve for a transitional Nusselt number scaling by equating δ_κ and δ_E, yielding $Nu_t \propto E^{-1/2}$. Thus, our hypothesis leads us to predict that convection will be dominated by the influence of rotation when $Nu < Nu_t$. Conversely, we expect non-rotating convection dynamics for $Nu > Nu_t$.

Rotating convection experiments allow us to vary the thickness of the thermal boundary layer by varying the heating rate, and that of the Ekman boundary layer by varying the rotation rate. To test our hypothesis, we carry out laboratory and numerical experiments spanning $2 \times 10^3 < Ra < 6 \times 10^9$ and $10^{-6} \leq E \leq \infty$ (see Supplementary Information, section 1). Heat transfer behaviour is shown in Fig. 2. Non-rotating ($E = \infty$) heat transfer data agree with the previously obtained $Nu \propto Ra^{2/7}$ scaling law[10,17,18]. Several different fluids are used, as characterized by the Prandtl number, $Pr = \nu/\kappa$. Fluids with different Prandtl numbers yield slightly different non-rotating scaling prefactors[23–25], but we do not consider this relatively weak effect here. When rotation is included, the onset of convection is delayed by the stabilizing effect of the Coriolis force[26]. Once convection begins, heat transfer exhibits a much steeper scaling, in agreement with the previously reported $Nu \propto Ra^{6/5}$ relationship[12–14]. More specifically, heat transfer is adequately described by $Nu = (Ra/Ra_c)^{6/5}$ in this convective regime, where $Ra_c = 6E^{-4/3}$ is the critical Rayleigh number for the onset of convection[26]. However, owing to the experimental limitations in accessing the rapidly rotating, strongly supercritical regime, this scaling is not well constrained. For strong enough thermal forcing (Ra) at a given rotation rate (E), our heat transfer data conform to the non-rotating scaling behaviour. Thus, we observe two distinct convective heat transfer regimes: the rotationally controlled regime, with $Nu \propto Ra^{6/5}$, and the non-rotating regime, with $Nu \propto Ra^{2/7}$.

We define the transition between these two regimes as the point of intersection between their respective scalings, $Nu = 0.16Ra^{2/7}$ and $Nu = (Ra/Ra_c)^{6/5}$. Equating the two, we solve for transitional Rayleigh and Nusselt numbers: $Ra_t = 1.4E^{-7/4}$ and $Nu_t = 0.18E^{-1/2}$. Figure 3a shows Nu normalized by the non-rotating scaling law versus Ra normalized by the transitional Rayleigh number. When $Ra < Ra_t$ ($Nu < Nu_t$), convection is constrained by the influence of rotation and heat transfer is less efficient than its non-rotating counterpart. When $Ra > Ra_t$ ($Nu > Nu_t$), heat transfer is not significantly affected by rotation and follows the non-rotating scaling. Indeed, our empirical results agree with the boundary layer transition hypothesis, which predicts that $Nu_t \propto E^{-1/2}$.

To further test our hypothesis, we measure the thicknesses of the two boundary layers from numerical experiments carried out at $E = 10^{-4}$ and $Pr = 7$ (Fig. 3b). Following refs 17, 27, we define the Ekman boundary layer thickness, δ_E, as the vertical position of the maximum value of the root-mean-square velocity, and the thermal boundary layer thickness, δ_κ, as the vertical position of the maximum value of the temperature variance (see Supplementary Information, section 2). Figure 3b illustrates that when $\delta_\kappa \approx \delta_E$, $Ra \approx Ra_t$ and the

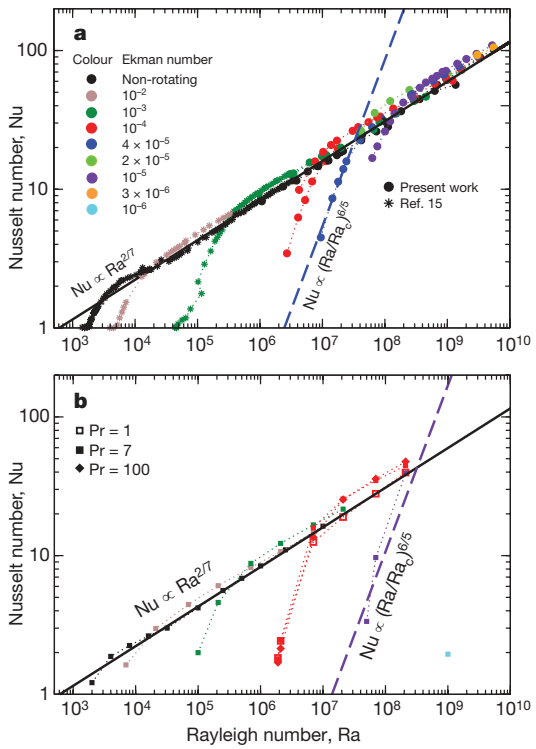

Figure 2 | Nusselt number versus Rayleigh number. **a**, Laboratory experiments; **b**, numerical simulations. Our laboratory experiments were carried out in cylinders with diameter-to-height ratios ranging from 6.25 to 1 using water ($Pr \approx 7$) and sucrose solution ($Pr \approx 10$). Included in **a** are results from ref. 15 in water. Numerical experiments are carried out in a Cartesian box with no-slip top and bottom boundaries and periodic sidewalls. Gravity and the rotation axis are both vertical. Non-rotating convection in laboratory experiments yields $Nu \propto Ra^{0.289 \pm 0.005}$ across more than five decades in Ra. Solid black lines represent the non-rotating scaling law $Nu = 0.16Ra^{2/7}$. Dashed black lines represent the rotationally controlled scaling law $Nu = (Ra/Ra_c)^{6/5}$, where $Ra_c = 6E^{-4/3}$ from ref. 26.

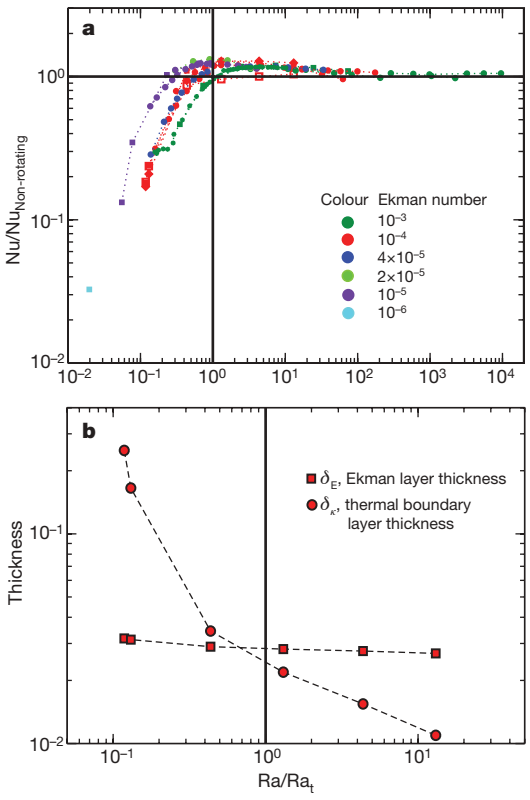

Figure 3 | The transition from rotationally controlled to non-rotating heat transfer behaviour. **a**, The heat transfer regime is determined by the transitional Rayleigh number, $Ra_t = 1.4E^{-7/4}$, for $E \leq 10^{-3}$ and $1 \leq Pr \leq 100$. Symbols are the same as in Fig. 2. The Nusselt number is normalized by its non-rotating value, $Nu_{Non\text{-}rotating} = 0.16Ra^{2/7}$. When $Ra/Ra_t > 1$, heat transfer follows the non-rotating scaling law. Near the transition, the data overshoot the non-rotating scaling law owing to Ekman pumping effects[9,30]. **b**, The numerically determined non-dimensional thicknesses of the competing boundary layers are shown as the Rayleigh number is varied for $E = 10^{-4}$ and $Pr = 7$. The dynamical transition at $Ra = Ra_t$ occurs when the relative thicknesses of the competing boundary layers are approximately equal, that is, when $\delta_\kappa = \delta_E$.

transition is in fact controlled by the relative thicknesses of the boundary layers. When the thermal boundary layer is thinner than the Ekman layer ($\delta_\kappa < \delta_E$, $Ra > Ra_t$), convection is manifested as turbulent, three-dimensional flow (Fig. 1b). Conversely, when the Ekman layer is thinner than the thermal boundary layer ($\delta_E < \delta_\kappa$, $Ra < Ra_t$), rotational effects control convection and constrain fluid motion (Fig. 1a).

It is often argued that the influence of rotation on turbulent convection dynamics is governed by the relative global magnitude of the relevant forces: the buoyancy force and the Coriolis force[7–12]. The ratio of these two global forces is represented by the convective Rossby number[7–12], $Ro_c = \sqrt{RaE^2\,Pr^{-1}}$. The force balance argument predicts a transition between rotationally controlled convection and non-rotating convection when $Ro_c \approx 1$ (see Supplementary Information, section 3), and thus predicts a transitional Rayleigh number that scales as E^{-2}, in comparison with the $E^{-7/4}$ scaling derived from our boundary layer arguments. These two scalings, when extrapolated to planetary settings, yield drastically different predictions for the importance of rotation. At a typical planetary value[12] of $E = 10^{-15}$, for example, the two scalings predict transitional Rayleigh numbers that differ by roughly four orders of magnitude. Figure 4 shows experimental heat transfer data (Nu) plotted against Ro_c. Should the force balance control the importance of rotation in convective heat transfer, we would expect the transitions to occur when $Ro_c \approx 1$. The heat transfer transitions observed in the data (Fig. 4) are not adequately explained by the global force balance, Ro_c, but are instead well described by our boundary-layer-controlled transition scaling. Furthermore, the force balance argument predicts a Pr-dependent transition, and no such dependence is observed. Our transition scaling also describes the disparate results from previous studies: those[12–14] finding the rotationally controlled $Nu \approx Ra^{6/5}$ heat transfer behaviour typically have $Ra < Ra_t$, whereas those[8–10] yielding the non-rotating scaling, $Nu \approx Ra^{2/7}$, typically have $Ra > Ra_t$, despite setting $Ro_c < 1$. To further test the validity of boundary layer control, future laboratory and numerical experiments must be able to access high Ra convection at lower values of E.

The boundary-layer-controlled transition scaling, Ra/Ra_t, is broadly applicable to natural convection systems (see Supplementary Information, section 4). The Rayleigh number, Ra, depends on a system's global density gradient (in thermal convection, the temperature gradient), which is often difficult to observe in nature. The flux-Rayleigh number, $Ra_f = RaNu$, depends instead on the overall buoyancy flux. For thermal convection, $Ra_f = \alpha_T g D^4 Q/\rho c_p \kappa^2 \nu$, where Q is the heat flux, ρ is the fluid's mean density and c_p is the fluid's specific heat. The product of Ra_t and Nu_t constitutes a transitional flux-Rayleigh number, $Ra_{f,t} = 0.25E^{-9/4}$.

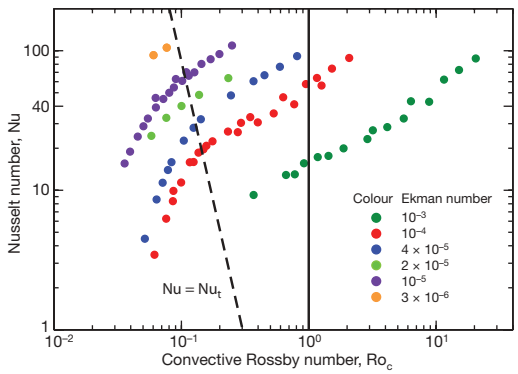

Figure 4 | Nusselt number versus the convective Rossby number for laboratory experiments in water ($Pr \approx 7$) with $3 \times 10^{-6} \leq E \leq 10^{-2}$. The convective Rossby number, Ro_c, characterizes the ratio of buoyancy forcing to the Coriolis force. Force balance arguments predict that rotation will dominate the system when $Ro_c < 1$. However, our heat transfer regime transitions follow the boundary-layer-controlled transitional Nusselt number, $Nu_t = 0.18E^{-1/2}$ (dashed line).

Thus, given the fluid properties, system size and rotation rate, as well as the emitted heat flux, a given body's convective regime can be determined. For example, a typical estimate[12,14] of the Ekman number in the Earth's liquid-metal outer core is $E \approx 10^{-15}$, which allows us to estimate a transitional flux-Rayleigh number of $Ra_{f,t} = 2 \times 10^{33}$ for the core. We estimate a flux-Rayleigh number of $Ra_f \approx 6 \times 10^{29}$ in the core using the following estimates[23,28]: $\alpha_T \approx 10^{-4}\,K^{-1}$; $g \approx 10\,m\,s^{-2}$; $D \approx 2 \times 10^6\,m$; $\rho \approx 10^4\,kg\,m^{-3}$; $c_p \approx 1{,}000\,J\,kg^{-1}\,K^{-1}$, $\kappa \approx 10^{-5}\,m^2\,s^{-1}$; $\nu \approx 10^{-6}\,m^2\,s^{-1}$; and a 4-TW superadiabatic heat flow from the core, corresponding to a superadiabatic $Q \approx 4 \times 10^{-2}\,W\,m^{-2}$. Using the empirical relation $Nu \approx (Ra/Ra_c)^{6/5}$, appropriate to convection with $Ra_f < Ra_{f,t}$, we provide the following estimate of the Rayleigh number in the Earth's core: $Ra \approx 7 \times 10^{24}$.

This estimate implies that core convection occurs just below the boundary layer transition, with $Ra/Ra_t \approx 3 \times 10^{-2}$, and this close proximity to the transition may be important for core dynamics. Recent work has shown that reversal frequencies of magnetic fields in dynamo simulations are linked to the decreasing importance of rotation[29]. Geomagnetic reversals may then depend on boundary layer dynamics and on the value of Ra/Ra_t in the core. To test the planetary and stellar applicability of our result, future work must investigate the influence of low-Pr fluids, fluid compressibility, strong magnetic fields, spherical geometry and internal heating on the boundary layer transition.

Received 27 June; accepted 28 October 2008.

1. Spiegel, E. A. Convection in stars. *Annu. Rev. Astron. Astrophys.* **9,** 323–353 (1971).
2. Ingersoll, A. P. & Porco, C. C. Solar heating and internal heat flow on Jupiter. *Icarus* **35,** 27–43 (1978).
3. Hathaway, D. H. A convective model for turbulent mixing in rotating convection zones. *Astrophys. J.* **276,** 316–324 (1984).
4. Busse, F. H. Convective flows in rapidly rotating sphere and their dynamo action. *Phys. Fluids* **14,** 1301–1314 (2002).
5. Heimpel, M., Aurnou, J. & Wicht, J. Simulation of equatorial and high-latitude jets on Jupiter in a deep convection model. *Nature* **438,** 193–196 (2005).
6. Aurnou, J., Heimpel, M., Allen, L., King, E. & Wicht, J. Convective heat transfer and the pattern of thermal emission on the gas giants. *Geophys. J. Int.* **173,** 793–801 (2008).
7. Gilman, P. A. Nonlinear dynamics of Boussinesq convection in a deep rotating spherical shell. *Geophys. Astrophys. Fluid Dyn.* **8,** 93–135 (1977).
8. Julien, K., Legg, S., McWilliams, J. & Werne, J. Hard turbulence in rotating Rayleigh-Bénard convection. *Phys. Rev. E* **53,** 5557–5560 (1996).
9. Julien, K., Legg, S., McWilliams, J. & Werne, J. Rapidly rotating turbulent Rayleigh-Bénard convection. *J. Fluid Mech.* **322,** 243–273 (1996).
10. Liu, Y. & Ecke, R. E. Heat transport in turbulent Rayleigh-Bénard convection: effects of rotation and Prandtl number. *Phys. Rev. Lett.* **79,** 2257–2260 (1997).
11. Aurnou, J. M., Heimpel, M. & Wicht, J. The effects of vigorous mixing in a convective model of zonal flow on the ice giants. *Icarus* **190,** 110–126 (2007).
12. Aurnou, J. M. Planetary core dynamics and convective heat transfer scaling. *Geophys. Astrophys. Fluid Dyn.* **101,** 327–345 (2007).
13. Christensen, U. R. Zonal flow driven by strongly supercritical convection in rotating spherical shells. *J. Fluid Mech.* **470,** 115–133 (2002).
14. Christensen, U. R. & Aubert, J. Scaling properties of convection-driven dynamos in rotating spherical shells and application to planetary magnetic fields. *Geophys. J. Int.* **166,** 97–114 (2006).
15. Rossby, H. T. A study of Bénard convection with and without rotation. *J. Fluid Mech.* **36,** 309–335 (1969).
16. Olson, P. L. & Christensen, U. R. Dipole moment scaling for convection-driven planetary dynamos. *Earth Planet. Sci. Lett.* **250,** 561–571 (2006).
17. Takeshita, T., Segawa, T., Glazier, J. A. & Sano, M. Thermal turbulence in mercury. *Phys. Rev. Lett.* **76,** 1465–1468 (1996).
18. Glazier, J. A., Segawa, T., Naert, A. & Sano, M. Evidence against ultrahard thermal turbulence at very high Rayleigh numbers. *Nature* **398,** 307–310 (1999).
19. Greenspan, H. P. *The Theory of Rotating Fluids* (Cambridge Univ. Press, 1968).
20. Hignett, P., Ibbetson, A. & Killworth, P. D. On thermal rotating convection driven by non-uniform heating from below. *J. Fluid Mech.* **109,** 161–187 (1981).
21. Boubnov, B. M. & Golitsyn, G. S. Temperature and velocity field regimes of convective motions in a rotating plane fluid layer. *J. Fluid Mech.* **219,** 215–239 (1990).
22. Read, P. L. Transition to geostrophic turbulence in the laboratory, and as a paradigm in atmospheres and oceans. *Surv. Geophys.* **22,** 265–317 (2001).
23. Tilgner, A. High-Rayleigh-number convection in spherical shells. *Phys. Rev. E* **53,** 4847–4851 (1996).
24. Verzicco, R. & Camussi, R. Prandtl number effects in convective turbulence. *J. Fluid Mech.* **383,** 55–73 (1999).

25. Schmalzl, J., Breuer, M. & Hansen, U. The influence of the Prandtl number on the style of vigorous thermal convection. *Geophys. Astrophys. Fluid Dyn.* **96,** 381–403 (2002).
26. Chandrasekhar, S. The instability of a layer of fluid heated below and subject to Coriolis forces. *Proc. R. Soc. Lond. A* **217,** 306–327 (1953).
27. Belmonte, A., Tilgner, A. & Libchaber, A. Temperature and velocity boundary layers in turbulent convection. *Phys. Rev. E* **50,** 269–279 (1994).
28. Nimmo, F., Price, G. D., Brodholt, J. & Gubbins, D. The influence of potassium on core and geodynamo evolution. *Geophys. J. Int.* **156,** 363–376 (2004).
29. Kutzner, C. & Christensen, U. R. From stable dipolar towards reversing numerical dynamos. *Phys. Earth Planet. Inter.* **131,** 29–45 (2002).
30. Kunnen, R. P. J., Clercx, H. J. H. & Geurts, B. J. Heat flux intensification by vortical flow localization in rotating convection. *Phys. Rev. E* **74,** 056306 (2006).

Supplementary Information is linked to the online version of the paper at www.nature.com/nature.

Acknowledgements Salary support for E.M.K., J.N. and J.M.A. was provided by the US National Science Foundation Earth Sciences Division Geophysics Program and the NASA Planetary Atmospheres Program. Support for S.S. and U.H. was provided by the German Research Foundation and for S.S. by the NASA Solar and Heliospheric Physics Program. Support for laboratory experiment fabrication was provided by the US National Science Foundation Instrumentation & Facilities Program. Computational resources were provided by the John von Neumann-Institut für Computing. E.M.K., J.N. and J.M.A. would like to thank J. Frydman, J. Neal, A. Yaghmaei and R. M. Aurnou for engineering support in experimental development. E.M.K. and J.M.A. would like to thank H. T. Rossby for making his thesis data available to them, J. McWilliams for discussion and S. R. Dickman for introducing them to geophysics.

Author Information Reprints and permissions information is available at www.nature.com/reprints. Correspondence and requests for materials should be addressed to E.M.K. (eric.king@ucla.edu).

LETTERS

The braincase and jaws of a Devonian 'acanthodian' and modern gnathostome origins

Martin D. Brazeau[1]

Modern gnathostomes (jawed vertebrates) emerged in the early Palaeozoic era[1], but this event remains unclear owing to a scant early fossil record. The exclusively Palaeozoic 'acanthodians' are possibly the earliest[2,3] gnathostome group and exhibit a mosaic of shark- and bony fish-like characters that has long given them prominence in discussions of early gnathostome evolution[1]. Their relationships with modern gnathostomes have remained mysterious, partly because their un-mineralized endoskeletons rarely fossilized. Here I present the first-known braincase of an Early Devonian (approximately 418–412 Myr BP) acanthodian, *Ptomacanthus anglicus*[4], and re-evaluate the interrelationships of basal gnathostomes. Acanthodian braincases have previously been represented by a single genus, *Acanthodes*[5], which occurs more than 100 million years later in the fossil record. The braincase of *Ptomacanthus* differs radically from the osteichthyan-like braincase of *Acanthodes*[5] in exhibiting several plesiomorphic features shared with placoderms[6,7] and some early chondrichthyans[8,9]. Most striking is its extremely short sphenoid region and its jaw suspension, which displays features intermediate between some Palaeozoic chondrichthyans and osteichthyans. Phylogenetic analysis resolves *Ptomacanthus* as either the most basal chondrichthyan or as the sister group of all living gnathostomes. These new data alter earlier conceptions of basal gnathostome phylogeny and thus help to provide a more detailed picture of the acquisition of early gnathostome characters.

Most of the recent hypotheses of acanthodian relationships expressed in cladistic terms have focused on their sister-group relations with chondrichthyans[10] or osteichthyans[5]. All of these studies have presupposed acanthodian monophyly and stereotyped acanthodian endoskeletal morphology on *Acanthodes*, the latest-occurring, and a highly apomorphic[1], genus. The assumption of acanthodian monophyly was initially based on their possession of paired and anal fin spines and a peculiar type of scale growth. A wealth of new data from unusual 'acanthodians' and acanthodian-like 'teleostomes' from northern Canada[3,11–13] and Australia[14], as well as discoveries of paired fin spines in basal chondrichthyans[15,16] and osteichthyans[17], have called acanthodian monophyly into question. This has placed acanthodians at the centre of the growing debate on gnathostome origins, but there remains a reluctance to attempt explicit cladistic solutions.

Ptomacanthus anglicus specimen NHM (Natural History Museum, London, UK) P 24919a (Fig. 1) was collected from the Wayne

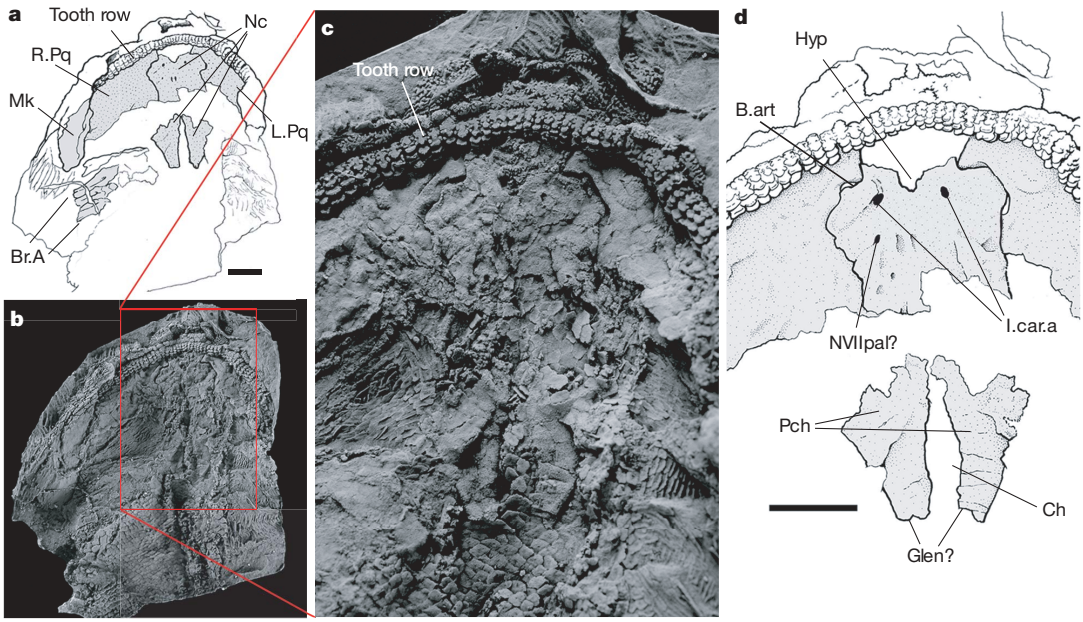

Figure 1 | *Ptomacanthus anglicus* NHM P 24919a. **a**, **b**, Interpretive sketch of specimen (**a**) with accompanying photograph (**b**). **c**, **d**, Close-up photograph of neurocranium, tooth row and anterior part of palatoquadrates (**c**) and interpretive sketch of neurocranium (**d**). B.art, basal articulation; Br.A, branchial arches; Ch, notochordal notch; Glen?, possible occipital glenoid; Hyp, hypophyseal opening; I.car.a, foramen for the internal carotid artery; L.Pq, left palatoquadrate; Mk, mineralized Meckelian cartilage; NVIIpal?, possible foramen for the palatine ramus of the facial nerve; Nc, neurocranial mineralizations; Pch, parachordal mineralizations; R.Pq, right palatoquadrate. Scale bar, 1 cm.

[1]Subdepartment of Evolutionary Organismal Biology, Department of Physiology and Developmental Biology, Evolutionary Biology Centre, Uppsala University, Norbyvägen 18A, SE-752 36 Uppsala, Sweden.

Herbert Quarry Lagerstätte[4] in Herefordshire, England, UK. The site is Lochkovian in age (approximately 418–412 Myr BP), placing *Ptomacanthus* among the earliest recorded articulated acanthodians. *Ptomacanthus* is assigned to the 'Climatiidae', a division of the 'Acanthodii', on the basis of its paired and median fin spine complement, paired pre-pelvic (or intermediate) fin spines and tessellated dermal cranial covering (further taxonomic review is found in the Supplementary Information). The specimen is a nearly complete, dorsoventrally flattened head and pharynx preserved as a natural mould in fine siltstone that has previously been acid etched and cast in rubber. Part and counterpart are preserved, with one side showing the specimen in palatal view, revealing the partial basicranium, the internal faces of the articulated palatoquadrates, the posterior half of the right Meckelian cartilage and several incomplete branchial arches.

The braincase is preserved in two portions: a basisphenoid region anteriorly, and paired, unfused parachordal plates posteriorly. When examined under a dissecting microscope, the tissue has a rough crystalline surface comparable to the mineralized jaws known from *Climatius*[4]. However, there is no evidence of prismatic calcified tesserae as in chondrichthyans, as no significant biomineral remains in the natural moulds.

The basisphenoid region is incompletely mineralized at its anterior end, but is delimited anteriorly by the intact tooth row. The anterior margin of this mineralization bears a deep medial notch corresponding to the hypophyseal opening. At the anterolateral margins of the basisphenoid are the articulations for the palatoquadrate. The sphenoid region narrows only slightly anterior to these articulations, suggesting that it continued forward between them to contact the ethmoid. The interorbital portion of the basisphenoid is otherwise very broad and extends only a short way anterior to the articulations compared with *Acanthodes*[5] and basal osteichthyans[18,19], in which it forms a narrow, elongate extension between the orbits[5] (Fig. 2). In these aspects, *Ptomacanthus* resembles some placoderms[7,20] which have very short ethmosphenoid regions. This is also seen in some early chondrichthyans[9,21], but even there the pre-hypophysial extension of the sphenoid is comparatively longer than in *Ptomacanthus*. Flanking either side of the hypophysial opening is a foramen that gives off a posterolaterally directed groove (most clearly visible on the anatomical right side of the specimen). The right groove (left in the figures) appears to continue as far as the lateral margin of the basicranium. These grooves and foramina are here interpreted as having accommodated the internal carotid arteries. This is based on their position near to the hypophysis and the angle of the associated grooves. A smaller but distinct groove extends anteriorly from the foramen for the right internal carotid and possibly carried the efferent pseudobranchial artery as in the arthrodire *Buchanosteus*[22] and the early osteichthyan braincase assigned to *Ligulalepis*[23,24]. Unlike basal osteichthyans[18,19,24] and *Acanthodes*[5], the basisphenoid of *Ptomacanthus* lacks evidence of spiracular grooves, again comparing more closely to chondrichthyans and placoderms.

The basicranial circulation of *Ptomacanthus* resembles that in arthrodire placoderms[6,7]. The internal carotid foramina are widely separate from one another on a platybasic neurocranium (see Supplementary Information for a discussion of the chondrichthyan *Pucapampella*, which *Ptomacanthus* also resembles). In most chondrichthyans and in *Acanthodes*[5], the internal carotid arteries share a common medial foramen, usually shared with the hypophyseal opening.

Some aspects of the basicranium cannot be identified with confidence but are worth mentioning. Evidence for a ventral cranial fissure is equivocal. Although the level corresponding to the position of this fissure in other gnathostomes (almost immediately posterior to the level of the hypophysis and postorbital processes) is mineralized, the large unpreserved region between the basisphenoid region and parachordals may correspond to this fissure. However, the dorsal portions of both palatoquadrates are missing from the specimen and their incomplete margins match closely the incomplete margins of the braincase. Thus, the unpreserved middle portion of the braincase may be taphonomic. Posterior to the anatomical right internal carotid opening is a smaller opening with a posterolaterally oriented groove. No corresponding feature can be confidently observed on the antimere, but the surface there is highly disrupted. Nevertheless, this foramen corresponds positionally to the opening for the palatine ramus of the facial nerve (N. VII) in many early gnathostomes[6,9]. Near the ventral midline of the basicranium is a pair of anteroposteriorly elongate depressions that match the position of the pituitary vein foramina in certain arthrodires. Confirmation of the identity of these structures will have to await the discovery of more complete material.

The paired palatoquadrate articulations are situated on anteriorly facing areas on the anterolateral corner of the basisphenoid, as in *Acanthodes*[5]. They are slightly anterior to the internal carotid foramina and are approximately at the same anteroposterior level as the hypophysial notch. This would, therefore, correspond to the basal articulation of osteichthyans, *Acanthodes* and the early chondrichthyan

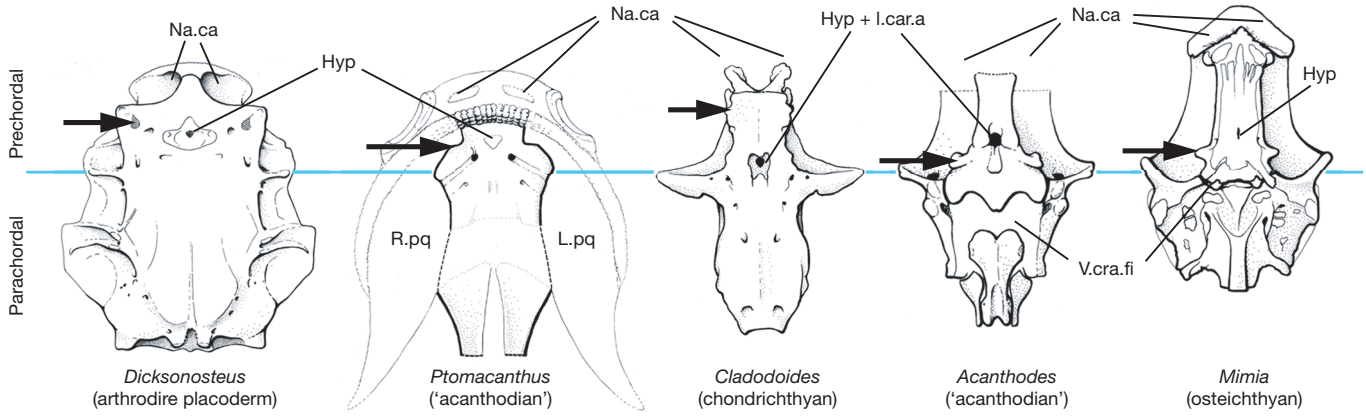

Figure 2 | Comparison of neurocranial proportions (ventral view) in early gnathostome taxa drawn to same anterior–posterior length. *Ptomacanthus* braincase (delimited by heavy black lines) is shown inside the reconstructed head skeleton (delimited by thin lines). Horizontal blue line demarcates the approximate boundary between prechordal and parachordal regions of the braincase, with the position of the postorbital process used as a proxy. Arrows indicate position of palatoquadrate articulation shown in Fig. 3. The position of this structure in *Ptomacanthus* is approximated by the position of the ascending process of the palatoquadrate. Illustrations modified after refs 5, 7, 9 and 18. Na.ca, nasal capsules, or their corresponding position; V.cran.fi, ventral cranial fissure.

Pucapampella[8]. However, they are situated very close to the ethmoid, as in early chondrichthyans (Figs 1 and 2).

The parachordals are represented by paired trapezoidal, unfused mineralizations. They taper posteriorly to squared-off posterior ends, but there is no evidence of paired glenoids or any blood-vessel foramina. The unfused nature of the elements implies an unmineralized floor of the notochordal tunnel. This forms a deep anteriorly tapering notch as seen in *Pucapampella*[8], but also some placoderms. Actinopterygians[18] and *Acanthodes* also exhibit partial fusion of the parachordals; however, the resulting notches are considerably smaller.

The neurocranium of *Ptomacanthus* is clearly distinct from its only other acanthodian counterpart, *Acanthodes*. In these respects, *Ptomacanthus* resembles more closely some placoderms and some basal chondrichthyans, rather than osteichthyans, suggesting that *Ptomacanthus* retains many plesiomorphic gnathostome attributes.

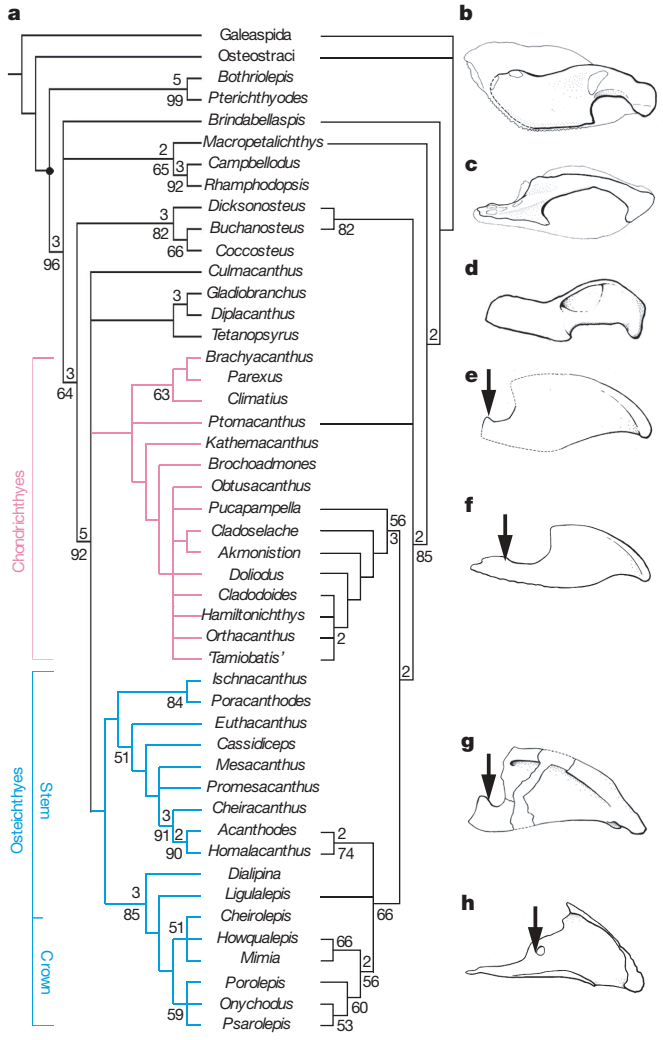

Figure 3 | Results of phylogenetic analyses and selected gnathostome palatoquadrates. **a**, Strict consensus trees of the 2,904 shortest trees from the global analysis (left; treelength: 318 steps; consistency index: 0.44; retention index: 0.76; rescaled consistency index: 0.34) and the 30 most parsimonious trees from the endocranial data set (right; treelength: 83 steps; consistency index: 0.64; retention index: 0.85; rescaled consistency index: 0.54). **b**, *Bothriolepis*. **c**, *Buchanosteus*. **d**, *Tetanopsyrus*. **e**, *Ptomacanthus*. **f**, *Cladodoides*. **g**, *Acanthodes*. **h**, *Mimia*. Vertical arrow shows position of palatoquadrate-braincase articulation that corresponds to the basipterygoid articulation shown in Fig. 2. Double digits indicate percentage bootstrap support; single digits show Bremer decay indices (when greater than 1). Illustrations are modified from refs 5 and 18 (also see Supplementary Information).

Furthermore, although the exocranial (that is, dermal) facial proportions of *Ptomacanthus* (and other similar 'climatiid' acanthodians)[4,5] are osteichthyan-like, this aspect is underlain by a neurocranium distinctly unlike any basal osteichthyan.

Partial left and right palatoquadrates (Figs 1 and 3) are preserved and articulated to the neurocranium at the basal articulations. Their shape is similar to those of most other acanthodians, and basal chondrichthyans and osteichthyans with a large otic expansion giving a 'cleaver-shaped' profile[25]. As in *Acanthodes*, the autopalatine region is short. Between the basal articulation and the ascending process of the palatoquadrate, the autopalatine exhibits a slight extension, by contrast with *Acanthodes* and basal osteichthyans, where the two are quite closely situated. The palatoquadrate of *Ptomacanthus* thus exhibits a process corresponding to the ethmoid/orbital process of certain Palaeozoic sharks, but articulating with a surface on the braincase clearly corresponding to the basal articulation of osteichthyans, *Acanthodes* and *Pucapampella*. This mosaic morphology supports the recently revived hypothesis that the orbital articulation and basal articulation are homologous structures[9].

Jarvik[19] cited the complete dental arcade of *Ptomacanthus* (Fig. 1) as evidence of a palatoquadrate symphysis, as in modern elasmobranchs. However, the palatoquadrates show no evidence of continuing mesially beneath the ethmoid. It is likely that the mesial part of the tooth row was supported on the ethmoid, a condition now considered to be plesiomorphic for chondrichthyans[26].

A cladistic analysis of 45 ingroup and two outgroup taxa was performed on the basis of 134 characters (see Supplementary Information). *Ptomacanthus* is placed as a basal stem chondrichthyan, but this result should be viewed with caution. A large part of the acanthodians, including *Acanthodes*, form a cohesive monophyletic group on the osteichthyan stem. However, the position of *Ptomacanthus* is problematical. Many of the supporting characters are not known or applicable in recognized crown-group chondrichthyans. Bayesian inference analysis (see Supplementary Information for results) does not resolve the position of *Ptomacanthus* beyond its relationships with the gnathostome crown node. The analysis was re-run for the endocranial character set and found that *Ptomacanthus* was resolved as the sister group of crown gnathostomes, on the basis of its short pre-hypophysial region. This subset may well be compromised by the inclusion of fewer data, but its resolution also reflects a greater proportion of characters for which polarity is well established by outgroups. As far as the material can be scored, the neurocranial data from *Ptomacanthus* exhibits no significant endocranial synapomorphies with either lineage of the gnathostome crown group.

Two additional significant results emerged from this analysis. First, *Ligulalepis*[23,24] and *Dialipina*[27] are recovered as stem osteichthyans, in agreement with a recent phylogenetic analysis of Osteichthyes[28]. Second, placoderms are resolved as a basal gnathostome grade, as suggested by some other recent work[28,29]. Also, the failure to resolve the position of 'diplacanthid' acanthodians results from several similarities with placoderms, such as the absence of an expanded otic process of the palatoquadrate (Fig. 3).

Current conceptions of gnathostome phylogeny depict a rather simplistic arrangement of nominally monophyletic and, apparently, morphologically disparate groups[1]. The emerging picture of acanthodian (and perhaps placoderm) paraphyly does not overturn a general consensus about gnathostome interrelationships. Instead, it populates the long, naked internal branches, revealing a much richer picture of character evolution in early gnathostomes.

METHODS SUMMARY

The global data set was analysed using the heuristic search option, 10,000 random addition sequence replicates with 'maxtrees' set to automatically increase. One character (character 33) was ordered, and one character (character 113) was parsimony-uninformative and excluded during all tree statistics calculations. Outgroup members were constrained as a paraphylum by inputting and

enforcing a topological constraint tree. Bayesian inference analysis used a standard data model with 1.5×10^7 generations sampled every 100 generations. The 15,000-generation 'burnin' period was discarded. Analysis of the endocranial data set used only taxa for which braincase data were adequately known. The search was performed using the branch-and-bound algorithm, outgroup constrained as a paraphylum, and 'maxtrees' set to increase automatically. Details of phylogenetic analyses are given in Supplementary Information.

Received 11 July 2007; accepted 15 September 2008.

1. Janvier, P. *Early Vertebrates* (Oxford Univ. Press, 1996).
2. Smith, M. M. & Sansom, I. J. Exoskeletal micro-remains of an Ordovician fish from the Harding Sandstone of Colorado. *Palaeontology* **40,** 645–658 (1997).
3. Hanke, G. F. *Paucicanthus vanelsti* gen. et sp. nov., an Early Devonian (Lochkovian) acanthodian that lacks paired fin-spines. *Can. J. Earth Sci.* **39,** 1071–1083 (2002).
4. Miles, R. S. Articulated acanthodian fishes from the Old Red Sandstone of England, with a review of the structure and evolution of the acanthodian shoulder-girdle. *Bull. Br. Mus. Nat. Hist. (Geol.)* **24,** 111–213 (1973).
5. Miles, R. S. in *Interrelationships of Fishes* (eds Greenwood, P. H., Miles, R. S. & Patterson, C.) 63–103 (Academic, 1973).
6. Stensiö, E. Anatomical studies on the arthrodiran head, part I. *Kungl. Svensk. Vetenskakad. Handl.* **9,** 1–419 (1963).
7. Goujet, D. *Les Poissons Placodermes du Spitsberg* (Cahiers de Paléontologie, Section Vertébrés, Centre National de la Recherche Scientifique, 1984).
8. Maisey, J. G. in *Major Events in Early Vertebrate Evolution* (ed. Ahlberg, P. E.) 263–288 (Taylor and Francis, 2001).
9. Maisey, J. G. Braincase of the Upper Devonian shark *Cladodoides wildungensis* (Chondrichthyes, Elasmobranchii), with observations on the braincase in early chondrichthyans. *Bull. Am. Mus. Nat. Hist.* **288,** 1–103 (2005).
10. Nelson, G. J. Gill arches and the phylogeny of fishes, with notes on the classification of vertebrates. *Bull. Am. Mus. Nat. Hist.* **141,** 475–552 (1969).
11. Gagnier, P.-Y. & Wilson, M. V. H. Early Devonian acanthodians from northern Canada. *Palaeontology* **39,** 241–258 (1996).
12. Hanke, G. F. & Wilson, M. V. H. in *Recent Advances in the Origin and Early Radiation of Vertebrates* (eds Arratia, G., Wilson, M. V. H. & Cloutier, R.) 189–216 (Pfeil, 2004).
13. Wilson, M. V. H., Hanke, G. F. & Märss, T. in *Major Transitions in Vertebrate Evolution* (eds Anderson, J. S. & Sues, H.-D.) 122–149 (Indiana Univ. Press, 2007).
14. Burrow, C. J. & Young, G. C. An articulated teleostome fish from the Late Silurian (Ludlow) of Victoria, Australia. *Rec. W. Aust. Mus.*, Suppl. 57, 1–14 (1999).
15. Young, G. C. Devonian sharks from south-eastern Australia and Antarctica. *Palaeontology* **25,** 817–843 (1982).
16. Miller, R. F., Cloutier, R. & Turner, S. The oldest articulated chondrichthyan from the Early Devonian period. *Nature* **425,** 501–504 (2003).
17. Zhu, M., Yu, X. & Janvier, P. A primitive fossil fish sheds light on the origin of bony fishes. *Nature* **397,** 607–610 (1999).
18. Gardiner, B. G. The relationships of the palaeoniscoid fishes, a review based on new specimens of *Mimia* and *Moythomasia* from the Upper Devonian of Western Australia. *Bull. Br. Mus. Nat. Hist. (Geol.)* **37,** 173–428 (1984).
19. Jarvik, E. *Basic Structure and Evolution of Vertebrates* (Academic, 1980).
20. Ørvig, T. in *Problèmes actuels de Paleontologie: Evolution des Vertébrés* (ed. Lehman, J. P.) 41–71 (Colloques Internationaux du Centre National de la Recherche Scientifique, 1975).
21. Schaeffer, B. The xenacanth shark neurocranium, with comments on elasmobranch monophyly. *Bull. Am. Mus. Nat. Hist.* **169,** 1–66 (1981).
22. Young, G. C. New information on the structure and relationships of *Buchanosteus* (Placodermi: Euarthrodira) from the Early Devonian of New South Wales. *Zool. J. Linn. Soc.* **66,** 309–352 (1979).
23. Basden, A. M., Young, G. C., Coates, M. I. & Ritchie, A. The most primitive osteichthyan braincase? *Nature* **403,** 185–188 (2000).
24. Basden, A. M. & Young, G. C. A primitive actinopterygian neurocranium from the Early Devonian of southeastern Australia. *J. Vertebr. Paleontol.* **21,** 754–766 (2001).
25. Schaeffer, B. in *Problèmes actuels de Paleontologie: Evolution des Vertébrés* (ed. Lehman, J. P.) 101–109 (Colloques Internationaux du Centre National de la Recherche Scientifique, 1975).
26. Maisey, J. G. An evaluation of jaw suspension in sharks. *Am. Mus. Novit.* **2706,** 1–17 (1980).
27. Schultze, H.-P. & Cumbaa, S. L. in *Major Events in Early Vertebrate Evolution* (ed. Ahlberg, P. E.) 315–332 (Taylor and Francis, 2001).
28. Friedman, M. *Styloichthys* as the oldest coelacanth: implications for early osteichthyan interrelationships. *J. Syst. Palaeontol.* **5,** 289–343 (2007).
29. Johanson, Z. Vascularization of the osteostracan and antiarch (Placodermi) pectoral fin: similarities, and implications for placoderm relationships. *Lethaia* **35,** 169–186 (2002).

Supplementary Information is linked to the online version of the paper at www.nature.com/nature.

Acknowledgements I thank M. Richter for loans of specimens and access to collections; S. Davis, M. Friedman, D. Goujet, J. Long, J. Maisey and G. Young for discussions on early gnathostome endocranial anatomy; P. Ahlberg and H. Blom for discussions and support during all phases of this work. Financial support for this work was provided by a Natural Sciences and Engineering Research Council of Canada Postgraduate Scholarship (NSERC PGS-D 331758-2006) awarded to the author. Thanks to J. Maisey, R. Miller and S. Turner for access to unpublished data on *Doliodus*.

Author Information Reprints and permissions information is available at www.nature.com/reprints. Correspondence and requests for materials should be addressed to M.D.B. (martin.brazeau@gmail.com).

LETTERS

A tunable synthetic mammalian oscillator

Marcel Tigges[1], Tatiana T. Marquez-Lago[1,2,3], Jörg Stelling[1,2,3] & Martin Fussenegger[1]

Autonomous and self-sustained oscillator circuits mediating the periodic induction of specific target genes are minimal genetic time-keeping devices found in the central and peripheral circadian clocks[1,2]. They have attracted significant attention because of their intriguing dynamics and their importance in controlling critical repair[3], metabolic[4] and signalling pathways[5]. The precise molecular mechanism and expression dynamics of this mammalian circadian clock are still not fully understood. Here we describe a synthetic mammalian oscillator based on an auto-regulated sense–antisense transcription control circuit encoding a positive and a time-delayed negative feedback loop, enabling autonomous, self-sustained and tunable oscillatory gene expression. After detailed systems design with experimental analyses and mathematical modelling, we monitored oscillating concentrations of green fluorescent protein with tunable frequency and amplitude by time-lapse microscopy in real time in individual Chinese hamster ovary cells. The synthetic mammalian clock may provide an insight into the dynamics of natural periodic processes and foster advances in the design of prosthetic networks in future gene and cell therapies.

Synthetic gene circuits that emulate the expression dynamics of living systems provide new insights into the connectivity of genes and proteins in the postgenomic era[6] and they advance our understanding of complex control networks. Circadian pacemakers[7,8] are of particular interest because they coordinate many periodic physiological activities. The mammalian circadian clock consists of a central pacemaker in the suprachiasmatic nuclei of mammalian brains[9], with subsidiary oscillators in most peripheral cell types[4,5,10]. In contrast to neurons in the suprachiasmatic nuclei, peripheral oscillators damp rapidly when disconnected from remote control by the suprachiasmatic nuclei[10]. However, both oscillators rely on a very similar gene circuitry that involves a set of transcriptional repressors (CRY and PER) and activators (BMAL1 and CLOCK) connected by mutual feedback[11]. Previously designed simple synthetic gene networks in bacteria showed self-sustained[12], damped[13] or metabolically controlled oscillations[14], but those oscillators lacked robustness and/or tunability. In mammalian cells, even synthetic clock replicas using natural components and network design have not provided oscillating transgene expression[15] as observed for reporter genes plugged

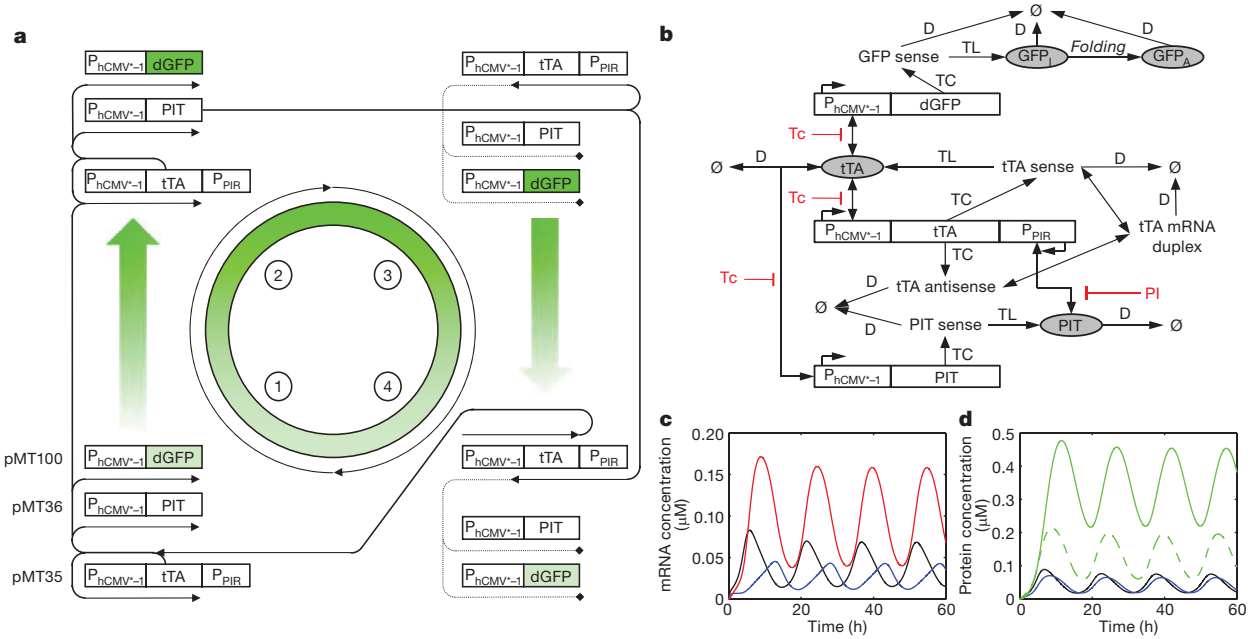

Figure 1 | Mammalian clock components and predicted oscillation dynamics. **a**, Core mammalian oscillator. Autoregulated $P_{hCMV*-1}$-driven tTA transcription triggers increasing expression of sense tTA (pMT35), Ub^{V76}–GFP (pMT100) and PIT (pMT36) (1). As Ub^{V76}–GFP and PIT levels reach a peak (2), PIT steadily induces P_{PIR}-driven tTA anti-sense expression (3), resulting in a gradual decrease in sense tTA, PIT and Ub^{V76}–GFP (4). **b**, Intracellular processes considered in the mathematical model. Abbreviations and symbols are as follows: single-headed arrows, irreversible reactions; double-headed arrows, reversible reactions; Ø, sinks for degradation processes; dGFP, destabilized GFP; Tc, tetracycline; PI, pristinamycin I; GFP_I, unfolded inactive GFP; GFP_A, folded active GFP; TC, transcription; TL, translation; D, degradation. **c**, **d**, Model predictions for the reference parameter set (plasmid ratios 1:1:1, no antibiotics) with mRNA concentrations (**c**) (black, tTA; blue, PIT; red, tTA-sense–antisense duplex) and protein concentrations (**d**) (black, tTA; blue, PIT; dashed green, unfolded GFP; solid green, active GFP).

[1]Department of Biosystems Science and Engineering, ETH Zurich, Mattenstrasse 26, CH-4058 Basel, Switzerland. [2]Institute of Computational Science and [3]Swiss Institute of Bioinformatics, ETH Zurich, CH-8092 Zurich, Switzerland.

into the natural circadian clock of peripheral fibroblasts[10]. This suggested that important details on how cellular clocks operate are still unknown.

Our synthetic core oscillator (Fig. 1a) consists of a sense–antisense expression unit encoding the tetracycline-dependent transactivator (tTA)[16]. tTA manages its sense transcription by means of an autoregulated feedback loop controlled by the tTA-specific tetracycline-responsive promoter ($P_{hCMV*-1}$; $P_{hCMV*-1}$→tTA; pMT35). Antisense transcription of tTA is driven by the pristinamycin-responsive promoter (P_{PIR}; $P_{hCMV*-1}$→tTA←P_{PIR}; pMT35) and triggered by the pristinamycin-dependent transactivator (PIT)[17], whose expression is induced by $P_{hCMV*-1}$ and thus feedback controlled by tTA ($P_{hCMV*-1}$→PIT; pMT36). tTA levels can be examined by tTA-specific $P_{hCMV*-1}$-driven expression of a fluorescent protein. For reasons given below, we used either the destabilized enhanced yellow fluorescent protein (d2EYFP; $P_{hCMV*-1}$→d2EYFP; pBP282 (ref. 18); see Supplementary Information) or the green fluorescent protein (GFP) variant Ub^{V76}–GFP ($P_{hCMV*-1}$→Ub^{V76}–GFP; pMT100), which have different half-lives. The network can be fine-tuned by modulating sense expression of tTA and PIT by tetracycline and by adjusting tTA antisense transcription by pristinamycin I (PI). In the absence of antibiotics $P_{hCMV*-1}$ and P_{PIR} are fully induced.

To analyse whether the circuit could function as a genetic oscillator, we developed a first deterministic mathematical model (see Supplementary Information). It describes in a simplified yet mechanistic fashion the processes shown in Fig. 1b. Biologically plausible model parameterization demonstrated the oscillatory capacity of the mammalian circuit (Fig. 1c, d). It can undergo autonomous and self-sustained oscillation of tTA expression by alternating the induction of tTA by means of its autoregulated feedback (tTA induces its own expression), with time-delayed repression of tTA mediated by the two-level tTA antisense transcription cascade (tTA triggers PIT expression; PIT then induces tTA antisense expression). The antisense-mediated decrease in tTA levels triggers the recovery of tTA sense expression and, hence, a second clock cycle.

A first oscillator implementation with the d2EYFP reporter provided evidence that the basic design could function *in vivo* (see Supplementary Information). For detailed circuit design, we adapted the model parameters to the experimental d2EYFP time courses from oscillating cells and controls. The refined model enabled us to make a semiquantitative description of the circuit behaviour by capturing all qualitative dynamic features, but not all quantitative aspects (Supplementary Fig. 1 and Supplementary Information). With the experimentally constrained model, we conducted simulation studies with varying model parameters and/or inputs to establish critical design features. The model predicted that the circuit should be robust to variations in protein and messenger RNA degradation and that the antibiotics may switch the oscillator on or off but not tune its behaviour gradually (Supplementary Fig. 2 and Supplementary Notes). Moreover, model analysis suggested that the synthetic network could sustain autonomous oscillations only at specific relative levels of the individual clock components (Fig. 2a, b). These levels are influenced by the relative amounts of expression vectors used to transfect mammalian cells[19]. The model predicted that, even when the ratios of oscillator components were held constant, absolute plasmid concentrations could be used to modify the period and amplitude of the oscillations (Fig. 2a, b). More intuitively, destabilization of the reporter was predicted to increase the relative signal amplitude (Fig. 2b, c). The model-based analysis therefore pointed to reporter stability and gene dosage as key variables for optimizing the circuit.

To reveal any rhythmic transcription control in single cell-based time-lapse microscopy studies, we implemented a second-generation oscillator by functionally plugging in a $P_{hCMV*-1}$-driven GFP variant engineered for a decreased half-life of a few minutes (Ub^{V76}–GFP; pMT100, $P_{hCMV*-1}$→Ub^{V76}–GFP). Co-transfection of pMT35 ($P_{hCMV*-1}$→tTA←P_{PIR}) and pMT100 resulted in a steady increase in green fluorescence, indicating that sense tTA was co-inducing its own expression as well as that of Ub^{V76}–GFP (Supplementary Fig. 3a). We observed a similar increase in Ub^{V76}–GFP expression after co-transfection of pMT100, pMT35 and pMT36 ($P_{hCMV*-1}$→PIT) when transfected populations were cultivated in the presence of PI, which inactivated PIT and prevented tTA antisense expression (Supplementary Fig. 3b). When the same population was exposed to tetracycline, Ub^{V76}–GFP expression was gradually shut off as a result of tTA inactivation (Supplementary Fig. 3c). Ub^{V76}–GFP expression was also shut off when co-transfecting pMT100 and pMT35 with the constitutive PIT expression vector pMF156 (P_{hCMV}→PIT)[17], which confirmed that PIT-mediated induction of P_{PIR}-driven tTA antisense expression outcompetes autoregulated tTA expression (Supplementary Fig. 3d). The individual feedback loops therefore operated as expected.

To test the complete synthetic oscillator we co-transfected pMT35, pMT36 and pMT100 at various ratios. Ratios of 2:1:1 or 3:1:1 resulted in imbalanced expression of clock components and constant expression of Ub^{V76}–GFP (Supplementary Fig. 3e, f). When pMT35, pMT36 and pMT100 were co-transfected at equimolar ratios (100 ng each) into Chinese hamster ovary (CHO-K1) cells cultivated without antibiotics, we observed spontaneous, autonomous, self-sustained and robust oscillations of Ub^{V76}–GFP fluorescence in single cells (Fig. 3 and Supplementary Video). The oscillations could only be disturbed deliberately by adding either tetracycline or PI (Supplementary Fig. 3b, c), or by constitutive PIT expression (Supplementary Fig. 3d). Fast Fourier transformation-based analysis (see Supplementary Information) of at least 20 CHO-K1 cells with oscillating Ub^{V76}–GFP expression collected from four independent experiments showed that oscillations occur at a frequency of 170 ± 71 min (mean $\pm$ s.d.), with an amplitude of 1.81 ± 1.96 fluorescence units (Fig. 3). The oscillations of the synthetic clock showed substantial variability between individual cells, even adjacent ones, suggesting that there is no functional coupling between oscillating cells.

Next, to check the model predictions on gene-dosage-dependent oscillator behaviour, we varied the DNA doses used for transfection. In comparison with the oscillations generated by co-transfection of 100 ng pMT35, pMT36 and pMT100 (Fig. 3), co-transfection of 200 ng of each clock vector resulted in oscillation with a higher frequency (period of 147 ± 58 min) but a reduced amplitude

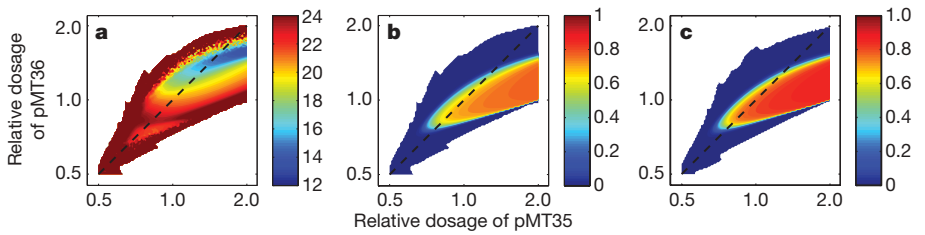

Figure 2 | Systems behaviour depending on gene dosage as predicted by the adapted model with variable transfection times. Panels show the colour-coded oscillator period (**a**; the colour bar gives the period in hours) and relative amplitude (**b**, **c**; normalized by maximal fluorescence) as a function of relative plasmid concentrations. In **a** and **b** the reporters are d2EYFP; in **c** the reporter is Ub^{V76}–GFP, a variant with a decreased half-life. The dashed line denotes a 1:1 plasmid ratio. No oscillations were observed in white areas.

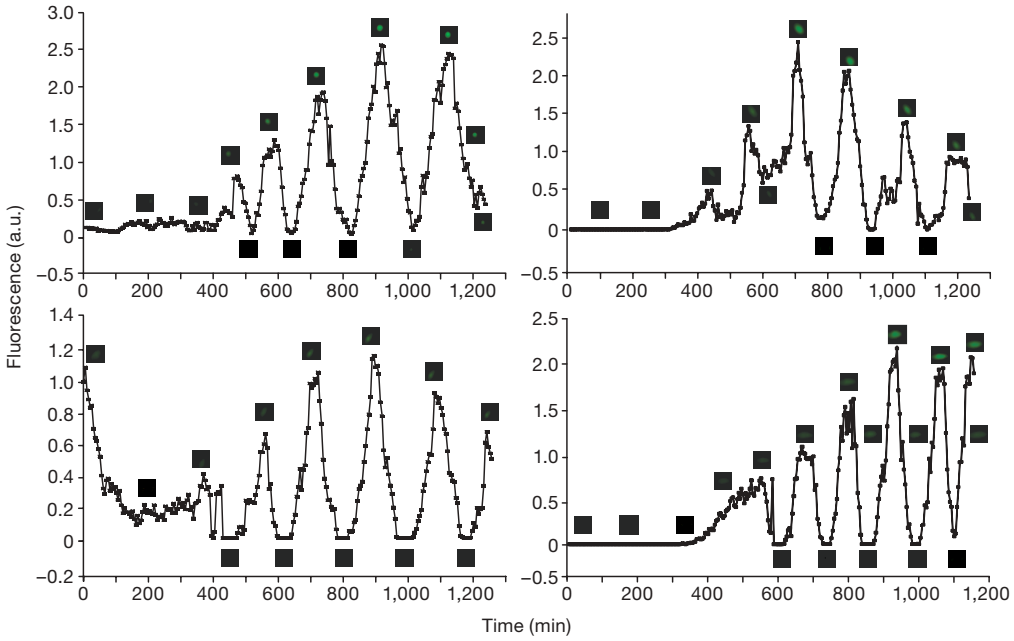

Figure 3 | Validation of the mammalian oscillator by time-lapse fluorescence analysis of transfected CHO-K1 cells. CHO-K1 cells were co-transfected at equimolar ratios (100 ng each) with pMT35 ($P_{hCMV*\text{-}1}$→tTA←P_{PIR}), pMT36 ($P_{hCMV*\text{-}1}$→PIT) and pMT100 ($P_{hCMV*\text{-}1}$→Ub^{V76}–GFP) and cultivated in the absence of antibiotics. The same four independent CHO-K1 cells showing oscillating Ub^{V76}–GFP are also shown, circled, in the Supplementary Video.

(1.44 ± 0.74 fluorescence units) (Fig. 4a), as predicted qualitatively by the model (Fig. 2a–c). When the plasmid doses were decreased to 50 ng each, the oscillation period increased (328 ± 162 min) and the amplitude decreased (0.96 ± 0.63 fluorescence units) (Fig. 4b), which confirms the model predictions on the tunability of the synthetic clock. Quantitative statistical analysis of single-cell data for various plasmid dosages revealed the dependences between gene dosage and oscillator frequency and amplitude shown in Fig. 4c, d. We used these experimental data together with the control experiments to establish a structurally refined mathematical model that could describe all experimental data quantitatively (see Supplementary Information). This deterministic model predicted non-intuitive relations between gene dosage and oscillator behaviour (Fig. 4c, d). Thus, our model-supported synthetic biology approach revealed a previously unknown correlation between oscillation frequency and gene dosage of clock components.

Variable timings of plasmid uptake constitute a major source of cell-to-cell variability of GFP expression. However, through the alignment of single-cell trajectories by using simplified models (see Supplementary Information), we estimated that GFP expression in control experiments varied by only about 20%. Previous studies pointed to stochasticity, or 'noise', as a principal reason for limiting accuracy in synthetic networks[20,21]. To estimate the impact of molecular noise on the mammalian oscillator, we established a detailed stochastic model (see Supplementary Information). Stochastic simulations show that, at least for low plasmid dosages, noise contributes substantially to the observed cell-to-cell variability in the period (Fig. 4c, d). The model predicts that not all cells will

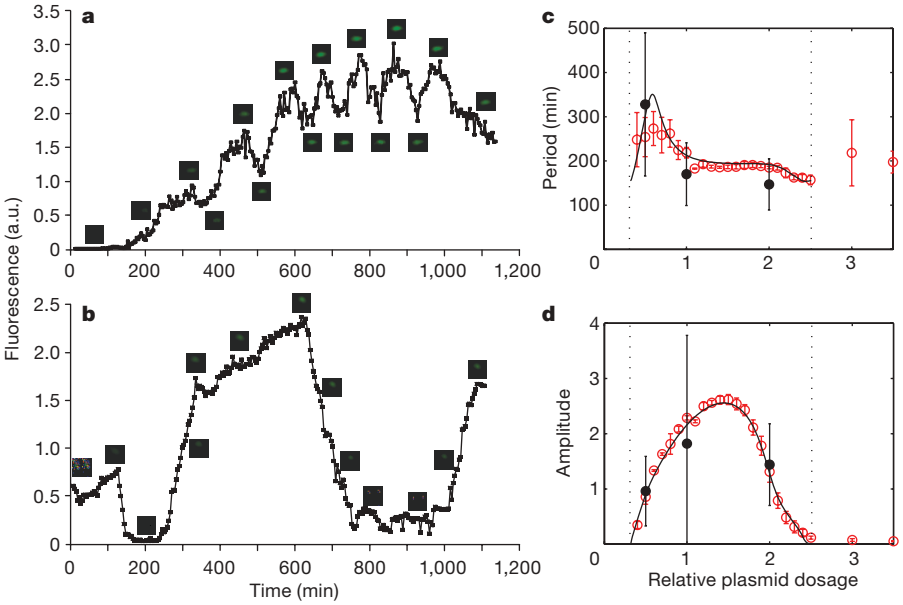

Figure 4 | Tunable oscillating gene expression in mammalian cells. Examples of oscillating CHO-K1 cells co-transfected at equimolar ratios (**a**, 200 ng each; **b**, 50 ng each) with pMT35, pMT36 and pMT100 in cultivation without antibiotics. **c**, **d**, Statistical data analysis and model predictions for oscillator period (**c**) and amplitude (**d**). Experimental data from at least 20 single-cell trajectories per plasmid dosage (filled black symbols; a relative plasmid dosage of one corresponds to 100 ng of DNA) and predictions from the refined deterministic model (black lines) and from stochastic simulations (red symbols) for a similar number of oscillations. Dotted lines indicate regions of oscillations for the deterministic model. Error bars indicate s.d.

oscillate under these conditions. In addition, we find low-amplitude noise-induced oscillations for high plasmid dosages that are similar to those predicted for simplified oscillators[21]. This underlines the importance of stochastic effects on the quantitative behaviour of systems with complicated dynamics[22].

Prokaryotic clocks that were constructed previously[12–14] employed only transcription control elements, and it was not obvious whether a post-transcriptional control component in a mammalian circuit could enable autonomous and self-sustained oscillations. The recent discovery of antisense clock-gene transcripts suggests that mechanisms of gene regulation operating through antisense RNA may also be integral to the circadian clockwork and be more important than previously anticipated[23]. Using a novel network design combining an autoregulated positive transcription feedback with a two-step transcription cascade producing non-coding antisense RNA for translation control, we achieved autonomous, self-sustained and tunable oscillation in mammalian cells. Besides providing insight into the dynamics of mammalian clocks, a more profound understanding of molecular time-keeping devices could foster therapeutic opportunities in clock-related pathologies such as Huntington's[24] and Alzheimer's[25] diseases.

METHODS SUMMARY

Design of expression vectors. pcDNA3.1-Ub^{V76}–GFP enables the constitutive expression of the destabilized GFP variant Ub^{V76}–GFP[26]. pMT35 ($P_{hCMV*\text{-}1}$→tTA←P_{PIR}) contains an expression unit for the $P_{hCMV*\text{-}1}$-driven sense and P_{PIR}-driven antisense expression of tTA[17,27]. pMT35 was constructed by replacing p27^{Kip1} of pMF226 (ref. 27) with tTA of pSAM200 by using EcoRI/HindIII. pMT36 ($P_{hCMV*\text{-}1}$-PIT), engineered for $P_{hCMV*\text{-}1}$-driven PIT[17] expression, was constructed by elimination of the NotI fragment from pMF125 (ref. 28). pMT100 ($P_{hCMV*\text{-}1}$-Ub^{V76}–GFP), enabling the tetracycline-responsive expression of Ub^{V76}–GFP, was designed by inserting Ub^{V76}–GFP, excised from pcDNA3.1-Ub^{V76}–GFP by NheI/NotI, into the corresponding sites of pMF111 (ref. 29). pMF156 encodes the constitutive expression of PIT (P_{hCMV}→PIT)[17].

Cell culture, transfection and gene regulation. CHO-K1 (ATCC CCL61) cells were cultivated in ChoMaster HTS (Cell Culture Technologies) supplemented with 5% fetal calf serum (lot no. P231902; Pan Biotech GmbH). Cells were cultivated at 30 °C in a humidified atmosphere containing 5% CO_2, and 35,000 cells were transfected with up to 1.2 μg of plasmid mixtures by using the FuGENE6 transfection reagent (lot no. 93535720; Roche Molecular Biochemicals).

Fluorescence imaging. Time-lapse fluorescence microscopy was performed with an inverted fluorescent microscope (DMI 6000B; Leica Microsystems) equipped with an incubation chamber, a DFC350FX R2 digital camera (Leica), a 10× objective (Obj. HC PL FL 10×/0.30 PH1 –/D 11.0; Leica) and a 488-nm/509-nm (B/G/R) Ub^{V76}–GFP-specific excitation/emission filter set. Time-lapse videos were produced with the LAS AF imaging software (FW4000-TZ; Leica) set to exposure times of 590–960 ms (auto-controlled depending to the mean fluorescence intensity level) every 3 min. Fluorescence was quantified with ImageJ software for at least 50 cells per condition.

Computational modelling. All details of mathematical models and computational methods are provided in Supplementary Information. Simulations were performed with MATLAB (MathWorks).

Received 26 July; accepted 4 November 2008.

1. Gillette, M. U. & Sejnowski, T. J. Physiology. Biological clocks coordinately keep life on time. *Science* **309,** 1196–1198 (2005).
2. Schibler, U. & Sassone-Corsi, P. A web of circadian pacemakers. *Cell* **111,** 919–922 (2002).
3. Lahav, G. The strength of indecisiveness: oscillatory behavior for better cell fate determination. *Sci. STKE* **2004,** pe55 (2004).
4. Kaasik, K. & Lee, C. C. Reciprocal regulation of haem biosynthesis and the circadian clock in mammals. *Nature* **430,** 467–471 (2004).
5. Covert, M. W., Leung, T. H., Gaston, J. E. & Baltimore, D. Achieving stability of lipopolysaccharide-induced NF-κB activation. *Science* **309,** 1854–1857 (2005).
6. Hasty, J., McMillen, D. & Collins, J. J. Engineered gene circuits. *Nature* **420,** 224–230 (2002).
7. Reppert, S. M. & Weaver, D. R. Forward genetic approach strikes gold: cloning of a mammalian clock gene. *Cell* **89,** 487–490 (1997).
8. Storch, K. F. *et al.* Extensive and divergent circadian gene expression in liver and heart. *Nature* **417,** 78–83 (2002).
9. Reppert, S. M. & Weaver, D. R. Coordination of circadian timing in mammals. *Nature* **418,** 935–941 (2002).
10. Nagoshi, E. *et al.* Circadian gene expression in individual fibroblasts: cell-autonomous and self-sustained oscillators pass time to daughter cells. *Cell* **119,** 693–705 (2004).
11. Gekakis, N. *et al.* Role of the CLOCK protein in the mammalian circadian mechanism. *Science* **280,** 1564–1569 (1998).
12. Atkinson, M. R., Savageau, M. A., Myers, J. T. & Ninfa, A. J. Development of genetic circuitry exhibiting toggle switch or oscillatory behavior in *Escherichia coli*. *Cell* **113,** 597–607 (2003).
13. Elowitz, M. B. & Leibler, S. A synthetic oscillatory network of transcriptional regulators. *Nature* **403,** 335–338 (2000).
14. Fung, E. *et al.* A synthetic gene–metabolic oscillator. *Nature* **435,** 118–122 (2005).
15. Chilov, D. & Fussenegger, M. Toward construction of a self-sustained clock-like expression system based on the mammalian circadian clock. *Biotechnol. Bioeng.* **87,** 234–242 (2004).
16. Gossen, M. & Bujard, H. Tight control of gene expression in mammalian cells by tetracycline-responsive promoters. *Proc. Natl Acad. Sci. USA* **89,** 5547–5551 (1992).
17. Fussenegger, M. *et al.* Streptogramin-based gene regulation systems for mammalian cells. *Nature Biotechnol.* **18,** 1203–1208 (2000).
18. Kramer, B. P. & Fussenegger, M. Transgene control engineering in mammalian cells. *Methods Mol. Biol.* **308,** 123–143 (2005).
19. Rossmanith, W., Chabicovsky, M., Herkner, K. & Schulte-Hermann, R. Cellular gene dose and kinetics of gene expression in mouse livers transfected by high-volume tail-vein injection of naked DNA. *DNA Cell Biol.* **21,** 847–853 (2002).
20. Rosenfeld, N., Young, J. W., Alon, U., Swain, P. S. & Elowitz, M. B. Gene regulation at the single-cell level. *Science* **307,** 1962–1965 (2005).
21. Vilar, J. M., Kueh, H. Y., Barkai, N. & Leibler, S. Mechanisms of noise-resistance in genetic oscillators. *Proc. Natl Acad. Sci. USA* **99,** 5988–5992 (2002).
22. Di Ventura, B., Lemerle, C., Michalodimitrakis, K. & Serrano, L. From *in vivo* to *in silico* biology and back. *Nature* **443,** 527–533 (2006).
23. Crosthwaite, S. K. Circadian clocks and natural antisense RNA. *FEBS Lett.* **567,** 49–54 (2004).
24. Morton, A. J. *et al.* Disintegration of the sleep–wake cycle and circadian timing in Huntingdon's disease. *J. Neurosci.* **25,** 157–163 (2005).
25. Wu, Y. H. *et al.* Pineal clock gene oscillation is disturbed in Alzheimer's disease, due to functional disconnection from the 'master clock'. *FASEB J.* **20,** 1874–1876 (2006).
26. Johnson, E. S., Ma, P. C., Ota, I. M. & Varshavsky, A. A proteolytic pathway that recognizes ubiquitin as a degradation signal. *J. Biol. Chem.* **270,** 17442–17456 (1995).
27. Fux, C. *et al.* Streptogramin- and tetracycline-responsive dual regulated expression of p27^{Kip1} sense and antisense enables positive and negative growth control of Chinese hamster ovary cells. *Nucleic Acids Res.* **29,** e19 (2001).
28. Moser, S. *et al.* Dual-regulated expression technology: a new era in the adjustment of heterologous gene expression in mammalian cells. *J. Gene Med.* **3,** 529–549 (2001).
29. Fussenegger, M., Schlatter, S., Datwyler, D., Mazur, X. & Bailey, J. E. Controlled proliferation by multigene metabolic engineering enhances the productivity of Chinese hamster ovary cells. *Nature Biotechnol.* **16,** 468–472 (1998).

Supplementary Information is linked to the online version of the paper at www.nature.com/nature.

Acknowledgements We thank H. Meyer for providing pcDNA3.1-Ub^{V76}–GFP; and B. Kramer, M. Gitzinger, D. Greber and W. Weber for conceptual input and/or critical comments on the manuscript. This work was supported by the Swiss National Science Foundation and the EC Framework 6 (COBIOS).

Author Information Reprints and permissions information is available at www.nature.com/reprints. Correspondence and requests for materials should be addressed to M.F. (fussenegger@bsse.ethz.ch) or J.S. (joerg.stelling@bsse.ethz.ch).

LETTERS

Experience leaves a lasting structural trace in cortical circuits

Sonja B. Hofer[1]†, Thomas D. Mrsic-Flogel[1]†, Tobias Bonhoeffer[1] & Mark Hübener[1]

Sensory experiences exert a powerful influence on the function and future performance of neuronal circuits in the mammalian neocortex[1–3]. Restructuring of synaptic connections is believed to be one mechanism by which cortical circuits store information about the sensory world[4,5]. Excitatory synaptic structures, such as dendritic spines, are dynamic entities[6–8] that remain sensitive to alteration of sensory input throughout life[6,9]. It remains unclear, however, whether structural changes at the level of dendritic spines can outlast the original experience and thereby provide a morphological basis for long-term information storage. Here we follow spine dynamics on apical dendrites of pyramidal neurons in functionally defined regions of adult mouse visual cortex during plasticity of eye-specific responses induced by repeated closure of one eye (monocular deprivation). The first monocular deprivation episode doubled the rate of spine formation, thereby increasing spine density. This effect was specific to layer-5 cells located in binocular cortex, where most neurons increase their responsiveness to the non-deprived eye[3,10]. Restoring binocular vision returned spine dynamics to baseline levels, but absolute spine density remained elevated and many monocular deprivation-induced spines persisted during this period of functional recovery. However, spine addition did not increase again when the same eye was closed for a second time. This absence of structural plasticity stands out against the robust changes of eye-specific responses that occur even faster after repeated deprivation[3]. Thus, spines added during the first monocular deprivation experience may provide a structural basis for subsequent functional shifts. These results provide a strong link between functional plasticity and specific synaptic rearrangements, revealing a mechanism of how prior experiences could be stored in cortical circuits.

Temporary closure of one eye induces adaptive changes of eye-specific responses in binocular visual cortex of juvenile[11–14] and adult mice[3,10,15,16], as neurons shift their preference towards the non-deprived eye. These ocular dominance shifts can be fully reversed by restoring binocular vision, and they become accelerated when the animal experiences a second monocular deprivation (MD) episode several weeks after the first[3]. Thus, a transient adaptation to altered visual input leaves a 'trace' in cortical circuits that facilitates similar adaptations in the future. This trace could take on multiple forms; here we investigate whether it could be morphological in nature, in which case potential synaptic restructuring during the initial experience[17] would outlast the functional changes to support later ocular dominance shifts.

We repeatedly imaged apical dendritic stretches of layer-5 (L5) and layer-2/3 (L2/3) pyramidal neurons in functionally defined regions of mouse visual cortex by combining two-photon laser scanning microscopy with optical imaging of intrinsic signals. Adult mice (postnatal day 45–100) expressing enhanced green fluorescent protein (GFP) sparsely in the cortex[18] were implanted with a glass window[6] through which the position of binocular visual cortex was first determined functionally using intrinsic signal imaging (Fig. 1a, b). Subsequently, starting on average 16 days after surgery, spine dynamics of labelled neurons in different cortical regions (see Supplementary Fig. 1 for positions of imaged neurons) were followed for up to eight weeks. Dendrites were imaged in layer 1 at four-day intervals while animals experienced repeated episodes of MD separated by periods of normal binocular vision (Fig. 1, Supplementary Fig. 2a). We also corroborated our previous findings on facilitated functional plasticity during repeated MD[3] in adult mice implanted with cranial windows: ocular dominance shifts caused by the first MD, as measured by intrinsic signal imaging, reversed completely after reopening the deprived eye. A second MD of three days in the same eye induced a stronger ocular dominance shift than the first three-day MD ($P = 0.009$; Fig. 1c, Supplementary Figs 2c, 3a, b).

Chronic two-photon imaging revealed that under normal conditions, $5.6 \pm 0.4\%$ (mean $\pm$ s.e.m.) of spines appeared (spine gain) and $6.7 \pm 0.4\%$ of spines disappeared (spine loss) on apical dendrites of L5 pyramidal neurons in the binocular visual cortex over a four-day period (Fig. 1d, e). Closing the eye contralateral to the imaged hemisphere increased spine gain rate in the binocular region during the first four days of MD and, to a lesser degree, during the subsequent four days, in comparison with baseline conditions or control animals (MD 0–4 d: $P < 0.002$; MD 4–8 d: $P < 0.03$; Fig. 1e, h). Spine loss rate, however, was not consistently altered by MD, with marginally fewer spines disappearing during the first four days of MD ($P = 0.03$, in comparison with baseline conditions; Fig. 1e; for a comparison of gain and loss in individual neurons, see Supplementary Fig. 4a). Consequently, spine number had increased by ~8% at the end of the eight-day MD episode (before MD: 399 ± 12.6 spines per millimetre; MD 8 d: 434 ± 11.9 spines per millimetre; $P < 0.002$; also see below). Notably, L5 neurons with more complex apical dendrites displayed a larger increase in spine density during MD than did neurons with simpler apical structures ($P < 0.001$; Supplementary Information and Supplementary Fig. 4b).

The selective increase in spine number could reflect either the reorganization of synaptic inputs associated with ocular dominance shifts or a non-specific, compensatory effect due to the loss of visual drive through the deprived eye. To distinguish between these possibilities, we quantified spine dynamics on neurons located in regions surrounding the binocular cortex. Neurons in monocular primary visual cortex, which receive input exclusively from the deprived eye, did not exhibit changes in spine turnover as a consequence of visual deprivation (Fig. 1f). Similarly, spine dynamics of neurons located laterally or frontally, outside the functionally defined borders of the binocular cortex and presumably in monocular parts of higher visual areas[19] (Supplementary Fig. 1), did not change during MD (Supplementary Fig. 5). Finally, neurons positioned at the border regions of the binocular cortex showed an intermediate effect: the

[1]Max Planck Institute of Neurobiology, D-82152 Martinsried, Germany. †Present address: Department of Physiology, University College London, London WC1 6JJ, UK.

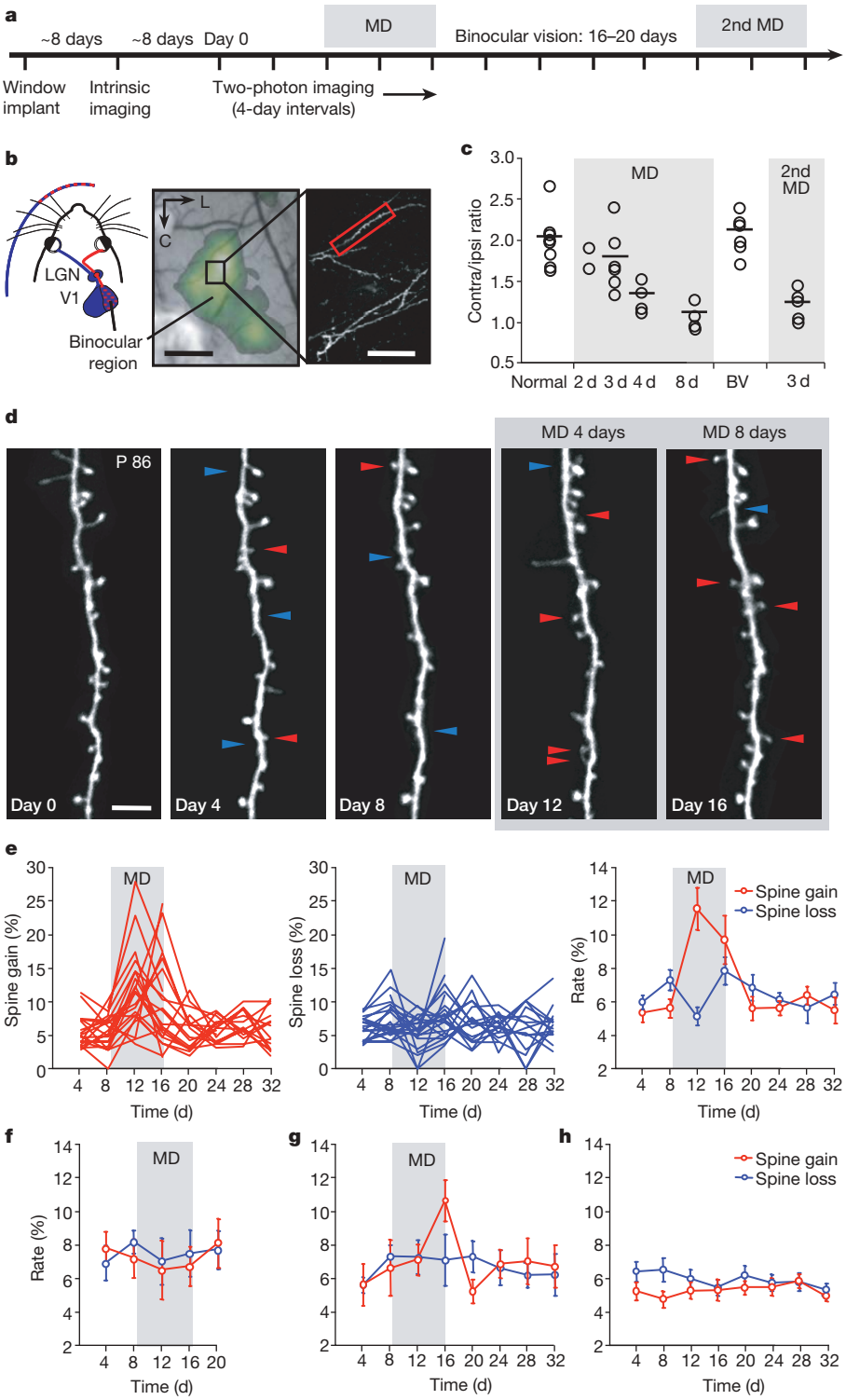

Figure 1 | Monocular deprivation in adult mice increases the rate of spine gain in L5 neurons in binocular cortex. **a**, Timeline of the experimental protocol. **b**, Schematic mouse visual system (left), intrinsic signal map of the binocular visual cortex (middle; scale bar, 500 μm) and low-magnification image of a L5 neuron apical dendrite (right; scale bar, 50 μm). LGN, lateral geniculate nucleus; V1, primary visual cortex; L, lateral; C, caudal. **c**, Ocular dominance shifts during contralateral-eye MD, 1–2 weeks after eye reopening (BV, binocular vision) and during a second MD, measured by intrinsic signal imaging and shown as ratio of contralateral-eye (contra) to ipsilateral-eye (ipsi) response strength. Circles depict data from individual mice; horizontal lines indicate mean values. **d**, High-magnification view of the dendritic stretch shown in **b** (red box), imaged every four days (depth, ~25 μm; soma depth, ~625 μm). MD in the contralateral eye was induced at the end of the third imaging session (day eight). Arrows point to spines appearing (red) or disappearing (blue), compared with the previous imaging session. Scale bar, 5 μm. **e**–**h**, Percentage of spines appearing (spine gain) and disappearing (spine loss) on L5 neurons between two imaging time points, plotted against time for different cortical regions or conditions: binocular visual cortex (**e**: left and middle, individual neurons; right, average data; 22 cells, 13 mice, 2,360 spines), monocular region of primary visual cortex (**f**: 7 cells, 6 mice, 754 spines), border of the binocular region (**g**: 9 cells, 9 mice, 984 spines) and control data from non-deprived mice (**h**: 21 cells, 11 mice, 2,468 spines). Error bars, s.e.m.

rate of spine gain increased only after eight days of MD (MD 4 d: $P > 0.2$; MD 8 d: $P < 0.02$; Fig. 1g). Therefore, the observed increase in spine number was specific to binocular cortex, indicating that the experience of imbalanced input from the eyes causes synaptic reorganization accompanying ocular dominance shifts in mature visual cortex. Overall, the net gain of spines during MD closely parallels the functional consequences of adult MD, whereby open-eye responses are selectively strengthened[3,10,20] (Supplementary Fig. 3a, b). Conversely, the negligible loss of spines matches the absence of substantial deprived-eye response weakening during adult ocular dominance plasticity[3,10,20].

We imaged a subset of mice at two-day intervals during MD to obtain a closer correlation between spine gain and ocular dominance shifts (Supplementary Fig. 3c). Most new spines appeared during a time when the strongest functional changes occurred, between days two and four of MD, whereas after day six, when the ocular dominance shift had reached saturation[3] (Fig. 1c), spine gain returned to baseline levels. The consistency between structural and functional data suggests that synaptic remodelling, implemented by the addition of new spines on L5 neurons, contributes to the strengthening of non-deprived-eye representation in binocular cortex.

By contrast with L5 neurons, spine dynamics on apical dendrites of L2/3 neurons did not change significantly during MD (spine gain: $P > 0.4$; spine loss: $P > 0.06$; Fig. 2). As cells in L2/3 exhibit robust ocular dominance shifts[3,15,16] in adults, more pronounced structural changes may occur on deeper parts of the dendritic trees[17], or different mechanisms of ocular dominance plasticity might prevail in the upper layers of mature visual cortex.

In adult mice, restoring binocular vision leads to complete functional recovery from an ocular dominance shift within a week following seven-day MD[3] (Fig. 1c). To determine whether MD-induced spine changes are also reversed during recovery, we reopened the deprived eye and continued imaging the same dendritic stretches on L5 neurons. The rate of spine formation in binocular cortex returned to baseline levels within four days of the contralateral eye being reopened (Fig. 1e), whereas the rate of spine loss did not change ($P > 0.3$; Fig. 1e); this resulted in spine numbers that remained elevated even after recovery from MD. To demonstrate that MD-induced structural changes indeed outlast the experience, we analysed data from only those cells that had been imaged over the entire recovery period following MD and which showed a clear change in spine dynamics during MD (14 cells, nine mice). The average spine density, which had increased progressively during the eight-day MD episode, declined only modestly in the following period of binocular vision (Fig. 3a, b). Two weeks later, spine densities were still substantially higher than they were before MD and in comparison with control animals ($P < 0.005$; Fig. 3b).

Tracking the long-term fate of individual spines revealed that the density of new spines that appeared during the eight days of MD and remained stable over the entire period of binocular vision following MD ('persistent new spines'[21]) was more than twice as high as that of control mice during a similar time period and of spines gained in the eight-day baseline period before MD ($P < 0.001$; Fig. 3c). The relative fraction of new spines that persisted during the weeks following MD did not significantly increase ($P > 0.05$; Fig. 3d), indicating that the efficiency of conversion of new spines into persistent spines was no different between control and deprived mice. In summary, MD in adult mice increases the number of spines, many of which remain when normal vision is restored. Thus, a structural correlate of the altered experience persists, even though changes in eye-specific response strength elicited by MD are completely reversed during recovery[3].

Inspired by work on plasticity in the barn owl midbrain[22,23], we previously showed that closure of the same eye for a second time leads to a faster and more persistent ocular dominance shift[3] (Fig. 1c). To test whether the extra spines induced by one MD episode could represent

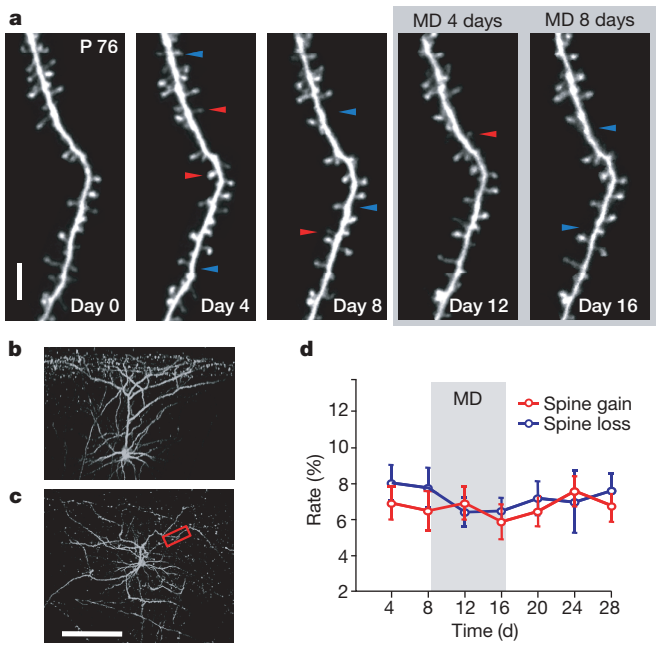

Figure 2 | Monocular deprivation in adult mice does not alter spine dynamics in L2/3 neurons. **a**, **b**, **c**, Repeatedly imaged dendritic stretch of a L2/3 pyramidal neuron (**a**: imaging depth, ~50 μm; soma depth, ~210 μm; scale bar, 5 μm) shown in **b** (side view) and **c** (top view; red box outlines dendritic stretch shown in **a**; scale bar, 100 μm). Arrows mark spine changes relative to previous imaging time point (red, spine gained; blue, spine lost). **d**, Average spine gain and loss on L2/3 pyramidal neurons in binocular visual cortex (7 cells, 4 mice, 1,101 spines). Error bars, s.e.m.

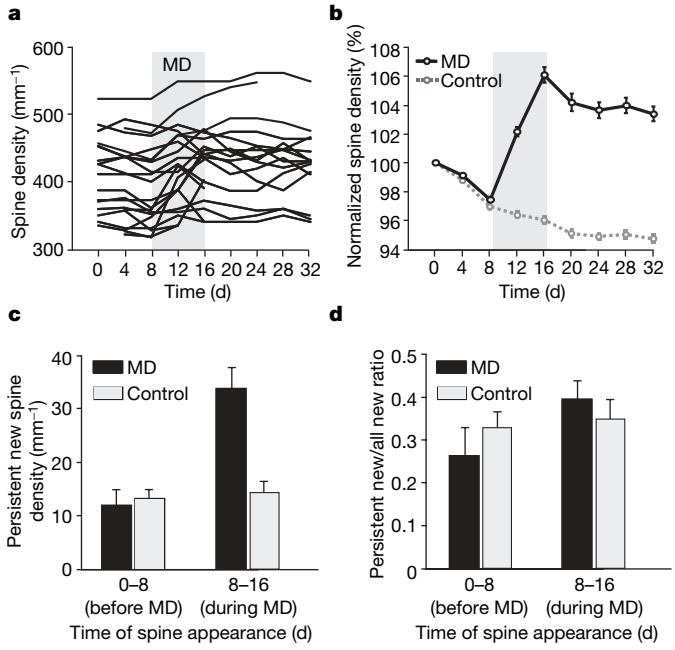

Figure 3 | MD-induced increase in spine density on L5 neurons outlasts the altered experience. **a**, Spine density as a function of time for all imaged L5 neurons in binocular visual cortex (22 cells, 13 mice, 2,360 spines). **b**, Average normalized spine density of L5 cells showing an increase in spine density during MD, imaged for at least 32 days (14 cells, 9 mice, 1,316 spines). **c**, Density of newly appeared spines that remain stable for a minimum of 16 days. The data have been split according to the time when the spines first appeared: before MD and during MD (and equivalent periods in control animals). **d**, Ratio of persistent new spines to all new spines before and during MD. Matched control data from non-deprived mice are shown in grey. Error bars, s.e.m.

the lasting 'memory trace' of earlier experience, we induced a second MD of the same eye after a two- to three-week period of normal vision. We found that the second MD neither altered spine dynamics nor increased spine density on L5 neurons in binocular cortex ($P > 0.2$; Fig. 4a, c). This stood out against the structural plasticity that occurred in conjunction with the first MD and could not be accounted for by greater age, the longer time since cranial window implantation, or the number of imaging sessions before the second deprivation episode: control mice that were matched for these parameters and which experienced only a single MD showed altered spine dynamics ($P < 0.02$; Fig. 4b) and increased spine density similar to those observed during the first MD in animals undergoing repeated MD episodes ($P > 0.7$; Fig. 4d; compare with Figs 1e and 3b).

The absence of structural plasticity during the second MD strongly contrasts with the presence of robust and even enhanced functional plasticity following repeated MD (Fig. 1c). When induced in adult mice, these ocular dominance shifts are implemented primarily by strengthening of non-deprived-eye responses[3] (Supplementary Fig. 3b). The new spines formed during the first MD most likely carry synapses[24,25], presumably contributing to the strengthening of non-deprived-eye responses. We suggest that these synapses are then weakened or silenced after eye re-opening, without retraction of the spines, thereby enabling full recovery of eye-specific responses. Their potentiation or reactivation may later allow for faster strengthening of non-deprived-eye responses during the second MD, as physical connections do not have to be re-established.

A robust correlation between spine size and synapse size and strength has been established in the literature[26,27], and strengthening or weakening of synaptic transmission has been shown to lead to spine enlargement or shrinkage, respectively[28–30]. We therefore followed the size of individual spines that appeared during, and outlasted, MD by measuring their integrated brightness (see Methods). On average, new spines became larger during deprivation and were similar in size to new spines in control animals ($P = 0.12$; MD spines: 50.0 ± 24.1 (mean brightness $\pm$ s.e.m., arbitrary units), $n = 34$; control spines: 57.3 ± 18.2, $n = 19$) and to other spines in the vicinity ($P = 0.38$, 63.1 ± 46.0, $n = 130$). However, spines that appeared during MD shrank after binocular vision had been restored and, notably, increased in size again during the second MD (analysis of variance, $P = 0.0002$; Fig. 4e, f, Supplementary Fig. 6). By contrast, persistent new spines in control animals grew and stabilized after their appearance (analysis of variance, $P = 0.72$; Fig. 4f, Supplementary Fig. 6). Thus, size changes of MD-induced spines correlate with the potentiation, depression and re-potentiation of non-deprived-eye responses during MD, recovery and subsequent MD, respectively, thereby supporting the idea that these new spines are functionally important as they are likely to bear synapses whose strength is modulated by visual experience. Calcium imaging in individual spines *in vivo* during eye-specific visual stimulation may provide final proof of the nature of synaptic inputs on these spines.

Overall, our experiments not only show that the rearrangement of intracortical connections by way of dendritic spines is one mechanism contributing to experience-dependent plasticity, but also that these spines embody the history of previous adaptations by cortical circuits. In this way, specific structural modifications may serve to store information about past experiences and thereby endow the cortex with an improved ability to adapt to similar experiences in the future.

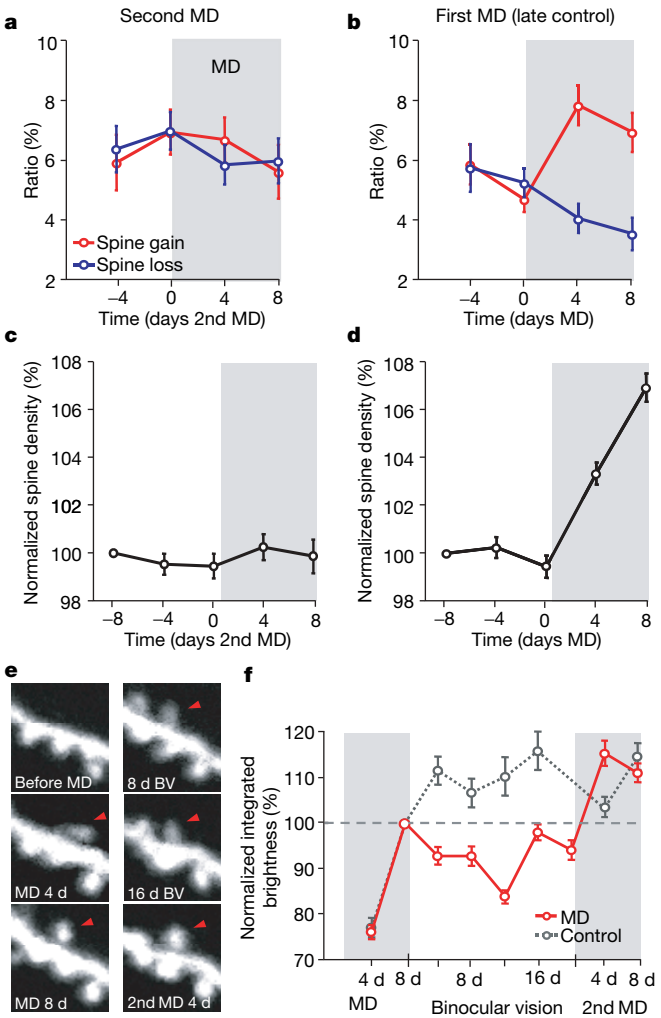

Figure 4 | A second MD increases the size of spines gained during the first MD, without additional spine gain. **a**, **b**, **c**, **d**, Rate of spine gain and loss (**a**, **b**) and normalized spine density (**c**, **d**) on L5 pyramidal neurons during a second period of contralateral-eye MD induced 2–3 weeks after the first (**a**, **c**: 14 cells, 9 mice, 1,316 spines), and during a single MD in control mice of similar implant duration and number of imaging sessions before the MD (**b**, **d**: 14 cells, 11 mice, 1,693 spines). **e**, Example of a spine that appeared during the first four days of MD and its brightness/size changes over time. BV, binocular vision. **f**, Average integrated brightness of persistent new spines that appeared during MD (red) or during the corresponding time period in non-deprived control animals (grey), normalized to the spine brightness value at the end of the first MD or the equivalent time point in control mice. Error bars, s.e.m.

METHODS SUMMARY

Adult mice expressing enhanced GFP in a small subset of cortical neurons (line GFP-M[18]) were implanted with a chronic imaging window[6] over the right visual cortex. Optical imaging of intrinsic signals during presentation of small, rapidly changing, drifting-grating stimuli was used to functionally identify the binocular region and to assess eye-specific responses and ocular dominance after different durations of MD, after re-opening of the eye and after a second MD, as described previously[3]. Apical dendritic stretches, 10–100 µm below the cortical surface, of L5 and L2/3 pyramidal neurons were repeatedly imaged every four days or every two days under ketamine–xylazine anaesthesia with two-photon laser scanning microscopy (custom-built microscope, Mai Tai Ti:sapphire laser (Spectra-Physics) at 910 nm, ×40 infrared Olympus objective). Spine dynamics were followed during alternating periods of normal, binocular vision and eight-day periods of contralateral-eyelid suture. In total, 10,548 spines from 100 cells were tracked over 5–14 imaging sessions. The percentages of spines appearing and disappearing on a cell between two successive imaging sessions, relative to the total spine number of the previous imaging session, were defined as the rates of spine gain and spine loss, respectively. For spine size measurements, the integrated brightness of all pixels comprising the spine was calculated (see Methods). *P* values were calculated with a non-parametric Wilcoxon rank-sum test or a Dunnett test for independent samples, and with a repeated-measures analysis of variance and Wilcoxon signed-rank test for paired samples.

Full Methods and any associated references are available in the online version of the paper at www.nature.com/nature.

Received 9 July; accepted 2 October 2008.
Published online 12 November 2008.

1. Wiesel, T. N. & Hubel, D. H. Single cell responses in striate cortex of kittens deprived of vision in one eye. *J. Neurophysiol.* **26,** 1003–1017 (1963).
2. Clark, S. A., Allard, T., Jenkins, W. M. & Merzenich, M. M. Receptive fields in the body-surface map in adult cortex defined by temporally correlated inputs. *Nature* **332,** 444–445 (1988).
3. Hofer, S. B., Mrsic-Flogel, T. D., Bonhoeffer, T. & Hübener, M. Prior experience enhances plasticity in adult visual cortex. *Nature Neurosci.* **9,** 127–132 (2006).
4. Bailey, C. H. & Kandel, E. R. Structural changes accompanying memory storage. *Annu. Rev. Physiol.* **55,** 397–426 (1993).
5. Yuste, R. & Bonhoeffer, T. Morphological changes in dendritic spines associated with long-term synaptic plasticity. *Annu. Rev. Neurosci.* **24,** 1071–1089 (2001).
6. Trachtenberg, J. T. *et al.* Long-term *in vivo* imaging of experience-dependent synaptic plasticity in adult cortex. *Nature* **420,** 788–794 (2002).
7. Grutzendler, J., Kasthuri, N. & Gan, W. B. Long-term dendritic spine stability in the adult cortex. *Nature* **420,** 812–816 (2002).
8. Majewska, A. K., Newton, J. R. & Sur, M. Remodeling of synaptic structure in sensory cortical areas *in vivo*. *J. Neurosci.* **26,** 3021–3029 (2006).
9. Holtmaat, A. J. *et al.* Transient and persistent dendritic spines in the neocortex *in vivo*. *Neuron* **45,** 279–291 (2005).
10. Sawtell, N. B. *et al.* NMDA receptor-dependent ocular dominance plasticity in adult visual cortex. *Neuron* **38,** 977–985 (2003).
11. Gordon, J. A. & Stryker, M. P. Experience-dependent plasticity of binocular responses in the primary visual cortex of the mouse. *J. Neurosci.* **16,** 3274–3286 (1996).
12. Hensch, T. K. *et al.* Local GABA circuit control of experience-dependent plasticity in developing visual cortex. *Science* **282,** 1504–1508 (1998).
13. Huang, Z. J. *et al.* BDNF regulates the maturation of inhibition and the critical period of plasticity in mouse visual cortex. *Cell* **98,** 739–755 (1999).
14. Mrsic-Flogel, T. D. *et al.* Homeostatic regulation of eye-specific responses in visual cortex during ocular dominance plasticity. *Neuron* **54,** 961–972 (2007).
15. Tagawa, Y., Kanold, P. O., Majdan, M. & Shatz, C. J. Multiple periods of functional ocular dominance plasticity in mouse visual cortex. *Nature Neurosci.* **8,** 380–388 (2005).
16. Fischer, Q. S., Graves, A., Evans, S., Lickey, M. E. & Pham, T. A. Monocular deprivation in adult mice alters visual acuity and single-unit activity. *Learn. Mem.* **14,** 277–286 (2007).
17. Mataga, N., Mizuguchi, Y. & Hensch, T. K. Experience-dependent pruning of dendritic spines in visual cortex by tissue plasminogen activator. *Neuron* **44,** 1031–1041 (2004).
18. Feng, G. *et al.* Imaging neuronal subsets in transgenic mice expressing multiple spectral variants of GFP. *Neuron* **28,** 41–51 (2000).
19. Wang, Q. & Burkhalter, A. Area map of mouse visual cortex. *J. Comp. Neurol.* **502,** 339–357 (2007).
20. Heimel, J. A., Hartman, R. J., Hermans, J. M. & Levelt, C. N. Screening mouse vision with intrinsic signal optical imaging. *Eur. J. Neurosci.* **25,** 795–804 (2007).
21. Holtmaat, A., Wilbrecht, L., Knott, G. W., Welker, E. & Svoboda, K. Experience-dependent and cell-type-specific spine growth in the neocortex. *Nature* **441,** 979–983 (2006).
22. Knudsen, E. I. Instructed learning in the auditory localization pathway of the barn owl. *Nature* **417,** 322–328 (2002).
23. Linkenhoker, B. A., der Ohe, C. G. & Knudsen, E. I. Anatomical traces of juvenile learning in the auditory system of adult barn owls. *Nature Neurosci.* **8,** 93–98 (2005).
24. Knott, G. W., Holtmaat, A., Wilbrecht, L., Welker, E. & Svoboda, K. Spine growth precedes synapse formation in the adult neocortex *in vivo*. *Nature Neurosci.* **9,** 1117–1124 (2006).
25. Nägerl, U. V., Kostinger, G., Anderson, J. C., Martin, K. A. & Bonhoeffer, T. Protracted synaptogenesis after activity-dependent spinogenesis in hippocampal neurons. *J. Neurosci.* **27,** 8149–8156 (2007).
26. Kasai, H., Matsuzaki, M., Noguchi, J., Yasumatsu, N. & Nakahara, H. Structure-stability-function relationships of dendritic spines. *Trends Neurosci.* **26,** 360–368 (2003).
27. Bourne, J. & Harris, K. M. Do thin spines learn to be mushroom spines that remember? *Curr. Opin. Neurobiol.* **17,** 381–386 (2007).
28. Matsuzaki, M., Honkura, N., Ellis-Davies, G. C. & Kasai, H. Structural basis of long-term potentiation in single dendritic spines. *Nature* **429,** 761–766 (2004).
29. Kopec, C. D., Li, B., Wei, W., Boehm, J. & Malinow, R. Glutamate receptor exocytosis and spine enlargement during chemically induced long-term potentiation. *J. Neurosci.* **26,** 2000–2009 (2006).
30. Zhou, Q., Homma, K. J. & Poo, M. M. Shrinkage of dendritic spines associated with long-term depression of hippocampal synapses. *Neuron* **44,** 749–757 (2004).

Supplementary Information is linked to the online version of the paper at www.nature.com/nature.

Acknowledgements We thank T. Keck for contributing control data for Supplementary Fig. 7a, and M. Sperling and B. Pichler for programming help. This work was supported by the Max Planck Society, the Wellcome Trust and the Humboldt Foundation.

Author Information Reprints and permissions information is available at www.nature.com/reprints. Correspondence and requests for materials should be addressed to M.H. (mark@neuro.mpg.de).

METHODS

Window implant surgery. C57BL/6 mice (postnatal day 45–100) expressing enhanced GFP under the *Thy-1* promoter in a small subset of cortical neurons (line GFP-M[18]) were anaesthetized with an intraperitoneal injection of ketamine (0.14 mg per gram of bodyweight) and xylazine (0.01 mg per gram of bodyweight). Atropine (0.01 ml at 0.1 mg ml^{-1}) and fortecortin (0.01 ml at 2 mg ml^{-1}) were injected subsequently. After resecting the scalp and cleaning the skull, a circular craniotomy (3–4-mm diameter) was performed over the posterior part of the right hemisphere. The intact dura was covered with a thin layer of agarose (1.2% in artificial cerebral spinal fluid) and a glass coverslip (no. 1, 5-mm diameter). Dental acrylic was applied to seal implant, skull and wound margins. A small metal bar was embedded in the acrylic for fixing the animal during imaging sessions. Animals were housed separately after surgery.

Intrinsic signal imaging. In all mice, the binocular region of the visual cortex was identified using optical imaging of intrinsic signals. In a subset of animals, shifts in ocular dominance were determined during repeated episodes of MD (for details, see ref. 3). Mice were anaesthetized with a mixture of fentanyl (0.05 mg kg^{-1}), midazolam (5.0 mg kg^{-1}) and medetomidine (0.5 mg kg^{-1}). Rectangular square-wave drifting gratings of changing orientations (0.03 cycles per degree, 2 cycles per second, 25° × 25° for identifying the binocular cortex, 18° × 18° for ocular dominance measurements) were presented to the eyes independently at neighbouring positions on a monitor in the central visual field of the mouse. Images (600-ms duration) of the cortex through the cranial window were taken with a cooled, slow-scan charged-coupled-device camera under illumination by 707-nm light. Three 'blank' images were acquired before the stimulus was shown for 7 s. Response maps were blank-corrected and averaged over 9–24 stimulus repetitions. Responses were combined in a maximum-response projection to visualize the binocular visual cortex. Response strength for the two eyes was determined as described previously[3]. The ratio of contralateral- to ipsilateral-eye response strength (contra/ipsi ratio) was calculated as a measure of ocular dominance.

Two-photon imaging and lid suture. Using two-photon laser scanning microscopy, dendritic stretches of L5 and L2/3 pyramidal neurons were repeatedly imaged every four days under ketamine–xylazine anaesthesia (70% of implant surgery dose), starting on average 16 days after surgery. A subset of mice was imaged at two-day intervals. High-resolution image stacks (1024 × 1024 pixel, 90 × 90 μm^2, 0.5-μm *z*-step size) of several apical dendrites 10–100 μm below the cortical surface (layer 1) were obtained with Fluoview software (Olympus), using a custom-built microscope, a 910-nm Mai Tai Ti:sapphire laser (Spectra-Physics) focused through a ×40 immersion objective (infrared, 0.8 numerical aperture, Olympus). Lower-magnification image stacks (512 × 512 pixel, 350 × 350 μm^2, 1–2-μm *z*-step size) of labelled cells were taken and matched to the blood vessel pattern on the brain surface, to relocate imaging regions and to determine the cortical depth of the cell bodies of imaged neurons.

To induce MD, the left lid (contralateral to the imaged hemisphere) was sutured shut immediately after the imaging session. The eye was reopened eight days later, immediately following the imaging session. In a subset of mice, a second eight-day MD in the same eye was induced two to three weeks later. Imaging was continued between deprivation periods. Another group of animals was imaged nine times every four days before an eye was closed for eight days to yield control data ('late control'; Fig. 4b, d).

Data analysis. All clear protrusions from the dendrite, irrespective of their orientation relative to the imaging plane, were included in the analysis, resulting in a total of 10,548 spines from 100 cells that were tracked over 5–14 imaging sessions. Spine analysis was carried out on raw image stacks using the ImageJ image processing program, blind with respect to cell position in the cortex. The rates of spine gain and loss are respectively the percentages of spines that appeared and disappeared between two successive imaging sessions (in a four-day or two-day period), relative to the total spine number of the previous imaging session. To investigate whether structural changes occurring during MD outlast the eight-day deprivation period (Figs 3b, c, d, 4a, c), only those cells were included that were imaged over at least nine time points and which showed a detectable effect on spine dynamics during MD.

Imaging stacks were aligned with the intrinsic signal response maps by means of the blood vessel pattern to determine the position of dendritic stretches and cell bodies with regard to cortical region (binocular visual cortex, monocular primary visual cortex, and outside primary visual cortex).

To follow the size of spines over time, only spines which clearly protruded from the dendritic shaft at all time points after their appearance were included in the analysis. In the best focal section, intensity values of all pixels comprising the spine were summed after background subtraction (taken from a region close to the spine which was devoid of GFP-labelled structures). This integrated spine intensity was divided by the mean intensity of the adjacent dendritic shaft to correct for varying imaging conditions. Repeating this analysis with a maximum-intensity projection of all sections containing the spine (instead of the best focal section) yielded very similar results. To compare the size of persistent new spines in deprived and control animals to other spines in their vicinity after eight days of MD (or the equivalent imaging time point for control animals), the integrated spine brightness values of ten spines on the same dendrite closest to a persistent new spine were included ($n = 130$ spines, 13 neurons).

P values were calculated using a non-parametric Wilcoxon rank-sum test for independent samples, with a repeated-measures analysis of variance and Wilcoxon sign-rank test for paired samples, and with a Dunnett test for comparing different groups with one reference group.

Vol 457|15 January 2009|doi:10.1038/nature07472

LETTERS

Role for Spi-C in the development of red pulp macrophages and splenic iron homeostasis

Masako Kohyama[1,2], Wataru Ise[1,2], Brian T. Edelson[1], Peter R. Wilker[1], Kai Hildner[1,2], Carlo Mejia[1,2], William A. Frazier[3], Theresa L. Murphy[1] & Kenneth M. Murphy[1,2]

Tissue macrophages comprise a heterogeneous group of cell types differing in location, surface markers and function[1]. Red pulp macrophages are a distinct splenic subset involved in removing senescent red blood cells[2]. Transcription factors such as PU.1 (also known as Sfpi1) and C/EBPα (Cebpa) have general roles in myelomonocytic development[3,4], but the transcriptional basis for producing tissue macrophage subsets remains unknown. Here we show that Spi-C (encoded by *Spic*), a PU.1-related transcription factor, selectively controls the development of red pulp macrophages. Spi-C is highly expressed in red pulp macrophages, but not monocytes, dendritic cells or other tissue macrophages. *Spic*$^{-/-}$ mice have a cell-autonomous defect in the development of red pulp macrophages that is corrected by retroviral Spi-C expression in bone marrow cells, but have normal monocyte and other macrophage subsets. Red pulp macrophages highly express genes involved in capturing circulating haemoglobin and in iron regulation. *Spic*$^{-/-}$ mice show normal trapping of red blood cells in the spleen, but fail to phagocytose these red blood cells efficiently, and develop an iron overload localized selectively to splenic red pulp. Thus, Spi-C controls development of red pulp macrophages required for red blood cell recycling and iron homeostasis.

Spi-C belongs to the Spi subfamily of Ets transcription factors, which includes PU.1 and Spi-B[5,6], and was initially reported to be expressed in B cells[5,7]. We compared expression of PU.1, Spi-B and Spi-C across a panel of immune cells such as B cells, bone marrow monocytes, dendritic cells and several types of resident tissue macrophages, including red pulp macrophages (RPMs; Fig. 1a, Supplementary Fig. 1). PU.1 was broadly expressed and Spi-B was predominantly restricted to B cells[8,9]. In contrast, Spi-C was highly expressed in RPMs, expressed at lower levels in B cells, and essentially absent in other cells. To test for a role of Spi-C in RPMs and B cells, we generated mice lacking *Spic* expression by gene targeting (Supplementary Fig. 2). Male and female *Spic*$^{-/-}$ mice are fertile and healthy, with a normal lifespan, but are born at a somewhat lower than expected Mendelian frequency (Supplementary Fig. 2). We also generated *Spic*$^{null/null}$ mice, in which the neomycin cassette was deleted from the targeted *Spic* allele (Supplementary Fig. 2).

RPMs have been defined as F4/80^{hi}CD68^{+}CD11b$^{lo/-}$ cells with strong autofluorescence[10,11]. Both *Spic*$^{-/-}$ mice and *Spic*$^{null/null}$ mice showed a phenotype characterized by the selective loss of RPMs (Fig. 1b and c, Supplementary Fig. 3a), but showed no abnormalities in the development of B cells, conventional dendritic cells, plasmacytoid dendritic cells (Supplementary Figs 3 and 4, and Supplementary Table 1) or T cells (Supplementary Fig. 5), and had normal serum immunoglobulin levels (Supplementary Fig. 4f). We confirmed the loss of RPMs by immunohistochemical analysis, finding an almost complete loss of F4/80^{+} cells in the splenic red pulp (Fig. 2a). In contrast, SIGN-R1 (also known as CD209a)-expressing marginal zone macrophages and MOMA-1 (also known as Siglec1)-expressing metallophilic marginal zone macrophages were present normally in the spleens of *Spic*$^{-/-}$ mice (Fig. 2a). *Spic*$^{-/-}$ mice had normal F4/80^{+} tissue macrophages in peritoneum and liver, normal macrophage and dendritic cell progenitors in bone marrow, and normal monocytes in bone marrow and blood (Supplementary Fig. 6).

Loss of RPMs could result either from a cell-autonomous defect or from the loss of a required extrinsic component such as a bone marrow or splenic stromal cell. To distinguish these possibilities, we generated haematopoietic chimaeras by transplanting bone marrow cells from CD45.2^{+} *Spic*$^{+/+}$ or *Spic*$^{-/-}$ mice into irradiated congenic CD45.1^{+}

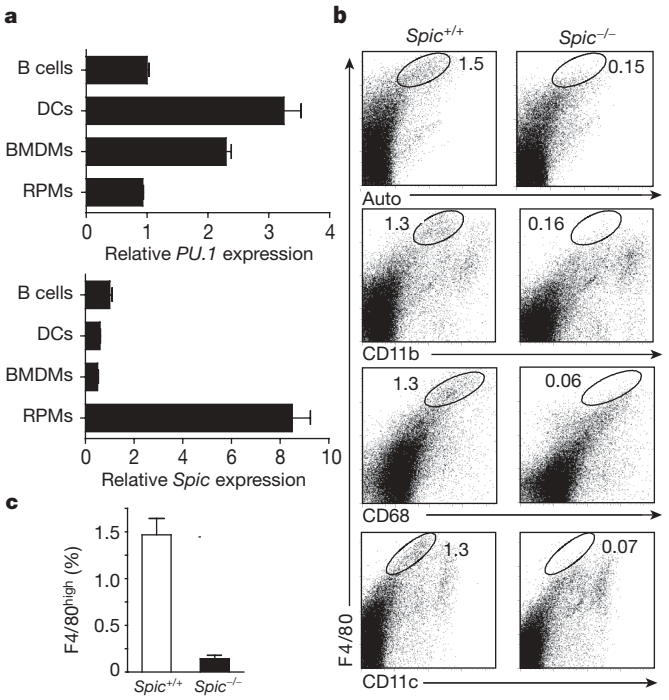

Figure 1 | *Spic*$^{-/-}$ mice have a selective loss of red pulp macrophages. **a**, *PU.1* and *Spic* expression was determined by quantitative polymerase chain reaction with reverse transcription (RT–PCR) in purified B cells, dendritic cells (DCs), bone-marrow-derived macrophages (BMDMs) and RPMs. Shown is the normalized messenger RNA expression relative to expression in B cells. **b**, *Spic*$^{+/+}$ and *Spic*$^{-/-}$ spleen cells were stained with antibodies to F4/80, CD11b, CD68 and CD11c and analysed by flow cytometry. Auto, autofluorescence. Numbers represent the percentage of cells in the indicated gate. **c**, Frequency of F4/80^{hi} cells in spleen was determined as the mean (and s.d., $n = 7$) from total splenocytes as shown in **b**.

[1]Department of Pathology and Immunology, [2]Howard Hughes Medical Institute, [3]Department of Biochemistry and Molecular Biophysics, Washington University School of Medicine, 660 S. Euclid Avenue, St Louis, Missouri 63110, USA.

recipients (Fig. 2b). In these chimaeras, F4/80$^+$ RPMs developed from *Spic*$^{+/+}$, but not from *Spic*$^{-/-}$, donor bone marrow (Fig. 2b). This defect was restricted to RPMs, because *Spic*$^{-/-}$ donor bone marrow generated normal B cells (Fig. 2b), CD11b$^+$ and CD11c$^+$ myeloid lineages, natural killer cells and T cells (Supplementary Fig. 6e). Development of F4/80$^+$ RPMs was restored when *Spic*$^{-/-}$ bone marrow was infected with a Spi-C-expressing retrovirus and allowed to develop in lethally irradiated hosts (Fig. 2c). These findings indicate that the loss of RPMs in *Spic*$^{-/-}$ mice results from an intrinsic haematopoietic defect.

Senescent red blood cells (RBCs) are normally phagocytosed by macrophages in spleen and liver, followed by degradation of their haemoglobin, and transport of the iron back into the circulation[12–14]. To study RBC clearance by splenic macrophages, we used the system of *Cd47*$^{-/-}$ RBCs[13]. We injected carboxy-fluorescein succinimidyl ester (CFSE)-labelled *Cd47*$^{-/-}$ RBCs into mice and examined their clearance and uptake by spleen and liver cells (Supplementary Fig. 7). The initial clearance of *Cd47*$^{-/-}$ RBCs from the circulation was similar between *Spic*$^{-/-}$ and *Spic*$^{+/+}$ mice (Supplementary Fig. 7a). However, we found differences in efficiency of phagocytosis of trapped RBCs by splenic macrophages between *Spic*$^{+/+}$ and *Spic*$^{-/-}$ mice. In *Spic*$^{+/+}$ mice, F4/80^{hi} CD68$^+$ RPMs showed more than tenfold higher uptake of CFSE than F4/80^{lo}CD68$^+$ cells (Supplementary Fig. 7c, d). In *Spic*$^{-/-}$ mice, which lacked F4/80^{hi}CD68$^+$ macrophages (Supplementary Fig. 7c), the remaining F4/80^{lo}CD68$^+$ macrophages showed the low level of phagocytosis seen in *Spic*$^{+/+}$ mice (Supplementary Fig. 7d). Liver cells did not take up labelled *Cd47*$^{-/-}$ RBCs in either wild-type or *Spic*$^{-/-}$ mice (Supplementary Fig. 7e). These results suggest that the absence of F4/80^{hi} RPMs in *Spic*$^{-/-}$ mice represents the loss of a functional macrophage subset that is normally responsible for efficient phagocytosis of RBCs in the spleen.

Spic$^{-/-}$ mice developed an age-dependent increase in the size and weight of the spleen not associated with increased numbers of splenocytes (Fig. 3a, b). Because mice with genetic defects in iron or haemoglobin metabolism can exhibit splenomegaly[15,16], we assessed the iron stores of *Spic*$^{-/-}$ mice. Serum and liver iron concentrations were normal in *Spic*$^{-/-}$ mice, but splenic tissue iron concentration was increased (Fig. 3c, d and Supplementary Fig. 8a, b). This iron accumulation was evident histologically in *Spic*$^{-/-}$ mice and largely confined to the red pulp (Fig. 3e and Supplementary Figs 8c and 9a), but was not observed in the liver or intestine (Supplementary Fig. 8d, and data not shown). *Spic*$^{-/-}$ mice did not exhibit abnormal erythroid parameters or morphology (Supplementary Table 2 and Supplementary Fig. 9c).

To identify potential Spi-C target genes, we compared global gene expression profiles of RPMs, alveolar and peritoneal macrophages, monocytes and dendritic cells (Fig. 4a). The haemoglobin scavenger receptor (*Cd163*)[17] and the iron transporter ferroportin 1 (*Slc40a1*)[18] were both highly expressed by RPMs relative to other macrophage subsets or B cells (Fig. 4a). Vascular cell adhesion molecule 1 (*Vcam1*) was also highly expressed in RPMs compared to peritoneal and alveolar macrophages (Fig. 4a), consistent with reported Vcam1 expression in the red pulp[19,20]. Vcam1 is most highly expressed in the red pulp of control spleens, but was virtually absent in *Spic*$^{-/-}$ spleens (Fig. 4b, Supplementary 10a, b). In *Spic*$^{+/+}$ spleens, Vcam1 was highly correlated with F4/80 expression (Supplementary Fig. 10a), both of which were substantially reduced in *Spic*$^{-/-}$ spleens. In contrast, other tissues did not show this coordinated expression of F4/80 and Vcam1 (Supplementary Fig. 10a). Peritoneal macrophages expressed high F4/80 without high Vcam1, and most F4/80$^+$ cells in lymph nodes expressed low levels of Vcam1 (Supplementary Fig. 10b). However, Vcam1 expression by B cells was reduced in *Spic*$^{-/-}$ mice compared to *Spic*$^{+/+}$ mice (Supplementary Fig. 10b). Bone marrow monocytes treated with M-CSF (colony stimulating factor 1, also known as Csf1)[21] induced both Spi-C and Vcam1 expression, whereas treatment with GM-CSF (also known as Csf2) caused much less induction of Spi-C and no induction of Vcam1 (Supplementary Fig. 10c). Consistently, *Spic*$^{-/-}$ bone marrow cells treated with M-CSF showed reduced levels of Vcam1 expression compared to wild-type cells (Supplementary Fig. 10d). Together, these results suggest the possibility that Spi-C may regulate the expression of Vcam1.

Reporter analysis and electrophoretic mobility shift assays (EMSAs) provide additional evidence that Spi-C regulates Vcam1 (Fig. 4c–e). PU.1 can augment FcγR2b promoter activity[22]. PU.1 and Spi-C each augment a Vcam1 reporter by a similar magnitude[22] (Fig. 4c). An Ets consensus element within the proximal Vcam1 promoter forms complexes with PU.1 and Spi-C in EMSAs (Fig. 4d), which are supershifted by anti-PU.1 or anti-Spi-C antisera, respectively (Fig. 4e). Formation of the Spi-C EMSA complex was specifically inhibited by an FcγR2b Ets probe and Vcam1 Ets probe, but not by a mutated Vcam1 Ets probe. Deletion of the Ets element within the Vcam1 promoter eliminated reporter augmentation by both PU.1 and Spi-C (Fig. 4c). To test whether Spi-C could induce

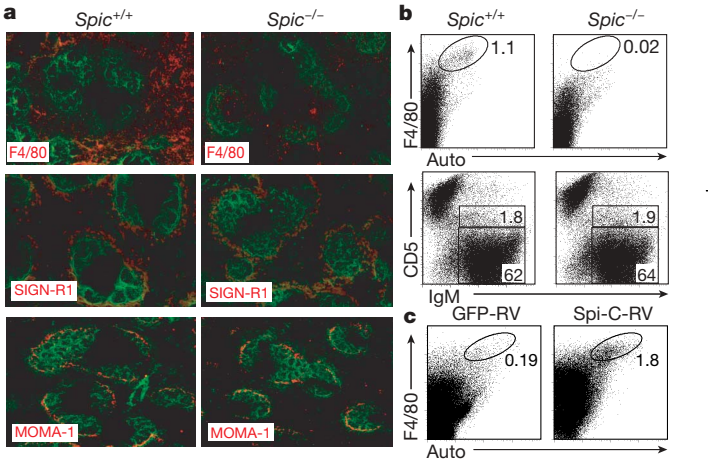

Figure 2 | *Spic*$^{-/-}$ mice have a cell-autonomous defect in red pulp macrophages. a, *Spic*$^{+/+}$ and *Spic*$^{-/-}$ spleens sections were stained for B220 (green) and F4/80, SIGN-R1 or MOMA-1 (red). **b**, Bone marrow cells from CD45.2$^+$ C57BL/6 *Spic*$^{+/+}$ or *Spic*$^{-/-}$ mice were transferred into irradiated CD45.1$^+$ B6.SJL mice. Splenocytes were stained for CD45.2, CD45.1, F4/80, CD5 and immunoglobulin (Ig)M. After 10 weeks, >97% of spleen cells were donor-derived (CD45.2$^+$CD45.1$^-$). Plots are gated on donor-derived cells. Numbers represent the percentage of donor-derived cells in the indicated gates. **c**, Bone marrow cells from CD45.2$^+$ C57BL/6 *Spic*$^{-/-}$ mice were infected with Spi-C-RV or control retrovirus (GFP-RV) and transferred into irradiated CD45.1$^+$ B6.SJL mice. After 6 weeks, spleen cells were stained for CD45.2, CD45.1 and F4/80. Plots are gated on donor-derived cells. Results are representative of four mice per group.

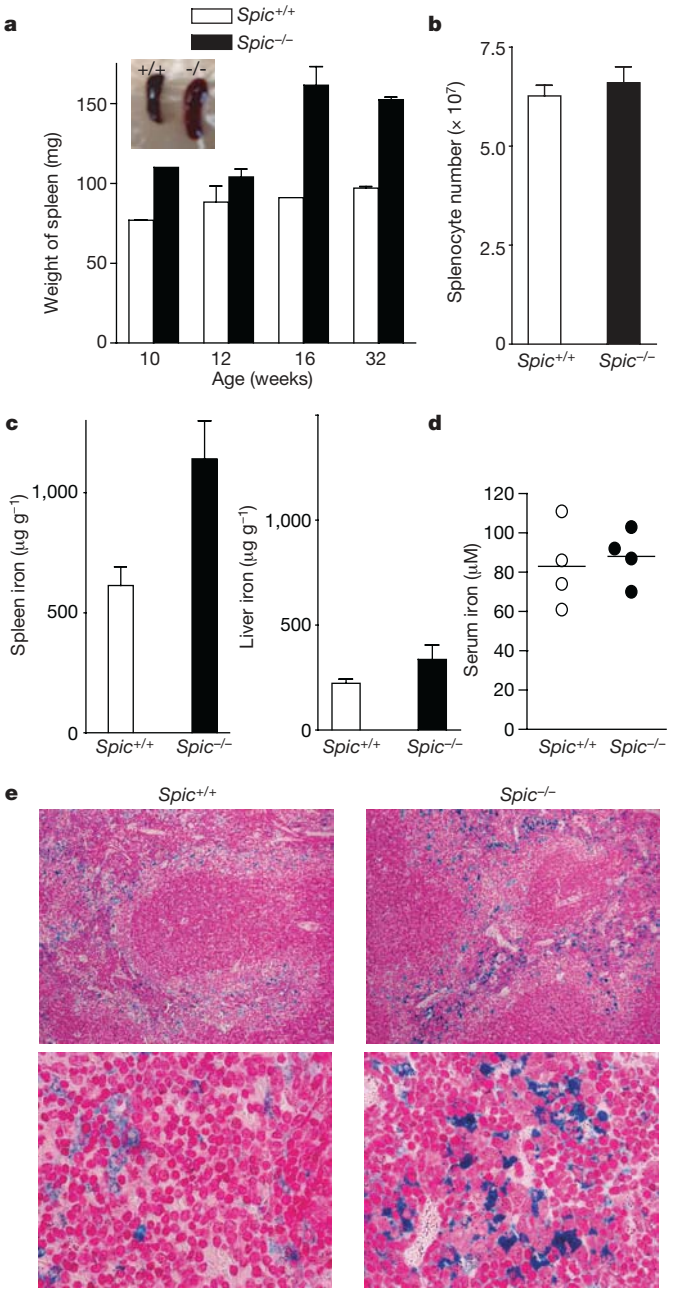

Figure 3 | *Spic*$^{-/-}$ mice have increased splenic iron stores. **a**, Spleens from *Spic*$^{+/+}$ and *Spic*$^{-/-}$ mice of the indicated age were weighed ($n = 3$ per time point). Representative spleens at 32 weeks are shown in the inset. **b**, Splenocytes from *Spic*$^{+/+}$ and *Spic*$^{-/-}$ mice were counted (mean and s.d., $n = 5$). **c**, Iron levels in spleen (left) and liver (right) of 129 SvEv background *Spic*$^{+/+}$ and *Spic*$^{-/-}$ male mice on a standard diet (mean and s.d., $n = 4$). **d**, Serum iron levels were determined for 32-week-old 129 SvEv background *Spic*$^{+/+}$ and *Spic*$^{-/-}$ male mice on a standard diet. **e**, Perl's Prussian blue stain for ferric iron in the spleens of 16-week old 129 SvEv *Spic*$^{+/+}$ and *Spic*$^{-/-}$ male mice.

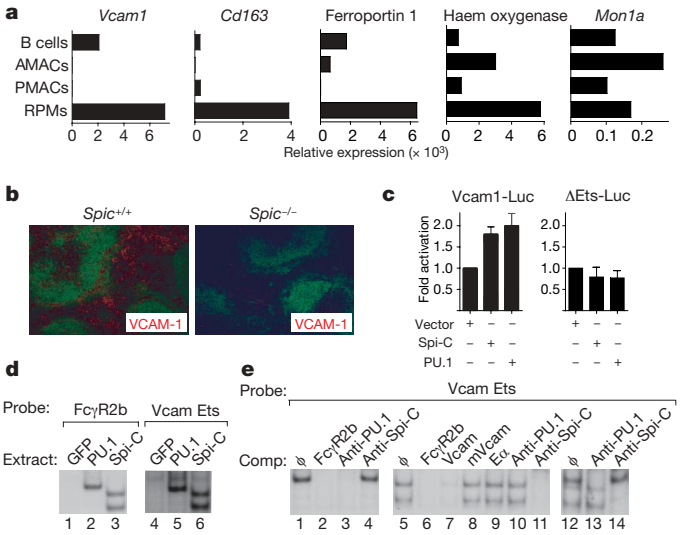

Figure 4 | Spi-C regulates Vcam1 expression. **a**, Normalized expression of *Vcam1*, *Cd163*, ferroportin I, haem oxygenase and *Mon1a* is shown for B cells, alveolar macrophages (AMACs), peritoneal macrophages (PMACs) and RPMs, assessed by expression microarrays. **b**, *Spic*$^{+/+}$ or *Spic*$^{-/-}$ spleen sections were stained for B220 (green) and Vcam1 (red). **c**, J774 cells were transfected with the Vcam1 reporter (Vcam1-Luc) or the ΔEts-Luc reporter, and with pEF4 (vector), Spi-C- or PU.1-expressing vectors. Cells were analysed for luciferase activity as described in the Supplementary Methods. Data are representative of four independent experiments (mean and s.d., $n = 3$). **d**, 293F/T cells were transiently transfected with GFP-RV (GFP), PU1-MIGR1 (PU.1) or Spi-C-RV (Spi-C), and whole-cell extracts were analysed for binding to the FcγR2b or the Vcam1 Ets probes. **e**, Extracts from PU.1-expressing cells (lanes 1–4), Spi-C-expressing cells (lanes 5–11) or mixtures of PU.1 and Spi-C extracts (lanes 12–14) were analysed for binding to the Vcam1 Ets probe. Shown are competitions (Comp) using unlabelled competitor oligonucleotides or supershifts using anti-sera against PU.1 or Spi-C as indicated. ϕ, no treatment; mVcam, mutated Vcam1 oligonucleotides.

Vcam1 in cell lines, we transfected the RAW264.7 macrophage cell line with Spi-C retrovirus (Spi-C-RV) or control retrovirus (Supplementary Fig. 10e). Control RAW264.7 cells do not express Spi-C or Vcam1, and treatment with M-CSF only weakly induced Vcam1. In Spi-C-expressing RAW264.7 cells, M-CSF strongly induced Vcam1, but not CD163, ferroportin, haem oxygenase or Mon1a. Thus, Vcam1 seems to be a target of Spi-C in macrophages.

Spi-C was initially identified as a PU.1-related transcription factor expressed in B cells, but its function was unknown[5,7]. An earlier report based on overexpression studies suggested Spi-C might regulate immunoglobulin E production[23]. Differential expression of Spi-C was suggested as evidence for independent ontogeny for splenic B cells and peritoneal B1a B cells[24]. We find *Spic*$^{-/-}$ mice to have normal B-cell development and antibody production, but do not exclude a subtle role for Spi-C in B-cell function. However, our evidence supports a critical role for Spi-C in the development of RPMs, and shows that this cell lineage is required for normal recycling of red blood cells and iron homeostasis in the spleen.

The known genetic defects of iron metabolism[14,25,26] frequently involve proteins that function as iron transporters/exporters (for example, ferroportin[18]), as receptors for iron-binding proteins (for example, transferrin receptor[27] and hemochtomatosis[28]), or to regulate the activity of these transporters or receptors (for example, hepcidin[29]). Such gene defects that directly alter iron transport can produce global changes in iron storage that may affect many tissues. In contrast, the transcription factor Spi-C is the first gene to affect iron metabolism by controlling the development of a particular cell lineage important for recycling red blood cells and their products. Future studies will be directed at analysis of the specific roles of transcriptional targets of Spi-C, such as Vcam1, in elaborating these functions of red pulp macrophages.

METHODS SUMMARY

Mice and reagents. *Spic*$^{-/-}$ mice were generated by deleting the entire protein-coding regions exons 2–6 of the *Spic* locus. The neomycin resistance cassette was deleted by intercrossing *Spic*$^{+/-}$ mice with CMV-Cre deletor mice to produce *Spic*$^{null/null}$ mice, as described in Supplementary Methods.

Histochemical analysis. Six-micrometre frozen tissue sections were fixed in cold acetone and blocked with 5% bovine serum albumin (Roche). The monoclonal antibodies used were biotinylated antibody against F4/80 (Caltag), Vcam1 (eBioscience), MOMA-1 (BMA Biomedicals) and SIGN-R1 (ER-TR9, BMA

Biomedicals), Alexa488-conjugated antibody against B220 (BD PharMingen) and streptavadin-Alexa555 (Invitrogen). For Perl's Prussian blue stain, tissues were fixed with 4% paraformaldehyde in 0.1 M phosphate buffer (pH 7.0), embedded in paraffin, and stained with Perl's Prussian blue and pararosaniline (Sigma).

Adoptive transfer of bone marrow cells. Recipient CD45.1$^+$ B6.SJL (Taconic) mice were lethally irradiated with 1,100 rads and injected intravenously with 10^7 bone marrow cells obtained from CD45.2$^+$ F4 or F5 *Spic*$^{+/+}$ or *Spic*$^{-/-}$ mice. Donor-derived cells in spleen (CD45.2$^+$) were analysed 10 weeks after transfer by fluorescence-activated cell sorting.

Measurement of iron content in spleen, liver and serum. Age- and gender-matched mice were analysed for non-haem iron as described[30]. Livers and spleens were weighed and digested in 3 M hydrochloric acid/10% trichloroacetic acid, at 65 °C for 20 h. Ten microlitres of each acid extract was mixed with 0.5 ml of chromagen reagent. The absorbance at 535 nm was measured by a DU Series 500 spectrophotometer (Beckman), and compared to an iron standard treated identically. For serum measurements[30], 20 µl of serum was incubated with 20 µl of acid reagent for 5 min. Supernatant was mixed with 40 µl chromagen reagent, and absorbance at 535 nm was measured as described above.

Received 26 August; accepted 30 September 2008.
Published online 26 November 2008.

1. Taylor, P. R. *et al.* Macrophage receptors and immune recognition. *Annu. Rev. Immunol.* **23,** 901–944 (2005).
2. Gordon, S. & Taylor, P. R. Monocyte and macrophage heterogeneity. *Nature Rev. Immunol.* **5,** 953–964 (2005).
3. Ye, M. & Graf, T. Early decisions in lymphoid development. *Curr. Opin. Immunol.* **19,** 123–128 (2007).
4. Friedman, A. D. Transcriptional control of granulocyte and monocyte development. *Oncogene* **26,** 6816–6828 (2007).
5. Bemark, M., Martensson, A., Liberg, D. & Leanderson, T. Spi-C, a novel Ets protein that is temporally regulated during B lymphocyte development. *J. Biol. Chem.* **274,** 10259–10267 (1999).
6. Carlsson, R., Hjalmarsson, A., Liberg, D., Persson, C. & Leanderson, T. Genomic structure of mouse SPI-C and genomic structure and expression pattern of human SPI-C. *Gene* **299,** 271–278 (2002).
7. Hashimoto, S. *et al.* Prf, a novel Ets family protein that binds to the PU.1 binding motif, is specifically expressed in restricted stages of B cell development. *Int. Immunol.* **11,** 1423–1429 (1999).
8. Lloberas, J., Soler, C. & Celada, A. The key role of PU.1/SPI-1 in B cells, myeloid cells and macrophages. *Immunol. Today* **20,** 184–189 (1999).
9. Su, G. H. *et al.* Defective B cell receptor-mediated responses in mice lacking the Ets protein, Spi-B. *EMBO J.* **16,** 7118–7129 (1997).
10. Taylor, P. R. *et al.* Dectin-2 is predominantly myeloid restricted and exhibits unique activation-dependent expression on maturing inflammatory monocytes elicited *in vivo*. *Eur. J. Immunol.* **35,** 2163–2174 (2005).
11. Taylor, P. R., Brown, G. D., Geldhof, A. B., Martinez-Pomares, L. & Gordon, S. Pattern recognition receptors and differentiation antigens define murine myeloid cell heterogeneity *ex vivo*. *Eur. J. Immunol.* **33,** 2090–2097 (2003).
12. Bratosin, D. *et al.* Cellular and molecular mechanisms of senescent erythrocyte phagocytosis by macrophages. A review. *Biochimie* **80,** 173–195 (1998).
13. Oldenborg, P. A. *et al.* Role of CD47 as a marker of self on red blood cells. *Science* **288,** 2051–2054 (2000).
14. De Domenico, I., McVey, W. D. & Kaplan, J. Regulation of iron acquisition and storage: consequences for iron-linked disorders. *Nature Rev. Mol. Cell Biol.* **9,** 72–81 (2008).
15. Biggs, T. E. *et al.* Nramp1 modulates iron homoeostasis *in vivo* and *in vitro*: evidence for a role in cellular iron release involving de-acidification of intracellular vesicles. *Eur. J. Immunol.* **31,** 2060–2070 (2001).
16. Tolosano, E. *et al.* Enhanced splenomegaly and severe liver inflammation in haptoglobin/hemopexin double-null mice after acute hemolysis. *Blood* **100,** 4201–4208 (2002).
17. Kristiansen, M. *et al.* Identification of the haemoglobin scavenger receptor. *Nature* **409,** 198–201 (2001).
18. Donovan, A. *et al.* The iron exporter ferroportin/Slc40a1 is essential for iron homeostasis. *Cell Metab.* **1,** 191–200 (2005).
19. Gurtner, G. C. *et al.* Targeted disruption of the murine *Vcam1* gene — essential role of Vcam-1 in chorioallantoic fusion and placentation. *Genes Dev.* **9,** 1–14 (1995).
20. Ulyanova, T. *et al.* VCAM-1 expression in adult hematopoietic and nonhernatopoietic cells is controlled by tissue-inductive signals and reflects their developmental origin. *Blood* **106,** 86–94 (2005).
21. Leon, B. *et al.* Dendritic cell differentiation potential of mouse monocytes: monocytes represent immediate precursors of CD8$^-$ and CD8$^+$ splenic dendritic cells. *Blood* **103,** 2668–2676 (2004).
22. Schweitzer, B. L. *et al.* Spi-C has opposing effects to PU.1 on gene expression in progenitor B cells. *J. Immunol.* **177,** 2195–2207 (2006).
23. Carlsson, R., Thorell, K., Liberg, D. & Leanderson, T. SPI-C and STAT6 can cooperate to stimulate IgE germline transcription. *Biochem. Biophys. Res. Commun.* **344,** 1155–1160 (2006).
24. Stoermann, B., Kretschmer, K., Duber, S. & Weiss, S. B-1a cells are imprinted by the microenvironment in spleen and peritoneum. *Eur. J. Immunol.* **37,** 1613–1620 (2007).
25. Hentze, M. W., Muckenthaler, M. U. & Andrews, N. C. Balancing acts: Molecular control of mammalian iron metabolism. *Cell* **117,** 285–297 (2004).
26. Wang, F. D. *et al.* Genetic variation in Mon1a affects protein trafficking and modifies macrophage iron loading in mice. *Nature Genet.* **39,** 1025–1032 (2007).
27. Fleming, R. E. *et al.* Targeted mutagenesis of the murine transferrin receptor-2 gene produces hemochromatosis. *Proc. Natl Acad. Sci. USA* **99,** 10653–10658 (2002).
28. Zhou, X. Y. *et al.* Knockout of the mouse HFE gene products hemochromatosis. *Gastroenterology* **114,** A1372 (1998).
29. Roetto, A. *et al.* Mutant antimicrobial peptide hepcidin is associated with severe juvenile hemochromatosis. *Nature Genet.* **33,** 21–22 (2003).
30. Torrance, J. D. & Bothwell, T. D. in *Methods in Hematology* Vol. 1 (ed. Cook, J. D.) 90–115 (1980).

Supplementary Information is linked to the online version of the paper at www.nature.com/nature.

Acknowledgements This work was supported by the Howard Hughes Medical Institute (K.M.M.), and the Burroughs Wellcome Fund Career Award for Medical Scientists (B.T.E.).

Author Contributions M.K. designed experiments, analysed and interpreted results, and wrote the manuscript; W.I. sorted cells and did retrovirus experiments; B.T.E. contributed gene expression microarray data for mouse tissues; P.R.W. did B cell analysis; K.H. did T cell differentiation analysis; M.A.F. provided *Cd47*$^{-/-}$ mice; T.L.M. did EMSA; and K.M.M. directed the study and wrote the manuscript.

Author Information Reprints and permissions information is available at www.nature.com/reprints. Correspondence and requests for materials should be addressed to K.M.M. (murphy@wustl.edu).

Vol 457|15 January 2009|doi:10.1038/nature07526

LETTERS

The insect nephrocyte is a podocyte-like cell with a filtration slit diaphragm

Helen Weavers[1]*, Silvia Prieto-Sánchez[2]*, Ferdinand Grawe[3], Amparo Garcia-López[4], Ruben Artero[4], Michaela Wilsch-Bräuninger[5], Mar Ruiz-Gómez[2], Helen Skaer[1] & Barry Denholm[1]

The nephron is the basic structural and functional unit of the vertebrate kidney. It is composed of a glomerulus, the site of ultrafiltration, and a renal tubule, along which the filtrate is modified. Although widely regarded as a vertebrate adaptation[1], 'nephron-like' features can be found in the excretory systems of many invertebrates, raising the possibility that components of the vertebrate excretory system were inherited from their invertebrate ancestors[2]. Here we show that the insect nephrocyte has remarkable anatomical, molecular and functional similarity to the glomerular podocyte, a cell in the vertebrate kidney that forms the main size-selective barrier as blood is ultrafiltered to make urine. In particular, both cell types possess a specialized filtration diaphragm, known as the slit diaphragm in podocytes or the nephrocyte diaphragm in nephrocytes. We find that fly (*Drosophila melanogaster*) orthologues of the major constituents of the slit diaphragm, including nephrin, NEPH1 (also known as KIRREL), CD2AP, ZO-1 (TJP1) and podocin, are expressed in the nephrocyte and form a complex of interacting proteins that closely mirrors the vertebrate slit diaphragm complex. Furthermore, we find that the nephrocyte diaphragm is completely lost in flies lacking the orthologues of nephrin or NEPH1—a phenotype resembling loss of the slit diaphragm in the absence of either nephrin (as in human congenital nephrotic syndrome of the Finnish type, NPHS1) or NEPH1. These changes markedly impair filtration function in the nephrocyte. The similarities we describe between invertebrate nephrocytes and vertebrate podocytes provide evidence suggesting that the two cell types are evolutionarily related, and establish the nephrocyte as a simple model in which to study podocyte biology and podocyte-associated diseases.

Filtration of blood in the vertebrate kidney occurs within the glomerulus of the nephron (Fig. 1a, b). The filtration barrier is formed by podocytes—specialized epithelial cells—which send out interdigitating foot processes to enwrap the glomerular capillaries. These processes are separated by 30–50-nm-wide slit pores spanned by the slit diaphragm[3,4], which, together with the glomerular basement membrane, form a size- and charge-selective filtration barrier (Fig. 1b). Disruption to this barrier in disease leads to leakage of blood proteins into the urinary space and to kidney failure[5].

Although invertebrate excretory systems are considered to lack nephrons, 'nephron-like' components, such as filtration cells and ducts in which the filtrate is modified, are widespread (Fig. 1c)[6,7]. Insect nephrocytes regulate haemolymph composition by filtration, followed by endocytosis and processing to sequester and/or secondarily metabolise toxic materials[7–9]. *Drosophila* have two types of nephrocytes: garland and pericardial nephrocytes (Fig. 1e–g). They are tethered to the oesophagus (Figs 1g, 2d and 3g) or heart (Fig. 1f), and are bathed in haemolymph. Extensive infolding of the plasma membrane generates a network of labyrinthine channels or lacunae flanked by nephrocyte foot processes (Fig. 1h). The channel entrances are narrow slits 30 nm in width, spanned by a single or double filament forming a specialized filtration junction—the nephrocyte diaphragm (Figs 1h, i and 3c). Each nephrocyte is enveloped by the basement membrane (Figs 1h and 3c). The nephrocyte diaphragm and basement membrane behave as a size- and charge-selective barrier[7,9] (Fig. 1d) and filtrate is endocytosed from the sides of the lacunae. Thus, the anatomies of the nephrocyte and podocyte filtration barriers are remarkably similar[3].

In view of this similarity, we investigated whether the nephrocyte diaphragm is molecularly related to the slit diaphragm. The major slit diaphragm components, the transmembrane immunoglobulin-domain superfamily proteins nephrin and NEPH1, are co-expressed in the podocyte and interact across the slit pore by homo- and heterotypic binding to form the diaphragm[4,10–16]. Mutations in *NPHS1*, as in human congenital nephrotic syndrome of the Finnish type[10], or in *NEPH1* (ref. 17) cause slit diaphragm loss and foot process effacement, resulting in breakdown of the filtration barrier and proteinuria.

Drosophila has two *NPHS1* orthologues—*sticks and stones* (*sns*) and *hibris* (*hbs*)—and two *NEPH1* orthologues—*dumbfounded* (*duf*, also known as *kirre*) and *roughest* (*rst*; Supplementary Table 1). Because *hbs* and *rst* are expressed in only a subset of nephrocytes (data not shown), we focus on *sns* and *duf*. Sns and Duf are expressed throughout life in both nephrocyte types (Figs 2a–g, adult data not shown), from mid-embryogenesis for garland cells (Supplementary Fig. 1 and Fig. 2a, b) and from the first larval instar for pericardial cells (Fig. 2c). Interestingly, the onset of Sns and Duf expression correlates in time with the appearance of the nephrocyte diaphragm at the ultrastructural level[18,19]. Both proteins localize to the plasma membrane (Fig. 2d–g) and double-labelling reveals precise co-localization (Fig. 2h). This finding is initially surprising because in most contexts Sns and Duf are expressed in complementary patterns and mediate interactions between cells of different types. The only other situation in which the two types of immunoglobulin-domain proteins are co-expressed in the same cell is the vertebrate podocyte[14]. We find that Sns and Duf are dependent on each other for stabilization at the plasma membrane. Loss or knockdown of either protein in embryonic (Fig. 2i–l) or larval (Fig. 2m–p) nephrocytes leads to a loss, severe reduction or mislocalization of the other. These data demonstrate an essential interaction between the two proteins in the same cell, similar to that between nephrin and NEPH1 in the podocyte[13–16]. The precise subcellular location of the proteins was revealed by immuno-electron microscopy. Both Sns and Duf specifically localize to the nephrocyte diaphragm (Fig. 2q–s) and

[1]Department of Zoology, University of Cambridge, Downing Street, Cambridge CB2 3EJ, UK. [2]Centro de Biología Molecular Severo Ochoa, CSIC, UAM, Cantoblanco, 28049 Madrid, Spain. [3]Institut für Genetik, Heinrich-Heine-Universität, Düsseldorf D-40225, Germany. [4]Department of Genetics, University of Valencia, Burjasot, Valencia 46100, Spain. [5]Max Planck Institute of Molecular Cell Biology and Genetics, Dresden D-01307, Germany.
*These authors contributed equally to this work.

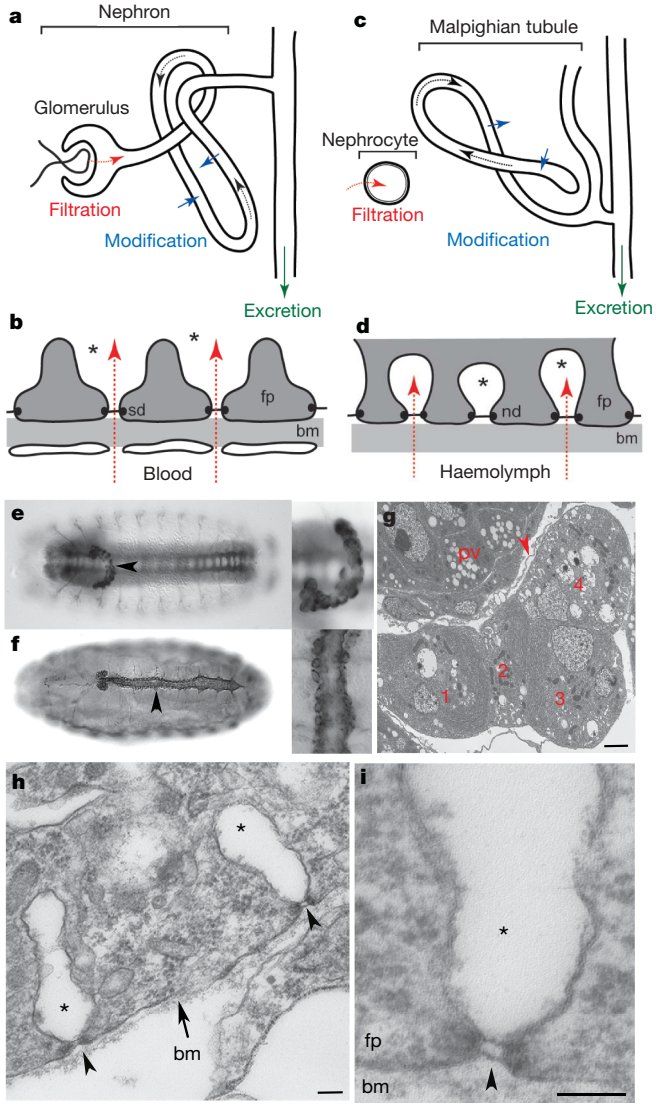

Figure 1 | The glomerular and nephrocyte filtration barriers are anatomically similar. **a**–**d**, Schematic drawings of the vertebrate nephron (**a**), glomerular filtration barrier (**b**), insect excretory system (**c**) and nephrocyte filtration barrier (**d**). Ultrafiltration (red arrow), filtrate flow (black arrow) and urinary space (**b**, asterisk) or extracellular lacunae (**d**, asterisk) are shown. bm, basement membrane; fp, foot process; nd, nephrocyte diaphragm; sd, slit diaphragm. **e**, **f**, *Drosophila* garland (anti-HRP, **e**) and pericardial (anti-pericardin, **f**) nephrocytes. Higher magnification images are shown to the right. **g**–**i**, Transmission electron micrographs of stage-16 embryonic garland nephrocytes. **g**, Four garland nephrocytes surrounding the proventiculus (pv); connective fibres (arrowhead). **h**, **i**, High magnification of the garland nephrocyte cell surface (**h**) and nephrocyte diaphragm (**i**) showing the nephrocyte diaphragm (arrowhead) and extracellular lacunae (asterisk). Scale bars: 2 μm (**g**) and 100 nm (**h**, **i**).

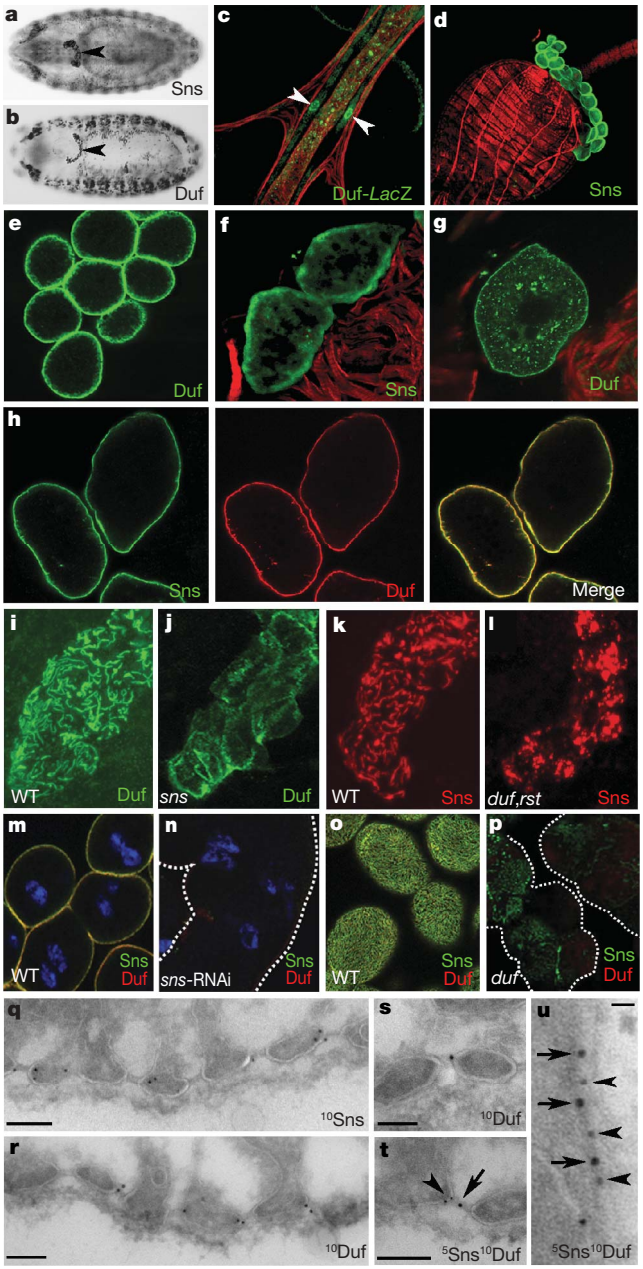

Figure 2 | Sns and Duf are expressed in *Drosophila* nephrocytes. **a**–**h**, Sns (**a**, **d**, **f**, **h**) and Duf (**b**, **c**, **e**, **g**, **h**) expression in garland (**a**, **b**, **d**, **e**) and pericardial (**c**, **f**, **g**, **h**) nephrocytes. Embryonic (**a**, **b**, arrowheads), first instar larva (**c**, green, arrowheads) and third instar larvae (**d**–**h**). The actin cytoskeleton has been counterstained in **c**, **d**, **f** and **g** (red). **h**, Sns (left, green) and Duf (centre, red) co-localize (right, yellow). **i**–**l**, Clusters of ~6–8 wild-type (WT; **i**, **k**), *sns* (**j**) or *duf,rst* (**l**) embryonic garland cells stained with anti-Duf (**i**, **j**) or anti-Sns (**k**, **l**). **m**–**p**, Wild-type (**m**, **o**), *sns*-RNAi (**n**) and *duf* (**p**) third instar garland cells stained for anti-Duf (red), anti-Sns (green; merge appears yellow) and DNA (blue). Single optical section (**m**, **n**) or *z*-projection of cell surface (**o**, **p**) are shown. **q**–**u**, Transmission electron micrographs of wild-type third instar garland cells immunogold-stained for anti-Sns (^{10}Sns, **q**) or anti-Duf (^{10}Duf, **r**, **s**), or that were double labelled (**t**, **u**). For double labelling, 5 nm (arrowhead) and 10 nm (arrow) gold particles are used for Sns and Duf, respectively. Scale bars: 100 nm (**q**–**t**) and 15 nm (**u**).

double-labelling reveals close co-localization between the two proteins (Fig. 2t, u).

Garland and pericardial nephrocytes are correctly specified in *sns* and *duf* mutants (Supplementary Fig. 2a–k). However, given the importance of the immunoglobulin-domain proteins in slit diaphragm formation, we examined the ultrastructure of the diaphragm in *sns* and *duf* mutants. In wild-type garland cells, nephrocyte diaphragms and associated lacunae appear during mid-embryogenesis (Supplementary Fig. 2l), progressively increasing in number (Fig. 1h). Diaphragms densely populate the cell periphery in third instar larvae (Fig. 3c). Notably, *sns* or *duf* mutant garland cells completely lack nephrocyte diaphragms at every stage, and lacunae are rarely detected (compare Fig. 3a, b with Fig. 1i, Fig. 3c with Fig. 3d, and Supplementary Fig. 2m, n with Supplementary Fig. 2l). Occasional infoldings do form, but are never bridged by diaphragms (Fig. 3b and Supplementary Fig. 2n). Instead, the nephrocyte surface contains frequent, small patches of electron-dense subcortical material (Fig. 3a,

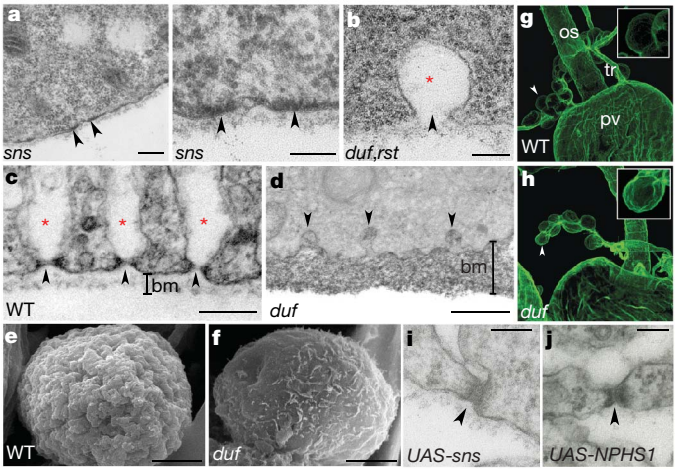

Figure 3 | Sns and Duf are required for nephrocyte diaphragm formation and normal morphology. **a**, **b**, *sns* (**a**) and *duf,rst* (**b**) embryonic garland cells lack diaphragms and lacunae. The right image of **a** is a higher magnification image of the left image, showing electron-dense subcortical material (arrowheads). Small lacunae (red asterisk) lacking diaphragms are occasionally found (**b**, arrowhead). **c**, **d**, Wild-type (WT, **c**) and *duf* (**d**) third instar garland cells. **c**, Diaphragms (arrowheads) and lacunae (red asterisks) densely populate the nephrocyte surface. **d**, *duf* nephrocytes have small lacunae (arrowheads) lacking diaphragms and a substantially thickened basement membrane (bm). **e**, **f**, Scanning electron micrographs of wild-type (**e**) and *duf* (**f**) third instar garland nephrocytes stripped of basement membrane by collagenase treatment. *duf* nephrocytes lack the furrows corresponding to diaphragm rows. **g**, **h**, Wild-type (**g**) and *duf* (**h**) Viking–GFP (collagen IV) third instar garland cells, stained with anti-GFP (green), showing greater Viking deposition around *duf* nephrocytes (arrowheads and inset). Garland cell number is also reduced in *duf* larvae, suggesting that mutant cells ultimately die. os, oesophagus; pv, proventriculus; tr, trachea. **i**, **j**, Diaphragm and foot process morphology are abnormal (arrowheads) in *sns* (**i**) and human *NPHS1* (**j**) embryonic overexpression. Scale bars: 200 nm (**a** (left), **c**, **d**), 100 nm (**a** (right), **b**), 50 nm (**i**, **j**) and 5 μm (**e**, **f**).

right)—possible remnants of undercoat normally associated with the wild-type diaphragm. These observations indicate that in the absence of the diaphragm, foot processes are unstable and undergo effacement. Scanning electron microscopy reveals the surface smoothing in mutant garland cells (compare Fig. 3e with Fig. 3f). These phenotypes are notably similar to those of podocytes lacking nephrin or NEPH1 (refs 5, 17). Thus, by analogy with nephrin and NEPH1 in the slit diaphragm, we suggest that Sns and Duf interact through their extracellular domains to form the nephrocyte diaphragm itself.

We noted that the basement membrane in *sns* knockdown and *duf* larval nephrocytes was irregular and markedly expanded (compare Fig. 3c to Fig. 3d). The basement membrane in *duf* nephrocytes has an average depth of 202 nm (±24 (s.e.m.), $n = 13$), compared with 57 nm (±4, $n = 11$) for the wild type. This results from an increase in deposition of the *Drosophila* collagen IV (Viking; Fig. 3g, h and Supplementary Fig. 3). However, this is unlikely to account for the fourfold thickening observed, and we suggest that a further contributing factor is accumulation of haemolymph proteins that clog the basement membrane owing to inefficient filtration.

Given the similarities between the morphology and molecular requirements for podocyte and nephrocyte diaphragms, we tested the ability of human *NPHS1* to rescue the *sns* mutant phenotype. However nephrocytes are sensitive to absolute levels of Sns, so even moderate overexpression produced abnormal phenotypes. We therefore compared the effects of overexpressing *Drosophila sns* with those of overexpressing human *NPHS1*. The resulting phenotypes are notably similar, including abnormal nephrocyte foot process morphology and marked thickening of diaphragm filaments (Fig. 3i, j). These data indicate that precise levels of Sns are critical for diaphragm formation and, more importantly, that human nephrin and *Drosophila* Sns function in equivalent ways.

Vertebrate nephrin and NEPH1 form a multi-protein complex at the slit diaphragm with zonula occludens-1 (ZO-1)[20], CD2-associated protein (CD2AP)[21,22] and podocin[23] (Supplementary Table 1). Mutations in these genes result in kidney disease[21,23,24]. We asked whether the fly orthologues (Supplementary Table 1) contribute to the nephrocyte diaphragm. *In situ* hybridization reveals that *pyd* (the orthologue of ZO-1), *CG31012* (CD2AP) and *Mec2* (*NPHS2*/podocin, Supplementary Fig. 4) are expressed in nephrocytes (Fig. 4a–f). Furthermore, Pyd–GFP (green fluorescent protein) precisely co-localizes with Duf to the membrane (Fig. 4g), mirroring co-localization of ZO-1 and NEPH1 in the podocyte[20].

Molecular interactions between these vertebrate slit-diaphragm-associated proteins have been established (Fig. 4h, black arrows)[11,20,22,25]. To test whether fly orthologues form a similar complex, we performed a yeast two-hybrid analysis with Sns and Duf intracellular domains (Fig. 4i). Sns interacts with Mec-2 (podocin) and Duf interacts with Pyd (ZO-1) (Fig. 4j). An interaction between Duf and Pyd was independently confirmed by co-immunoprecipitation (Fig. 4k). A previous report established direct association between Sns and Duf[26]. These interactions between the fly proteins (Fig. 4h, red arrows) closely resemble those described for slit-diaphragm-associated proteins (Fig. 4h, black arrows). These data, taken together with those described above, provide strong evidence that the nephrocyte diaphragm (Fig. 4l) and slit diaphragm are molecularly homologous structures.

Insect nephrocytes are size- and charge-selective in their sequestration of materials from the haemolymph. Selectivity is based on the characteristics of the diaphragm and basement membrane, which act together as a filtration barrier[7,9]. To test the filtration capacity of the *Drosophila* nephrocyte diaphragm, we assayed the passage of fluorescently labelled dextrans of different sizes. If the nephrocyte diaphragm acts as a size-selective filter, we reasoned that, like the vertebrate slit diaphragm[27], it would allow free passage of small (molecular mass of 10,000 Da) but exclude large (molecular mass of 500,000 Da) dextrans (Fig. 5b). In agreement with our expectations, uptake of the 500,000 Da dextran in wild-type nephrocytes is significantly lower than that of the 10,000 Da dextran (1:3.6, $n = 20$; Fig. 5a, f). These data strongly suggest that the nephrocyte diaphragm functions as a size-based filtration diaphragm (endocytosis from foot process tips could account for low levels of large dextran uptake, Fig. 5b). We anticipated higher uptake of the large dextran in immunoglobulin-domain mutant nephrocytes because they lack diaphragms. However, although the level of uptake of the small dextran in *duf* or *sns* nephrocytes is unaltered compared to wild type, we found a marked reduction in large dextran uptake (Fig. 5c, d, f); the large-to-small ratio is 1:22.5 ($n = 20$) for *duf* and 1:15.3 ($n = 19$) for *sns*. Instead, the large dextran appears as a halo surrounding the cell (Fig. 5c, d). The thickening of basement membrane observed in *duf* nephrocytes (Fig. 3d) could explain the exclusion of the large dextran (Fig. 5e). This highlights a further parallel between nephrocytes and podocytes. An endocytosis-based clearance mechanism in podocytes prevents clogging of the glomerular basement membrane with blood plasma proteins; the slit-diaphragm-associated protein CD2AP has been implicated in this process[24,28]. We suggest that an equivalent clearance mechanism exists in nephrocytes, and that this mechanism requires Sns and Duf.

Whatever the causes of reduction in filtration capability, the animal's haemolymph physiology will be disturbed. We tested this hypothesis by feeding larvae silver nitrate, a toxin endocytosed and concentrated in nephrocytes (Fig. 5h). At low concentrations of silver nitrate, viability of control larvae is not compromised (82% eclose as adults, Fig. 5i), but *duf* larvae show a greatly reduced viability (26% eclose, Fig. 5i). A previous study showed a requirement for nephrocytes in the face of toxic stress[29]. Our data show that immunoglobulin-domain proteins are essential for this function.

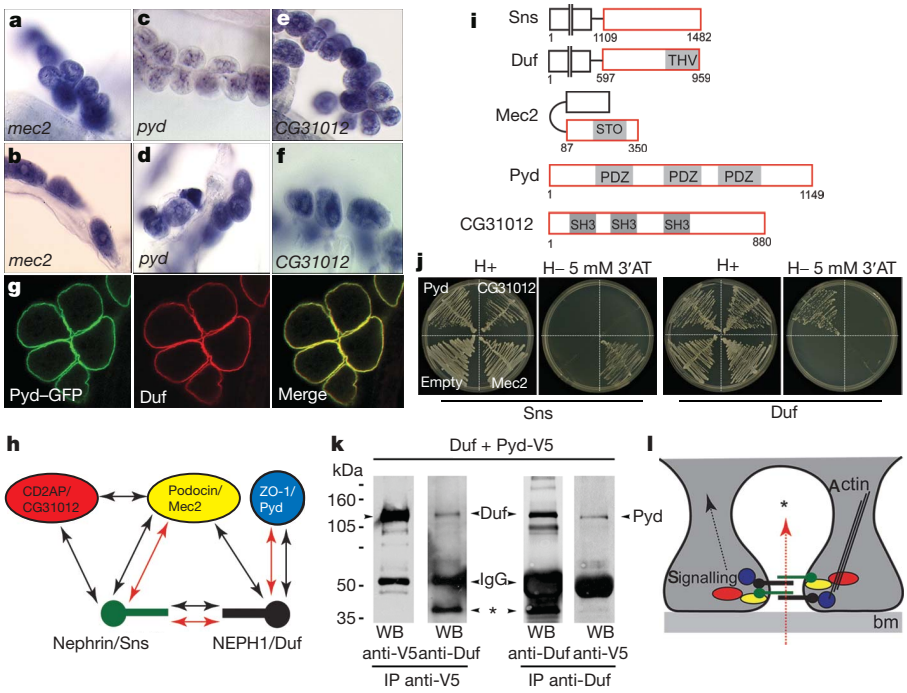

Figure 4 | Analysis of slit-diaphragm-associated protein orthologues in the fly nephrocyte. **a**–**f**, Third instar garland (**a**, **c**, **e**) and pericardial (**b**, **d**, **f**) nephrocytes hybridized with probes directed against *Mec2* (**a**, **b**), *pyd* (**c**, **d**) and *CG31012* (**e**, **f**). **g**, Pyd (left, green) and Duf (centre, red) co-localize (right, yellow) in third instar garland nephrocytes. **h**, Schematic of the main components of the podocyte slit diaphragm (black arrows) and nephrocyte diaphragm (described here and elsewhere, red arrows). **i**, Schematic of *Drosophila* orthologues of slit-diaphragm-associated proteins: PDZ-binding domain (THV), PDZ domain (PDZ), stomatin domain (STO) and SH3 domain (SH3). The region of the protein used in the yeast two-hybrid analysis is outlined in red. **j**, Yeast two-hybrid analysis of Sns or Duf with Pyd, CG31012, Mec2 and negative control (empty vector). Direct protein interaction is indicated by growth of yeast on selective media (H− 5 mM 3′AT). **k**, Duf and Pyd-V5 co-immunoprecipitate with each other from *Drosophila* cells (the unlabelled arrowhead on the left corresponds to Pyd; the asterisk indicates cleaved form of Duf that is also co-immunoprecipitated with Pyd). **l**, Schematic of molecular interactions at the nephrocyte diaphragm; Sns (green), Duf (black), Mec2 (yellow), Pyd (blue), CG31012 (red), direction of filtration (red arrow), extracellular lacuna (asterisk). Putative links to signalling or the actin cytoskeleton based on analogy with the equivalent complex at the slit diaphragm are shown. bm, basement membrane.

We have highlighted similarities between podocytes and nephrocytes; however, podocytes are an integral part of the nephron (Fig. 1a) whereas the nephrocyte is spatially separated from its renal (Malpighian) tubule (Fig. 1c). Such differences have contributed to the traditional view that vertebrate and invertebrate excretory systems are unrelated[1]. Nevertheless, nephron-like features are present

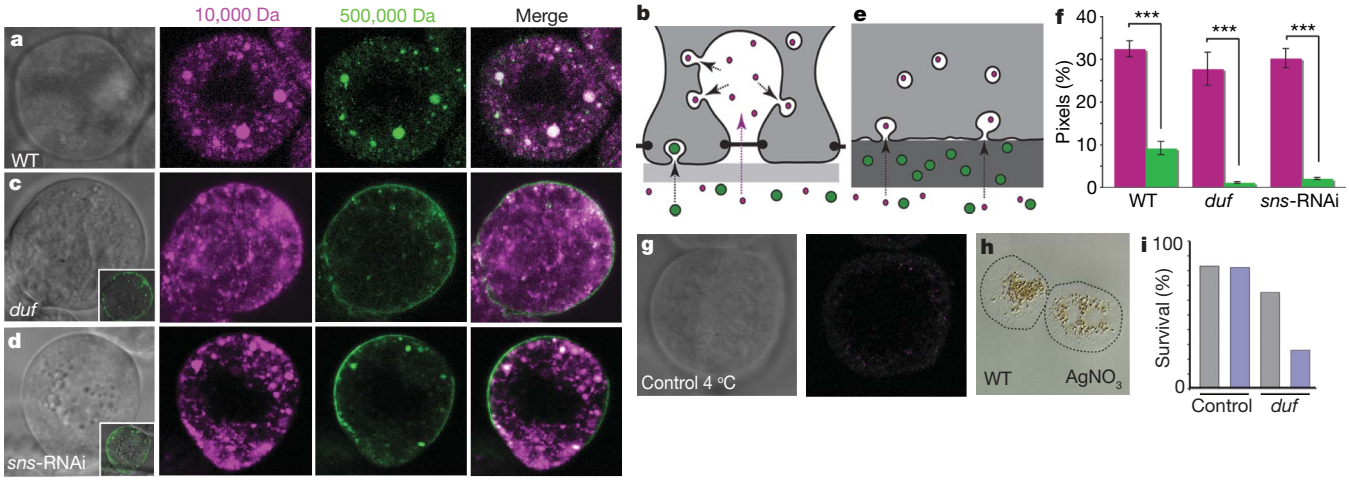

Figure 5 | Sns and Duf are required for nephrocyte filtration. **a**, **c**, **d**, Third instar garland nephrocytes from wild-type (WT, **a**), *duf* (**c**) and *sns*-RNAi knockdown (**d**) animals co-incubated with 10,000 Da (magenta) and 500,000 Da (green) fluorescently labelled dextran. Inset in **c** and **d** shows a merged image of transmitted light and 500,000 Da channels. **b**, **e**, Schematic drawing of filtration and endocytosis in wild-type (**b**) and *sns* or *duf* mutant (**e**) nephrocytes. **f**, Quantification of small (magenta) and large (green) dextran uptake in wild-type, *duf* and *sns*-RNAi knockdown garland cells. The percentage pixel number exceeding the threshold per unit area is shown on the *y*-axis (error bars, s.e.m.). Triple-asterisks indicate significance of $P < 0.001$. Please note, the molar ratio of dye to dextran is 1:1 (for 10,000 Da) and 64:1 (for 500,000 Da). **g**, A control nephrocyte incubated with fluorescent dextran at 4 °C showing no uptake (right image). **h**, Ten-micrometre section of garland nephrocytes from a wild-type larva fed with $AgNO_3$ (brown granular staining). **i**, The percentage of eclosing sibling control or *duf* adults fed yeast paste (grey) or yeast paste with $AgNO_3$ (blue; $n = 65$, 68, 55 and 57).

in the excretory systems of a wide variety of invertebrates and in the protochordate *Amphioxus*, suggesting a common origin[2]. The molecular parallels between nephrocytes and podocytes described here support this hypothesis, and it will be of interest to determine whether nephrin- and NEPH1-like protein complexes are found in other invertebrate filtration diaphragms.

Defects in the slit diaphragm complex underlie human diseases for which the unifying feature is proteinurea and kidney failure. These symptoms result from defective filtration, but in addition the nephrin–NEPH1 complex regulates podocyte behaviours such as cell survival, polarity, actin dynamics and endocytosis[30]. How these functions of the slit diaphragm relate to disease pathologies is currently unclear. The fly nephrocyte also depends on the activity of a nephrin–NEPH1 complex for survival, shape and selective endocytosis, and thus provides a simple and genetically tractable model in which the multiple roles of the slit diaphragm complex can be addressed.

METHODS SUMMARY

Fly strains. Flies were reared on standard food at room temperature (~22 °C), 18 °C or 25 °C. The strains used are listed in the Methods.

Nephrocyte filtration assay. Garland cells were dissected, incubated with AlexaFluor568-dextran (10,000 Da) and fluorescein-dextran (500,000 Da; Molecular Probes) at a concentration of 0.33 mg ml^{-1} at 25 °C for 5 min, washed on ice, fixed and mounted. Dextran uptake was quantified by counting the pixel number exceeding the background threshold per unit area using Volocity software.

Toxin stress assay. First instar larvae of the appropriate genotype were transferred to agar-only plates supplemented with yeast paste or with yeast paste containing $AgNO_3$ (2 g yeast in 3.5 ml of 0.003% $AgNO_3$), and allowed to develop at 25 °C. The percentage of eclosing adults was scored.

Antibodies. Antibodies used were: anti-Sns (1:200, from S. Abmayr), anti-Kirre (1:200, K. Fischbach), anti-Duf extracellular (1:50, M.R.-G.), anti-Duf intracellular (1:500, M.R.-G.), anti-βgal (1:1,000, ICN Biomedicals), anti-HRP (1:200, Jackson ImmunoResearch), anti-pericardin (1:2, DSHB) and anti-GFP (1:500, Invitrogen Molecular Probes).

Confocal and electron microscopy. Confocal and electron microscopy were carried out using standard techniques. For immuno-electron microscopy, dissected larval garland cells were fixed in 4% formaldehyde plus 0.05% glutaraldehyde, embedded in gelatin, cryosectioned, and incubated with anti-Duf extracellular (1:5), anti-Kirre (1:20) or anti-Sns (1:20) followed by 10 nm (for single stains) or both 5 nm and 10 nm (for double stains) gold-conjugated secondary antibody.

Yeast two-hybrid analysis. The intracellular domains of Sns and Duf were tested for interaction with Pyd (isoform f), CD2AP (SD08724) and the C-terminal cytoplasmic domain of Mec2 using the Clontech Matchmaker GAL4 two-hybrid system. Interaction was indicated by growth in the absence of histidine. 5 mM 3-amino-1,2,4-triazole (3′AT, Sigma) was included to titrate residual autoactivation from the bait fusion proteins.

Co-immunoprecipitation experiments. *Drosophila* S2 cells transiently co-transfected with pMK33/pMtHy-duf and pAC5.1V5-His-pyd were induced for 20 h with 0.7 mM $CuSO_4$. Total cell lysate was split and each half immunoprecipitated with either anti-V5 or anti-Duf intracellular antibodies and probed with anti-Duf intracellular antibodies and anti-V5 following standard protocols.

Full Methods and any associated references are available in the online version of the paper at www.nature.com/nature.

Received 4 August; accepted 8 October 2008.
Published online 29 October 2008.

1. Smith, H. W. *From Fish to Philosopher* (Little, Brown, 1953).
2. Ruppert, E. E. Evolutionary origin of the vertebrate nephron. *Am. Zool.* **34,** 542–533 (1994).
3. Rodewald, R. & Karnovsky, M. J. Porous substructure of the glomerular slit diaphragm in the rat and mouse. *J. Cell Biol.* **60,** 423–433 (1974).
4. Wartiovaara, J. *et al.* Nephrin strands contribute to a porous slit diaphragm scaffold as revealed by electron tomography. *J. Clin. Invest.* **114,** 1475–1483 (2004).
5. Patrakka, J. *et al.* Congenital nephrotic syndrome (NPHS1): features resulting from different mutations in Finnish patients. *Kidney Int.* **58,** 972–980 (2000).
6. Berridge, M. J. & Oschman, J. L. *Transporting Epithelia* 11–15 (Academic, 1972).
7. Crossley, A. C. in *Comprehensive Insect Physiology, Biochemistry and Pharmacology* (eds Kerkut, G. A. & Gilbert, L. I.) 487–515 (Pergamon, 1985).
8. Kowalevsky, A. Ein Beitrag zur Kenntnis der Excretions-organe. *Biol. Centralbl.* **9,** 74–79 (1889).
9. Locke, M. & Russell, V. W. in *Microscopic Anatomy of Invertebrates* (eds Harrison, F. W. & Locke, M.) 687–709 (Wiley, 1998).
10. Kestila, M. *et al.* Positionally cloned gene for a novel glomerular protein—nephrin—is mutated in congenital nephrotic syndrome. *Mol. Cell* **1,** 575–582 (1998).
11. Sellin, L. *et al.* NEPH1 defines a novel family of podocin interacting proteins. *FASEB J.* **17,** 115–117 (2003).
12. Ruotsalainen, V. *et al.* Nephrin is specifically located at the slit diaphragm of glomerular podocytes. *Proc. Natl Acad. Sci. USA* **96,** 7962–7967 (1999).
13. Gerke, P., Huber, T. B., Sellin, L., Benzing, T. & Walz, G. Homodimerization and heterodimerization of the glomerular podocyte proteins nephrin and NEPH1. *J. Am. Soc. Nephrol.* **14,** 918–926 (2003).
14. Barletta, G. M., Kovari, I. A., Verma, R. K., Kerjaschki, D. & Holzman, L. B. Nephrin and Neph1 co-localize at the podocyte foot process intercellular junction and form *cis* hetero-oligomers. *J. Biol. Chem.* **278,** 19266–19271 (2003).
15. Khoshnoodi, J. *et al.* Nephrin promotes cell–cell adhesion through homophilic interactions. *Am. J. Pathol.* **163,** 2337–2346 (2003).
16. Liu, G. *et al.* Neph1 and nephrin interaction in the slit diaphragm is an important determinant of glomerular permeability. *J. Clin. Invest.* **112,** 209–221 (2003).
17. Donoviel, D. B. *et al.* Proteinuria and perinatal lethality in mice lacking NEPH1, a novel protein with homology to NEPHRIN. *Mol. Cell. Biol.* **21,** 4829–4836 (2001).
18. Tepass, U. & Hartenstein, V. The development of cellular junctions in the *Drosophila* embryo. *Dev. Biol.* **161,** 563–596 (1994).
19. Rugendorff, A., Younossi-Hartenstein, A. & Hartenstein, V. Embryonic origin and differentiation of the *Drosophila* heart. *Rouxs Arch. Dev. Biol.* **203,** 266–280 (1994).
20. Huber, T. B. *et al.* The carboxyl terminus of Neph family members binds to the PDZ domain protein zonula occludens-1. *J. Biol. Chem.* **278,** 13417–13421 (2003).
21. Shih, N. Y. *et al.* Congenital nephrotic syndrome in mice lacking CD2-associated protein. *Science* **286,** 312–315 (1999).
22. Shih, N. Y. *et al.* CD2AP localizes to the slit diaphragm and binds to nephrin via a novel C-terminal domain. *Am. J. Pathol.* **159,** 2303–2308 (2001).
23. Boute, N. *et al.* NPHS2, encoding the glomerular protein podocin, is mutated in autosomal recessive steroid-resistant nephrotic syndrome. *Nature Genet.* **24,** 349–354 (2000).
24. Kim, J. M. *et al.* CD2-associated protein haploinsufficiency is linked to glomerular disease susceptibility. *Science* **300,** 1298–1300 (2003).
25. Schwarz, K. *et al.* Podocin, a raft-associated component of the glomerular slit diaphragm, interacts with CD2AP and nephrin. *J. Clin. Invest.* **108,** 1621–1629 (2001).
26. Galletta, B. J., Chakravarti, M., Banerjee, R. & Abmayr, S. M. SNS: Adhesive properties, localization requirements and ectodomain dependence in S2 cells and embryonic myoblasts. *Mech. Dev.* **121,** 1455–1468 (2004).
27. Kramer-Zucker, A. G., Wiessner, S., Jensen, A. M. & Drummond, I. A. Organization of the pronephric filtration apparatus in zebrafish requires Nephrin, Podocin and the FERM domain protein Mosaic eyes. *Dev. Biol.* **285,** 316–329 (2005).
28. Akilesh, S. *et al.* Podocytes use FcRn to clear IgG from the glomerular basement membrane. *Proc. Natl Acad. Sci. USA* **105,** 967–972 (2008).
29. Das, D., Aradhya, R., Ashoka, D. & Inamdar, M. Post-embryonic pericardial cells of *Drosophila* are required for overcoming toxic stress but not for cardiac function or adult development. *Cell Tissue Res.* **331,** 565–570 (2008).
30. Huber, T. B. & Benzing, T. The slit diaphragm: a signaling platform to regulate podocyte function. *Curr. Opin. Nephrol. Hypertens.* **14,** 211–216 (2005).

Supplementary Information is linked to the online version of the paper at www.nature.com/nature.

Acknowledgements We thank F. Evers, Z. Cseresnyes, M. Guerra and E. Salvador for technical assistance, and S. Abmayr, L. Cooley, C. Doe, M. Affolter, K. Fischbach and K. Tryggvason for reagents. We thank V. Hartenstein, M. Inamdar, A. Woolf, I. Miguel-Aliaga, F. Evers, M. Landgraf and members of the Skaer laboratory for discussions, and E. Knust and W. B. Huttner for their support. This work was supported by Wellcome Trust grants awarded to H.S. (072441 and 079221; H.W., B.D. and H.S.); Deutsche Forschungsgemeinschaft SFB 590 awarded to E. Knust (F.G.) and ARC 1242 (H.W., B.D., H.S. and F.G.); an MEC grant awarded to M.R.-G. (BFU2007-62201; S.P.-S. and M.R.-G.); a Fundación Ramón Areces grant to the CBMSO (M.R.-G.); EC grant LSHG-CT-2004-511978 to MYORES (M.R.-G.); and an FPU fellowship from the MEC awarded to A.G.-L.

Author Contributions B.D., H.S. and M.R.-G. designed and directed the project. B.D., H.W., M.R.-G. and S.P.-S. performed the experiments. F.G. and M.W.-B. provided technical assistance. A.G.-L. and R.A. provided materials. B.D. and H.S. wrote the paper. All authors discussed results and commented on the manuscript.

Author Information Reprints and permissions information is available at www.nature.com/reprints. Correspondence and requests for materials should be addressed to H.S. (hs17@cam.ac.uk).

METHODS

Fly strains. The following fly genotypes were used: OregonR (wild-type strain); sns^{XB3} and *UAS-sns* (gift from S. Abmayr); $Df(1)w^{67k30}$ hemizygotes for embryonic analysis of *duf*; $Df(1)w^{67k30}/Df(1)N^{5419}$ transheterozygotes or $Df(1)duf^{ps\text{-}1}$ (small deficiency removing the *duf* locus only, a description of this allele will be published elsewhere, S.P.-S. *et al.*, in preparation) for larval analysis of *duf*; *rP298* (*duf-LacZ*); *UAS-Pyd-GFP* (gift from M. Affolter); *Viking-GFP* (gift from L. Cooley); *UAS-sns-RNAi* (a 1,047 bp fragment was obtained by PCR from *sns* complementary DNA using primers 5′-CCAGTTCGTATAATGACACCG-3′ and 5′-CCTACAGCTATACGAGGTGTC-3′ and used to make intron-spliced hairpin RNA according to ref. 31); *UAS-NPHS1* (human *NPHS1* cDNA, gift from K. Tryggvason, cloned into pUAST); *G447.2-GAL4* (embryonic garland cell driver; gift from R. Reuter); and *Prospero-Gal4* (larval garland cell driver; gift from C. Doe). Fly crosses were maintained at 25 °C except for the overexpression experiment in which animals were maintained at 29 °C to ensure maximum transgene expression. Marked balancer chromosomes (Krüppel–Gal4, UAS–GFP) and/or PCR genotyping[32] from carcasses remaining after dissection were used to identify appropriate genotypes.

Nephrocyte filtration assay. Garland nephrocytes (including a small portion of oesophagus and the proventriculus) were dissected from third instar larvae in Shields and Sang medium (Sigma), and were then transferred to media containing AlexaFluor568-dextran (10,000 Da) and fluorescein-dextran (500,000 Da; Molecular Probes) at a concentration of 0.33 mg ml^{-1}, and incubated at 25 °C for 5 min. The cells were washed on ice for 10 min in cold PBS, fixed in 4% formaldehyde for 10 min at room temperature (~22 °C), rinsed once in PBS and then mounted in vectashield (Vector labs). All post-dissection procedures were carried out in the dark. A single confocal section of the cell midpoint was taken using a Leica SP1 confocal microscope, and dextran uptake was quantified by counting the pixel number exceeding the background threshold per unit area using Volocity software. The average fluorescence from the proventriculus epithelium (where dextran uptake does not occur) was used to set the background threshold. The same threshold was used for all experiments. Control cells incubated with dextran on ice showed no uptake. Results were analysed statistically using the Shapiro–Wilk normality test followed by the paired *t*-test or Kruskal–Wallis Rank Sum test as appropriate.

Toxin stress assay. Flies of the appropriate genotype were allowed to lay on standard apple juice plates supplemented with yeast. After approximately 24 h, freshly emerging first instar larvae from this plate were transferred to agar-only plates supplemented with yeast paste or with yeast paste containing $AgNO_3$ (2 g yeast in 3.5 ml of 0.003% $AgNO_3$), and allowed to develop at 25 °C. The percentage of eclosing adults was scored.

***In situ* hybridization and immunohistochemistry.** Whole-mount *in situ* hybridization and immunohistochemistry to embryos and third instar nephrocytes were carried out using standard techniques. Antibodies used were: anti-Sns (1:200, gift from S. Abmayr), anti-Kirre (1:200, gift from K. Fischbach), anti-Duf extracellular (1:50), anti-Duf intracellular (1:500, the generation of both antisera will be published elsewhere), anti-βgal (1:1,000, ICN Biomedicals), anti-HRP (1:200, Jackson ImmunoResearch), anti-pericardin (1:2, DSHB), anti-GFP (1:500, Invitrogen Molecular Probes), AlexaFluor 488 phalloidin and AlexaFluor 568 phalloidin (1:20, Invitrogen Molecular Probes), and TOTO3 and TO-PRO-3 (1:100, Invitrogen Molecular Probes).

Confocal and electron microscopy. Confocal microscopy, transmission electron microscopy and scanning electron microscopy were carried out using standard techniques. For immuno-electron microscopy, dissected garland cells were fixed in 4% formaldehyde plus 0.05% glutaraldehyde, embedded in gelatin, and cryosectioned and incubated with anti-Duf extracellular (1:5), anti-Kirre (1:20), or anti-Sns (1:20) followed by 10 nm (for single stains) or both 5 nm and 10 nm (for double stains) gold-conjugated secondary antibody. In some cases, confocal images correspond to *z*-projections from a series of confocal sections.

Collagenase treatment. Third instar garland cells were incubated in 0.1% collagenase type I in PBS for 3 min at 37 °C.

Yeast two-hybrid assays. The intracellular domains of Sns and Duf were used as bait (cloned into pGBKT7, Clontech) and tested for interaction with Pyd (isoform f), CD2AP (SD08724), and C-terminal cytoplasmic domain of Mec2 (all cloned into pGADT7, Clontech). Interaction was indicated by growth in absence of histidine. 5 mM 3′AT (Sigma) was included to titrate residual auto-activation from the bait fusion proteins.

Co-immunoprecipitation experiments. *Drosophila* S2 cells transiently co-transfected with pMK33/pMtHy-duf and pAC5.1V5-His-pyd were induced for 20 h with 0.7 mM $CuSO_4$. Total cell lysate was split and each half immunoprecipitated with either anti-V5 or anti-Duf, and probed consecutively with anti-Duf and anti-V5 or anti-V5 and anti-Duf, respectively, following standard protocols.

31. Nagel, A. C., Maier, D. & Preiss, A. Green fluorescent protein as a convenient and versatile marker for studies on functional genomics in *Drosophila*. *Dev. Genes Evol.* **212**, 93–98 (2002).
32. Strunkelnberg, M. *et al. rst* and its paralogue *kirre* act redundantly during embryonic muscle development in *Drosophila*. *Development* **128**, 4229–4239 (2001).

LETTERS

Altered circadian rhythms regulate growth vigour in hybrids and allopolyploids

Zhongfu Ni[1]*†, Eun-Deok Kim[1]*, Misook Ha[1,2,3], Erika Lackey[1], Jianxin Liu[1], Yirong Zhang[1]†, Qixin Sun[5] & Z. Jeffrey Chen[1,2,3,4]

Segregating hybrids and stable allopolyploids display morphological vigour[1–3], and *Arabidopsis* allotetraploids are larger than the parents *Arabidopsis thaliana* and *Arabidopsis arenosa*[1,4]—the mechanisms for this are unknown. Circadian clocks mediate metabolic pathways and increase fitness in animals and plants[5–8]. Here we report that epigenetic modifications of the circadian clock genes *CIRCADIAN CLOCK ASSOCIATED 1* (*CCA1*) and *LATE ELONGATED HYPOCOTYL* (*LHY*)[9–11] and their reciprocal regulators *TIMING OF CAB EXPRESSION 1* (*TOC1*) and *GIGANTEA* (*GI*)[10,12,13] mediate expression changes in downstream genes and pathways. During the day, epigenetic repression of *CCA1* and *LHY* induced the expression of *TOC1*, *GI* and downstream genes containing evening elements[14] in chlorophyll and starch metabolic pathways in allotetraploids and F_1 hybrids, which produced more chlorophyll and starch than the parents in the same environment. Mutations in *cca1* and *cca1 lhy* and the daily repression of *cca1* by RNA interference (RNAi) in *TOC1::cca1*(*RNAi*) transgenic plants increased the expression of downstream genes and increased chlorophyll and starch content, whereas constitutively expressing *CCA1* or ectopically expressing *TOC1::CCA1* had the opposite effect. The causal effects of CCA1 on output traits suggest that hybrids and allopolyploids gain advantages from the control of circadian-mediated physiological and metabolic pathways, leading to growth vigour and increased biomass.

Polyploidy (whole genome duplication) is an evolutionary innovation in many plants and some animals. Several important crops such as wheat, cotton and canola are of allopolyploidy that contains two or more divergent genomes[15,16], and some plants and animals exist as interspecific hybrids[17]. The common occurrence of polyploids suggests an evolutionary advantage in having additional genetic materials for growth and adaptation. Moreover, heterozygosity and new genomic interactions in allopolyploids induce phenotypic variation and growth vigour[16].

In stable allotetraploids that were resynthesized by interspecific hybridization between *A. thaliana* and *A. arenosa* (Supplementary Fig. 1)[4], over 1,400 genes (>5% and up to 9,800 genes or ~38%) were non-additively expressed[1]. Non-additive expression indicates that the expression level of a gene in an allotetraploid is not equal to the sum of two parental loci ($1 + 1 \neq 2$), leading to activation (>2), repression (<2), dominance or overdominance[16]. Many genes involved in energy and metabolism including photosynthesis and starch pathways are upregulated[1], coinciding with growth vigour in the allotetraploids. This morphological vigour is commonly observed[18], and phenotypic variations among allotetraploids are related to genetic and epigenetic mechanisms[16].

Among 128 genes upregulated in the allotetraploids, 86 genes (~67%) each contains at least one CCA1 binding site (CBS; AAAAATCT) or evening element (AAAATATCT)[14] within the ~1,000-base pair (bp) upstream region (Supplementary Table 1), which is significantly higher than all genes containing a putative evening element and CBS (~47%, $\chi^2 = 19.56$, $P \leq 9.7 \times 10^{-6}$). These evening-element- and CBS-containing genes are probably the targets of CCA1 and LHY[9,11,19].

CCA1 and LHY are MYB-domain transcription factors and have partially redundant but incompletely overlapping functions[9,10]. They negatively regulate *TOC1* and *GI* expression, whereas TOC1 and GI positively regulate *CCA1* and *LHY* expression[10,12,13]. This circular feedback regulation affects central oscillation as well as input and output pathways that maintain the rhythms, amplitude and/or phase of circadian clock in *Arabidopsis*[20]. Disrupting oscillator control alters the expression of ~10% of *Arabidopsis* genes[14], whereas maintaining circadian clock regulation increases CO_2 fixation, growth and fitness[5,8].

We found that *CCA1* and *LHY* were repressed and *TOC1* and *GI* were upregulated at noon in the allotetraploids[1]. As in the parents, both *CCA1* and *LHY* showed diurnal expression patterns in the allotetraploids (Fig. 1a, Supplementary Fig. 2a and Supplementary Table 2). Their expression peaked at dawn (Zeitgeber time 0, ZT0), decreased 6 h after dawn (ZT6), and continued declining until dusk (ZT15). Notably, *CCA1* and *LHY* were expressed 2–4-fold lower in the allotetraploids than the mid-parent value (MPV) at ZT6–12 and higher than the MPV at dusk (ZT15). *TOC1* and *GI* expression was inversely correlated with *CCA1* and *LHY* expression (Fig. 1b and Supplementary Fig. 2b), suggesting feedback regulation in the allotetraploids as in the diploids[10,12,13]. However, *TOC1* and *GI* expression fluctuated in the allotetraploids, indicating that other factors may be involved[20]. The expression changes of these genes from noon to dusk in the allotetraploids may alter the amplitude but not the phase of circadian clock, as they quickly gained the expression levels similar to the MPV after dusk (ZT18–24).

To determine how *CCA1* and *LHY* expression was repressed, we examined the expression patterns of *A. thaliana* and *A. arenosa* loci in the allotetraploids using polymerase chain reaction with reverse transcription (RT–PCR) and cleaved amplified polymorphic sequence analyses[1] that are discriminative of locus-specific expression patterns (Supplementary Table 3). Although *A. thaliana* and *A. arenosa* loci were equally expressed in respective parents, in both allotetraploids (Allo733 and Allo738) *A. thaliana CCA1* (*AtCCA1*) expression was downregulated ~3-fold, whereas *A. arenosa CCA1* (*AaCCA1*) expression was slightly reduced (Fig. 1c). Similarly, *AtLHY* expression was

[1]Section of Molecular Cell and Developmental Biology, [2]Institute for Cellular and Molecular Biology, [3]Center for Computational Biology and Bioinformatics, and [4]Section of Integrative Biology, The University of Texas at Austin, One University Station, A-4800, Austin, Texas 78712, USA. [5]Department of Plant Genetics and Breeding, China Agricultural University, Yuanmingyuan Xilu No. 2, Beijing, 100094, China. †Present address: Department of Plant Genetics and Breeding, China Agricultural University, Yuanmingyuan Xilu No. 2, Beijing, 100094, China.
*These authors contributed equally to this work.

dramatically reduced (~3.3-fold), whereas *AaLHY* expression was decreased ~2-fold in the allotetraploids. Conversely, *AtTOC1* and *AtGI* loci were upregulated in the allotetraploids. These data suggest that *A. thaliana* genes are more sensitive to expression changes in the allotetraploids, probably through *cis*- and *trans*-acting effects and chromatin modifications as observed in other loci[18].

We examined chromatin changes in the upstream regions (~250-bp) of *CCA1*, *LHY*, *TOC1*, and *GI* (Supplementary Table 4) using antibodies against histone H3-Lys 9 acetylation (H3K9Ac) and H3-Lys 4 dimethylation (H3K4Me2)—two marks for gene activation[21]. H3K9Ac and H3K4Me2 levels in the *CCA1* and *LHY* promoters were 2–3-fold lower in the allotetraploids than in *A. thaliana* and *A. arenosa* (Fig. 1d), consistent with *CCA1* and *LHY* repression. Likewise, *TOC1* and *GI* upregulation correlated with increased levels of H3K9Ac and H3K4Me2. Changes in H3K9Me2, a heterochromatic mark[21], were undetectable (data not shown). These data suggest that the diurnal expression changes of *LHY*, *CCA1*, *TOC1* and *GI* are associated with euchromatic histone marks. Alternatively, autonomous pathways and other factors such as ELF4 may mediate *TOC1* and *GI* expression[20,22].

To test the downstream effects of *CCA1* and *LHY* repression, we examined the expression of two subsets of evening-element- and CBS-containing genes (Fig. 2a). One subset consists of the *PORA* and *PORB* genes that encode protochlorophyllide oxidoreductases a and b, which mediate the only light-requiring step in chlorophyll biosynthesis in higher plants[23]. *PORA* and *PORB* are strongly expressed in seedlings and young leaves, and their upregulation increases chlorophyll a and b content[24]. Both *PORA* and *PORB* were upregulated in the allotetraploids (Fig. 2d). The total chlorophyll content in both allotetraploids was ~60% higher than in *A. thaliana* and ~15% higher than in *A. arenosa* (Fig. 2b). Chlorophyll a increased more than chlorophyll b, and the allotetraploids accumulated ~70% more chlorophyll a than *A. thaliana*.

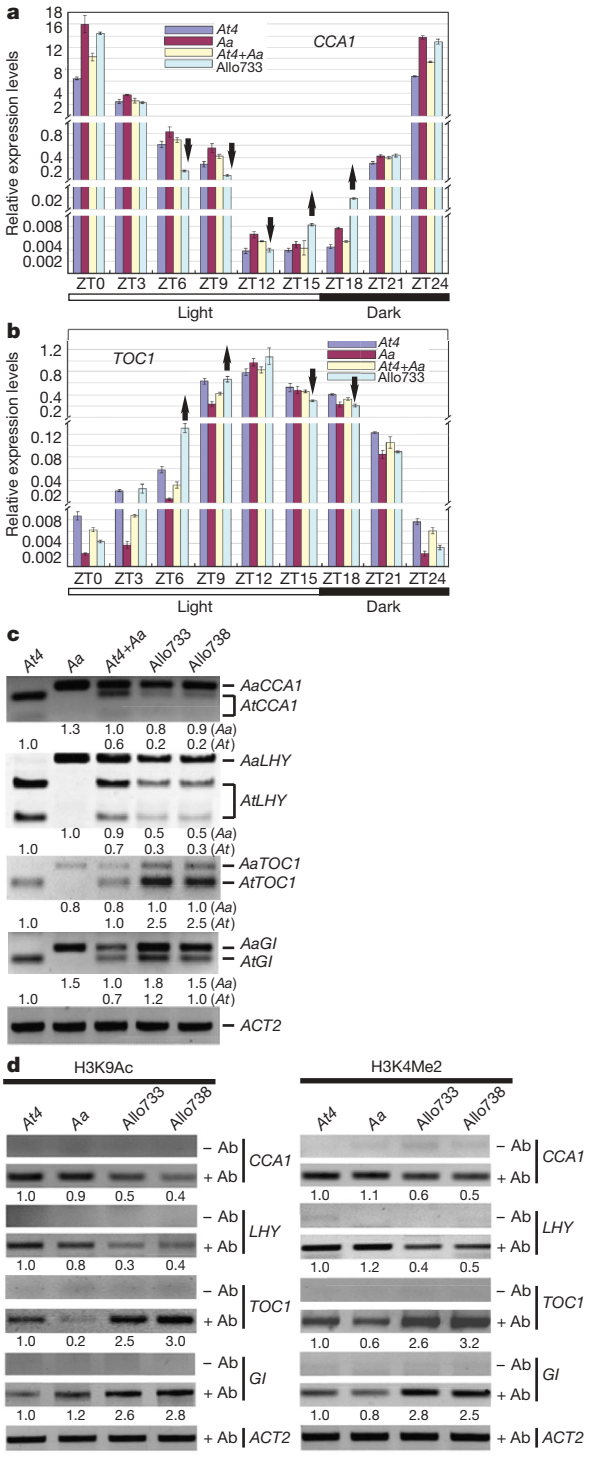

Figure 1 | Locus-specific and chromatin regulation of circadian clock genes in the allotetraploids. **a**, **b**, Quantitative RT–PCR analysis of *CCA1* (**a**) and *TOC1* (**b**) expression ($n = 3$, *ACT2* as a control) in a 24-h period (light/dark cycles) starting from dawn (ZT0, 6:00); arrows indicate up- and downregulation. *Aa*, *A. arenosa*; Allo733, allotetraploid; *At4*, *A. thaliana*. **c**, Repression of *A. thaliana CCA1* and *LHY*, and upregulation of *A. thaliana TOC1* and *GI* in the allotetraploids. RT–PCR products were digested with AvaII (*CCA1*), AflIII (*LHY*), SspI (*TOC1*) and SpeI (*GI*). **d**, ChIP analysis of *CCA1*, *LHY*, *TOC1* and *GI* using antibodies (Ab) against H3K9Ac and H3K4Me2 ($n = 2$).

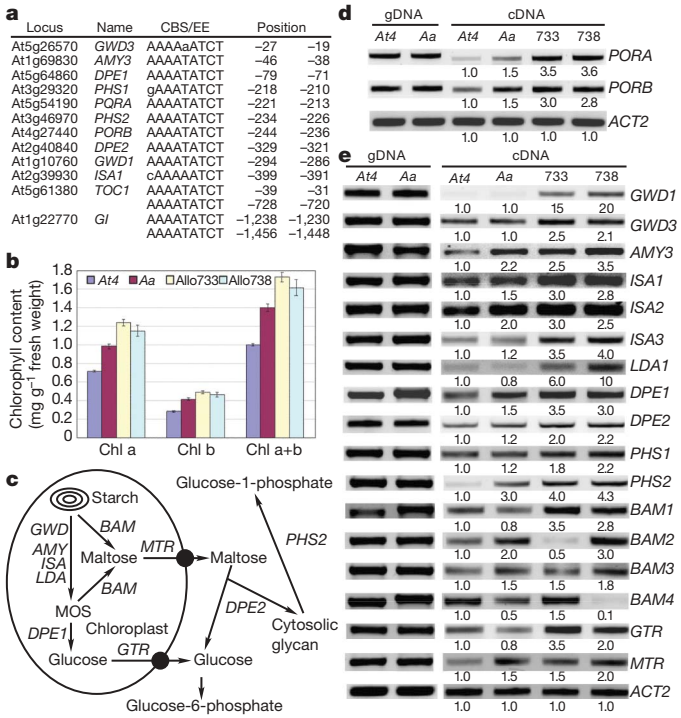

Figure 2 | Increase in chlorophyll content and upregulation of the genes involved in chlorophyll and starch biosynthesis in allotetraploids. **a**, Locations of CBS or evening element (EE) in the downstream genes (Supplementary Table 1). Lower-case letters denote nucleotide variation. **b**, Increase in chlorophyll (chl; a, b and total) content in the allotetraploids ($n = 3$). **c**, Starch metabolic pathways (modified from ref. 26) in the chloroplast (circled) and cytoplasm. MOS, maltose oligosaccharide. **d**, Upregulation of *PORA* and *PORB* in the allotetraploids (733 and 738) at ZT6 ($n = 2$). *ACT2* was used as a loading control; gDNA, genomic PCR. **e**, Upregulation of starch metabolic genes in allotetraploids ($n = 2$) at ZT6. See Supplementary Table 5 for gene names.

The other subset of evening-element- and CBS-containing genes encodes enzymes involved in starch metabolism and sugar transport[25,26], many of which show strong diurnal rhythmic expression patterns[14,27]. Starch metabolism involves the genes encoding AMY3, BAM1, 2 and 3, DPE1 and 2, GTR, GWD1 and 3, ISA1, 2 and 3, LDA, MEX1, and PHS1 and 2 (refs 25 and 26; Fig. 2c and Supplementary Table 5). Many contained an evening element or CBS (Fig. 2a) and were upregulated 1.5–4-fold in the allotetraploids (Fig. 2e) when *CCA1* and *LHY* were downregulated (Fig. 1a, c). *MTR*, *BAM3* and *BAM4*, which all lacked an evening element or CBS, showed little expression changes suggesting that their expression is independent of clock regulation or undergoes post-transcriptional regulation[26].

As a result, allotetraploids accumulated more starch than the parents in both mature and immature leaves as measured using iodine-staining (Fig. 3a) and quantitative assays (Fig. 3b). In the mature leaves, allotetraploids accumulated 2-fold more starch than *A. thaliana* and 70% more than *A. arenosa*. In the immature leaves, allotetraploids contained 4-fold more starch than *A. thaliana* and 50–100% more sugar content than the parents (Fig. 3c), mainly due to increases in glucose and fructose content, suggesting high rates of starch and sugar accumulation in young leaves. The sucrose content in allotetraploids was similar to *A. arenosa* but higher than in *A. thaliana* in immature leaves, and similar among all lines tested in mature leaves (data not shown), indicating that rapid transport and metabolism of sucrose occurs—especially in the mature leaves. Together, chlorophyll, starch and sugar amounts were consistently high in the allotetraploids.

We further tested whether circadian clock regulation is altered in F_1 hybrids as in the interspecific hybrids and allotetraploids. At ZT6 (noon), *CCA1* and *LHY* were repressed ~2-fold, whereas *TOC1* was upregulated ~2-fold in the F_1 hybrids relative to the parents (C24 and Columbia; Supplementary Fig. 3). At ZT15, *CCA1* and *LHY* were upregulated in the hybrids, whereas *TOC1* was repressed. The F_1 hybrids showed morphological vigour (Fig. 3d) and contained ~12% more total chlorophylls and ~10% more starch than the higher parent (Fig. 3e).

To determine how CCA1 regulates downstream genes and output traits, we examined the function of CCA1 in the allotetraploids and their parents. CCA1 protein amounts in these lines were high at dawn (ZT0) and low at noon (ZT6; Fig. 3f), corresponding to the *CCA1* transcript levels (Fig. 1a). CCA1 levels were constantly high in *A. thaliana* constitutive CCA1-overexpression (*CCA1-OX*) lines[11]. Electrophoretic mobility shift assays (EMSA) indicated specific binding of recombinant CCA1 to evening-element-containing fragments of the target genes *TOC1*, *PORB*, *PORA*, *DPE1* and *GWD3* (Fig. 3g, Supplementary Fig. 4 and Supplementary Table 6). Using antibodies against CCA1 in chromatin immunoprecipitation (ChIP) assays[18], we further demonstrated that endogenous CCA1 in the *TOC1* promoter was ~2.5-fold lower at noon (ZT6) than at dawn (ZT0; Fig. 3h), which is inversely correlated with the *TOC1* expression levels that were higher at noon than at dawn (Fig. 1b).

These data collectively suggest that CCA1 directly affects *TOC1* and downstream genes in clock regulation, photosynthesis and starch metabolism. Clock-dependent upregulation of output genes[14,27] may lead to growth vigour. Indeed, overexpression of *PORA* and *PORB* increases chlorophyll content, seedling viability and growth vigour in *A. thaliana*[24], whereas mutants of starch metabolic genes show reduced starch content and growth vigour[26].

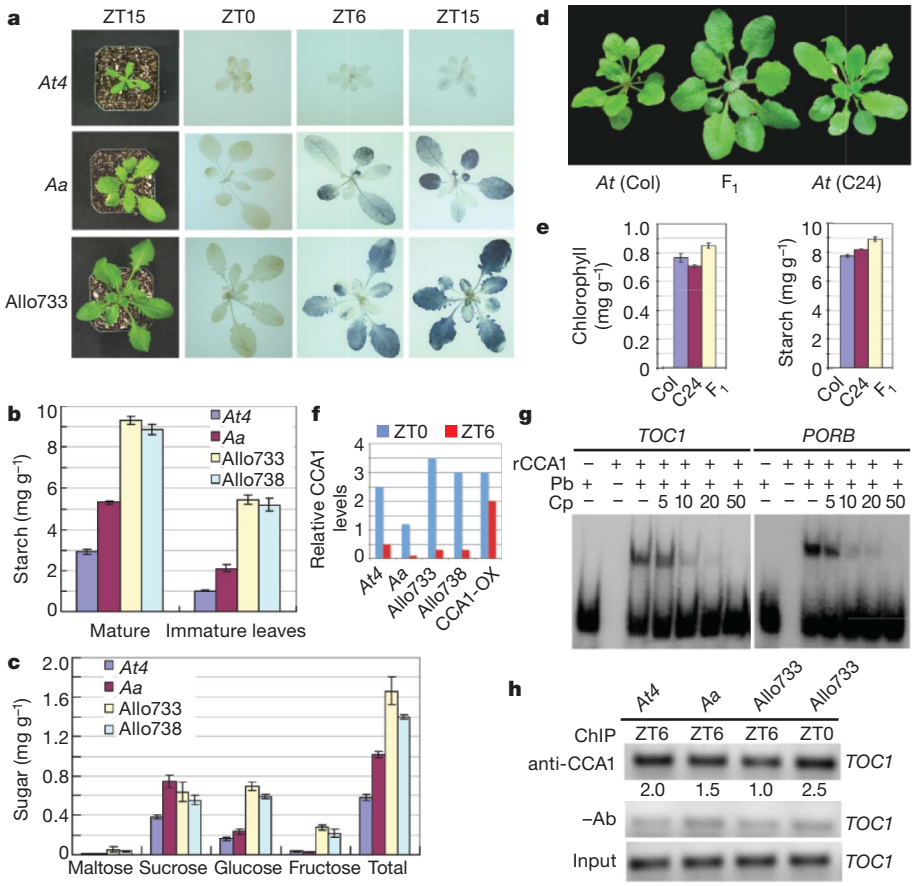

Figure 3 | CCA1 function and increased amounts of chlorophyll, starch and sugar in allotetraploids and F_1 hybrids. **a**, Starch staining in *A. thaliana* tetraploid (*At4*), *A. arenosa* (*Aa*) and allotetraploid (Allo733) at ZT0, ZT6 and ZT15. **b**, **c**, Increased starch content (**b**) and increased sugar content (**c**) in allotetraploids at ZT6. **d**, Morphological vigour in F_1 hybrids between *A. thaliana* diploid (*At*) Columbia (Col) and C24. **e**, Increased chlorophyll (ZT6, left) and starch (ZT15, right) accumulation in F_1. **f**, CCA1 protein levels changed at ZT6 and ZT0. **g**, Specific CCA1 binding activity to evening elements of downstream genes (*TOC1* and *PORB*) *in vitro*. Cp, cold probes; Pb, ^{32}P-labelled evening-element-containing probes (Supplementary Table 6). **h**, ChIP assays of endogenous CCA1 binding to the *TOC1* promoter. The levels were normalized using input DNA ($n = 2$).

If *CCA1* repression promotes growth, *CCA1* overexpression would reduce growth vigour in diploids. Indeed, *TOC1::CCA1* transgenic plants expressing *CCA1* under the clock-regulated *TOC1* promoter (Supplemental Fig. 5) displayed 3-fold induction of *CCA1* expression at noon (Fig. 4a, left) and 1.5–30-fold repression of the downstream genes *PORA*, *PORB*, *AMY*, *DPE1* and *GWD3* (Supplementary Fig. 6a), resulting in ~14% and ~17% reduction of chlorophyll (Fig. 4a, middle) and starch (Fig. 4a, right) contents, respectively. *CCA1-OX* had ~20% reduction of chlorophyll content in seedlings (Supplementary Fig. 5c) and may affect various regulators in clock and other pathways related to growth vigour. For example, *gi* mutants in *A. thaliana* increase starch content and flower late[28], but *GI* induction in the allotetraploids correlates with starch accumulation. *CCA1-OX* lines also flowered late[11] and may increase chlorophyll and starch content in late stages.

To test whether *CCA1* repression has positive effects on growth vigour in diploids as in the hybrids and allotetraploids (Figs 2b and 3a–e), we examined the starch content in *cca1* single and *cca1 lhy* double mutants[9,22,29]. *CCA1* expression was not completely abolished in these mutants (Fig. 4b) probably because of the T-DNA insertion near the ATG codon[29]. The five downstream genes examined were upregulated 1.5–12.5-fold in the mutants (Supplementary Fig. 6b), and the starch content was doubled in the *cca1* mutant (Fig. 4b). The starch content was lower in the double mutant than in *cca1*, indicating a metabolic penalty of severely lacking clock regulation[5]. Furthermore, to reduce *CCA1* expression during the day, we expressed *cca1*(*RNAi*) driven by the TOC1 promoter (Supplementary Fig. 6c). In the *TOC1::cca1*(*RNAi*) transgenic plants, CCA1 messenger RNA and protein amounts were downregulated 2–10-fold (Fig. 4c, left) and 1.4–3-fold (Fig. 4c, right), respectively. Consequently, four downstream genes examined were upregulated in the *TOC1::cca1*(*RNAi*) lines (Supplementary Fig. 6e), and the starch content increased ~28% (Fig. 4d). Taken together, the data suggest a mechanistic role of *CCA1* repression in promoting downstream pathways, increasing chlorophyll synthesis, starch metabolism and growth vigour.

We propose a model that explains the growth vigour and increased biomass in allotetraploids and hybrids (Fig. 4e). Correct circadian regulation enhances fitness and metabolism[5,6,8]. In the allotetraploids the expression of clock regulators is altered by autonomous regulation[20] and chromatin modifications (Fig. 1d)[16], including rhythmic changes in histone H3 acetylation in the *TOC1* promoter[30]. During the day, *A. thaliana CCA1* (and *LHY*) is epigenetically repressed, leading to upregulation of evening-element- and CBS-containing downstream genes in photosynthesis and carbohydrate metabolism. As a result the entire network is reset at high amplitude during the day, increasing chlorophyll synthesis and starch metabolism. At night, *CCA1* is derepressed and resumes normal oscillation. Although little is known about why the *A. thaliana* genes are repressed during the day[16], the repression is probably associated with *cis*- and *trans*-acting effects on homologous loci in the allotetraploids, as observed in flowering-time genes[18]. Interestingly, modulation of circadian clock regulators in allopolyploids and hybrids is reminiscent of switching gene expression during dawn- and evening-phased rhythmic alternation[14,20] that is required for properly maintaining

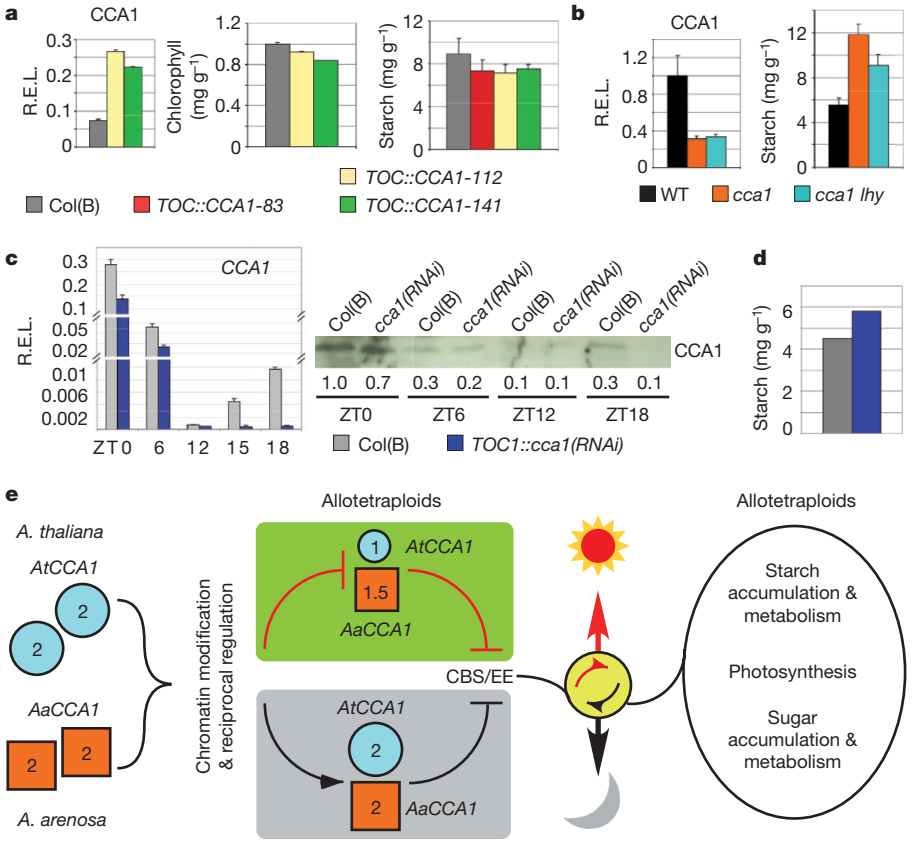

Figure 4 | A role of CCA1 in growth vigour in allotetraploids and hybrids. **a**, Relative expression levels (R.E.L.) of *CCA1* (ZT6, left), and reduced chlorophyll (ZT9, middle) and starch (ZT15, right) accumulation in *TOC1::CCA1* lines ($n = 3$; Supplementary Fig. 4). Col(B), Columbia transformed with Basta gene. **b**, Reduced *CCA1* expression (ZT6, left) and increased starch content (ZT15, right) in *cca1-11* and *cca1-11 lhy-21* mutants[9,29] ($n = 3$). Wild type (WT): Wassilewskija (Ws) or Columbia. **c**, Decreased expression of *CCA1* mRNA (left, $n = 3$) and protein (right, $n = 2$; ZT0-18, T2) in *TOC1::cca1*(*RNAi*) transgenic plants. **d**, Increased starch content in *TOC1::cca1*(*RNAi*) lines (ZT15, $n = 2$). **e**, A model for growth vigour and increased biomass. Chromatin-mediated changes in internal clock regulators (for example, *AtCCA1*) in allotetraploids lead to up- and downregulation (red and black arrows, respectively) and normal oscillation (yellow circle) of gene expression and output traits (photosynthesis, starch and sugar metabolism) at noon (sun) and dusk (moon). EE, evening element.

homoeostasis in clock-mediated metabolic pathways in diploids[9,19]. Hybrids and allopolyploids simply exploit epigenetic modulation of parental alleles and homologous loci of the internal clock regulators and use this convenient mechanism to alter the amplitude of gene expression and metabolic flux and gain advantages from clock-mediated photosynthesis and carbohydrate metabolism. Epigenetic regulation of a few regulatory genes induces cascade changes in downstream genes and physiological pathways and ultimately growth and development, which provides a general mechanism for growth vigour and increased biomass[2,3,16] that are commonly observed in the hybrids and allopolyploids produced within and between species.

METHODS SUMMARY

Allotetraploids were resynthesized as previously described[1,4], and hybrids were made by crossing C24 with Columbia. Unless otherwise noted, 8–15 plants (grown under 22 °C and 16-h light/day cycles) from each of 2–3 biological replications were pooled for the analysis of DNA, RNA, protein, chlorophyll, starch and sugar. *TOC1::CCA1* and *TOC1::cca1*(*RNAi*) transgenic plants were produced using pEarlygate303 (CD694) and pCAMBIA (CD3-447) derivatives, respectively. *cca1-11* (CS9378) and *ccal-11 lhy-21* (CS9380) mutants[9,22,29] were obtained from *Arabidopsis* Biological Resource Center (ABRC). Protein blot, EMSA and ChIP assays were performed as previously described[11,18].

Full Methods and any associated references are available in the online version of the paper at www.nature.com/nature.

Received 13 April; accepted 2 October 2008.
Published online 23 November 2008.

1. Wang, J. *et al.* Genomewide nonadditive gene regulation in *Arabidopsis* allotetraploids. *Genetics* **172,** 507–517 (2006).
2. Lippman, Z. B. & Zamir, D. Heterosis: revisiting the magic. *Trends Genet.* **23,** 60–66 (2007).
3. Birchler, J. A., Auger, D. L. & Riddle, N. C. In search of the molecular basis of heterosis. *Plant Cell* **15,** 2236–2239 (2003).
4. Comai, L. *et al.* Phenotypic instability and rapid gene silencing in newly formed *Arabidopsis* allotetraploids. *Plant Cell* **12,** 1551–1568 (2000).
5. Dodd, A. N. *et al.* Plant circadian clocks increase photosynthesis, growth, survival, and competitive advantage. *Science* **309,** 630–633 (2005).
6. Wijnen, H. & Young, M. W. Interplay of circadian clocks and metabolic rhythms. *Annu. Rev. Genet.* **40,** 409–448 (2006).
7. Panda, S., Hogenesch, J. B. & Kay, S. A. Circadian rhythms from flies to human. *Nature* **417,** 329–335 (2002).
8. Michael, T. P. *et al.* Enhanced fitness conferred by naturally occurring variation in the circadian clock. *Science* **302,** 1049–1053 (2003).
9. Mizoguchi, T. *et al. LHY* and *CCA1* are partially redundant genes required to maintain circadian rhythms in *Arabidopsis. Dev. Cell* **2,** 629–641 (2002).
10. Alabadi, D. *et al.* Reciprocal regulation between *TOC1* and *LHY/CCA1* within the *Arabidopsis* circadian clock. *Science* **293,** 880–883 (2001).
11. Wang, Z. Y. & Tobin, E. M. Constitutive expression of the *CIRCADIAN CLOCK ASSOCIATED 1* (*CCA1*) gene disrupts circadian rhythms and suppresses its own expression. *Cell* **93,** 1207–1217 (1998).
12. Strayer, C. *et al.* Cloning of the *Arabidopsis* clock gene *TOC1*, an autoregulatory response regulator homolog. *Science* **289,** 768–771 (2000).
13. Park, D. H. *et al.* Control of circadian rhythms and photoperiodic flowering by the *Arabidopsis GIGANTEA* gene. *Science* **285,** 1579–1582 (1999).
14. Harmer, S. L. *et al.* Orchestrated transcription of key pathways in *Arabidopsis* by the circadian clock. *Science* **290,** 2110–2113 (2000).
15. Leitch, A. R. & Leitch, I. J. Genomic plasticity and the diversity of polyploid plants. *Science* **320,** 481–483 (2008).
16. Chen, Z. J. Genetic and epigenetic mechanisms for gene expression and phenotypic variation in plant polyploids. *Annu. Rev. Plant Biol.* **58,** 377–406 (2007).
17. Rieseberg, L. H. & Willis, J. H. Plant speciation. *Science* **317,** 910–914 (2007).
18. Wang, J., Tian, L., Lee, H. S. & Chen, Z. J. Nonadditive regulation of *FRI* and *FLC* loci mediates flowering-time variation in *Arabidopsis* allopolyploids. *Genetics* **173,** 965–974 (2006).
19. Alabadi, D., Yanovsky, M. J., Mas, P., Harmer, S. L. & Kay, S. A. Critical role for CCA1 and LHY in maintaining circadian rhythmicity in *Arabidopsis. Curr. Biol.* **12,** 757–761 (2002).
20. McClung, C. R. Plant circadian rhythms. *Plant Cell* **18,** 792–803 (2006).
21. Jenuwein, T. & Allis, C. D. Translating the histone code. *Science* **293,** 1074–1080 (2001).
22. Doyle, M. R. *et al.* The *ELF4* gene controls circadian rhythms and flowering time in *Arabidopsis* thaliana. *Nature* **419,** 74–77 (2002).
23. Reinbothe, S., Reinbothe, C., Lebedev, N. & Apel, K. PORA and PORB, two light-dependent protochlorophyllide-reducing enzymes of angiosperm chlorophyll biosynthesis. *Plant Cell* **8,** 763–769 (1996).
24. Sperling, U., van Cleve, B., Frick, G., Apel, K. & Armstrong, G. A. Overexpression of light-dependent PORA or PORB in plants depleted of endogenous POR by far-red light enhances seedling survival in white light and protects against photooxidative damage. *Plant J.* **12,** 649–658 (1997).
25. Lloyd, J. R., Kossmann, J. & Ritte, G. Leaf starch degradation comes out of the shadows. *Trends Plant Sci.* **10,** 130–137 (2005).
26. Smith, A. M., Zeeman, S. C. & Smith, S. M. Starch degradation. *Annu. Rev. Plant Biol.* **56,** 73–98 (2005).
27. Smith, S. M. *et al.* Diurnal changes in the transcriptome encoding enzymes of starch metabolism provide evidence for both transcriptional and posttranscriptional regulation of starch metabolism in *Arabidopsis* leaves. *Plant Physiol.* **136,** 2687–2699 (2004).
28. Eimert, K., Wang, S. M., Lue, W. I. & Chen, J. Monogenic recessive mutations causing both late floral initiation and excess starch accumulation in *Arabidopsis. Plant Cell* **7,** 1703–1712 (1995).
29. Hall, A. *et al.* The *TIME FOR COFFEE* gene maintains the amplitude and timing of *Arabidopsis* circadian clocks. *Plant Cell* **15,** 2719–2729 (2003).
30. Perales, M. & Mas, P. A functional link between rhythmic changes in chromatin structure and the *Arabidopsis* biological clock. *Plant Cell* **19,** 2111–2123 (2007).

Supplementary Information is linked to the online version of the paper at www.nature.com/nature.

Acknowledgements We are grateful to E. Tobin for her gifts of the CCA1-overexpression (*CCA1-OX*) line and antibodies against CCA1. We thank H. Y. Chen for advice on recombinant CCA1 production, D. W. Ng for western blot analysis, T. Juenger for insightful discussions on life history traits in *Arabidopsis*, and D. Y. Chen and E. Huq for careful readings of the manuscript. The work was supported by the grants from the National Science Foundation Plant Genome Research Program (DBI0733857 and DBI0624077) and the National Institutes of Health (GM067015; Z.J.C.) and National Basic Research Program of China (2007CB109000; Q.S.).

Author Contributions Z.N. examined gene expression, ChIP, chlorophyll, starch and sugars in allotetraploids and hybrids. E.-D.K. analysed *CCA1* mRNA, protein, chlorophyll and starch in the transgenic plants and mutants. M.H. conducted statistical tests. E.L. performed EMSA. J.L. assayed western blots and ChIP. Y.Z. assisted cloning. Q.S. discussed the experiments. Z.J.C. conceived the project, analysed the data and wrote the paper.

Author Information Reprints and permissions information is available at www.nature.com/reprints. Correspondence and requests for materials should be addressed to Z.J.C. (zjchen@mail.utexas.edu).

METHODS

Plant growth. Plant materials included *A. thaliana* autotetraploid (*At4*, ABRC accession CS3900), *A. arenosa* (*Aa*, CS3901), and two independently resynthesized allotetraploid lineages (Allo733 and Allo738; CS3895-96; F_7 to F_8). All plant materials were generated as previously described[1,4]. Plants for 24-h rhythm analysis were grown for 4 weeks in 16/8-h (light/dark) cycles and collected at indicated Zeitgeber time (ZT0 = dawn)[20]. For each genotype, mature leaves from five plants were collected every 3 h for a period of 48 h and frozen in liquid nitrogen. The data from the first 24-h period were shown because the second-period data were the same. Leaves were collected before bolting (6–8 rosette leaves in *A. thaliana*, 10–12 leaves in *A. arenosa*, and 12–15 leaves in allotetraploids) to minimize developmental variation among genotypes[31,32]. Unless noted otherwise, analyses for gene expression, chlorophyll, starch and sugars were performed at ZT6 (noon), ZT9 and ZT15.

CCA1 transgenic plants. The constitutive *CCA1*-overexpression line (*CCA1-OX*) was provided by E. Tobin at University of California, USA. We amplified a *TOC1* (At5g61380.1) promoter fragment using *A. thaliana* Columbia genomic DNA and the primer pair 5′-GGGAATTCCGTGTCTTACGGTGGATGAAGTTGA-3′ (EcoRI; in which the restriction site is underlined) and 5′-GGGGATCCGTTTT GTCAATCAATGGTCAAATTATGAGACGCG-3′ (BamHI) and a full-length *CCA1* cDNA fragment using the primer pair 5′-GCGGCCGGATCCATGGAGACAAATTCGTCTGG AG-3′ (BamHI) and 5′-GGCCGCTCTAGATCATGTGGAAGCTTGAGTTTC-3′ (XbaI). The *TOC1* promoter fragment was fused to *CCA1* cDNA and cloned into pBlueScript. The inserts were validated by sequencing and subcloned into pEarlyGate303 (CD694) using the primer pair 5′-GGGGACAAGTTTGTACAAAA AAGCAGGCTTACGTGTCTTACGGTGGATGAAGTTGA -3′ and 5′-GGGGACCACTTTG TACAAGAAAGCTGGGTCTGTGGAAGCTTGAGTTTCCAACCG-3′. The construct (*ProTOC1::CCA1*) was transformed into *A. thaliana* (Columbia) plants[33] (Supplementary Fig. 4b). One-week old T1 seedlings (two true leaves) were sprayed with Basta solution (~100 mg l^{-1}), and the positive plants were genotyped (Supplementary Fig. 4). T2 transgenic plants (*TOC1::CCA1*) were subjected to chlorophyll, starch, and gene expression analysis.

To make the *TOC1::cca1*(*RNAi*) construct, we amplified a *TOC1* promoter fragment (*ProTOC1*) using the primer pair F-EcoRI-*ProTOC1* 5′-GGGAATTCCGTGTCTTACGGTGGATGAAGTTGA-3′ and R-*ProTOC1*-NcoI 5′-GCGGCCCCATGGGTTTTGTCAATCAATGGTCAAATTATGAGACGCG-3′ and replaced the 35S promoter with *ProTOC1* in pFGC5941 (CD3-447; Supplementary Fig. 5c). A 250-bp *CCA1* fragment was amplified using the primer pair F-*CCA1*(*RNAi*)-XbaI–AscI 5′-GCGGCCTCTAGAGGCGCGCCTCTGGAAAACGGTAATGAGCAAGGA-3′ and R-*CCA1*(*RNAi*)–BamHI–SwaI 5′-GGCCGCCCTAGGTAAATTTACACCACTAGAATCGGGAGGCCAAA-3′. We subcloned the BamHI–XbaI fragment and then the AscI–SwaI fragment into the same vector, generating two CCA1 fragments in opposite orientations (*proTOC1::cca1*(*RNAi*); Supplementary Fig. 5c). Four *TOC1::cca1*(*RNAi*) T1 transgenic plants were used to analyse gene expression and starch content.

We obtained mutant seeds of *cca1-11* (CS9378) and *cca1-11 lhy-21* (CS9380)[22,29] from ABRC. Gene expression, chlorophyll and starch assays were performed when the mutant plants were about 3–4 weeks old and had 6–8 true leaves under 16/8 h of day/night before bolting[9].

Note that the *CCA1-OX* and *TOC1::CCA1* lines flowered late (Supplementary Fig. 4)[11], whereas *cca1* and *cca1 lhy* mutants flowered early[9,29]. A few *TOC1::cca1*(*RNAi*) lines flowered early, whereas some flowered late (Supplementary Fig. 5d), which may be related to various secondary and systematic effects on the downstream genes related to flowering time. All assays in mutant and transgenic plants were performed before bolting.

DNA and RNA analysis. Genomic DNA was extracted using a modified protocol[32]. Total RNA was extracted using RNeasy plantmini kits (Qiagen). The first-strand cDNA synthesis was performed using reverse transcriptase Superscript II (Invitrogen). An aliquot (1/100) of cDNA was used for quantitative RT–PCR analysis using the primer pairs for *LHY*, *CCA1*, *TOC1* and *GI* (Supplementary Table 2) in an ABI7500 machine (Applied Biosystems) as previously described[34], except that *ACT2* was used as a control to estimate the relative expression levels in three biological replications.

To distinguish locus-specific expression patterns, the RT–PCR products were amplified using the primer pairs (Supplementary Table 3) and subjected to cleaved amplified polymorphism sequence analysis[32].

Semi-quantitative RT–PCR was used to determine the expression levels of the genes in chlorophyll a and b biosynthesis and starch metabolism (Supplementary Table 5).

Chlorophyll, starch and sugar contents. Chlorophyll was extracted in dark with 5 ml of acetone (80%) at 4 °C from 300 mg 4-week-old seedlings. The chlorophyll content was calculated using spectrophotometric absorbance (A) at light wavelengths of 603, 645 and 663 nm and 80% acetone as a control[35] and shown as milligram of chlorophyll per gram of fresh leaves.

$$\text{Chlorophyll a (mg g}^{-1}) = 12.7 \times A_{663} - 2.69 \times A_{645}$$

$$\text{Chlorophyll b (mg g}^{-1}) = 22.9 \times A_{645} - 4.86 \times A_{663}$$

$$\text{Chlorophyll a+b (mg g}^{-1}) = 8.02 \times A_{663} + 20.20 \times A_{645}$$

Starch content was measured from leaves of five plants (about 600 mg fresh weight). The leaves were boiled in 25 ml 80% (v/v) ethanol. The decoloured leaves were stained in an iodine solution or ground with a mortar and pestle in 80% ethanol[36,37]. Total starch in each sample was quantified using 30 µl of the insoluble carbohydrate fraction using a kit from Boehringer Mannheim (R-Biopharm).

To quantify soluble sugars, 600 mg fresh leaves were extracted with 80% ethanol according to a published protocol[38]. The sugar concentration was determined enzymatically using Maltose/Sucrose/D-Glucose and D-Glucose/D-Fructose kits (Boehringer Mannheim, R-Biopharm) and shown as milligram of sugar per gram of fresh leaves.

Promoter motif analysis. DNA sequences from ~1,000-bp upstream of the transcription start sites of the upregulated genes identified in the allotetraploids[1] were extracted and evening elements (AAAATATCT) or CBSs (AAAAATCT)[10,11,39] were searched for. The same method was used to analyse motifs in all genes in the *Arabidopsis* genome[40]. The list of 128 upregulated genes and motif locations is provided in Supplementary Table 1.

Chromatin immunoprecipitation. The ChIP assays were performed using a modified protocol[41,42]. We used one-tenth of the chromatin solution as input DNA to determine DNA fragment sizes (0.3–1.0 kb). The remaining chromatin solution was diluted 10-fold and divided into two aliquots; one aliquot was incubated with 10 µl of antibodies (anti-dimethyl-H3-Lys4, anti-dimethyl-H3-Lys9 and anti-acetyl-H3-Lys9 (Upstate Biotechnology); or anti-CCA1), and the other was incubated with protein beads. The immunoprecipitated DNA was amplified by semi-quantitative PCR using the primers designed from the conserved sequences of the *CCA1*, *LHY*, *TOC1* and *GI* upstream of the ATG codon from both *A. thaliana* and *A. arenosa* loci (Supplementary Table 4). Two independent experiments were performed and analysed.

Electrophoretic mobility shift assay. A *CCA1* full-length cDNA was amplified from *A. thaliana* cDNA using a primer pair attB1-*CCA1*-F-XhoI (in which the attachment sequences are underlined) GGGGACAAGTTTGTACAAAAAAGCAGGCTCCCTCGAGATGGAGACAAATTCGTCT-3′ and *CCA1*-R-Avr2-attB2 5′-GGGGACCACTTTGTACAAGAAAGCTGGGTCCCCTAGGTCATGTGGAAGCTTGAGTTTC-3′. The cDNA was cloned into pDONR221 and validated by sequencing. The resulting insert was transferred by recombination into pET300/NT-DEST expression vector (Invitrogen Corp.,) and expressed in *Escherichia coli* Rosetta-gami B competent cells (Novagen). Recombinant CCA1 protein was purified and subjected to EMSA[39] in 6% native polyacrylamide gels using recombinant CCA (rCCA1; 10 fmoles) and ^{32}P-labelled double-stranded oligonucleotides (10 fmoles; Supplementary Table 6). The cold probe concentrations were 0 (−), 50 (5×), 100 (10×), 200 (20×) and 500 (50×) fmoles.

Western blot analysis. Protein crude extracts were prepared from fresh leaves as previously described[11]. The immunoblots were probed with anti-CCA1, and antibody binding was detected by ECL (Amersham).

31. Madlung, A. *et al.* Remodeling of DNA methylation and phenotypic and transcriptional changes in synthetic *Arabidopsis* allotetraploids. *Plant Physiol.* **129,** 733–746 (2002).
32. Wang, J. *et al.* Stochastic and epigenetic changes of gene expression in *Arabidopsis* polyploids. *Genetics* **167,** 1961–1973 (2004).
33. Clough, S. J. & Bent, A. F. Floral dip: a simlified method for Agrobacterium-mediated transformation of *Arabidopsis thaliana*. *Plant J.* **16,** 735–743 (1998).
34. Lee, H. S. *et al.* Sensitivity of 70-mer oligonucleotides and cDNAs for microarray analysis of gene expression in *Arabidopsis* and its related species. *Plant Biotechnol. J.* **2,** 45–57 (2004).
35. Mochizuki, N., Brusslan, J. A., Larkin, R., Nagatani, A. & Chory, J. *Arabidopsis genomes uncoupled 5* (*GUN5*) mutant reveals the involvement of Mg-chelatase H subunit in plastid-to-nucleus signal transduction. *Proc. Natl Acad. Sci. USA* **98,** 2053–2058 (2001).
36. Yu, T. S. *et al.* The *Arabidopsis sex1* mutant is defective in the R1 protein, a general regulator of starch degradation in plants, and not in the chloroplast hexose transporter. *Plant Cell* **13,** 1907–1918 (2001).
37. Smith, A. M. & Zeeman, S. C. Quantification of starch in plant tissues. *Nature Protocols* **1,** 1342–1345 (2006).
38. Focks, N. & Benning, C. *wrinkled1*: A novel, low-seed-oil mutant of *Arabidopsis* with a deficiency in the seed-specific regulation of carbohydrate metabolism. *Plant Physiol.* **118,** 91–101 (1998).
39. Harmer, S. L. & Kay, S. A. Positive and negative factors confer phase-specific circadian regulation of transcription in *Arabidopsis*. *Plant Cell* **17,** 1926–1940 (2005).

40. The Arabidopsis Genome Initiative. Analysis of the genome sequence of the flowering plant *Arabidopsis thaliana*. *Nature* **408,** 796–815 (2000).
41. Bastow, R. *et al.* Vernalization requires epigenetic silencing of *FLC* by histone methylation. *Nature* **427,** 164–167 (2004).
42. Tian, L. *et al.* Reversible histone acetylation and deacetylation mediate genome-wide, promoter-dependent and locus-specific changes in gene expression during plant development. *Genetics* **169,** 337–345 (2005).

Vol 457|15 January 2009|doi:10.1038/nature07510

LETTERS

Transcription inactivation through local refolding of the RNA polymerase structure

Georgiy A. Belogurov[1], Marina N. Vassylyeva[2], Anastasiya Sevostyanova[1], James R. Appleman[3], Alan X. Xiang[3], Ricardo Lira[3], Stephen E. Webber[3], Sergiy Klyuyev[2], Evgeny Nudler[4], Irina Artsimovitch[1] & Dmitry G. Vassylyev[2]

Structural studies of antibiotics not only provide a shortcut to medicine allowing for rational structure-based drug design, but may also capture snapshots of dynamic intermediates that become 'frozen' after inhibitor binding[1,2]. Myxopyronin inhibits bacterial RNA polymerase (RNAP) by an unknown mechanism[3]. Here we report the structure of dMyx—a desmethyl derivative of myxopyronin B[4]—complexed with a *Thermus thermophilus* RNAP holoenzyme. The antibiotic binds to a pocket deep inside the RNAP clamp head domain, which interacts with the DNA template in the transcription bubble[5,6]. Notably, binding of dMyx stabilizes refolding of the β′-subunit switch-2 segment, resulting in a configuration that might indirectly compromise binding to, or directly clash with, the melted template DNA strand. Consistently, footprinting data show that the antibiotic binding does not prevent nucleation of the promoter DNA melting but instead blocks its propagation towards the active site. Myxopyronins are thus, to our knowledge, a first structurally characterized class of antibiotics that target formation of the pre-catalytic transcription initiation complex—the decisive step in gene expression control. Notably, mutations designed in switch-2 mimic the dMyx effects on promoter complexes in the absence of antibiotic. Overall, our results indicate a plausible mechanism of the dMyx action and a stepwise pathway of open complex formation in which core enzyme mediates the final stage of DNA melting near the transcription start site, and that switch-2 might act as a molecular checkpoint for DNA loading in response to regulatory signals or antibiotics. The universally conserved switch-2 may have the same role in all multisubunit RNAPs.

Our data show that myxopyronins efficiently inhibit formation of transcription initiation complexes by both *Escherichia coli* and *T. thermophilus* RNAPs (Supplementary Fig. 1). The crystal structure of dMyx bound to the *T. thermophilus* RNAP holoenzyme (Fig. 1, Supplementary Fig. 2 and Supplementary Table 1) has been refined at 2.7 Å resolution to the final $R_{factor}/R_{free} = 0.240/0.270$. Comparison with the apo-RNAP (Protein Data Bank (PDB) accession 2A6E) showed a subtle but systematic dMyx-induced ~2.0–3.7 Å shift of the β′-subunit amino-terminal domain (residues β′1–600) and the σ-subunit in the RNAP–dMyx complex (Methods and Supplementary Fig. 3). This shift, however, did not change either the pattern of the σ/core-RNAP interactions, or the arrangement of and the distance between the σ-regions 2 and 4 which recognize the −10 and −35 promoter elements[5]. The configuration of the fork formed by the σ-regions 2.3–2.4 and 2.5–3.1 at the upstream entrance to the RNAP main channel (where melting of the DNA duplex is thought to start[6–8]) is also largely unaffected by dMyx. In the RNAP–dMyx complex, the width of the main channel is reduced by ~4 Å as compared to that in one of the two crystallographically independent molecules in the apo-RNAP. If systematic, this constriction could affect accommodation of the upstream DNA duplex and/or DNA melting. However, the second apo-RNAP molecule also had the narrowed channel, indicating the inherent flexibility of the neighbouring domains and suggesting that the main channel width is unlikely to be a limiting factor for open complex formation (Supplementary Fig. 4).

dMyx binds in the pocket deep inside the RNAP clamp head domain (Fig. 1a, b), which constitutes the wall of the main channel opposite the catalytic centre and forms crucial contacts with the DNA template strand in the elongation complex[9,10]. Although hydrophobic contacts probably have a dominant role in binding, most of the dMyx polar groups also form specific interactions with the protein (Fig. 1d and Supplementary Fig. 5). The most important and notable change observed in the presence of dMyx is refolding of the highly conserved β′ switch-2 segment (β′602–621; Fig. 1c): the α-helix, interrupted in the middle by four flipped-out residues, is straightened, whereas its carboxy-terminal portion (~two-helical turns) unwinds and refolds into a loop (Fig. 1e, f). This loop extends towards the active site, where it approaches the σ hairpin loop[11] (σ317–333; Fig. 1a, b).

To verify the dMyx-binding determinants revealed by the structure and to probe the role of switch-2 refolding in the dMyx mechanism, we performed *in vitro* mutational analysis of *E. coli* RNAP (Supplementary Information). As anticipated, substitutions of three residues (Ser β1322, Glu β1279 and Lys β′345, numbered as in *E. coli*; Fig. 1d) making crucial interactions with dMyx conferred resistance to the antibiotic (Fig. 2 and Supplementary Fig. 6). On the other hand, after the switch-2 refolding Lys 334 forms only weak van der Waals interactions with dMyx whereas Arg 337 and Arg 339 do not interact with the inhibitor at all (Fig. 1d). Consistently, substitutions of these residues for Ala do not substantially affect inhibition by dMyx (Fig. 2). To design switch-2 variants with altered refolding properties, we used the following considerations. First, we selected residues without essential direct contacts with dMyx. Second, deletion of two flipped-out residues, Lys 334 and Gln 335 (the integration of which into an α-helix probably initiates refolding; Fig. 1e), would prevent both opening of the inhibitor-binding site and formation of the C-terminal loop. Third, in the structures without dMyx, Phe 338 is integrated into the hydrophobic core that probably stabilizes the original switch-2 conformation (Supplementary Fig. 7). The Phe/Ala substitution, as well as a deletion of 338–341 residues, would weaken these interactions, thereby presumably favouring refolding. Fourth, although in both conformations Gly 336 is located at the junction between the α-helical and unfolded portions, its main chain angles (ϕ, ψ) appear in the disallowed and favourable (for the amino acids with side chains) regions of the Ramachadran plot for the original

[1]Department of Microbiology, The Ohio State University, 484 West 12th Avenue, Columbus, Ohio 43210, USA. [2]Department of Biochemistry and Molecular Genetics, University of Alabama at Birmingham, Schools of Medicine and Dentistry, 720 20th Street South, Birmingham, Alabama 35294, USA. [3]Anadys Pharmaceuticals, Inc., 3115 Merryfield Row, San Diego, California 92121, USA. [4]Department of Biochemistry, New York University School of Medicine, 550 First Avenue, New York, New York 10016, USA.

and refolded configurations, respectively, suggesting that its substitution for Ala would favour the refolded conformation. In support of structural considerations, the Δ334–335 was resistant, whereas the Δ338–341, F338A and G336A variants were hypersensitive to dMyx (Fig. 2).

Switch-2 refolding may be pivotal for the dMyx action. Refolding opens the entry to the otherwise inaccessible dMyx-binding site (Supplementary Fig. 8). Also, Arg β′610 and Gln β′611 are flipped out of the helix in the original switch-2 configuration and form hydrogen bonds with the DNA template in the elongation complex (and presumably in the initiation complex, where they may be crucial for stability of the transcription bubble) but lose these contacts on refolding (Fig. 1e, f). This change may inhibit DNA melting beyond the register −3. Furthermore, the newly formed C-terminal loop would clash with the DNA template strand if melting propagates to register +1 (Supplementary Fig. 9). This clash can hardly be avoided: although the upstream DNA (registers −2 to −10, and so on) may show relatively large deviations between the initiation and elongation complexes, the position of the acceptor template ($i+1$) is strongly restrained by base pairing with the incoming substrate and thus is probably identical in both states.

To complement the lack of structural information on the DNA conformation in the dMyx-inhibited complex, we tested this model using biochemical approaches. The model suggests that the properly positioned template strand would preclude refolding and thus Myx binding; indeed, dMyx failed to inhibit transcription if added to the preformed open promoter complex (Supplementary Fig. 1b). We then tested the effect of dMyx on RNAP–DNA contacts and the DNA strand separation in λP_R promoter complexes using DNaseI and $KMnO_4$ footprinting, respectively. Consistent with published data[12–14], the non-template strand thymidine residues at positions −4, −3 and +2 were hypersensitive to $KMnO_4$ modification in the absence of dMyx (Fig. 3a). In the presence of inhibitor, the +2 position became strongly protected. DNaseI probing showed that dMyx induced a loss of protection (4–5 base pairs (bp)) at the downstream footprint boundary (on both DNA strands; Fig. 3a and data not shown). Similar patterns were observed in complexes trapped at intermediate steps of open complex formation[7,14,15].

Our structural data did not show any considerable antibiotic-dependent alterations of the RNAP structure that may affect DNA loading into the main channel at the upstream (−10) promoter region. Consistently, our footprinting analysis demonstrates that dMyx does not prevent RNAP binding to promoter, nucleation of melting at approximately −11, or entry of the double-stranded downstream DNA into the enzyme. The antibiotic imposes a block to DNA melting only beyond register −3, in which the direct interactions with switch-2 are predicted by modelling (assuming that the DNA trajectory is not markedly changed between the initiation and elongation complexes). Moreover, dMyx inhibited transcription on the artificially melted promoters (Supplementary Fig. 10); thus, it precludes the correct loading of the template DNA into the main channel even after complete strand separation. Overall, our present data favour a mechanism (Fig. 3b) in which local dMyx-stabilized refolding of switch-2 disrupts potentially critical interactions with and/or sterically occludes accommodation of the melted template DNA near the transcription start site, resulting in misplaced downstream DNA and inhibition of the strand separation. Further allosteric effects (for example, on the clamp opening/closing) of dMyx binding cannot be ruled out, but our study fails to demonstrate any indications of their importance in antibiotic action. A more detailed

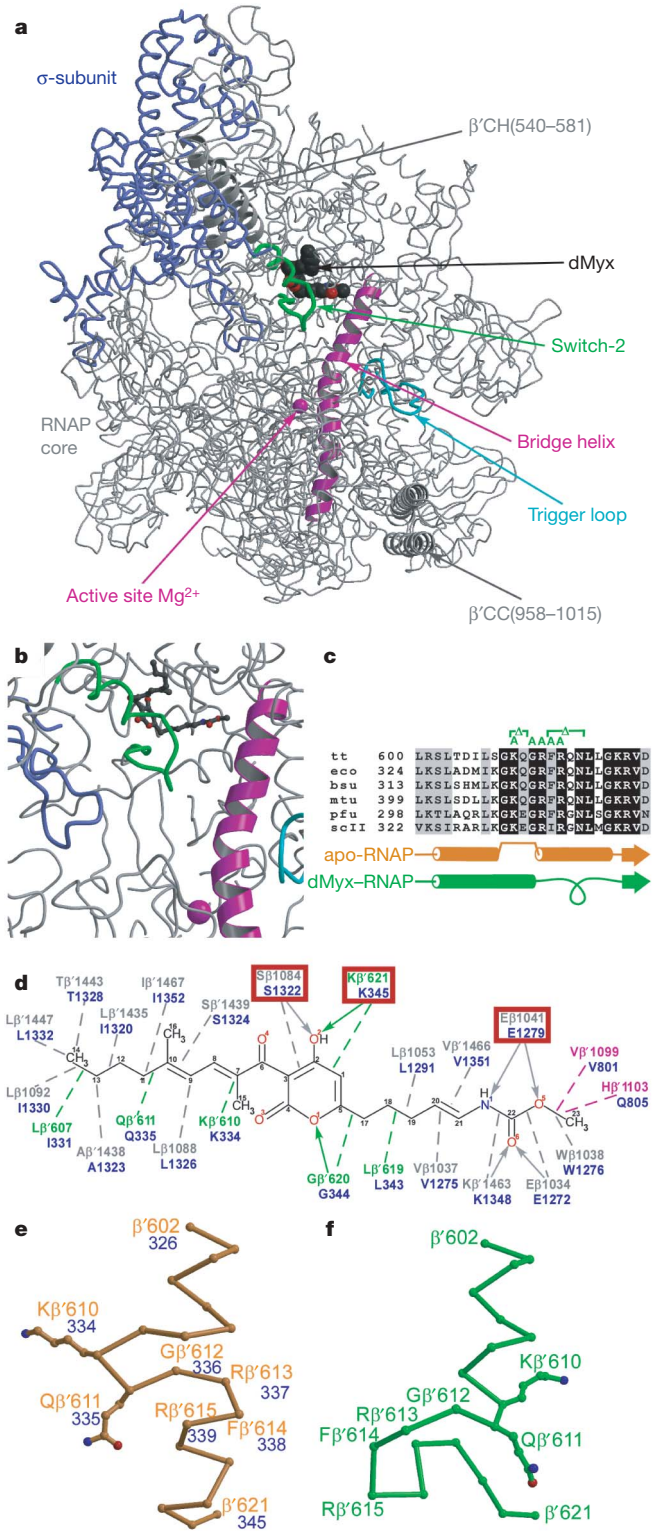

Figure 1 | Structure of the RNAP–Myx complex. The same colour scheme is used in all figures throughout this manuscript. The σ-subunit, bridge helix, trigger loop and the remainder of the RNAP molecule are in blue, magenta, cyan and grey, respectively. The switch-2 segments in the Myx-free and Myx-bound structures are in orange and green, respectively. dMyx is in black. The Mg^{2+} ion is shown as magenta sphere. **a**, The overall view of the complex is shown. CC, coiled–coil; CH, clamp helices. **b**, Close-up view of the dMyx binding site. **c**, Sequence alignment of the switch-2 segment from bacterial (bsu, *Bacillus subtilis*; eco, *E. coli*; mtu, *Mycobacterium tuberculosis*; tt, *T. thermophilus*), archaeal (pfu, *Pyrococcus furiosis*) and yeast *Saccharomyces cerevisiae* pol II (scII) enzymes. Substitutions constructed in this work are shown above the sequence in green. **d**, Schematic drawing of the protein–dMyx interactions. The polar and van der Waals interactions are shown as solid arrows and dashed lines, respectively. The mutated residues are indicated by the red boxes. **e**, **f**, Conformations of the switch-2 segment in the Myx-free (**e**) and Myx-bound (**f**) holo-RNAP structures. In the panels **d** and **e** the *E. coli* residue numbers are shown in blue.

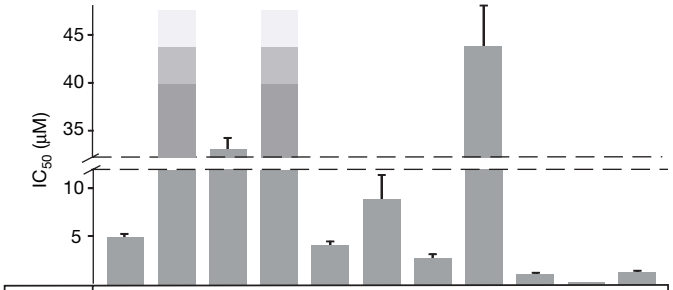

RNAP	Wild type	β S1322E (1084)	β E1279A (1041)	β′ K345A (621)	β′ K334A (610)	β′ R337A (613)	β′ R339A (615)	β′ Δ334–5 (610–1)	β′ G336A (612)	β′ F338A (614)	β′ Δ338–41 (614–7)
IC_{50}	4.99 ±0.45	63.3 ±12.3	33.1 ±1.1	>100	4.13 ±0.61	8.99 ±2.58	2.76 ±0.53	43.9 ±4.6	1.05 ±0.25	0.264 ±0.020	1.27 ±0.29

Figure 2 | Effect of RNAP mutations on dMyx activity. The half-maximal inhibitory concentration (IC_{50}) values were measured *in vitro* with purified RNAP variants (see Methods). The data is for all variants tested in this study. The IC_{50} could not be determined for the highly resistant β′ K345A variant. The *T. thermophilus* residue numbers are shown in brackets. Errors are standard deviations of the best fit estimates for IC_{50} and were calculated by nonlinear regression of the RNA synthesis measurements versus dMyx concentration assuming a hyperbolic dependence.

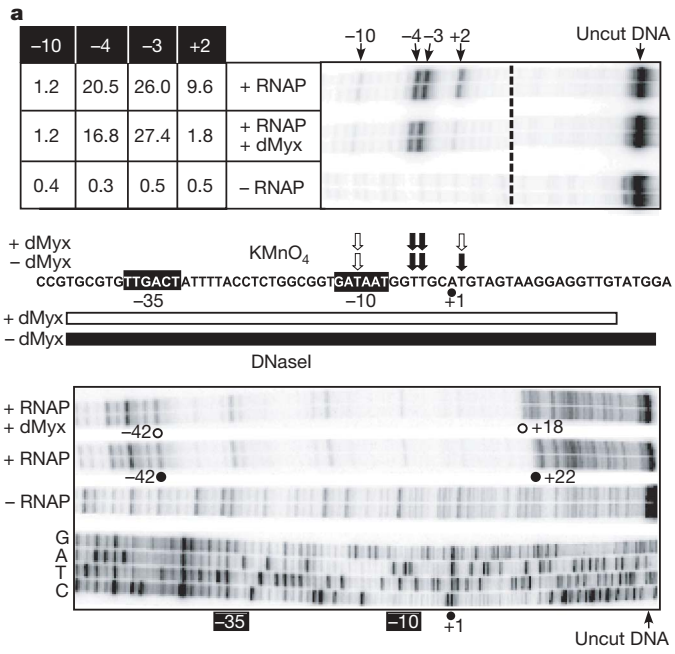

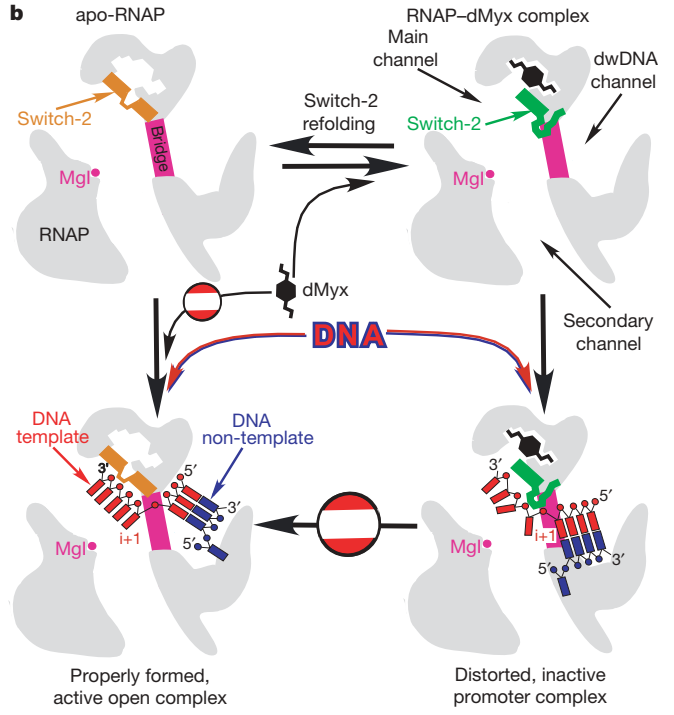

Figure 3 | A mechanism of the dMyx action. a, Myx alters the contacts between RNAP and λP_R promoter DNA. A linear DNA fragment encompassing positions −81 to +70 of the λP_R promoter was generated by polymerase chain reaction (PCR); the non-template DNA strand was end-labelled with [^{32}P]-γATP (see Methods). The sequence from −44 to +23 is shown. The −35 and −10 hexamers are indicated by black boxes, the start site (+1) is shown by a black dot. The top panel shows probing of the non-template strand by piperidine-induced cleavage of the permanganate-modified T residues. Reactivities of −10, −4, −3 and +2 residues (quantification described in Methods) are shown to the left of the gel and summarized above the promoter sequence where black and white arrows indicate high and low reactivity, respectively. The bottom panel shows protection of the non-template DNA strand from DNaseI digestion. The footprint boundaries in the promoter region shown are indicated on the gel and by black (RNAP alone) and white (RNAP with the inhibitor) bars below the promoter sequence; the dideoxy-sequencing ladder is shown for reference. In the gels shown, independent reaction repeats were analysed for consistency. **b**, Schematic drawing of the putative mechanism of the dMyx action. dwDNA, downstream DNA.

understanding of the mechanism awaits the high resolution structures of the RNAP open complex with and without dMyx. Discovery of the dMyx-binding determinants and the mechanism of its action would guide rational design of more potent dMyx derivatives (Supplementary Information).

Our results, together with conformational transitions in switch-2 observed in eukaryotic RNAP[16,17], suggest that this region is inherently flexible and may influence the open complex formation in the absence of inhibitors. To test this hypothesis, we used $KMnO_4$ footprinting analysis of the λP_R promoter complexes formed by switch-2 variants with altered refolding properties (Fig. 4). In contrast to the wild-type RNAP, which formed a stable complex with the melted region extended to the +2 position, the two mutants lacking the Phe 338 side chain (that probably stabilizes the original switch-2 configuration) demonstrated prominent melting defects. The Δ338–341 enzyme alone behaves as the wild-type RNAP in the presence of dMyx: DNA melting at +2 is blocked, DNaseI footprint is shortened, and the complex is heparin sensitive (Supplementary Fig. 11). In F338A RNAP, the pattern of permanganate sensitivity is shifted further upstream: the +2 position is not melted and the −10 position becomes unprotected. Notably, addition of dMyx shifted all complexes into the same state (Fig. 4). Taken together our data indicate that changes in the switch-2 designed to promote its refolding stabilize promoter intermediates in different states from the properly formed open complex, but are active on addition of substrates. Judging by the similarity of $KMnO_4$ footprints it is tempting to suggest that these states structurally resemble initiation intermediates of wild-type RNAP trapped by altering reaction conditions[7,12,14].

Although several arguments favour a hypothesis that the switch-2 state observed in the presence of dMyx resembles a 'physiological' (dMyx-independent) intermediate as opposed to an antibiotic-induced dead-end complex (Supplementary Information), we cannot definitively prove this notion. Thus, the detailed understanding of the effects of the substitutions used in this work requires further structural and biochemical characterization. However, our present findings support a mechanism of open complex formation that involves sequential bending of the promoter DNA upstream and downstream of the RNAP main channel as the pivotal transitions. The upstream bend is thought to originate from the σ-subunit–DNA contacts and induces upstream DNA melting ~60 Å away from the catalytic centre[7,11,13]. In contrast, the subsequent step is probably σ-independent and is set near the active site, in which interactions of DNA with the core enzyme

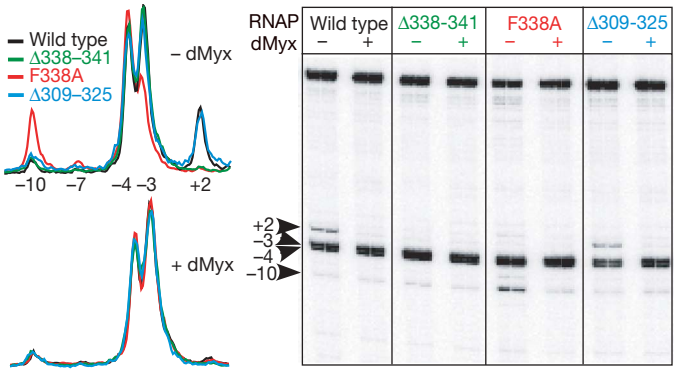

Figure 4 | Mutations in switch-2 affect the open complex formation. Accessibility of the non-template DNA strand residues to permanganate modification probed as in Fig. 3a. Wild-type and mutant RNAPs differ in their patterns of reactivity in the absence of dMyx (top traces) but are nearly identical in the presence of 10 μM dMyx (bottom traces). Notably, β′Δ309–325 that removes the entire rudder loop (which is inserted in the same helix as switch-2, but is unlikely to interfere with the nucleic acids) has no effect on DNA melting, suggesting that a melting defect of a different rudder deletion[19] might be due to changes in the adjacent switch-2 instead.

introduce a sharp kink in the template strand[9,10] that may facilitate opening of the DNA duplex at the downstream edge, thereby finalizing the opening of the transcription bubble. Although the mechanisms of initiation of DNA melting are vastly different between bacterial and eukaryotic enzymes, the final (core-mediated) step of the DNA melting and the template strand loading into the active site is presumably fundamentally conserved, to give rise to essentially identical 'final' states observed in the structures of the active transcription complexes.

METHODS SUMMARY

dMyx was synthesized as described previously[4]. Crystallization of the complex was carried out under essentially the same conditions as for the apo-RNAP holoenzyme[18]. The structure was refined to a final R_{factor}/R_{free} of 0.240/0.270 at 2.7 Å resolution (Supplementary Fig. 2 and Supplementary Table 1). *Escherichia coli rpoB* and *rpoC* mutant vectors were constructed by side-directed mutagenesis and purified as described previously[18]. Footprinting analysis was performed using standard protocols[6,12]. See Methods for detailed experimental procedures.

Full Methods and any associated references are available in the online version of the paper at www.nature.com/nature.

Received 29 July; accepted 6 October 2008.
Published online 22 October 2008.

1. Brueckner, F. & Cramer, P. Structural basis of transcription inhibition by α-amanitin and implications for RNA polymerase II translocation. *Nature Struct. Mol. Biol.* **15,** 811–818 (2008).
2. Vassylyev, D. G. *et al.* Structural basis for substrate loading in bacterial RNA polymerase. *Nature* **448,** 163–168 (2007).
3. Irschik, H., Gerth, K., Hofle, G., Kohl, W. & Reichenbach, H. The myxopyronins, new inhibitors of bacterial RNA synthesis from *Myxococcus fulvus* (Myxobacterales). *J. Antibiot. (Tokyo)* **36,** 1651–1658 (1983).
4. Lira, R. *et al.* Syntheses of novel myxopyronin B analogs as potential inhibitors of bacterial RNA polymerase. *Bioorg. Med. Chem. Lett.* **17,** 6797–6800 (2007).
5. Paget, M. S. & Helmann, J. D. The σ^{70} family of sigma factors. *Genome Biol.* **4,** 203 (2003).
6. Artsimovitch, I., Kahmeyer-Gabbe, M. & Howe, M. M. Distortion in the spacer region of Pm during activation of middle transcription of phage Mu. *Proc. Natl Acad. Sci. USA* **93,** 9408–9413 (1996).
7. Chen, Y. F. & Helmann, J. D. DNA-melting at the *Bacillus subtilis* flagellin promoter nucleates near −10 and expands unidirectionally. *J. Mol. Biol.* **267,** 47–59 (1997).
8. Li, X. Y. & McClure, W. R. Stimulation of open complex formation by nicks and apurinic sites suggests a role for nucleation of DNA melting in *Escherichia coli* promoter function. *J. Biol. Chem.* **273,** 23558–23566 (1998).
9. Kettenberger, H., Armache, K. J. & Cramer, P. Complete RNA polymerase II elongation complex structure and its interactions with NTP and TFIIS. *Mol. Cell* **16,** 955–965 (2004).
10. Vassylyev, D. G., Vassylyeva, M. N., Perederina, A., Tahirov, T. H. & Artsimovitch, I. Structural basis for transcription elongation by bacterial RNA polymerase. *Nature* **448,** 157–162 (2007).
11. Murakami, K. S., Masuda, S., Campbell, E. A., Muzzin, O. & Darst, S. A. Structural basis of transcription initiation: an RNA polymerase holoenzyme–DNA complex. *Science* **296,** 1285–1290 (2002).
12. Craig, M. L. *et al.* DNA footprints of the two kinetically significant intermediates in formation of an RNA polymerase-promoter open complex: evidence that interactions with start site and downstream DNA induce sequential conformational changes in polymerase and DNA. *J. Mol. Biol.* **283,** 741–756 (1998).
13. Davis, C. A., Bingman, C. A., Landick, R., Record, M. T. Jr & Saecker, R. M. Real-time footprinting of DNA in the first kinetically significant intermediate in open complex formation by *Escherichia coli* RNA polymerase. *Proc. Natl Acad. Sci. USA* **104,** 7833–7838 (2007).
14. Suh, W.-C., Ross, W. & Record, M. T. Jr. Two open complexes and a requirement for Mg^{2+} to open the λ PR transcription start site. *Science* **259,** 358–361 (1993).
15. Severinov, K. & Darst, S. A. A mutant RNA polymerase that forms unusual open promoter complexes. *Proc. Natl Acad. Sci. USA* **94,** 13481–13486 (1997).
16. Cramer, P., Bushnell, D. A. & Kornberg, R. D. Structural basis of transcription: RNA polymerase II at 2.8 ångstrom resolution. *Science* **292,** 1863–1876 (2001).
17. Gnatt, A. L., Cramer, P., Fu, J., Bushnell, D. A. & Kornberg, R. D. Structural basis of transcription: an RNA polymerase II elongation complex at 3.3 Å resolution. *Science* **292,** 1876–1882 (2001).
18. Belogurov, G. A. *et al.* Structural basis for converting a general transcription factor into an operon-specific virulence regulator. *Mol. Cell* **26,** 117–129 (2007).
19. Kuznedelov, K., Korzheva, N., Mustaev, A. & Severinov, K. Structure-based analysis of RNA polymerase function: the largest subunit's rudder contributes critically to elongation complex stability and is not involved in the maintenance of RNA–DNA hybrid length. *EMBO J.* **21,** 1369–1378 (2002).

Supplementary Information is linked to the online version of the paper at www.nature.com/nature.

Acknowledgements We thank T. Townes for critical reading of the manuscript and R. Saecker for many stimulating discussions. Use of the Advanced Photon Source was supported by the US Department of Energy, Office of Energy Research under contract No. W-31-109-Eng-38. This work was supported by National Institutes of Health grants to I.A. and D.G.V.

Author Contributions J.R.A., A.X.X., R.L. and S.E.W. synthesized the antibiotic. G.A.B. constructed, purified and analysed the properties of mutationally altered RNAPs. M.N.V. performed crystallization. M.N.V. and S.K. carried out data collection and processing. A.S. performed footprinting analysis. I.A. carried out vector construction, performed biochemical assays, and supervised functional analysis of the dMyx mechanism. E.N. contributed to data analysis. D.G.V. has determined, refined, analysed the structure and supervised the project. D.G.V. and I.A. jointly wrote the manuscript.

Author Information The atomic coordinates and structure factors have been in deposited in the PDB under accession number 3EQL. Reprints and permissions information is available at www.nature.com/reprints. Correspondence and requests for materials should be addressed to I.A. (artsimovitch.1@osu.edu) or D.G.V. (dmitry@uab.edu).

METHODS

Structure determination and refinement. The *T. thermophilus* RNAP holoenzyme was purified and crystallized as described previously[20]. To obtain the complex crystals, the crystals of the apo-holoenzyme were transferred for 3 h into the drops containing collection buffer and 2 mM of dMyx[4]. The data were collected at beam line GM/CA-CAT (Advanced Photon Source, Argonne, USA). The crystals, although belonging to the same space group $P3_2$, had distinct unit cell parameters, $a = b = 235$ Å, $c = 255$ Å, as compared to the two previously studied *T. thermophilus* RNAP crystal forms; form I ($a = b = 236$ Å, $c = 250$ Å)[20–22] and form II ($a = b = 240$ Å, $c = 253$ Å)[23–25]. The data were processed using the HKL2000 data processing package (Supplementary Table 1)[26]. As for all previous holo-RNAP crystals, the crystals of the RNAP–dMyx complex were characterized by the perfect merohedral twinning coupled with the non-crystallographic symmetry[20]. Refinement, therefore, was carried out using the twinning option of the CNS program (Supplementary Table 1)[27]. The RNAP structure from the RNAP–Tgt complex (PDB accession 2BE5), from which the bridge helix (β′1067–1104) and the switch-2 segment (β′602–621) were omitted, was used as a starting model. Zonal scaling correction[10] substantially improved the initial R_{free} and the quality of the electron density. The $|2F_{obs} - F_{calc}|$ electron density map calculated after the rigid body and B-factor refinement steps revealed the undistorted bridge helix (characteristic of the crystal form II, see earlier), straightening of the switch-2 α-helix and a very clear electron density for dMyx. However, the unfolded C-terminal portion of the switch-2 (residues β′613–619) structure was represented by a fragmentary electron density that allowed for alternative interpretations. After several trials, using the reduced level of the electron density (~0.8σ, which was still above the noise) we were able to build a proper model that was characterized by a good, continuous electron density in the $|2F_{obs} - F_{calc}|$ electron density map for both the side- and main-chain atoms (note that all the previous partially wrong models did not improve the quality of the electron density in this region). After modelling of dMyx and switch-2 structures in the omit electron density, several rounds of the B-factor, positional, simulated annealing refinements and water 'pick' and water 'delete' procedures, alternating by manual model building using the program O[28] yielded a final R_{factor} of 24.0% and R_{free} of 27.0% for the RNAP–dMyx complex at 2.7 Å resolution (Supplementary Table 1). The final model was of high quality as shown by the simulated annealing omit electron density map calculated for dMyx and the switch-2 motif (Supplementary Fig. 1). Structural figures were prepared using programs Molscript[29], Bobscript[30] and Raster3D[31].

Isolation and assay of mutant *E. coli* RNAPs. Core wild-type and mutationally altered RNAPs were purified as described previously[18] except that the ionic strength was maintained at or above 0.2 M at all chromatographic steps. Overexpression plasmids for β′ R339A (pIA830), β E1279A (pIA870), β S1322E (pIA878), β′ G336A (pIA880), β′ F338A (pIA881), β′ K345A (pIA882), β′ Δ334-335 (pIA883), β′ K334A (pIA879), β′ Δ338–341 (pIA890) and β′ R337A (pGB055) were constructed by site-directed mutagenesis and the sequenced fragments were recloned into pVS10-based vectors[18]. Holoenzymes were reconstituted with the twofold molar excess of σ^{70}. For steady-state abortive initiation assays, holo RNAP (20 nM) in 16 μl of 20 mM Tris-acetate, 20 mM sodium acetate, 2 mM magnesium acetate, 5% glycerol, 1 mM dithiothreitol (DTT), 0.1 mM EDTA, pH 7.9, 1 μM σ^{70}, were supplemented with desired concentration of dMyx (2 μl) and incubated for 15 min at 37 °C. Transcription was initiated by adding linear T7A1 promoter template (100 nM), ApU (200 μM), CTP (25 μM) and 3 μCi [α^{32}P]-CTP (final reaction volume 20 μl). Reactions were allowed to proceed for 15 min at 37 °C and quenched by the addition of an equal volume of saturated urea in 90 mM Tris-borate, pH 8.3, 20 mM EDTA. Products were analysed on 7 M urea, 12% (w/v) acrylamide:bisacrylamide (19:1) denaturing gels and RNA quantities were determined from Phosphorimager scans of the gels. dMyx IC_{50} values for wild-type and variant RNAPs were determined by fitting concentration dependencies to hyperbolic function. The assay was repeated at least three times for each variant tested.

Footprinting analysis. A linear 153-bp DNA fragment containing λP_R promoter was made by PCR amplification using pIA226 (ref. 25) as a template with primers 17 (5′-CGTTAAATCTATCACCGCAAGGG) and 138 (5′-ATCGCCTGAAAGACTAGTCAGG). The top (non-template) DNA strand primer (number 17) was end-labelled with [^{32}P]-γATP (Perkin Elmer) and polynucleotide kinase (Epicentre) and purified using G-50 spin columns (GE Healthcare). PCR products were gel-purified using a kit (Promega). Sequencing reactions were performed using the same labelled primer with a SequiTherm kit (Epicentre). For DNaseI protection experiments, wild-type holo *E. coli* RNAP (400 nM) was preincubated with 1 μM of Myx or an equal volume of 50% ethanol for 15 min at 37 °C in GBB buffer (20 mM Tris-HCl, 14 mM $MgCl_2$, 20 mM NaCl, 5% glycerol, 1 mM DTT, 0.1 mM EDTA, pH 7.9) supplemented with 1 mM $CaCl_2$. A labelled λP_R promoter fragment was added (at 20 nM) and the reaction was incubated for a further 10 min. Samples were shifted to room temperature (22 °C) and treated with 0.002 U of DNaseI (Roche, 10 U μl^{-1}) for 1 min. The reaction was stopped by the addition of an equal volume of buffer containing 15 mM EDTA and 8 M urea. For potassium permanganate probing, holo RNAP (400 nM) was preincubated with 1 μM of myxopyronin or an equal volume of 50% ethanol, 0.5% dimethylsulphoxide for 15 min at 37 °C in GBB buffer without reducing agents. Labelled λP_R promoter fragment was added (at 20 nM), and the reaction was incubated for a further 10 min. Samples were shifted to room temperature and treated with $KMnO_4$ at a final concentration of 10 mM for 60 s. The reaction was stopped by the addition of 5× stop buffer (1.5 M sodium acetate, pH 5.2, 80 mM EDTA, 6 M β-mercaptoethanol), samples were subjected to phenol-chloroform extraction and precipitated with ethanol. The pellet was dissolved in 20 μl of water and incubated with 100 μl of 0.5 M piperidine at 95 °C for 20 min. After another round of ethanol precipitation, DNA was dissolved on 96% formamide. Samples were heated at 95 °C for 3 min and analysed on 7 M urea, 8% (w/v) acrylamide:bisacrylamide (19:1) denaturing gels.

20. Vassylyeva, M. N. *et al.* Purification, crystallization and initial crystallographic analysis of RNA polymerase holoenzyme from *Thermus thermophilus*. *Acta Crystallogr. D* **58,** 1497–1500 (2002).
21. Artsimovitch, I. *et al.* Structural basis for transcription regulation by alarmone ppGpp. *Cell* **117,** 299–310 (2004).
22. Vassylyev, D. G. *et al.* Crystal structure of a bacterial RNA polymerase holoenzyme at 2.6 Å resolution. *Nature* **417,** 712–719 (2002).
23. Artsimovitch, I. *et al.* Allosteric modulation of the RNA polymerase catalytic reaction is an essential component of transcription control by rifamycins. *Cell* **122,** 351–363 (2005).
24. Temiakov, D. *et al.* Structural basis of transcription inhibition by antibiotic streptolydigin. *Mol. Cell* **19,** 655–666 (2005).
25. Vassylyev, D. G. *et al.* Structural basis for transcription inhibition by tagetitoxin. *Nature Struct. Mol. Biol.* **12,** 1086–1093 (2005).
26. Otwinowski, Z. & Minor, W. Processing X-ray diffraction data collected in oscillation mode. *Methods Enzymol.* **276,** 307–326 (1997).
27. Brunger, A. T. *et al.* Crystallography & NMR system: A new software suite for macromolecular structure determination. *Acta Crystallogr. D* **54,** 905–921 (1998).
28. Jones, T. A., Zou, J. Y., Cowan, S. W. & Kjeldgaard, M. Improved methods for building protein models in electron density maps and the location of errors in these models. *Acta Crystallogr. A* **47,** 110–119 (1991).
29. Kraulis, P. J. MOLSCRIPT: a program to produce both detailed and schematic plots of protein structures. *J. Appl. Crystallogr.* **24,** 946–950 (1991).
30. Esnouf, R. M. Further additions to MolScript version 1.4, including reading and contouring of electron-density maps. *Acta Crystallogr. D* **55,** 938–940 (1999).
31. Merritt, E. A. & Bacon, D. J. Raster3D: photorealistic molecular graphics. *Methods Enzymol.* **277,** 505–524 (1997).

Vol 457|15 January 2009|doi:10.1038/nature07512

LETTERS

Dynamics of DNA replication loops reveal temporal control of lagging-strand synthesis

Samir M. Hamdan[1], Joseph J. Loparo[1], Masateru Takahashi[1], Charles C. Richardson[1] & Antoine M. van Oijen[1]

In all organisms, the protein machinery responsible for the replication of DNA, the replisome, is faced with a directionality problem. The antiparallel nature of duplex DNA permits the leading-strand polymerase to advance in a continuous fashion, but forces the lagging-strand polymerase to synthesize in the opposite direction. By extending RNA primers, the lagging-strand polymerase restarts at short intervals and produces Okazaki fragments[1,2]. At least in prokaryotic systems, this directionality problem is solved by the formation of a loop in the lagging strand of the replication fork to reorient the lagging-strand DNA polymerase so that it advances in parallel with the leading-strand polymerase. The replication loop grows and shrinks during each cycle of Okazaki fragment synthesis[3]. Here we use single-molecule techniques to visualize, in real time, the formation and release of replication loops by individual replisomes of bacteriophage T7 supporting coordinated DNA replication. Analysis of the distributions of loop sizes and lag times between loops reveals that initiation of primer synthesis and the completion of an Okazaki fragment each serve as a trigger for loop release. The presence of two triggers may represent a fail-safe mechanism ensuring the timely reset of the replisome after the synthesis of every Okazaki fragment.

The 'trombone model' as proposed in ref. 3 provides an elegant model for coupling many rounds of Okazaki fragment synthesis on the lagging strand of the replication fork to the continuous production of DNA on the leading strand. The looping back of the lagging strand onto the replisome allows both leading- and lagging-strand DNA polymerases to synthesize in the same direction and facilitates recycling of the lagging-strand DNA polymerase by virtue of its proximity to the RNA primers newly synthesized at the fork. The visualization of replication intermediates of the T4 and T7 bacteriophage replication systems by electron microscopy demonstrated the existence of replication loops and allowed a characterization of their length distributions[4,5]. Biochemical studies revealed a number of molecular scenarios that explain how formation and release of replication loops may be regulated[6–14]. However, no dynamic characterization has been reported and the timeline controlling the various enzymatic activities at the fork is not entirely understood.

In this study, we report the reconstitution of T7 replisomes and the observation of coordinated leading- and lagging-strand synthesis at the single-molecule level. The T7 replisome consists of only four proteins and it displays all the important features of more complicated replication systems[15] (Fig. 1a). These proteins are the T7 DNA polymerase, a 1:1 complex of T7 gene 5 protein (gp5) and *Escherichia coli* thioredoxin processivity factor, T7 gene 4 helicase–primase protein (gp4), and T7 gene 2.5 single-stranded DNA binding protein (gp2.5). In previous work, we used single-molecule techniques to study the activity of partially assembled replisome proteins mediating only leading-strand synthesis in both T7 and *E. coli*[16–18]. Here we describe the observation of T7 replication complexes undergoing coordinated leading- and lagging-strand synthesis, allowing for kinetic characterization of many rounds of replication loop formation and release. Replication is studied at the single-molecule level by monitoring the length of individual, tethered DNA molecules. Briefly, the lagging strand of a forked-duplex phage-λ DNA molecule (48.5 kilobases (kb) long) is attached by one end to the surface of a glass flow cell and the other end to a bead[19] (Fig. 1b; Supplementary Information). A laminar flow exerts a well-controlled drag force on the beads and stretches the DNA molecules. Figure 1c shows the length of an individual DNA molecule as a function of time in the flow of a buffer containing purified gp4, T7 DNA polymerase, gp2.5, Mg^{2+}, four deoxynucleoside 5′-triphosphates and the ribonucleotides adenosine triphosphate (ATP) and cytidine triphosphate (CTP) required for primase activity[13]. The single-molecule trajectories show repeated cycles of DNA shortening (Fig. 1c, blue arrow) followed by rapid lengthening to the original DNA length (Fig. 1c, red arrow).

In the presence of a saturating concentration of gp2.5, which is required to coordinate leading- and lagging-strand synthesis[13,20], single-stranded DNA (ssDNA) is equal in length to double-stranded DNA (dsDNA) (Supplementary Information). Because the bead is attached to the surface by the lagging strand, the formation of a replication loop in this strand will decrease the apparent DNA length by an amount equal to the DNA length stored in the loop. Several lines of evidence support the notion that the observed DNA shortening is a result of coupled DNA replication and loop formation. First, the loop length is comparable to that observed in electron microscopy studies. Figure 1d shows the wide distribution of loop lengths observed for 115 individual replisomes. This distribution can be described using a single-exponential distribution with a decay constant of 1.4 ± 0.1 kb, which is close to the average length of 2 kb obtained in previous electron microscopy studies[5].

The observation that inhibition of either the primase or DNA polymerase activity abrogates DNA shortening provides further confirmation that the observed events are related to coupled replication (Supplementary Information). Furthermore, the average rate of DNA shortening observed during loop growth (146 ± 50 bp s^{-1}; Fig. 1e) is nearly twice the rate observed for leading-strand polymerization alone under similar experimental conditions (80 bp s^{-1}) (Supplementary Information)[16], consistent with the notion that loop growth is supported by both leading- and lagging-strand synthesis with a net rate that contains the contributions of the two polymerases. Also, we observe multiple DNA shortening events (an average of 3 ± 2 loops per replication event, with 25% of replisomes displaying more than 4 loops; Supplementary Information) that occur in rapid succession on a small fraction of surface-tethered DNA molecules (5%). This pattern indicates the presence of stably assembled and processive replisomes, as opposed to the distributive activity of replication proteins leading to isolated looping events. Also, loop length and the number of successive loops formed per

[1]Department of Biological Chemistry and Molecular Pharmacology, Harvard Medical School, 240 Longwood Avenue, Boston, Massachusetts 02115, USA.

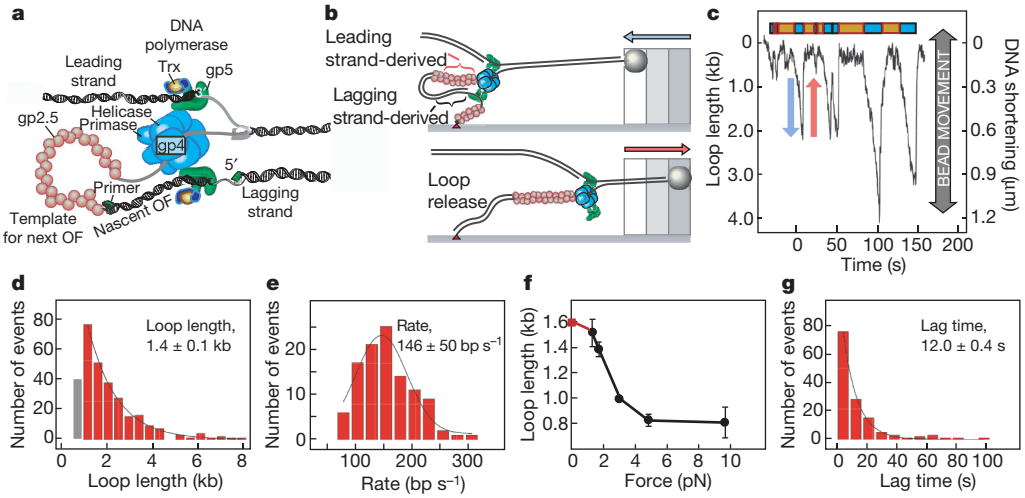

Figure 1 | Observation of replication loops. **a**, Organization of the T7 replication fork. Gene 4 protein (gp4) encircles the lagging strand and mediates both the unwinding of double-stranded DNA through its helicase domain and the synthesis of RNA primers through the primase domain. The T7 DNA polymerases are stably bound to gp4 and incorporate nucleotides on the leading and lagging strands. The DNA polymerase is a 1:1 complex of the T7 gene 5 protein (gp5) and *E. coli* thioredoxin (trx). The ssDNA extruded behind the helicase is coated by the ssDNA-binding protein gp2.5. A replication loop is formed in the lagging strand to allow the polymerase to synthesize in the same direction. The lagging-strand DNA polymerase initiates the replication of Okazaki fragments (OFs) using RNA primers synthesized by the primase domain of gp4. **b**, Depiction of the overall length change of tethered DNA as a result of replication loop formation and release. The blue and red arrows correspond to shortening and lengthening of the DNA; see **c**. **c**, Change over time of the length of a single DNA molecule during replication (see Supplementary Information for more examples). The loop growth and lag phases are shown as cyan and orange boxes, respectively. **d**, Histogram of the replication loop length (bars; $n = 288$) fitted with a single-exponential decay (solid line). The grey bar represents loop lengths below 1 kb, which are under sampled owing to noise in the length measurements. These loops were not included in the fitting of loop size distributions. **e**, Histogram of rate of loop growth (bars; $n = 107$) fitted with a normal distribution (solid line). The rate of loop growth is determined from the slope of the DNA shortening phase. **f**, Dependence of replication loop length on stretching force ($n = 108, 288, 158, 64, 26$ at forces of 1.4, 1.7, 3.0, 4.8 and 9.5 pN, respectively). The replication loop length at zero force (red square) is derived from the Okazaki fragment length as measured in bulk-phase experiments (Supplementary Information). **g**, Histogram of lag times (bars; $n = 135$) fitted with a single-exponential decay (solid line). All reported mean values are obtained using the maximum-likelihood-estimation method. Uncertainties (**d**, **e**, **g**) and error bars (**f**) correspond to the standard deviation of the distribution (**e**) or to the error of fitting the loop length (**d**, **f**) and lag time (**g**) distributions with exponential decay functions.

replisome are reduced by increasing force (Fig. 1f). This observation is consistent with the prediction that the applied force will be exerted directly on the protein interactions that hold the loop together.

Finally, fluorescence time-lapse microscopy on individual, replicating DNA molecules demonstrates that DNA is synthesized on both the leading and the lagging strand (Fig. 2). In these experiments, λ DNA templates were stained with a fluorescent, dsDNA-specific dye and the fluorescent DNA was imaged while flow-stretched and replicated by the T7 replisome. The growth of a leading-strand product, its continuous movement along DNA, and the double-stranded nature of the lagging-strand product demonstrate that both leading and lagging strands are being replicated. Further confirmation of the presence of both leading- and lagging-strand synthesis is obtained by a bulk-phase analysis of replication products obtained under conditions identical to those used in the single-molecule experiments (Supplementary Information). The length of Okazaki fragments (0.8 kb) corresponds well with half of the mean loop length as measured in the single-molecule experiments (0.5×1.4 kb $= 0.7$ kb), in agreement with the fact that half of the replication loop consists of the nascent Okazaki fragment produced by the lagging-strand DNA polymerase and the other half consists of ssDNA extruded by the helicase[5].

Observation of replication loop formation and release provides us with kinetic information that is inaccessible using bulk-phase assays. The stochastic and sequential nature of the many enzymatic processes involved causes the synchronicity of a population of reactions to be lost quickly and will obscure kinetic information about the short-lived, intermediate steps. Our single-molecule experiments reveal the presence of lag times between the release of one replication loop and formation of the next, a step unobservable in bulk-phase assays. The distribution of the lag times follows a single-exponential dependence with a decay constant of 12.0 ± 0.4 s (Fig. 1g). The

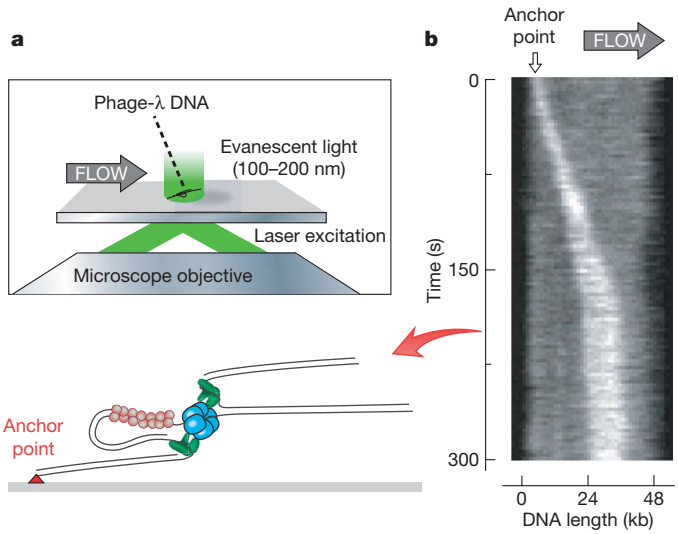

Figure 2 | Fluorescence imaging of coordinated DNA replication. **a**, The experimental design. Individual DNA molecules are fluorescence-stained by means of intercalating dye, stretched by flow and imaged through total-internal-reflection fluorescence (TIRF) microscopy. As the replication reaction proceeds, the leading-strand product will grow and be flow-stretched along the parental DNA. **b**, Kymograph of an individual DNA molecule undergoing coordinated replication (see Supplementary Movie). The grey scale indicates the fluorescence intensity. The intensity is doubled where the leading strand overlaps the parental strand. Growth of the leading strand and its movement along the DNA indicate processive replication. The double-stranded nature of the DNA between anchor point and leading strand indicate synthesis at the lagging strand.

appearance of a lag time after replication loop release suggests the requirement for intermediate steps before the formation of a new replication loop. At least three steps are necessary for a loop to be formed: the recognition by the primase of a priming site in the lagging strand, the synthesis of a primer and its handover to the lagging-strand DNA polymerase. The importance of primer synthesis in regulating the timing of the events at the replication fork is clear from several studies that found an effect of primase activity on the size of Okazaki fragments in T7, T4 and *E. coli* replisomes[10,12,13]. However, the timing of primer synthesis and its causal relation with loop release has not been established.

By changing the concentration and nature of the ribonucleotides required by the primase, we can modulate the observed loop dynamics and extract a timeline of enzymatic events during the replication cycle. T7 DNA primase recognizes four sequences, namely 5′-GGGTC-3′, 5′-TGGTC-3′, 5′-GTGTC-3′ and 5′-TTGTC-3′, and requires only ATP and CTP to synthesize primers (5′-ACCC-3′, 5′-ACCA-3′, 5′-ACAC-3′ and 5′-ACAA-3′) complementary to the four nucleotides at the 5′ end of the recognition sequence[21]. Reducing the ATP and CTP concentrations from the optimal 300 μM to 30 and 10 μM, respectively, shows an increase in loop length from 1.4 ± 0.1 kb to 3.6 ± 0.5 kb (Fig. 3). The lag time between loops also increases significantly, from 12.0 ± 0.4 s to 28.6 ± 2.8 s (Fig. 3). The observation that changing the kinetics of primer synthesis alters the loop lengths as well as the length of the lag times led us to consider how the different steps in primer synthesis have a role in the timing of the events that lead to both loop release and loop formation. Primer synthesis takes place in two distinct steps[22–24]. First, the primase condenses ATP and CTP to form pppAC, the triphosphate diribonucleotide that is present as the starting nucleotide pair in all four possible primers. Subsequently, pppAC is extended in a much slower step to a full-length, tetraribonucleotide primer in a sequence-dependent manner[22–24]. T7 DNA primase can utilize pAC, the monophosphate AC diribonucleotide, and extend it efficiently using only ATP and CTP[23]. Therefore, by providing the coupled replication reaction with a pre-made pAC, we can bypass the requirement of the condensation step. At low ATP (30 μM) and CTP (10 μM) concentrations, the presence of 300 μM pAC nearly restored the loop length to that observed at optimal ATP and CTP concentrations (Fig. 3). The lag time, however, remains unaffected by the presence of pAC. These results demonstrate that the first step in primer synthesis, condensation of ATP and CTP to form pppAC, triggers loop release. As a consequence, the lag time has to include the slow extension step of pppAC to a full tetraribonucleotide.

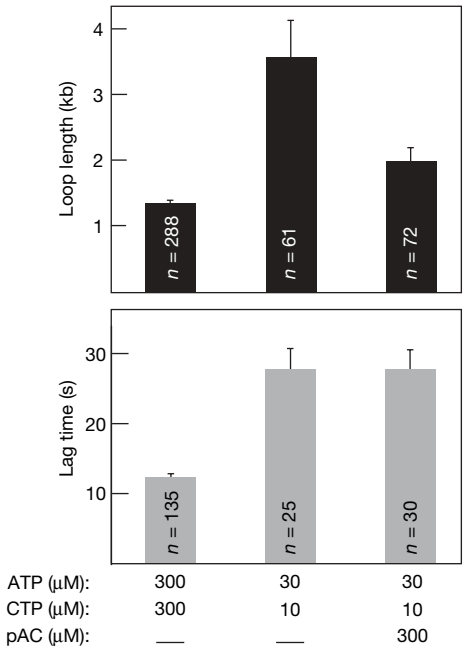

Figure 3 | Replication loop dynamics depend on primase activity. Loop growth and lag times are compared for different concentrations of ribonucleotides. Replication loop lengths and lag times were determined as described in Fig. 1.

Our observation that replication loop length is determined by primer synthesis and previously reported dependencies of Okazaki fragment length on primase activity[10,12,13] suggests a signalling mechanism by which the primase controls the timing of the cycle of enzymatic events at the fork. The observation that the average Okazaki fragment length as observed in the bulk phase does not decrease on introduction of pAC (Supplementary Information) demonstrates that pAC triggers loop release before the nascent Okazaki fragment is completed, explaining previous observations of ssDNA gaps in electron microscopy and bulk-phase assays[10,11]. Primer synthesis and loop release before completion of the Okazaki fragment will result in a length decrease of the ssDNA template available for the next Okazaki fragment. Consequently, a gradual decrease in replication loop length is predicted as the replisome progresses. However, a length comparison between subsequent replication loops formed by individual replisomes suggests no apparent trend in loop size (mean length difference is 0.17 ± 0.3 kb).

In an alternative model, the encounter of the lagging-strand DNA polymerase with the 5′ terminus of the previously synthesized Okazaki fragment triggers dissociation of the polymerase and subsequent loop release[6–9]. In this collision model, leading-strand synthesis needs to continue after loop release to allow the primase to search for its recognition sequence. In this case, the size of the subsequent Okazaki fragment is expected to increase by the extra amount of ssDNA generated during the primase search. Therefore, the collision model predicts a gradual increase in Okazaki fragment size as the replisome progresses. To address the possibility that both signalling and collision models are operative, preventing a net change in loop length, we test a number of predictions for the behaviour of the lag times between loops in the two different mechanisms. In both mechanisms, the lag time will contain the primer extension step and handover of the primer to the lagging-strand DNA polymerase. In the collision mechanism, however, the lag time will also include additional leading-strand synthesis mediating the search of the primase for a priming sequence. A lack of length contrast between ssDNA and dsDNA prevents us from directly observing leading-strand synthesis during the lag phase. Because further leading-strand synthesis will give rise to a lengthening of the Okazaki fragment produced during the next cycle and collision-mediated loop release requires completion of the fragment, we predict a positive correlation between the lag time and the increase in loop length. Similarly, we predict no correlation between lag time and loop length change in the case of a signalling mechanism. Inefficient primer utilization and a subsequent increase in single-stranded DNA template size may result in an increase in Okazaki fragment size, but loop release will still be triggered by the stochastic condensation of ATP and CTP and will remain uncorrelated with lag time.

To test the presence of both signalling and collision mechanisms, we divide all observed loop pairs into two categories, solely on the basis of whether the second loop of a pair is longer or shorter than the first loop of the pair, and determine the correlation between lag time and loop length change for each of the two groups. We see a correlation between lag time and loop length change in the data set that showed loop growth ($r = 0.55$, $n = 50$; the probability that a similarly sized data set of two uncorrelated variables would produce this correlation coefficient is less than 0.05%), but not in the group of loop pairs that showed a decrease in length ($r = -0.05$, $n = 49$) (Fig. 4). A slightly longer lag time between loop pairs that showed a length increase (collision controlled; 13.3 ± 1.5 s) and pairs that showed a length reduction (signalling controlled; 11.2 ± 0.8 s) lends further support to the notion that after collision-mediated release, extra leading-strand synthesis is required

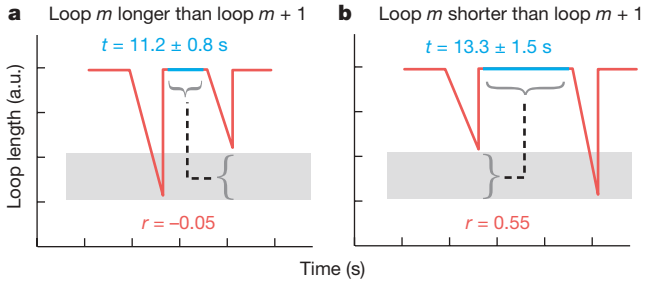

Figure 4 | Signalling and collision mechanisms both serve to trigger loop release. a, Correlation ($r = -0.05$, $n = 49$) between the lag time and the size change of the second loop for the pairs of loops in which loop $m + 1$ is smaller than loop m. **b**, Correlation ($r = 0.55$, $n = 50$) between the lag time and the size change of the second loop for the pairs of loops in which loop $m + 1$ is larger than loop m. a.u., arbitrary units.

to facilitate the search for a primer site. Additionally, experiments done under conditions that disfavour the collision mechanism by increasing the Okazaki fragment size while maintaining the pAC synthesis kinetics as a loop release signal result in the absence of any correlation between lag time and loop length (Supplementary Information). Taken together, these results suggest that the signalling and collision mechanisms are both operative during coupled replication.

In previous single-molecule studies, we have demonstrated that primase search is a stochastic process, with there being a limited probability of the primase recognizing and using a priming sequence during its scan of the lagging strand[16]. The random nature of primase activity poses a fundamental challenge to coordinating the timing of primer synthesis with the release of the replication loop. The utilization of both the signalling mechanism and the collision mechanism to release a replication loop and initiate formation of a new one provides an elegant mechanism that allows the replisome to cope with the stochastic nature of the primase activity. The signalling mechanism will release the replication loop if the primase locates one of its sequences before the nascent Okazaki fragment is finished. On the other hand, if the nascent Okazaki fragment is finished without the primase having engaged a recognition sequence, then the collision mechanism acts as a fail-safe mechanism to trigger loop release and ensure that the cycle of enzymatic events at the replication fork is properly reset.

METHODS SUMMARY

Single-molecule DNA stretching. A biotinylated fork was introduced at one end of phage-λ DNA to attach it to the streptavidin-coated glass surface of a flow cell. The other DNA end was functionalized with a digoxigenin moiety to couple it to a 2.8-μm-diameter anti-digoxigenin-coated bead[16]. A laminar flow was introduced to exert a well-defined drag force on the bead, resulting in a stretching of the DNA molecules. Coordinated DNA synthesis was carried out in a flow of purified gp4 helicase–primase[25], T7 DNA polymerase[26], gp2.5[27] and nucleotides. Beads were imaged onto a charge-coupled device using dark-field microscopy and their positions tracked using particle-tracking software. For a detailed description, see Methods and Supplementary Information.

Fluorescence imaging. DNA was tethered at the forked end to functionalized coverslips as described above, but beads were omitted. In the presence of dsDNA-specific stain, the hydrodynamically stretched DNA was imaged using through-objective TIRF microscopy (Methods and Supplementary Information).

Full Methods and any associated references are available in the online version of the paper at www.nature.com/nature.

Received 16 April; accepted 3 October 2008.
Published online 23 November 2008.

1. Benkovic, S. J., Valentine, A. M. & Salinas, F. Replisome-mediated DNA replication. *Annu. Rev. Biochem.* **70,** 181–208 (2001).
2. Johnson, A. & O'Donnell, M. Cellular DNA replicases: components and dynamics at the replication fork. *Annu. Rev. Biochem.* **74,** 283–315 (2005).
3. Alberts, B. M. *et al.* Studies on DNA replication in the bacteriophage T4 in vitro system. *Cold Spring Harb. Symp. Quant. Biol.* **47,** 655–668 (1983).
4. Chastain, P. D., Makhov, A. M., Nossal, N. G. & Griffith, J. D. Analysis of the Okazaki fragment distributions along single long DNAs replicated by the bacteriophage T4 proteins. *Mol. Cell* **6,** 803–814 (2000).
5. Park, K., Debyser, Z., Tabor, S., Richardson, C. C. & Griffith, J. D. Formation of a DNA loop at the replication fork generated by bacteriophage T7 replication proteins. *J. Biol. Chem.* **273,** 5260–5270 (1998).
6. Carver, T. E., Sexton, D. J. & Benkovic, S. J. Dissociation of bacteriophage T4 DNA polymerase and its processivity clamp after completion of Okazaki fragment synthesis. *Biochemistry* **36,** 14409–14417 (1997).
7. López de Saro, F. J., Georgescu, R. E. & O'Donnell, M. A peptide switch regulates DNA polymerase processivity. *Proc. Natl Acad. Sci. USA* **100,** 14689–14694 (2003).
8. Hacker, K. J. & Alberts, B. M. The rapid dissociation of the T4 DNA-polymerase holoenzyme when stopped by a DNA hairpin helix: a model for polymerase release following the termination of each Okazaki fragment. *J. Biol. Chem.* **269,** 24221–24228 (1994).
9. Li, X. & Marians, K. J. Two distinct triggers for cycling of the lagging strand polymerase at the replication fork. *J. Biol. Chem.* **275,** 34757–34765 (2000).
10. Yang, J., Nelson, S. W. & Benkovic, S. J. The control mechanism for lagging strand polymerase recycling during bacteriophage T4 DNA replication. *Mol. Cell* **21,** 153–164 (2006).
11. Nossal, N. G., Makhov, A. M., Chastain, P. D., Jones, C. E. & Griffith, J. D. Architecture of the bacteriophage T4 replication complex revealed with nanoscale biopointers. *J. Biol. Chem.* **282,** 1098–1108 (2007).
12. Wu, C. A., Zechner, E. L., Reems, J. A., McHenry, C. S. & Marians, K. J. Coordinated leading-strand and lagging-strand synthesis at the *Escherichia coli* DNA-replication fork: primase action regulates the cycle of Okazaki fragment synthesis. *J. Biol. Chem.* **267,** 4074–4083 (1992).
13. Lee, J., Chastain, P. D., Griffith, J. D. & Richardson, C. C. Lagging strand synthesis in coordinated DNA synthesis by bacteriophage T7 replication proteins. *J. Mol. Biol.* **316,** 19–34 (2002).
14. Tougu, K. & Marians, K. J. The interaction between helicase and primase sets the replication fork clock. *J. Biol. Chem.* **271,** 21398–21405 (1996).
15. Richardson, C. C. Bacteriophage T7: minimal requirements for the replication of a duplex DNA molecule. *Cell* **33,** 315–317 (1983).
16. Lee, J. B. *et al.* DNA primase acts as a molecular brake in DNA replication. *Nature* **439,** 621–624 (2006).
17. Tanner, N. A. *et al.* Single-molecule studies of fork dynamics in *Escherichia coli* DNA replication. *Nature Struct. Mol. Biol.* **15,** 170–176 (2008).
18. Hamdan, S. M. *et al.* Dynamic DNA helicase-DNA polymerase interactions assure processive replication fork movement. *Mol. Cell* **27,** 539–549 (2007).
19. van Oijen, A. M. *et al.* Single-molecule kinetics of lambda exonuclease reveal base dependence and dynamic disorder. *Science* **301,** 1235–1238 (2003).
20. Lee, J., Chastain, P. D., Kusakabe, T., Griffith, J. D. & Richardson, C. C. Coordinated leading and lagging strand DNA synthesis on a minicircular template. *Mol. Cell* **1,** 1001–1010 (1998).
21. Frick, D. N. & Richardson, C. C. DNA primases. *Annu. Rev. Biochem.* **70,** 39–80 (2001).
22. Qimron, U., Lee, S. J., Hamdan, S. M. & Richardson, C. C. Primer initiation and extension by T7 DNA primase. *EMBO J.* **25,** 2199–2208 (2006).
23. Kusakabe, T. & Richardson, C. C. Gene 4 DNA primase of bacteriophage T7 mediates the annealing and extension of ribo-oligonucleotides at primase recognition sites. *J. Biol. Chem.* **272,** 12446–12453 (1997).
24. Frick, D. N., Kumar, S. & Richardson, C. C. Interaction of ribonucleoside triphosphates with the gene 4 primase of bacteriophage T7. *J. Biol. Chem.* **274,** 35899–35907 (1999).
25. Notarnicola, S. M., Mulcahy, H. L., Lee, J. & Richardson, C. C. The acidic carboxyl terminus of the bacteriophage T7 gene 4 helicase/primase interacts with T7 DNA polymerase. *J. Biol. Chem.* **272,** 18425–18433 (1997).
26. Tabor, S., Huber, H. E. & Richardson, C. C. *Escherichia coli* thioredoxin confers processivity on the DNA polymerase activity of the gene 5 protein of bacteriophage T7. *J. Biol. Chem.* **262,** 16212–16223 (1987).
27. Hyland, E. M., Rezende, L. F. & Richardson, C. C. The DNA binding domain of the gene 2.5 single-stranded DNA-binding protein of bacteriophage T7. *J. Biol. Chem.* **278,** 7247–7256 (2003).

Supplementary Information is linked to the online version of the paper at www.nature.com/nature.

Acknowledgements We thank J.-B. Lee for technical advice and S. Moskowitz for illustrations. This work was supported by the National Institutes of Health (grants GM-077248 to A.M.v.O. and GM-54397 to C.C.R.) and the National Science Foundation (CAREER grant 0543784 to A.M.v.O.). J.J.L. acknowledges the Jane Coffin Childs Memorial Fund for a postdoctoral fellowship.

Author Contributions S.M.H. performed the single-molecule bead experiments; S.M.H. and J.J.L. performed the single-molecule fluorescence experiments; S.M.H. and M.T. performed the bulk-phase experiments; S.M.H., C.C.R. and A.M.v.O. designed the experiments, analysed the data and wrote the manuscript.

Author Information Reprints and permissions information is available at www.nature.com/reprints. Correspondence and requests for materials should be addressed to A.M.v.O. (antoine_van_oijen@hms.harvard.edu).

METHODS

Single-molecule stretching and length measurements. Phage-λ DNA molecules were annealed and ligated to modified oligonucleotides to introduce a biotinylated fork on one end of the DNA and a digoxigenin moiety on the other end. The resulting DNA molecules were attached, by the 5′ terminus of the bifurcated end, to the streptavidin-coated glass surface of a flow cell and, by the 3′ end of the same strand, to a 2.8-μm-diameter anti-digoxigenin-coated paramagnetic bead (Dynal) (Supplementary Information). To prevent non-specific interactions between the beads and the surface, a 1-pN upward magnetic force was applied on the bead by positioning a permanent magnet above the flow cell. Beads were imaged with a charge-coupled-device camera at a time resolution of 500 ms and their positions were determined by particle-tracking software (Semasopht). Coordinated DNA synthesis in the flow cell was carried out by flowing gp4 helicase–primase (10 nM hexamers), T7 DNA polymerase (a purified 1:1 complex of gp5 and thioredoxin, 80 nM), and gp2.5 (750 nM) in buffer A (40 mM Tris–HCl (pH 7.5), 10 mM $MgCl_2$, 10 mM DTT, 50 mM potassium glutamate (pH 7.5), 0.1 mg-ml^{-1} BSA), 600 μM dATP, 600 μM dCTP, 600 μM dGTP, 600 μM dTTP, 300 μM ATP and 300 μM CTP. Traces were corrected for instabilities in the flow by subtracting traces corresponding to tethers that were not enzymatically altered. Brownian motion and residual fluctuations resulted in a 300-bp error in DNA length measurement.

Fluorescence imaging. DNA was tethered at the forked end to functionalized coverslips as described above, but beads were omitted. Instead, the hydrodynamic drag on the DNA itself was used to extend the molecule. In the presence of 100 nM Sytox Orange dsDNA-specific stain (Invitrogen), the stretched DNA was imaged using through-objective TIRF microscopy (Olympus IX-71; ×60, 1.45 numerical aperture). A continuous-wave 532-nm diode laser (CrystaLaser) was used to excite stain at power densities sufficiently low to minimize photo-induced cleavage of stained DNA over the timescale of an experiment. Protein and nucleotide concentrations were identical to those used to replicate the bead-tethered DNA molecules (see above). Single-molecule bead-tethering assays demonstrated that the kinetics of leading-strand synthesis and coordinated replication were not influenced by the presence of the stain (Supplementary Information).

CORRIGENDUM

doi:10.1038/nature07628

Microfibre–nanowire hybrid structure for energy scavenging

Yong Qin, Xudong Wang & Zhong Lin Wang

Nature 451, 809–813 (2008)

It has been drawn to our attention that an error was made in calculating the output power of our fibre nanogenerator. The correct output power density of the fabric is expected to be 4–16 mW per square metre rather than 20–80 mW per square metre as originally claimed. This correction does not affect the main conclusions of our paper.

naturejobs

THE CAREERS MAGAZINE FOR SCIENTISTS

A new job site called CareerCast.com recently ranked the top 200 professions in the United States. Interestingly, mathematician took first prize, and biologist came fourth. In fact, several science-related professions scored quite well. Statistician was third, physicist thirteenth, meteorologist ranked fifteenth and astronomer twentieth. But the list did not consider job satisfaction or experience needed, which might unfairly skew its results.

The site used five core criteria to draw up its list: environment, income, outlook, physical demands and stress. Yet none of these looked at what it takes to become a 'biologist' — the many years of hard work, schooling, stress and intense competition. If the entire career path were taken into account, some jobs could lose their lustre.

Perhaps more significant was a bias towards desk jobs. Consider some of the worst-ranked professions. At number 200 was lumberjack, seaman ranked 197 and ambulance workers (emergency medical technicians) 196. The rankings tend to classify these jobs as unsafe or arduous; but arduous can be a good thing.

Under environment, for example, one of the criteria scored was 'physical components'. And the stress criteria included 'hazards encountered', 'initiative required' and 'stamina required'. The more points a job received, the worse its rank. This could be misleading. Emergency medical technicians might find their job tremendously rewarding, despite the stress. The same goes for less highly ranked field scientists who might have more taxing daily duties. The pages of *Naturejobs* include many examples of research and postdoc positions that push scientists' physical as well as mental capacities (see, for example, *Nature* **446,** 226–228; 2007).

Rankings such as these are intriguing, but not bias-free. Ideally, they should relate their results to a survey on job satisfaction. After all, the best jobs are the most satisfying, not necessarily those with the lowest stress. Mathematicians may be expected to have good jobs, but are they happy? Lumberjacks are paid little and encounter danger on a daily basis. But, as they dodge falling trees amid the dense aroma of cedar, are they really that miserable?

Gene Russo is editor of *Naturejobs*.

CONTACTS
Editor: Gene Russo
Assistant editor: Karen Kaplan
e-mail: naturejobseditor@naturedc.com

European Head Office, London
The Macmillan Building,
4 Crinan Street, London N1 9XW, UK
Tel: +44 (0) 20 7843 4961
Fax: +44 (0) 20 7843 4996
e-mail: naturejobs@nature.com

European Sales Manager:
Dan Churchward (4966)
e-mail: d.churchward@nature.com
Assistant European Manager:
Nils Moeller (4953)
***Nature*events:**
Ghizlaine Ababou (+44 (0) 20 7014 4015)
e-mail: g.ababou@nature.com
Southwest UK/RoW:
Alexander Ranken (4944)

Northeast UK/Ireland:
Matthew Ward (+44 (0) 20 7014 4059)
France/Switzerland/Belgium:
Muriel Lestringuez (4994)
Scandinavia/Spain/Portugal/Italy:
Evelina Rubio-Hakansson (4973)
North Germany/The Netherlands/Eastern Europe: Kerstin Vincze (4970)
South Germany/Austria:
Hildi Rowland (+44 (0) 20 7014 4084)
Advertising Production Manager:
Stephen Russell
To send materials use London address above.
Tel: +44 (0) 20 7843 4816
Fax: +44 (0) 20 7843 4996
e-mail: naturejobs@nature.com
***Naturejobs* web development:** Tom Hancock
***Naturejobs* online production:** Dennis Chu

US Head Office, New York
75 Varick Street, 9th Floor,
New York, NY 10013-1917
Tel: +1 800 989 7718
Fax: +1 800 989 7103
e-mail: naturejobs@natureny.com
US Sales Manager: Ken Finnegan

India
Vikas Chawla (+91 1242881057)
e-mail: v.chawla@nature.com

Japan Head Office, Tokyo
Chiyoda Building, 2-37 Ichigayatamachi,
Shinjuku-ku, Tokyo 162-0843
Tel: +81 3 3267 8751
Fax: +81 3 3267 8746

Asia-Pacific Sales Manager:
Ayako Watanabe (+81 3 3267 8765)
e-mail: a.watanabe@natureasia.com
Business Development Manager, Greater China/Singapore:
Gloria To (+852 2811 7191)
e-mail: g.to@natureasia.com

FEAR FACTOR

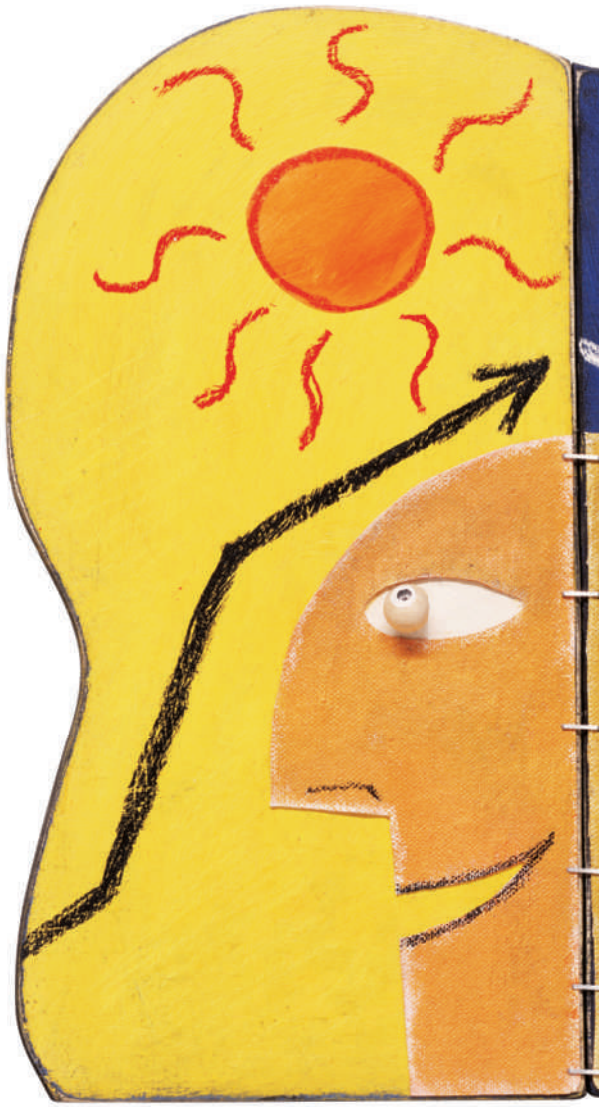

RECESSION WATCH

Job prospects are looking gloomy as the economic downturn runs its course, but there are bright spots for some. **Genevive Bjorn** reports on ways to shelter from the storm.

As if years of shrinking budgets hadn't created a competitive enough postdoctoral job market in many fields and sectors, the worldwide economic downturn is now making some difficult-to-navigate career paths downright treacherous. Although hard data are yet to emerge, anecdotal evidence suggests that the slowdown has stymied the efforts of many postdoctoral jobseekers.

"The situation has changed so dramatically, so quickly, that it is difficult to know how to react," says Marc Kastner, dean of the school of science at the Massachusetts Institute of Technology (MIT) in Cambridge. He says he is "very concerned" about the prospects for young scientists.

Many prospective employers had placed adverts and received applications before the crunch. But as hiring freezes and suspended candidate searches become more common worldwide, fewer jobs will be filled than initially planned, predicts Roger Davies, chairman of the physics department at the University of Oxford, UK. "We won't know the numbers until the jobs are filled in the first four months of the year," he says.

The finances of US universities have taken a big hit (see 'Universities struggle as value of endowments falls' *Nature* **457,** 11–12; 2009). MIT is making 5% spending cuts, but some US universities are taking more drastic steps. In December, Harvard University announced a hiring freeze, and others have followed suit.

Kevin Covey, a third-year Spitzer fellow at Harvard's Center for Astrophysics in Cambridge, Massachusetts, recently applied for a junior faculty position at Johns Hopkins University in Baltimore, Maryland. "About an hour after I sent in the application, the job was cancelled," he says. He is now applying for about a dozen other faculty and postdoc positions.

Public funding not guaranteed

Universities in Europe have so far avoided a freeze on recruitment, largely because most are publicly funded and don't rely on interest payments from large endowments to cover operating costs. Still, cuts may be coming as government revenues decline. And even before the economic slowdown, notes Davies, the UK Engineering and Physical Sciences Research Council had planned to reduce its grants portfolio for physics from £137 million (US$206 million) for 2006–2007 to £97 million for 2008–2009.

"I'm using a blanket strategy of applying for every suitable post in the United Kingdom, which amounts to only half a dozen openings," says Daniel Mortlock, an astrophysics postdoc at Imperial College London.

Publicly funded research institutions have reason to be wary. The Gemini Observatory in Hilo, Hawaii, recently suspended searches for two postdoc positions, even though its 2009 budget — which funded those positions — was approved in November. Gemini is supported by a consortium of Argentina, Australia, Brazil, Britain, Canada, Chile and the United States.

Seekers: Daniel Mortlock (top) and Maja Zavaljevski.

Its administrators are worried that the promised funding may not come through. "This is absolutely related to the current economic turmoil," says deputy director Jean-René Roy. "Government revenues are falling in various countries, and shortfalls roll down to funding for scientific research." He adds that Gemini has resumed one search and still hopes to be able to fill both positions.

There are striking exceptions to the belt-tightening, however. The European Space Agency (ESA) received strong support from European ministers during a 25–26 November meeting in The Hague. They agreed to spend €9.9 billion (US$13.5 billion) on space-science projects for 2009–2013, thus stabilizing ESA's workforce (see 'Space agency funding defies downturn' *Nature* **456,** 552; 2008). "ESA does not see a reason to deviate from the human-resources policy that it applied before the global economic crisis," says Andreas Diekman, head of ESA's office in Washington DC.

New careers, new competition

Mortlock says he may soon face the reality of having to leave astrophysics research for another field of science, or even of leaving science altogether. However, Clare Jones, a careers adviser for postgraduates in the career development centre at the University of Nottingham, UK, warns that this is not the best time to attempt a complete switch into another field.

IMAGES.COM/CORBIS

Although non-traditional career paths have promise, science PhDs and postdocs may find themselves competing with more and more jobseekers who have MBAs and master's degrees. According to the US Bureau of Labor Statistics, the unemployment rate for advanced-degree holders jumped to 3.1% in November from 2.5% in September; overall unemployment in the United States stands at 6.7% of the workforce.

Professional, scientific and technical services (the category that includes science PhDs employed as consultants, managers and researchers) took a hard hit in October and November, losing 15,727 jobs. Along with the collapse of financial services and layoffs in the drug and biotech industries, this means postdocs are now competing with seasoned insiders for fewer jobs.

N. WALKER/UNIV. NOTTINGHAM

Advisers: Clare Jones (top) and Ryan Wheeler.

One postdoc in virology (who asked to remain anonymous) applied for some 100 consulting jobs early last autumn. "Where I did get interviews, I was interviewing alongside MBAs from Chicago who had just been laid off from Bear Stearns," he says. "It's hard enough for science PhDs to break into consulting, let alone compete with seasoned investment bankers." But his persistence eventually paid off, as he recently received a job offer.

Maja Zavaljevski, a postdoc in haematology at the University of Washington in Seattle, has been dismayed by her biotech job search. "I'm competing with experienced industry PhDs who've been recently laid off," she says. US chemical manufacturing, a category that includes the drug industry, employed 851,000 in November 2008, down from 860,500 people a year earlier.

Unexpected opportunities

Jones says many of her clients are nervous and discouraged. She advocates 'creative job searching'. For example, seek tips from former colleagues who have moved into industry and might spot an opening in the company before it is posted. Jones also recommends seeking possible moves within one's own institution, for example looking into scientific management, business development or careers advising.

Academics have other options, according to Matthias Haury, coordinating manager of the European Molecular Biology Laboratory's International Centre for Advanced Training in Heidelberg, Germany. Many companies in Europe, he says, still need qualified scientists to work as consultants, because so many academics disdain positions other than 'pure research'.

One result of the economic crunch could simply be longer job-search times, notes Ryan Wheeler, manager of the postdoctoral services office at the Scripps Research Institute in La Jolla, California. He suspects that most postdocs will weather the storm relatively unharmed by staying in their current jobs or negotiating postdoc extensions. Indeed, unemployment rates among scientists remain low compared with many professions (see *Nature* **452,** 777; 2008). Wheeler suggests using any extra downtime to scrutinize one's skills, interests and values, perhaps through coaching or mentoring (see 'Personal postdoc coaching'). "The whole process," says Wheeler, "is less daunting if you have a better idea of what's important to you in a job." ■

Genevive Bjorn is a freelance writer in Maui, Hawaii.

PERSONAL POSTDOC COACHING

Anxious postdoc jobseekers in the United States have a new resource to help jumpstart their careers. Starting this month, the National Postdoc Association (NPA) will offer its members personal coaching services in conjunction with YouPlus, a coaching company.

Interested postdocs will be able to get advice primarily via the telephone with follow-up and additional support by e-mail. The coaching process often involves homework assignments in combination with telephone counselling services. These phone conversations encourage introspection and reflection while discussing the postdoc's passions and strengths, and the available career options.

NPA members will be eligible to buy personal coaching services from YouPlus at discounted rates. The usual hourly rate is $90 an hour; NPA executive director Cathee Johnson-Phillips declined to reveal the discounted price.

Although it had been under discussion for some time, the agreement came after the financial downturn pushed negotiators to expedite the process. Johnson-Phillips and others in the NPA are trying to meet a long-felt need: members have, for some time, been asking for more help in developing their skills, in the hope of feeling more comfortable pursuing all the available career options.

Postgraduate researchers often benefit from one-to-one confidential career discussions, says Clare Jones, of the career development centre at the University of Nottingham, UK.

"They feel free to express their concerns," she says. "They don't worry that it's going to have any impact on how others view them or their work." **G.B.**

Making memories

You must remember this ...

John Frizell

Ellie relived the moment — her break from the pack, her shot on goal, the shocked look of the goalie as the ball soared past him, just out of reach, and the deafening roar of the crowd, so powerful that she could feel it like waves drumming on her body — and shook her head. This was a boy's memory. The other players were all male and the leg that had kicked the winning goal was hairy. Yuck.

Something cold was creeping into her stomach. A thing like this could only have come from Jamie. Jamie was probably the most irritating younger brother in the world but he was still her brother.

She knocked on the door of his room and then stepped well back. You never knew what might be on the other side.

Jamie's room was even weirder than when Ellie had visited last. There were more computers, many of them torn open, and other machines she could not identify. Jamie was working on one that looked different. It was scuffed white instead of matt black or grey and its open top and missing side revealed rows of tiny cylinders interconnected with coils of thin tubing.

There was something that looked like a big mechanical dog wedged between two boxes of parts on the floor. She placed her feet carefully, partly out of general caution, partly because she had just treated herself to a new pair of shoes.

She gave him her best no-nonsense stare, modelled on the one Mum used on them. He flinched.

"I remember kicking the winning goal in a big football game."

"Oops. It must have leaked out. I'll put a towel under the door next time."

The olfactory nerve is a direct extension of the brain so memories were administered in nasal sprays. The thought of Jamie's bootleg memories wafting down the hall frightened her.

"Jamie!"

The dog had come to life. She pointed at it. Its head turned, tracking the movement of her hand. It had fangs.

"Don't move. It can only see things that move quickly."

Jamie reached out slowly and smoothly and hit a key on his computer. The dog collapsed, inert.

"Where did you get that memory?"

"Made it."

Her stomach lurched. Only doctors and the police were allowed to manufacture memories. Even teachers had to have forms signed and countersigned before they could so much as *administer* a memory. This was serious stuff, worse than drugs. The police could arrest Jamie for this, *would* arrest him if they found out. Jamie would go to jail if they caught him.

JACEY

Implanted memories made society work. Someone who was aggressive was given memories of peaceful acts, a cheat was given memories of honesty. Sometimes it had to be done many times before the person's behaviour changed to match what they remembered. But society had to control what was implanted, not individuals. She had learnt that at school.

"We need to talk."

"Can't talk now. Big fight comin' up." He was loading two ugly bricks of scarred metal and plastic into a bag. They had armoured wheels and sharp things that slid out of their interiors. Every week he went off to fight these things against ones made by other boys almost as weird as him.

"You need to tell me now."

He kept on loading the bag with batteries, tools and spare parts as he talked. The story came out in bits and pieces. He had found the machine while scavenging at the local tip. It was broken and obsolescent, discarded by a research lab. The tip attendant had no idea of what it was and accepted £5 for it as scrap.

"It wasn't hard to fix. Just a blown motor-driver chip and a pump that seized when its motor stopped working."

"It's got to go."

"No way. This is a once-in-a-lifetime thing. I'll be careful. Besides ..." He pointed at the banks of tiny cylinders in his prize, each with its own bar code. "When the reagents run out, that's it. These chemicals aren't something you can order without attracting attention." He shouldered the bag; they went out into the hall and then he turned. "Do you want to come and watch me fight?"

After he was gone she went back to her room and had a long hard think about what to do.

Ellie woke the next morning feeling pleased with herself. She hadn't liked the idea of sneaking into Jamie's room but some things just had to be done. She relived the memory — she had crept into the room, moving slowly, careful to disturb nothing, and had triple-wrapped the machine in black plastic garbage bags. It had made a series of crashes, each fainter than the last, as it tumbled down the garbage chute. She would have to face Jamie at breakfast but at least he hadn't been pounding on her door or phoning her.

She brushed her hair and put on her best dressing gown. Ellie knew she had done the right thing and had saved Jamie from the consequences of his very silly actions. But he would be disappointed and angry, and was probably sulking. Still, he deserved an explanation and she wanted to get it over with. She knocked on his door.

"Go away Ellie. I'm busy."

She glanced down. There was a towel stuffed under the door. ■

John Frizell trained in biochemistry and works on oceans conservation for Greenpeace. In his spare time he walks, builds robots and writes short stories.

FUTURES